Vacuum Infusion (VI) Process Modeling and Material Characterization with Viscoelastic Compaction Models

by

Bekir Yenilmez

A Thesis Submitted to the
Graduate School of Engineering
in Partial Fulfillment of Requirements
for the Degree of

Doctor of Philosophy
in
Mechanical Engineering

Koc University

September, 2014

Koc University

Graduate School of Sciences and Engineering

This is to certify that I have examined this copy of a doctoral thesis by

Bekir Yenilmez

and have found that it is complete and satisfactory in all respects,

and that any and all revisions required by the final

examining committee have been made.

Committee Members:

____

Assoc. Prof. E. Murat Sözer

____

Assoc. Prof. B. Erdem Alaca

____

Assoc. Prof. Nuri Ersoy

____

Asst. Prof. Melis Şerefoğlu Kaya

____

Assoc. Prof. A. Tuğrul Seyhan

Date: ______________________

This page intentionally left blank.

Abstract

In the Vacuum Infusion (VI) process, a dry fabric preform is compacted between a single-sided mold half and a vacuum bag, and then impregnated with thermoset resin to manufacture polymeric fiber-reinforced composite parts. Use of vacuum bag as the upper mold half reduces the cost, but more importantly it allows to manufacture large parts such as wind turbine blades. Compared to two-sided mold manufacturing processes such as Resin Transfer Molding (RTM), VI suffers from significant thickness variation because of the non-stiff upper mold half. Manufacturing of parts with small dimensional tolerances require compaction characterization of the fabric preforms which can be used in the process modeling by coupling fabric preform and the resin flow.

Viscoelastic models have advantage over elastic models since they have the ability to model the time dependent compaction of the fabric. Since the fabric undergoes significant change in thickness with time even at constant pressure especially during relaxation stage, using elastic models greatly decreases the accuracy of the VI simulation. With viscoelastic models, it is possible to model both filling and post filling stages of the VI process with a greater accuracy than with elastic models. With this increased accuracy, filling time and final thickness distribution can be estimated correctly.

This study contributes to the composite manufacturing literature with the following achievements: (1) a compaction characterization procedure is designed to mimic the compaction behavior of fiber reinforcements used in VI; (2) an automated characterization experimental setup is constructed to reduce human error and increase the repeatability; (3) experimental characterization data allows to have a database for two fabric types (random and woven); (4) five viscoelastic compaction models (Maxwell, Kelvin-Voigt, Zener, General Maxwell and Burgers) with dampers and nonlinear spring elements, and an elastic compaction model are used to investigate different stages of VI; (5) comparison of the models allows to study the contribution of different elements of the compaction models and thus understand their physical responses in different stages.

8 different sets of experiments are conducted on each fabric type to investigate the effect of different compaction parameters (such as loading/unloading rates, relaxation pressure and whether the specimen is dry or wet) on the results.

Differential equation (DE) solvers are used on the derived system equations stage by stage to overcome discontinuity problems at the stage transitions.

It is seen that Burgers model outperforms other 4 models in terms of the parameter count and R^2. However, Burgers model undergoes infinite deformation under a constant load, which is not physically correct. Hence, Generalized Maxwell model with $n = 2$, which mimics the plastic deformation with slow viscous response, should be used if prolonged time of settling is expected.

By coupling a resin flow model and a viscoelastic compaction model (preferably Generalized Maxwell with n=2 or Burgers depending on which stage(s) of VI is desired to be modeled) in a complete VI process model, it is possible to simulate more accurate gradual pressure and thickness changes with time during the application of control actions in VI post-filling stage. Elastic models fail in these situations because they cannot model time dependent response, and thus viscoelastic models of this study should be preferred.

Özet

Vakum infüzyon (VI) imalat usulünde, kuru elyaf yatağı tek taraflı kalıp parçası ve vakum torbası arasında sıkıştırılır, daha sonra termoset reçine infüzyonuyla elyaf takviyeli kompozit parça imal edilir. Vakum torbasının üst kalıp parçası olarak kullanılması imalat masraflarını düşürür, fakat daha önemlisi rüzgâr tribünü kanatları gibi büyük parçaların imalatına olanak sağlar. Çift katı parçalı kalıpla imalat usullerine (Reçine Transfer Kalıplama, RTM gibi) kıyasla, rijit olmayan üst kalıp parçası sebebiyle VI parçalarında önemli miktarda kalınlık varyasyonu olmaktadır. Parça boyut toleranslarının düşük olması gerektiği durumlarda elyaf yatakların sıkışma karakterizasyonunun yapılması gerekmektedir. Sıkışma ve reçine akış modelleri birlikte çözülerek imalat usulü modellenmesi mümkün olur.

Elastik modellere kıyasla viskoelastik modeller, elyaf kumaşların zamana bağla sıkışma davranışını temsil edebildiği için avantajlıdır. Sabit baskı basıncında bile, elyaf kumaşların önemli miktarda kalınlık değişimine uğraması nedeniyle, elastik model kullanılması VI simülasyonunun doğruluğunu azaltmaktadır. Elastik modellere kıyasla viskoelastik model kullanarak, daha yüksek doğrulukla VI'ın kalıp dolumu ve dolum sonrası fazlarının modellenmesi mümkündür. Bu, kalıp dolum süresini ve son parça kalınlık dağılımını tahmin etmeyi mümkün kılar.

Parametre sayısı ve R^2 göz önüne alındığında, Burgers modelinin diğer 4 modelden daha yüksek performanslı olduğu gözlenmiştir. Fakat Burgers modeli, sabit yük altında fiziksel olarak gerçekçi olmadığı halde sonsuz deformasyona uğramaktadır. Eğer simülasyonda uzatmalı yerleşme zamanı bekleniyorsa, yavaş viskoz davranışlı plastik deformasyonu temsil eden Generalized Maxwell modeli (n=2) kullanılmalıdır.

Bu çalışma kompozit imalat literatürüne aşağıdaki katkıları sağlamaktadır: (1) VI da kullanılan elyaf takviye yataklarının sıkışma davranışını temsil eden sıkışma karakterizasyon deney prosedürü tasarlanmıştır; (2) işçilik hatalarını azaltmak ve tekrarlanabilirliğini arttırmak için otomasyona geçirilmiş karaterizasyon deney düzeneği kurulmuştur; (3) keçe ve dokuma elyaf yatak tipleri için, karaterizasyon veri tabanı elde edilmiştir; (4) damper ve lineer olmayan yay kullanan 5 viskoelastik

sıkıştırma modeli (Maxwell, Kelvin-Voigt, Zener, Generalized Maxwell ve Burgers) ve 1 elastik model kullanılarak VI'nın farklı fazları incelenmiştir; (5) modellerin karşılaştırmaları yapılarak, farklı elemanların sıkıştırma modeline etkisi ve parametrelerin fiziksel tepkiye katkısı çalışılmıştır.

Her bir elyaf tipi için 8 farklı deney seti yapılarak farklı sıkıştırma parametrelerinin (yükleme/boşaltma hızı, relaksiyon basıncı ve numunenin kuru ya da ıslak olması) karakterizasyona etkisi incelenmiştir.

VI'ın her bir fazı için diferansiyel denklem çözümleyicilerinin sistem denklemleri üzerinde kullanılmasıyla fazlar arasındaki süreksizlik problemi bertaraf edilmiştir.

Reçine akış modeli ve bir viskoelastik modelin (modellemesi istenen VI fazına bağlı olarak tercihen Generalized Maxwell (n=2) veyahut Burgers modeli) beraber kullanılmasıyla, VI dolum sonrası fazında kontrol aksiyonları sonucu oluşan basınç ve kalınlık dağılımı zamana bağlı geçişleri daha yüksek hassasiyetle simüle etmek mümkün olmaktadır. Elastik modeller zamana bağlı tepki veremedikleri için bu durumlarda başarısız olmakta bu sebeple bu çalışmada verilen viskoelastik modeller tercih edilmektedir.

To my family

Acknowledgement

I would like to express my sincere gratitude to my supervisor Murat Sözer for all his guidance, efforts and continued support. Additionally, I wish to extend my gratitude to the members of my thesis committee for their critical reading, invaluable feedback and insightful comments.

I also wish to offer my sincerest thanks to the members of my research group; Barış Çağlar and Akif Yalçınkaya for their endless support both as colleagues, and as friends during my years in the composite material manufacturing lab.

My heartfelt appreciation goes to my family for their endless love and support, also to my friends for helping me get through the difficult times, and for all the emotional support, camaraderie, entertainment and caring they have provided. All the good times that I had with my friends during these difficult times, will not be forgotten, even after lost friendships. I also would like to express my gratitude to Miraç Ünlüer who is always there willing to support me as a good friend.

I would also like to thank to the staff of College of Engineering and Graduate School of Sciences & Engineering for their support. Many thanks are also due to TÜBİTAK (The Scientific and Technical Research Council of Turkey) for their scholarship at Koç University, Istanbul, Turkey.

Table of Contents

List of Tables

List of Figures

1 Introduction

1.1 LCM Processes

In Liquid Composite Molding (LCM) processes, a dry fiber preform is compacted in a mold cavity, and liquid thermoset resin is injected to impregnate the empty spaces between the fibers. The composite part is demolded after partial or complete cure of the resin. The dimensions of the mold cavity do not change with time during the injection if the mold plates are made of thick and stiff materials eliminating bending of the plates. Resin Transfer Molding (RTM) uses a double sided mold with rigid mold parts and/or stiffening bars; thus a small dimensional tolerance in thickness can be achieved. However, the tooling cost is high, and large parts cannot be manufactured due to the in-plane dimensional limitations in machining the mold parts using conventional milling machines. Large parts with in-plane dimensions of tens of meters can be readily manufactured in single-sided mold applications of LCM such as Vacuum Infusion.

1.2 Vacuum Infusion

In Vacuum Infusion (VI, a.k.a. Vacuum Assisted RTM, VARTM or Resin Infusion, RI), and its derivatives such as FASTRAC and VIPR processes, the fiber preform is compacted between a lower rigid mold half and a vacuum bag which functions as the upper mold half. The resin pressure changes spatially and with time as it propagates, and thus the compaction pressure on the fiber preform changes accordingly. As a result, the part thickness changes both spatially and with time. One needs to understand the compaction behavior of a fiber preform in VI, if a process model and control is applied to minimize the variation in the part thickness.

In this study, a viscoelastic model will be used to fit a set of compaction characterization experiments that is designed to mimic the fiber compaction during the pre-injection, injection and post-injection stages of VI. A through analysis of the viscoelastic model reveals the elastic and time-dependent viscous response of the preform at different compaction pressures and rates, and allows modeling the fiber compaction so that manufacturing of parts with tight dimensional tolerances will be possible.

1.2.1 Thickness Monitoring Methods in the Literature

To investigate the compaction behavior of an uncured composite part (fiber preform and liquid resin), various experimental monitoring schemes, characterization models and simulations have been studied in the literature. Commonly used methods for thickness monitoring include using (i) dial gauges [1–5], (ii) linear variable differential transducers (LVDT) [6–16], (iii) laser displacement sensors [8,17,18], (iv) digital speckle photography (DSP) [19–21], and (v) 3D scanners (i.e. cameras that can capture 3D point cloud) [5,22]. In addition to monitoring of the thickness distribution, pressure sensors were used in the setups [1–3,5,7–10,12,14,20] to see the coupled effect between the pressure and the thickness.

1.3 Literature on Compaction Modeling

Compaction characterization experiments and models relate a fabric preforms' thickness (and thus fiber volume fraction) and compressive stress applied in the thickness direction. The experimental data could be in the form of a graph, look-up table or a function. Various compaction models are either elastic or viscoelastic with different stiffness and damper arrangements. The experimental data or model fit to experiments can be used to calculate the clamping forces in an RTM mold, or to simulate single-sided mold processes such as VI, in which the thickness of the preform changes spatially and with time due to varying resin pressure within a rigid mold half and a vacuum bag. Depending on the process type (i.e. whether the thickness is constant or not), characterization method may differ as well as ranges of fiber volume fraction and compaction pressure. From now on, to be consistent with mechanics literature, the compaction pressure, P, applied on the fabric will be called the (compaction) stress, σ, and thickness change will be considered in terms of absolute true strain, ε, which is $\ln(h_0/h)$.

1.3.1 Compaction Modeling Based on Characterization Parameters

a. Dry vs. wet vs. dry/wet fabric

Previous studies done by Yenilmez and Sozer [1,2,18] presents that the compaction behavior of a fabric preform may change significantly after saturation. In these studies, it is seen that the thickness of a random fabric decreases significantly after wetting due to the lubrication effect of the resin. On the other hand, the change in thickness due to wetting was negligible for woven and biaxial fabrics. Thus, depending on the fabric type, it may be necessary to conduct experiments on both dry and wet fabrics. Alternatively, the fabric can be wetted at an intermediate stage of a characterization experiment (rather than starting with already wetted fabric) to mimic the VI process and have more realistic experimental data to characterize the fabric.

Compaction characterization experiments can be used to investigate different stages of the RTM and VI processes: (1) compaction stress, $\sigma(t)$ varies with time if $h(t) =$

$h(t = 0) = c$, constant as in the entire RTM process; (2) part thickness, $h(t)$ varies with time if σ is fixed as in the fiber settling (during pre-infusion) and relaxation stages (during post filling) of VI; (3) part thickness, $h(t)$ varies with time if σ varies with time during the mold filling stage due to the coupling of compaction and resin flow. Item (1) can be studied to determine the mold closing force in RTM. Some studies used dry fabric characterization [10,23–33], whereas the characterization of wet fabrics was also included in [7,8,15,34–47]. In all of these studies, the fabric specimen is either dry or wet (fully saturated) throughout the characterization experiment. In VI process, dry data are used for modeling pre-infusion stage, and wet data are used during and after mold filling stages. To mimic the VI process better, the recent studies start characterization with a dry fabric specimen and saturates the fabric during the experiments [1,2,4,9,12,18,48,49]. The transition corresponds to the resin arrival to a location in VI. At this transition, a sudden change in thickness may be observed at constant compaction pressure due to lubrication effect of the resin.

b. Strain- and stress-controlled experiments

There are two control approaches while conducting the characterization experiments. Either, strain is controlled and resulting thickness is measured, or vice versa. Details of each test method are given below.

i. Strain-controlled experiments

A strain-controlled characterization setup consists of a compression chamber or a press which has an accurate positioning system and a stress measuring sensor. While decreasing the specimen thickness (i.e. chamber height) usually with a computer controlled predefined scheme, the corresponding resisting force (or stress) applied as a reaction by the preform specimen is measured and recorded. Thus, the resulting compression stress versus strain data can be obtained. Displacement of the chamber is usually achieved using an electro-mechanical system. An extensometer (which can be either contact or non-contact type such as laser) is used to measure the chamber height. The stress is monitored by measuring the resisting force with a load cell. The common practice is to use a universal testing machine (UTM) equipped with a custom compression chamber.

Majority of the studies in the literature used strain-rate (or displacement) controlled equipment. These experiments are mainly conducted for characterizing mold (tool) closure force in RTM [25,50–53], where the fabric is dry and the compaction pressure is in the range of MPas. The availability and reliability of UTMs allowed researchers to use strain-controlled experiments even for the characterization of the VI process. Early and some analytical studies characterized only dry fabrics [24–26,28–31,33], whereas some recent studies [36,37,39,41,44–46,50] used both dry and wet specimens.

In strain rate controlled characterization using UTMs, wet data is generally obtained by saturating the fabric before the experiment. However, dry to wet transition was also studied in [50].

The most important aspect of a strain-controlled characterization experiment is its similarity with the nature of the fiber compaction in RTM. After the preform is placed inside an RTM mold, the mold is closed to a specific final thickness value. As the fabric is compacted under press or mechanical clamping forces, the fabric resists the motion very similar to the strain-controlled characterization experiment. Thus, a strain-rate controlled experiment is the most appropriate characterization approach to estimate RTM mold closure force and to calculate the required clamping force to compact the preform to a specific thickness (thus fiber volume fraction).

The data can be extended to a wide range of fiber volume fractions by repeating the experiments at different final thicknesses. One may measure the instantaneous stress only for an elastic approach; or record the time-dependent stress value to investigate the viscoelastic behavior. This strain-rate controlled experimental approach can be used not only for RTM, but also for similar processes such as compression molding and compression resin transfer molding (CRTM) in which the mold cavity thickness is set to a final value, and the stress is dependent on the thickness (and thus strain), but not vice-versa.

Another advantage of this control approach is the suitability of a standard test equipment (universal test machine, UTM) integrated to a custom-made chamber, which is usually a small RTM mold. UTMs are typically more reliable and precise than custom-made stress-controlled testing equipment.

ii. Stress-controlled experiments

In stress-controlled characterization experiments, the compaction stress is controlled as the independent variable, and the displacement (i.e. the change in thickness), thus the strain of the specimen, is measured. Either feedback controlled (closed loop) mechanical presses (e.g. UTMs) are used, or stress is applied with a hydraulic, pneumatic or vacuum system. The displacement is usually measured with an extensometer similar to the strain-controlled setups. To measure the initial thickness, a minor load is applied on a specimen. One could ideally try to measure the initial thickness at zero loading, i.e. as the loose fabric layers rest over each other freely without any force exerted on them. However, this may involve large statistical variations depending on inconsistent placement of the layers. To eliminate this, a fixed and minor load is applied and corresponding thickness is considered as the initial thickness. This minor load depends on the machine used and also defines the lower limit of the characterization range.

Since stress-controlled characterization should be preferred for VI compaction modeling, majority of the studies conducted these experiments using a typical VI setup [7,8,14,23,49]. The pressure is varied and the thickness of the specimen is measured by using a dial-gauge, LVDT or a similar sensor. In stress-controlled setups, wetting can be done by infusion as in the actual VI process. Some studies only used dry fabrics [23,31,32]; and some used both dry and wet fabric [4,7,8,12,14,38,43,48,49] similar to strain-controlled characterization. Some researchers also included dry to wet transition [4,48,49] by impregnating the specimen with resin after loading and fiber settling stages. Besides using an actual VI setup for stress-controlled characterization, some researchers [32,43,48] used UTMs where the applied stress can be controlled by closed loop control.

RTM mold allows strain-controlled fabric compaction due to fixed mold gap. VI experimental setup allows stress-controlled compaction characterization if the user adjusts the vacuum pressure and measures the part thickness. Since this thesis aims to model VI process, stress-controlled compaction characterization will be preferred by using an experimental setup which is a VI setup integrated with some sensor systems and a quick radial injector (it will be described in the proceeding sections).

A vacuum is applied to compact the fabric preform at a pressure level (atmospheric pressure minus the vacuum pressure) set by the experimentalist, and the part thickness changes because the upper mold (vacuum bag) is free to move. The resulting thickness is measured by using an appropriate sensor.

1.3.2 Elastic models

In the literature, static (elastic) models have been commonly used for fabric compaction characterization. Elastic models are easier to fit the results of characterization experiments. Especially power-law fit is preferred for analysis because of the ease of manipulation in analytical formulations, such as derivation and integration.

Elastic models are also easier to characterize. They relate strain directly to stress. There is no time dependence, or simply, the rate or history of applied strain has no effect on the instantaneous stress value.

a. Power law fit

Power law fit for fabric compaction is commonly written as,

$$V_f = A + B\,P^C \qquad \textbf{(1.1)}$$

where V_f is the fiber volume fraction, P is the compaction pressure and A, B, C are the empirical constants obtained by fitting to the experimental data [42,47]. Notice that A is the fiber volume fraction at the zero compaction pressure. Some studies [1,4,5,24,34–36,40,46] used a simpler form where $A = 0$ and thus $B = V_{f,0}$. It should be noted that the function grows rapidly at high pressures, thus care should be taken if the fitted parameters will be used outside of the characterization pressure domain. That means the user of this model should be cautious while extrapolating the data.

b. Analytical models

In the literature, analytical compaction models are available for fabrics with well-defined unit cell geometries [54,55]. A unit cell is a periodic fiber structure in the fabric specimen. The solution of the analytical model is usually tedious; and may not result in a better solution than experimental characterization. This is usually due to the assumptions made both in the unit cell geometry and compaction model.

c. Other empirical models

Besides the power law fit (Equation **(1.1)**), the following empirical models were used:

$$V_f = \frac{(1-\phi)V_{f0}}{1-\epsilon}$$

$$\epsilon_{wet} = a + b\,\frac{P}{P+c} \tag{1.2}$$

$$\epsilon_{dry} = a(\,1 - e^{b\,P})$$

in [8,9] where a, b, c are model constants.

$$V_f = k\left(\frac{P}{P_i}\right)^m \tag{1.3}$$

in [24] where k and m are model constants.

d. Using database

Instead of using an empirical formula such as Equations **(1.2)** and **(1.3)**, the results of compaction characterization experiment can be organized as a look-up table [1]. If the look-up table has a fine increment, the interpolation between two data points may not result in a significant error, no matter what the interpolating function is. Similar to empirical equations, the user should be cautious when extrapolating the table data.

1.3.3 Viscoelastic models

Viscoelastic models are heavily dependent on strain-rate and applied stress history, which makes them time-dependent. The advantage of a better model fit comes with a cost which is the requirement of larger set of experimental data as a result of more parameters (due to time-dependency). To capture the true behavior of the fabric accurately, in other words to fit model as close as possible, multiple experiments with varying strain rates, relaxation/settling times and major or minor strain/stress values at these stages must be conducted. Moreover, viscoelastic models are usually in the form of ODE making it very hard to obtain analytical solutions. Thus, numerical methods are used to solve equations containing viscoelastic models.

a. Empirical models

Empirical models are obtained by fitting a mathematical formula to the experimental data. The formula can be selected intuitively. In [15], an empirical relaxation model is used to have viscoelastic response of carbon-epoxy pre-preg. Similarly, [27] decomposed the model to strain and strain-rate components and fitted to the experimental data. These models were shown to fit experimental data well for specific applications with predefined input (i.e. constant rate compaction and constant thickness relaxation); however, the use of the model is questionable for different applications or inputs.

b. Mechanical models

Mechanical viscoelastic models are composed of springs and damper connected in various configurations. Elastic response is obtained with spring; and viscous response is obtained by damper. The most known and basic two models are Kelvin-Voigt and Maxwell models. More complicated models include Kelvin chain, Zener, Burgers, generalized Maxwell and fractional element models. In composite material literature, mechanical viscoelastic models are relatively new. In 2006, Kelly et.al. [39] used standard linear solid model (a.k.a. Zener) to model constant rate compaction and stress relaxation of dry fabric. In the same year, Sajn [28] compared the performance of the well-known viscoelastic models (Maxwell, modified SLS, Alfrey's, 2 and 3 component Maxwell models) along longitudinal (wrapping) direction. He used this model while studying fabric winding into cloth batch. In 2008, Echaabi [45] compared relaxation performance of Burgers, Zener, and Maxwell models for a fabric under constant strain. In 2012, Somashekar et.al. [33] used "5 element Maxwell model" for relaxation behavior.

These models were specifically used for the modeling of stress relaxation stage in RTM only. This thesis contributes to the literature by modeling not only RTM (with strain-controlled characterization) but also all stages of VI (with stress-controlled characterization). A detailed comparison of the five models will be studied as well.

1.4 Literature on Coupled Flow and Compaction Modeling

By using Darcy's law and the relation between compaction pressure and permeability in the continuity equation, a process model for VI can be obtained. Most of the studies [23,34,36,56,57] used well accepted Kozeny-Carman equation,

$$K = A\frac{\left(1 - V_f\right)^3}{V_f^2} \qquad \textbf{(1.4)}$$

to fit the experimental permeability data to fiber volume fraction. Some of the researchers [1,40,58] used power-law fits for permeability and/or compaction:

$$K = a\left(V_f\right)^b \qquad \textbf{(1.5)}$$

$$h = c\, P^n \qquad \textbf{(1.6)}$$

We [2] used experimentally collected compaction database data with dry to wet transition. Our results showed that the lubrication effect upon resin arrival is significant for random type of fabrics but not for woven or biaxial, and it should be accounted for a realistic process simulation.

1.5 Literature on Process Control

As mentioned in the introduction, the compaction pressure on a fiber preform changes as the flow propagates thus the thickness of the part varies with time and spatial coordinate. To have a uniform thickness throughout the part, numerous methods are used to control the process.

To reduce the thickness variation, the most commonly used method is resin bleeding [59]. In resin bleeding, the injection gate is closed and vacuuming is continued through the ventilation port after complete mold filling. As the resin exits, the fiber volume fraction and final mechanical properties increase. One other major advantage of resin bleeding is to decrease the overall thickness variation.

It is also observed in [60] that, fiber tows having a lower permeability than the bulk preform is allowed to saturate by applying bleeding. As a result, undesired micro voids are reduced. The cause of thickness variation remaining after bleeding is explained by Yenilmez et. al. [2]. We showed that, for the three different types of fabrics (random, woven, and biaxial), steady-state equilibrium for thickness could not be obtained under static loading even after 15 minutes. This is due to the fact that the fabric preform's compaction is viscoelastic; that means not elastic only. For this reason, bleeding alone cannot eliminate the thickness variation unless very long relaxation is allowed.

Heider et al. [61] investigated the effect of debulking. The repeated compression-relaxation cycles applied on of the preform to increase the packing of fiber (i.e. increase in fiber volume fraction) and to decrease the thickness variation. Their experimental results also showed that debulking reduces the spring-back effect of the preform as much as 40%. As a result, reduced thickness variation was observed after full injection.

2 Materials

In this chapter, materials used in this study are listed and technical specifications are given. In the first half, characterized fabric types and configurations are presented. In the second half, saturating medium is documented, since the type of fluid also affects the response behavior.

2.1 Fabrics

Fabrics are the reinforcement materials in a composite part. They are responsible for carrying the applied loads, and hence define the strength of the material. Most commonly used material types are glass and carbon fibers, followed by aramid (Kevlar). Carbon is preferred for its high strength to weight ratio and aramid is preferred where impact toughness is the key design parameter. On the other hand, glass fiber is preferred for its lower cost, where above mentioned qualities are not critical for the application.

Fibers can either be continuous or discontinuous. Parts containing discontinuous fibers are called short/long fiber reinforcement plastics. Discontinuity of the fibers reduce the overall strength of the part while making it suitable for injection processes.

In this study, continuous fibers in the form of fabrics are used, in which the manufactured parts are called advanced composites due to their high strength.

The important parameters for selecting the fabric are summarized as type, superficial density and fiber orientation (if not random fabric is used). Fabric type directly affects the strength and toughness of the material. Superficial density is the areal density of fabric which represents the amount of reinforcement material available per square area. Independent of fabric tow orientation, this measure gives a rough estimate of the strength of the part. And lastly, the fabric orientation is important for part strength characteristics. Unlike traditional materials such as metals, composites are not isentropic in nature. Strength characteristics can differ significantly when using directional fabrics like non-crimp stitched fabrics. As a result of aforementioned reasons; fabric type, superficial density and orientation of fiber tows (unless random) are need to be specified for any fabric. In proceeding section, these parameters will be documented.

2.1.1 Random (Continuous fiber mat) fabric

Random fabrics made with continuous fiber tows laid at random directions like a mat that is why it is also called continuous fiber mat. They can be either stitched or chemically bonded to keep the fabric structure. Random fiber mats preferred when there is no specific loading direction or ease of fabric preparation can be preferred over strength of material. Laying the fabric on the mold is much simpler, compared to woven and axial fabrics, especially on convex mold geometries.

Although random fabric expected to have more consistency with more isotropic properties, large variations (more than 50%) observed especially within roll stacks [2,62].

In this study, Fibroteks brand stitched random fabric has been used, which is shown in Figure 2-1. It is an E-glass type fabric with a superficial density of 450 g/m^2. The average fiber length is 50 mm. The applied sizing makes this fabric compatible with polyester, epoxy and vinyl-ester resins.

Figure 2-1. Fibroteks E-glass Stitched Random Fabric.

2.1.2 Woven fabric

Woven fabrics have superior directional strength properties. Since it consists of continuous tows along two main directions (0 and 90 degrees), load carrying capacity is maximum at these directions. Depending of the application, multiple layers of woven fabric stacked with an offset in degrees and named accordingly. As an example 45 degree offset of one layer will result in high loading capacity along 4 (0, 45, 90, 135 degree) directions.

Woven fabrics defined by its warp/weft ratio and superficial density. High density fabrics used for structural element, whereas low density (fine) fabrics commonly used at outer layers for smoother surface finish.

As shown in Figure 2-2, Fibroteks brand E-glass type woven fabric with a warp/weft ratio of 1:1 is used in this study. Superficial density of the fiber is 500 g/m^2. Sizing is the same with random fabric, which makes this compatible for polyester, vinyl-ester and epoxy.

Type and sizing of the two fabrics are selected to be the same to avoid extra variables and just focus on fabric configuration. However, there is 10% difference on superficial densities between the two fabrics, which will only affect geometrical properties but not chemical interaction with resin.

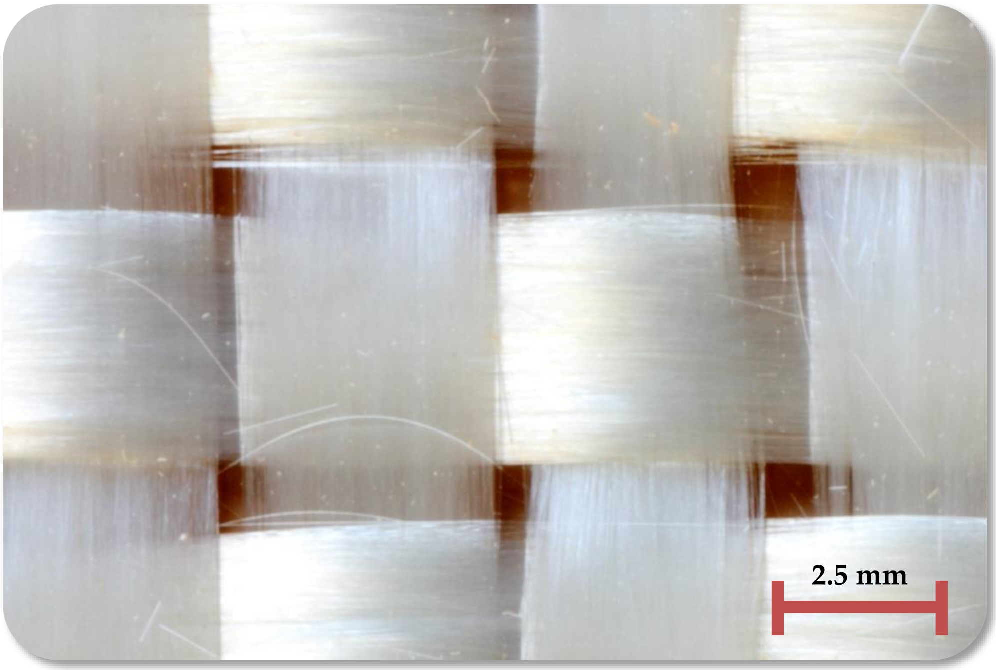

Figure 2-2. Fibroteks E-glass Woven Fabric.

2.1.3 Core

In some VI applications, flow speed is not sufficient for desired mold filling time. Operator must either increase pressure difference, decrease resin viscosity, or increase permeability of fabric to overcome this issue. Pressure difference that is used to drive the resin can be theoretically set to 100 kPa at maximum. Practically this limit is around 80 kPa (may differ depending on resin additives) to avoid cavitation and formation of bubbles in the resin. Resin viscosities are roughly in a range of 150-500 mPa.s for RTM and VI applications. Due to these limitations, permeability of fabric is altered to decrease process time. As mentioned in the first chapter, either flow mesh or core material can be used.

In CMML laboratories, polypropylene (PP) core material seen on Figure 2-3 is used. The core material is manufactured by Metyx and has a superficial density of 250 g/m^2.

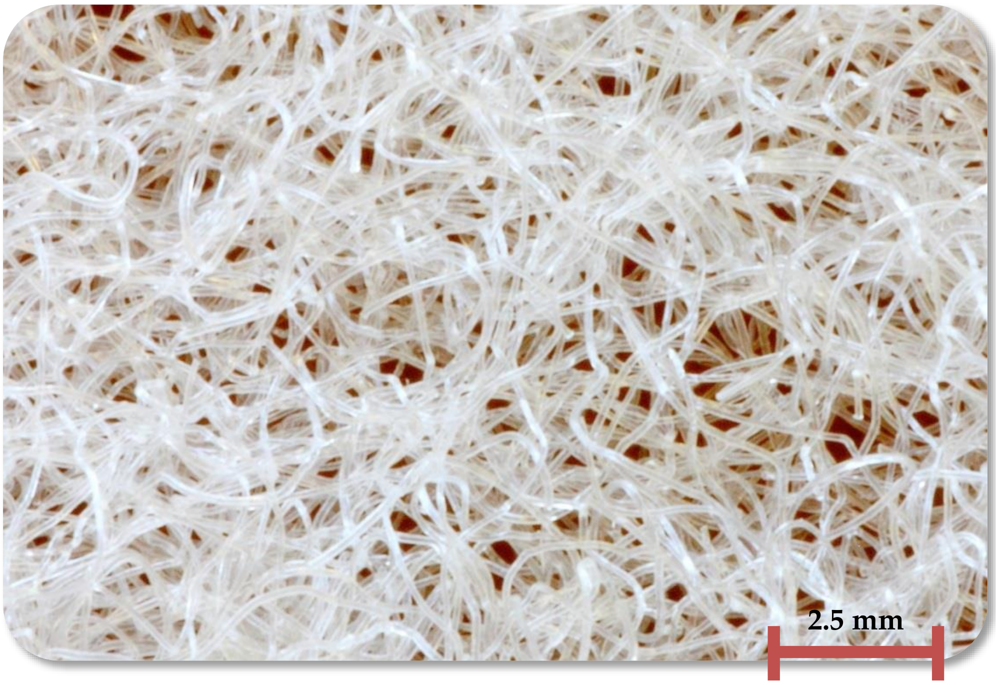

Figure 2-3. Metyx Meticore 250PP core.

2.2 Test Fluid

For either of the actual VI experiments or material characterization experiments, one can either use an actual resin system appropriate for LCM processes (such as polyester resin or epoxy) or a dummy test fluid. Previous studies [1,2,18] have demonstrated that the major requirement for a test fluid to be used in characterization is the similarity (indeed equality) of viscosity values of the test fluid and the actual resin system. However, some studies [63] have also showed that not only the viscosity, but also the surface energy of the fluids should be comparable.

2.2.1 Polyester Resin

In Koc University CMML, general purpose polyester resin, Poliya Polipol 337 is commonly used to manufacture fiber reinforced composite parts. It has a density of 1096 kg/m^3 and viscosity varies between 190 and 300 mPa.s, depending on the temperature and the age of the batch. It is a room temperature curable polyester resin with addition of cure agents (MEK peroxide and Cobalt solution).

2.2.2 Diluted Corn Syrup

Dealing with actual resin system requires tedious cleaning and long cycle time especially if curing occurs. Additionally, if appropriate ventilation is not applied, it may be harmful to human health, especially when high volumes are used. To ease the characterization experiments, and to reduce the health risks mentioned above, diluted corn syrup was used as the test fluid in this study.

The thick corn syrup was diluted with water so that its viscosity is set to a value of 200 mPa.s, which is a typical viscosity value measured for available polyester resin batch. Corresponding density of the corn syrup is measured as 1080 kg/m^3.

3 Experiments

Two types of experiments are conducted in this study: (i) Actual VI experiments, and (ii) Compaction characterization experiments. VI experiments are conducted to observe how the thickness of a fabric preform changes during a typical VI process. The thickness data is shown to be dependent on pressure and time. Also, the instant thickness decrease upon resin arrival can be seen for some types of fabrics, and not significantly in some other types of fabrics.

In the compaction experiments, compaction material behavior of different fabric types is investigated by controlling the independent variable and measuring the dependent variable. The experimental setup and the procedure are given below in detail.

3.1 VI Experiments

The compaction on the fabric changes during the VI process. As explained before, the flexible upper mold (i.e. vacuum bag) allows the fabric to move freely. The change in thickness is heavily dependent on the type of the fabric structure. Well packed fabrics, such as stitched non-crimp fabrics, do not show as significant change in thickness as random fabrics due to both (i) change in pressure, and (ii) lubrication effect caused by wetting.

The experiments conducted in this section investigate the thickness variation during a VI process. The thickness distribution along a 1-D mold is measured at fixed time intervals as the flow propagates. Measurements are continued even after complete mold filling, to investigate how the thickness changes at an almost constant pressure distribution.

3.1.1 Experimental Setup

The experimental setup is shown in Figure 3-1 and it consists of a flat lower mold plate with two inlet (injection) and two exit (ventilation) ports. Two infusions are done simultaneously side by side in [64]. On the left (Figure 3-1a) the fabric is covered with a vacuum bag. On the right (Figure 3-1b), it is also covered with a vacuum bag but additionally the thickness is constraint at its minimum value (initial thickness value) with an acrylic lid. The thickness of the left mold is monitored using a laser displacement sensor Omron Z4M-W40RA. The thickness distribution is obtained with the rail-car mechanism moving this sensor along the flow direction. The movement of the car on the rail is obtained with a stepper motor, which is interfaced to a PC running Matlab. With the help of Matlab, the thickness distribution can be seen in real-time.

The arrival time of flow fronts of both molds are recorded visually at each 20 mm mark. On the right mold, the flow arrival time can be used to get permeability data since the gate (inlet and vent) pressures and thickness is known. The differences on the flow arrival times also gives a general idea of how safe it is to assume constant thickness in a VI simulation for that type of fabric at used pressure range (i.e. between the range of inlet and vent pressure.).

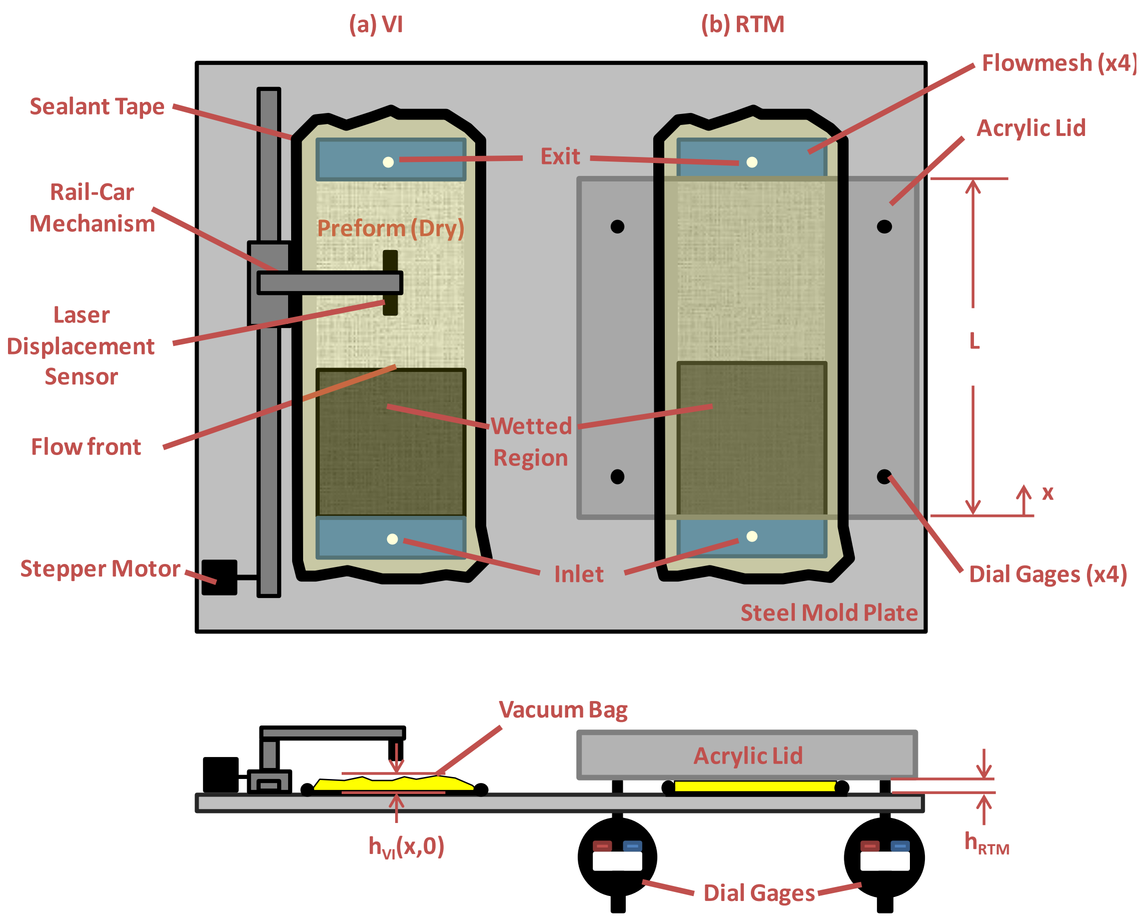

Figure 3-1. VI Experiment setup [64].

3.2 Compaction Characterization Experiments

As mentioned in the literature review, some researchers [7,8,14,23,49] related compaction pressure and thickness by using an actual VI experimental setup. After the compaction pressure is set to a particular value and it almost settles, the thickness is measured. In this approach, a static relationship is obtained resulting in an elastic compaction model. However, as seen from the results in the previous section, the thickness varies significantly with time under a constant pressure, and thus one needs to use a viscoelastic model instead of an elastic model to capture a more realistic response. The following process parameters are varied to investigate the dependency of the thickness on those parameters: Compaction and de-compaction pressure rates; the maximum compaction pressure; the number of fabric layers; and the type of fabric.

3.2.1 Former Setups

The setups that are used by the author in the current and the previous studies [1,2] are strain-controlled type. A predefined stress is applied on a fabric specimen and the resulting thickness is measured.

a. Setup with manual loading and external wetting

The first version of the previous setup, which was used in [1], is shown in Figure 3-2. This experimental setup consists of a piston cylinder pair, where a fabric specimen is placed in the cylinder prior to the experiment. The stress on the fabric is applied by adding weight over the piston. The resulting thickness is measured by using 4 dial-gauges which are attached between the piston and the cylinder.

The experiments were conducted at a constant loading and unloading rates and also at constant settling and relaxation pressures. The drawback of the setup in [1] was that, the wetting was done manually by removing the piston (i.e. actually unloading it completely) and then dipping the fabric specimen into the resin. The rest of the experiment was continued after the specimen was placed back in the cylinder and loaded almost instantaneously to the major load.

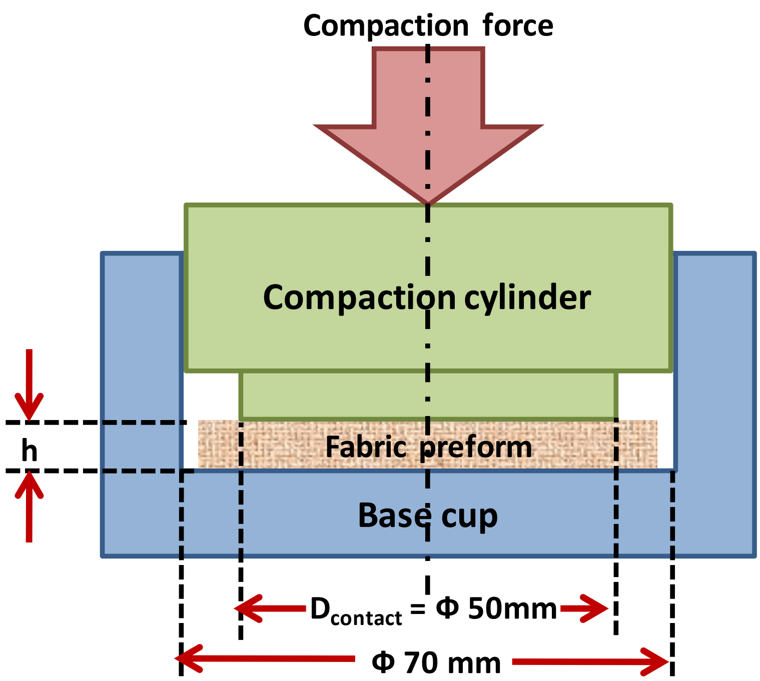

Figure 3-2. Compaction characterization setup used in [1].

b. Setup with manual loading and internal wetting

The previous setup was modified in the author's next study [2] as shown in Figure 3-3. The minor (minimum) pressure was decreased by using a lightweight piston (by changing the material and also making it hollow instead of solid one). This resulted the minor pressure to decrease from 5 kPa down to 2 kPa. To saturate the fabric without removing the cylinder, and hence removing the compaction stress, an injection port was added at the center of the base cup. Moreover, channels are opened on the compaction cylinder to remove the air and the excess resin, so the pressure will not build up during resin injection, otherwise it may lift the compaction cylinder up.

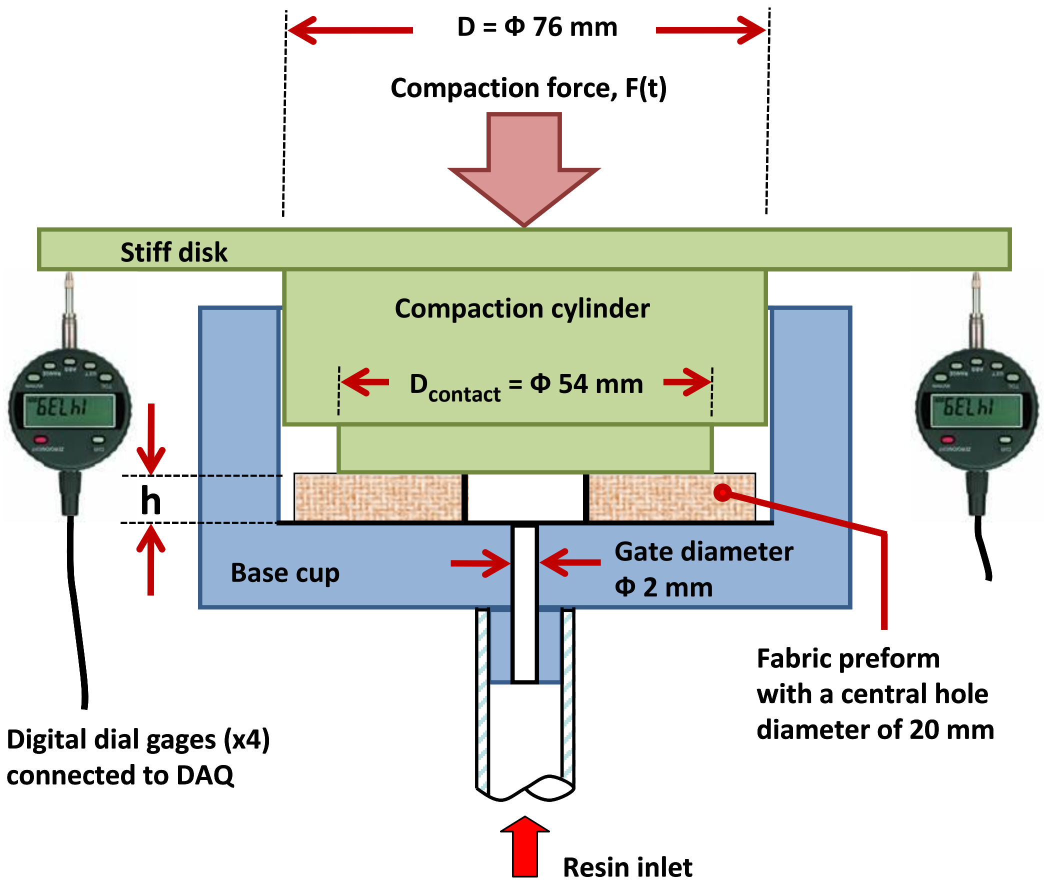

Figure 3-3. Compaction characterization setup used in [2].

This setup was successfully used in [2] to monitor the thickness while varying the pressure. The time dependent behavior was also monitored during relaxation stage. User interaction was needed to start and stop the loading and unloading stages. Hence, inherent human error can significantly affect the values of time dependent viscoelastic model parameters. The following section describes an automated setup which eliminates this drawback.

3.2.2 Automated setup with vacuum assisted wetting

An automated experiment setup was made to eliminate the human error involved in previous setups. This automation is necessary to accurately start and end stages of characterization experiment, which will be crucial when determining the parameters of a time dependent (e.g., viscoelastic) model. Also, it increases the repeatability of the experiments by eliminating the user interaction and thus human errors as much as possible. To automate the experimental procedure, the previous compaction characterization setups are discarded and a new setup is made out of scratch.

a. Mechanical System

The schematic of the experimentalal setup is given in Figure 3-4. The setup consists of 3 identical molds shown in the schematic which have inlet/vent ports, slots to increase flow (hence decrease wetting duration), and a vacuum bag to serve as an upper mold.

The compaction stress on a fabric specimen is obtained by applying a regulated vacuum in the mold. The regulated vacuum is obtained using a closed-loop controlled proportional valve connected to a vacuum pump. A single vacuum and resin system (pump, proportional valve, solenoid valves, vacuum reservoir, resin trap and resin reservoir) is used for all 3 molds. Solenoid valves are used to isolate, or to apply pressure differential between reservoirs, which are used for self-calibration and wetting stages, respectively.

The thickness is measured using a non-contact laser displacement sensor, Omron Z4M-W40. Thus, measurement is taken without disturbing the fabric. To avoid measuring local dents or peaks, a plastic disc with a diameter of 40 mm and a thickness of 1.30 mm is placed over the specimen, to measure the average thickness of the center of the specimen.

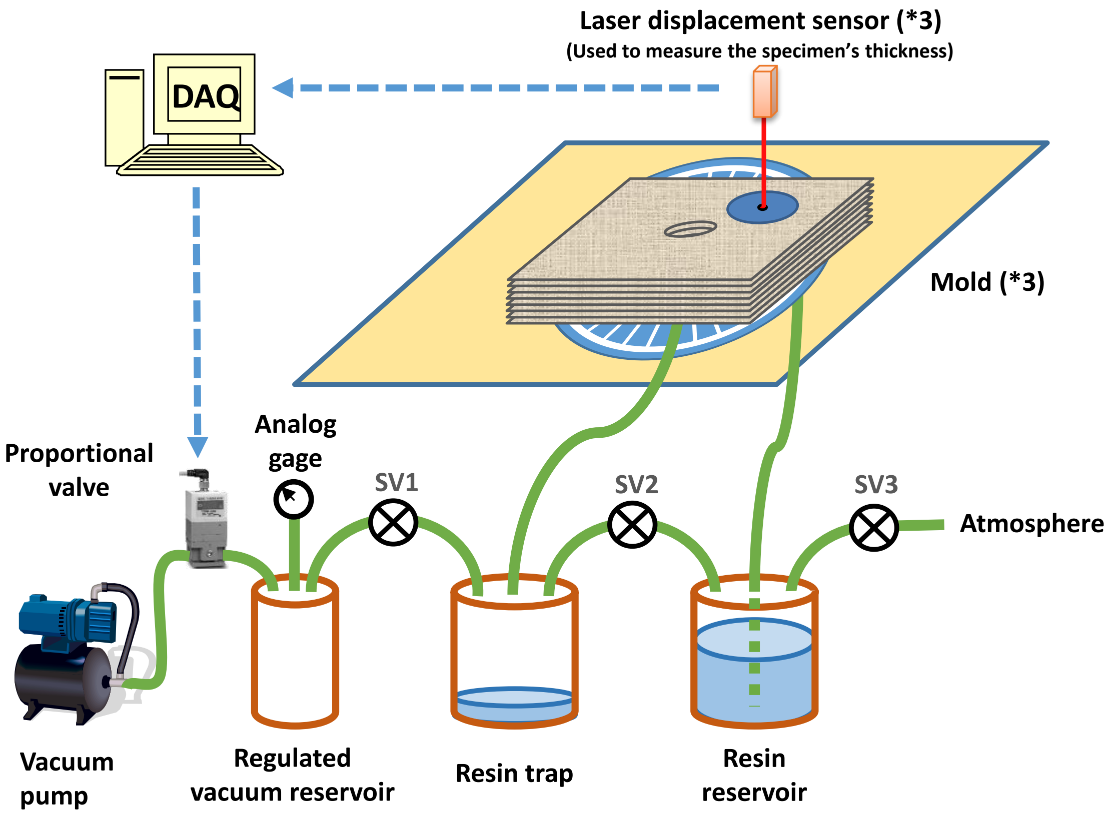

Figure 3-4. The automated compaction characterization setup with vacuum-assisted wetting.

b. Control System

The entire system is controlled in real-time by a computer running a Matlab code. The experimental setup is interfaced to the computer using NI USB-6008 data acquisition card (DAQ). DAQ card is controlled with Matlab using a DAQ-mx interface software. A PID loop in the code controls the proportional valve to obtain desired vacuum level at the vacuum trap. The feedback for PID loop is obtained from the piezoelectric pressure sensor located in the regulated vacuum reservoir. Another loop controls the stages of the experimental procedure. The precision of the pressure sensor and laser displacement sensors are 0.25 kPa and 0.015 mm, respectively. The accuracy of the vacuum pressure using the closed loop system is approximately 1 kPa. Ideally, the vacuum pressure can reach up to 100 kPa when there is no leakage, but it typically reaches up to 99 kPa during the experiments due to air leakage.

Solenoid valves are also controlled by the same DAQ card, and activated to do either one of the following: (i) to seal the mold (during compaction, settling, unloading and relaxation stages); (ii) to infuse the resin (after settling stage to saturate the specimen); or (iii) to exhaust the mold (at the end of the experiment).

c. Wetting

The wetting stage is done by changing the pressure of the resin reservoir. Initially, the resin reservoir is at the same pressure level with the resin trap since the solenoid valve, SV2, which connects the two reservoirs, is open. This valve is closed and the next solenoid valve, SV3 is opened which opens the resin reservoir to the atmosphere causing the pressure inside the reservoir to rise to atmospheric pressure. Due to the pressure difference between the two reservoirs, resin flows from the container with a higher pressure to the container with a lower pressure, i.e. from the resin reservoir to the resin trap. This valve configuration, where the resin reservoir is opened to the atmosphere instead of being connected to the vacuum trap, is kept for 10 seconds. After a duration of 10 seconds has passed, SV3 is closed and SV2 is opened so that the resin reservoir is connected to the vacuum trap once again, hence the pressure equalizes between the two reservoirs which is expected to stop the resin flow. However, resin flow can be visually monitored for a while. The resistance of the pipes and valves delays the equalization of the pressure, thus flow continues for a short time after switching the valves. But, the major cause for this resin flow is that, the excess resin in the mold is removed as the compaction pressure in the mold reaches to 100 kPa again. Wetting process continues in this configuration for another 20 seconds. After 30 seconds of wetting stage, the fabric is fully wetted and no more flow is observed.

One of the drawbacks of this wetting system is as follows. Due to the sudden pressure change at the start of wetting, and vacuum pump's capacity; the pressure in the vacuum trap also drops for a short duration. This can be observed in the experiment results clearly. One should note that, the compaction pressure in the mold also drops, which increases the thickness for a short duration. On the other hand, one may prefer this method as this increases the permeability of the fabric specimen during this pressure drop, and thus the wetting is completed in shorter time.

Another drawback is that, the pipes connecting the resin reservoir to the molds should be cleaned after each experiment. It is visually seen that resin remaining from previous experiment may partially wet the fabric unintentionally before the wetting stage. Also, even if multiple solenoid valves are switched simultaneously, one valve can trigger with a delay of fraction of a second, causing instantaneous unwanted pressure differential, and thus unwanted wetting. Automated schedule can handle the problems with simultaneous the valve switching by activating them sequentially with slight delay rather than controlling them in a single command. On the other hand, the operator must still be cautious for the excess resin remaining in the system after each experiment.

3.2.3 Automated setup with pump assisted wetting

Due to the aforementioned problems with vacuum assisted wetting setup, the automated setup is modified to wet the fabric using liquid pumps instead of pressure differential obtained with vacuum. The modifications of mechanical part of the setup and the control system is detailed in following headings.

a. Mechanical system

The schematic of the modified setup is shown in Figure 3-5. The resin reservoir is disconnected from the setup and reconnected to molds using separate fluid pumps. Peristaltic pumps with silicone tubes are preferred for resin compatibility. The reservoir is placed above the pump level to ensure the gravity feed, and to avoid the air bubbles. By using separate pumps, it is ensured that each specimen is wetted equally and at the same time. The pipes connecting the pumps to the molds is kept as short and thin as possible (< 5 cm with 2 mm diameter) so that the fabrics start to get wet as soon as the pumps are energized.

b. Control System

The pressure regulation of the control system is used without any modification. The only modification was done on solenoid valve SV3. SV3 is removed and the same output on DAQ card is used to control the pumps via a relay. An external adjustable power supply is used to energize the pumps, which gives the flexibility to adjust the motor running voltage.

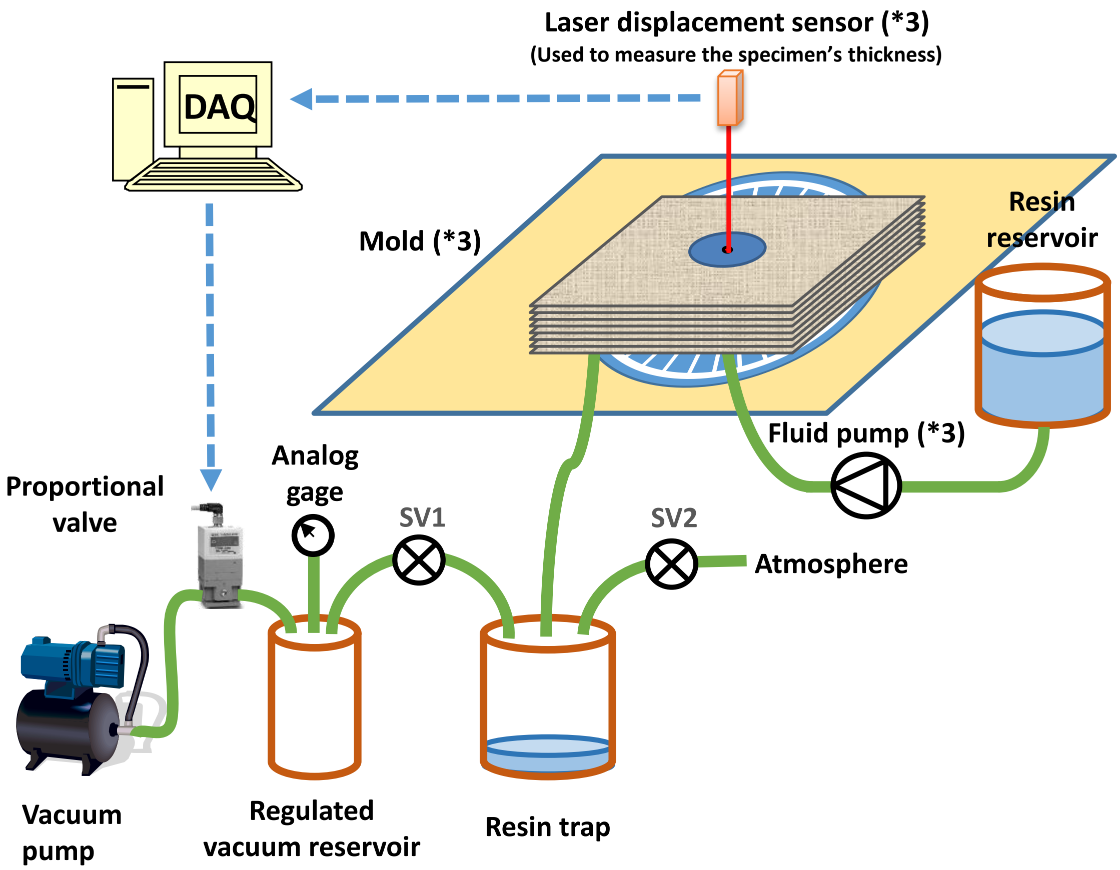

Figure 3-5. The new automated compaction characterization setup with pump-assisted wetting.

c. Wetting

By using electric pumps, flow rate can be controlled by changing the pump motor voltage, and total flow can be controlled with the duration of the pump motor energized. With these two parameters (pump motor voltage, and running duration), excess resin amount is kept as low as possible which allows the use of much smaller resin trap. Together with a smaller vacuum reservoir, the pressure can be changed much faster compared to previous setup, which is required for step response experiments. In practice, all excess resin stays at the outer pool in the molds, and no resin reaches to the resin trap while ensuring that the center of the specimen is totally saturated.

3.2.4 Automated setup advantages

For both setups (vacuum- and pump-assisted compaction characterization), compaction, self-test and calibration stages are the same, and detailed as follows.

i. Stress-controlled compaction

Using the vacuum pressure for the fabric compaction is a major improvement over previous setups. Loading a fabric specimen with a weight, a mechanical or a hydraulic press is the same in theory; however the corresponding compaction stresses may not be accurate in all cases. For example, when a specimen is loaded with a weight as in [1,2], the stress may vary significantly from one specimen to another as the surface area of the specimen may vary due to (i) human error (considering how easily fiber bundles may fall from a dry fabric specimen), or (ii) non-uniformity of the fabric structure. This issue could be eliminated by using a press in which the compaction stress was controlled no matter what the surface area of the specimen is. Controlling the compaction stress is expected to yield more accurate results than controlling the force as in the piston-cylinder approach, in which the corresponding compaction stress is calculated as F/A (i.e. the force divided by the area of the fabric specimen) where the area A may have a significant scatter. Moreover, this approach is very similar to VI process, where the vacuum bag does not restrain the movement of fabric. Thus, the fabric can freely thicken during the relaxation stage, which is required to capture the relaxation behavior correctly.

ii. Self-tests and Calibration

Compaction characterization of fabric specimens requires a large number of sampling since the variance of the fabrics superficial density is very high especially for the random fabric. This high variance makes it hard to decide if any outliner data is due to experimental error, or just variation in the specimens. To minimize the experimental error, self-test and self-calibration routines are performed. The self-test routine, which is repeated before each experiment, and self-calibration, which is repeated periodically are explained below.

The self-test routine checks the vacuum pump by measuring the pressure at the vacuum chamber. This is done before each experiment by closing the first solenoid valve, SV1, which results in isolation of vacuum chamber from the experiment setup. After isolation, the vacuum pump is started and the proportional valve is completely opened without any feedback control mechanism. The system checks if the vacuum pressure can reach over 98 kPa; if not, it stops the experiment and warns the user. This failure can be caused by either (i) degrading performance of the vacuum pump, or (ii) incorrect calibration. One can use a redundant analog pressure gauge to decide what causes the failure. If the pressure gauge displays a value over 98 kPa of vacuum pressure but the system gives an error message, then calibration must be done. If the gauge displays a value less than 98 kPa, then the vacuum pump should be inspected.

The self-calibration routine is done before starting a batch of experiments. During self-calibration, voltage values corresponding to the two pressure values are recorded (the system records the data for 10 seconds and takes the average). These two voltage values are used to map the voltage values read from the sensor to the pressure values linearly. The two pressure values are selected as the lower (full vacuum) and upper limit (atmospheric pressure) to cover the whole pressure range used in the experiment. By using analog pressure gauge, a user should confirm that 100 kPa of vacuum pressure is observed during calibration. Once the full vacuum is confirmed with the analog gauge by the user, the calibration is completed.

3.2.5 Specimens

In the previous studies [1,2], the specimens were circular since they were required to fit in a cylindrical cup and also be in contact with a circular compaction cylinder. It is not easy to cut circular specimens manually, hence a punch was used. Punching helps for size consistency, but on the other hand, may cause some fabric types such as woven fabrics to deform. One could prefer a square specimen since cutting it instead of a circular one is easier and it causes less deformation on fiber structure. However, placement of a square specimen in a piston-cylinder test setup would require a larger diameter.

In this study, a new approach was taken to compact a fabric specimen. Instead of compacting it in a two sided mold (male part: piston, female: cylinder), a single-sided mold as in the actual VI process was used. This configuration allows the use of specimen in any geometry. This approach has an advantage of using a specimen in any geometry, and it is not affected if some fiber tows may have been deformed or fallen down during the preparation (cutting and placement). This is due to the compaction pressure is created by the vacuum applied, which is uniform in the mold. This allows repeatable experiments by setting the same vacuum level in each experiment. On the other hand, in the previous setup, the compaction pressure is equal to the applied force divided by the contact area. It is vulnerable to the fact that as the dimensions or geometry varies from one experiment to another, or the edges are deformed during the preparation, the effective contact area varies and thus the compaction pressure deviates from the expected value.

In the first study [1], the specimen was saturated outside of the chamber by dipping it into the resin. To avoid removing a specimen from the setup during the experiment, an inlet gate was added in [2]. Without removing the specimen, resin is forced into the cavity through the gate using an injector. Two sets of specimens were used in this study: specimens with and without center holes (20 mm diameter). A center hole in a specimen allows quicker saturation by the resin, however the plastic disc placed on the vacuum bag may deflect slightly in the center region due to the less support underneath. Considering this issue, all experimental results and the corresponding model fits were done on specimens with no holes on them.

a. Square specimen with center hole

In automated setup with vacuum assisted wetting, which is shown in Figure 3-4, square specimens are used with a center hole as shown in Figure 3-6. The center hole is punched to create a resin pool at the inlet. This greatly reduces the wetting duration. It takes about 7 seconds only.

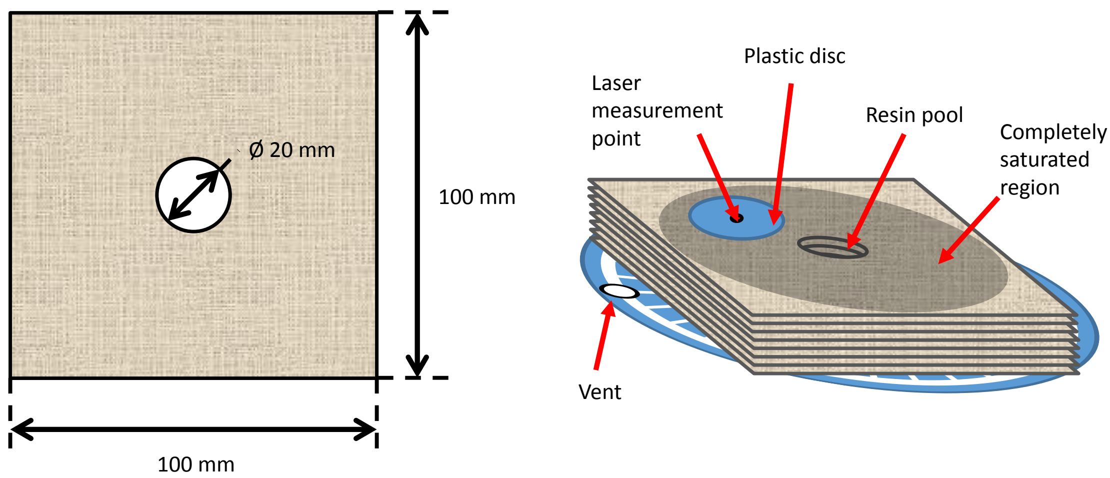

Figure 3-6. Compaction characterization specimen with a center hole.

It must be noted that the plastic disc, which is placed beneath the laser measurement point, must be away from the center hole. This disc is used to measure the effective thickness of an area instead of a local point which varies between dents and peaks of the fabric. If the plastic disc is placed on the center hole even partially, the compaction pressure will deviate from the vacuum pressure and this will cause an error in the characterization. This will be explained below with a case analysis.

Two different cases are shown in Figure 3-7. In (a), the plastic disc is placed on the center hole so that its contact area with the specimen is smaller than its surface area. As schematically shown in the figure and also detailed below, this causes the compaction pressure to be higher than the expected value. By considering the equilibrium of the forces on both sides of the disc, one can obtain the pressure applied on the fabric (which is also called as the compaction pressure) as follows:

$$F_{upper} = F_{lower}$$

$$P_{upper}\, A_{upper} = P_{lower}\, A_{lower}$$

$$P_{fabric} = P_{atm} \frac{A_{upper}}{A_{lower}} > \ P_{atm}$$

since $\frac{A_{upper}}{A_{lower}} > 1$. With a disc of 40mm diameter and 20mm hole, actual pressure applied on the fabric beneath the disc becomes 135 kPa at full vacuum. Thus, the operator should be aware of this, and place the specimen such that the plastic disc must be placed by not overlapping with the center hole as illustrated in Figure 3-7b, in which $P_c = P_{atm} - P_{vac}$ as designed in this approach.

It is visually observed that the vacuum bag applies additional stress over the edge of the hole while it dents over it. This is shown schematically in Figure 3-7b. The dent causes tension on the vacuum bag. It is best to place the disc not so close to the hole; however it should not be too far away from the center as it may take longer during the wetting.

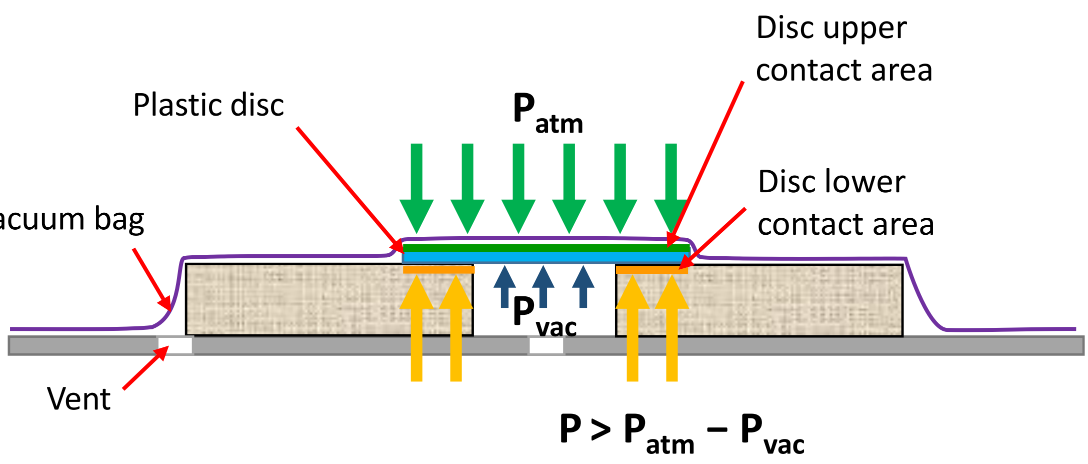

(a)

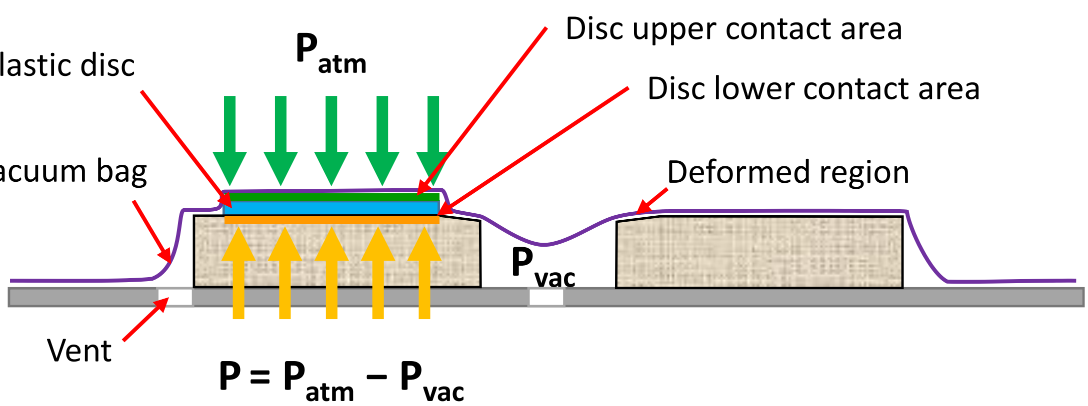

(b)

Figure 3-7. Compaction pressure applied on the fabric specimen under the disc when the disk is placed (a) at the center and (b) at the edge of the hole.

b. Square specimen without center hole

The results on specimens with holes showed a large variance mostly caused by the operator during the specimen placement. Those results will not be presented here. Instead, experiments were repeated on specimens with no holes on them (as shown in Figure 3-8) to avoid aforementioned problems, and their results will be used in this study.

The lack of resin pool at the inlet causes longer wetting duration than wetting of a specimen with a center hole. To overcome this problem, the setup is modified (as mentioned in Section 3.2.3) by using pumps instead of vacuum pressure which resulted in higher injection flow rate and shorter wetting duration.

The only drawback of this final approach compared to the previous specimen and setup is that, pressure builds up at the injection port during wetting. Pressure caused by the fluid pump rises the plastic disc for a short period of time, which can be observed from the experiment results. Similar to the pressure drop caused in vacuum assisted setup, this results in an increase in fabric thickness (a bulge is observed at the center region) hence increase in permeability. It becomes easier to saturate fabric. Recall that this stage mimics wetting of specimen with resin upon resin arrival in VI. However, the change in local thickness (bulge) is caused artificially due to the wetting approach in this material characterization approach. Thus, this short interval of the experiment will be excluded in the compaction model calculations.

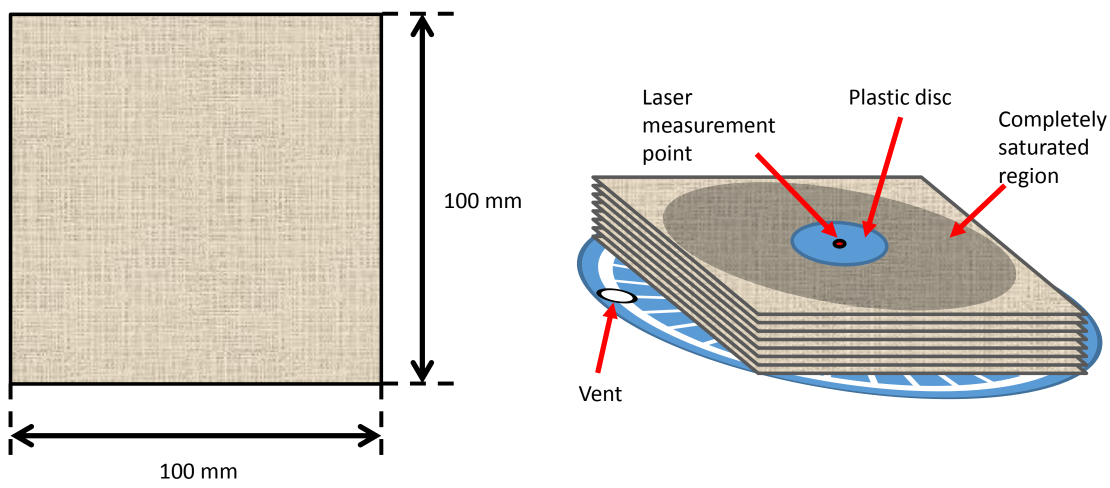

Figure 3-8. Compaction characterization specimen without center hole.

3.2.6 Procedure

The compaction experiments were conducted as originally detailed in the previous study of the author, [1] and [2]. There are four main stages in a characterization experiment. Each stage mimics a main part of the VI process. The four main stages (loading, settling, unloading and relaxation) are discussed below.

Loading stage: This stage mimics the initial vacuuming of the preform during the VI process. Initially there is no compaction pressure acting on the preform. Induced by the application of vacuum inside the mold cavity, the internal pressure decreases, resulting in a pressure differential between inside and the outside of the vacuum bag. Depending on the pump capacity and the mold size, this stage can take from a few seconds to minutes.

In characterization tests, the compaction pressure on the fabric is increased from P_{minor} to P_{major} with a constant rate which is denoted as dP/dt. It should be noted that in the actual process, the magnitude of dP/dt decreases as the compaction pressure increases (i.e. the change in pressure occurs fast at the beginning of the vacuuming stage, and slows down as the pressure comes close to the full vacuum). In characterization experiments, dP/dt is selected to be constant to simplify the modeling.

The base value for the compaction rate is selected as 2 kPa/s, the same as in previous studies [1] and [2]. This rate corresponds to a stage duration of 50 s from atmospheric pressure to full vacuum.

Settling stage: After vacuuming the mold cavity, the preform is kept under constant pressure to compact the fabric and exit as much air out of the mold as possible. Also, the mold is inspected for leaks during this stage. Depending on the mold, size and the complexity of the mold this stage can take in the order of minutes to hours. Moreover, since this stage ends with wetting upon the resin flow front arrival to a location (i.e. dry parts of the fabric will be at maximum vacuum pressure until wetting), the duration of this stage varies spatially in the fabric preform.

The specimen is kept under a major pressure, P_{major}, during settling stage. It is selected as 100 kPa in characterization experiments. The duration of this stage is taken as 15 minutes. It is shown in [2] that, the woven, biaxial or random fabric preform continues to deform even after 15 minutes. However, there is a tradeoff between experiment duration and amount of useful data collected. The magnitude of deformation rate decreases quickly in the first few minutes and at 15 minutes this rate becomes very small. To keep the experiment duration short, 15 minutes of settling is taken as in [2].

Unloading stage: During the VI process, this stage starts with wetting and ends with complete mold filling. With the arrival of resin flow front, the compaction pressure on that spatial location starts to decrease. This continues until the mold is filled or any modification is done on injection and ventilation port condition or configuration. If the gates are not modified, compaction pressure at a specific location reaches its steady value at the end of the mold filling. This steady value can be between $P_{atm} - P_{inj}$ and $P_{atm} - P_{vent}$ depending on the location.

The compaction pressure decreases nonlinearly with time in typical VI process. But in the characterization experiments, the compaction pressure is varied linearly as in the loading stage, from P_{major} to P_{relax}. The magnitude of the rate of unloading is taken the same as the loading rate in all experiments. The final compaction pressure is varied in some experiments to observe its effect on the compaction. Due to these, the duration of this stage in characterization setup is both dependent on the pressure rate dP/dt and final pressure.

Relaxation stage: This stage corresponds to what happens to the preform after the complete mold filling in VI process. Compaction pressure does not vary with time afterwards. During this period, even though the compaction pressure does not change, the fabric continues to deform until curing. In practice, this stage ends before curing by applying a control action, such as resin bleeding. A control action will result in a change in the compaction pressure and causes to end this stage. To avoid wasting of resin as much as possible, this stage is kept short. However, in multiple injection/ventilation gate scenarios, some regions of the mold can stay under relaxation while the rest of the mold is still being filled. For example, in a rectangular mold with a central injection gate and two ventilation gates at the farther ends, resin may reach the ventilation port on the left before it reaches on the right. In this case, the left side of the mold is under the relaxation stage until the complete mold filling occurs.

In characterization experiments, relaxation stage duration is taken as 15 minutes to be consistent with the settling stage. The relaxation pressure, P_{relax} is varied in different experiments to see its effect on the compaction.

Besides these four main stages used originally in [1] and [2], additional stages are added for both more consistent experiments (initial settling stage) and additional data (debulking stage). These minor stages are summarized below:

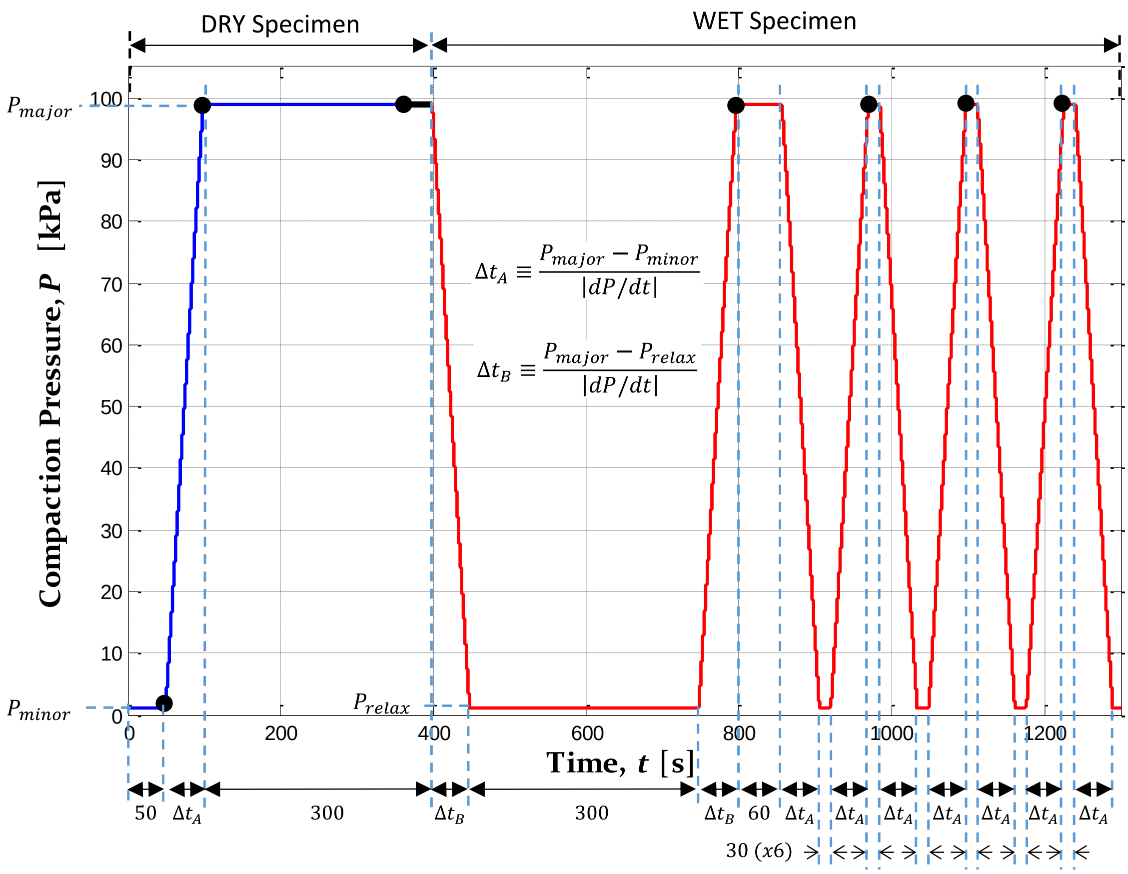

Figure 3-9. The compaction pressure versus time applied in Experiment Set 1 (baseline). The input pressure is similar in other experiment sets where the time scale changes due to change in dP/dt or P_{relax}. Some instances are marked to show corresponding response in the thickness graph.

Initial settling stage: The specimens are prepared by placing the layers of fabrics. No pressure is applied while stacking by the operator. Then, a minor compaction pressure, P_{minor} of 1 kPa is applied before the loading stage to have more consistent specimens between the experiments. No pressure is applied to stack the preform by the operator. This initial settling stage makes it possible for specimens to be stacked consistently. Since the pressure is very low, it is seen that specimens' thickness becomes almost steady in about 2-3 minutes. 5 minutes of initial settling is selected in this study to be on the safe side.

Debulking stage: After the main stages are completed, experiments are continued to have additional data for the analysis of different aspects such as effect of debulking. In this stage, four main stages of a single cycle is repeated three times with shorter durations than the initial cycle. Analyzing the collected data, fabrics response to multiple cycles can be observed. It should be noted that, the debulking data is not used in compaction model fitting, but in verification of the model. The performance of the model after the first cycle can be calculated with this additional stage.

The compaction pressure versus time for the base experiment is shown in Figure 3-9. It should be noted that the first 250 s of the initial settling stage is discarded and not shown in any of the results since it is redundant. The last 50 seconds shows that the fabric reaches a steady value before actual cycle starts.

A representative thickness graph is given in Figure 3-10 corresponding to the pressure input in Figure 3-9. The beginning of the experiment; the beginning of each settling cycle, and the wetting are all shown with black markers. Note that, without synchronized pressure and thickness graph, it is not possible to distinguish the stages by looking at the thickness graph alone since the stage transitions are smooth. That is why autonomous characterization setup is a necessity, to record the beginning and end of stages accurately.

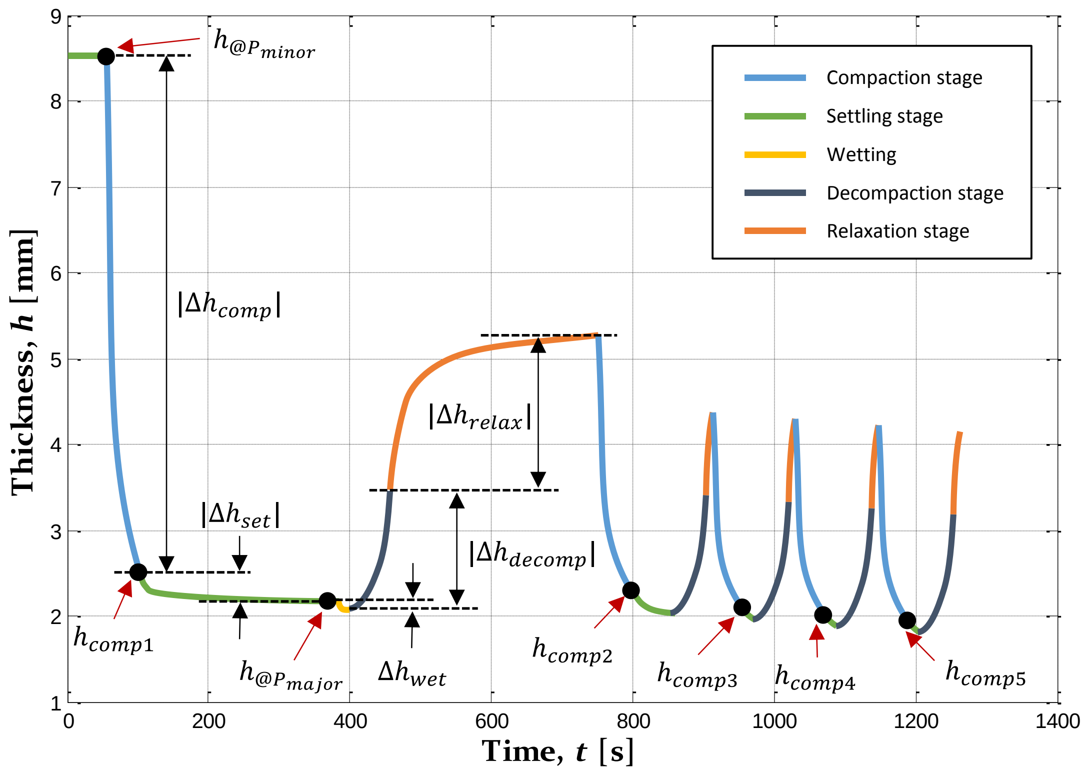

Figure 3-10. A representative thickness response for the Experiment Set 1 (baseline). Each stage is color coded and corresponding instances marked similar to compaction graph.

The common parameters for all these experiments and used materials are listed in Table 3-1. 8 layers of fabric are used for both random and woven fabric specimens. The corn syrup is diluted with water to have a viscosity close to actual polyester resin used in the lab.

Table 3-1 Material properties and parameters used in characterization experiments.

Fabric	1. Random e-glass (Fibroteks), 450 g/m^2 2. Woven e-glass, 500 g/m^2
Number of layers in the preform	8, $[0^o]_8$
Test fluid for wet decompaction	Diluted corn syrup, 1.05 g/cm^3, 0.20 Pa.s
Minor compaction pressure, P_{minor}	1 kPa
Major compaction pressure, P_{major}	100 kPa
Duration of minor pressure, Δt_{minor}	300 s
Duration of settling, $\Delta t_{settling}$	300 s
Duration of wetting, Δt_{wet}	30 s (approximately)
Duration of relaxation, Δt_{relax}	300 s

By using the parameters tabulated in Table 3-2, 12 characterization experiments were conducted for each sets listed in proceeding headings. The compaction pressure input versus time is shown in Figure 3-11 for different experiment sets. In Figure 3-11a, the difference for the input compaction pressure is shown for various dP/dt rates corresponding to Experiment Sets 3 and 4. Similarly, the effect of using different relaxation pressures in Experiment Sets 5-7 are shown in Figure 3-11b. In the last plot, the all dry experiment is shown in Figure 3-11c.

Table 3-2 Experimental parameters for each set in characterization experiments.

Experiment Sets	***Wetting before decompaction***	P_{relax} [kPa]	dP/dt [kPa/s]	***Debulking***
Set 1: Dry/Wet	Yes	1	2	Yes
Set 2: Dry/Dry	**No**	1	2	Yes
Set 3: dP/dt = 1 kPa/s	Yes	1	**1**	Yes
Set 4: dP/dt = 4 kPa/s	Yes	1	**4**	Yes
Set 5: P_{relax} = 5 kPa	Yes	**5**	2	**No**
Set 6: P_{relax} = 10 kPa	Yes	**10**	2	**No**
Set 7: P_{relax} = 40 kPa	Yes	**40**	2	**No**

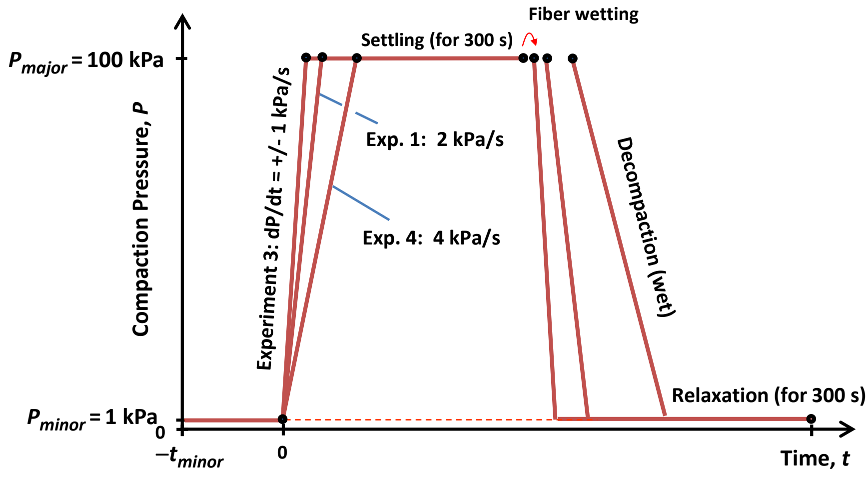

(a) Characterization experiments by varying *dP/dt*

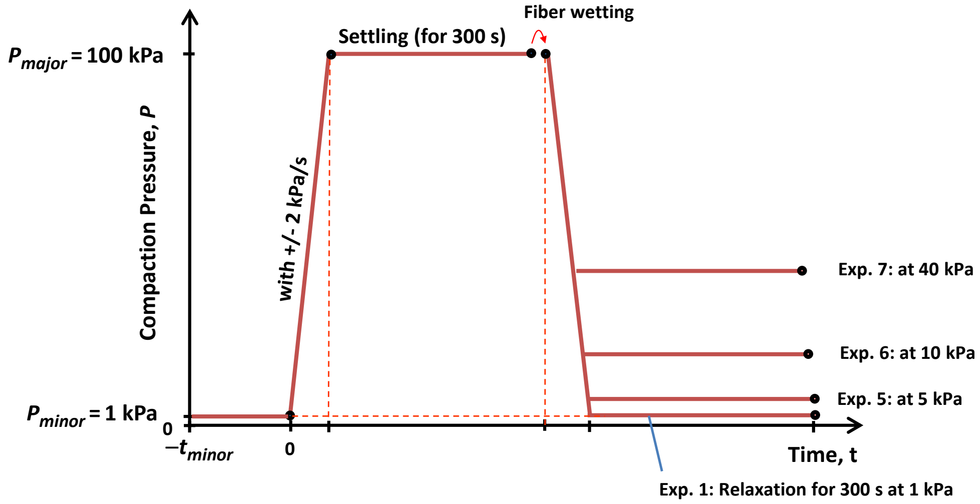

(b) Characterization experiments by varying P_{relax}

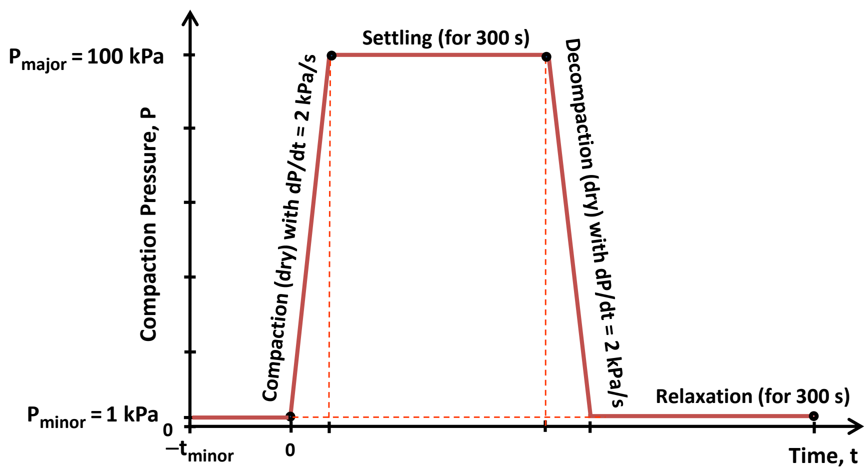

(c) Dry Compaction/Dry Decompaction (Exp. Set 2)

Figure 3-11. Investigation of the effect of three parameters on the characterization: (a) dP/dt, (b) P_{relax} and (c) wetting. Note that each experiment (say Experiment 1, 2 and 3 in part (a)) is a set of 12 experiments using separate specimens to investigate statistical variation.

3.2.7 Experimental sets

As mentioned in the procedure section, some of the experimental parameters are modified between experiment sets to see their corresponding effect on the characterization. The modifications and the motivation behind them is given in the following separate headings.

a. Dry to wet transition

Experiment Set 2 is the same as the baseline experiment (Set 1) except that the specimen is not wetted after the first settling stage. It was shown that the compaction behavior of the fabric changes significantly after wetting [1,2,18] even though some researches in the literature do not consider this fact in their characterization and/or model by conducting the experiments on dry specimens [10,23–28,32]. By conducting both dry/wet and dry/dry experiments, it is planned to see if the model parameters differ significantly, and also if different types of fabrics behave differently after being wetted.

One could alternatively conduct an experiment by using a wet specimen starting from the beginning to model the behavior of a saturated fabric; however this approach does not mimic the actual wetting and compaction of a fabric specimen in VI, and thus not used here. Instead, a dry/wet characterization experiment is designed such that a specimen is dry initially, during the loading and settlement stages; and then it is wetted just before the unloading (decompaction) stage. The rationale for this approach is to capture the compaction/decompaction behavior of a specimen in VI in which the fabric preform undergoes the same stages (loading, settling, wetting, unloading and relaxation). In VI, a dry fabric specimen is compacted during the pre-injection; it is locally wetted by the resin after the arrival of resin flow front. This is followed by an increase in the resin pressure (thus decrease in the compaction pressure) as the resin propagates. Thus, in dry/wet experiments, a specimen is dry at the beginning where the pressure is constant (at the vacuum pressure applied in the process).

b. Effect of compaction pressure rate (dP/dt)

Viscoelastic models can capture not only the settling/relaxation behavior at a constant pressure, but also the delay in the response when the pressure is changing. To include this effect in characterization, experiments are repeated with different rates of compaction pressure. The base experiment set (Experiment Set 1) had $dP/dt = 2$kPa/s. dP/dt is halved in Experiment Set 3, and doubled in Experiment Set 4; resulting in 1kPa/s and 4 kPa/s compaction pressure rates, respectively.

As dP/dt goes to zero, quasi-static equilibrium can be obtained, which means there will be no viscous behavior, but only elastic response. As observed in our previous studies [1,2], even after 15 minutes of full vacuuming (settling stage), a fabric preform continues to compact, i.e. its thickness decreases with time, which makes it impractical to perform quasi-static experiments. On the other hand, as dP/dt goes to infinity, the pressure input becomes a step input, which results in dominantly viscous response.

c. Effect of relaxation pressure

The main reason of the thickness variation in the final part is due to relaxation of the fabric at different compaction pressure values throughout the part. During mold filling, the compaction pressure decreases from the initial compaction pressure to a lower value depending on time and the spatial location. As the resin pressure increases with time at a particular location, the compaction pressure decreases and thus, the part thickens. This corresponds to the decompaction stage of the characterization experiment. The resin pressure is settled after the mold is completely filled, but the part keeps thickening. This stage in VI corresponds to the relaxation stage in compaction characterization. Keeping in mind that resin pressure varies spatially within the mold at the mold filling time and fabric relaxes at different pressures, the relaxation characterization is conducted on multiple specimens at various relaxation pressures. Since the thickness of the fabric changes significantly at low compaction pressures, these relaxation pressures are taken as 5, 10, 40 kPa in Experiment Sets 5, 6, and 7, respectively (also recall that the base Experiment Set 1 had its relaxation at 2 kPa).

d. Effect of debulking

Fabric preforms tend to compact more after each cycle of compaction/ decompaction. To decrease the thickness (thus, increase the fiber volume fraction), a fabric preform is compacted and released several times in some VI applications, which is called debulking. To see the effect of debulking, in this study, specimens are compacted 4 more times after the main experiment cycle. $|dP/dt|$ is the same during the main and the additional cycles. After the first compaction, a specimen is kept at 100 kPa during the settling stage for 60 seconds. In each of the last 3 cycles, the full compaction is kept for 15 seconds.

e. Step input response

To investigate the purely viscous behavior of the specimens (by excluding its elastic behavior as much as possible), compaction pressure input is selected so that dP/dt approaches to infinity, i.e. $P(t)$ converges to a step input as seen in Figure 3-12. Practically speaking, this input cannot be obtained exactly due to the flow rate limitations of the pump. Even if a powerful pump is used (or very large accumulator tank), resistance in the pipes will result in a limited flow rate and thus, the input will not be a perfect step input.

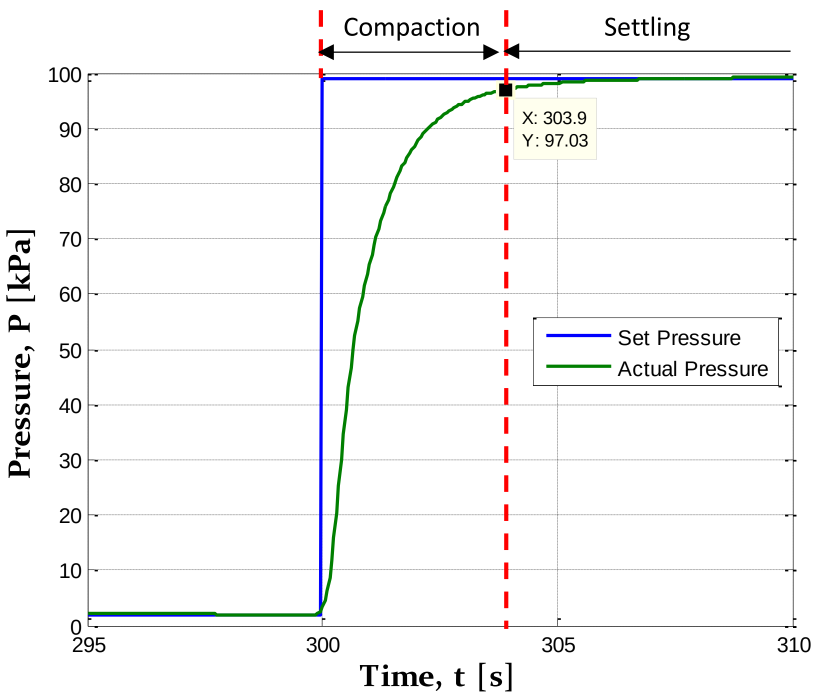

Figure 3-12. Set and actual pressures applied during a typical step input experiment

As seen in Figure 3-12, the set pressure is set to a value of 100 kPa at 50 s. However, it takes 4 seconds for pressure to rise %2 margin (~97 kPa). dP/dt significantly decreases as the compaction pressure increases. This is mainly due to the pump's capacity rather than the resistances in the piping. It is possible to conduct these experiments at a lower compaction pressure such as 80 kPa to have a steeper step input.

However, it is known that the viscous effect of fabric compaction is slow and it takes much longer time. Thus, 4 seconds of rise time is sufficiently small to capture the response of a specimen in this characterization.

3.2.8 System performance and raw data format

The raw data obtained from the setup are presented in this section. For brevity, only the results of the Experiment Set 1 is given in this chapter. Results for the other experiment sets are given in the Appendix B.

In Figure 3-13, the set pressure and resulting actual pressure in the vacuum trap is shown. As explained in the wetting of the specimen, pressure drops inside the trap at the beginning of the wetting process, but later the set pressure is reached again. Another thing to notice is that, the system cannot keep up the pressure rate (2 kPa/s) at higher vacuum pressure levels (over 97 kPa). At the end of compaction, pressure changes slowly due to vacuum pumps limited capacity, resulting in a smooth transition. Ideally, there should be a sharp transition, resulting in sharp change in thickness, which can be seen during curve fitting section.

In Figure 3-14, the thickness versus time for random specimens is shown, corresponding to the pressure input presented in Figure 3-13. The effect of the lubrication can be seen during wetting (the thickness decreases, due to further stacking of the fibers). There is a slight increase in thickness after a few seconds which is expected to be caused by the pressure drop mentioned in the previous paragraph and does not contradicts the expected lubrication effect.

It is also seen that, debulking helps a fabric specimen to compact and increase its fiber volume fraction. However, by visually comparing the slow compaction in the first settling stage, and the minimum thickness values at debulking, it is not easy to decide if debulking has an advantage over a longer settling. In other terms, the answer for the following question is not clear: “Will three debulking cycles taking 300 s will compact the fiber more compared to 300s settling under constant compaction pressure?”. The answer to this question will be discussed in the Results section.

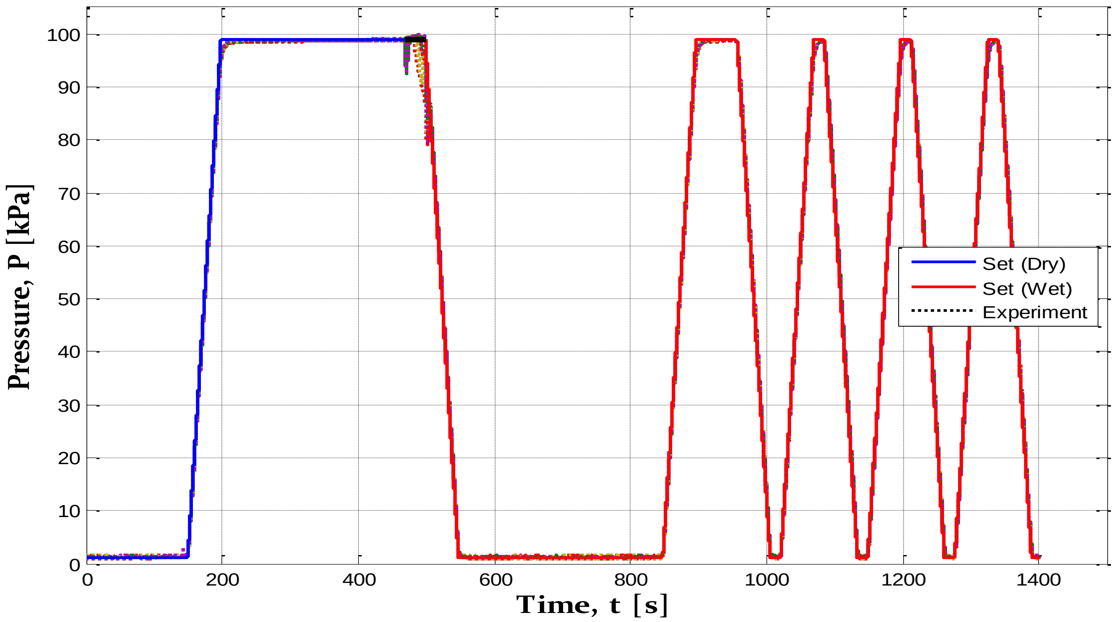

Figure 3-13. Compaction pressure applied on the specimens.

a. Random

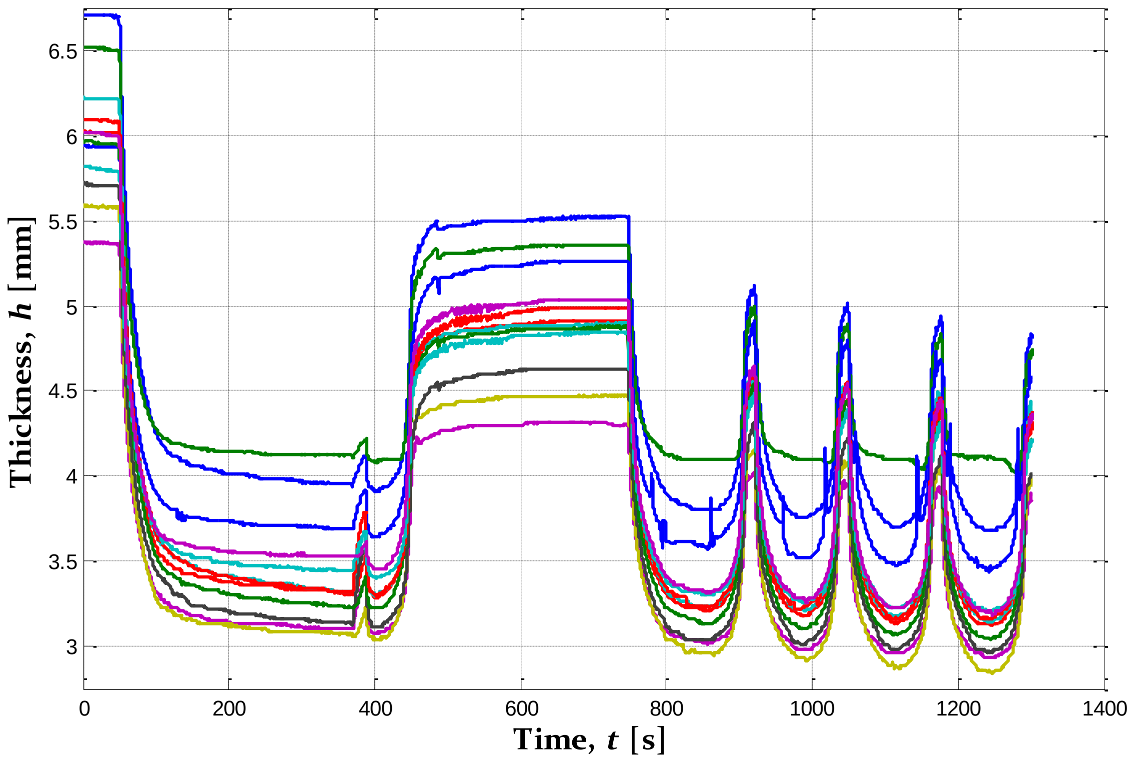

Figure 3-14. Random fabric, Dry/Wet (Base) experiment thickness vs. time.

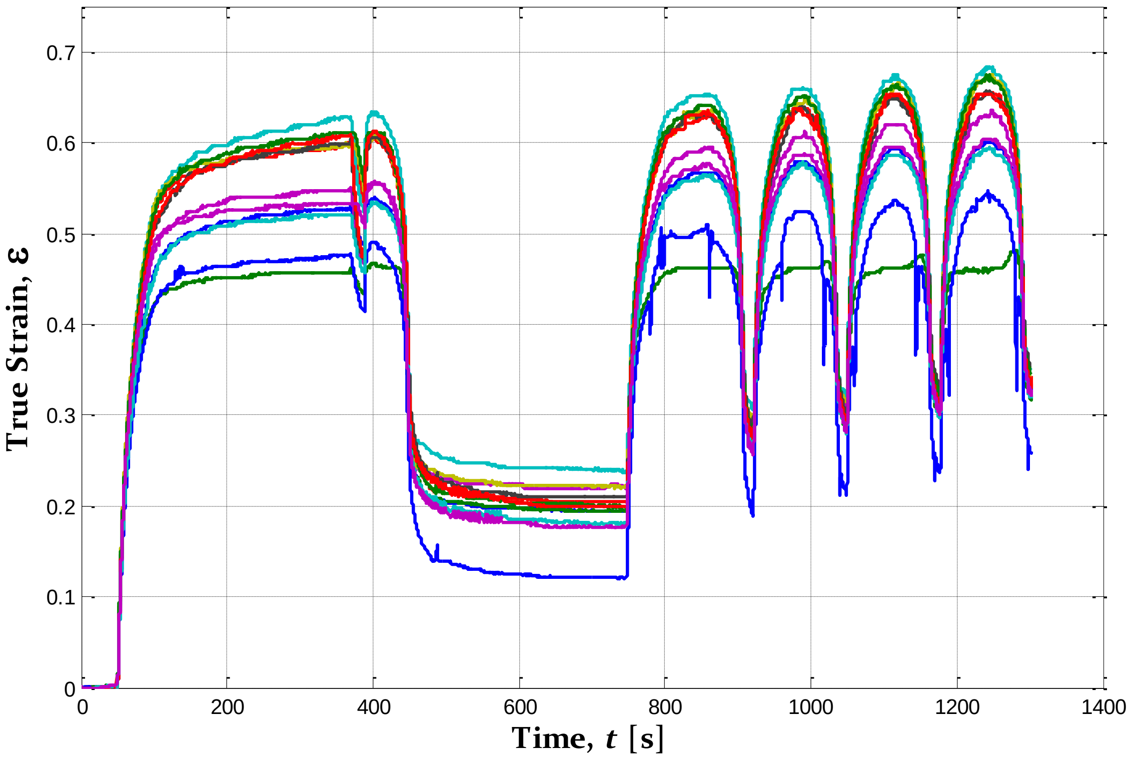

Figure 3-15. Random fabric, Dry/Wet (Base) experiment strain vs. time.

b. Woven

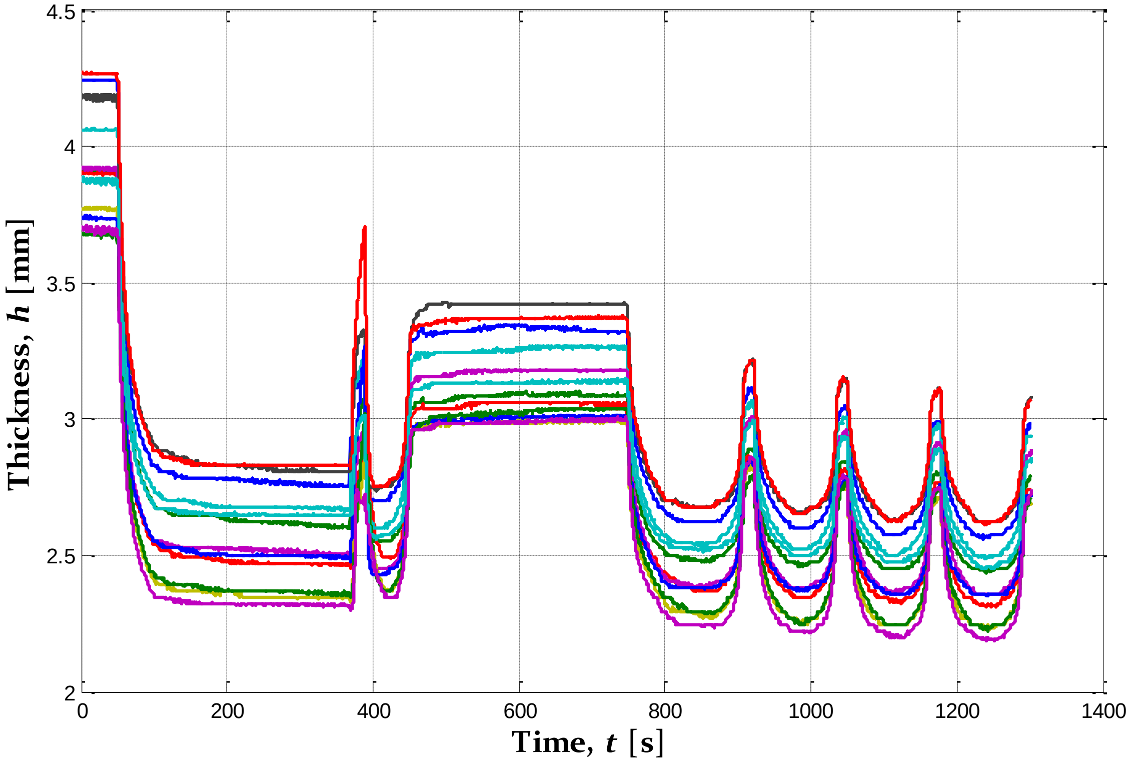

Figure 3-16. Woven fabric, Dry/Wet (Base) experiment thickness vs. time.

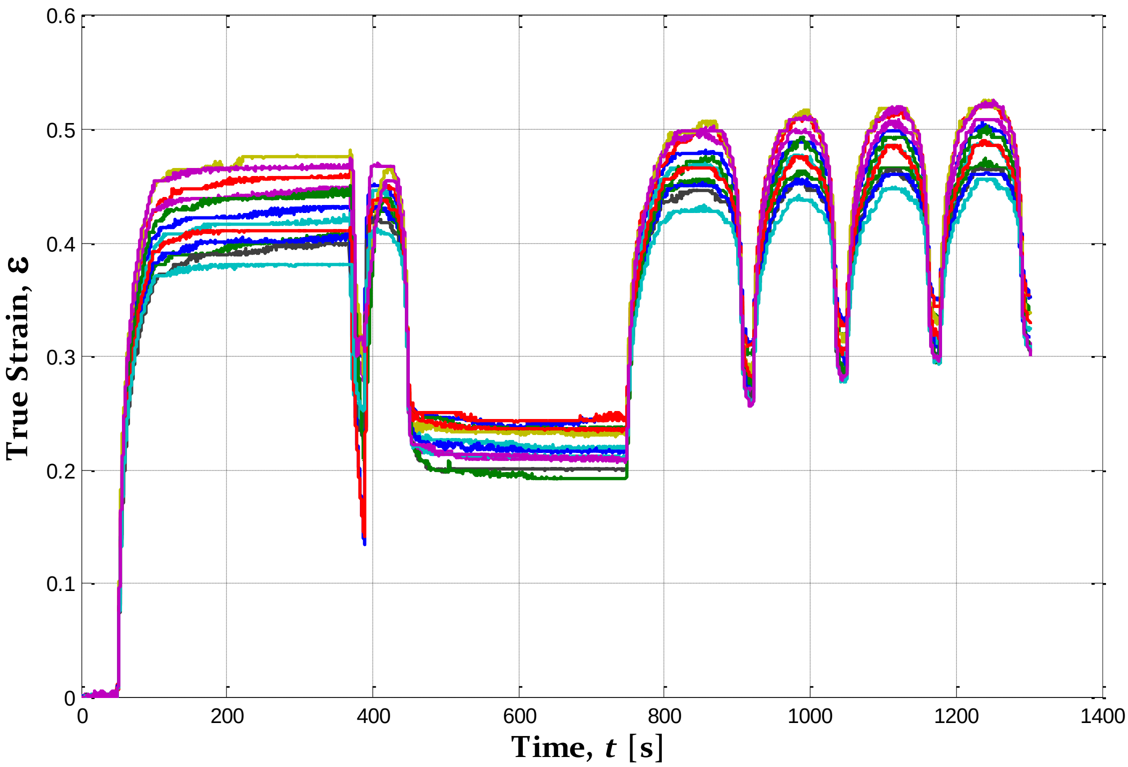

Figure 3-17. Woven fabric, Dry/Wet (Base) experiment strain vs. time.

Figure 3-15 shows the true strain of the random specimens calculated using the thickness data in $\varepsilon = \ln(\frac{h_0}{h})$. In each experiment, the reference thickness value (h_0) is taken as the average of the first 150 s of the experiment (during the pre-loading stage), i.e. $h_0 = \frac{1}{150}\int_0^{150} h(t)dt$. Notice that $h(t)$ data shows a significant scatter initially due to the inherent variations induced by non-uniform fabric structure, and fabric cutting and preparation. However, this scatter is reduced when $\varepsilon(t)$ is used in the analysis as seen in Figure 3-15.

By observing the change in strain under constant load (settling/relaxation stages), it is much easier to see that specimens have viscous behavior, it continues to strain with time under constant load.

Figure 3-16 and Figure 3-17 show the thickness and strain graphs for the woven specimens. The general trend is similar to the random specimens, however this fabric compacts less than the random fabric.

For both random and woven fabrics, the variation among the experiments is very significant due to the variation in the fabric itself. For random fabrics, it is seen that even in the same roll, the superficial density changes from one location to another. This will be documented in Chapter 7 by comparing the initial specimen weights.

4 Compaction Modeling

In this chapter, viscoelastic models and their numerical solution are studied to represent the compaction behavior of porous media in VI applications. The modeling parameters (spring and damper constants) and the variables (stress and strain) are defined; and the system equations are given relating the stress and strain. This chapter also discusses the mathematical issues caused by singularity of the system equations and the discontinuity in the input functions of the independent variable.

4.1 Models

An elastic model includes only springs, and the response occurs instantaneously when the system is disturbed externally. On the other hand, a viscoelastic model includes springs and dampers in many different configurations (series or parallel), and the response has two components: elastic (instantaneous) and viscous (time-varying). Each model will be studied by developing and examining its (1) mechanical analogue, (2) typical strain response to a stress input, and (3) formulation of system equations. Figure 4.1 illustrates a fabric preform and its mechanical analogue by using a sample viscoelastic model that will be studied in detail later in this chapter.

This sample mechanical analogue has a left branch with a single spring, a right branch with a spring and a damper in series. There are three nodes, 0, 1 and 2. Node 0 is the reference node (which can be referred as ground node). This reference node is assumed fixed resembling the fixed bottom surface of the fabric specimen contacting the rigid mold surface. The other two nodes are called floating nodes. The position of Node 2 physically represents the position of the top surface of the specimen. Thus, the distance between Nodes 0 and 2 physically represents the thickness, h of specimen. Node 1 is a virtual node which does not have a physical correspondence.

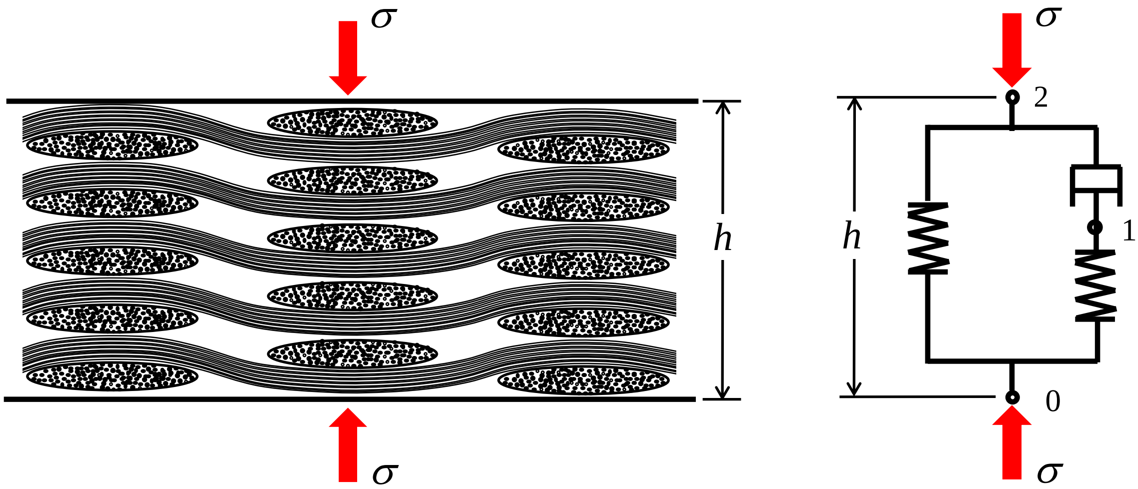

Figure 4-1. A fabric preform under compaction, and its sample mechanical analogue.

System equations are obtained as follows:

- **"Constitutive relations"** of springs and dampers are defined by relating stress, strain and time derivative of strain. These relations may be linear, polynomial or exponential.
- Assuming massless nodes, quasi-static equilibrium is considered at any instant by equating the stresses on each node, except the reference node. That means, if the system has N nodes (including the reference), N-1 "**equilibrium equations**" are written.
- "**Kinematic equations**" are written by considering the equality of displacements (or strains) in different branches. For example, in the sample mechanical analogue given in Figure 4.1, which has two parallel branches, the strain in the left branch (between

Nodes 0 and 2) is equal to the summation of the two strains (the strain between Nodes 0 and 1, and the strain between Nodes 1 and 2).

- Constitutive relations are rewritten by replacing the element's strain with nodes' strains.
- Constitutive relations are substituted in equilibrium equations; and these equations are called system equations.

The stress applied on the fabric preform is called the compaction pressure, P. P is caused by the difference between the outer atmospheric pressure, P_{atm} and inner pressure of the mold, P_{vent}. P_{vent} is created by the vacuum pump applied from the vent.

P causes the preform to compact and decrease its thickness. The constitutive equation for a fabric specimen can be formed by relating thickness, h to P, or true strain, ε to P. Since true strain is conventionally accepted in material deformation studies, the latter relation (between ε and P) will be used here too. In this study, true strain, ε is defined positive for compression, and negative for tension (opposite of mechanics convention). Thus, the equation for calculating true strain is written as follows

$$\varepsilon(t) = \ln\left(\frac{h(0)}{h(t)}\right) \quad \textbf{(4.1)}$$

where $h(0)$ is the initial thickness. Note that preform consists of fabric layers, which are cut and stacked on top of each other. Considering loose nature of stacked layers, it is not practical to define and measure a repeatable initial thickness unless some compaction is applied. Hence, $h(0)$ is measured under a minor compaction pressure, P_{minor}. To accommodate for this initial pressure, and ensure zero stress at zero strain, the stress is defined as:

$$\sigma(t) \equiv P(t) - P_{minor} = [P_{atm} - P_{vent}(t)] - P_{minor} \quad \textbf{(4.2)}$$

In the following subsections, five different viscoelastic models will be introduced, and their mathematical models will be developed. To clearly see the differences between their responses, two conventional stress inputs (step and ramp) will be applied as seen in Figure 4-2. Notice that, the input functions mimic the following stages of VI:

- *Initial zero level* represents the pre-vacuum condition of the specimen.
- *Rise of stress* represents the increase in compaction pressure during the application of vacuuming of the mold cavity.
- *Constant maximum stress* mimics the stress state at holding duration which is done in VI to achieve pressure equilibrium in the mold cavity while keeping the vacuum on.
- *Fall of stress (unloading)* represents the decrease in compaction after the resin arrival to a particular location.
- *Final zero level (or final lowest level)* corresponds to the unloaded fabric specimen after the resin pressure reaches its maximum value at any particular location (thus the compaction pressure reaches its minimum value there). Note that in VI, the compaction pressure near injection ports will behave as this input pressure; however, as getting away from injection ports, the compaction pressure will be non-zero. The reader should recall from Chapter 3 that in the characterization experiments different levels of compaction pressures (1, 5, 10, 40 kPa) were applied. These correspond to compaction stresses, σ of 0, 4, 9, 39 kPa since $P_{minor} = 1\ kPa$.

Since it allows seeing the elastic and viscous components separately of response induced by the step input, all the labeling is done for the step input; and shown with solid blue line Figure 4-2. For completeness of the graphs in the following subsections, the responses of different models to the ramp input are also given with dashed red line in the same figures.

Model parameters in these graphs are chosen arbitrarily. Both stress and strain are normalized by dividing them with their maximum values. The maximum value for input stress, σ_{max} is 100 kPa. Maximum strain values, ε_{max} and the values of the selected parameters for each model are given in Appendix A.I.

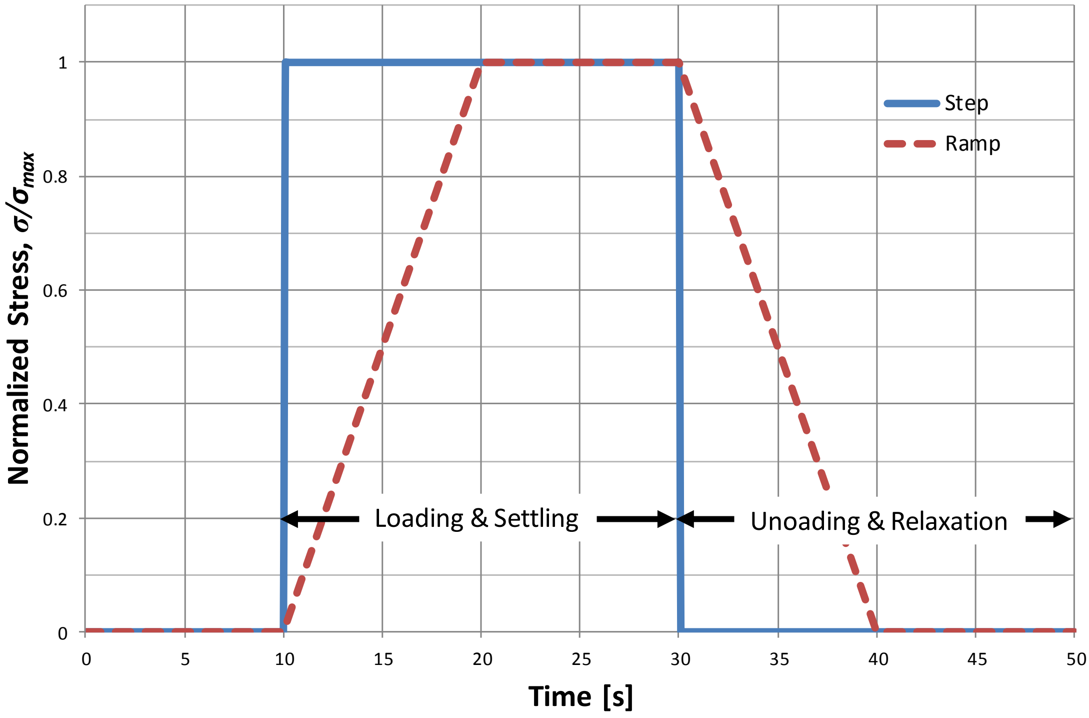

Figure 4-2. Stress applied on viscoelastic models for the sample run.

In the next subsections, the following five different viscoelastic models will be studied: Maxwell, Zener, Kelvin-Voigt, Generalized Maxwell and Burgers. The responses of the five mentioned models for different stages to step-input compaction experiment is summarized in Table 4-1. The details of the models are given in proceeding sections.

Table 4-1 Response of five viscoelastic models to the step stress input.

<table>
<tr><th></th><th>Step Loading</th><th>Settling</th><th>Step Unloading</th><th>Relaxation</th></tr>
<tr><td>Maxwell</td><td>Elastic response happens instantly.</td><td>Strain increases continuously at a constant rate.</td><td>Elastic response happens instantly.</td><td>No relaxation is observed.</td></tr>
<tr><td>Kelvin-Voigt</td><td>No instantaneous response.</td><td rowspan="3">Strain increases with time and converges to the steady state value.</td><td>No instantaneous response.</td><td rowspan="3">Strain decreases with time and converges to zero.</td></tr>
<tr><td>Zener</td><td rowspan="2">Elastic response happens instantly.</td><td rowspan="2">Elastic response happens instantly.</td></tr>
<tr><td>Generalized Maxwell</td></tr>
</table>

Burgers		Strain increases continuously and with a decreasing rate which converges to a constant rate.		Strain decreases with time and converges to a non-zero permanent value.

4.1.1 Maxwell

A viscoelastic model should contain at least one elastic (spring) and one viscous (damper) elements. There are two configurations: series and parallel. The series configuration is called Maxwell model [65–74] as seen in Figure 4-3. The damper in series causes stress to decay to zero under a constant strain. Thus, this model can be used for stress relaxation. On the other hand, damper continues to deform at a constant rate for a given stress, which makes it not suitable for modeling creep. In the next subsection, the parallel configuration, which is called Kelvin-Voigt model, will be studied.

Usually, springs are assumed linear (i.e. stress is a linear function of strain, which is usually called Hooke's law). In this study, nonlinear springs are used since it is known that the responses of fabric preforms are highly nonlinear [1,2].

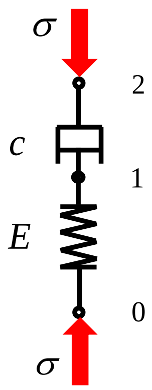

Figure 4-3. Schematic representation of Maxwell model.

The constitutive relation for the non-linear spring element shown in Figure 4-3 is given below

$$\sigma_s = E\, \varepsilon_s^m \tag{4.1}$$

where E is the stiffness of the spring, m is the nonlinearity constant, σ_s and ε_s are stress and strain of the spring.

Note that the nonlinear term results in a complex number if the strain, ε_s is negative and the power term, m is not an integer. To avoid complex results, absolute value of strain is used in Equation **(4.1)**. Sign function is added to include the direction information of the applied stress. Recall that, in this study, compressive stress is positive and tensile stress is negative as discussed in the previous section.

$$\sigma_s = E\text{sign}(\varepsilon_s)|\varepsilon_s|^m \tag{4.3}$$

The viscous damper is chosen to be linear (Newtonian) and its constitutive relation is defined as:

$$\sigma_d = c\dot{\varepsilon}_d \tag{4.4}$$

The subscript d denotes the damper, σ_d is the stress and $\dot{\varepsilon}_d$ is the strain-rate of the damper (i.e. $d\varepsilon_d/dt$).

The system equation can be obtained by following the guideline given in the previous section. The kinematic equation gives:

$$\begin{aligned} \varepsilon_s &= \varepsilon_1 \\ \varepsilon_d &= \varepsilon_2 - \varepsilon_1 \end{aligned} \tag{4.5}$$

where ε_1 and ε_2 are the strains at Nodes 1 and 2, respectively. It should be noted that strain at Node 2 corresponds to the strain on fabric whereas Node 1 is a virtual node required for the viscoelastic response of the material.

The equilibrium equation will be written at Nodes 1 and 2:

Node 1:
$$\sigma_s = \sigma_d \tag{4.6}$$

Node 2:
$$\sigma_d = \sigma \tag{4.7}$$

After replacing the local strains (ε_s and ε_d) in Equations **(4.3)** and **(4.4)** with node strains, ε_1 and ε_2 in Equation **(4.5)**, the resulting equations are substituted in equilibrium Equations **(4.6)** and **(4.7)** to obtain the following two system equations:

$$E\text{sign}(\varepsilon_1)|\varepsilon_1|^m - c(\dot{\varepsilon}_2 - \dot{\varepsilon}_1) = 0 \qquad \textbf{(4.8)}$$

$$c(\dot{\varepsilon}_2 - \dot{\varepsilon}_1) = \sigma \qquad \textbf{(4.9)}$$

The system equations can be written in the matrix form:

$$\begin{bmatrix} c & -c \\ -c & c \end{bmatrix} \begin{Bmatrix} \dot{\varepsilon}_1 \\ \dot{\varepsilon}_2 \end{Bmatrix} + \begin{bmatrix} E & 0 \\ 0 & 0 \end{bmatrix} \begin{Bmatrix} \text{sign}(\varepsilon_1)|\varepsilon_1|^m \\ \varepsilon_2 \end{Bmatrix} = \begin{Bmatrix} 0 \\ \sigma \end{Bmatrix} \qquad \textbf{(4.10)}$$

$$\mathbf{M}\dot{\boldsymbol{\varepsilon}} + \mathbf{E}g(\boldsymbol{\varepsilon}) = \mathbf{f} \qquad \textbf{(4.11)}$$

In the matrix form, the first matrix, **M** containing dampers constants is usually called the mass matrix. The origin of the name comes from rigid-body dynamics, where the matrix contains mass values. Following the conventional terminology, that matrix will be called mass matrix in this study. The second matrix, **E** containing elastic moduli is called elasticity matrix. The vector on the right hand side, **f** is called force vector and g is a function of $\boldsymbol{\varepsilon}$.

It should be noted that the mass matrix in Equation **(4.10)** is singular (i.e. its determinant is zero). This is caused by the dependency of the two equations. Addition of Equations **(4.8)** and **(4.9)** results in the following algebraic equation rather than a differential equation:

$$E\text{sign}(\varepsilon_1)|\varepsilon_1|^m = \sigma \qquad \textbf{(4.12)}$$

One can use either Equation **(4.10)** alone, or use Equations **(4.8)** and **(4.12)** to define the system. If a system has differential equations and an algebraic equation these types of equations are called differential algebraic equations (DAE). The details of DAE will be given in the proceeding sections.

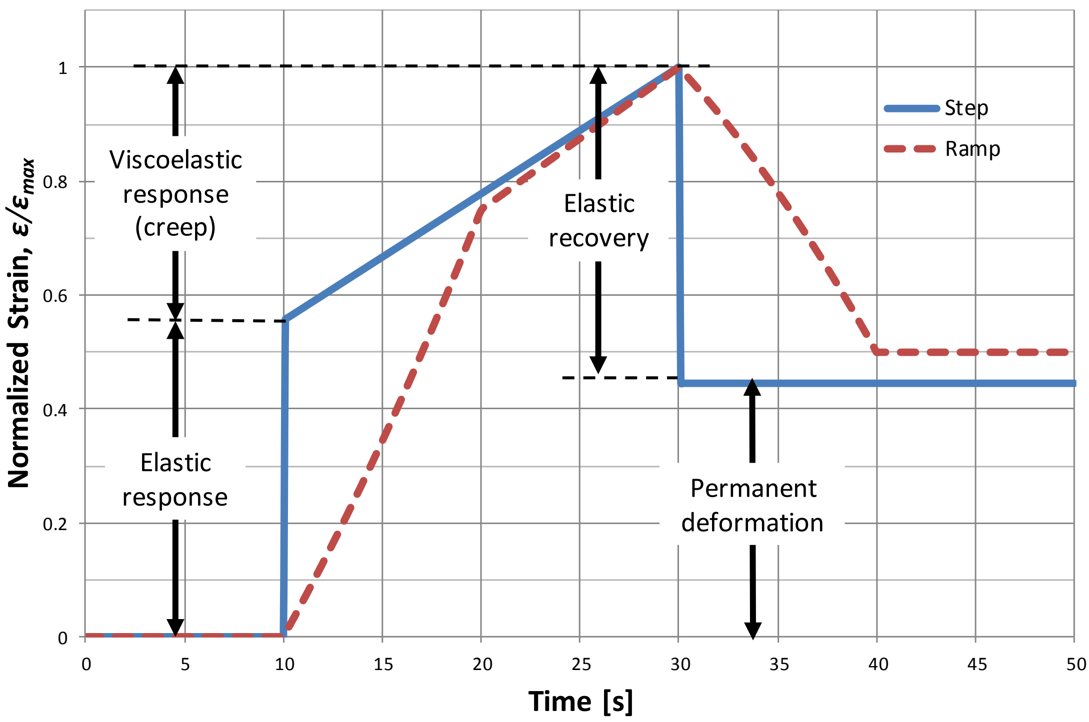

Figure 4-4. The strain response of the Maxwell model.

The solution of the system equation **(4.10)** is illustrated in Figure 4-4 for a set of model parameters (E, m and c). The values of these parameters and the maximum strain, ε_{max} are given in Appendix A.I.

Although this model is one of the two simplest models that will be studied here, it can adequately simulate the elastic and viscous behavior of a specimen as explained in the following two paragraphs.

Elastic deformation occurs instantaneously due to the step rise, and elastic recovery occurs instantaneously due to step fall, both in equal magnitude.

Viscous deformation is the change in strain with time under a constant stress; it rises linearly with time in this model. But, there is no viscous recovery at the relaxation stage where the stress is set to zero. The permanent strain is equal to

$$\varepsilon_{permanent} = \varepsilon_{elastic\ deformation} + \varepsilon_{viscous\ deformation} - \varepsilon_{elastic\ recovery}$$

Since $\varepsilon_{elastic\ deformation} = \varepsilon_{elastic\ recovery}$,

$$\varepsilon_{permanent} = \varepsilon_{viscous\ deformation}$$

If strain input is used as independent variable and stress is solved, the stress decays exponentially in this model (it will be shown in Chapter 5 in more detail). The slope of $\log(\sigma)$ versus time is called relaxation time and defined as $\tau = c/E$ [65]. This study mainly focuses on stress-controlled deformation, however the solution procedure for strain-controlled experiments is described in Chapter 5 for completeness purpose.

4.1.2 Kelvin-Voigt

Kelvin-Voigt (a.k.a. Kelvin or Voigt separately) model consists of a spring connected to a damper in parallel [65–77] as shown in Figure 4-5. It allows simulating creep behavior well, but cannot model stress relaxation. The time dependent response is linear in the previous Maxwell model; and it is nonlinear here. This difference is due to the fact that the spring in Maxwell model is strained instantaneously, whereas in Kelvin-Voigt model, stress and strain in the spring develop with time.

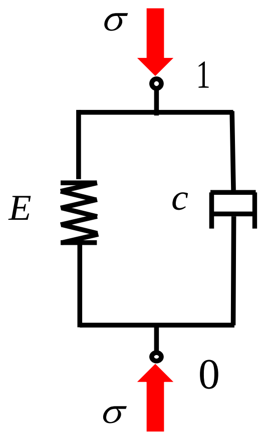

Figure 4-5. Schematic representation of Kelvin-Voigt model.

Moreover, the model is defined with an ODE, thus it is computationally easier to solve Kelvin-Voigt model than Maxwell model which is defined with a DAE.

Recall that stress relaxation is an important stage in the compaction characterization experiments. One needs to set the strain of the fabric to a constant value, and observe the change in stress with time. Modeling of this characterization cannot be achieved by using Kelvin-Voigt model. Note that, the strain at Node 1 represents the strain of the fabric which has to be kept fixed during this stage. By fixing that node, the model cannot result in a response varying in time because the damper branch is restrained. Thus, stress relaxation cannot be studied with this model. Yet, this model can effectively study the viscous recovery of the material as follows. If the characterization procedure is designed based on stress control instead of strain control, one needs to measure the strain at Node 1 by keeping the stress fixed. Thus, Kelvin-Voigt model along with this approach can be adequately used to determine fiber-settling (at high stresses) and fiber-relaxation (at low stresses).

Similar to Maxwell model, the spring is selected to be nonlinear in this study, and it has the same constitutive relation as written in Equation **(4.17)**. The damper is Newtonian and constitutive relation is given in Equation **(4.4)**. The stress equality at the floating Node 1 can be written as follows:

$$\sigma_s + \sigma_d = \sigma \tag{4.13}$$

There is only a single node and both constitutive equations **(4.4)** and **(4.17)** are written using the same strain, hence no kinematic equation is necessary. By substituting the constitutive relations into the stress equality, the system equation is obtained:

$$E\text{sign}(\varepsilon)|\varepsilon|^m + c\dot{\varepsilon} = \sigma \tag{4.14}$$

which can be reorganized as follows:

$$\dot{\varepsilon} = \frac{\sigma - E\text{sign}(\varepsilon)|\varepsilon|^m}{c} \tag{4.15}$$

Recall that Node 1 is a physical node, where the stress (and thus strain) applied on it is non-negative ($\sigma \geq 0$ and $\varepsilon \geq 0$) for VI process. That means, the fabric can be only compressed under vacuum, but tension cannot be applied on it. So the sign function and absolute value can be dropped to simplify the calculations:

$$\dot{\varepsilon} = \frac{(\sigma - E\varepsilon^m)}{c}, \quad \varepsilon \geq 0 \tag{4.16}$$

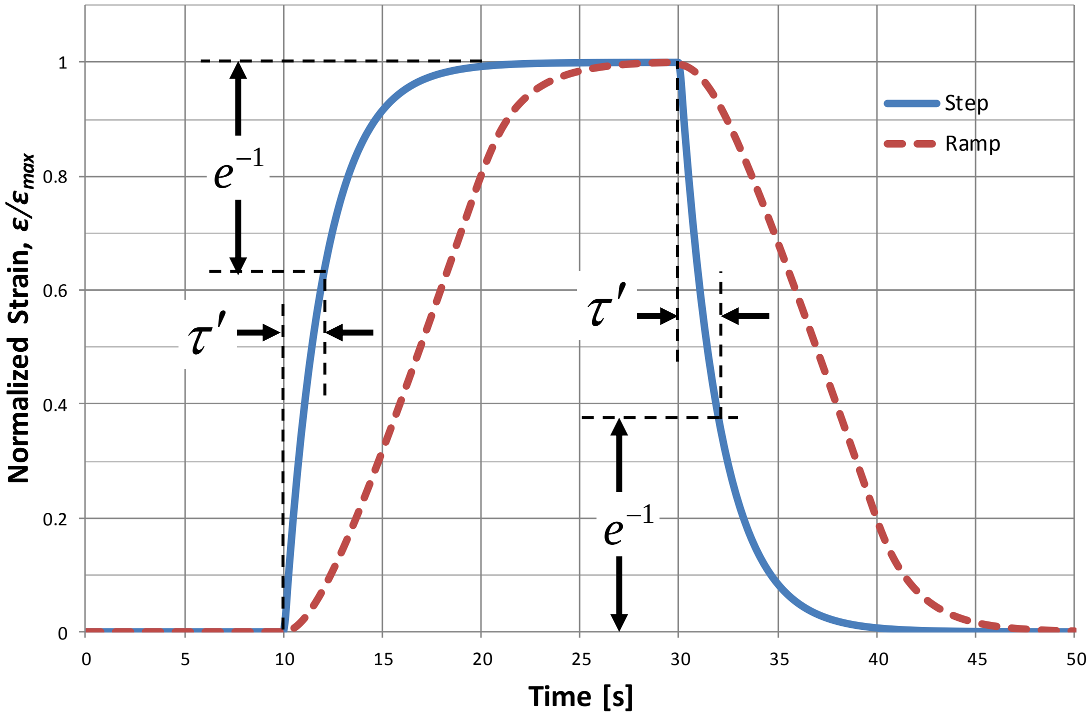

Figure 4-6. The strain response of the Kelvin-Voigt model.

The solution of the system equation **(4.16)** is illustrated in Figure 4-6. Similar to the previous model, the model parameters and ε_{max} are given in Appendix A.I. This simple model can also adequately simulate the features in the following two paragraphs.

There is no instantaneous *elastic deformation*. *Viscous deformation* and *viscous recovery* occur gradually with a decreasing rate. Strain converges to zero as time increases during the relaxation stage; therefore this model allows full strain recovery.

Time constant (a.k.a. retardation time) is a measure of how quickly the response of a system reaches its equilibrium state. In this model, it is defined as $\tau' = c/E$ [65,66,71,77]. This is the time required for strain to reach to a certain value of its equilibrium, which is 62.9% ($= 1 - e^{-1}$) for a system consisting of linear elements (i.e. for $m = 1$). For the arbitrarily chosen model parameters here, $\tau' = 2s$ as seen in Figure 4-6.

4.1.3 Zener

Zener model (a.k.a. 3-element solid, or 3-parameter solid, standard linear solid) consists of a Maxwell element connected in parallel with an elastic spring [65,68,69,78] as shown in Figure 4-7. The advantage of this model is that it can simulate both creep and stress relaxation. But, in turn, it introduces computational complexity.

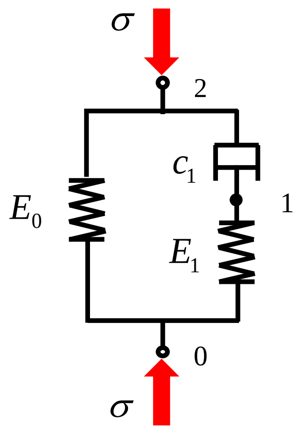

Figure 4-7. Schematic representation of Zener model.

The two springs are selected to be non-linear (i.e. $m \neq 1$) and the constitutive relations are given below

$$\sigma_{si} = E_i \text{sign}(\varepsilon_{si})|\varepsilon_{si}|^{m_i}, \quad i = 0,1 \tag{4.17}$$

where E_i is the stiffness of the spring, m_i is the nonlinearity constant, $\sigma_{s,i}$ and $\varepsilon_{s,i}$ are stress and strain of the i^{th} spring, respectively. The damper is the same as in Maxwell model introduced in Equation **(4.4)**.

To obtain the solution of the system, stress equilibrium at the floating Nodes 1 and 2 can be written as follows:

Node 1:
$$\sigma_{s1} = \sigma_d \tag{4.18}$$

Node 2:
$$\sigma_{s0} + \sigma_d = \sigma \tag{4.19}$$

where σ is the external stress applied on the preform.

Kinematic equations can be written as follows

$$
\begin{aligned}
\varepsilon_{s0} &= \varepsilon_2 \\
\varepsilon_{s1} &= \varepsilon_1 \\
\varepsilon_d &= \varepsilon_2 - \varepsilon_1
\end{aligned}
\tag{4.20}
$$

These equations are substituted into the constitutive relations defined in Equations **(4.4)** and **(4.17)**, and the resulting equations are substituted into Equations **(4.18)** and **(4.19)**. The two equations defining the system response are obtained:

$$E_1 \text{sign}(\varepsilon_1)|\varepsilon_1|^{m_1} - c_1(\dot{\varepsilon}_2 - \dot{\varepsilon}_1) = 0 \tag{4.21}$$

$$E_0 \text{sign}(\varepsilon_2)|\varepsilon_2|^{m_0} + c_1(\dot{\varepsilon}_2 - \dot{\varepsilon}_1) = \sigma \tag{4.22}$$

Equations **(4.21)** and **(4.22)** can be written in matrix form as follows:

$$\begin{bmatrix} c_1 & -c_1 \\ -c_1 & c_1 \end{bmatrix} \begin{Bmatrix} \dot{\varepsilon}_1 \\ \dot{\varepsilon}_2 \end{Bmatrix} + \begin{bmatrix} E_1 & 0 \\ 0 & E_0 \end{bmatrix} \begin{Bmatrix} \text{sign}(\varepsilon_1)|\varepsilon_1|^{m_1} \\ \text{sign}(\varepsilon_2)|\varepsilon_2|^{m_0} \end{Bmatrix} = \begin{Bmatrix} 0 \\ \sigma \end{Bmatrix} \tag{4.23}$$

In the literature, some studies prefer representing Equation **(4.23)** as follows:

$$\begin{bmatrix} c_1 & -c_1 \\ -c_1 & c_1 \end{bmatrix} \begin{Bmatrix} \dot{\varepsilon}_1 \\ \dot{\varepsilon}_2 \end{Bmatrix} = \begin{Bmatrix} -E_1 \text{sign}(\varepsilon_1)|\varepsilon_1|^{m_1} \\ \sigma - E_0 \text{sign}(\varepsilon_2)|\varepsilon_2|^{m_0} \end{Bmatrix} \tag{4.24}$$

In this notation, it is not as easy to see the contributions of spring elements on each node as in Equation **(4.23)**.

The solution of the system for the previously mentioned step and ramp input functions are given in Figure 4-8. The advantage of this model compared to the previous two models consisting of two elements only becomes significant with this sample response graph. This model simply combines instantaneous *elastic deformation/recovery* of Maxwell model with *viscous deformation/recovery* of Kelvin-Voigt model. Both branches contribute to the instantaneous deformation, and the magnitude of the corresponding strain for linear springs can be obtained with $\varepsilon = \sigma/(E_0 + E_1)$.

Since the effect of both Maxwell and Kelvin-Voigt models are included in this model, both relaxation and retardation time should be defined. Maxwell element branch alone causes the stress relaxation, hence the relaxation time is $\tau = c/E_1$. But both branches contribute to creep, hence retardation time must be redefined as $\tau' = (c/E_0 + c/E_1)$ [65].

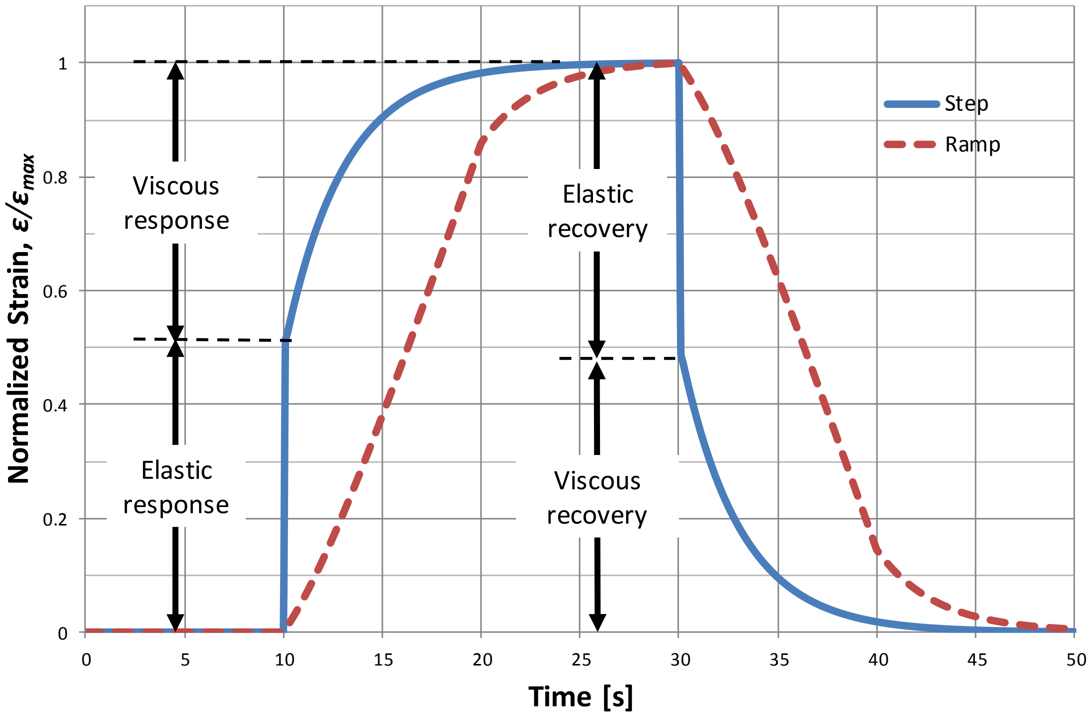

Figure 4-8. The strain response of the Zener model.

4.1.4 Generalized Maxwell

Generalized Maxwell (a.k.a. Wiechert) model includes multiple Maxwell elements and a single spring all connected in parallel [68–72,74–76] as shown in Figure 4-9. It is an expansion of Zener model.

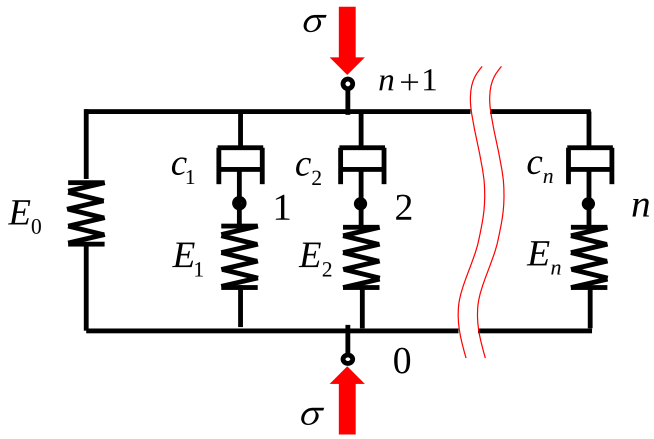

Figure 4-9. Schematic representation of Generalized Maxwell model.

Viscoelastic materials can have response with more than one time constant. If the system responses in such a way that it does not have a single time constant, it becomes hard to define the behavior of the material with previously discussed models. In mechanical viscoelastic models, the time dependent response and hence the time constant is captured using the Maxwell element. The idea behind Generalized Maxwell model is to use n Maxwell elements connected in parallel to account for n different time dependent responses reaching equilibrium at different instants depending on their relaxation times. With multiple relaxation times, it is possible to include both long term (high relaxation time) and short term (low relaxation time) responses in the model. Debulking of a fabric can be modeled with a high relaxation time; and the time dependent relaxation can be modeled with a low relaxation time. To avoid infinite deformation, a spring (E_0) is connected in parallel with the Maxwell elements.

As mentioned earlier in this chapter, Zener model is a generalized Maxwell model with a single Maxwell branch ($n = 1$). Hence, the derivation of the model is very similar. For this application, the springs are non-linear, but viscous dampers are Newtonian:

$$\sigma_{si} = E_i \operatorname{sign}(\varepsilon_{si})|\varepsilon_{si}|^{m_i}, \quad i = 0,1,\dots,n \tag{4.25}$$

$$\sigma_{di} = c_i \dot{\varepsilon}_{di}, \quad i = 1,\dots,n \tag{4.26}$$

The stress equality at each node location results in the following:

Node *1,…,n*:

$$\sigma_{sn} = \sigma_{dn} \tag{4.27}$$

Node *n+1*:

$$\sigma_{s0} + \sum_{i=1}^{n} \sigma_{di} = \sigma \tag{4.28}$$

Kinematic equations can be written as follows

$$\begin{aligned} &\varepsilon_{s0} = \varepsilon_{n+1} \equiv \varepsilon \\ &\varepsilon_{si} = \varepsilon_i, \qquad i = 1,\dots,n \\ &\varepsilon_{di} = \varepsilon - \varepsilon_i, \qquad i = 1,\dots,n \end{aligned} \tag{4.29}$$

After substituting constitutive relations **(4.25)** and **(4.26)** into Equation **(4.29)**, and then combining them with equilibrium equations **(4.27)** and **(4.28)**, the system of equations are obtained

$$\begin{gathered} E_1 sign(\varepsilon_1)|\varepsilon_1|^{m_1} - c_1(\dot{\varepsilon} - \dot{\varepsilon}_1) = 0 \\ E_2 sign(\varepsilon_2)|\varepsilon_2|^{m_2} - c_2(\dot{\varepsilon} - \dot{\varepsilon}_2) = 0 \\ \vdots \\ E_n sign(\varepsilon_n)|\varepsilon_n|^{m_n} - c_1(\dot{\varepsilon} - \dot{\varepsilon}_n) = 0 \\ E_0 sign(\varepsilon)|\varepsilon|^{m_0} - \sum_{i=1}^{n} c_i(\dot{\varepsilon} - \dot{\varepsilon}_i) = \sigma \end{gathered} \tag{4.30}$$

Equation **(4.30)** is rewritten in matrix form below; and it allows showing how the constant matrices **M** and **E** are formed in a systematic way:

$$\begin{bmatrix} c_1 & 0 & \cdots & 0 & -c_1 \\ 0 & c_2 & & 0 & -c_2 \\ \vdots & & \ddots & & \vdots \\ 0 & 0 & & c_n & -c_n \\ -c_1 & -c_2 & \cdots & -c_n & \sum_{i=1}^{n} c_i \end{bmatrix} \begin{Bmatrix} \dot{\varepsilon}_1 \\ \dot{\varepsilon}_2 \\ \vdots \\ \dot{\varepsilon}_n \\ \dot{\varepsilon} \end{Bmatrix} + \begin{bmatrix} E_1 & 0 & \cdots & 0 & 0 \\ 0 & E_2 & & 0 & 0 \\ \vdots & & \ddots & & \vdots \\ 0 & 0 & & E_n & 0 \\ 0 & 0 & \cdots & 0 & E_0 \end{bmatrix} \begin{Bmatrix} \mathrm{sign}(\varepsilon_1)|\varepsilon_1|^{m_1} \\ \mathrm{sign}(\varepsilon_2)|\varepsilon_2|^{m_2} \\ \vdots \\ \mathrm{sign}(\varepsilon_n)|\varepsilon_n|^{m_n} \\ \mathrm{sign}(\varepsilon)|\varepsilon|^{m_0} \end{Bmatrix} = \begin{Bmatrix} 0 \\ 0 \\ \vdots \\ 0 \\ \sigma \end{Bmatrix} \tag{4.31}$$

The non-zero terms in **M** and **E** correspond to the dampers and springs, respectively. Each damper adds its positive damper constant to its connecting nodes (i.e. a damper "k" connected between Nodes i and j adds $+c_k$ to $\mathbf{M}_{i,i}$ and $\mathbf{M}_{j,j}$) and negative value to off-diagonal terms (i.e. $-c_k$ to $\mathbf{M}_{i,j}$ and $\mathbf{M}_{j,i}$). Similarly, springs contribute to **E** matrix. In other words, if there is a damper, c_k between Nodes i and j, $\mathbf{M}_{i,i} = \mathbf{M}_{j,j} = c_k$, and $\mathbf{M}_{i,j} = \mathbf{M}_{j,i} = -c_k$. If Node i is connected to an additional damper c_p between Nodes i and q, the contributions to the mass matrix will be: $\mathbf{M}_{i,i} = c_k + c_p$, $\mathbf{M}_{j,j} = c_k$, $\mathbf{M}_{q,q} = c_p$, $\mathbf{M}_{i,j} = \mathbf{M}_{j,i} = -c_k$ and $\mathbf{M}_{i,q} = \mathbf{M}_{q,i} = -c_p$. Similar rules apply to the construction of **E** matrix. Since one node of each spring is connected to the reference ground node, only one term appears per spring in **E**. Notice that this systematic formation of matrix form is also applicable to other models. This methodology is introduced here since the number of nodes is high, and regular formulation can be more tedious.

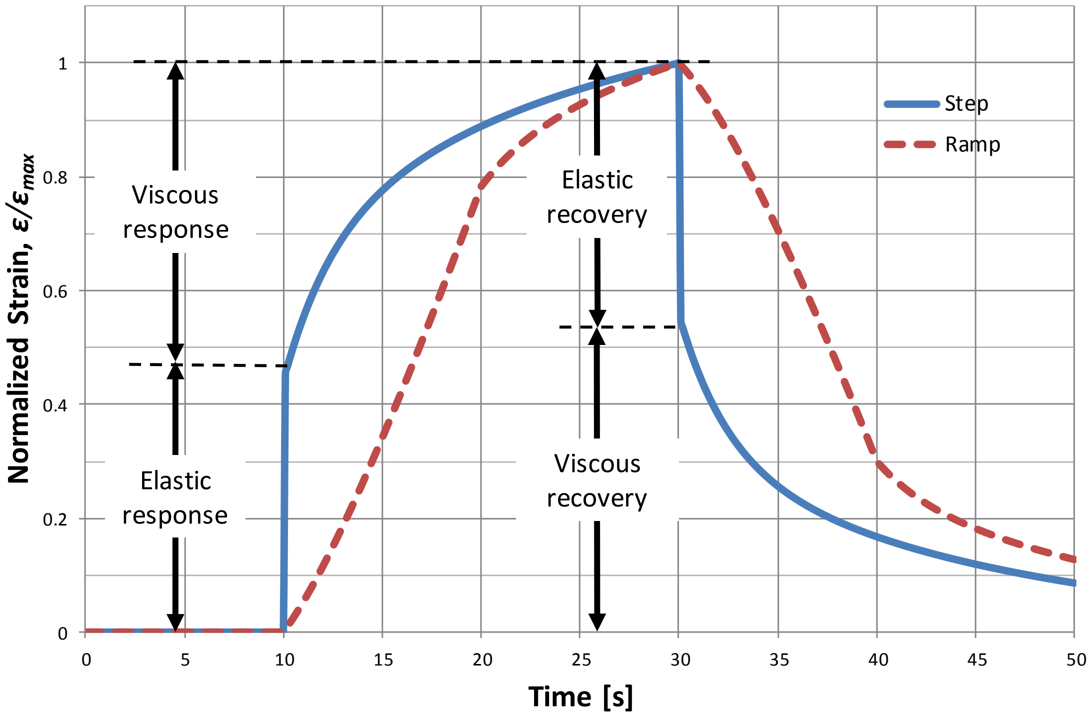

Figure 4-10. The strain response of the Generalized Maxwell model.

The determinant of the mass matrix is zero, which makes it a singular matrix. This is an indication of a DAE. The response of the model to the two input stress functions (given in Figure 4-2) is shown in Figure 4-10.

The response is very similar to Zener model, which is simply a Generalized Maxwell model with $n = 1$. Different from Zener model, the system has multiple relaxation times as a result of multiple Maxwell elements. The relaxation time constants are defined similar to the Maxwell model. For each branch, the relaxation time is $\tau_i = c_i/E_1$, $i = 0, \ldots, n$. On the other hand, there is a single retardation time, τ'. In the literature, τ' is usually evaluated as the time required for strain to reach 62.9% ($= 1 - e^{-1}$) of its equilibrium value.

4.1.5 Burgers

Burgers (a.k.a. 4-element creep) model, which is shown in Figure 4-11, is obtained by connecting a Maxwell element to a Kelvin-Voigt model in series [66,71,73–75,77]. This serial Maxwell element means that there is a damper connected in series. Because of this damper, the model does not recover completely after the load is removed and a non-zero equilibrium is reached. In other words, a permanent (plastic) deformation takes place.

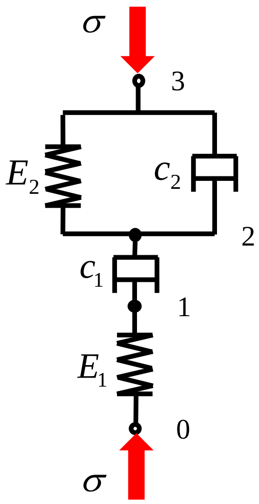

Figure 4-11. Schematic representation of Burgers model.

The constitutive relations for the springs and dampers are given in Equation **(4.17)** and **(4.26)** (for $n = 2$). The stress equality at each node location results in the following equations

Node 1: $$\sigma_{s1} = \sigma_{d1} \tag{4.32}$$

Node 2: $$\sigma_{d1} = \sigma_{s2} + \sigma_{d2} \tag{4.33}$$

Node 3: $$\sigma_{s2} + \sigma_{d2} = \sigma \tag{4.34}$$

Kinematic equations can be written as follows:

(4.35)

$$\varepsilon_{s1} = \varepsilon_1$$

$$\varepsilon_{s2} = \varepsilon_{d2} = \varepsilon_3 - \varepsilon_2$$

Substituting constitutive relations and Equations (4-21) and (4-22) into Equation **(4.35)** results in:

$$\begin{aligned} E_1 \operatorname{sign}(\varepsilon_1)|\varepsilon_1|^{m_1} - c_1(\dot{\varepsilon}_2 - \dot{\varepsilon}_1) &= 0 \\ c_1(\dot{\varepsilon}_2 - \dot{\varepsilon}_1) - E_2 \operatorname{sign}(\varepsilon_3 - \varepsilon_2)|\varepsilon_3 - \varepsilon_2|^{m_2} - c_2(\dot{\varepsilon}_3 - \dot{\varepsilon}_2) &= 0 \\ E_2 \operatorname{sign}(\varepsilon_3 - \varepsilon_2)|\varepsilon_3 - \varepsilon_2|^{m_2} + c_2(\dot{\varepsilon}_3 - \dot{\varepsilon}_2) &= \sigma \end{aligned} \qquad \textbf{(4.36)}$$

Rearranging Equation **(4.36)** in matrix form results in:

$$\begin{bmatrix} c_1 & -c_1 & 0 \\ -c_1 & c_1 + c_2 & -c_2 \\ 0 & -c_2 & c_2 \end{bmatrix} \begin{Bmatrix} \dot{\varepsilon}_1 \\ \dot{\varepsilon}_2 \\ \dot{\varepsilon}_3 \end{Bmatrix} = \begin{Bmatrix} -E_1 \operatorname{sign}(\varepsilon_1)|\varepsilon_1|^{m_1} \\ E_2 \operatorname{sign}(\varepsilon_3 - \varepsilon_2)|\varepsilon_3 - \varepsilon_2|^{m_2} \\ \sigma - E_2 \operatorname{sign}(\varepsilon_3 - \varepsilon_2)|\varepsilon_3 - \varepsilon_2|^{m_2} \end{Bmatrix} \qquad \textbf{(4.37)}$$

Note that Spring 2 is connected between the two floating nodes, whereas in the previous models, one port of the spring is connected to ground/reference. Thus, that spring stress contains two strain terms ε_2 and ε_3, which is not separable in matrix form. That means the system of equation cannot be written in the form of Equation **(4.10)**.

The response for the sample input is given in Figure 4-12. The Burgers model can simulate both elastic deformation/recovery and viscous deformation/recovery as in Zener model. Additionally, it has one more element (damper connected in series) compared to a Zener model, which allows modeling a permanent deformation. There are two independent relaxation times present in the system, and they are defined as: $\tau_1 = c_1/E_1$ and $\tau_2 = c_2/E_2$ [66]. On the other hand, there is a single retardation time, and it is defined as: $\tau' = c_2/E_2$.

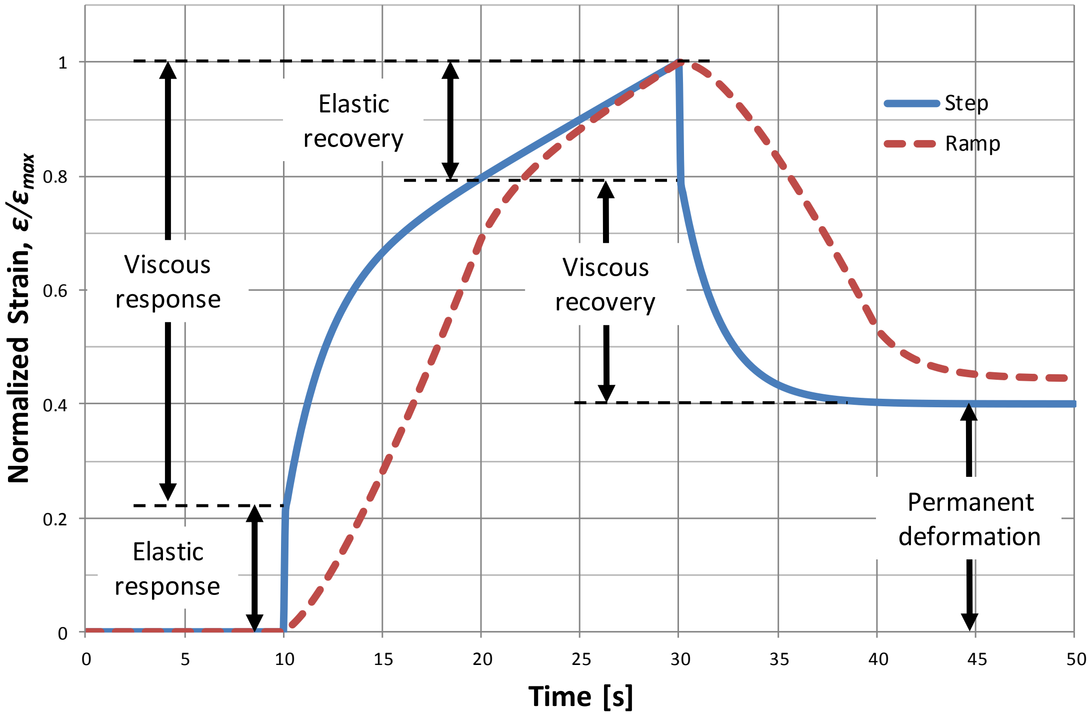

Figure 4-12. The strain response of the Burgers model.

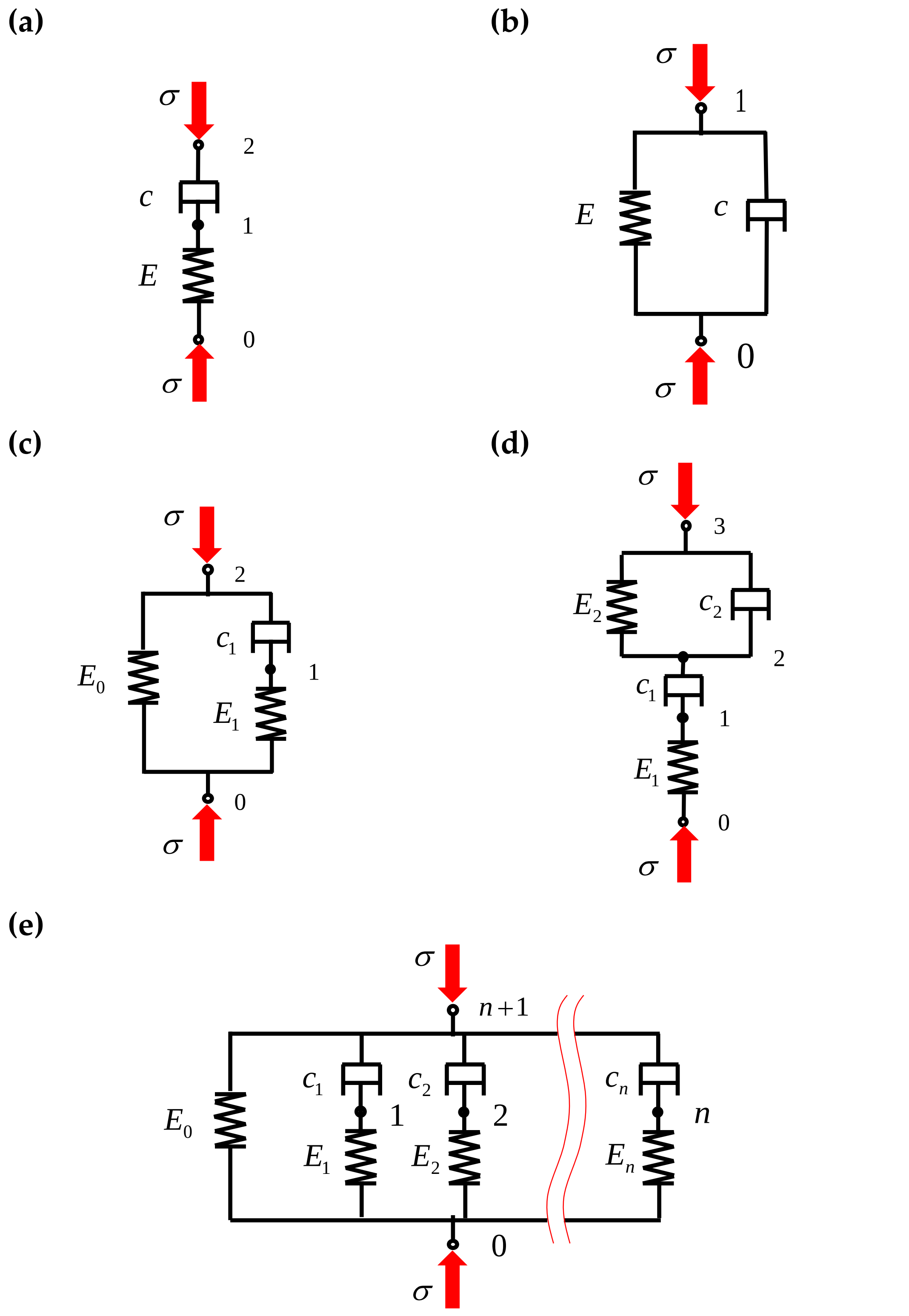

Figure 4-13. Schematic representation of the five viscoelastic models: (a) Maxwell, (b) Kelvin-Voigt, (c) Zener, (d) Burger's and (e) Generalized Maxwell model.

4.2 Solution of Strain for a Given Stress Input

For a given arbitrary stress input, σ, the response of the system (i.e. strain, ε) can be solved by using the system equations given in the previous section. The system equations that will be used in this section are summarized below for all five viscoelastic models introduced earlier.

Maxwell, Equation **(4.10)**:

$$\begin{bmatrix} c & -c \\ -c & c \end{bmatrix} \begin{Bmatrix} \dot{\varepsilon}_1 \\ \dot{\varepsilon}_2 \end{Bmatrix} + \begin{bmatrix} E & 0 \\ 0 & 0 \end{bmatrix} \begin{Bmatrix} \mathrm{sign}(\varepsilon_1)|\varepsilon_1|^m \\ \varepsilon_2 \end{Bmatrix} = \begin{Bmatrix} 0 \\ \sigma \end{Bmatrix}$$

Kelvin-Voigt, Equation **(4.16)**:

$$\dot{\varepsilon} = \frac{(\sigma - E\varepsilon^m)}{c}, \quad \varepsilon \geq 0$$

Zener, Equation **(4.23)**:

$$\begin{bmatrix} c_1 & -c_1 \\ -c_1 & c_1 \end{bmatrix} \begin{Bmatrix} \dot{\varepsilon}_1 \\ \dot{\varepsilon}_2 \end{Bmatrix} + \begin{bmatrix} E_1 & 0 \\ 0 & E_0 \end{bmatrix} \begin{Bmatrix} \mathrm{sign}(\varepsilon_1)|\varepsilon_1|^{m_1} \\ \mathrm{sign}(\varepsilon_2)|\varepsilon_2|^{m_0} \end{Bmatrix} = \begin{Bmatrix} 0 \\ \sigma \end{Bmatrix}$$

Generalized Maxwell, Equation **(4.31)**:

$$\begin{bmatrix} c_1 & 0 & \cdots & 0 & -c_1 \\ 0 & c_2 & & 0 & -c_2 \\ \vdots & & \ddots & & \vdots \\ 0 & 0 & & c_n & -c_n \\ -c_1 & -c_2 & \cdots & -c_n & \sum_{i=1}^{n} c_i \end{bmatrix} \begin{Bmatrix} \dot{\varepsilon}_1 \\ \dot{\varepsilon}_2 \\ \vdots \\ \dot{\varepsilon}_n \\ \dot{\varepsilon} \end{Bmatrix} + \begin{bmatrix} E_1 & 0 & \cdots & 0 & 0 \\ 0 & E_2 & & 0 & 0 \\ \vdots & & \ddots & & \vdots \\ 0 & 0 & & E_n & 0 \\ 0 & 0 & \cdots & 0 & E_0 \end{bmatrix} \begin{Bmatrix} \mathrm{sign}(\varepsilon_1)|\varepsilon_1|^{m_1} \\ \mathrm{sign}(\varepsilon_2)|\varepsilon_2|^{m_2} \\ \vdots \\ \mathrm{sign}(\varepsilon_n)|\varepsilon_n|^{m_n} \\ \mathrm{sign}(\varepsilon)|\varepsilon|^{m_0} \end{Bmatrix} = \begin{Bmatrix} 0 \\ 0 \\ \vdots \\ 0 \\ \sigma \end{Bmatrix}$$

Burgers, Equation **(4.37)**:

$$\begin{bmatrix} c_1 & -c_1 & 0 \\ -c_1 & c_1+c_2 & -c_2 \\ 0 & -c_2 & c_2 \end{bmatrix} \begin{Bmatrix} \dot{\varepsilon}_1 \\ \dot{\varepsilon}_2 \\ \dot{\varepsilon}_3 \end{Bmatrix} = \begin{Bmatrix} -E_1 \mathrm{sign}(\varepsilon_1)|\varepsilon_1|^{m_1} \\ E_2 \mathrm{sign}(\varepsilon_3-\varepsilon_2)|\varepsilon_3-\varepsilon_2|^{m_2} \\ \sigma - E_2 \mathrm{sign}(\varepsilon_3-\varepsilon_2)|\varepsilon_3-\varepsilon_2|^{m_2} \end{Bmatrix}$$

Note the similarity between Maxwell, Zener and Generalized Maxwell models' equations. As mentioned in their corresponding sections, Maxwell and Zener models are special cases of Generalized Maxwell model. The number of Maxwell elements in these two models is one, hence $n = 1$. If $n = 1$ is defined in the Generalized Maxwell model equation, it effectively becomes Zener equation. On the other hand, in Maxwell model, there is no spring connected in parallel to the Maxwell element, which means $E_0 = 0$ should be set. Considering these, the solution of Equation **(4.31)** will be used for not only the Generalized Maxwell model, but also for Maxwell and Zener models simply by adjusting model parameters, n and E_0. There is no simplification for Kelvin-Voigt and Burgers model.

4.2.1 Numerical Solution

The five models discussed in previous sections consist of dampers and springs, and they are called mechanical viscoelastic models. The equations for these models are differential equations. Among these five, Kelvin-Voigt model is an ODE with a single variable and the other four are DAE. A DAE can be rearranged to an ODE, if all the elements are linear. The dampers are linear in this study. Additionally, if the springs are linear, $\sigma = E\varepsilon$ the previous condition is satisfies and thus the conversion from DAE to ODE can be done. The nonlinear elements (i.e. springs in this study) increase complexity, and it might make it impossible to obtain uncoupled ODEs.

Since some models do not result in ODEs, and analytical solutions of some system equations may not be available, numerical solution methods will be sought in this study. As it will be illustrated in this section, the numerical solution procedure for all these five models will be similar. Thus, any other viscoelastic model can also be investigated readily simply by developing its system equation and following the same numerical solution model.

In this study, a single numerical solution method will be used to solve strain in all of the five model system equations, whether the system equation is an ODE or DAE. It should be noted that a DAE can be written as two sets of equations, one of which is ODE and the other is algebraic equation. The algebraic equation can be a null function, which means an ODE can be written as a DAE. Thus, a DAE solver can be used for both DAEs and ODEs, whereas the opposite is not true.

In this study, MATLAB's ode15s solver is used to solve the equations numerically. This solver is specifically used for stiff differential equations and DAEs. The details of the solver are given in the proceeding sections.

a. Differential Algebraic Equations (DAE)

A DAE (a.k.a. algebro-differential system, implicit differential equations, or singular system) is a set of differential equations which have an algebraic constraint [79]. One example of algebraic constraint was given in Equation **(4.12)** while discussing the Maxwell model.

The simplest DAE can be shown in a semi-explicit form:

$$\begin{aligned} \dot{y}(t) &= f(x(t), y(t), t) \\ 0 &= g(x(t), y(y), t) \end{aligned} \qquad \textbf{(4.38)}$$

where f and g are the functions defining the system, y is the dependent variable to be solved, x is the independent variable, and t is time. $\dot{y}$ denotes the time derivative, dy/dt. A DAE cannot be solved directly using integration algorithms for ordinary differential equations (ODE). It is possible to solve f function first then substitute the partial solution into g to get the system solution. However, it is crucial to find consistent initial values satisfying the function g, and also it should be noted that algebraic equation must hold for the whole time domain. Also, this leads initial value problems for computationally expensive f functions [80].

As discussed above, if DAEs can be transformed into ODEs, a solution can be obtained. If they cannot be transformed, one approach could be to reduce DAE by differentiation, which results in ODEs with fewer variables [79].

The models used in this study have nonlinear springs. The corresponding DAEs cannot be transformed into ODE because of the power term appearing on the node strains which makes the variables in the equations non-separable. For special case of linear springs, the transformation could be achieved only if DAEs are reformulated.

DAE to ODE transformation could be achieved by numerical differentiation even if the springs are nonlinear. The number of differentiations required to transform DAE to ODE is called differentiation index. The index defines the complexity of the system. Index-0 system is simply an ODE. The solution of index-1 system requires the initial time derivatives of system variables. Whereas a DAE with an index of 2 or higher, which is called a higher-index DAE, requires additional initial values which may not correspond to the physical system variables, they are usually called hidden variables [81].

b. Solution of DAEs

The solution of DAEs is not straightforward for systems with coupled equations or nonlinearities; and the detail of the solution procedure is beyond the scope of this study. The system equations in this study can be written with a set of differential equations and a single algebraic equation. A single algebraic equation requires one differentiation to convert the system into ODE. In other words, the index of DAE is 1. A solution method for handling index-1 DAEs is available in Matlab; and thus it is sufficient to solve the system equations given in this study.

The solution can be found for index-1 systems if the input is continuous by following differentiation procedure. If there exists a discontinuity (i.e. a sudden change in the input function), the derivative is not defined at that point. This causes the method to fail even if the index of the system is 1. To overcome this problem, one of the two following approaches can be used:

- The input function is written piecewise in sub-time domains between the singular points. The end value of a subdomain is used as the initial value of the next subdomain.
- The input function is filtered or smoothed out to remove the discontinuities and the usual procedure is followed.

c. Initial condition estimation

For characterization experiments, the initial conditions are taken as zero. These initial conditions are the strains between the nodes, and their first time derivatives. Recall that the fabric specimen is compacted under the minor load initially for five minutes, and the corresponding strain at that minor load is defined as zero. Experimentally it was observed that $d\varepsilon/dt$ is insignificant and assumed to be negligible toward the end of the minor loading stage (see the first 50 seconds of Figure 3-14); and thus steady state (i.e. $d\varepsilon/dt = 0$) is assumed in the modeling.

If one is interested in solving an intermediate stage only, still the complete problem must be solved starting from the initial time by using the initial condition unless one could estimate the condition at the beginning of that particular intermediate stage. For example, if the modeling is needed for the wetted stage only, solution of the system equation must start at the wetting time. This dry to wet transition usually takes place under high vacuum in the actual VI process. Thus, the initial conditions cannot be taken as zero. Considering that the wetting takes place after the fabric is kept at the same vacuum level for a reasonably long time (five minutes in the characterization experiments), and a steady state is almost achieved at this high compaction pressure toward the end of the five minutes; thus $d\varepsilon/dt = 0$ is assumed. The initial conditions of the strains are directly calculated by substituting $\dot{\varepsilon}_i(0) = 0$ into the system equation. Among the five models studied here, Kelvin-Voigt, Zener and Generalized Maxwell models result in unique solution, however Maxwell and Burger's models (where there is a permanent deformation as seen in Figure 4-4 and Figure 4-12) result in non-unique solution. For these two models, the only way to solve the model is to start with "the original initial conditions". That means, instead of investigating a separate wet stage only, one must consider the solution by starting from the minor loading applied to the dry specimen; and then continue with the dry loading/settling, and eventually the wet unloading.

d. Numerical Solution

To solve the system equations, MATLAB's built-in solver, ode15s is used. Among the built-in ode## solvers of MATLAB, ode15s was chosen because of its ability to solve DAEs. This solver is specifically designed for DAEs and stiff ODEs. The accuracy of the solver is listed as low to medium. The detailed description of how this solver works is given in **Error! Reference source not found.**. Its brief description is as follows: "ode15s s a variable order solver based on the numerical differentiation formulas (NDFs). Optionally, it uses the backward differentiation formulas (BDFs, also known as Gear's method) that are usually less efficient. Like ode113, ode15s is a multistep solver." [82]

The use of this solver for a continuous input stress function is illustrated below for a sample model (Generalized Maxwell Model).

1. Set the parameter vector, P which contains E_i and m_i for $i = 0, \ldots, n$ and c_i for $i = 1, \ldots, n$.
2. Assign the mass matrix:

$$\mathbf{M} = \begin{bmatrix} c_1 & 0 & \cdots & 0 & -c_1 \\ 0 & c_2 & & 0 & -c_2 \\ \vdots & & \ddots & & \vdots \\ 0 & 0 & & c_n & -c_n \\ -c_1 & -c_2 & \cdots & -c_n & \sum_{i=1}^{n} c_i \end{bmatrix}$$

3. Define $\vec{\mathbf{F}}$ vector:

$$\vec{\mathbf{F}} = \begin{Bmatrix} 0 \\ 0 \\ \vdots \\ 0 \\ \sigma \end{Bmatrix} - \begin{bmatrix} E_1 & 0 & \cdots & 0 & 0 \\ 0 & E_2 & & 0 & 0 \\ \vdots & & \ddots & & \vdots \\ 0 & 0 & & E_n & 0 \\ 0 & 0 & \cdots & 0 & E_0 \end{bmatrix} \begin{Bmatrix} \mathrm{sign}(\varepsilon_1)|\varepsilon_1|^{m_1} \\ \mathrm{sign}(\varepsilon_2)|\varepsilon_2|^{m_2} \\ \vdots \\ \mathrm{sign}(\varepsilon_n)|\varepsilon_n|^{m_n} \\ \mathrm{sign}(\varepsilon)|\varepsilon|^{m_0} \end{Bmatrix}$$

4. Set the optional parameters of the solver:

   `MaxStep = 1` → Maximum time step = 1 s.

   `MStateDependence = "none"` → Mass matrix is independent of strain.

   ```
   Options = odeset('MaxStep',1,'Mass', M(P),'MStateDependence','none');
   ```

5. Define continuous input stress function, $\sigma(t)$:

   An input file is constructed for the procedure given in Figure 4-2.

6. Define time domain, $t = 0, \ldots, t_{final}$
7. Set the initial conditions for strains depending on the discussion given in the previous section:

$$\vec{\boldsymbol{\varepsilon}}(0) = \begin{Bmatrix} 0 \\ 0 \\ \vdots \\ 0 \\ \varepsilon(0) \end{Bmatrix} \qquad \text{or} \qquad \vec{\boldsymbol{\varepsilon}}(0) = \begin{Bmatrix} 0 \\ 0 \\ \vdots \\ 0 \\ \left(\frac{\sigma}{E_0}\right)^{1/m_0} \end{Bmatrix}$$

8. The solver is run, and ε is obtained as the output:

```
[t,ε] = ode15s( F, t, ε(o), options);
```

If the input function is discontinuous (such as having discontinuous derivatives between the stages of characterization procedure as shown in Figure 4-2), the procedure described between 1 and 5 will be followed exactly. Steps 6-8 will be revised as follows

6'. Define piecewise time domain, $t = \begin{cases} 0, \dots, t_1 \\ t_1, \dots, t_2 \\ \vdots \\ t_{N-1}, \dots, t_{final} \end{cases}$

7′-8′. Follow Steps 7 and 8 above for the first time sub-domain. Use the final values of strains, $\varepsilon(t_1)$ and their derivatives, $\dot{\varepsilon}(t_1)$ as the initial conditions of the next time subdomain. This step is continued in a loop until t_{final} is reached.

4.2.2 Special case: Linear elements

In the literature, viscoelastic materials are commonly modeled with linear elements [27,33,39] (resulting in linear models). For solid materials under small deformation and for liquid materials, this approach gives acceptable results. However a fabric preform undergoes large deformations. The fit of the model can be improved by using more complex models, such as generalized Maxwell model with $n = 3$. This will most likely give a better estimate than generalized Maxwell model with $n < 3$ or Kelvin-Voigt model. On the other hand, it is sometimes seen that the simplest models with non-linear elements give a better result than a complex model with linear elements. The comparison of the same model's performances when it has (1) linear and (2) non-linear elements (springs in our case) will be detailed in Chapter 7.

a. Numerical solution of linear models

$m = 1$ is set in the nonlinear system equations to solve linear equations, and exactly the same solution procedure for the nonlinear equations is followed.

b. Analytical solution of linear models

Using linear elements in the models results in differential equations where there is no power term in unknown variables as the name linear model implies. For the analysis of viscoelastic materials, the most common method used to solve the differential equation is to use Laplace transform. It should be noted that the input must be known and well defined or in other words must be represented with an analytical function. Considering the input in characterization experiments are defined as simple functions where the pressure either stays constant or changes with a fixed rate, Laplace transformation can be used in parameter estimation (model fitting). On the other hand, numerical methods must be used if the compaction model is embedded in a complete process simulation where the input (pressure) is not predefined.

Analytical solution done in Matlab environment

The system equation of a model can be transformed into the Laplace domain by hand readily because of the nature of the system equations and input. However, once the solution is obtained, the inverse Laplace operation must be made in Matlab environment. Since the input function will change for different scenarios, it is not feasible to make these transformations by hand.

Matlab symbolic toolbox has ability to take both Laplace and inverse Laplace transforms of the systems equation and the input function. To simplify the system equation and as a result to decrease the CPU load, the Laplace transform of the system equation is taken manually and the system of equations is decreased to a single equation. For each model a single expression is obtained (see Appendix C) and used in analytical solution.

5 Solution of Stress

The previous chapter studied the solution of strain when the stress is an input. That means, stress was the independent variable and strain was the dependent. Here, in this chapter, the opposite will be considered. These two different approaches were discussed in detail earlier in the Introduction chapter.

For a given arbitrary strain input, $\varepsilon(t)$, the response of the system (i.e. stress, $\sigma(t)$) can be solved by rearranging the system equations given in the previous chapter in such a way that (i) the unknowns, σ (the stress on the specimen) and components of the strain, ε_i are collected on the LHS and the prescribed input strain input $\varepsilon(t)$ is on the RHS of the equations; and (ii) the terms including $\dot{\varepsilon}$ were also included in RHS and $\dot{\sigma}$ was included on the LHS. The corresponding equations are given below for each of the five models.

Maxwell:

$$\begin{bmatrix} c & 0 \\ c & 0 \end{bmatrix} \begin{Bmatrix} \dot{\varepsilon}_1 \\ \dot{\sigma} \end{Bmatrix} + \begin{bmatrix} E & 0 \\ 0 & 1 \end{bmatrix} \begin{Bmatrix} \operatorname{sign}(\varepsilon_1)|\varepsilon|^m \\ \sigma \end{Bmatrix} = \begin{Bmatrix} c\dot{\varepsilon}_2 \\ c\dot{\varepsilon}_2 \end{Bmatrix} \quad \textbf{(5.1)}$$

Kelvin-Voigt:

$$\sigma = E\mathrm{sign}(\varepsilon)|\varepsilon|^m + c\dot{\varepsilon} \tag{5.2}$$

Zener:

$$\begin{bmatrix} c & 0 \\ c & 0 \end{bmatrix} \begin{Bmatrix} \dot{\varepsilon}_1 \\ \dot{\sigma} \end{Bmatrix} + \begin{bmatrix} E & 0 \\ 0 & 1 \end{bmatrix} \begin{Bmatrix} \mathrm{sign}(\varepsilon_1)|\varepsilon|^m \\ \sigma \end{Bmatrix} = \begin{Bmatrix} c\dot{\varepsilon}_2 \\ c\dot{\varepsilon}_2 + E_0\mathrm{sign}(\varepsilon_2)|\varepsilon_2|^{m_0} \end{Bmatrix} \tag{5.3}$$

Generalized Maxwell:

$$\begin{bmatrix} c_1 & 0 & \cdots & 0 & 0 \\ 0 & c_2 & 0 & 0 & 0 \\ \vdots & & \ddots & & \vdots \\ 0 & 0 & 0 & c_n & 0 \\ c_1 & c_2 & \cdots & c_n & 0 \end{bmatrix} \begin{Bmatrix} \dot{\varepsilon}_1 \\ \dot{\varepsilon}_2 \\ \vdots \\ \dot{\varepsilon}_n \\ \dot{\sigma} \end{Bmatrix} + \begin{bmatrix} E_1 & 0 & \cdots & 0 & 0 \\ 0 & E_2 & 0 & 0 & 0 \\ \vdots & & \ddots & & \vdots \\ 0 & 0 & 0 & E_n & 0 \\ 0 & 0 & \cdots & 0 & 1 \end{bmatrix} \begin{Bmatrix} \mathrm{sign}(\varepsilon_1)|\varepsilon_1|^{m_1} \\ \mathrm{sign}(\varepsilon_2)|\varepsilon_2|^{m_2} \\ \vdots \\ \mathrm{sign}(\varepsilon_n)|\varepsilon_n|^{m_n} \\ \sigma \end{Bmatrix} = \begin{Bmatrix} \dot{\varepsilon}c_1 \\ \dot{\varepsilon}c_2 \\ \vdots \\ \dot{\varepsilon}c_n \\ \dot{\varepsilon}\sum_{i=1}^{n} c_i + E_0\mathrm{sign}(\varepsilon)|\varepsilon|^{m_0} \end{Bmatrix} \tag{5.4}$$

Burgers:

$$\begin{bmatrix} c_1 & -c_1 & 0 \\ -c_1 & c_1 + c_2 & 0 \\ 0 & -c_2 & 0 \end{bmatrix} \begin{Bmatrix} \dot{\varepsilon}_1 \\ \dot{\varepsilon}_2 \\ \dot{\sigma} \end{Bmatrix} = \begin{Bmatrix} -E_1\mathrm{sign}(\varepsilon_1)|\varepsilon_1|^{m_1} \\ E_2\mathrm{sign}(\varepsilon_3 - \varepsilon_2)|\varepsilon_3 - \varepsilon_2|^{m_2} + c_2\dot{\varepsilon}_3 \\ \sigma - E_2\mathrm{sign}(\varepsilon_3 - \varepsilon_2)|\varepsilon_3 - \varepsilon_2|^{m_2} + c_2\dot{\varepsilon}_3 \end{Bmatrix} \tag{5.5}$$

In all system equations of the five models, multiplication coefficients of $\dot{\sigma}$ are zero as seen in **M** matrices. This is simply because $\dot{\sigma}$ does not appear in the system equations, but included here for a formal representation of DAE.

Similar to the previous section, Generalized Maxwell model can also be used for Maxwell (by setting $n = 1$ and $E_0 = 0$) and Zener (by setting $n = 1$) models.

All system equations given above, except for Kelvin-Voigt, are DAEs and their solution may not be straightforward as explained earlier. One can notice that, for a given model, all the equations except the last equation are uncoupled. Since $\dot{\sigma}$ is a dummy term with a zero coefficient, the last equation is simply an algebraic equation. Therefore, each

DAE can be rearranged as a set of ODEs and an algebraic equation. The solution can be obtained first by solving the ODEs and then substituting the results into the algebraic equation. Notice that Equation **(5.5)** of Burgers model has coupled ODEs due to the appearance of $\dot{\varepsilon}_1$ and $\dot{\varepsilon}_2$ in the same equation. However this relation can be removed readily by algebraic manipulations.

The final forms of the equations are given below for each model.

Maxwell:

$$\dot{\varepsilon}_1 = \dot{\varepsilon}_2 - \frac{E\text{sign}(\varepsilon_1)|\varepsilon_1|^m}{c} \quad \textbf{(5.6)}$$

$$\sigma = c\dot{\varepsilon}_2 - c\dot{\varepsilon}_1 \quad \textbf{(5.7)}$$

Kelvin-Voigt:

$$\sigma = E\text{sign}(\varepsilon)|\varepsilon|^m + c\dot{\varepsilon} \quad \textbf{(5.8)}$$

Zener:

$$\varepsilon_1 = \dot{\varepsilon}_2 - \frac{E\text{sign}(\varepsilon_1)|\varepsilon|^m}{c} \quad \textbf{(5.9)}$$

$$\sigma = c\dot{\varepsilon}_2 - c\dot{\varepsilon}_1 + E_0\text{sign}(\varepsilon_2)|\varepsilon_2|^{m_0} \quad \textbf{(5.10)}$$

Generalized Maxwell:

$$\dot{\varepsilon}_i = \dot{\varepsilon} - \frac{E_i\text{sign}(\varepsilon_i)|\varepsilon|^{m_i}}{c_i},\ i = 1,..,n \quad \textbf{(5.11)}$$

$$\sigma = \dot{\varepsilon}\sum_{i=1}^{n} c_i - \sum_{i=1}^{n} \varepsilon_i c_i + E_0 \mathrm{sign}(\varepsilon)|\varepsilon|^{m_0} - \sum_{i=1}^{n} \varepsilon_i c_i \tag{5.12}$$

Burgers:

$$\begin{aligned} \dot{\varepsilon}_2 &= \dot{\varepsilon}_3 + \frac{E_2 \mathrm{sign}(\varepsilon_3 - \varepsilon_2)|\varepsilon_3 - \varepsilon_2|^{m_2} - E_1 \mathrm{sign}(\varepsilon_1)|\varepsilon_1|^{m_1}}{c_2} \\ \dot{\varepsilon}_1 &= \dot{\varepsilon}_3 + \frac{c_1 E_2 \mathrm{sign}(\varepsilon_3 - \varepsilon_2)|\varepsilon_3 - \varepsilon_2|^{m_2} - (c_1 + c_2) E_1 \mathrm{sign}(\varepsilon_1)|\varepsilon_1|^{m_1}}{c_1 c_2} \end{aligned} \tag{5.13}$$

$$\sigma = E_2 \mathrm{sign}(\varepsilon_3 - \varepsilon_2)|\varepsilon_3 - \varepsilon_2|^{m_2} - c_2\dot{\varepsilon}_2 + c_2\dot{\varepsilon}_3 \tag{5.14}$$

5.1 Stress response

To see the stress responses of the five viscoelastic models, two conventional strain inputs (step and ramp) will be applied as seen in Figure 5-1. One can realize that, the input functions do not mimic the physical stages of VI. For example, *constant maximum strain* stage may be mistakenly used to represent the full vacuum condition on the specimen. The strain is kept constant, and the stress is expected to change (decrease) with time; however this is not the case in VI. In VI, one expects the opposite to occur, i.e. the stress is fixed, and the strain changes with time.

Stress responses of the five viscoelastic models are given in Figure 5-2 to Figure 5-8. All the labeling is done for the step input. The same model parameters are used as in the stress input case in the previous chapter. The stress values are normalized with its maximum value. The values of the selected parameters and σ_{max} are given in Appendix A.I. The characteristics of five models are summarized in Table 5-1. Other important aspects of the models are described below.

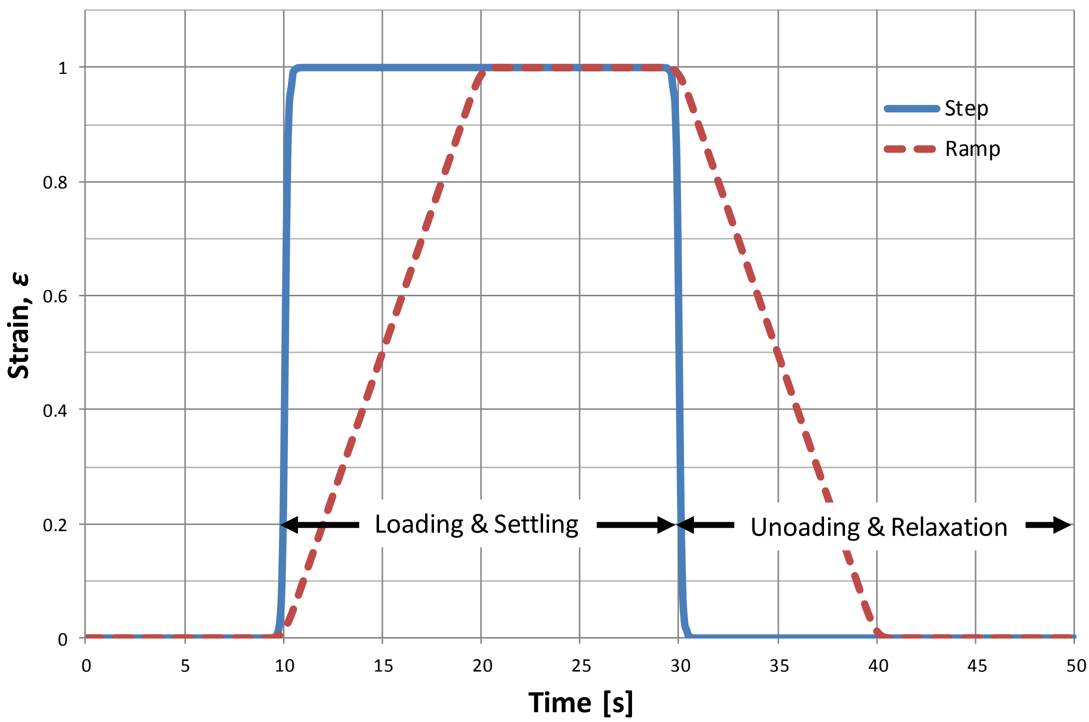

Figure 5-1. Input strain applied on the viscoelastic models for the sample run.

Table 5-1. Response characteristics of five viscoelastic models for step strain input.

<table>
<tr><th></th><th>Step Loading</th><th>Settling</th><th>Step Unloading</th><th>Relaxation</th></tr>
<tr><td>Maxwell</td><td rowspan="5">Instant rise in stress.</td><td>Complete stress relaxation occurs exponentially, i.e. stress converges to zero as time goes to infinity.</td><td rowspan="5">Instant fall in stress; note that $|\Delta\sigma_{unloading}| = |\Delta\sigma_{loading}|$</td><td>Complete stress relaxation occurs exponentially, i.e. stress converges to zero as time goes to infinity.</td></tr>
<tr><td>Kelvin-Voigt</td><td rowspan="3">Partial stress relaxation occurs; stress decreases with time and converges to a non-zero value.</td><td rowspan="4">Complete stress relaxation occurs non-exponentially.</td></tr>
<tr><td>Zener</td></tr>
<tr><td>Generalized Maxwell</td></tr>
<tr><td>Burgers</td><td>Complete stress relaxation occurs non-exponentially.</td></tr>
</table>

5.1.1 Maxwell

When a sudden deformation takes places on a Maxwell model, stress value jumps to a certain value, σ_0 and decreases exponentially over time. This can be seen in Figure 5-2. The initial stress value for a step input can be formulated as, $\sigma_0 = E\varepsilon_0$. The exponential decrease can be observed since the logarithmic plot of the stress response is linear as seen in Figure 5-3. The decrease in stress continues until the stress converges to zero. The slope of the stress can be written in terms of time constant as $-1/\tau$, where the time constant is $\tau = c/E$ as mentioned in Chapter 4. The stress response can be written as:

$$\sigma(t) = \sigma_0 e^{-t/\tau} \quad \textbf{(5.15)}$$

It should be noted that τ shown in Figure 5-3 is normalized since the stress value is normalized.

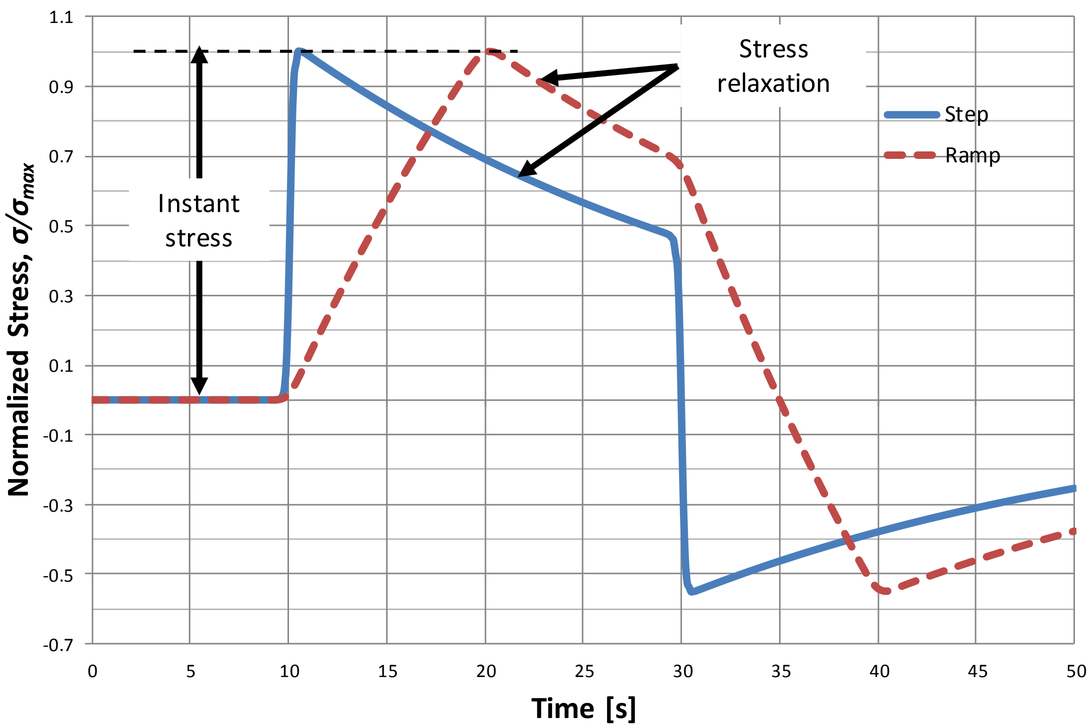

Figure 5-2. The stress response of the Maxwell model.

5.1.2 Kelvin-Voigt

The response of a Kelvin-Voigt model is shown in Figure 5-4. As mentioned in previous chapter, this model cannot model stress relaxation. There is only one floating node. When a strain is applied, the node is constrained (i.e. this floating node is fixed over time). Thus, the response of the system becomes independent of time. By investigating Figure 5-4, it can be seen that stress value is constant (i.e. not varying with time) when the strain is constant since the relationship is given as $\sigma = E\varepsilon^m$. In the step response, peaks occur at the instant the strain is applied and removed. In the ramp response, the constant rate strain deformation adds a constant stress value ($c\dot{\varepsilon}$) to the elastic response of $\sigma = E\varepsilon^m$. These relations can be seen in Equation **(5.8)**.

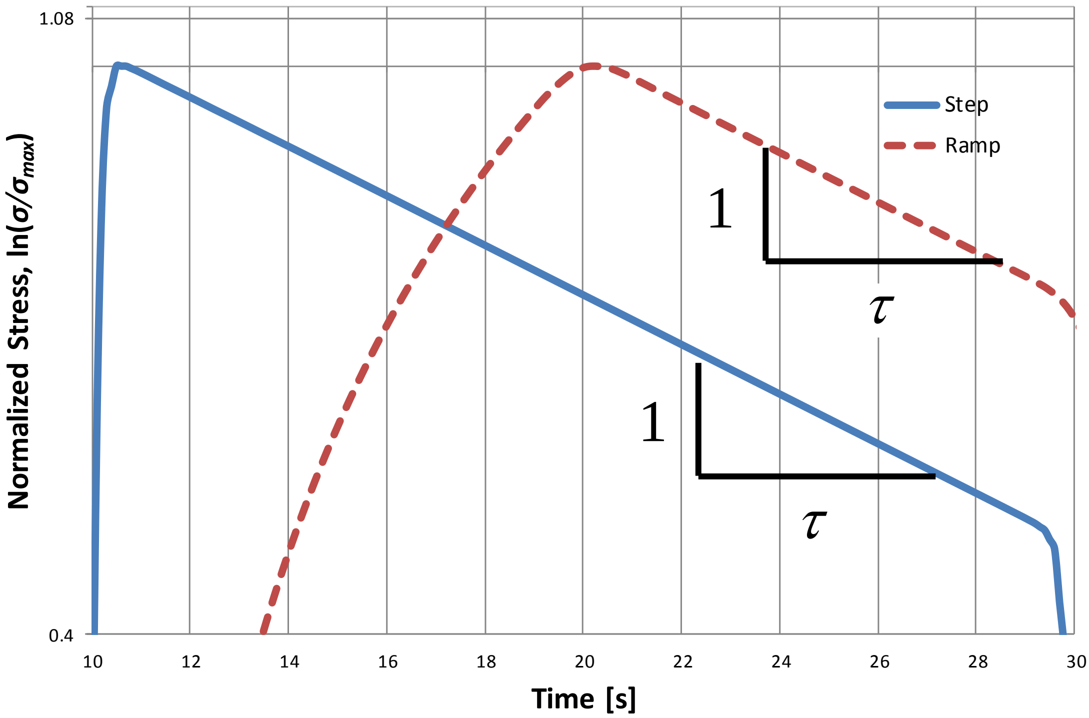

Figure 5-3. Logarithmic plot of Figure 5-2.

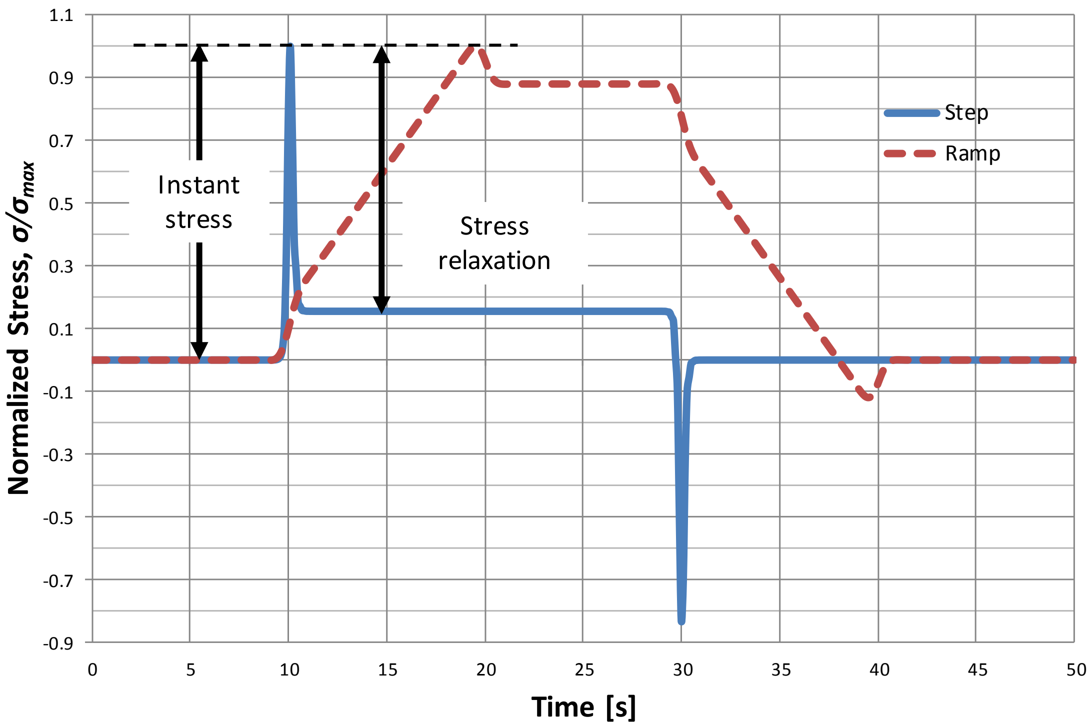

Figure 5-4. The stress response of the Kelvin-Voigt model.

5.1.3 Zener

Recall that a Zener model consists of a Maxwell model and a spring connected in parallel. Moreover, when the elements are connected in parallel between two fixed nodes (ground node is always fixed and in strain-controlled case the last node is also fixed), the total stress at that node can be calculated by adding the stresses on the two parallel braches. In other words, the stress response of a Zener model can be obtained by adding the stress response of the Maxwell model and the stress response of the parallel spring. As seen in Figure 5-5, the overall response consists of a constant value caused by the spring ($E_0\varepsilon^m$) and a decreasing value as a result of the Maxwell element ($E_o\varepsilon e^{tE_1/c_1}$). Notice that Zener's time constant is significantly lower than Maxwell element's time constant (due to typically lower damping coefficient, c in Zener than Maxwell). As a result, stress converges to a steady value in a shorter time in Zener than in Maxwell. There is a single time constant, which can be seen as the slope in Figure 5.6 similar to the Maxwell model.

5.1.4 Generalized Maxwell

Compared to Zener, Generalized Maxwell model has additional Maxwell elements connected in parallel. As a result, all the discussion in previous section applies to this model. The only exception is that, the Generalized Maxwell has multiple time constants, resulting in multiple exponential decays stacked on top of each other in the stress response. A sample response graph with two Maxwell elements ($n = 2$) is given in Figure 5-6.

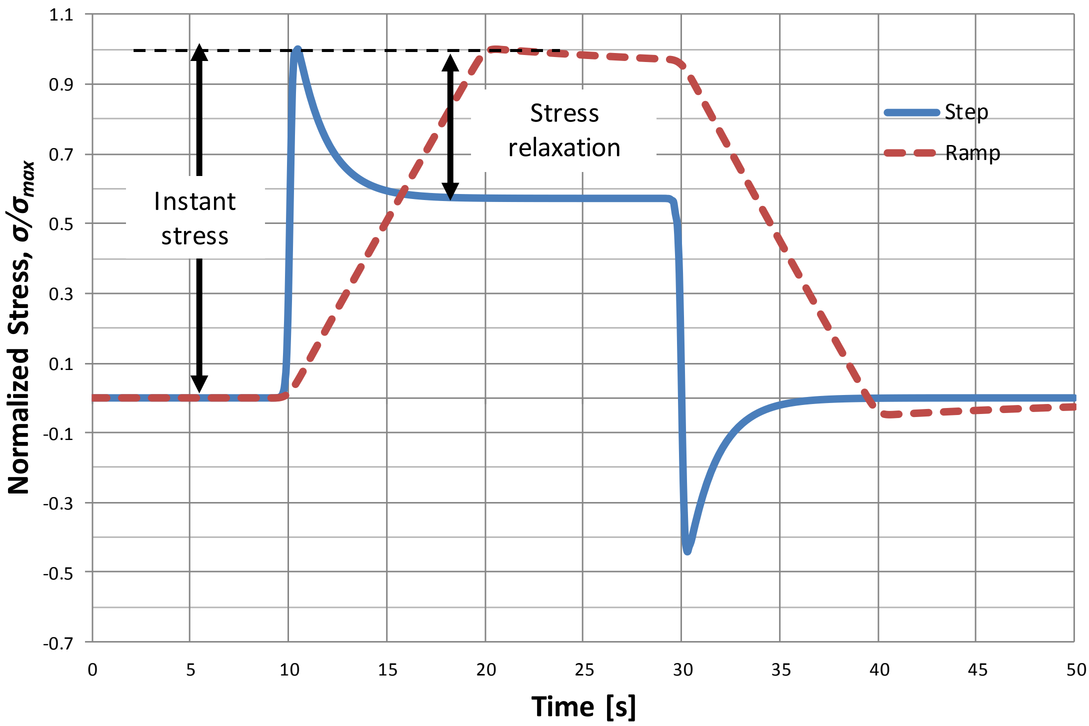

Figure 5-5. The stress response of the Zener model.

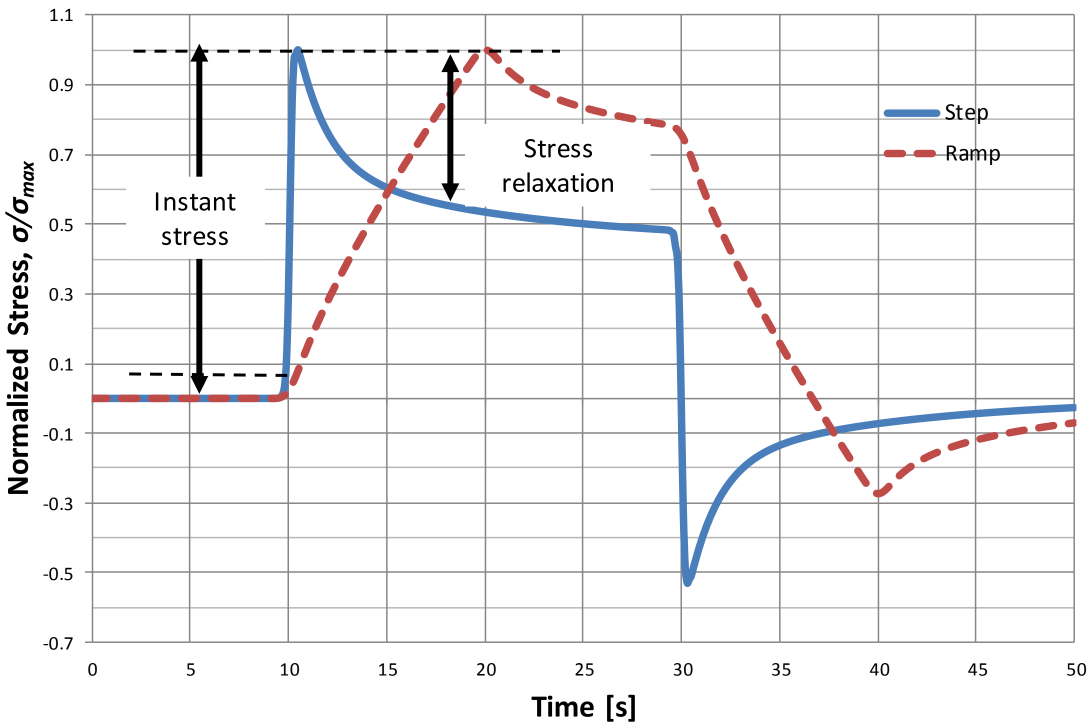

Figure 5-6. The stress response of the Generalized Maxwell model.

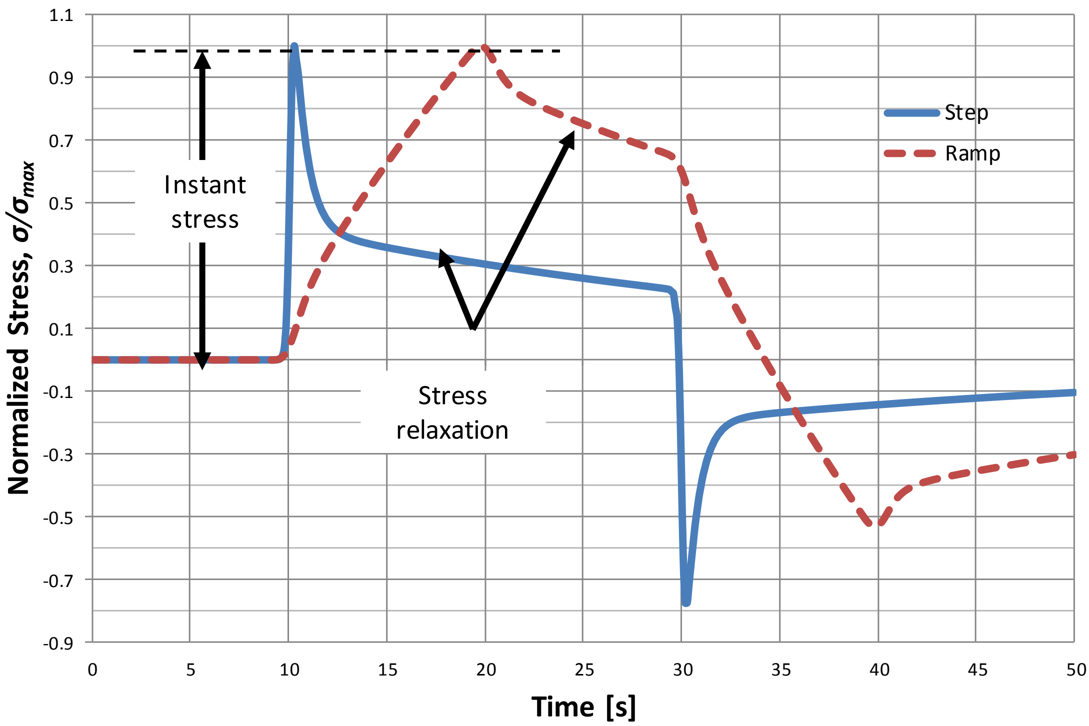

Figure 5-7. The stress response of the Burgers model.

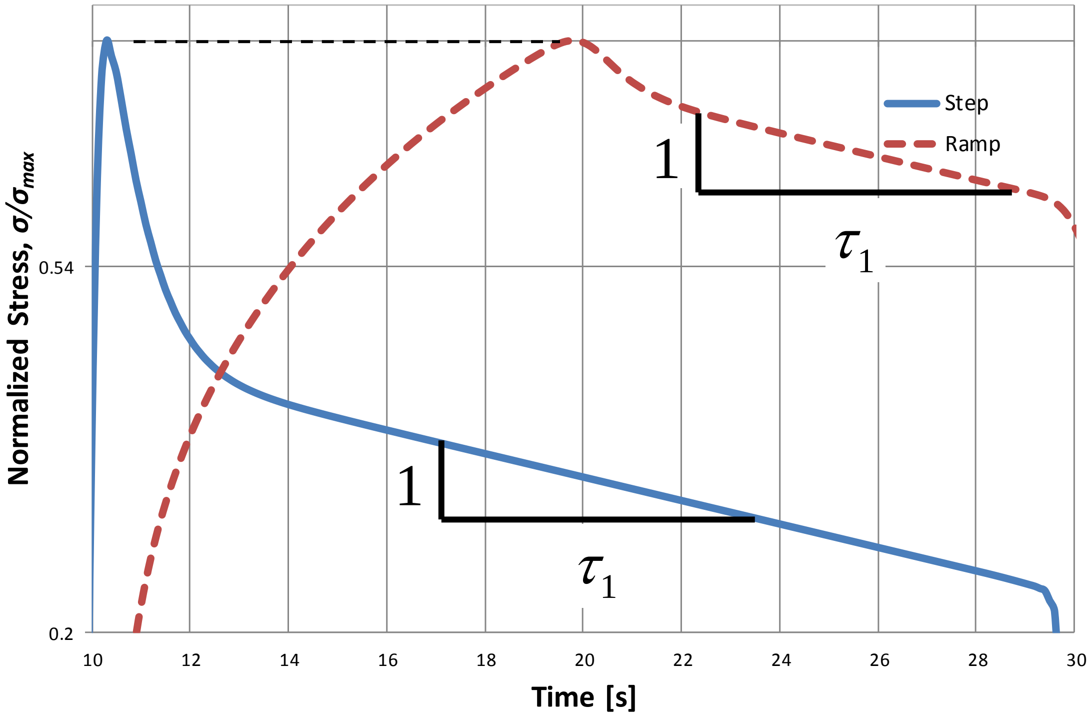

Figure 5-8. Logarithmic plot of Figure 5-7.

5.1.5 Burgers

Burgers model is the combination of a Kelvin-Voigt model and a Maxwell model in series connection. Spring 1 (E_1) and Damper 1 (c_1) correspond to Maxwell; Spring 2 (E_2) and Damper 2 (c_2) correspond to Kelvin-Voigt model. When a deformation is applied on a Burgers model, all the elements contribute to the stress response whereas some elements of Kelvin-Voigt model may not contribute when a constant strain is applied. An initial jump occurs which is followed by stress relaxation as shown in Figure 5-7. The decay rate of the stress is not constant initially, but it decays at a constant rate at late times. Notice the linear response in the logarithmic plot in Figure 5-8 which proves that the tress relaxation response is exponential. These two regions with different decay rates are caused by two time constants mentioned in the previous chapter.

6 Parameter Estimation

6.1 Curve Fitting Method

Curve fitting is an optimization problem where a mathematical function is fitted to an experimental data. Function is fitted by iterating the parameters (constants), in the function. The error is defined as a measure of how close the function is to a given data (related with the difference between the model function and the experimental data), which is also called residual error. The "best" curve fit is obtained by minimizing the error, hence obtaining the function parameters that result in the function as close to the experimental data as possible. Curve fitting can be done either analytically or numerically.

The unknown constants appearing in the system equations of this study are determined by using numerical curve fitting methods. An iterative solution is used, in which the error is minimized by modifying the parameters iteratively. The overview of this procedure is illustrated in Figure 6-1. The steps of curve fitting are summarized below:

- Initial estimates of the parameters are substituted into the differential system equation, and the response of the dependent variable is calculated by numerical integration (i.e. $\sigma(t)$ is calculated if $\varepsilon(t)$ is defined; or vice versa).
- The error, which is a measure of the difference between experimental and fitted data, is calculated.
- The parameters are modified iteratively to decrease the error, and these steps are repeated until a stop condition is satisfied (i.e. specific number of iterations, or a threshold error value).

The details of optimization, including error definition and algorithms, are given in the proceeding sections.

6.1.1 Error definition

As discussed, the numerical optimization requires an error to be defined. In the simplest case the error can be defined at a data-point $x = x_i$ as the difference between the fitted data, $f(x_i)$ and the experimental data, $y = y_i$ as below:

$$r(x_i, P) = y_i - f(x_i, P) \qquad \textbf{(6.1)}$$

where x is the independent variable, y is the dependent variable (experimental data), f is the function (i.e. mathematical model) to be fitted, P is a vector containing the parameters to be fitted, and subscript i denotes i^{th} data point. $r(x_i, P)$ is called the residual.

For the curve fitting problem, an error must be defined, which accounts for all the data points in the experimental data. Basically, the error at data-points can be summed to have an overall error for a function. To avoid negative errors canceling the positive errors, the absolute value of the residual may be used.

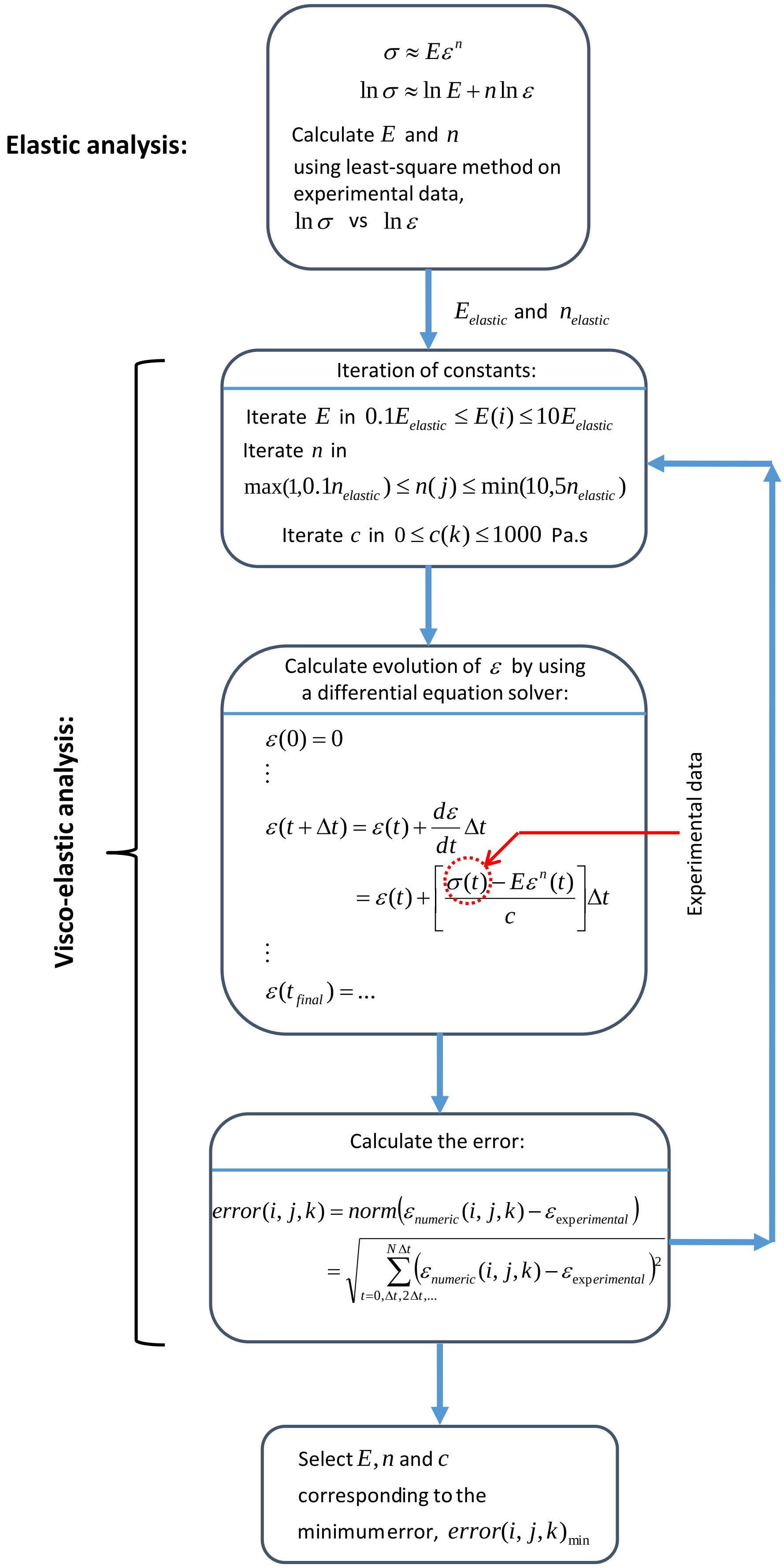

Figure 6-1. Flow chart for the parameter estimation.

$$e_{linear}(P) = \sum_i |r(x_i, P)| = \sum_i |y_i - f(x_i, P)| \qquad \textbf{(6.2)}$$

This linear error definition can be used for a curve fit; but commonly, the squares of the error are used so that large differences have more effect on the error than the small differences. Squared error definition can be written as:

$$e(P) = \sum_i r^2(x_i, P) = \sum_i \left(y_i - f(x_i, P)\right)^2 \qquad \textbf{(6.3)}$$

The curve fit obtained by searching P that minimizes the error $e(P)$, is called the least squares fit. It is the most commonly used curve fitting method. One should be careful that error, $e(P)$ increases with the number of data points. The error for different data sets should not be compared (as a performance of curve fit) unless they have the same number of data points. Otherwise, a bad curve fit evaluated at small number of data points, may result in smaller $e(P)$ than an almost perfect curve fit evaluated at many points. To avoid this, a conventional approach will be used to compare curve fits as explained in the next section.

6.1.2 R-squared (Coefficient of determination, R^2)

To obtain a scalar value representing the quality of fit, the R-squared (a.k.a. R^2 or coefficient of determination) is commonly used in statistics. It is defined as the proportion of variability within a dataset [83]. For curve fitting, it can be defined as one minus the ratio of the summed square errors to a reference fit, e_r:

$$R^2 = 1 - \frac{e(P)}{e_r} = 1 - \frac{\sum_i (f(x_i) - y_i)^2}{\sum_i (g(x_i) - y_i)^2} \qquad \textbf{(6.4)}$$

where g is a particular curve fit function used as a reference. A common approach is to use $g(x) = \bar{y}$ where $\bar{y}$ is the mean value of the data-points and can be calculated as $\bar{y} = \frac{1}{n}\sum_{i=1}^{n} y_i$. Substituting this particular $g(x)$ into Equation **(6.4)**, R^2 can be formulized as given below:

$$R^2 = 1 - \frac{\sum_i (f(x_i, P) - y_i)^2}{\sum_i (\bar{y} - y_i)^2} \tag{6.5}$$

$R^2 = 1$ means there is a direct correlation between fit and data points, and thus, a perfect fit. Whereas $R^2 = 0$ means that, there is no correlation between x and y using the function f. Mathematically, it means current fit is numerically equal to the mean value of the dataset. The fits with $R^2 < 0$ should not be considered because they are worse than using the mean value for the entire domain. An acceptable R^2 value is dependent on the application. For this study, R^2 values higher than 0.7 are considered acceptable.

In this study, R^2 is modified such that it compares current fit with the (a) mean value of each stage and (b) the best elastic fit (i.e. model without viscous elements). This modification is done by adjusting the reference function $g(x)$ in the Equation **(6.4)** and modified variables are named as R_a^2 and R_e^2 respectively.

a. Calculating R_a^2

Traditionally, the reference fit, g, in Equation **(6.4)** is set equal to the average of the entire dataset, $\bar{y}$. However, this approach is not very suitable for discontinuous (piece-wise) curve fit problems. In our case, while the system equations (differential equation set) are continuous, the input (compaction pressure) becomes discontinuous during stage transitions. Besides, this approach is not fair since the compaction trends are very different in different stages. These will be explained below.

For example, consider the contribution of the sample experimental data point given in Figure 6-2a to the error, e. Two different error analysis approaches are illustrated in that figure: (1) $g = \bar{y}$, i.e. the reference fit is set to the average of the entire ε dataset (from t = 0 till the end of the entire characterization including the base and debulking cycles), and (2) the reference fit is a piecewise function set to the average of each stage separately as $g_1 = \bar{y}_{@P_{minor}}$, $g_2 = \bar{y}_{compaction}$, … in the related time intervals. Figure 6-2b illustrates the two sample curve fits corresponding to the two approaches, (1) and (2) explained above. In this study, the latter approach is used, i.e. a reference fit is used by setting it to the average of each stage separately in a piecewise manner.

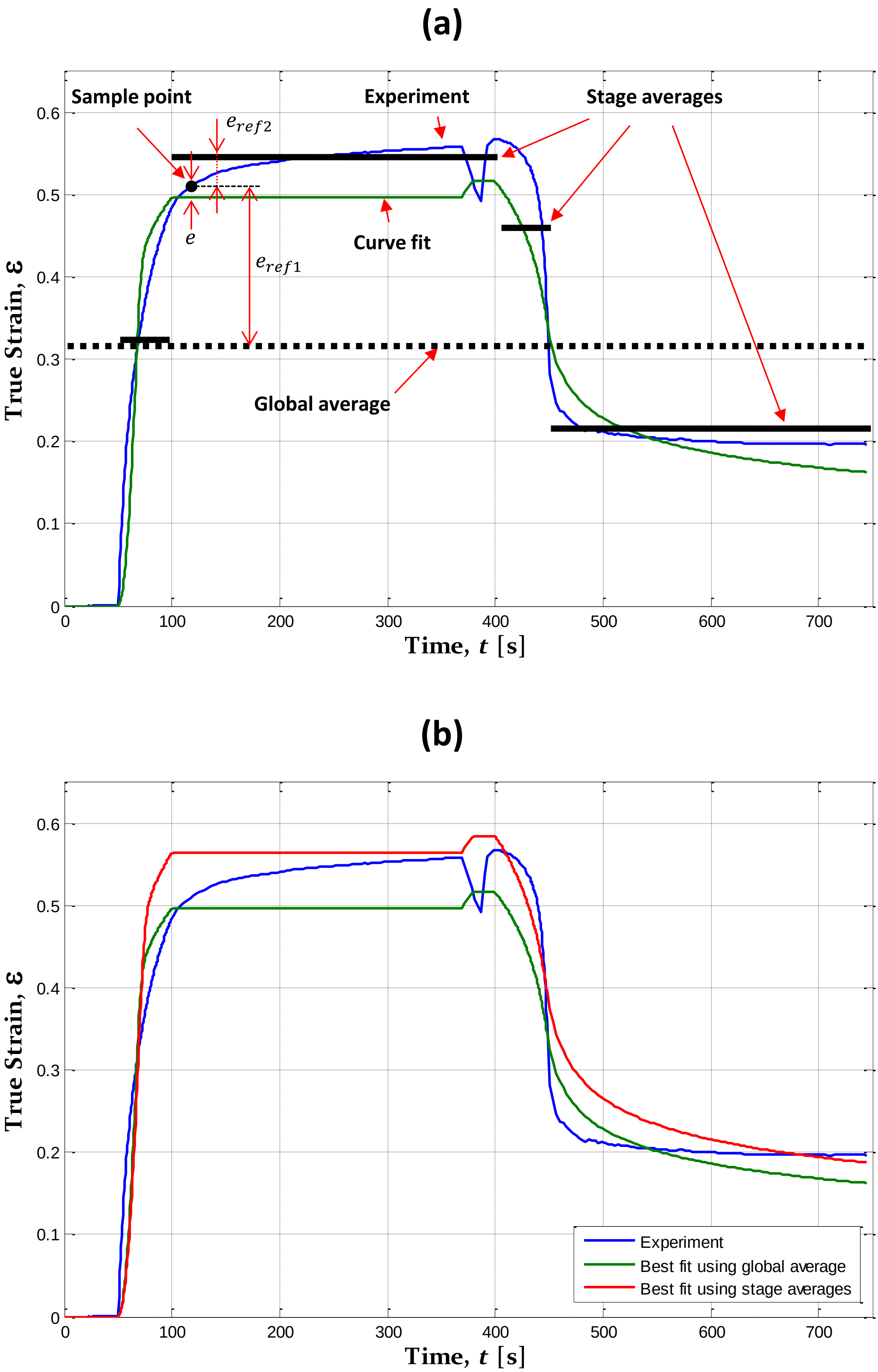

Figure 6-2. Comparison of calculating error with reference to (1) global and (2) stage average.

Thus Equation **(6.4)** is replaced with

$$R_a^2 = 1 - \sum_k \frac{\sum_i \left(f\left(x_{k,i}, P\right) - y_{k,i}\right)^2}{\sum_i \left(\overline{y_k} - y_{k,i}\right)^2} \quad \textbf{(6.6)}$$

where ***k*** represents stages of the characterization experiment.

b. Calculating R_e^2

By considering a nonlinear spring the reference elastic fit is assumed to be in the following form:

$$g(x) = \varepsilon_{elastic}(x) = \left(\frac{\sigma(x)}{A}\right)^{1/B} \quad \textbf{(6.7)}$$

The values of A and B are obtained using least squares fit to the experimental data. Notice that this equation is equivalent to the constitutive equation of the springs used in the viscoelastic models. By substituting Equation **(6.7)** into Equation **(6.4)**, the following is obtained:

$$R_e^2 = 1 - \frac{\sum_i (f(x_i) - y_i)^2}{\sum_i (AP_c(x)^B - y_i)^2} \quad \textbf{(6.8)}$$

The R_e^2 term indicates the performance of a viscoelastic model compared to an elastic model. R_e^2 varies between 0 and 1. $R_e^2 = 0$ means the viscoelastic model has no advantage over elastic model, and the performance of the viscoelastic model gets better over the elastic model as it approaches to 1.

R_a^2 or R_e^2 can be used as a measure of error in curve fitting as follows:

$$err(P) = 1 - R_a^2 \quad \textbf{(6.9)}$$

or

$$err(P) = 1 - R_e^2 \quad \textbf{(6.10)}$$

In the following parts of this study, Equation **(6.9)** will be used for the error analysis.

6.1.3 Weighted errors

Compaction modeling can be done for various stages of an LCM process either separately or for the complete cycle. The compaction characteristics of a fabric preform in RTM and VI differ very significantly. To mimic these two different types of compaction in corresponding characterization experiments, strain-rate controlled experiments should be preferred for RTM mold closing simulations to calculate compaction stress required to achieve a part thickness desired; and stress-rate controlled experiments should be preferred for VI simulations to calculate the resulting thickness distribution at a calculated/measured resin pressure distribution (and thus compaction pressure distribution).

One could be interested in modeling a particular stage or stages of the compaction cycle instead of the complete cycle. For example, if one is interested in calculating mold closing/holding pressure in RTM, the model is desired to fit the initial compaction stage more closely than fitting the rest of the cycle. Similarly, if the model will be used to simulate the mold filling in VI, the model is desired to fit the unloading stage more closely than fitting the rest of the cycle. Recall that wet unloading stage of the characterization experiment mimics the fabric behavior during the mold filling stage of VI. If compaction simulation during post filling is desired, the model is expected to fit the relaxation stage more closely than the rest of the stages. Thus, one should select the curve fitting error such that the model fits more closely the desired stage of the compaction cycle than the others.

In this study, a weighting function, w is introduced into the error function as follows:

$$e_w(P) = \frac{\sum_i w_i (f(x_i) - y_i)^2}{\sum_i w_i (g(x_i) - y_i)^2} \tag{6.11}$$

where w_i is defined as follows:

$$w_i = \begin{cases} w_{loading} & \text{during loading stage} \\ w_{settling} & \text{during settling stage} \\ w_{unloading} & \text{during unloading stage} \\ w_{relaxation} & \text{during relaxation stage} \end{cases} \tag{6.12}$$

If no specific weight is defined, then $w_i = 1$. When the model is desired to fit a particular stage more dominantly than other stages, either the weight corresponding to that region is increased, or the rest of the weights are decreased.

Even if one wants to solve the model for any intermediate stage (e.g. relaxation) or final stage, the system of differential equations must be solved by starting from the initial condition at $t = 0$. One should set the weights of the other stages to zero and set the weight of that particular stage to 1. This approach will minimize the error of the curve fit in that stage only and will not seek any minimization in the others. However, the differential equation is solved for the whole time domain.

6.1.4 Curve fitting function

Three Matlab optimization functions (*fminsearch*, *fmincon* and *patternsearch*) will be used to optimize the parameters used in a curve fitting model by minimizing an error function. One of the error functions, Equation **(6.9)** or **(6.10)** will be used for this purpose. The mentioned optimization functions are selected because they allow user to input a user-defined nonlinear and multivariable error function. One could attempt using Matlab's curve fitting functions such as *lsqcurvefit* for this purpose; however it calculates the error using its own error definition and thus it does not allow the user to input Equation **(6.9)** or **(6.10)**. Because of the non-flexibility of *lsqcurvefit*, it is not used here. Details of each function is given below.

Fminsearch is an unconstrained nonlinear optimization function. It performs search in an open domain, which means that no boundary is defined for the optimized parameters. Moreover, *fminsearch* is a direct search method, where a given error function is used directly to find the optimum point instead of requiring derivative of the function. In other word, in contrast to indirect search methods, it does not require analytical or numerical gradient to converge to a solution. Note that the error functions

(Equations **(6.9)** and **(6.10)**) are nonlinear relations between the experimental data and the solution of a DAE which is also nonlinear. Recall that the input (the applied pressure or strain) to the DAE function is discontinuous and not necessarily linear, also the solution of the function could not be obtained analytically but numerically. Considering all of these, obtaining an analytical solution for the gradient of this error function is not possible. By trying alternative methods, it is also seen that numerical gradient estimates do not always perform well for the mentioned error functions. Thus, *fminsearch* is preferred to confirm the solution of any other function is used initially. If *fminsearch* solution differs from other minimization function's solution, the additional inputs (such as convergence criteria or numerical calculation tolerances) supplied to other minimization functions are checked.

Fminsearch finds the optimum parameters by using Lagarias et al.'s [84] simplex search method. As the name implies, *fminsearch* searches a solution in a simplex, which is a triangle for 2 parameters, pyramid (tetrahedron) for 3 parameters, and so on. A new point near the current simplex is selected. If the error at this new point is smaller than the error at any of the existing simplex corners, it replaces that corner of the simplex. The diameter of simplex decreases if a smaller error values are found inside the simplex, and increases if they are outside of the simplex. This procedure continues until the diameter of the simplex is smaller than the defined tolerance (if the tolerance is not defined by a user, a default value of 0.001 is used). The advantage of *fminsearch* is that it can handle discontinuity of the error function unless it occurs near the solution.

Fmincon is a constrained nonlinear optimization function. The search domain can be open (unbounded) or closed (bounded). The user can supply linear inequalities for search parameters, if available, to speed up the search. *Fmincon* uses either numerically estimated, or user-supplied analytical derivative function to find the new iteration point, rather than randomly selecting points near the iteration point. *Fmincon* can use one of the four different solution algorithms available. In this study, the most suitable algorithm is selected by comparing their performances (their convergence speed). The default algorithm "trust-region-reflective" performs well in the error functions used in this study.

Patternsearch is another direct search method similar to *fminsearch*, but it also accepts closed (bounded) domains. This method creates a mesh around the initial estimate, and calculates the error at neighbor nodes. If a neighbor node has a smaller error than the current point, this iteration is called “successful”. The point with smallest error is selected as the new iteration point and also the mesh size is increased (doubled by default). If none of the neighbor node has smaller error, then this iteration is “unsuccessful”; and the same node is used for the next iteration but this time the mesh size is decreased (halved by default). Iteration continues until the element size of the mesh is below the convergence tolerance.

The optimal parameter is searched by using a “coarse search” in *fmincon*; and then a “fine search” in *fminsearch* or *patternsearch*. Inputting an initial estimate of parameter set, *fmincon* function is used with large tolerances to find an optimum parameter set. This search is repeated for multiple initial estimates. The parameter set which gives the minimum error is then used in *fminsearch*. *Fminsearch* is used with a smaller tolerance than the one used in *fmincon* to obtain a more accurate result. If *fminsearch* results in a nonphysical solution (negative spring or damping constants), the solution is discarded and the fine search is repeated using a different Matlab function, *patternsearch*. These three minimization functions (*fminsearch*, *fmincon* and *patternsearch*) are used for different purposes or solution stages. *Fmincon* performs well with large tolerances. *Fminsearch* and *patternsearch* give the accuracy needed, and they converge quickly when the solution is near initial estimate.

All three minimization functions (*fmincon*, *fminsearch* and *patternsearch*) will converge to an optimal parameter set with the minimum error close to the initial estimate. It does not necessarily mean that all three functions will converge to the same result even if the same initial estimate is used. A function may converge to the closest local minimum or pass over it and converge to another parameter set. This is dependent not only the function used but also the minimization parameter such as convergence criteria and step size.

To confirm that the computed set is the globally optimum solution (has the minimum error), these optimization functions must be executed multiple times starting with different initial estimates. After these multiple searches, the set giving the minimum error is selected as the optimum solution. In this study, two Matlab solver functions, *MultiStart* and *GlobalSearch* are used. *Multistart* calls the optimization (minimization) function for either user supplied or randomly generated initial estimate sets. Once the optimization is done for all initial estimates, best n-number of parameter sets are listed.

The initial estimates of the parameter set can be selected at the nodes of a coarse search mesh. However, here in this study, the following method is used to converge quickly.

A set of randomly generated parameter sets are used for the initial estimates such that only the sets with an error smaller than a tolerance are kept. In other words, the following steps are repeated: (1) randomly generate a set in the search domain, (2) evaluate the error function, and (3) include that estimate in the set if the error is smaller than the tolerance. This procedure continues until a desired number of sets are found. Once the set is completed, *MultiStart* is used.

GlobalSearch is a more efficient solver than *MultiStart*, in terms of CPU time. It uses a similar approach mentioned above in three steps, except that the solver selects the initial sets (i.e. cannot be set by the user). The initial estimates set is created by the solver function, and they could be updated during the optimization. The advantage of using *GlobalSearch* is that it works faster than *MultiStart* since it does not run minimization function for all sets and it requires less user input and coding. The downside is no initial estimate set can be input to the *GlobalSearch*. The parameter set for a specific model and fabric is expected to change between different characterization experiments' schedules (variations in the parameters) are considered. However, this change is expected to be slight; and thus a unique set of parameters will be searched to model all these schedules.

Once the initial estimates of the parameter set for a base characterization experiment is selected according to the criteria explained above, the same set is used for the proceeding experiments (Experiment Sets) instead of randomly generating different sets. This will decrease the CPU time considerably. In this study, 7 different experiment sets are performed; and the same parameter set can be used for all 7 experiment sets to decrease the optimization time.

6.2 Parameter Search Domain

Optimization algorithms mentioned in Section 6.1 need a search domain for parameters. The domain could be open (unbounded) between plus/minus infinity, or closed (bounded) if the user estimates the order of magnitude of the parameters. When a search domain is closed, it is called constrained optimization. If there is no search domain specified (i.e. the domain is open), it is called unconstrained optimization.

Non-physical results (negative spring or damper constants) are avoided by selecting non-negative search domain such as $0 < E_i < E_{upper}$, $0 < c_i < c_{upper}$, $1 < m_i < m_{upper}$ where the subscript "*upper*" denotes the maximum value expected (upper limit) for parameters. Moreover, the user can narrow down the search domain if the parameters were already determined for a different type of fabric. The upper value of the new search domain is set to a value which is in the same order of magnitude of the previous fabric type.

The user must be cautious if the constrained search is applied, and if the solution is found near or at the domain boundaries. In that case, the domain must be widened.

In this study, unconstrained algorithms are also used, either for comparison or for verification purpose. An example for open domain (unconstrained) search algorithm is Matlab's built-in function "*fminsearch*", in which only an initial estimate is given. To avoid unrealistic results, in other words negative spring or damper constants, a pseudo domain is defined. A pseudo domain is set by assigning the error as infinity (or a very high value) if any parameter is outside the desired bounds. Usually this approach is used successfully and a converged result is found; however no converged result is found if the solution is near one of the boundaries caused by the discontinuity at that boundary. A wider search domain should be selected, similar to the constrained search algorithm.

6.3 Weights of Stages in Curve Fitting

In this section, different approaches are described such that model fits either (1) a particular stage dominantly, or (2) to some or all stages by deciding on the number of data points to be used in the curve fitting and/or using stage weights in the optimization procedure.

6.3.1 Number of Data Points in Curve-Fitting

The thickness versus time data in an experiment is acquired at a constant frequency of 10 Hz. By using a conventional approach, the error of a curve fit can be computed using all the experimental data points available. But, it should be noted that, different stages have different durations. As a result, when all the data points are taken into account, the lengthier stages like settling and relaxation have more dominant effect over the shorter stages like compaction and decompaction. This can be avoided by skipping some data in the lengthy stages and/or using equal number of data in each stage. Thus the model can be fairly representing all stages of the characterization experiment instead of representing the lengthy stages dominantly. As another extreme case, a modeler can prefer the opposite of this approach, i.e. represent a particular stage more dominantly than the others simply by intentionally extending the duration of that stage and/or taking more data in that stage than the others. For example, much more data points in the relaxation stage than the others can be used in the curve-fitting procedure if one is interested in modeling the relaxation behavior better.

6.3.2 Fixed Number of Data at Each Stage

To overcome the dominance of some stages over the others caused by fixed time-step approach in curve fitting, data points are resampled so that each stage has the same number of data points. Recall that a base (default) characterization experiment has the following stages and durations: compaction (49 s), settling (300 s), decompaction (49 s) and relaxation (300 s). If one uses all the data collected at a fixed frequency, then the number of data in settling and relaxation stages will be approximately 6 times of the compaction and decompaction stages. Is this desired? The answer is dependent on what the modeler is interested in. If one is interested in viscous behavior of the specimens, which requires to investigate material response during settling and relaxation stages, this approach should be accepted. However, if one is interested in elastic behavior, then the model is required to represent the loading and unloading stages better than the others. Thus, one needs to do resampling of the experimental data which can be achieved either by increasing the number of compaction/decompaction data by using interpolation of the actual data, and/or by decreasing the number of settling and relaxation data by skipping some data or using interpolation method. With this approach, experimenter do not have to reconsider the fitting performance when a change is made in time schedule of an experiment. It allows the use of different dP/dt and different relaxation pressures as done here; or longer/shorter settling and relaxation durations for different material characterization design can be investigated by keeping in mind that a particular stage is not dominant, and all stages influence the curve fitting equally.

6.3.3 Adding weight for specific stages

Another approach that can be used to avoid long stages to become dominant in the curve fitting is the use of weights. Instead of resampling, the weight of shorter stages such as loading and unloading can be increased in the error calculation. These weights can be selected intuitively or by calculating the ratio of the number of data points to a reference number of data points. For example, the settling stage, which usually has a constant duration, can be selected as a reference. The weight of this stage will be w. For example, if the number of data points in compaction and decompaction stages is 1/6 of the data points in settling stage, these two stages should have $6w$ as weights.

It should be noted that, while this approach uses all the data-points, the use of weights gives a similar result as resampling stages with a fixed number of data points. Another point to keep in mind that, the main motivation for this study is to have model parameters that mimic the complete VI process. As mentioned before, some stages may be preferred to have dominance during curve fit.

One can alternatively use either one of these two methods explained in Sections 6.3.2 and 6.3.3 to fairly and consistently analyze the error contribution of each stage. In this study, a combination of these two methods is used. First, the data points in each stage are resampled to a fixed value of 100. Then, a consistent user supplied weights are used for each stage (as detailed in Chapter 7) so that the model fits particular stages better than others to mimic more crucial stages of VI. This hybrid approach allows the user to have more control over the curve fit, since the weights can be adjusted and a consistent analysis is repeated between different experiments and different models.

6.4 Case Studies: Estimating Fabric Response for Various Parameters

The viscoelastic models have dampers and springs attached in different configurations (parallel or series). When multiples of these elements are used, it is not obvious how they contribute to the fabric's response. Since a mass-spring-damper system is very commonly studied in the literature, one can expect to see what happens when the damping coefficient increases or decreases while keeping the others fixed. However, when many dampers and springs are used, as done here in compaction models, one needs to find a way of determining how each component contributes to the overall response of the system.

The experimental procedure may affect the model parameters. The values of the model parameters (E's, c's and m's) calculated as a result of the curve fitting will be dependent on the chosen values of different experimental parameters (minor/major compaction pressures, compaction/ decompaction rates, relaxation pressure, duration of each stage). To have a clearer image of how experimental parameters affect the result, multiple experiments are conducted by varying those parameters and recording the results. Proceeding sections inspect each parameter separately.

6.4.1 Compaction Rate

As the compaction/decompaction rate, $|dP/dt|$ increases, viscous effect increases. $|dP/dt|$ was selected as one of the experimental parameter to investigate its effect on the compaction model. It was varied as 1, 2 (base) and 4 kPa/s in the ramp stress input function in experiment sets 3, 1 and 4, respectively.

The curve fitting is done, first to each experiment individually, and then to all seven experiments (sets 1-7) simultaneously. The comparison of individually fitted parameters sets show how different rates affect the result. The response to a step input (set 8) is also investigated. This experiment is expected to yield the most dominant viscous response of a viscoelastic model.

6.4.2 Relaxation Pressure

In the literature, it is known that the scatter in fabric thickness increases as the compaction pressure decreases to zero [18]. This behavior also results that, the thickness variation is maximum near a resin inlet, where the compaction pressure is at the lowest level. Near the resin exit ports (vents), the fabric is compacted at the highest level. Thus, an accurate process simulation requires that the compaction characterization should not be done at one fixed level, but at various levels.

Note that the low compaction and thus thickening stage corresponds to the late instants after the resin arrival to a particular point in the preform in VI (relaxation stage is after the wetting and unloading stages in a characterization experiment).

Besides the base experiment with a final relaxation at 2 kPa (set 1), additional relaxation experiments are conducted at 5 kPa, 10 kPa, and 40 kPa (sets 5, 6 and 7, respectively).

7 Results

This chapter is divided into two main sections. In Section 7.1, the results of the compaction experiments are given, and in Section 7.2, the results of the model fits are presented.

7.1 Compaction Experiment Results

Figure 7-1 to Figure 7-12 are the results of all experiments done by compacting the specimens according to the input stress (see Figure 3.9 and Figure 3.13). In Figure 7-1 and Figure 7-2, the evolution of thickness $h(t)$ as a result of the input compaction pressure (Figure 3-9) is shown for random specimens.

Figure 7-3 and Figure 7-4 show the thickness graphs for the woven specimens. The general trend is similar to the random specimens, however the thickness values are lower (e.g. the average initial thickness is 6.02 mm for the random and 3.95 mm for the woven fabric specimens). During the compaction stage, the random fabric compacts from 6.02 to 3.74 mm which corresponds to $\Delta h = 2.28$ mm and $\Delta V_f = 14.7$ %, whereas the random fabric compacts from 3.95 to 2.67 mm which corresponds to $\Delta h = 1.28$ mm and $\Delta V_f = 16.9$ %.

In Figure 7-1 to Figure 7-4, the grey circles indicate the average data, and the vertical bars attached show plus/minus the standard deviation of the data. Figure 7-5 to Figure 7-12, which will be introduced in proceeding paragraphs, show the average of all sets with the blue line and standard deviation bound of all sets with the dashed red lines. Similarly in Figure 7-1 to Figure 7-4, the graphs use blue and red dashed lines to plot the average data and standard deviation limits, respectively.

The variation in physical properties (h, V_f and ρ_{sup}) and relative changes (such as Δh and ΔV_f) of fabric are given in Figure 7-5 to Figure 7-12 and in Table 7-1 to Table 7-4. Discussion of each figure and table will be given in the proceeding paragraphs.

Considering more definite nature of the woven fabric structure compared to the random fabric, it is expected to have a smaller scatter in the results of woven compared to random fabric specimens. It is also expected that different levels of nesting may occur in each experiment while stacking fabric layers during the preform preparation which results in a significant thickness variation.

The spacing between the strands is not uniform by observation. It is also very difficult to manufacture two identical preforms due to the inherent variations in labor and non-uniform fabric roll.

Before the compaction stage starts, the initial thickness values, $h_{@P_{minor}}$ are recorded after the specimens are kept under the minor load for 5 minutes. The recorded values are shown in Figure 7-5a and Table 7-1 for random fabric, and in Figure 7-6a and Table 7-2 for woven fabric. The standard deviation of the thickness (σ_h) for all specimens (7 x 12 = 84 specimens) is calculated as 0.34 mm and 0.18 mm for random and woven fabrics, respectively. The average thickness values ($\bar{h}$) are 6.02 mm and 3.95 mm, for random and woven fabrics, respectively. The corresponding initial fiber volume fractions are 23.99% and 35.05%, respectively. The woven fabric has a lower σ_h, but also has a lower $\bar{h}$ than random fabric. The variation in thickness (σ_h) itself may be misleading, thus the relative standard deviation can be used, which is defined as:

$$RSD = |\sigma/\bar{x}|$$

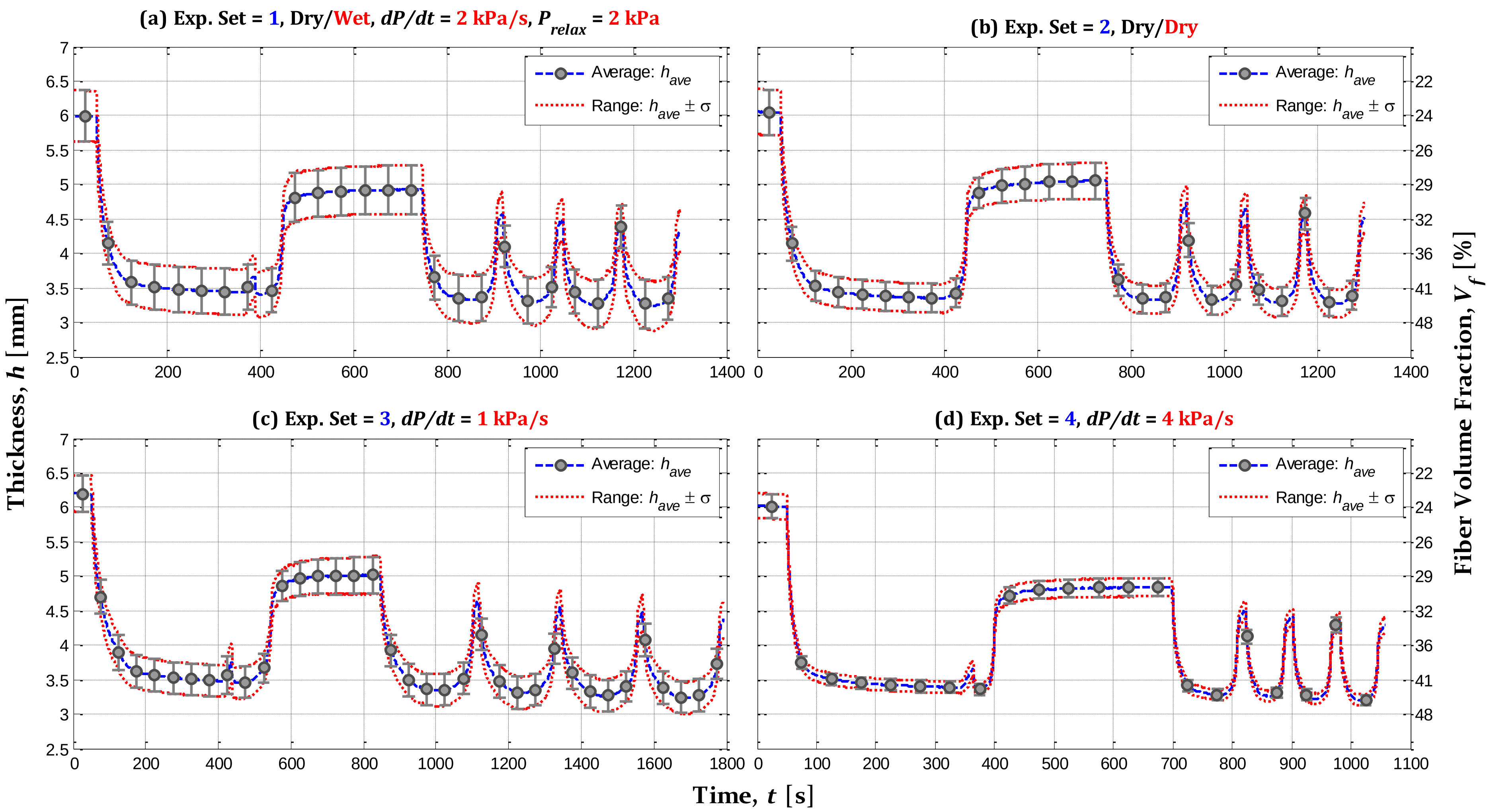

Figure 7-1. Experiment Sets 1-4 for **Random** fabric. In each set, 12 specimens were characterized separately.

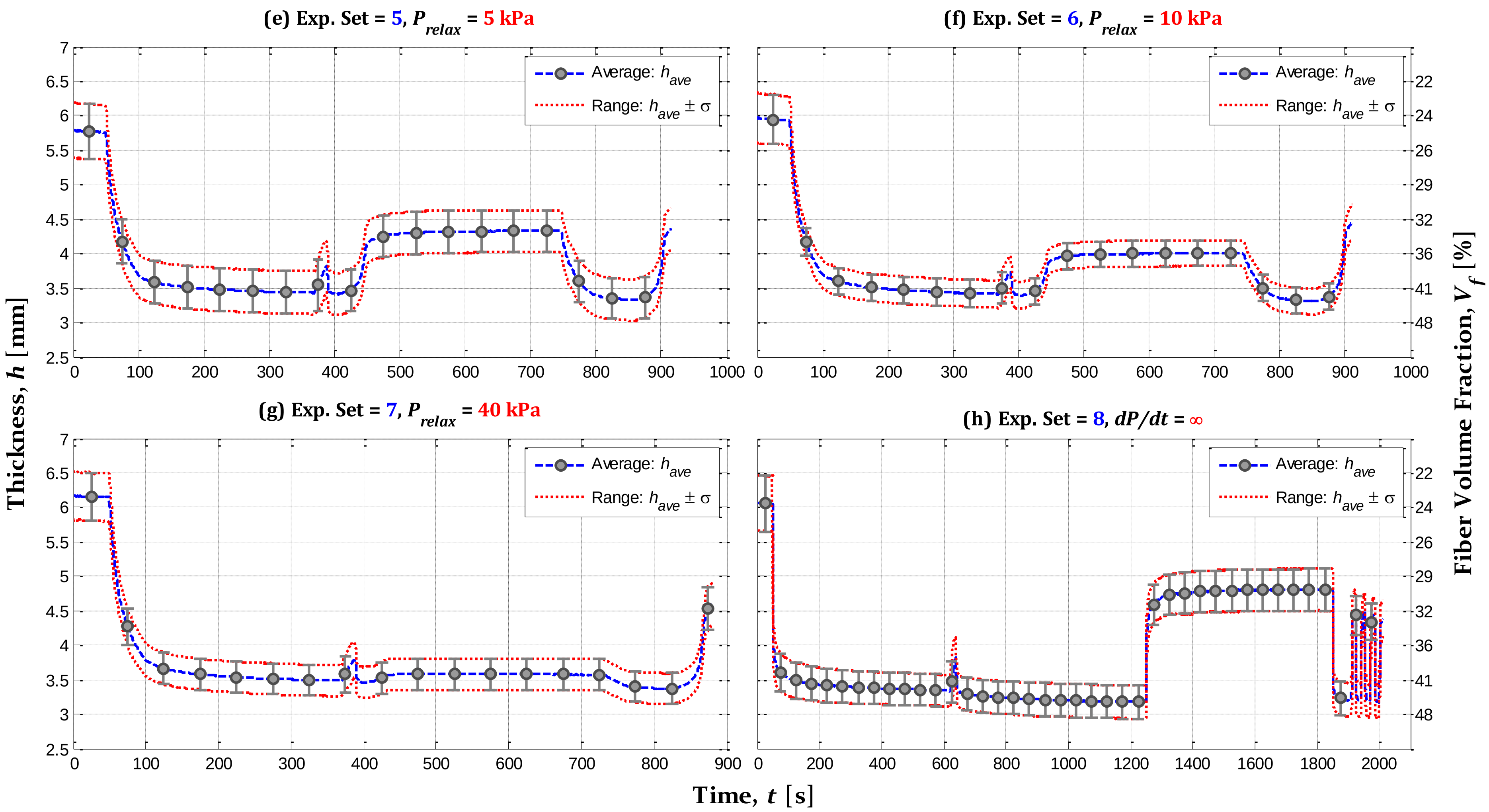

Figure 7-2. Experiment Sets 5-8 for **Random** fabric. In each set, 12 specimens were characterized separately.

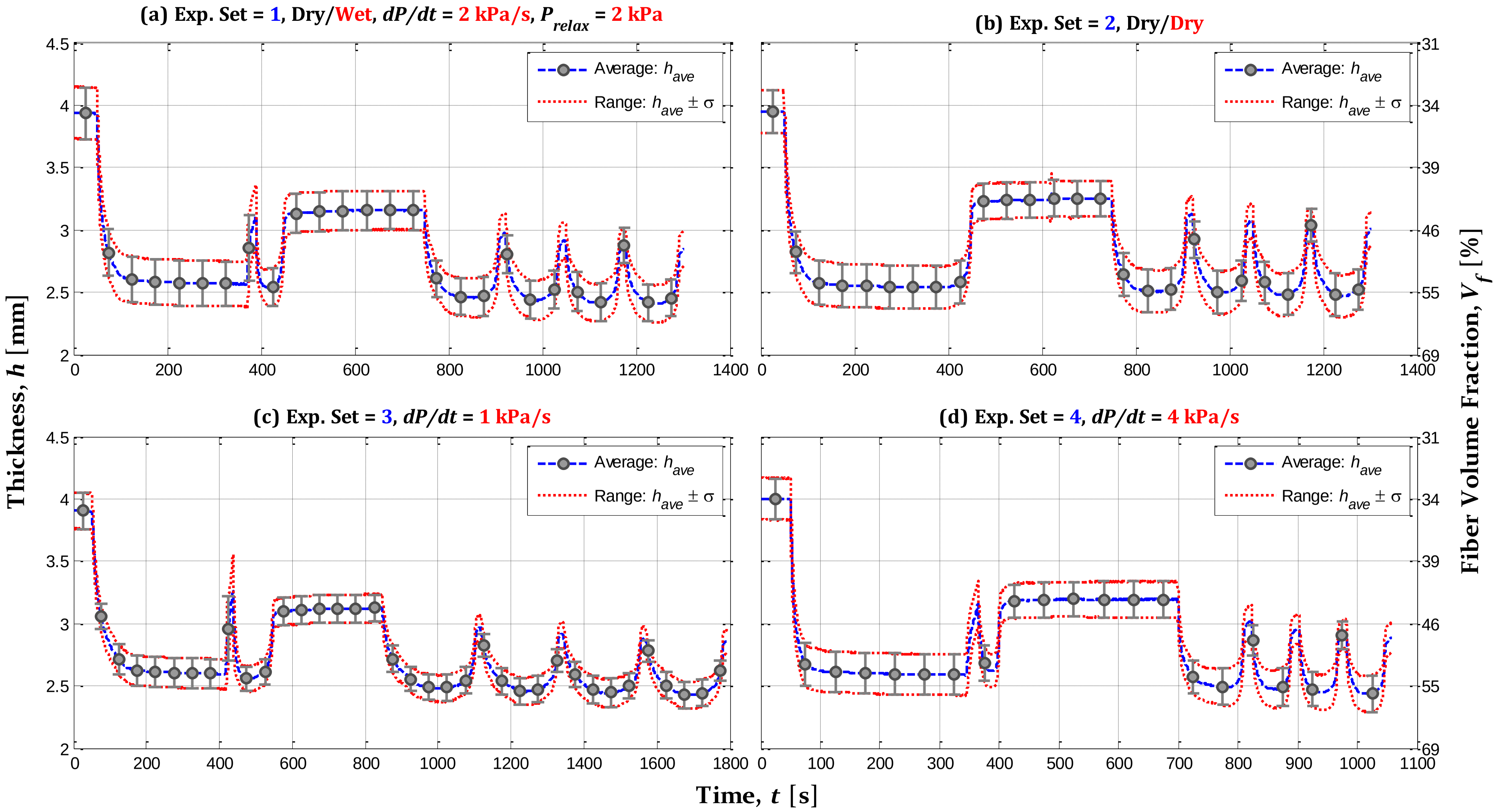

Figure 7-3. Experiment Sets 1-4 for **Woven** fabric. In each set, 12 specimens were characterized separately.

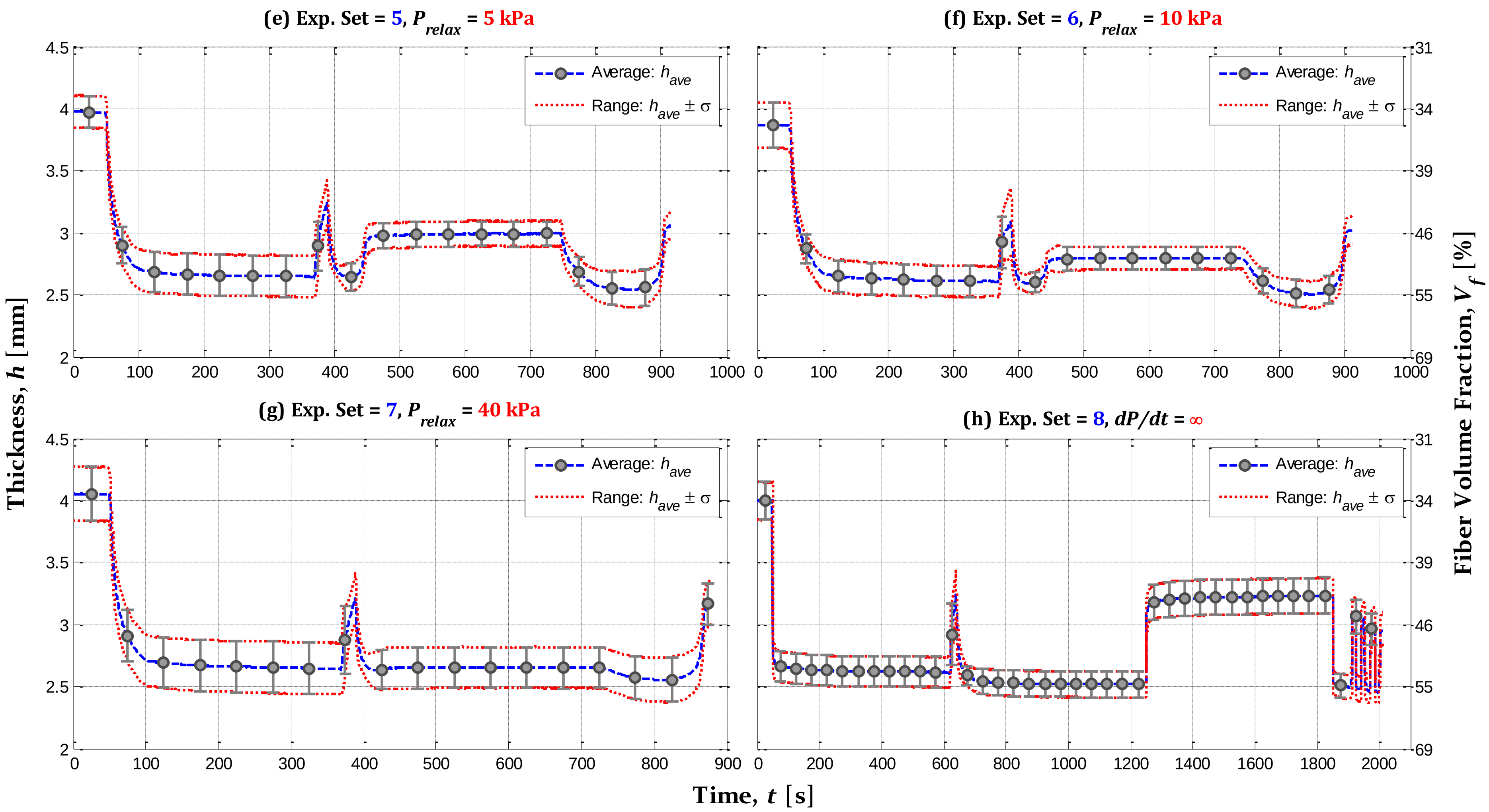

Figure 7-4. Experiment Sets 5-8 for **Woven** fabric. In each set, 12 specimens were characterized separately.

Table 7-1. Average values and standard deviation bounds of the parameters and variables for **random** fabric.

Exp. Set	1	2	3	4	5	6	7	Overall
Initial thickness, $h_{@P_{minor}}$ **[mm]**	5.99 ± 0.37	6.05 ± 0.33	6.20 ± 0.26	6.01 ± 0.18	5.77 ± 0.40	5.94 ± 0.36	6.15 ± 0.35	**6.02 ± 0.34**
Initial f. vol. frac., $V_{f@P_{minor}}$ **[%]**	23.60 ± 0.84	23.52 ± 1.36	23.32 ± 1.23	23.80 ± 1.20	24.73 ± 1.45	24.44 ± 1.21	24.55 ± 1.65	**23.99 ± 1.36**
Compacted thickness, $h_{@P_{major}}$ **[mm]**	3.58 ± 0.32	3.35 ± 0.21	3.63 ±0.28	3.53 ± 0.13	3.64 ± 0.39	3.59 ± 0.25	3.66 ± 0.27	**3.57 ± 0.28**
Compacted f. vol. frac., $V_{f@P_{major}}$ **[%]**	39.57 ± 2.17	42.46 ± 2.14	39.97 ± 2.82	40.56 ± 2.24	39.35 ± 2.93	40.56 ± 2.90	41.32 ± 3.12	**40.54 ± 2.74**
Superficial density, ρ_{sup} **[gr/m2]**	3590.00 ± 237.41	3609.17 ± 234.31	3670.83 ± 236.31	3632.50 ± 138.38	3614.17 ± 175.21	3683.33 ± 178.19	3833.33 ± 280.01	**3661.90 ± 222.00**
Effect of wetting, Δh_{wet} **[mm]**	-0.03 ± 0.02	**N/A**	-0.02 ± 0.01	-0.02 ± 0.02	-0.02 ± 0.02	-0.02 ± 0.01	-0.02 ± 0.01	**-0.02 ± 0.02**
Effect of wetting, $\Delta V_{f,wet}$ **[%]**	0.35 ± 0.22	**N/A**	0.28 ± 0.16	0.29 ± 0.20	0.19 ± 0.21	0.19 ± 0.17	0.25 ± 0.13	**0.26 ± 0.19**
Compaction stage, Δh_{comp} **[mm]**	-2.28 ± 0.17	-2.36 ± 0.18	-2.48 ± 0.13	-2.22 ± 0.15	-2.06 ± 0.27	-2.21 ± 0.29	-2.34 ± 0.21	**-2.28 ± 0.23**
Compaction stage, $\Delta V_{f,comp}$ **[%]**	14.66 ± 1.43	15.13 ± 1.08	15.69 ± 1.43	14.17 ± 0.85	13.81 ± 1.75	14.60 ± 1.85	15.15 ± 1.43	**14.74 ± 1.51**
Settling stage, Δh_{set} **[mm]**	-0.26 ± 0.06	-0.33 ± 0.06	-0.23 ± 0.05	-0.37 ± 0.04	-0.27 ± 0.04	-0.31 ± 0.03	-0.32 ± 0.03	**-0.30 ± 0.06**
Settling stage, $\Delta V_{f,set}$ **[%]**	3.01 ± 0.87	3.79 ± 0.64	2.55 ± 0.55	4.18 ± 0.40	3.12 ± 0.66	3.52 ± 0.41	3.66 ± 0.38	**3.40 ± 0.76**
Decompaction stage, Δh_{decomp} **[mm]**	0.85 ± 0.10	0.95 ± 0.07	0.99 ± 0.08	0.79 ± 0.08	0.61 ± 0.07	0.42 ± 0.06	0.09 ± 0.02	**N/A**
Decompaction stage, $\Delta V_{f,decomp}$ **[%]**	-8.37 ± 1.36	-9.39 ± 0.96	-9.40 ± 1.31	-8.13 ± 0.90	-6.41 ± 1.18	-4.77 ± 0.94	-1.15 ± 0.28	**N/A**
Relaxation stage, Δh_{relax} **[mm]**	0.66 ± 0.07	0.75 ± 0.07	0.56 ± 0.13	0.65 ± 0.06	0.30 ± 0.02	0.18 ± 0.03	0.02 ± 0.01	**N/A**
Relaxation stage, $\Delta V_{f,relax}$ **[%]**	-4.50 ± 0.47	-4.89 ± 0.39	-3.61 ± 0.69	-4.66 ± 0.40	-2.49 ± 0.28	-1.75 ± 0.26	-0.21 ± 0.14	**N/A**

Table 7-2. Average values and standard deviation bounds of the parameters and variables for **woven** fabric.

Exp. Set	1	2	3	4	5	6	7	Overall
Initial thickness, $h_{@P_{minor}}$ **[mm]**	3.94 ± 0.21	3.95 ± 0.17	3.90 ± 0.14	4.00 ± 0.17	3.97 ± 0.13	3.87 ± 0.18	4.05 ± 0.22	**3.95 ± 0.18**
Initial f. vol. frac., $V_{f@P_{minor}}$ **[%]**	34.99 ± 1.74	35.13 ± 1.36	35.95 ± 1.63	35.04 ± 1.49	34.61 ± 1.24	35.83 ± 1.74	33.80 ± 2.07	**35.05 ± 1.71**
Compacted thickness, $h_{@P_{major}}$ **[mm]**	2.96 ± 0.25	2.54 ± 0.17	3.05 ± 0.21	2.97 ± 0.18	3.03 ± 0.16	2.99 ± 0.22	3.00 ± 0.19	**2.94 ± 0.25**
Compacted f. vol. frac., $V_{f@P_{major}}$ **[%]**	46.67 ± 3.78	54.77 ± 3.45	46.15 ± 3.62	47.26 ± 3.23	45.43 ± 2.62	46.42 ± 3.41	45.72 ± 3.01	**47.49 ± 4.42**
Superficial density, ρ_{sup} **[gr/m²]**	3490.83 ± 45.62	3519.17 ± 49.44	3559.17 ± 62.59	3555.00 ± 62.30	3490.00 ± 94.29	3510.83 ± 72.80	3468.33 ± 76.02	**3513.33 ± 72.70**
Effect of wetting, Δh_{wet} **[mm]**	-0.04 ± 0.02	**N/A**	-0.02 ± 0.02	-0.01 ± 0.01	-0.02 ± 0.02	-0.02 ± 0.02	-0.04 ± 0.03	**-0.03 ± 0.02**
Effect of wetting, $\Delta V_{f,wet}$ **[%]**	0.78 ± 0.44	**N/A**	0.39 ± 0.45	0.22 ± 0.21	0.36 ± 0.39	0.48 ± 0.45	0.74 ± 0.51	**0.50 ± 0.45**
Compaction stage, Δh_{comp} **[mm]**	-1.30 ± 0.08	-1.32 ± 0.13	-1.26 ± 0.13	-1.31 ± 0.11	-1.26 ± 0.13	-1.18 ± 0.20	-1.32 ± 0.11	**-1.28 ± 0.14**
Compaction stage, $\Delta V_{f,comp}$ **[%]**	17.38 ± 2.14	17.83 ± 2.75	17.14 ± 2.33	17.35 ± 2.42	16.19 ± 2.51	15.75 ± 2.88	16.59 ± 2.41	**16.89 ± 2.51**
Settling stage, Δh_{set} **[mm]**	-0.07 ± 0.02	-0.08 ± 0.03	-0.05 ± 0.01	-0.09 ± 0.02	-0.07 ± 0.01	-0.08 ± 0.03	-0.08 ± 0.02	**-0.07 ± 0.02**
Settling stage, $\Delta V_{f,set}$ **[%]**	1.47 ± 0.42	1.74 ± 0.60	1.08 ± 0.32	1.82 ± 0.47	1.33 ± 0.40	1.52 ± 0.53	1.53 ± 0.47	**1.50 ± 0.50**
Decompaction stage, Δh_{decomp} **[mm]**	0.35 ± 0.09	0.48 ± 0.08	0.28 ± 0.14	0.25 ± 0.12	0.12 ± 0.15	0.11 ± 0.09	-0.07 ± 0.14	**N/A**
Decompaction stage, $\Delta V_{f,decomp}$ **[%]**	-6.23 ± 1.51	-8.78 ± 2.13	-4.96 ± 2.49	-4.50 ± 2.21	-2.13 ± 2.67	-2.08 ± 1.76	1.41 ± 2.84	**N/A**
Relaxation stage, Δh_{relax} **[mm]**	0.21 ± 0.04	0.22 ± 0.04	0.15 ± 0.04	0.24 ± 0.03	0.11 ± 0.03	0.05 ± 0.03	0.01 ± 0.01	**N/A**
Relaxation stage, $\Delta V_{f,relax}$ **[%]**	-3.18 ± 0.73	-3.19 ± 0.53	-2.29 ± 0.55	-3.63 ± 0.44	-1.81 ± 0.60	-0.85 ± 0.43	-0.18 ± 0.29	**N/A**

in statistics where σ is the standard deviation and $\bar{x}$ is the mean value of dataset x. The RSD of overall $h_{@P_{minor}}$ is $RSD(h_{@P_{minor}}) = 5.65$ % for random fabric, and $RSD(h_{@P_{minor}}) = 4.56$ % for woven fabric.

The compacted thickness values, $h_{@P_{major}}$ are shown in Figure 7-5b and Table 7-1 for random fabric, and in Figure 7-6b and Table 7-2 for woven fabric. One would expect that $h_{@P_{major}}$ should have been nearly the same in all 7 sets of experiments of each fabric type since (i) all specimens are dry until the end of compaction and relaxation stage, and (ii) the relaxation stage is long enough to compensate different levels of compaction induced by different dP/dt rates in different experiment sets (2 kPa/s in the sets 1,2,5-7; 1 kPa/s in experiment set 3; and 4 kPa/s in the set 4). As seen in Table 7-1, for random fabric, the mean $h_{@major}$ value in 7 sets varies between 3.35 mm and 3.66 mm; and its standard deviation varies between 0.13 mm and 0.32 mm. The mean value of all (7 * 12 = 84) experiments is 3.57 mm and its standard deviation is 0.28 mm. For woven fabric, the Table 7-2 shows the mean $h_{@major}$ values in 7 sets vary between 2.54 mm and 3.05 mm; and their standard deviation vary between 0.16 mm and 0.25 mm. The mean value of all (7 * 12 = 84) experiments is 2.94 mm and its standard deviation is 0.25 mm. RSD values can be used to compare the fabric types. $RSD\left(h_{@P_{major}}\right)_{random} = 7.84$ % and $RSD\left(h_{@P_{major}}\right)_{woven} = 8.50$ %. Woven fabric has slightly more variation than random fabric which is different than $RSD(h_{@P_{minor}})$.

The main cause for variation between specimens is the inconsistency of the fabric preform (its non-homogenous structure and preparation). The local superficial density, ρ_{sup} in a roll can vary from the catalogue value, which are $450 g/m^2$ and $500 g/m^2$ per a single layer of random and woven fabric (i.e. $3600 g/m^2$ and $4000 g/m^2$ for 8 layers of random and woven specimens). Thus, significant variations in h can be linked to the variation in the fabric's ρ_{sup}. For that purpose, before the start of a characterization experiment, each specimen's weight was measured to calculate the ρ_{sup} of each specimen. The calculated data is shown in Figure 7-5c and Table 7-1 for random fabric, and in Figure 7-6c and Table 7-2 for woven fabric.

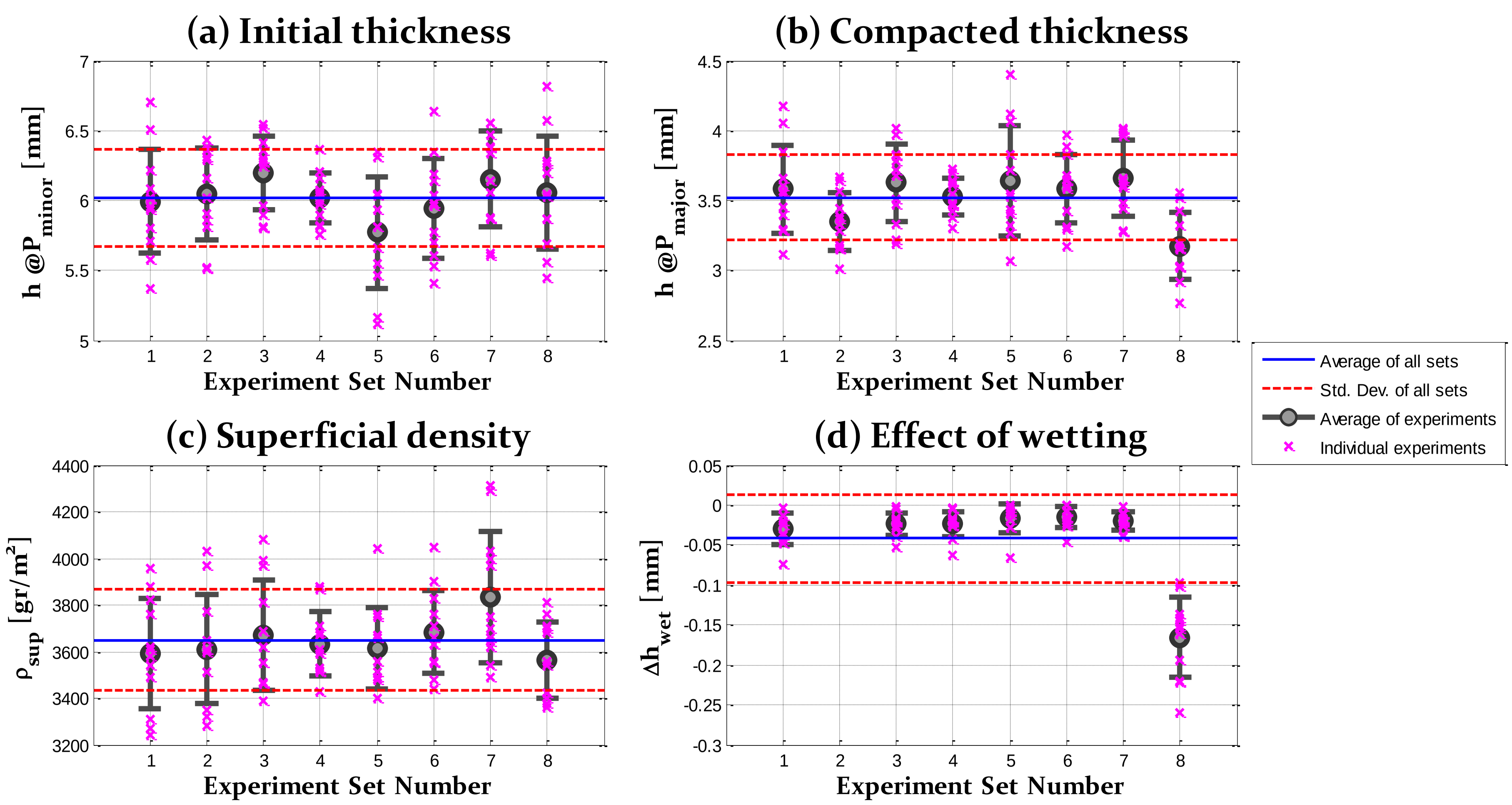

Figure 7-5. Variation in fabric parameters within experiments for **Random** fabric.

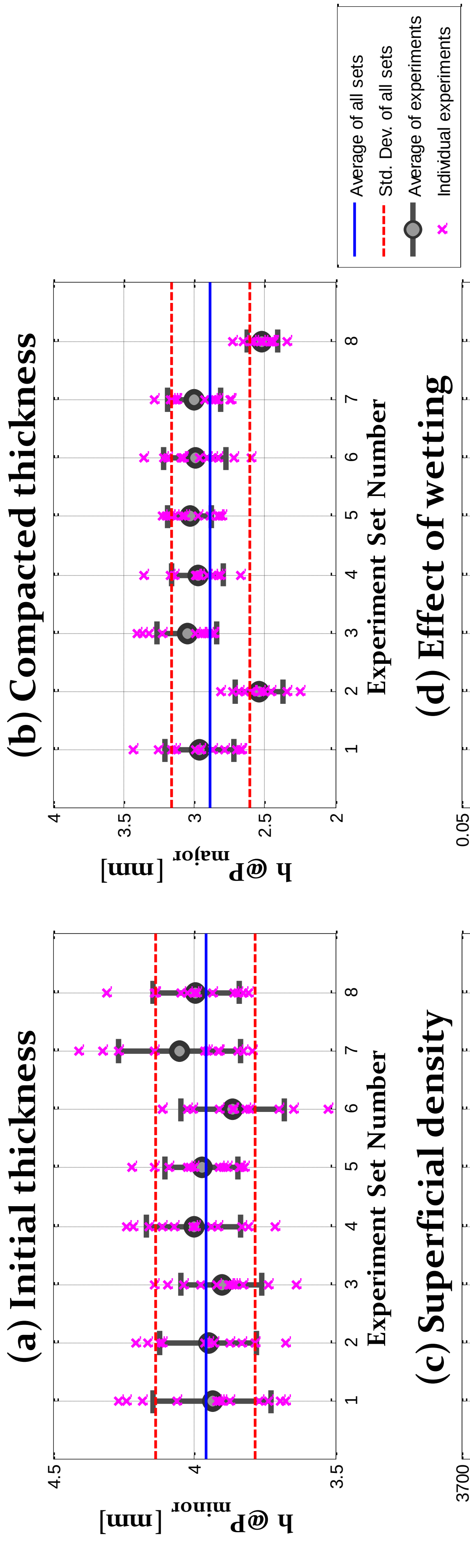

Figure 7-6. Variation in fabric parameters within experiments for **Woven** fabric.

Table 7-3. Relative standard deviation (RSD) for given variables.

		Fabric	
		Random	**Woven**
Initial	$RSD(h_{@P_{minor}})$	5.65 %	4.56 %
	$RSD(V_{f_{@P_{minor}}})$	5.67 %	4.88 %
Compacted	$RSD(h_{@P_{major}})$	7.84 %	8.50 %
	$RSD(V_{f_{@P_{major}}})$	6.76 %	9.31 %
Superficial density	$RSD(\rho_{sup})$	6.06 %	2.07 %

It is found that the random fabric has a mean superficial density of 3662 g/m^2 with a standard deviation of 222 g/m^2, and woven fabric has a mean superficial density of 3513 g/m^2 with a standard deviation of 72.7 g/m^2. They correspond to 6.06 % and 2.07 % variance compared to the mean values (RSD) for random and woven fabrics, respectively.

If h varies from one experiment to another, one may question the cause of this variation. One should not forget that the variance in the superficial density, ρ_{sup} may contribute to this variation in h. Recall that V_f is inversely proportional to h as given by $V_f = \frac{\rho_{sup}}{\rho_{bulk}}\frac{1}{h}$. As usually done in the literature, analyzing V_f instead of h is more meaningful for compaction characterization. In this study, both h and V_f will be documented in tables.

RSD values for V_f is given below:

$$RSD\left(V_{f_{@P_{minor}}}\right)_{random} = 5.67\ \% \qquad RSD\left(V_{f_{@P_{minor}}}\right)_{woven} = 4.88\ \%$$

$$RSD\left(V_{f_{@P_{major}}}\right)_{random} = 6.76\ \% \qquad RSD\left(V_{f_{@P_{major}}}\right)_{woven} = 9.31\ \%$$

RSD values of initial h and V_f, compacted h and V_f and ρ_{sup} are listed in Table 7-3. For the random fabric type, $RSD(\rho_{sup}) = 6.06\ \%$ and $RSD(h_{@P_{minor}}) = 5.65\%$ are close to each other and one may conclude that the variation in ρ_{sup} is the major reason of the variation in h. For the same random fabric, $RSD(h)$ increases to 7.84% at the end of settling stage of the main first compaction cycle. This shows that some other effects induced by inconsistent fabric preparation could also play a role in the thickness variation. Indeed, this can be seen for the other fabric type (woven) in the Table 7-3 that $RSD(h)$ and $RSD(V_f)$ are $4.56\ \%$ and $4.88\ \%$, respectively whereas $RSD(\rho_{sup})$ is only $2.07\ \%$. The following list are suspected to be the other minor causes of the experimental variations in h and V_f:

- Specimen preparation: Inconsistent placement of layers and thus different level of fiber tow nesting (this is especially important for the woven fabric);
- Potential leaks through the sealing of the setup, which may cause lower compaction pressure than the set (vacuum trap) pressure;
- Noise in the set pressure caused by the closed loop control system.

Figure 7-5d and Figure 7-6d show the change in thickness after wetting. In all experiment sets, except experiment set 2, the specimen is saturated after the first compaction cycle, right after $h_{@P_{major}}$ value is recorded. The wetting process takes place and change in thickness is measured. Ideally, no difference was expected between the experiment sets (for the same fabric) as the settling stage is the same for all experiments and the wetting procedure is the same. The wetting causes random fabric to decrease $0.02 \pm 0.02\ mm$ in thickness and $0.26 \pm 0.19\ \%$ in fiber volume fraction. For woven fabric, the decrease is $0.03 \pm 0.02\ mm$ in thickness and $0.50 \pm 0.45\ \%$ in fiber volume fraction. This effect is known as lubrication effect in the literature, where the liquid resin helps tows of fabric to slip over each other, thus fabric can be compacted further. The variation of the values for all experiment sets is shown in Table 7-1 and Table 7-2. One can argue that the effect of wetting on the compaction exists, but not too significant due to the magnitude of thickness or fiber volume fraction change.

The bottom halves of Table 7-1 and Table 7-2 show the change in thickness (Δh) and fiber volume fraction (ΔV_f) for each characterization stage. The characterization stages, and the definition of the variables used in the tables can be seen in Figure 3-10. Instead of comparing the full experimental data of different sets using a common time scale, ($0 < t < t_{final}$ seen in Figure 7-1 to Figure 7-4) h and V_f values at particular instants were compared. The reason for that is the transition instants between different stages and also the final time (t_{final}) vary between the experiment sets due to different dP/dt and P_{relax} values.

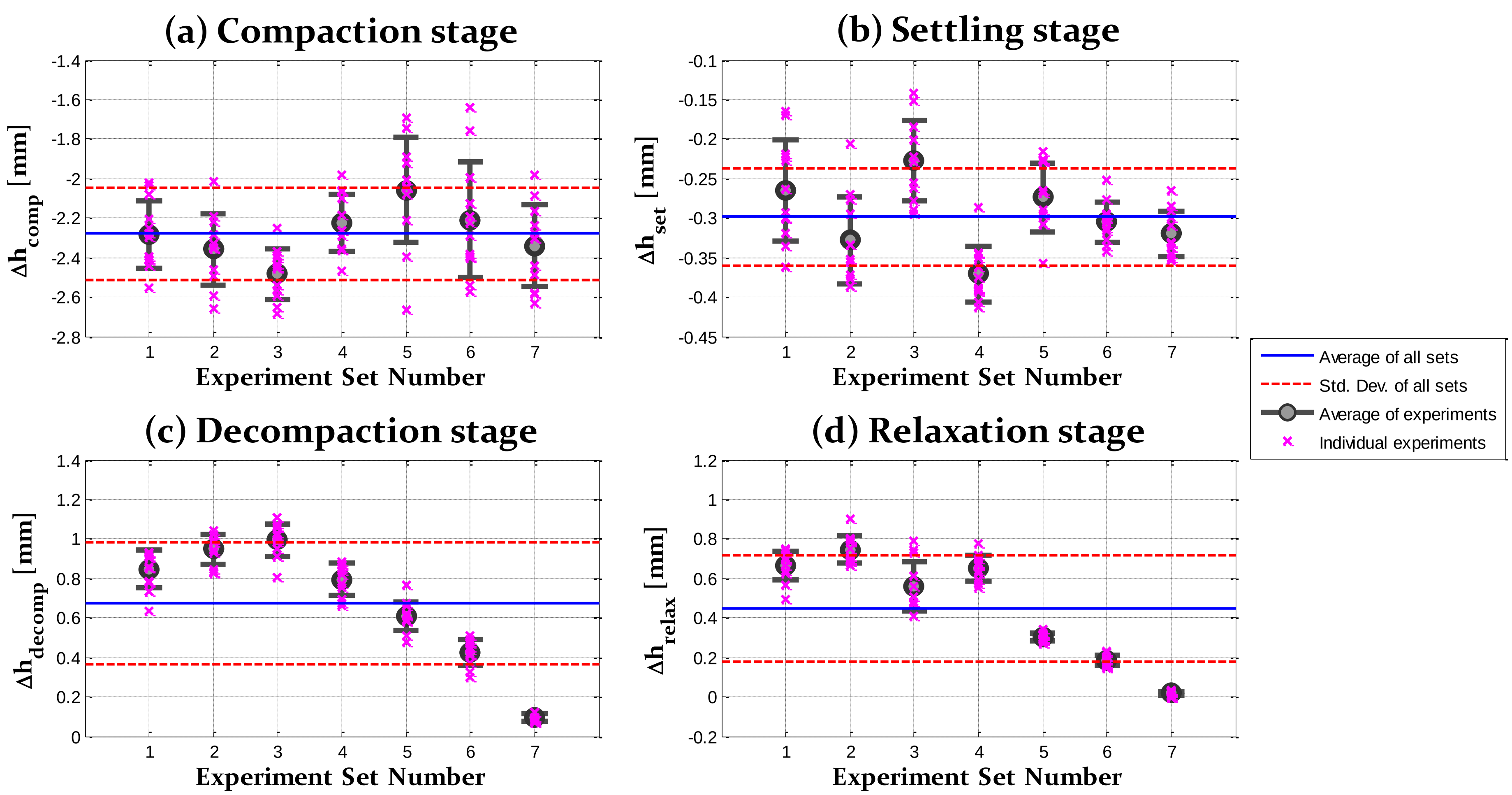

Figure 7-7. Change in thickness during main stages for **Random** fabric excluding Experiment Set 8 (step input).

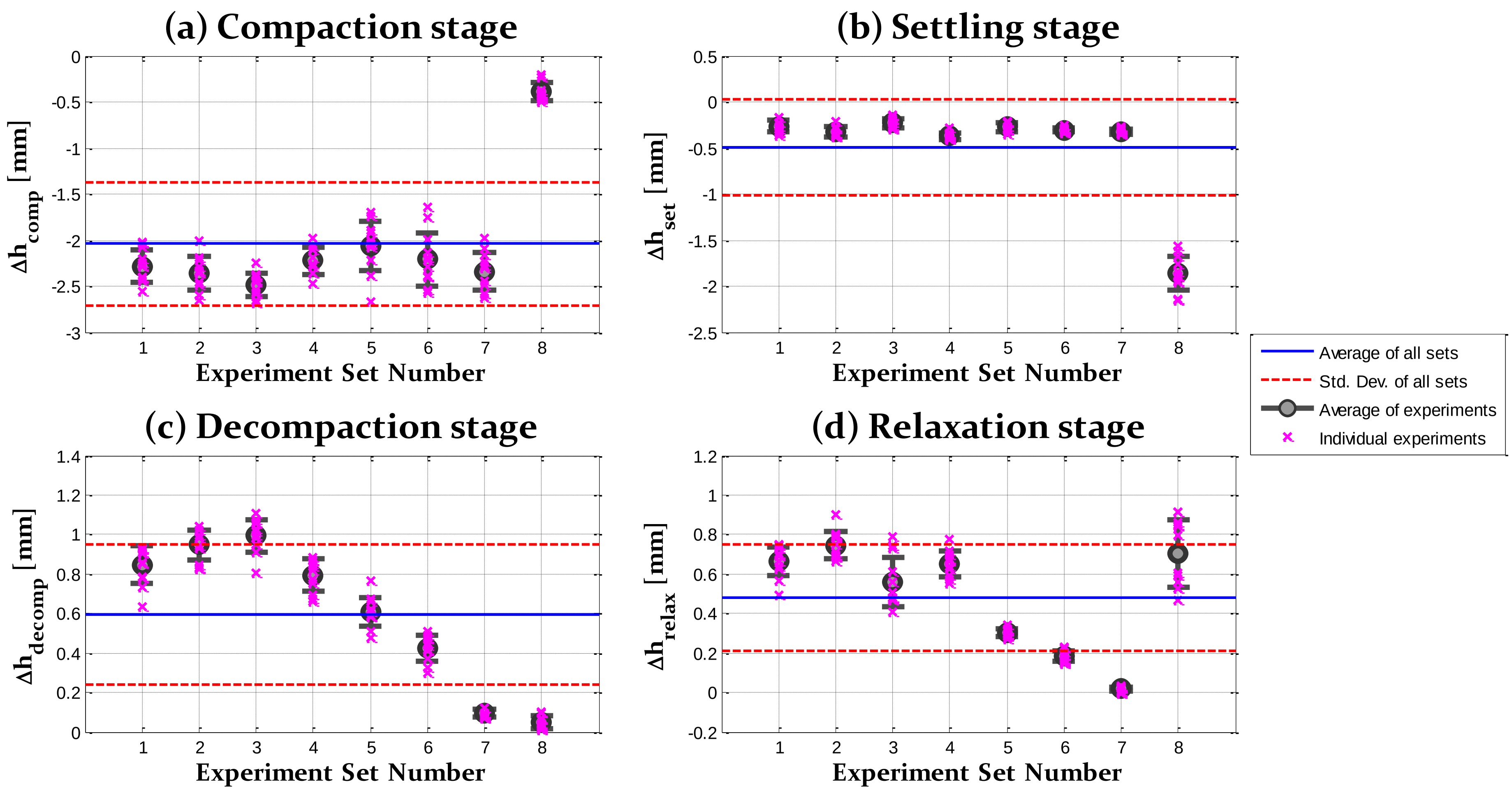

Figure 7-8. Change in thickness during main stages for **Random** fabric <u>including</u> Experiment Set 8 (step input).

Table 7-4. Average and standard deviation values of h and V_f after each compaction cycle.

Random Fabric

	1, Dry/Wet		2, Dry/Dry		3, $dP/dt = 1\ kPa/s$		4, $dP/dt = 4\ kPa/s$	
Cycle	h_{comp} [mm]	$\boldsymbol{V}_{f,comp}$ [%]	h_{comp} [mm]	$\boldsymbol{V}_{f,comp}$ [%]	h_{comp} [mm]	$\boldsymbol{V}_{f,comp}$ [%]	h_{comp} [mm]	$\boldsymbol{V}_{f,comp}$ [%]
1	3.70 ± 0.32	38.30 ± 1.63	3.68 ± 0.22	38.70 ± 1.96	3.71 ± 0.25	39.05 ± 2.13	3.75 ± 0.09	38.13 ± 1.66
2	3.43 ± 0.33	41.33 ± 2.18	3.40 ± 0.21	41.89 ± 2.19	3.42 ± 0.23	42.37 ± 2.20	3.42 ± 0.08	41.80 ± 1.72
3	3.33 ± 0.33	42.61 ± 2.32	3.33 ± 0.20	42.69 ± 2.25	3.33 ± 0.24	43.50 ± 2.33	3.30 ± 0.08	43.40 ± 1.82
4	3.29 ± 0.34	43.16 ± 2.47	3.31 ± 0.20	42.97 ± 2.30	3.28 ± 0.23	44.09 ± 2.34	3.26 ± 0.08	43.93 ± 1.79
5	3.26 ± 0.35	43.52 ± 2.63	3.29 ± 0.21	43.30 ± 2.34	3.25 ± 0.23	44.54 ± 2.36	3.23 ± 0.08	44.33 ± 1.87

Woven Fabric

	1, Dry/Wet		2, Dry/Dry		3, $dP/dt = 1\ kPa/s$		4, $dP/dt = 4\ kPa/s$	
Cycle	h_{comp} [mm]	$\boldsymbol{V}_{f,comp}$ [%]	h_{comp} [mm]	$\boldsymbol{V}_{f,comp}$ [%]	h_{comp} [mm]	$\boldsymbol{V}_{f,comp}$ [%]	h_{comp} [mm]	$\boldsymbol{V}_{f,comp}$ [%]
1	2.63 ± 0.18	52.41 ± 3.66	2.62 ± 0.17	52.98 ± 3.34	2.65 ± 0.12	53.10 ± 3.14	2.67 ± 0.17	52.52 ± 3.48
2	2.50 ± 0.15	55.09 ± 3.12	2.53 ± 0.17	54.89 ± 3.52	2.51 ± 0.10	55.90 ± 2.97	2.57 ± 0.13	54.48 ± 2.81
3	2.45 ± 0.16	56.34 ± 3.57	2.50 ± 0.17	55.54 ± 3.56	2.47 ± 0.11	56.85 ± 3.19	2.49 ± 0.14	56.39 ± 3.36
4	2.43 ± 0.15	56.77 ± 3.50	2.49 ± 0.17	55.95 ± 3.66	2.45 ± 0.11	57.42 ± 3.36	2.46 ± 0.14	56.95 ± 3.38
5	2.41 ± 0.15	57.12 ± 3.49	2.48 ± 0.17	56.19 ± 3.67	2.43 ± 0.11	57.72 ± 3.32	2.44 ± 0.13	57.46 ± 3.32

Figure 7-7 and Figure 7-9 show the change in thickness for the first 4 stages of the experiment: (a) compaction, (b) settling, (c) decompaction and (d) relaxation. From these graphs, the elastic and viscous behaviors of the fabrics can be seen. The thickness change in compaction and decompaction stages is due to the change in compaction pressure. The change in thickness, Δh during the compaction stage is higher than during the decompaction since the fabric is compressed for the first time during the compaction stage and fibers and tows slide into each other and stack more freely than during the decompaction stage which will resist more due to the initial compaction.

Figure 7-11 and Figure 7-12 show the thickness values at the end of compaction stage of each compaction/settling/decompaction/relaxation cycle which are also tabulated in Table 7-4. Note that there is total of 5 cycles. The specimen is dry during the first compaction stage, but it is wet during the remaining four cycles except experiment set 2. Both fabrics (random and woven) compact more after each consecutive cycle, however the change in thickness between cycles decreases as the cycle number increases. Also, for both fabrics saturation has no significant effect on the debulking behavior (i.e. the change in thickness decreases faster or slower).

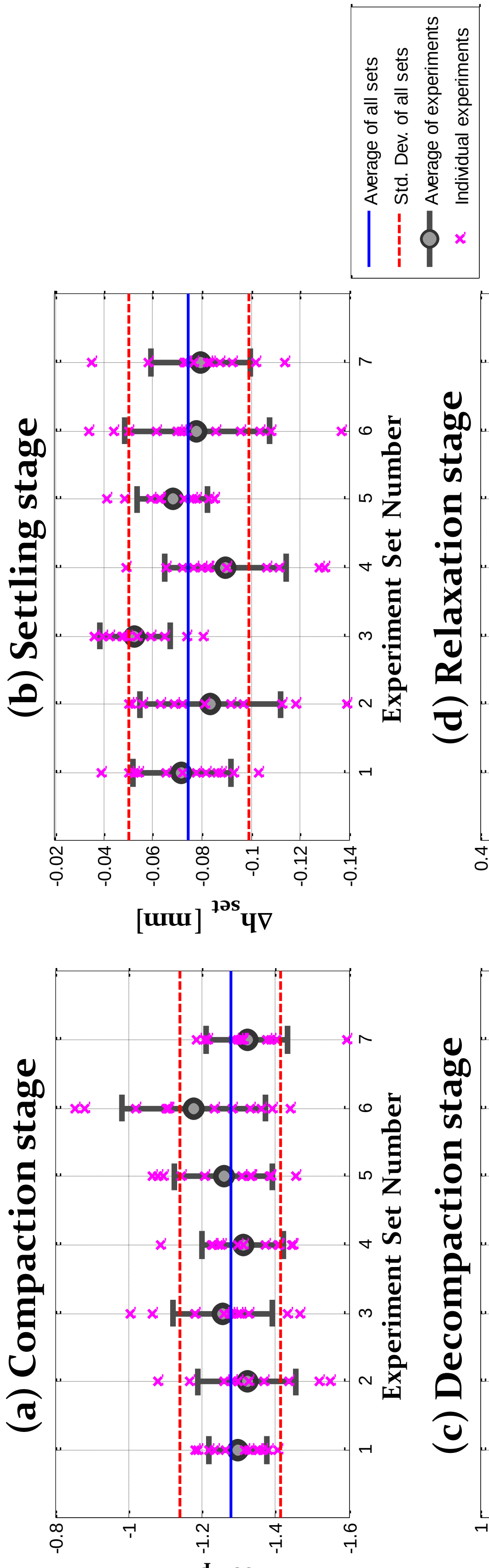

Figure 7-9. Change in thickness during main stages for **Woven** fabric <u>excluding</u> Experiment Set 8 (step input).

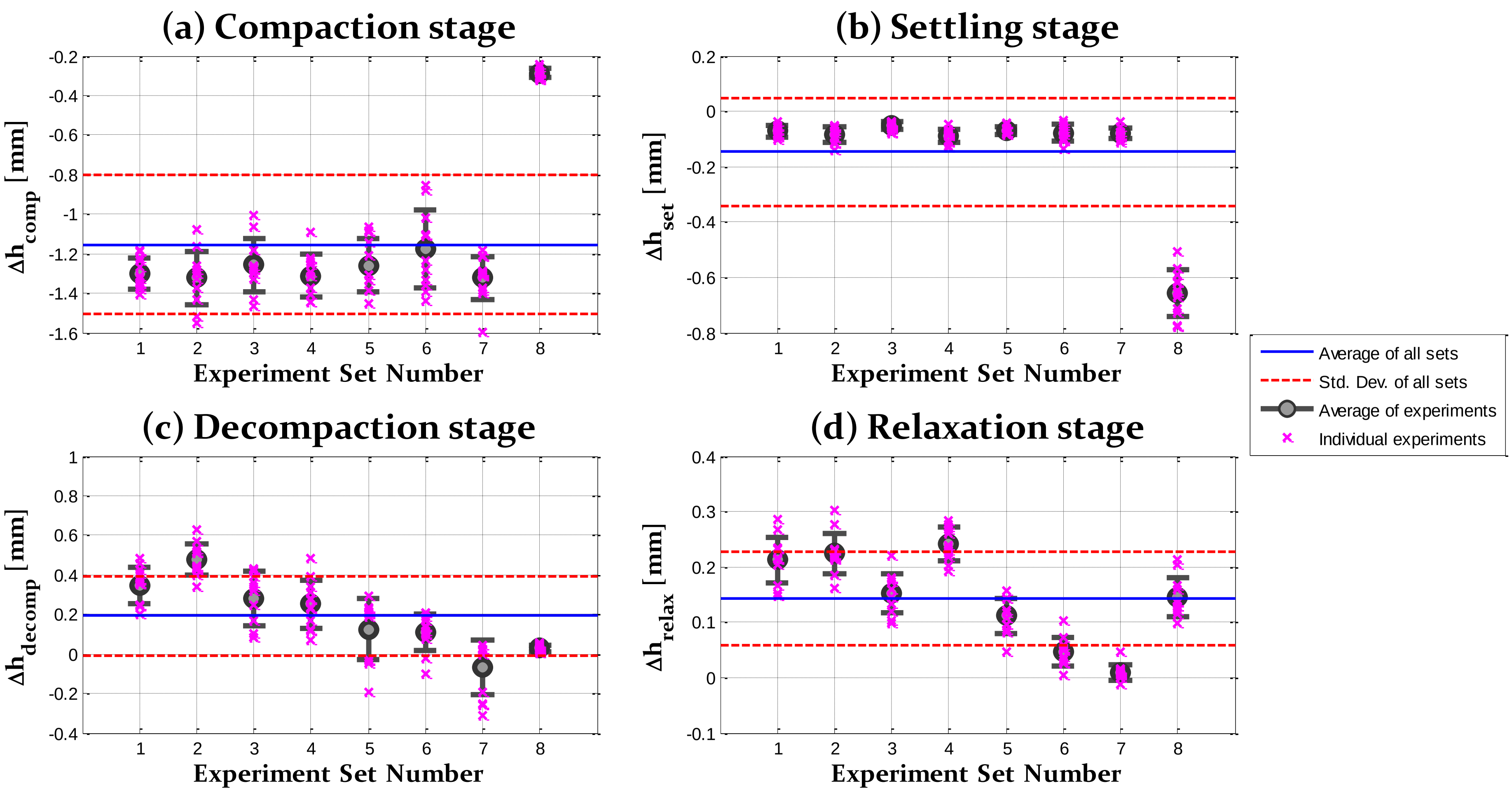

Figure 7-10. Change in thickness during main stages for **Woven** fabric including Experiment Set 8 (step input).

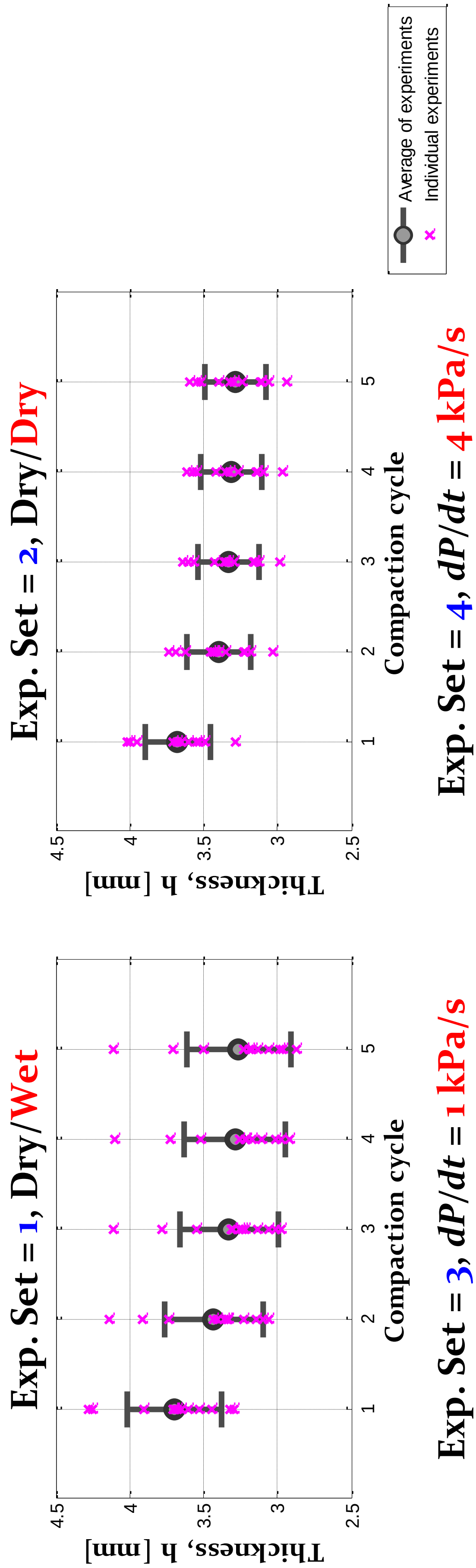

Figure 7-11. Effect of debulking shown for **Random** fabric with the thickness value after each compaction stage.

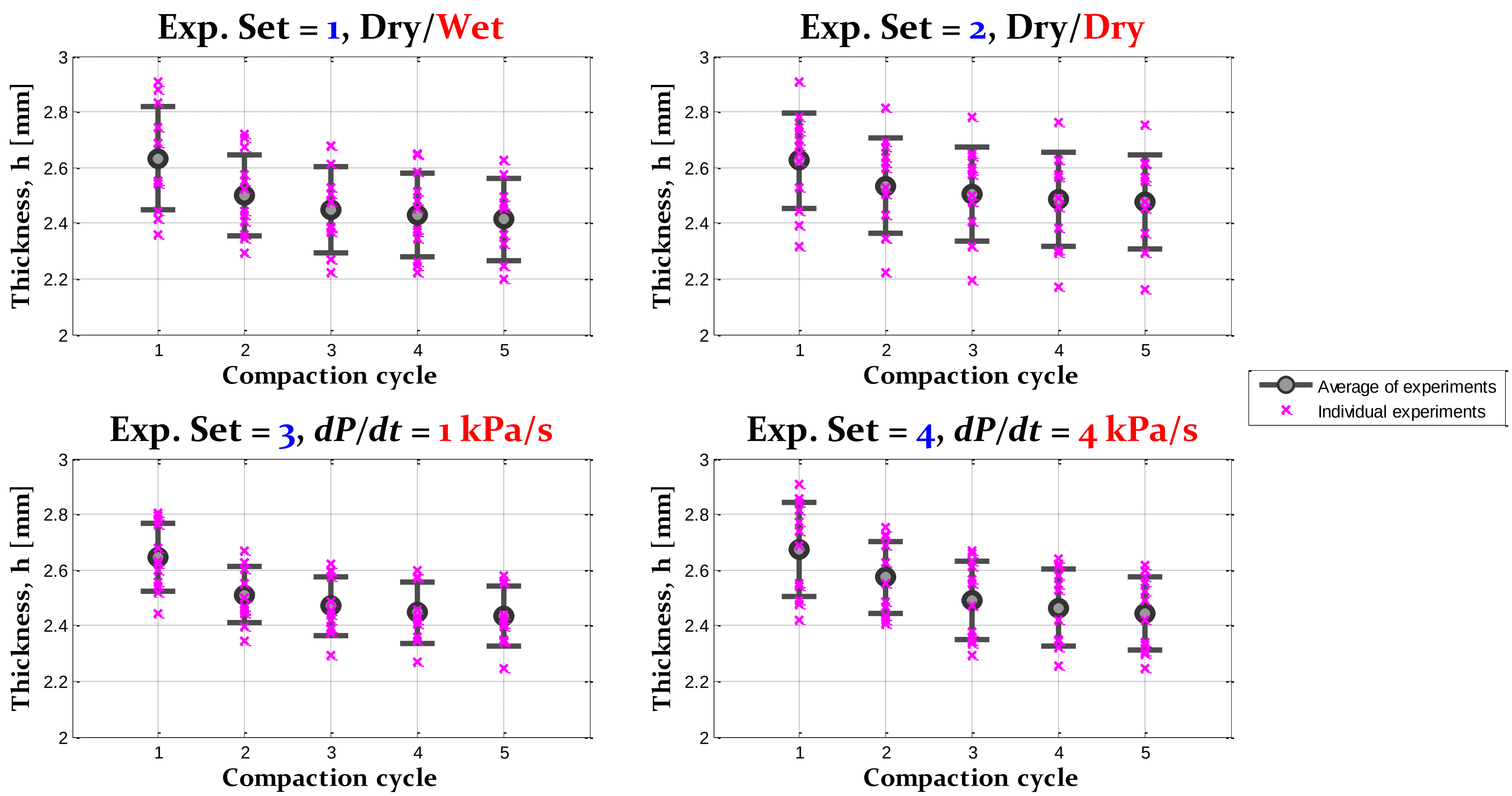

Figure 7-12. Effect of debulking shown for **Woven** fabric with the thickness value after each compaction stage.

7.2 Effects of the experimental parameters

7.2.1 Effect of wetting

Figure 7-5d and Figure 7-6d show the change in thickness after wetting. In all experiment sets, except experiment set 2, the specimen is saturated after the first compaction cycle, right after $h_{@P_{major}}$ value is recorded. The wetting process takes place and change in thickness is measured. Ideally, no difference is expected between the experiment sets (for the same fabric) as the settling stage is the same for all experiments and the wetting procedure is the same. The wetting causes random fabric to decrease $0.02 \pm 0.02\,mm$ in thickness and $0.26 \pm 0.19\,\%$ in fiber volume fraction. For woven fabric, the decrease is $0.03 \pm 0.02\,mm$ in thickness and $0.50 \pm 0.45\,\%$ in fiber volume fraction. This effect is known as lubrication effect in the literature where the liquid resin helps tows of fabric to slip over each other, thus fabric can be compacted further. The variation of the values for all experiment sets is shown in Table 7-1 and Table 7-2. One can argue that the effect of wetting on the compaction exists, but not too significant due to the magnitude of thickness or fiber volume fraction change.

Figure 7-13 illustrates the summed response in h and V_f during loading (compaction + settling) and unloading (decompaction + relaxation) for the random fabric. Ideally, one would expect that the loading results should be the same in all sets (except 3, 4 and 8) considering that the specimens in all sets are still dry during the entire loading (compaction and settling stages). However, there is a slight variation between them, which could be linked to variations in fabric. Similarly, Figure 7-14 is for the woven fabric. One can notice that the variation in “summed response during loading” for the woven fabric is less than the random fabric.

When the first two columns of unloading (decompaction and relaxation stages) in Figure 3-11 are compared, wetted random specimens have smaller “summed response during unloading” than dry specimens. The same is said for the woven fabric by examining the first two columns of Figure 7-14.

(a)

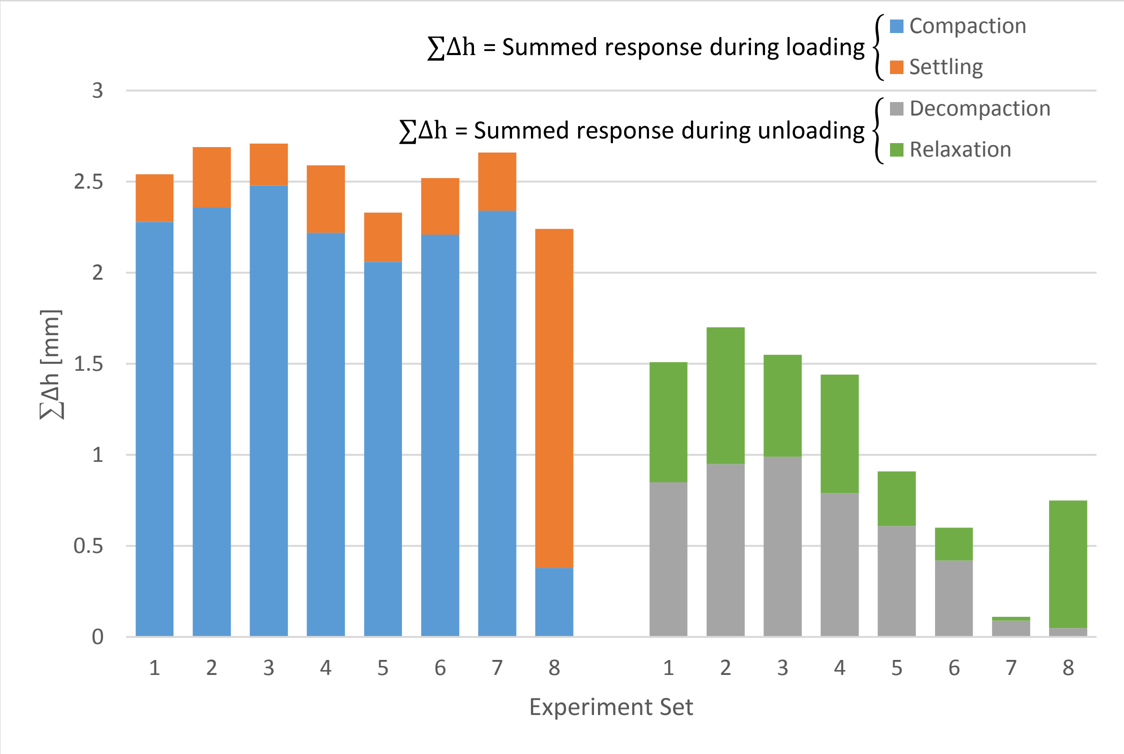

(b)

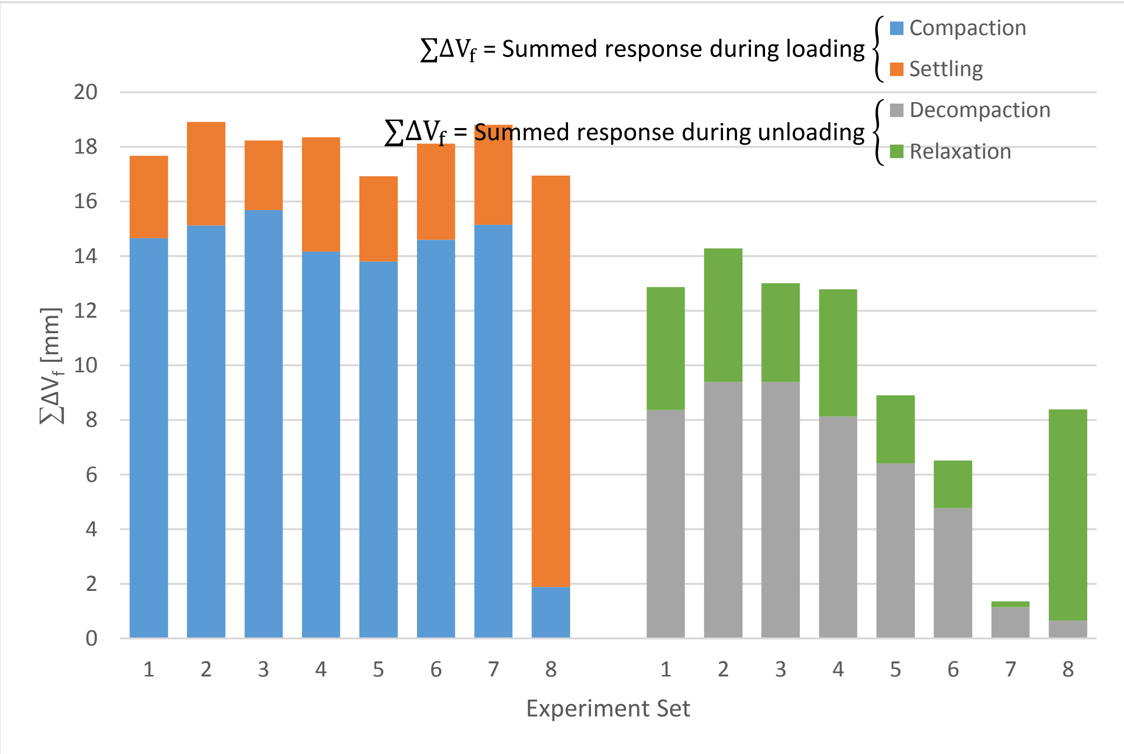

Figure 7-13. Summed response for both (a) thickness and (b) fiber volume fraction during loading and unloading stages for **random** fabric.

(a)

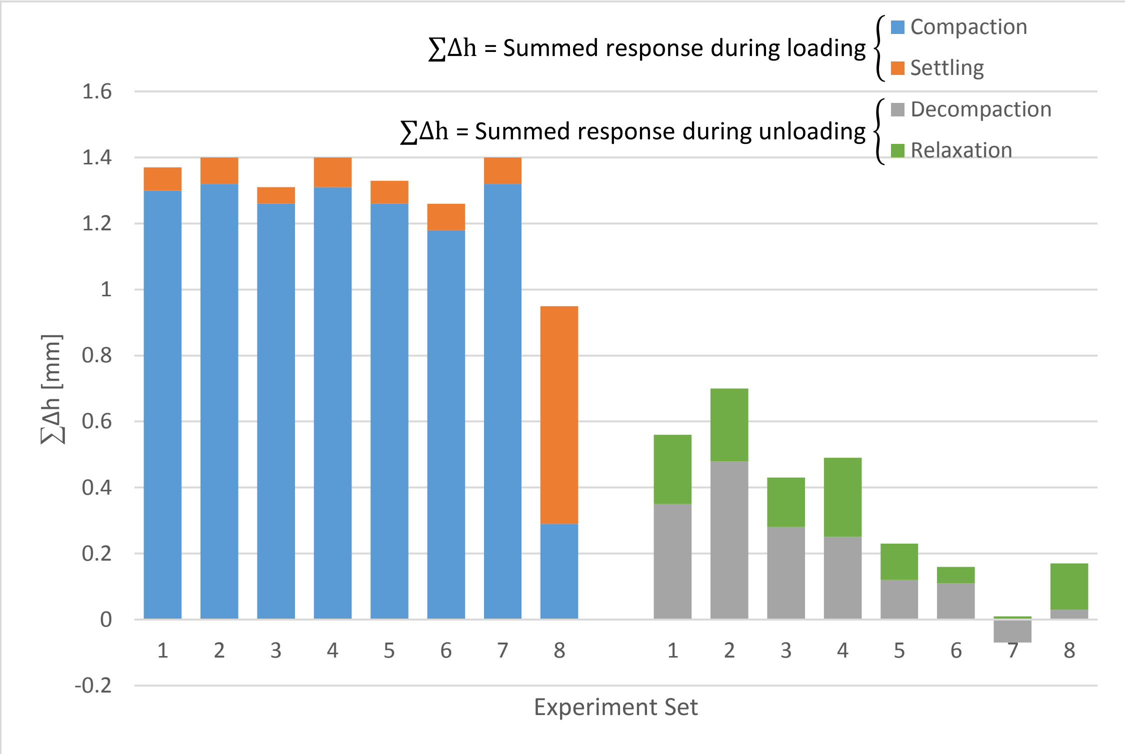

(b)

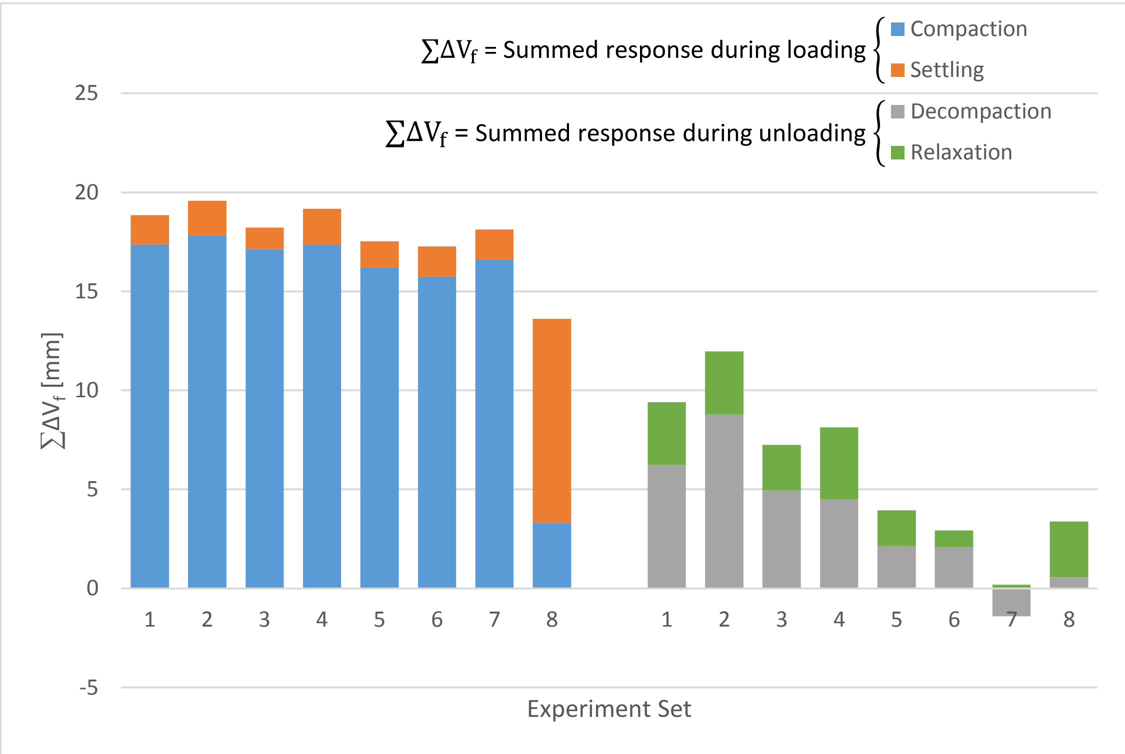

Figure 7-14. Summed response for both (a) thickness and (b) fiber volume fraction during loading and unloading stages for **woven** fabric.

7.2.2 Effect of dP/dt

To investigate the effect of dP/dt on h and V_f, experiment sets 3 and 4 were conducted. dP/dt was halved and doubled in experiment sets 3 and 4 compared to the base experiment set 1. One can briefly investigate this effect by seeing Figures 7.17-20.

a. Random fabric

The effect of the compaction/decompaction rate can be seen in Figure 7-13 as a summed response and in Figure 7-15 for each stage separately. From the summed response graph, there is an insignificant difference between experiments for loading. However, it is also seen that as the dP/dt increases, the Δh in compaction stage decreases while the Δh in settling stage decreases. This suggests that, as the duration of compaction stage decreases fabric cannot compact faster (as a result of viscous behavior of the fabric) and the deformation expected in this stage happens in the proceeding stage (settling). To support this idea one can use Figure 7-1a, c and d showing the thickness values at the end of relaxation stage which are almost the same for 1 kPa/s and 2 kPa/s. The thickness is larger for 4 kPa/s in comparison but the large variance makes it hard to state that this is due to the pressure rate. The results of the step input case also support this statement, the deformation in compaction stage is very low since it takes only about 4 seconds, but there is significant deformation in settling stage, making the summed response during loading comparable to other experiment sets.

During unloading, increase dP/dt results in decrease in Δh for the decompaction state similar to compaction. However, Δh in relaxation stage does not increase in the same order. Thus the summed response in thickness decreases as dP/dt increases during unloading.

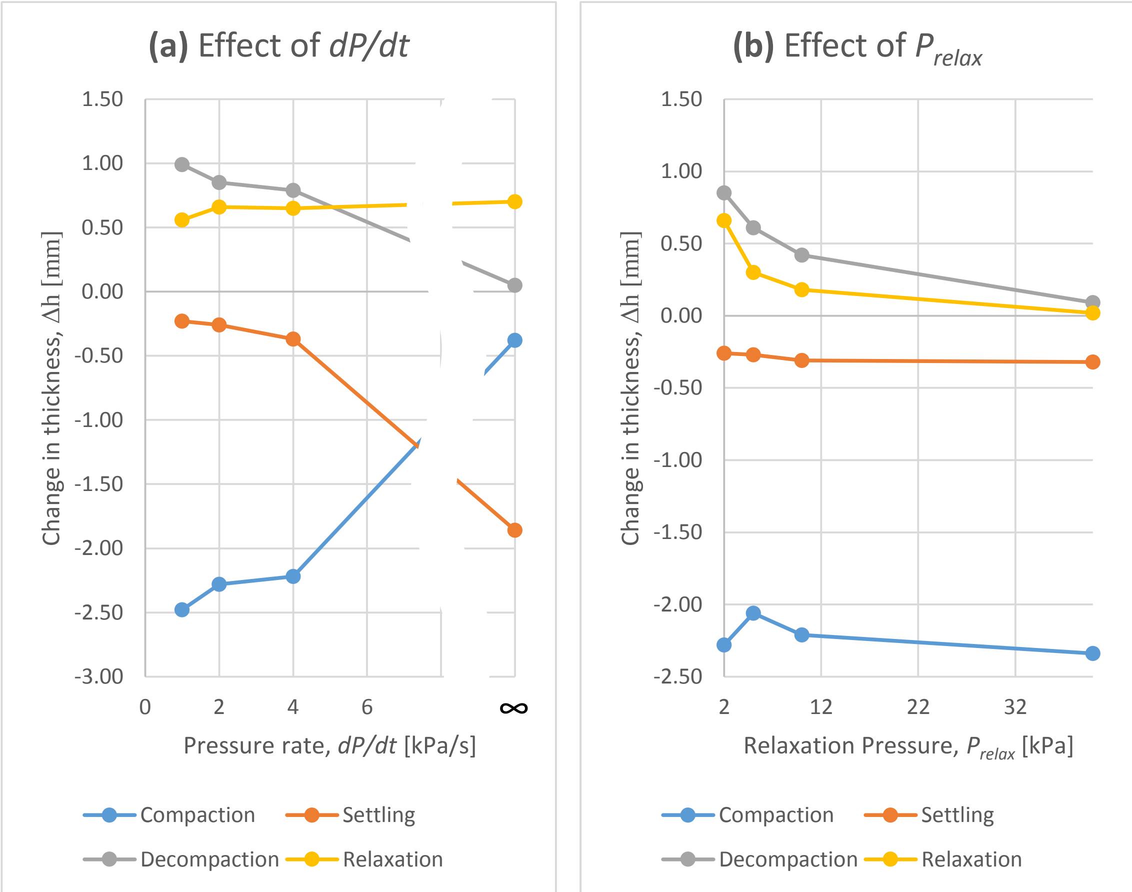

Figure 7-15. The effect of dP/dt and P_{relax} on Δh for **random** fabric.

b. Woven fabric

The change in thickness values for each stage versus dP/dt are shown in Figure 7-16. The trend for woven fabric looks similar to random fabric at first glance. However, there is no monotonic relation in woven fabric except the settling stage. It should be noted that the variation in the specimens are large and only 4 data points are available for dP/dt analysis, and the values of the first three points are close to each other.

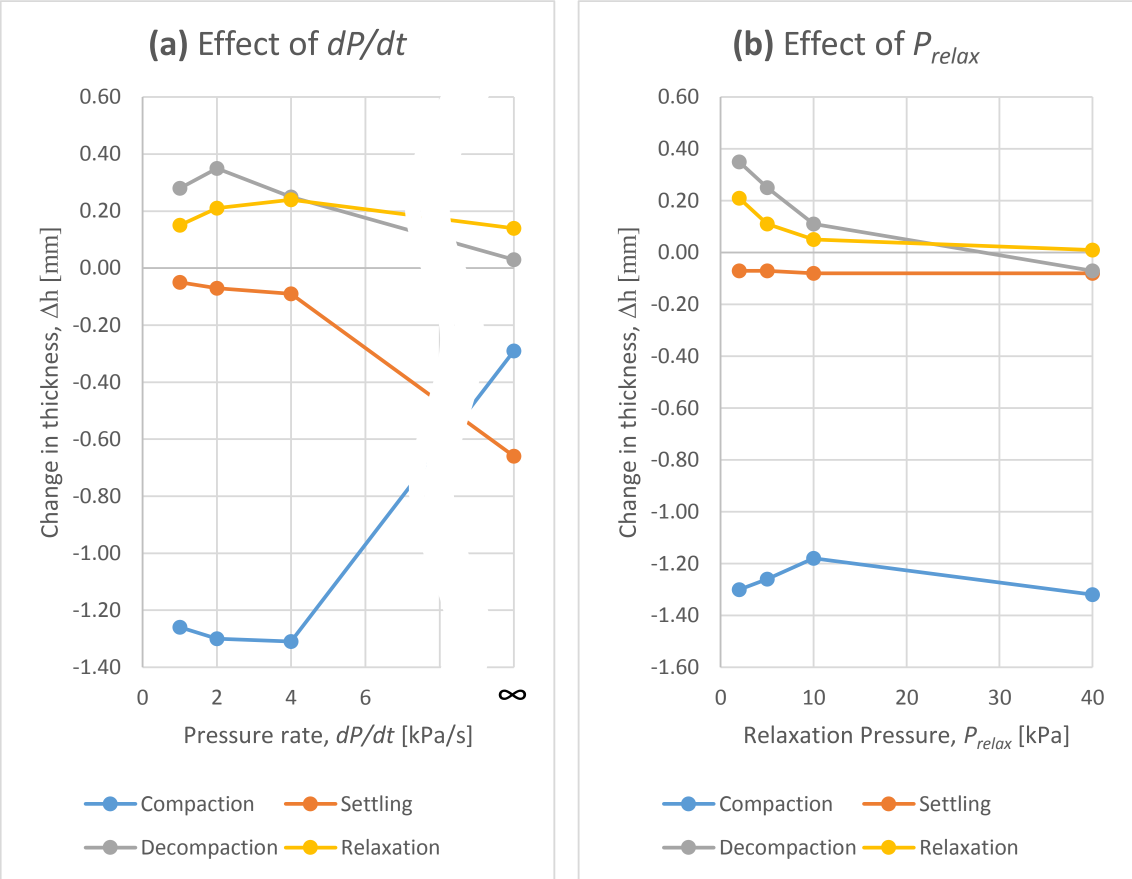

Figure 7-16. The effect of dP/dt and P_{relax} on Δh for **woven** fabric.

7.2.3 Effect of P_{relax}

Experiment Sets 5-7 were used to investigate the effect of P_{relax} on h and V_f. The relaxation pressures were taken as 5, 10, 40 kPa for the Experiment Set 5, 6 and 7 respectively, compared to the base experiment in which the relaxation pressure was 1 kPa. The effects can be seen in Figure 7-13 to Figure 7-16.

a. Random fabric

In Figure 7-13, it is seen that relaxation pressure directly affects summed response during unloading. The unloading rate, dP/dt is the same but the end pressures are different in decompaction stage. Thus the duration of the decompaction rate decreases as relaxation pressure increases, resulting in less recovery during decompaction. The amount of recovery in relaxation stage also decreases as relaxation pressure increases. However, the change in decompaction stage is larger compared to relaxation stage.

The change in thickness versus relaxation pressure is shown in Figure 7-15b. Note that pressure input in the compaction and settling stages are the same. The differences in change in thickness between experiment sets are due to variation in the fabric, thus redundant. In decompaction and relaxation stages, it is seen that relaxation pressure affect the change in thickness significantly at lower pressures than higher pressures.

b. Woven fabric

The results for woven fabric is given in Figure 7-13. Woven fabric responds the change in P_{relax} similar to the random fabric. However, the thickness continues to decrease in Experiment Set 7 in woven fabric, which is not expected during unloading. The cause of this decrease is that, the decompaction stage starts right after wetting. It takes some time for fabric to stack during which thickness may continue to decrease even the compaction force is reduced as in Experiment Set 7. On the other hand, thickness increases during relaxation stage and summed response during unloading becomes positive as expected.

Figure 7-16b shows that increase relaxation pressure results decrease in change in thickness very similar to the random fabric. Settling stage is unaffected as expected but there is redundant variation in compaction stage. Again this should be discarded as the compaction pressure and applied pressure history input is the same during compaction stage.

7.3 Curve Fit Results

The results for the curve fits obtained through parameter estimation is tabulated in Appendix D.I. The weights for stages are taken as 1, 3, 5 and 10 for loading, settling, unloading and relaxation stages respectively. Curve fits are obtained by using the total duration of the first 7 stages of the characterization experiments (i.e. 1: minor loading; 2: dry loading; 3: dry settling; 4: wet unloading; 5: wet relaxation; 6: wet re-loading; and 7: wet re-settling). First, a curve is fitted for each experiment set separately and the corresponding model parameters are determined which minimizes the *error* as explained in Chapter 6. Then a single curve fit is found to fit all experiments, and this one is marked as "All" in the tabulated results.

It should be noted that the first 4 experiment sets have the remaining debulking stages (i.e. the remaining stages after the 7th stage mentioned above) which are not used during the curve fit. Using the model parameters determined, model response is extrapolated for the remaining stages for verification purpose. R^2 is calculated by comparing this extrapolated model result and the experiment set in the whole time domain. The determined model parameters are tabulated in Appendix D.II and corresponding curve fits are plotted in Appendix D.II presenting both thickness and strain versus time. In these figures, experimental results are shown with the mean values in dashed blue lines and standard deviation bounds with red dotted lines. The curve fits are shown with black continuous lines. Results of random fabric is given for each model followed by the woven fabric. For each model, two sets of figures are given: (1) curves fitted separately for each set, and (2) global fits which are obtained by fitting the curve to all experiment sets using a single set of parameters. In each case, both thickness and strain versus time are plotted.

As a sample of all results, the results of Zener model (the most commonly used model in the literature) for global fit to all random fabric experiment sets is shown in Figure 7-17 and Figure 7-18. The parameter estimation results are given below

$E_0 = 1.195e3$ kPa $\quad m_0 = 4.66$

$E_0 = 2.720e4$ kPa $\quad m_1 = 3.88$

$c_1 = 3.158e3$ kPa.s

The results of the remaining models are detailed in Appendix E.II.

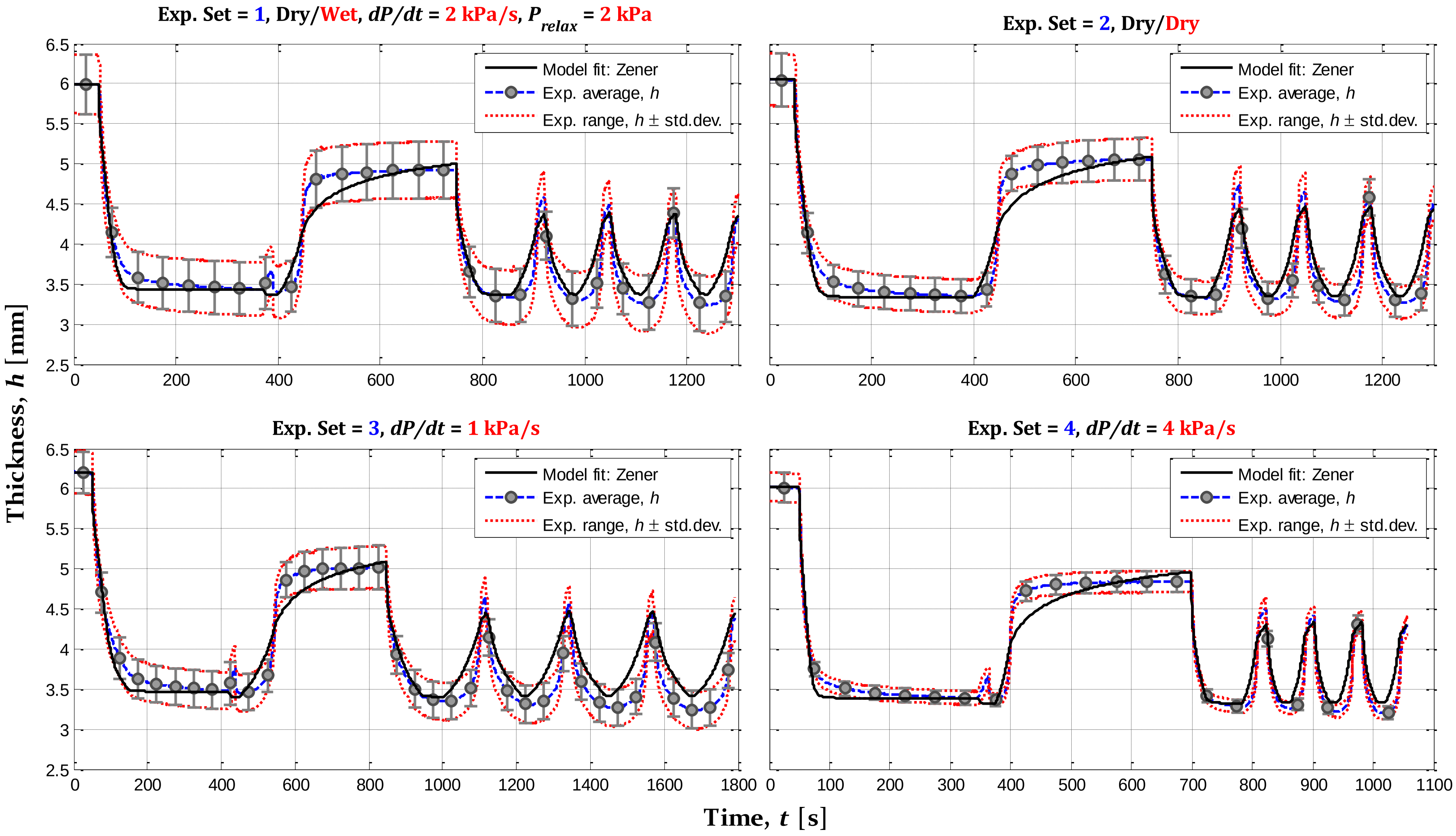

Figure 7-17. Thickness graph for Random fabric using *Zener model* fitted to all experiment sets using a single parameter set.

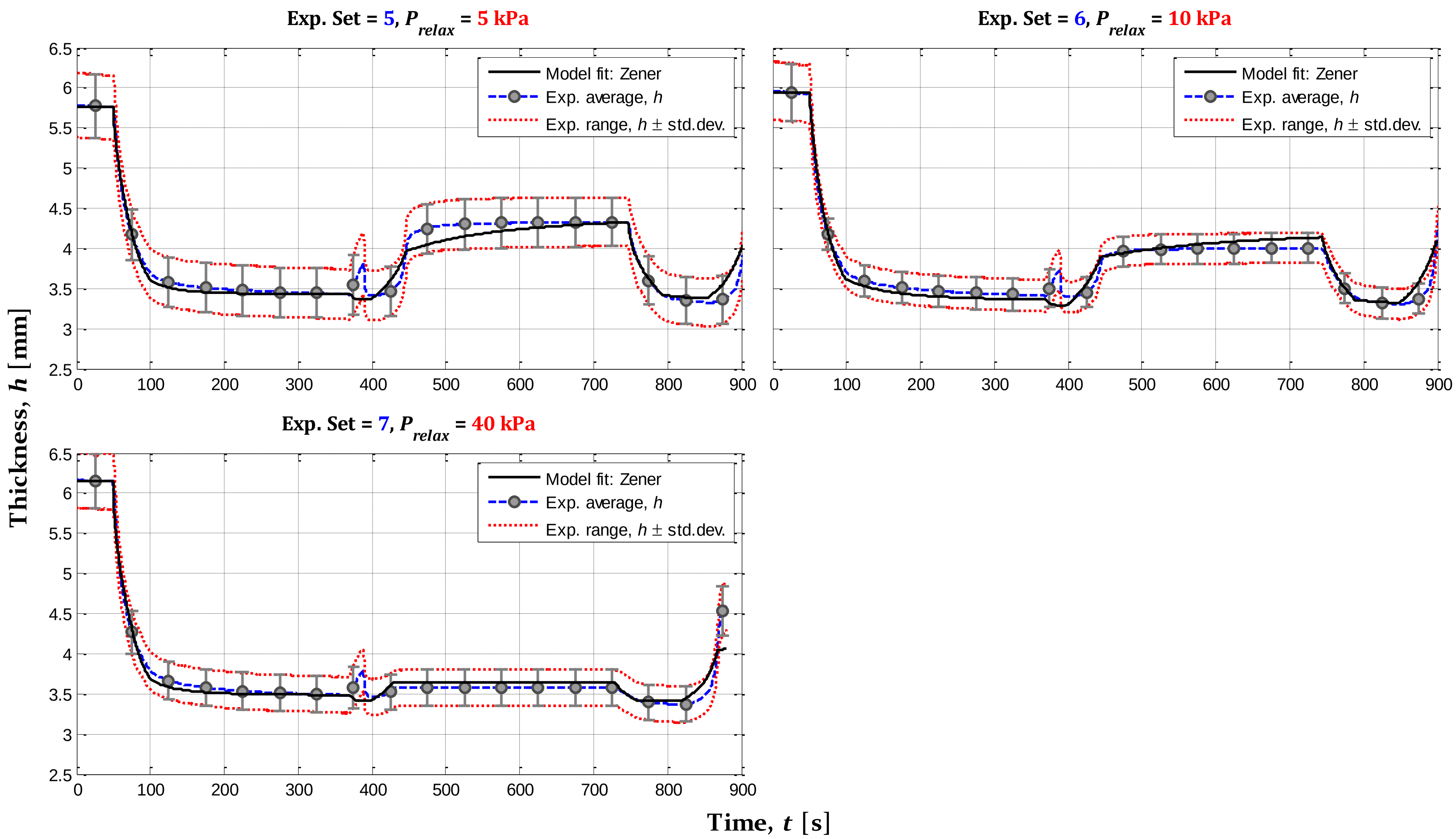

Figure 7-18. (cont.) Thickness graph for Random fabric using *Zener model* fitted to all experiment sets using a single parameter set.

8 Discussions & Conclusions

8.1 Performance of models in terms of R^2

In the results chapter, the fitted parameters and their corresponding R^2 are given for all models. These values are tabulated in Table 8-1 with models sorted in increasing parameter count. As the number of parameters increases, a model is expected to fit better in the cost of increased complexity of curve fitting. However, this may not be the case, and it will be investigated here.

The simplest two viscoelastic models are Maxwell and Kelvin-Voigt consisting of a single spring and a single damper. These two elements are in series and parallel configuration in Maxwell and Kelvin-Voigt models, respectively. There are 3 parameters, two of them are for the nonlinear spring and one of them is for the damper. By inspecting Table 8-1, it is seen that Kelvin-Voigt model has higher performance (i.e.

higher R^2) than Maxwell model. Thus, Kelvin-Voigt model should be used if low number of parameters are preferred.

As the number of parameters increases, R^2 value increases as expected. In practice, after 6 parameters, the performance stays the same or decreases depending on the fabric. This is mainly due to the increased complexity of the optimization problem. As the number of parameters increases, it is harder to find the globally optimum parameters. Instead of the global minimum, the optimization function may converge to a local minimum.

This is especially true for Generalized Maxwell models where the difference between models with n=2 and n=3 is an additional Maxwell element. The performance of the curve fit should increase in theory (or at least should not decrease), because if the 3 additional parameters are selected to be zero, the model should give the same performance. As these additional parameters are optimized, performance should increase. However, recall that during the optimization, one hundred randomly selected initial points are used to find the global minimum. It is still possible that none of these points may converge to the global solution. The number of initial points can be increased to overcome this problem in the cost of optimization time.

Table 8-1. Tabulated R^2 values for the viscoelastic models fitted to all experiment sets using a single parameter set.

Model	*# of parameters*	*R^2 for Random*	*R^2 for Woven*
Maxwell	3	0.874	0.736
Kelvin-Voigt	3	0.921	0.917
Zener	5	0.930	0.904
Burgers	6	0.962	0.942
G. Maxwell n=2	8	0.962	0.940
G. Maxwell n=3	11	0.961	0.922

Notice that Burgers and G. Maxwell n=2 give almost the same R^2 values for both random and woven fabric. Note that the two models have different configuration of springs and dampers and thus the characteristics of the models should be taken into account as detailed in Section 8.3.

8.2 Comparison between viscoelastic and elastic model

To show the advantage of viscoelastic over an elastic behavior, an elastic model with only a spring is used to fit its response to the base experiment (Experiment Set 1). The spring is selected to be nonlinear. As a result, there are two parameters (spring constant E and nonlinearity constant m) to optimize for the curve fit.

To be consistent, the same error function and weights are used in both viscoelastic and elastic model curve fits. First 7 stages are used during curve fitting and the rest is used to confirm the curve fit (the same as in the viscoelastic model fits). The optimum parameters and resulting curve fits are given in Appendix E.

The elastic model fails (i.e. the model response deviates from the experimental data) especially at low pressure values after the first compaction stage. This is due to the plastic deformation of the fabric. After the unloading stage, the compaction pressure decreases to the initial value (minor loading value). However, thickness value does not recover its original (initial) value. For example, h of random fabric at the end of unloading stage is approximately 1 mm thinner than the original (initial) value. An elastic model does not have an ability to model this response with a permanent plastic deformation. In the literature, different model constants are used to overcome this problem. A different set of constants are used for the dry region of the fabric (not initially compacted) and another one for the wet region (fully compacted under major pressure and lubricated). Since the wetting takes place after settling, the plastic deformation caused by both compaction and lubrication is accounted for with this approach. However, notice that even the elastic model is simpler than viscoelastic model, 4 parameters are required for this approach and a discontinuity occurs at dry/wet transition which increases complexity for embedding in a simulation package.

8.3 Modeling of plastic deformation

The comparison of the models can be made by using only the results of the curve fits presented Appendix D. To understand why some models behave differently than the others, the spring-damper configuration must be known.

Maxwell and Burgers models show a linear strain response during the settling stage which results in an infinite strain if the time goes to infinity. That means there is no steady state value for settling; this certainly does not represent the actual compaction nature of the actual fabric specimens which settle at a finite value after a while. The rest of the models give a converging settling response (i.e. the strain and thickness converges to a finite value as the time goes to infinity). Recall that the model configurations are summarized in Figure 4.13, and suggested to review that figure to understand the differences between the model responses. In both Maxwell and Burgers models, there is a damper serially connected to the main branch of the models. As mentioned before, this damper models plastic deformation. The continuously decreasing thickness in the settling stage is a result of this damper in these models.

During the VI process, a fabric specimen undergoes plastic deformations during both the first compaction stage (due to necking) and wetting stage (due to lubrication). The effect of lubrication is measured using the data obtained from Experiment Set 8, where the fabric is kept under the same load after wetting. The plastic deformation due to necking can be seen in Figure B-1 (from the experimental result of Set 2 where the fabric is kept dry). In relaxation stage, it is seen that the fabric reached an almost steady value at the end of relaxation, but still compacted about 1 mm more compared to its initial thickness. This clearly suggests that fabric is deformed plastically between these stages. One may argue that if the specimen is kept under relaxation for infinite time, then it may recover fully. However, within typical VI processing durations (in the order of several hours or shorter), this is not the case as seen in [2,18] and here.

The plastic deformation due to wetting is modeled as an increase in strain for all models. The plastic deformation due to nesting is modeled truly only by Maxwell and Burgers models. This explains the good fit and thus high R^2 value of Burgers model which is comparable to G. Maxwell with n=2 value although Burgers model has 2 lower number of parameters than G. Maxwell with n=2. The rest of the models try to mimic plastic deformation with very viscous (slow) response and highly nonlinear springs (i.e. their m is higher). As m increases, the spring force becomes very small in low compaction pressures. Because the balancing force is small, it takes very long time for the system to reach a steady state value, which is basically zero strain in zero relaxation pressure.

Due to these two distinct ways of modeling of plastic deformation, viscoelastic model should be selected depending on the application as explained below. Prolonged settling stages may result in overestimating the compaction with Burgers and Maxwell model. On the other hand, prolonged relaxation stages with Kelvin-Voigt, Zener and G. Maxwell models can overestimate relaxation. Also, a characterization experiment should be carefully set depending on the application.

Notice that plastic deformation occurs linearly with time during the settling stage in Maxwell and Burgers models. If Maxwell or Burgers model is preferred, settling stage duration in characterization must be comparable to the duration expected in the simulation. In experiments, the amount of plastic deformation does not differ much (i.e. $\Delta\varepsilon_{plastic}$ is almost constant) when the settling duration is in the order of minutes to hours as previously studied in [1,2,18]. If $\Delta t_{settling}$ used in a model is very different than in the characterization, the model can over or underestimate $\Delta\varepsilon_{plastic}$.

8.4 Physical Significance of Parameters

As the complexity of the compaction model increases, the response of each individual element cannot be predicted easily. To see the effects clearly, each parameter of the five models is perturbed -50, -25, 0, 25 and 50% from its optimal result, and the corresponding cases are labeled as k = 0.50, 0.75, 1.00, 1.25 and 1.50 indicating the ratio of the parameter value and its optimal result found earlier. The resulting response graphs are given for the base experiment (Experiment Set 1) from Figure 8-1 to Figure 8-5.

8.4.1 Maxwell

Recall that in Maxwell model, the damper models the plastic deformation. In Figure 8-1, it is seen that the perturbation in c changes the thickness at the relaxation stage, which supports this statement. E and m affect the elastic part of the model. This is seen by observing that amounts of compaction/decompaction vary as k varies in E and m, but not in c.

8.4.2 Kelvin-Voigt

In Kelvin-Voigt model, there is a single spring, which models the elastic part, and a single damper, which models the viscous part of the response. c affects the relaxation stage only (where the viscous effect is dominant) in this model, whereas it affects the amount of plastic deformation in Maxwell model. The same reasoning can be done for E and m in the two models.

8.4.3 Zener

By investigating Figure 8.3, the parameters of parallel spring E_0 and m_0, which models the elastic part, is dominant in response. The effect of m_1 is significant during the unloading to relaxation transition. An increase in m_1 results in sharper transition. c_1 determines how fast the model converges in relaxation stage similar to Kelvin-Voigt model.

8.4.4 Generalized Maxwell

In Figure 8.4 and Figure 8.5, $n = 2$ which means there is an extra Maxwell element connected in parallel in comparison to the Zener model. Notice that E_0 and m_0 are similar in response to E_0 and m_0 of Zener model. However, viscous response is divided into two branches. E_1, c_1 and m_1 do not only affect relaxation stage, but also the settling stage. On the other hand, E_2, c_2 and m_2 result in similar response as E_1, c_2 and m_1 in Zener model but with less effect (compare Figure 8.3 and 8.5).

8.4.5 Burgers

Recall that the spring (with parameters E_1, m_1) and damper (with parameter c_1) in this model are connected serially which in fact forms a Maxwell model. The second spring (with parameters E_2, m_2) and second damper (with parameter c_2) are connected in parallel forming a Kelvin-Voigt model. Then, these two parts are connected in series resulting in a viscoelastic model that can both model plastic deformation and stress relaxation.

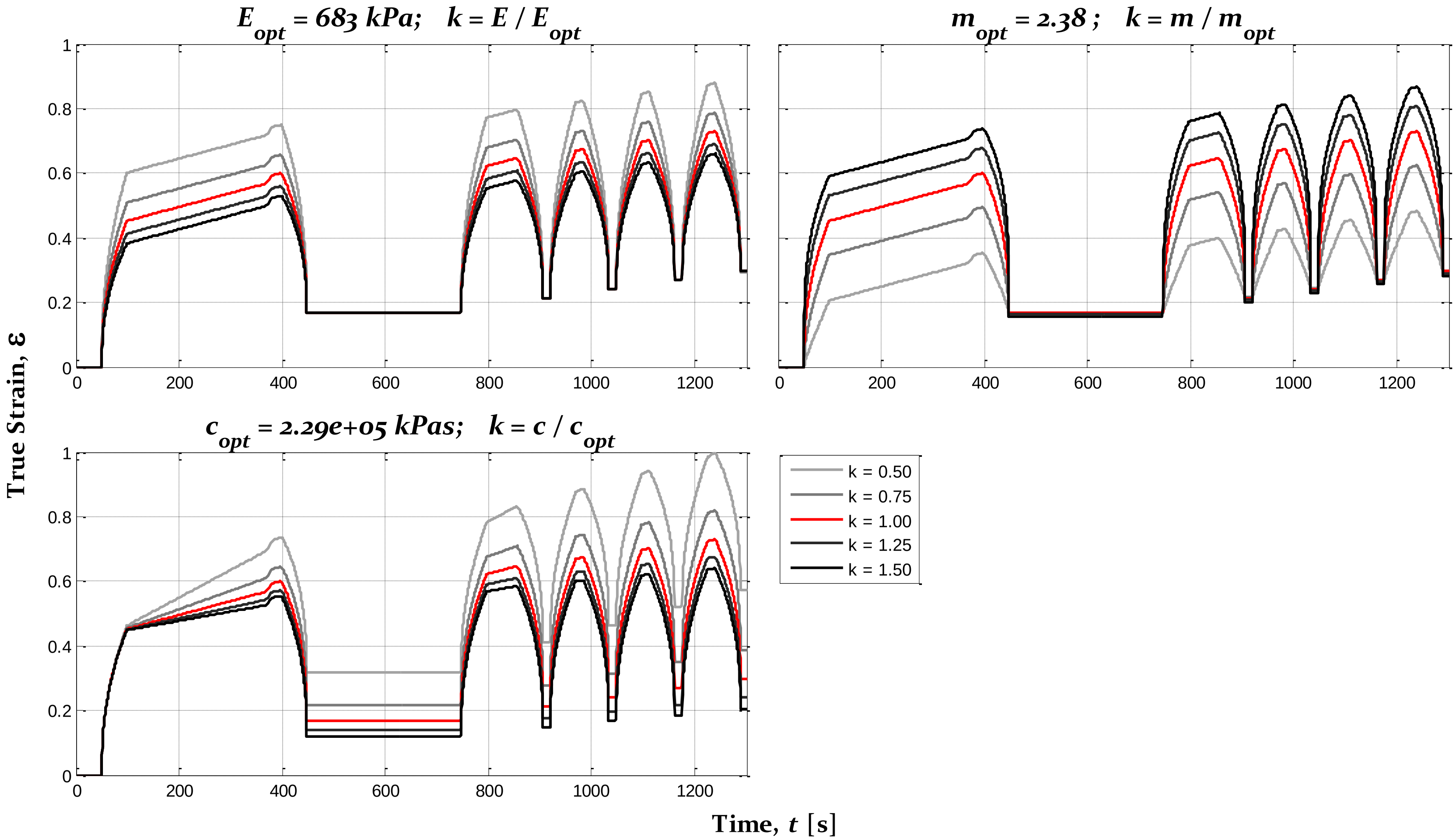

Figure 8-1. The effect of each parameter in Maxwell model for the base experiment.

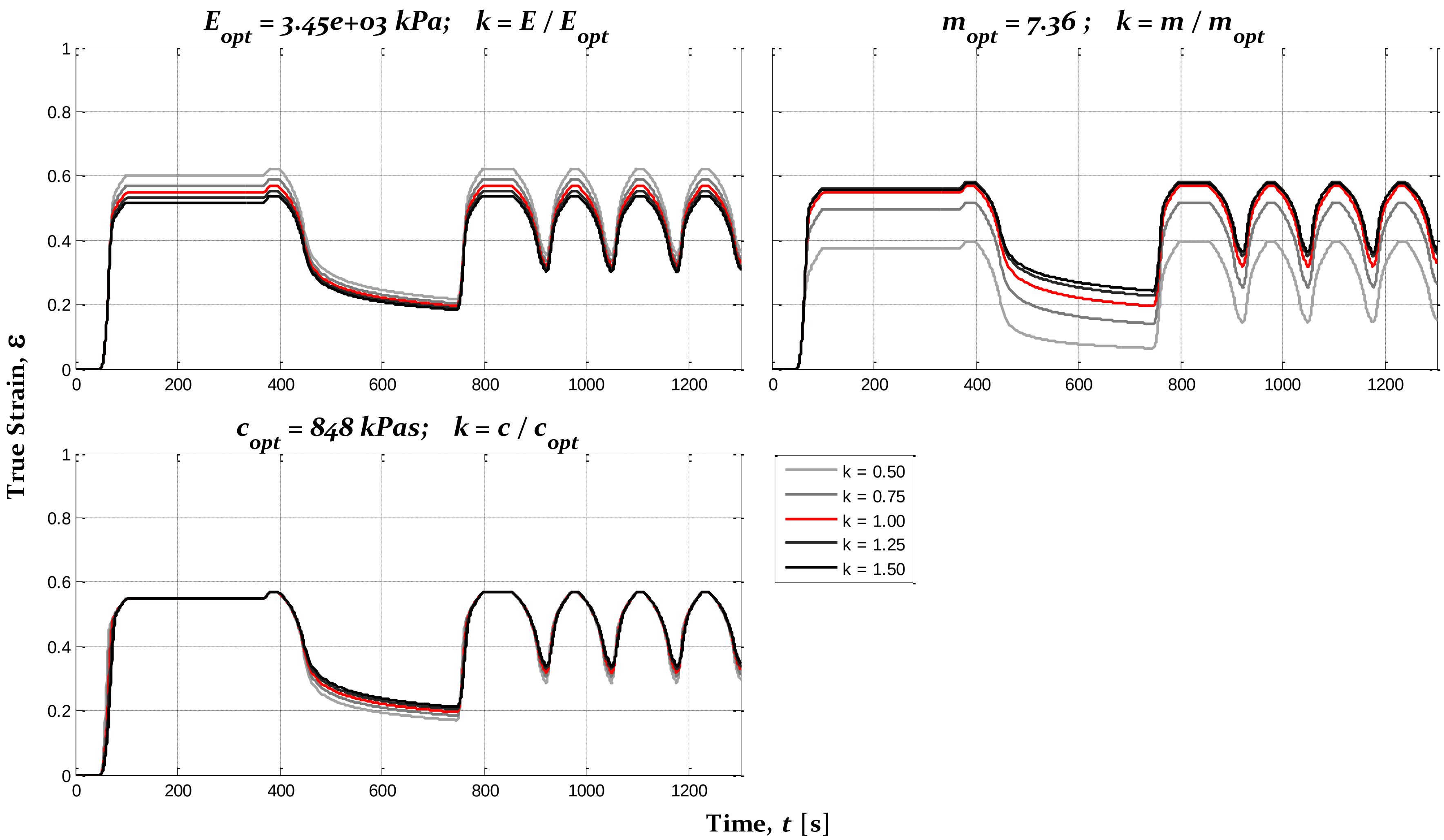

Figure 8-2. The effect of each parameter in Kelvin-Voigt model for the base experiment.

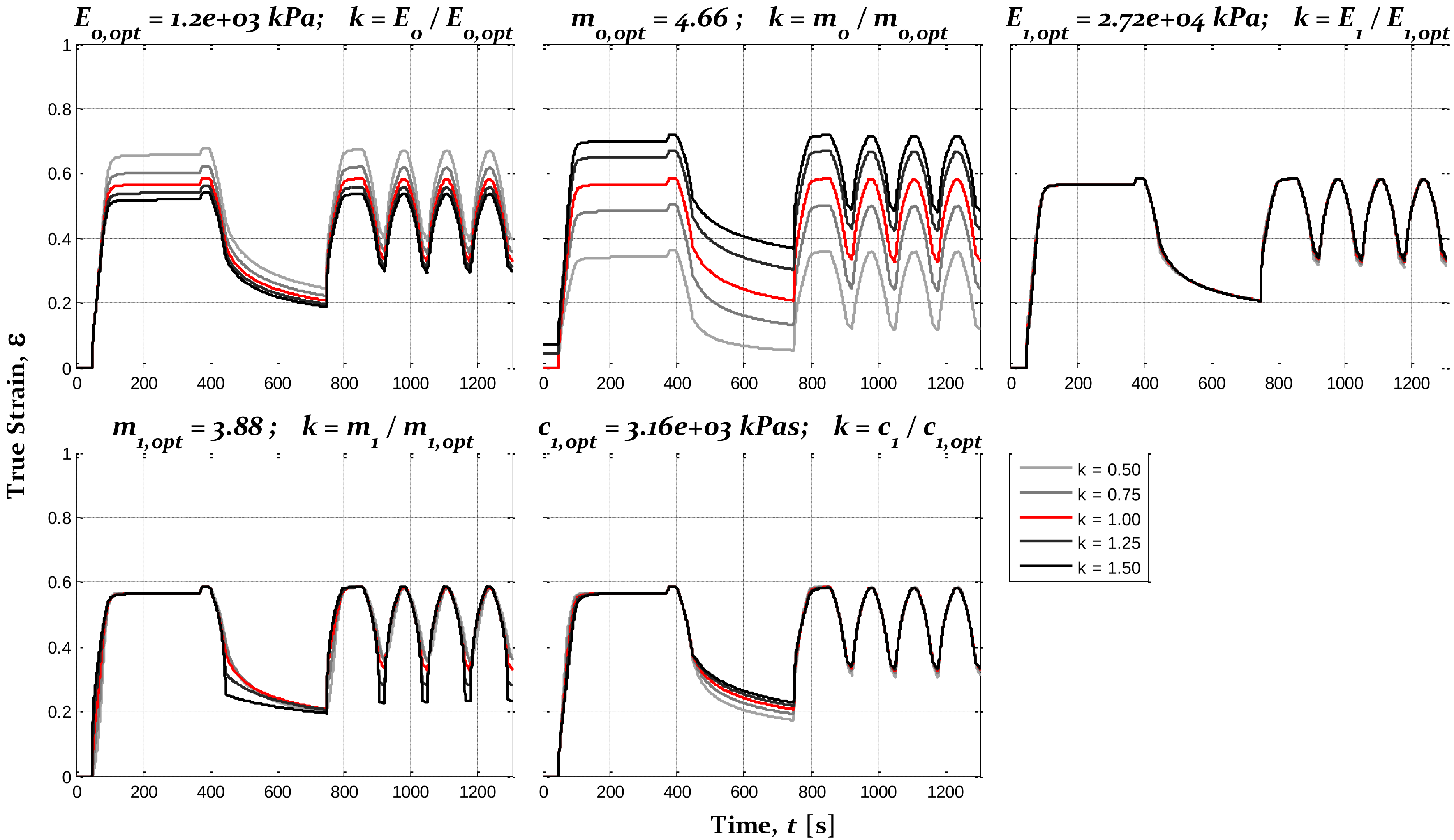

Figure 8-3. The effect of each parameter in Zener model for the base experiment.

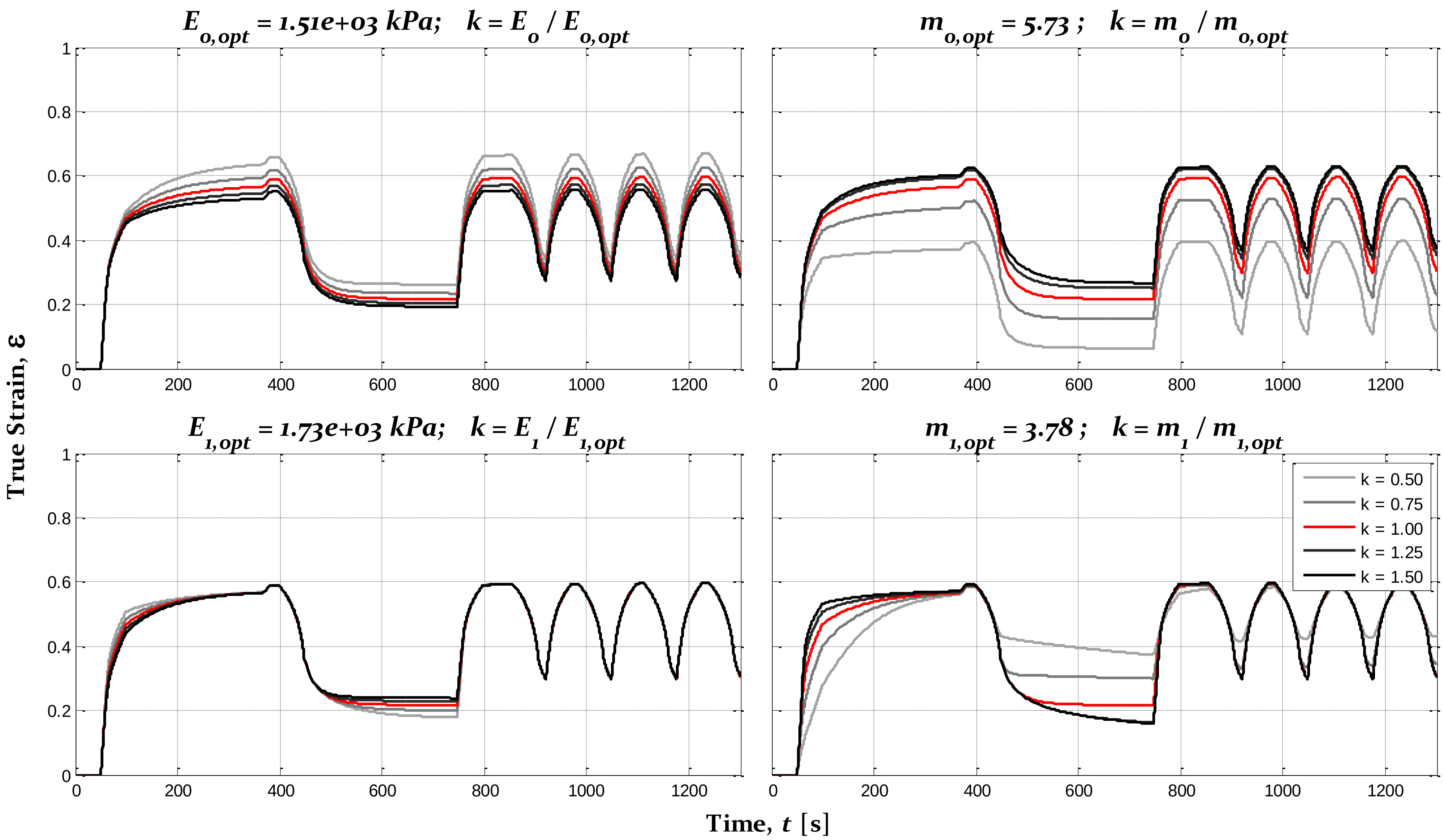

Figure 8-4. The effect of first four parameter in Generalized Maxwell (n=2) model for the base experiment.

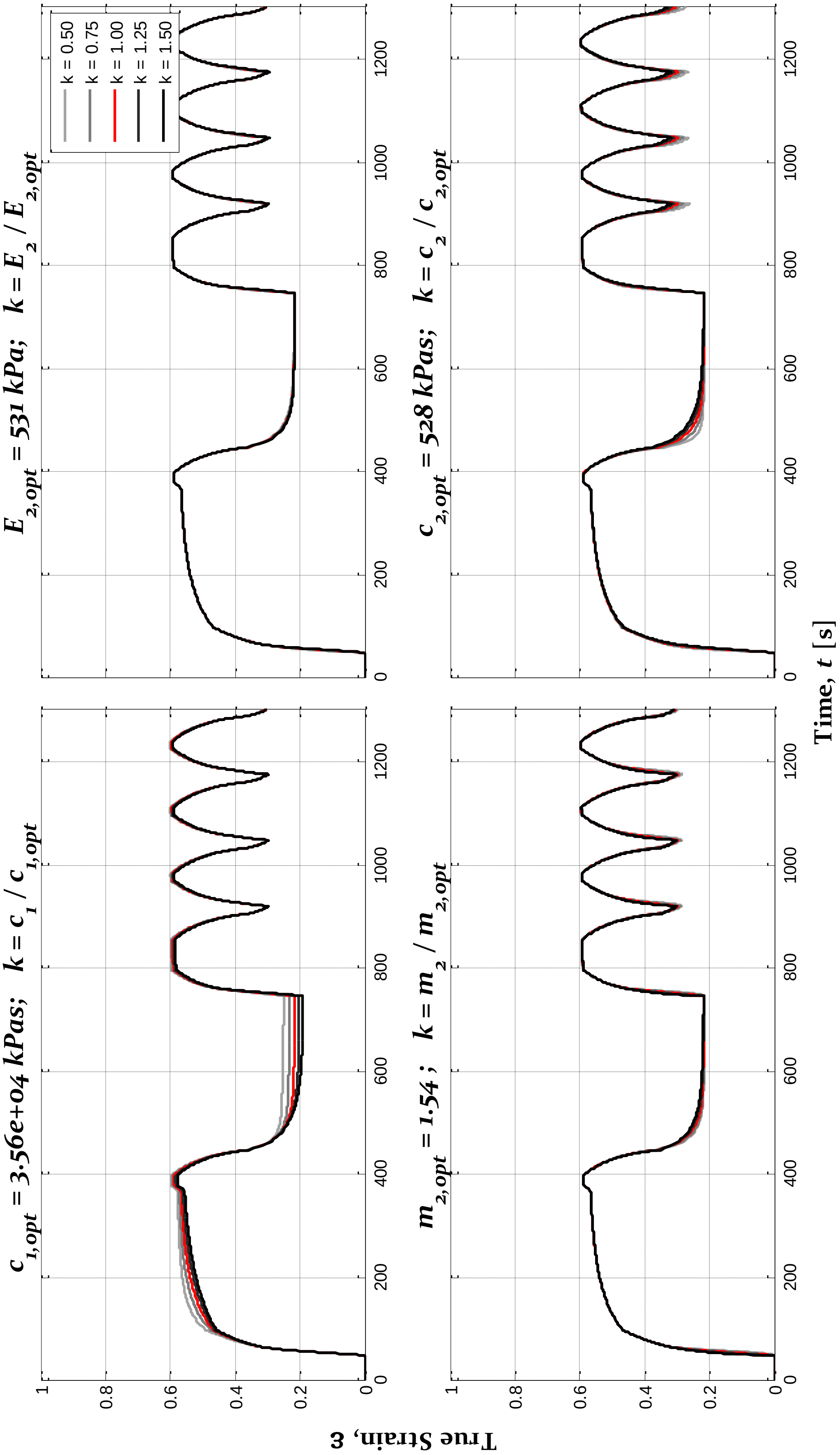

Figure 8-5. The effect of last four parameter in Generalized Maxwell (n=2) model for the base experiment.

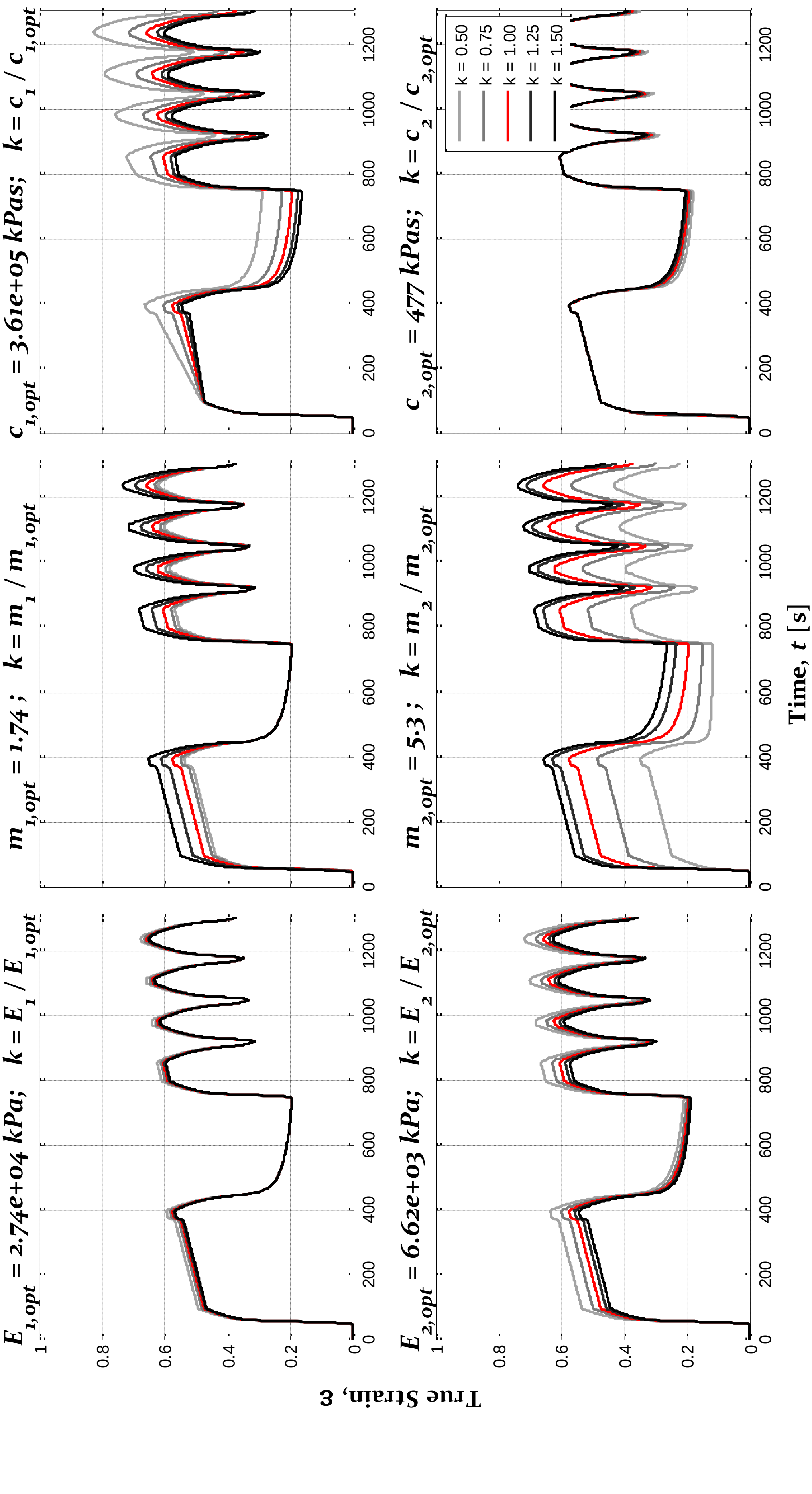

Figure 8-6. The effect of each parameter in Burgers model for the base experiment.

The perturbation in c_1 (see Figure 8.6) results in a change in the amount of plastic deformation. Spring constants E_1, m_1, E_2, m_2 all affect the amounts of compaction and decompaction. Similar to Kelvin-Voigt model, c_2 models the relaxation part. The spring in parallel part (i.e. Kelvin-Voigt element) has dominance over spring in series part (i.e. Maxwell element).

8.5 Sensitivity analysis

In the previous section, the model parameters are perturbed to show their effects on the model response by visually comparing the results. In this section, sensitivity of the model on each parameter is examined by calculating R^2 for the following five cases. (1-4): each of the four stages separately (loading, unloading, settling, relaxation) in repeated compaction cycles, and also (5) for the whole experiment. Sensitivity graphs are given in Figure 8-7 to Figure 8-11. R^2 is chosen to show the performance of the model fit instead of *error* definition used during fitting, because it is a commonly used and well known error measure in the literature.

In some of these figures, the optimal solution (corresponding to the maximum R^2) is not exactly at $\delta = 0$ where δ is the percentage perturbation on any model parameter. Note that k used in the previous section and δ related as follows: $k = 1 + 0.01\delta$.

Note that these figures use classical R^2 axes rather than the *error* function used in the parameter estimation. The *error* function uses different weights for each stage to make the curve fit suitable for the VI process. Hence, plots obtained by taking only some stages into account or taking all stages with a constant weight ($w_i = 1$) may result in a different optimal solution.

8.5.2 Loading stage

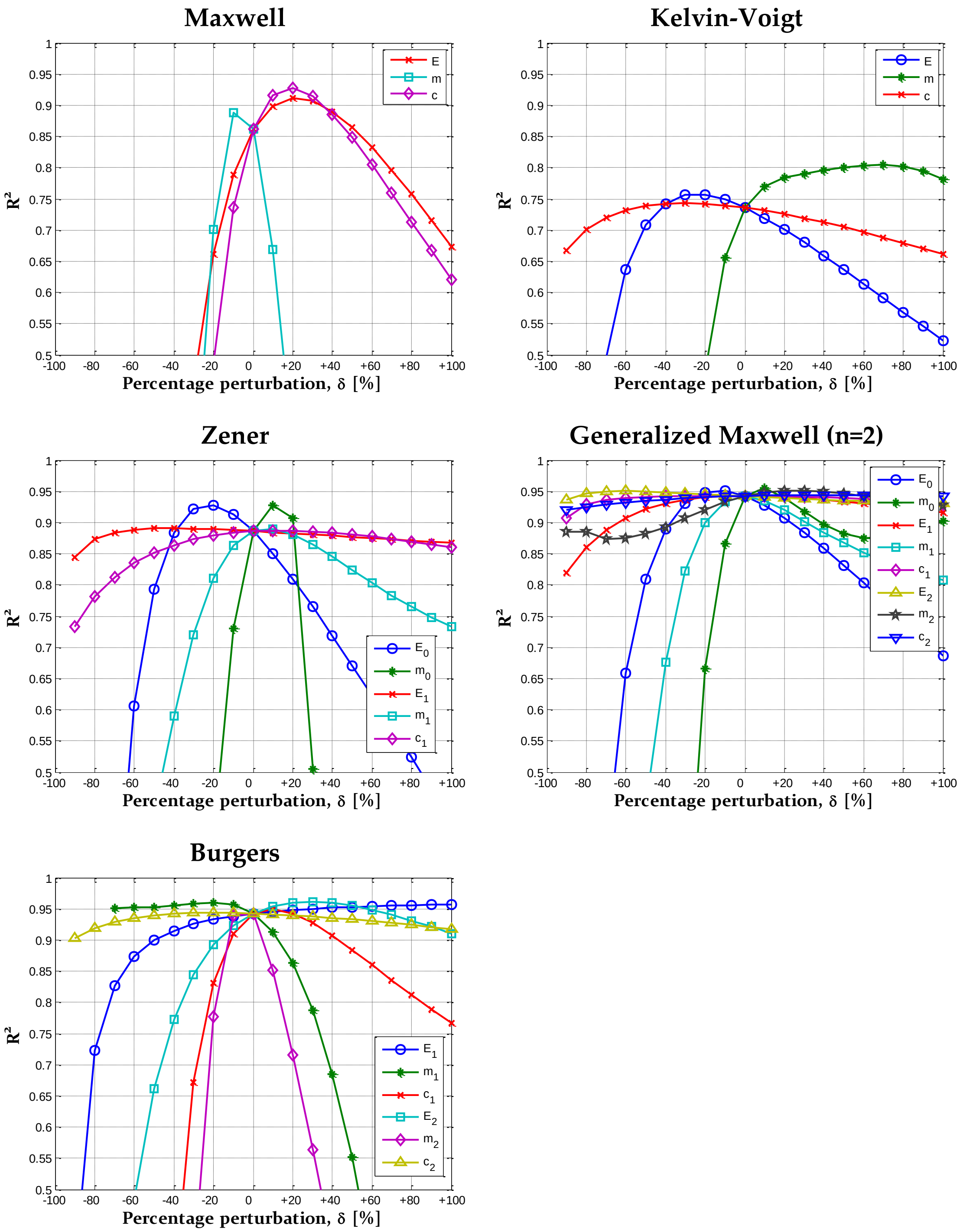

Figure 8-7. Effect of δ on R^2 for each parameter calculated only on loading stages.

From the sensitivity point of view, the following conclusions can be reached.

Maxwell:

- m is the dominant parameter. That means, R^2 is affected (deviates from the optimal value) the most when m is perturbed compared to the other parameters.

- The value of c is larger than the ones in the other models as a result of series connection and hence has comparable sensitivity effect with E.

Kelvin-Voigt:

- Dominant parameters are E and m.

Zener:

- The parallel spring is dominant (m_0 and E_0).
- In Maxwell element, m_1 has more effect than the other 2 parameters: E_1 and c_1.

Generalized Maxwell (n=2):

- Parallel spring and first Maxwell element are very similar to the Zener model.
- 2nd Maxwell element has less effect compared to 1st.
- Each additional Maxwell element is expected to improve result (results in a better curve fit and thus higher R^2), but with smaller contribution compared to the previous element.

Burgers:

- The model is sensitive to all parameters comparably except c_2.
- Comparable contribution to model behavior means an efficient model.

8.5.4 Settling stage

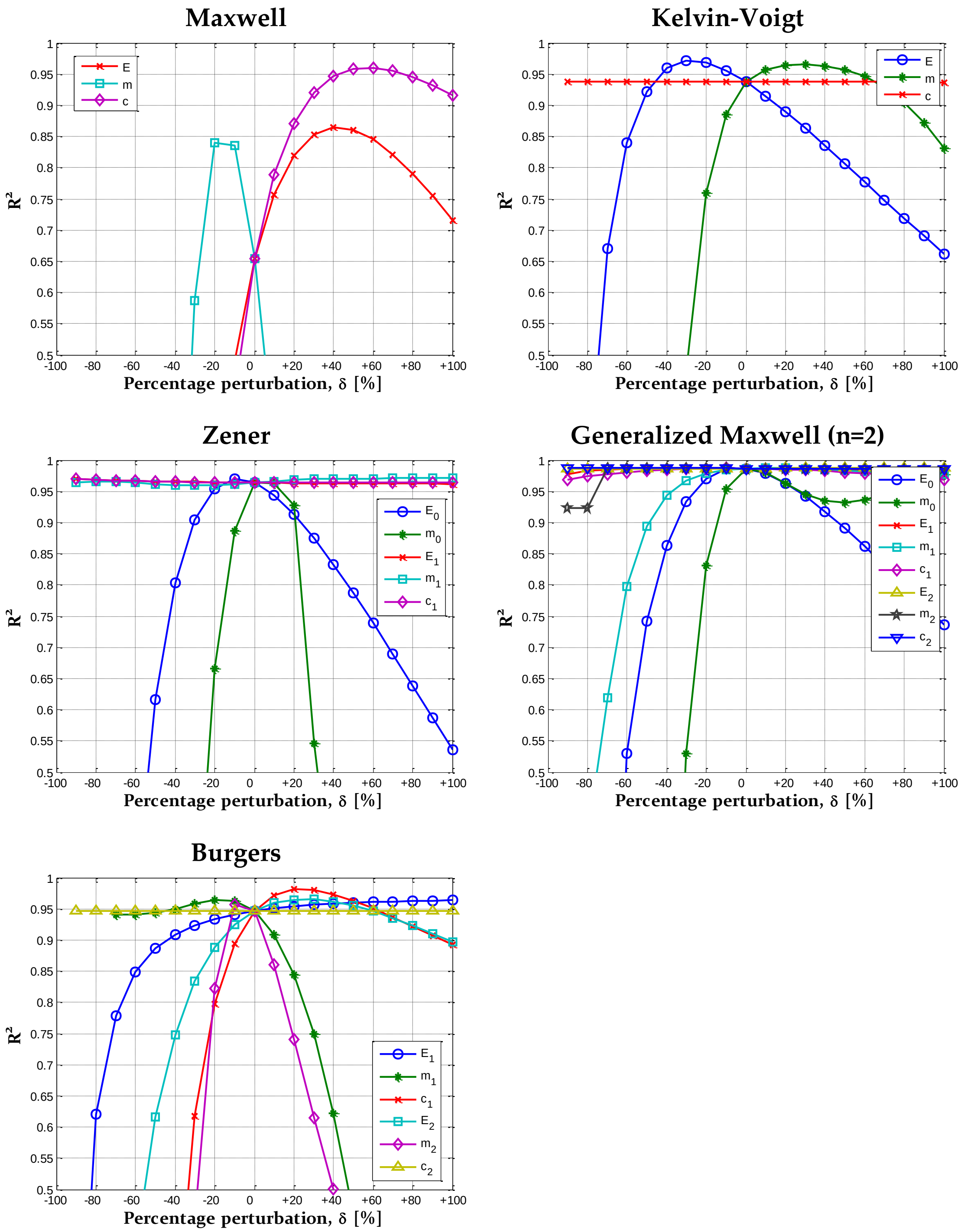

Figure 8-8. Effect of δ on R^2 for each parameter calculated only on settling stages.

Maxwell:

- Sensitivity is very similar to the loading stage.
- Perturbation on all parameters result in significantly higher R^2 in this settling stage. This can be explained as follows. The optimal parameters for the complete

cycle is more affected by the other stages than settling. In other words, if one is interested in modeling of the settling stage only, it is suggested to curve fit this stage only.

Kelvin-Voigt:

- c has no effect in this stage since this model cannot model settling (i.e. model settles very quickly to steady value).

Zener:

- Parameters of the Maxwell element has no effect due to quick settling (similar to K.V. model).

Generalized Maxwell (n=2):

- Only the first Maxwell element contributes to the settling stage, additional Maxwell element has almost no effect.

Burgers:

- Very similar to the loading stage.

8.5.6 Unloading stage

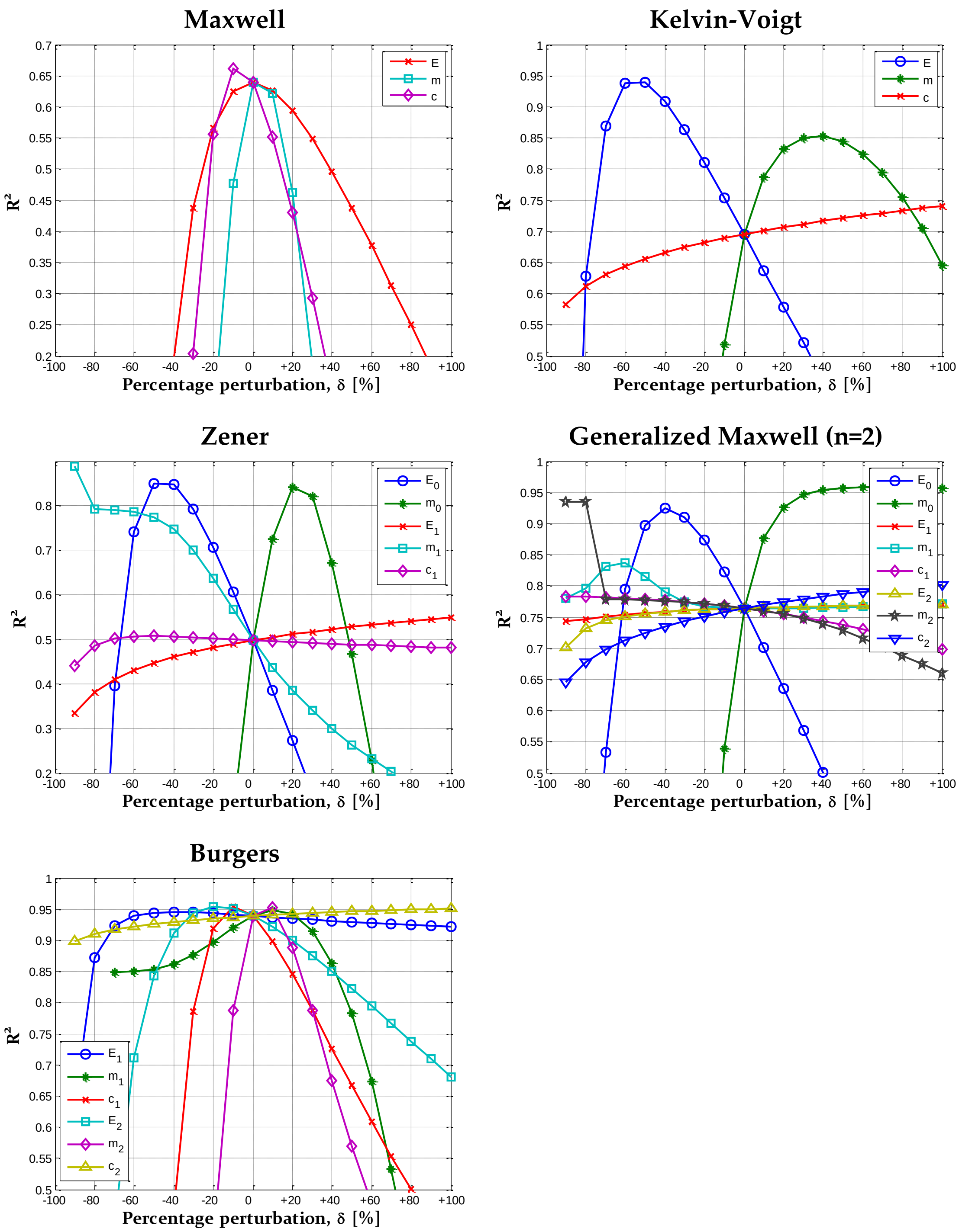

Figure 8-9. Effect of δ on R^2 for each parameter calculated only on unloading stages.

Maxwell & Burgers:

- All parameters' sensitivities are very comparable with each other in each model.
- Notice that, only these two models' R^2 are close to maximum around $\delta = 0$.

Kelvin-Voigt:

- Perturbation on all parameters result in significantly higher R^2 in this unloading stage.
- E and m are dominant during unloading since they model the elastic response.

Zener:

- Similar to Kelvin-Voigt model, perturbation on all parameters result in significantly higher R^2 in this unloading stage.
- All parameters except c_1 affect R^2 significantly.

8.5.8 Relaxation stage

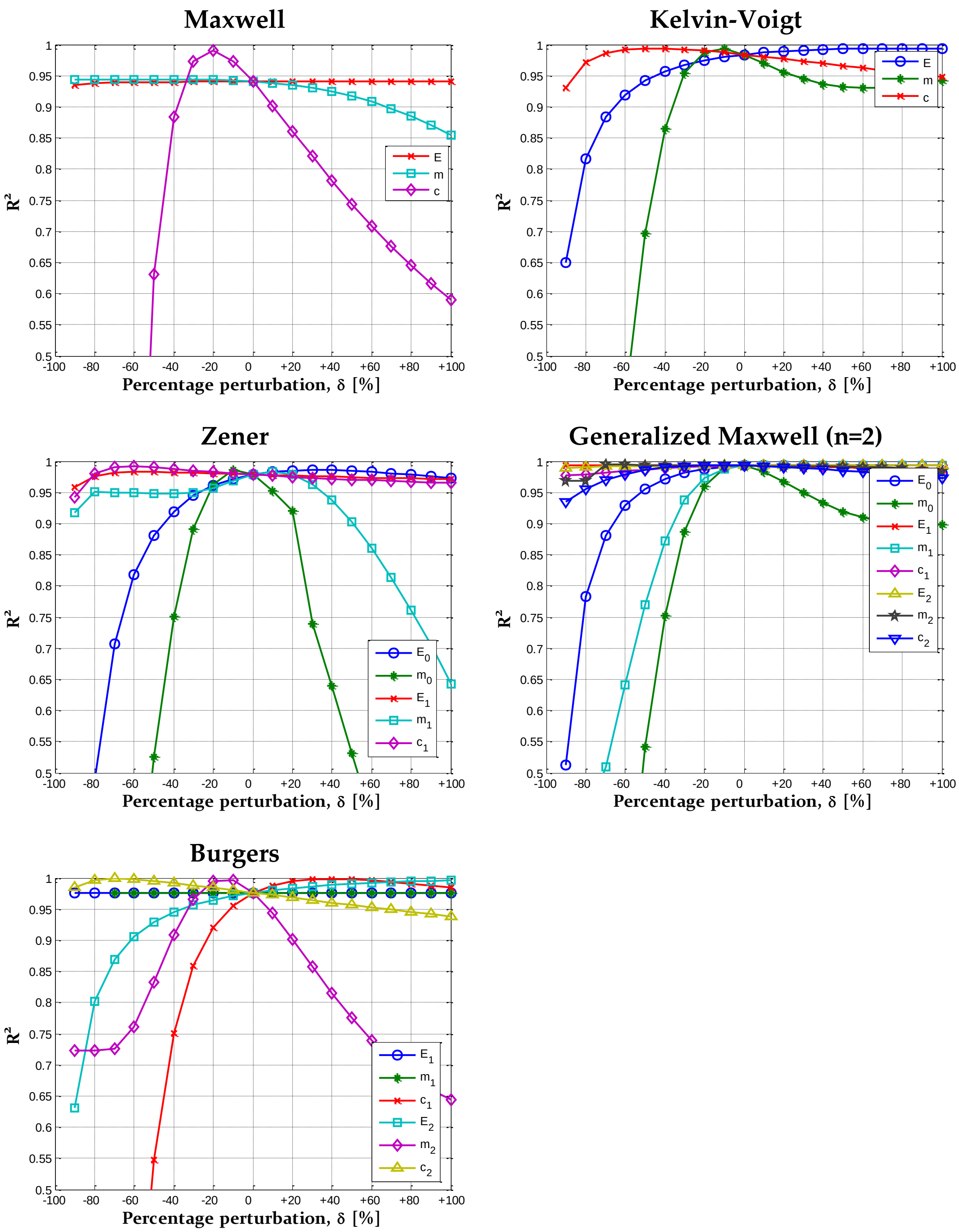

Figure 8-10. Effect of δ on R^2 for each parameter calculated only on relaxation stages.

Note that this stage has the highest weight during parameter estimation, hence R^2s of the models are expected to be highest at this stage.

Maxwell:

- Viscous component c has the highest sensitivity contribution to the response.
- Perturbation on c results in significantly higher R^2.

Kelvin-Voigt & Zener & Generalized Maxwell (n=2):

- Unexpectedly, elastic components are still dominant over the viscous components in relaxation stage.

Burgers:

- E_1 and m_1 have almost no effect, and c_2 has small effect during this stage.
- c_1 and m_2 are the main components that dominate response during relaxation stage.

8.5.9 Entire experiment

When all stages are considered, the trend is not very different than individual stages.

Although the complexity of a model increases as the number of elements and thus the parameters increase, Figure 8.11 suggests that some parameters are not dominant (i.e. R^2 is not affected significantly when the parameters are perturbed). In other words, the elements corresponding to these parameters can be removed and still almost the same quality of fit and thus R^2 can be achieved. For example, the second Maxwell element in G. Maxwell model can be removed to simplify it to a Zener model with no significant loss in the quality of the fit. Similarly, c_2 in Burgers model can be removed to decrease the number of parameters.

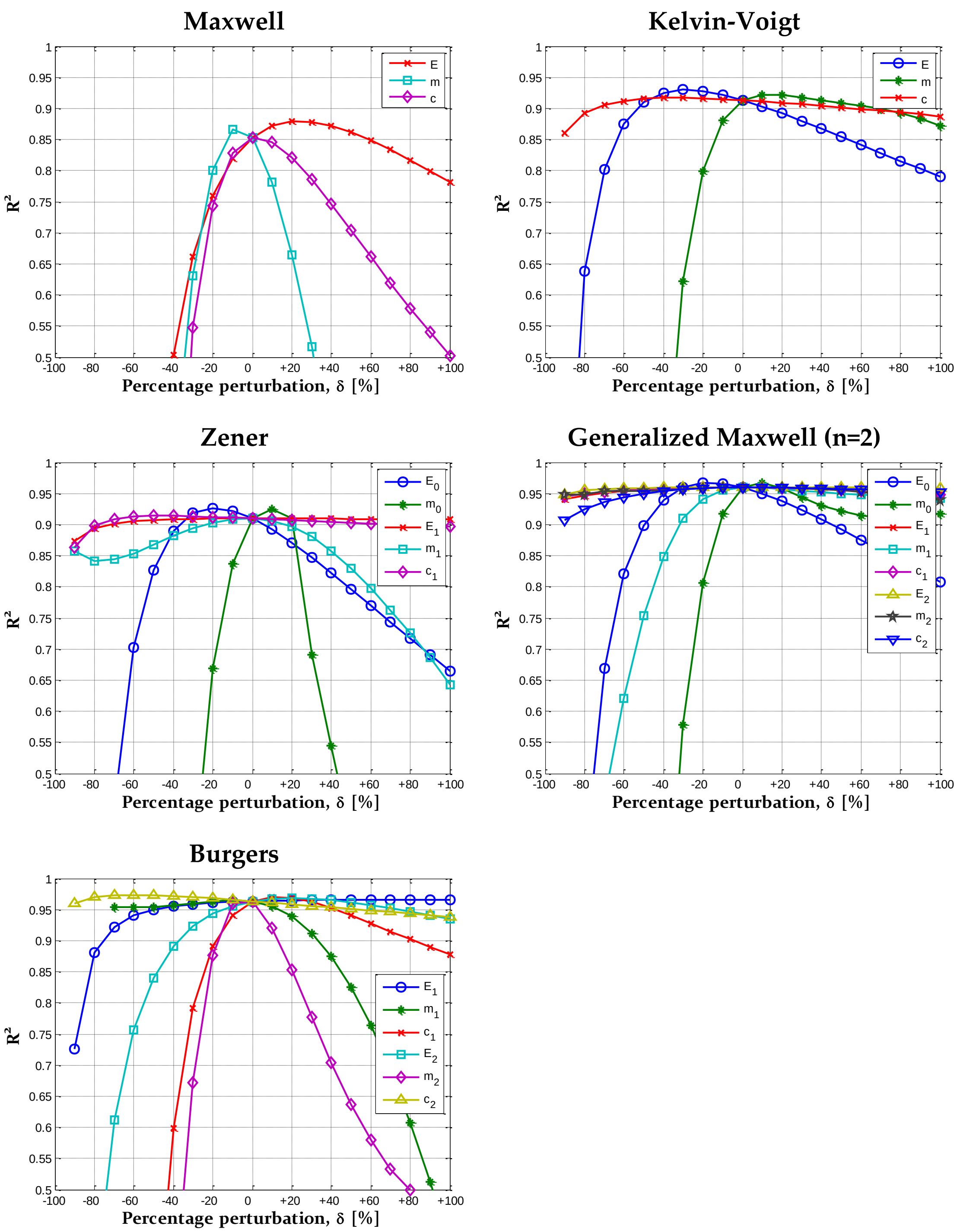

Figure 8-11. Effect of δ on R^2 for each parameter calculated for the entire experiment.

8.6 Conclusions

Viscoelastic models have advantage over elastic models since they have the ability to model the time dependent compaction response of the fabric. Since the fabric undergoes significant change in thickness with time even at constant pressure especially during relaxation stage, approximating with elastic models greatly decreases the accuracy of the VI simulation. With viscoelastic models, it is possible to model both filling and post filling stages of the VI process with a greater accuracy than with elastic models. With this increased accuracy, not only filling time and final thickness profile can be estimated correctly, but also excess resin amount can be minimized.

In this study, the compaction characterization of fabric preforms are done using five different viscoelastic models. Only two of these models (Kelvin-Voigt and Zener) were previously used in the composite literature for compaction characterization and only with linear springs. By using more complicated models and nonlinear springs, it is shown that fabric behavior can be modelled much better.

Two different fabric types (random and woven) have been studied. Specimens are prepared by stacking 8 layers. Fabric specimens undergo a predefined compaction cycle using an automated setup. Different sets of experiments are conducted by varying the relaxation pressure, compaction/decompaction rate and saturation (i.e. dry or wet).

Five viscoelastic models (Maxwell, Kelvin-Voigt, Zener, Generalized Maxwell and Burgers) are fitted to the experimental data by repetitively modifying parameters to reduce the custom error function. The custom error function calculates the error stage by stage first by normalizing (down-sampling data for each stage to 100 points) then by multiplying with a user defined weight. Applying the weight after normalizing allows a user to use the same weights for different experiment sets having different stage durations. For the curve fit, an initial estimate for the parameters are used, and the next guess is obtained by evaluating system equation and feeding the resulting error to the optimization function. Once the parameters are found, fitted curves and experimental data are presented on the graph with classical fit performance criteria R^2. It is seen that if more experiment sets are used to obtain a single set of parameters, extrapolated data become more accurate.

The effect of each parameter of the model on the model response is investigated by adding a perturbation to the optimal solution. The results of perturbations are shown both graphically and numerically using R^2. These results show that the models can be further improved for a specific stage if full VI simulation is not required.

It is seen that Burgers model outperforms other 4 models in terms of the parameter count and R^2 (0.962 for random and 0.942 for woven fabric) of the fitted curves. Generalized Maxwell model (when $n = 2$) has the same R^2 value (0.962 for random and 0.940 for woven fabric) but has 2 more parameters than Burgers model. This is the ability of Burgers model to simulate the plastic deformation. However, Burgers model undergoes infinite deformation at constant load, which is not physically correct. Hence, Generalized Maxwell model with $n = 2$, which mimics the plastic deformation with slow viscous response, should be used if prolonged time of settling is expected in simulation.

The viscoelastic models used in this study do not include any discontinuous element such as elements with hysteresis, thus these models can be embedded in classical VI simulation software for more accurate flow and thickness profile modeling.

This study contributes to the composite manufacturing literature with the following achievements: (1) a compaction characterization procedure is designed to mimic the compaction behavior of fiber reinforcements used in VI; (2) an automated characterization experimental setup is constructed to reduce human error and increase the repeatability; (3) experimental characterization data allows to have a database for two fabric types (random and woven); (4) five viscoelastic compaction models (Maxwell, Kelvin-Voigt, Zener, General Maxwell and Burgers) and an elastic compaction model are used to investigate different stages of VI; (5) comparison of the models allows to study the contribution of different elements of the compaction models and thus understand their physical responses in different stages. By coupling a resin flow model and a viscoelastic compaction model (preferably Generalized Maxwell with n=2 or Burgers depending on which stage(s) of VI is desired to be modeled) in a complete VI process model, it is possible to simulate more accurate gradual pressure and thickness changes with time during the application of control actions in VI post-filling stage.

Elastic models fail in these situations because they cannot model time dependent response, and thus viscoelastic models of this study should be preferred.

Bibliography

[1] Yenilmez B, Senan M, Sozer EM. Variation of part thickness and compaction pressure in vacuum infusion process. Compos Sci Technol 2009;69:1710–9.

[2] Yenilmez B, Sozer EM. Compaction of e-glass fabric preforms in the Vacuum Infusion Process, A: Characterization experiments. Compos Part A Appl Sci Manuf 2009;40:499–510.

[3] Senan M. Monitoring of Part Dimensions and Fiber Content in Vacuum Assisted Resin Transfer Molding (VARTM) Process. Koc University, 2007.

[4] Yang J, Xiao J, Zeng J, Jiang D, Peng C. Compaction Behavior and Part Thickness Variation in Vacuum Infusion Molding Process. Appl Compos Mater 2011;19:443–58.

[5] Li J. Modeling, design and control of vacuum assisted resin transfer molding (vartm) for thickness variation reduction. Florida State University, 2006.

[6] Tackitt K, Walsh SM. Experimental Study of Thickness Gradient Formation in the VARTM Process. Mater Manuf Process 2005;20:607–27.

[7] Grimsley BW, Song X, Hubert P, Cano RJ, Pipes RB, Loos AC. Flow and compaction during the vacuum assisted resin transfer molding process. Int. SAMPE Tech. Conf., vol. 33, Citeseer; 2001, p. 140–53.

[8] Grimsley BW. Characterization of the Vacuum Assisted Resin Transfer Molding Process for Fabrication of Aerospace Composites. Virginia Polytechnic Institute and State University, 2005.

[9] Song X. Vacuum assisted resin transfer molding (VARTM): model development and verification. Virginia Polytechnic Institute and State University, 2003.

[10] Luo Y, Verpoest I. Compressibility and relaxation of a new sandwich textile preform for liquid composite molding. Polym Compos 1999;20:179–91.

[11] Parnas RS, Walsh SM. Vacuum-assisted resin transfer molding model. Polym Compos 2005;26:477–85.

[12] Loos AC. RESIN INFUSION OF LARGE COMPOSITE STRUCTURES MODELING AND MANUFACTURING PROCESS. Proc. 27th Risø Int. Symp. Mater. Sci., Roskilde, Denmark: 2006, p. 29–47.

[13] Carrion JE, LaFave JM, Hjelmstad KD. Experimental behavior of monolithic composite cuff connections for fiber reinforced plastic box sections. Compos Struct 2005;67:333–45.

[14] Grimsley BW, Cano R, Hubert P, Loos AC. Preform characterization in VARTM process model development. SAMPE 2004, Long 2004.

[15] Hubert P, Poursartip a. A method for the direct measurement of the fibre bed compaction curve of composite prepregs. Compos Part A Appl Sci Manuf 2001;32:179–87.

[16] Laurent-Mounier A, Binétruy C, Krawczak P. Multipurpose carbon fiber sensor design for analysis and monitoring of the resin transfer molding of polymer composites. Polym Compos 2005;26:717–30.

[17] Li W. Process and Performance Evaluation of the Vacuum-Assisted Process. J Compos Mater 2004;38:1803–14.

[18] Yenilmez B, Sozer EM. Compaction of e-glass fabric preforms in the vacuum infusion process: (a) use of characterization database in a model and (b) experiments. J Compos Mater 2012;47:1959–75.

[19] Andersson HM. Vacuum Infusion of Polymer Composites. Lulea University of Technology, 2001.

[20] Govignon Q, Bickerton S, Morris J, Kelly PA. Full field monitoring of the resin flow and laminate properties during the resin infusion process. Compos Part A Appl Sci Manuf 2008;39:1412–26.

[21] Andersson HM, Lundström TS, Gebart BR, Synnergren P. Application of digital speckle photography to measure thickness variations in the vacuum infusion process. Polym Compos 2003;24:448–55.

[22] Li J, Walsh SM, Zhang C, Liang R, Wang B, Ground AP. Modeling and Analysis of Thickness Gradient and Variations in Vacuum-Assisted Resin Transfer Molding Process. Control 2008.

[23] Koefoed MS. Modeling and Simulation of the VARTM Process for Wind Turbine Blades. Aalnorg University, 2003.

[24] Robitaille F, Gauvin R. Compaction of textile reinforcements for composites manufacturing. I: Review of experimental results. Polym Compos 1998;19:198–216.

[25] Bickerton S, Buntain MJ, Somashekar AA. The viscoelastic compression behavior of liquid composite molding preforms. Compos Part A Appl Sci Manuf 2003;34:431–44.

[26] Somashekar AA, Bickerton S, Bhattacharyya D. Exploring the non-elastic compression deformation of dry glass fibre reinforcements. Compos Sci Technol 2007;67:183–200.

[27] Kelly PA. A viscoelastic model for the compaction of fibrous materials. J Text Inst 2011;102:689–99.

[28] Sajn D, Gersak J, Flajs R. Prediction of Stress Relaxation of Fabrics with Increased Elasticity. Text Res J 2006;76:742–50.

[29] Chen B, Cheng AHD, Chou T-W. A nonlinear compaction model for fibrous preforms. Compos Part A Appl Sci Manuf 2001;32:701–7.

[30] Kim YR, McCarthy SP, Fanucci JP. Compressibility and relaxation of fiber reinforcements during composite processing. Polym Compos 1991;12:13–9.

[31] Chen B, Lang EJ, Chou T-W. Experimental and theoretical studies of fabric compaction behavior in resin transfer molding. Mater Sci Eng A 2001;317:188–96.

[32] Batch GL, Cumiskey S, Macosko CW. Compaction of fiber reinforcements. Polym Compos 2002;23:307–18.

[33] Somashekar AA, Bickerton S, Bhattacharyya D. Modelling the viscoelastic stress relaxation of glass fibre reinforcements under constant compaction strain during composites manufacturing. Compos Part A Appl Sci Manuf 2012;43:1044–52.

[34] Modi D, Johnson M, Long A, Rudd C. Analysis of pressure profile and flow progression in the vacuum infusion process. Compos Sci Technol 2009;69:1458–64.

[35] Robitaille F, Correia NC, Long A, Rudd C, Advani SG, Simacek P. Analysis of the vacuum infusion moulding process: I. Analytical formulation. Compos Part A Appl Sci Manuf 2005;36:1645–56.

[36] Hammami A, Gebart BR. Analysis of the Vacuum Infusion Molding Process. Polym Compos 2000;21:28–40.

[37] Hammami A. Effect of reinforcement structure on compaction behavior in the vacuum infusion process. Polym Compos 2001;22:337–48.

[38] Kruckenberg T. Static and vibration compaction and microstructure analysis on plain-woven textile fabrics. Compos Part A Appl Sci Manuf 2008;39:488–502.

[39] Kelly PA, Umer R, Bickerton S. Viscoelastic response of dry and wet fibrous materials during infusion processes. Compos Part A Appl Sci Manuf 2006;37:868–73.

[40] Saunders RA. Compression in the processing of polymer composites 2. Modelling of the viscoelastic compression of resin-impregnated fibre networks. Compos Sci Technol 1999;59:1483–94.

[41] Binétruy C, Krawczak P, Comas-Cardona S, Legrognec P. Unidirectional compression of fibre reinforcements. Part 1: A non-linear elastic-plastic behaviour. Compos Sci Technol 2007;67:507–14.

[42] Simacek P, Eksik Ö, Heider D, Gillespie JW, Advani SG, Gillespie Jr. JW. Post-filling flow in vacuum assisted resin transfer molding processes: Theoretical analysis. Compos Part A Appl Sci Manuf 2009;40:370–80.

[43] Robitaille F, Gauvin R. Compaction of textile reinforcements for composites manufacturing. III: Reorganization of the fiber network. Polym Compos 1999;20.

[44] Saunders RA, Lekakou C, Bader MG. Compression and microstructure of fibre plain woven cloths in the processing of polymer composites. Compos Part A Appl Sci Manuf 1998;29:443–54.

[45] Echaabi J, Nziengui M, Hattabi M. Compressibility and relaxation models for fibrous reinforcements in Liquid Composites Moulding. Int J Mater … 2008:851 – 854.

[46] Saunders RA, Lekakou C, Bader MG. Compression in the processing of polymer composites 1. A mechanical and microstructural study for different glass fabrics and resins. Compos Sci Technol 1999;59:983–93.

[47] Simacek P, Eksik Ö, Heider D, Gillespie JW, Advani SG. Experimental validation of post-filling flow in vacuum assisted resin transfer molding processes. Compos Part A Appl Sci Manuf 2012;43:370–80.

[48] Govignon Q, Bickerton S, Kelly P a. Simulation of the reinforcement compaction and resin flow during the complete resin infusion process. Compos Part A Appl Sci Manuf 2010;41:45–57.

[49] Yuexin D, Zhaoyuan T, Yan Z, Jing S. Compression Responses of Preform in Vacuum Infusion Process. Chinese J Aeronaut 2008;21:370–7.

[50] Buntain MJ, Bickerton S. Modeling forces generated within rigid liquid composite molding tools. Part A: Experimental study. Compos Part A Appl Sci Manuf 2007;38:1729–41.

[51] Francucci G, Rodriguez ES, Vazquez A. Experimental study of the compaction response of jute fabrics in liquid composite molding processes. J Compos Mater 2012;46:155–67.

[52] Francucci G, Rodriguez ES. Modeling of the compaction response of jute fabrics in liquid composite molding processes. J Appl Polym … 2012;124:4789–98.

[53] Francucci G, Vazquez a., Rodriguez ES. Key differences on the compaction response of natural and glass fiber preforms in liquid composite molding. Text Res J 2012;82:1774–85.

[54] Chen B, Chou T-W. Compaction of woven-fabric preforms: nesting and multi-layer deformation. Compos Sci Technol 2000;60:2223–31.

[55] Chen B, Chou T-W. Compaction of woven-fabric preforms in liquid composite molding processes: single-layer deformation. Compos Sci Technol 1999;59:1519–26.

[56] Advani SG, Simacek P, Acheson JA. The implications of fiber compaction and saturation on fully coupled VARTM simulation. Compos Part A Appl Sci Manuf 2004;35:159–69.

[57] Arbter R, Beraud JM, Binétruy C, Bizet L, Bréard J, Comas-Cardona S, et al. Experimental determination of the permeability of textiles: A benchmark exercise. Compos Part A Appl Sci Manuf 2011.

[58] Toll S. Packing mechanics of fiber reinforcements. Polym Eng Sci 1998;38:1337–50.

[59] Caglar B, Yenilmez B, Sozer EM. Modeling of post-filling stage in vacuum infusion using compaction characterization. J Compos Mater 2014.

[60] Kuentzer N, Walsh SM, Simacek P, Advani SG. Permeability characterization of dual scale fibrous porous media. Compos Part A Appl Sci Manuf 2006;37:2057–68.

[61] Heider D, Gillespie JW. Manufacturing of composite parts via vartm. Security 2003:0–48.

[62] Parnas RS. A permeability database for composites manufacturing. Polym Compos 1997:623–33.

[63] Williams JG, Morris CEM, Ennis BC. Liquid flow through aligned fiber beds. Polym Eng Sci 1974;14:413–9.

[64] Yalçınkaya MA. Effect of Part Thickness Variation on the Mold Filling in Vacuum Infusion Process. Koç University, 2012.

[65] Bower DI. An Introduction to Polymer Physics. Cambridge: Cambridge University Press; 2002.

[66] Malkin AY, Isayev AI. Rheology: Concepts, Methods & Applications. Toronto: ChemTec Publishing; 2006.

[67] Ziegler F. Mechanics of Solids and Fluids. 2nd ed. NY: Springer; 1995.

[68] Haddad Y. Viscoelasticity of Engineering Materials. London: Chapman & Hall; 1995.

[69] Wineman AS, Rajagopal KR. Mechanical Response of Polymers: An Introduction. Cambridge: Cambridge University Press; 2000.

[70] Dealy JM, Larson RG. Structure and Rheology of Molten Polymers: From Structure To Flow Behavior and Back Again. Ohio: Hanser; 2006.

[71] Thomas G. Mezger. The Rheology Handbook: For Users of Rotational and Oscillatory Rheometers. 2nd ed. Isernhagen: Vincentz; 2006.

[72] Shaw MT, MacKnight WJ. Introduction to Polymer Viscoelasticity. 3rd ed. New Jersey: John Wiley & Sons; 2005.

[73] Tropea C, Yarin AL, Foss JF. Springer Handbook of Experimental Fluid Mechanics, Volume 1. Berlin: Springer; 2007.

[74] Barnes HA, Hutton JF, Walters K. An Introduction to Rheology. San Diego: Elsevier; 1989.

[75] Betten J. Creep Mechanics. 3rd ed. Berlin: Springer; 2008.

[76] Dai L, Jazar RN. Nonlinear Approaches in Engineering Applications. NY: Springer; 2011.

[77] Mitchell BS. An Introduction to Materials Engineering and Science for Chemical and Materials Engineers. New Jersey: John Wiley & Sons; 2003.

[78] Sharpe WNJ. Springer Handbook of Experimental Solid Mechanics. NY: Springer; 2008.

[79] Kunkel P, Mehrmann V. Differential-Algebraic Equations: Analysis and Numerical Solution. Zurich: European Mathematical Society; 2006.

[80] Mathworks. Differential Equations in MATLAB 2014.

[81] Simeon B. Differential-Algebraic Equations (DAEs). TU Kaiserslautern, Fachbereich Mathematik; 2012.

[82] Mathworks. ode15s 2014.

[83] Peck R, Olsen C, DeVore J. Introduction to Statistics and Data Analysis. 3rd ed. Cengage Learning; 2008.

[84] Lagarias J, Reeds J, Wright M, Wright P. Convergence properties of the Nelder-Mead simplex method in low dimensions. SIAM J Optim 1998;9:112–47.

Vita

BEKIR YENILMEZ was born in Ankara, Turkey on August 2, 1984. He received his B.Sc. degree in Mechanical Engineering from Middle East Technical University, Ankara in 2006. Then, he has enrolled in the M.Sc. program in Mechanical Engineering at Koc University, Istanbul with full TUBITAK scholarship, as both a teaching and research assistant. He has completed his M.Sc. degree with thesis titled “Real-Time Monitoring of Resin Transfer Molding Using a Grid of Dielectric Sensors” on 2008. He has pursued his career on with PhD in the same faculty with full TUBITAK scholarship. He has published six papers in refereed (peer-reviewed) journals during his PhD career. His most recent thesis, “Vacuum Infusion (VI) Process Modeling and Material Characterization with Viscoelastic Compaction Models” acts as a complement to his numerous other RTM and VARTM related works.

Appendix A *Appendix A*

A.I Parameters used in sample model runs

Model	ε_{max} Step input	ε_{max} Ramp input	Parameters		
Maxwell	0.90	0.80	$E = 200$	$n = 1$	$c = 5000$
Kelvin-Voigt	1.00	1.00	$E = 100$	$n = 1$	$c = 200$
Zener	1.00	0.99	$E_0 = 100$ $E_1 = 100$	$n_0 = 1$ $n_1 = 1$	 $c_1 = 150$
Kelvin Chain, n=3	1.98	1.95	$E_1 = 100$ $E_2 = 100$ $E_3 = 50$	$n_1 = 1$ $n_2 = 1$ $n_3 = 1$	$c_1 = 200$ $c_2 = 300$ $c_3 = 200$
Generalized Maxwell, n=2	0.89	0.85	$E_0 = 100$ $E_1 = 100$ $E_2 = 50$	$n_0 = 1$ $n_1 = 1$ $n_2 = 1$	 $c_1 = 150$ $c_2 = 50$
Burgers	4.99	4.50	$E_1 = 100$ $E_2 = 50$	$n_1 = 1$ $n_2 = 1$	$c_1 = 1000$ $c_2 = 100$

Appendix B *Characterization experiment results*

Below results are from the additional experiments where the parameters are modified from the base experiment. The base is also referred as Set 1 : Dry/Wet experiments where the default parameters are:

$\boldsymbol{P_{minor}} = \boldsymbol{P_{relax}} = 1$ kPa

$\boldsymbol{dP/dt}$ (loading/unloading rate) = 2 kPa/s

$\boldsymbol{t_{settle}} = \boldsymbol{t_{relax}} = 300$ s

$\boldsymbol{P_{settle}}$ == 99 kPa

Note that saturation (wetting) is started in the last 30 s of settling. As explained in the body text, injection trap is opened to atmosphere for 10 s, and then trap is sealed as saturation continuous until both traps pressure equalizes.

In Dry/Dry experiment (Set 2), the same parameters are taken but without saturating the fabric at the end of settling. In rest of the experiments, only one of the parameters modified as written on respective headings.

B.I Set 2: Dry/Dry

i. Random

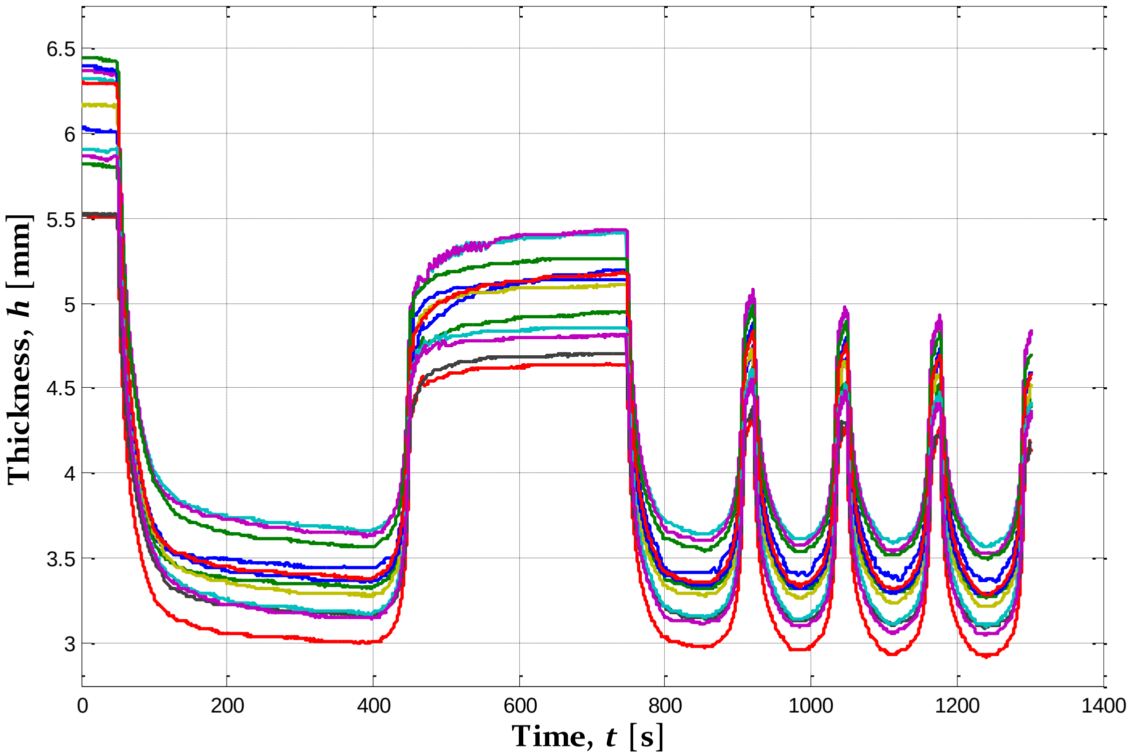

Figure B-1. Random fabric, Dry/Dry experiment thickness vs. time.

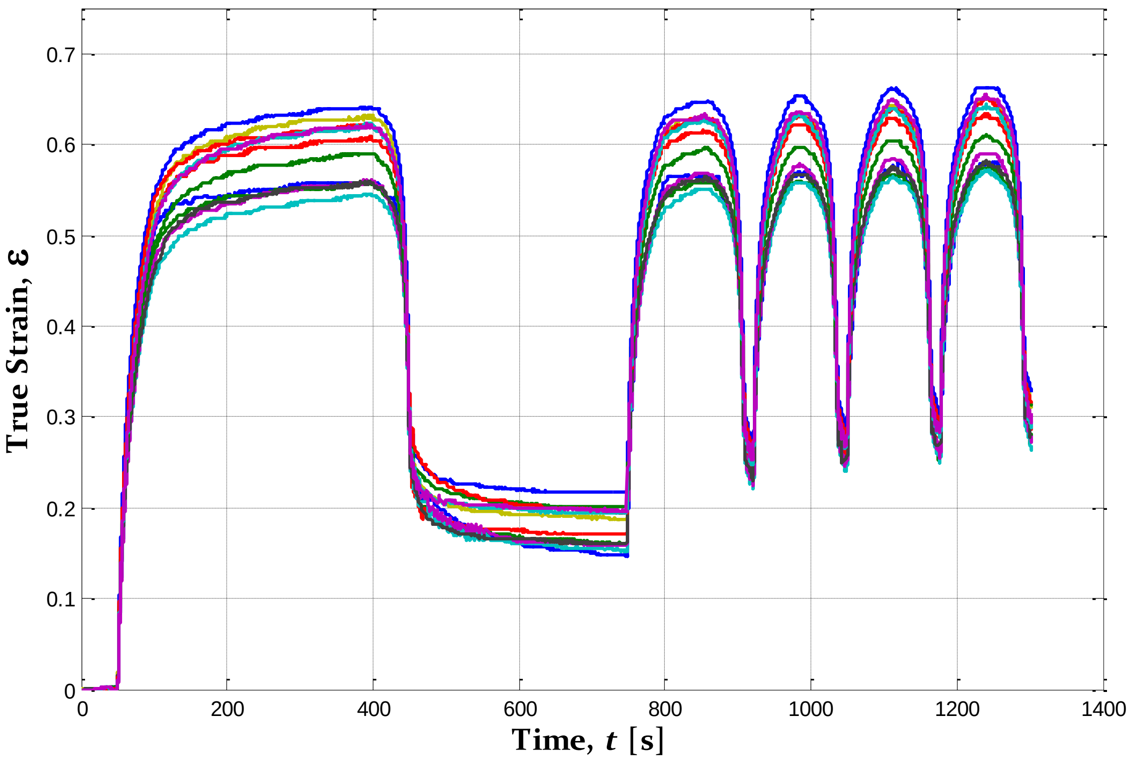

Figure B-2. Random fabric, Dry/Dry experiment true strain vs. time.

ii. Woven

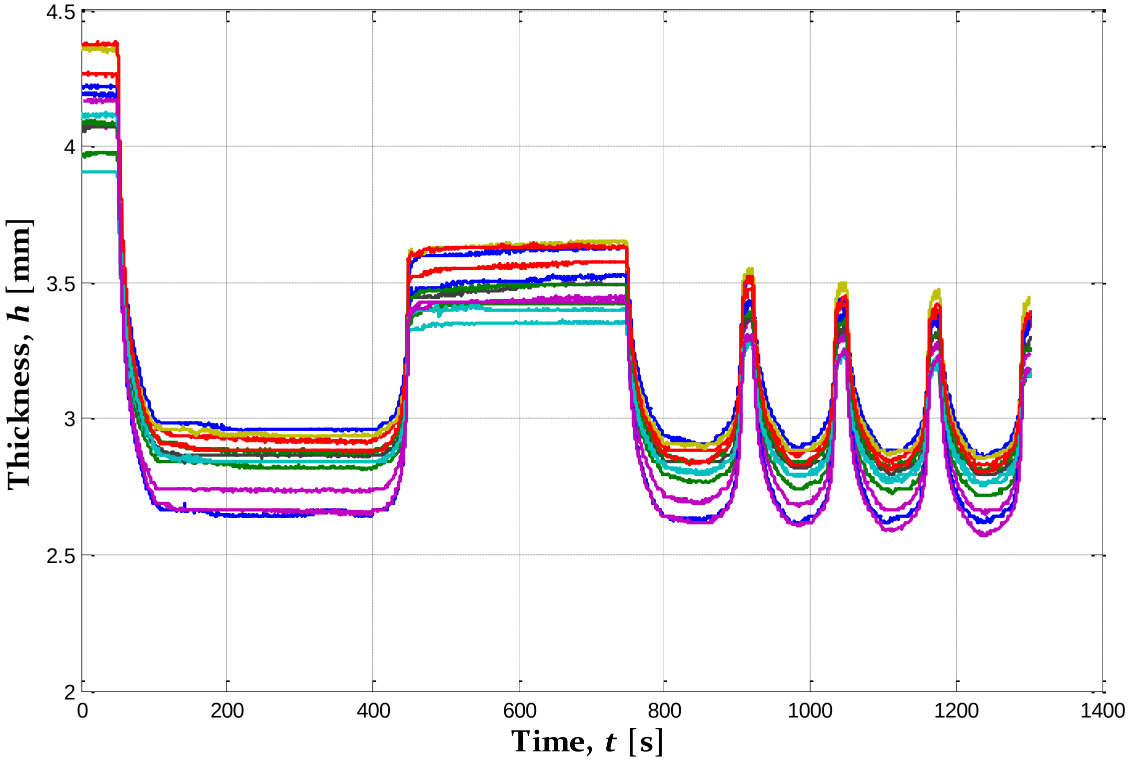

Figure B-3. Woven fabric, Dry/Dry experiment thickness vs. time.

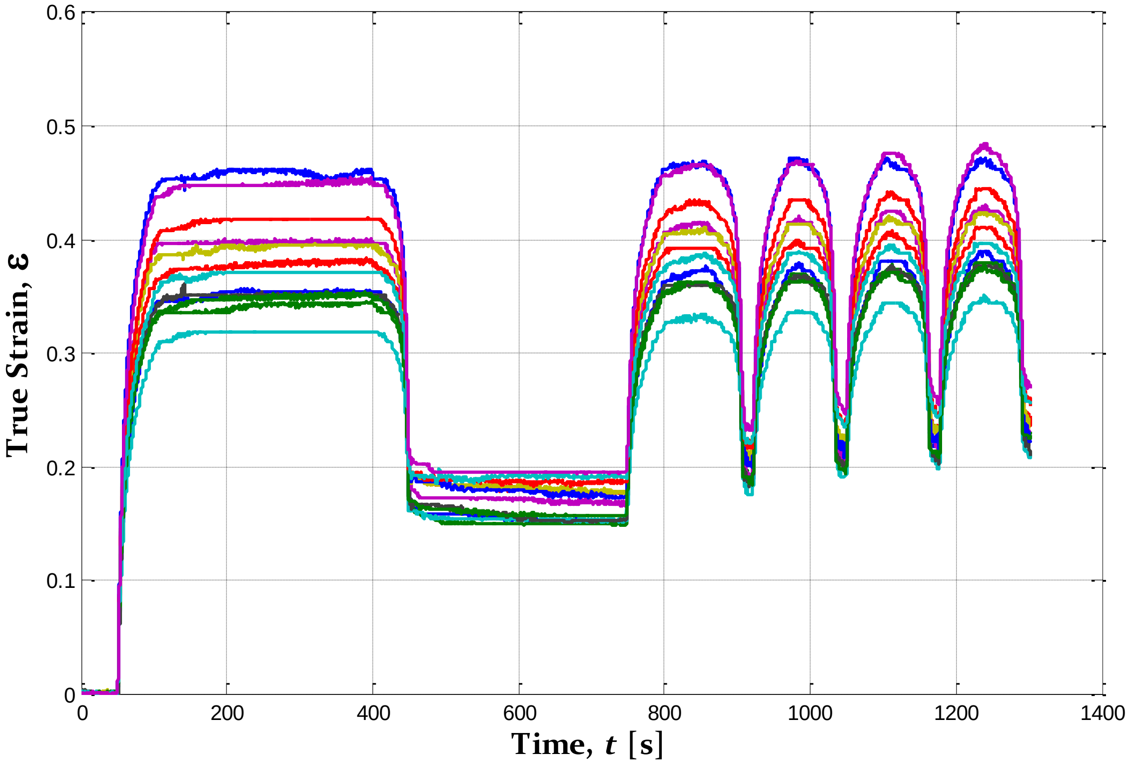

Figure B-4. Woven fabric, Dry/Dry experiment true strain vs. time.

B.II Set 3: $dP/dt = 1$ kPa/s

i. Random

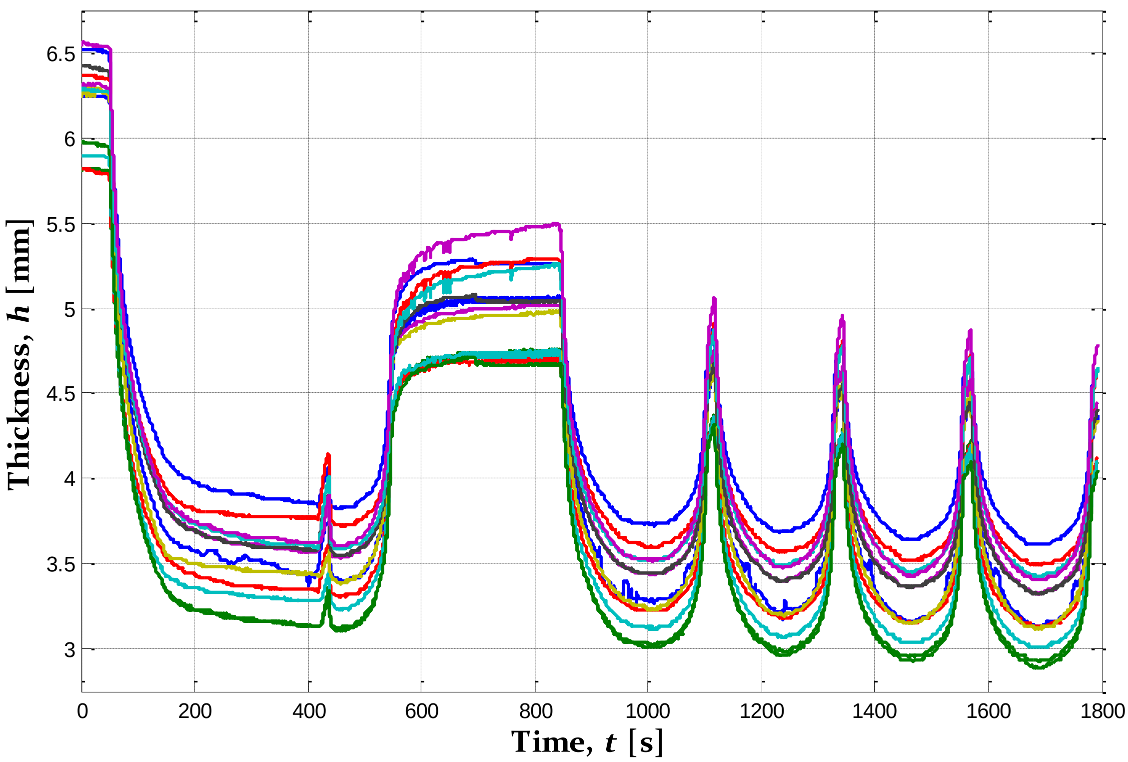

Figure B-5. Random fabric, dP/dt = 1 kPa/s experiment thickness vs. time.

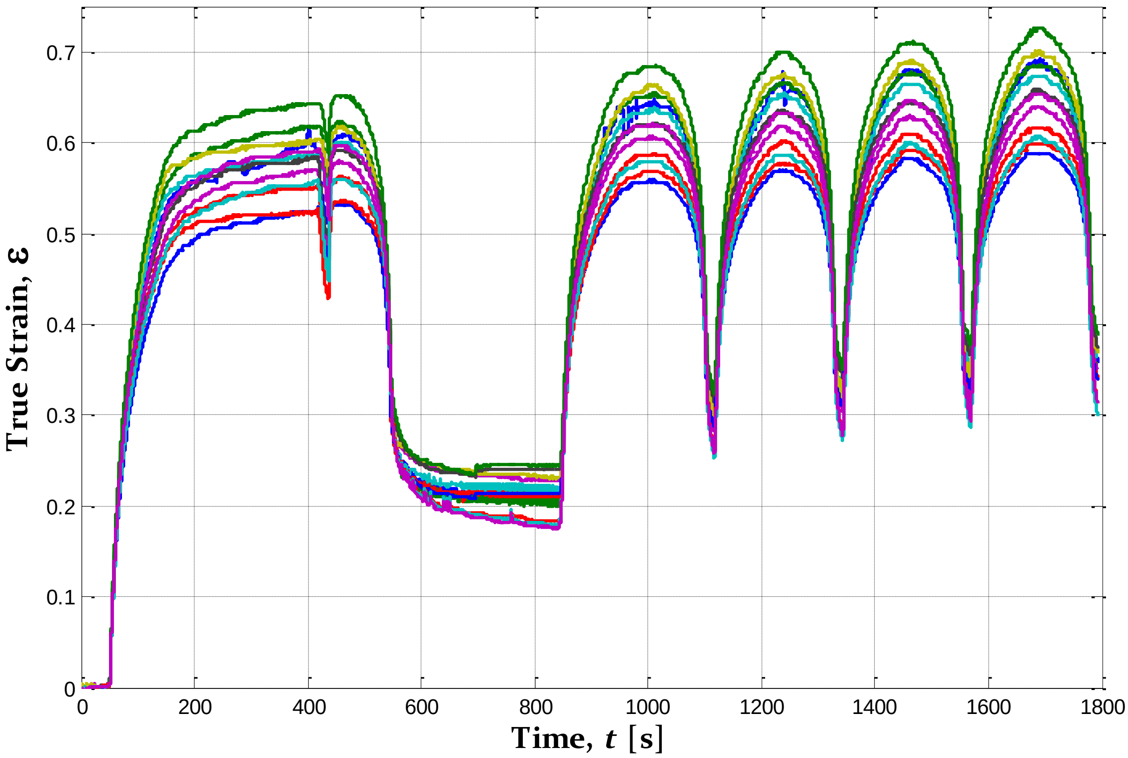

Figure B-6. Random fabric, dP/dt = 1 kPa/s experiment true strain vs. time.

ii. Woven

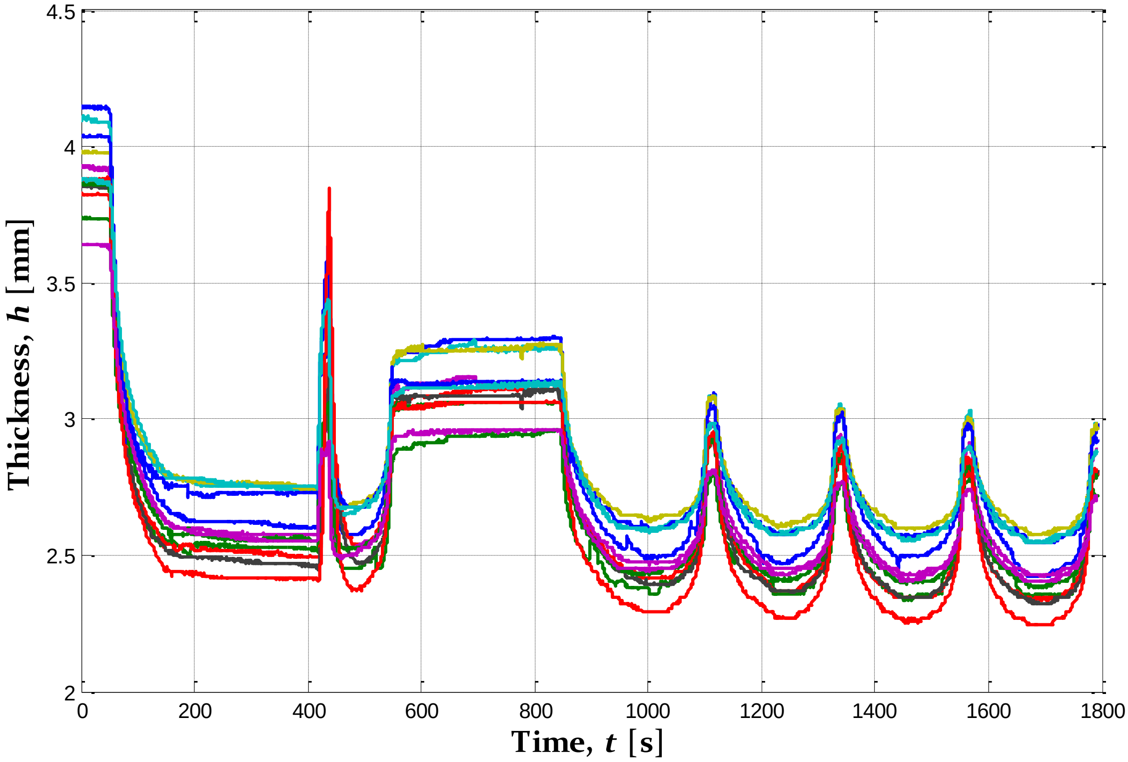

Figure B-7. Woven fabric, dP/dt = 1 kPa/s experiment thickness vs. time.

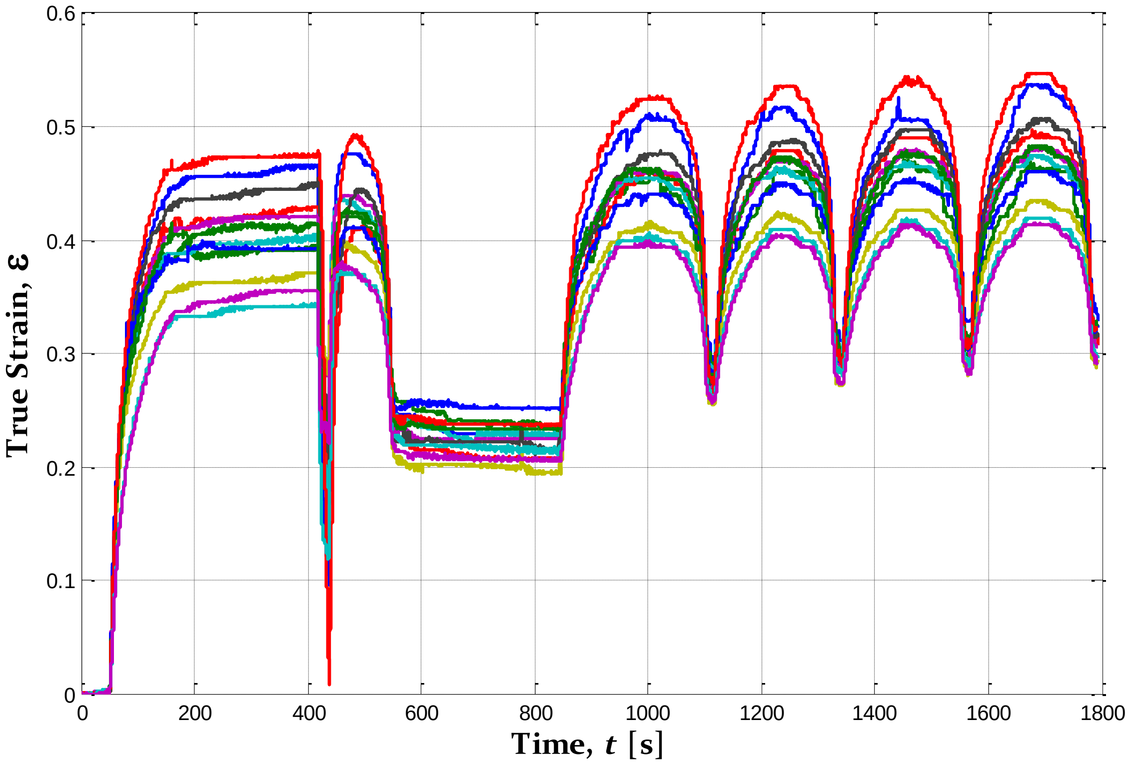

Figure B-8. Woven fabric, dP/dt = 1 kPa/s experiment true strain vs. time.

B.III Set 4: dP/dt = 4 kPa/s

i. Random

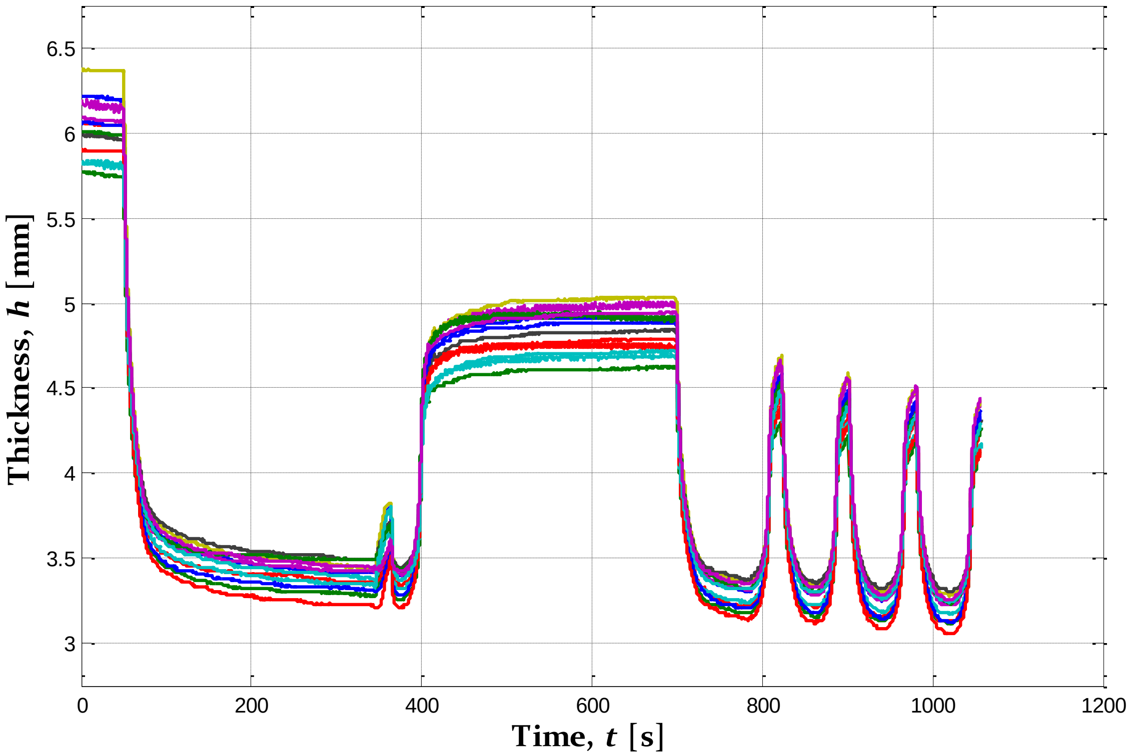

Figure B-9. Random fabric, dP/dt = 4 kPa/s experiment thickness vs. time.

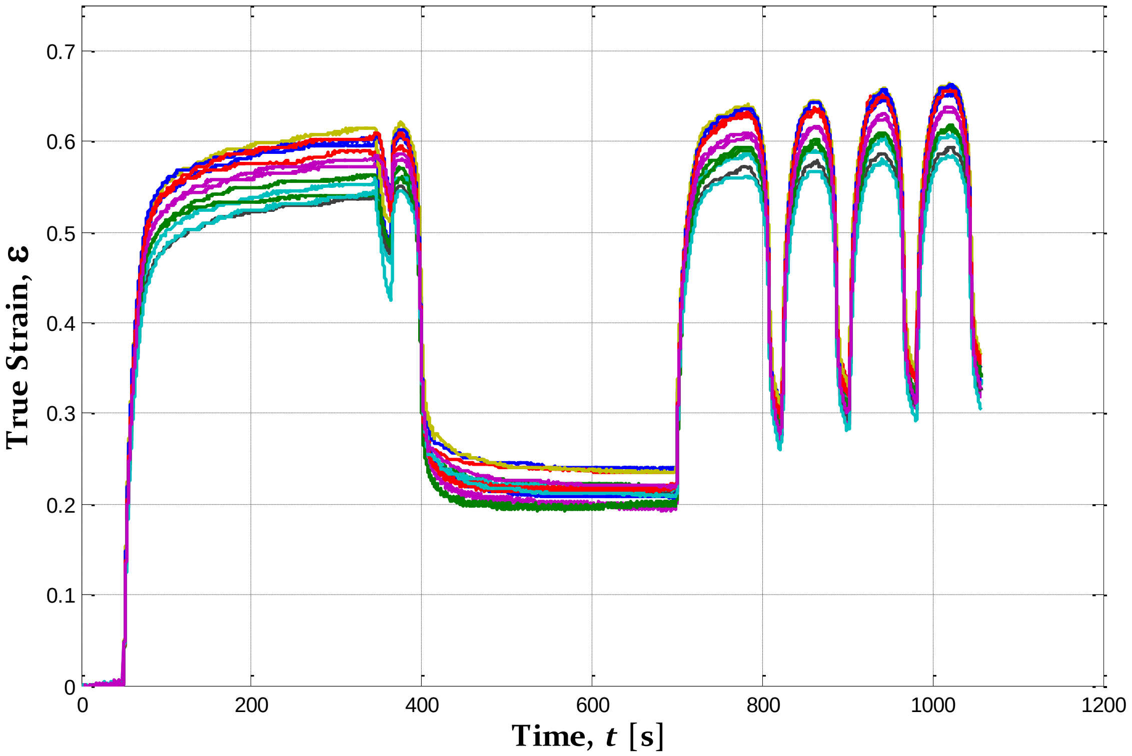

Figure B-10. Random fabric, dP/dt = 4 kPa/s experiment true strain vs. time.

ii. Woven

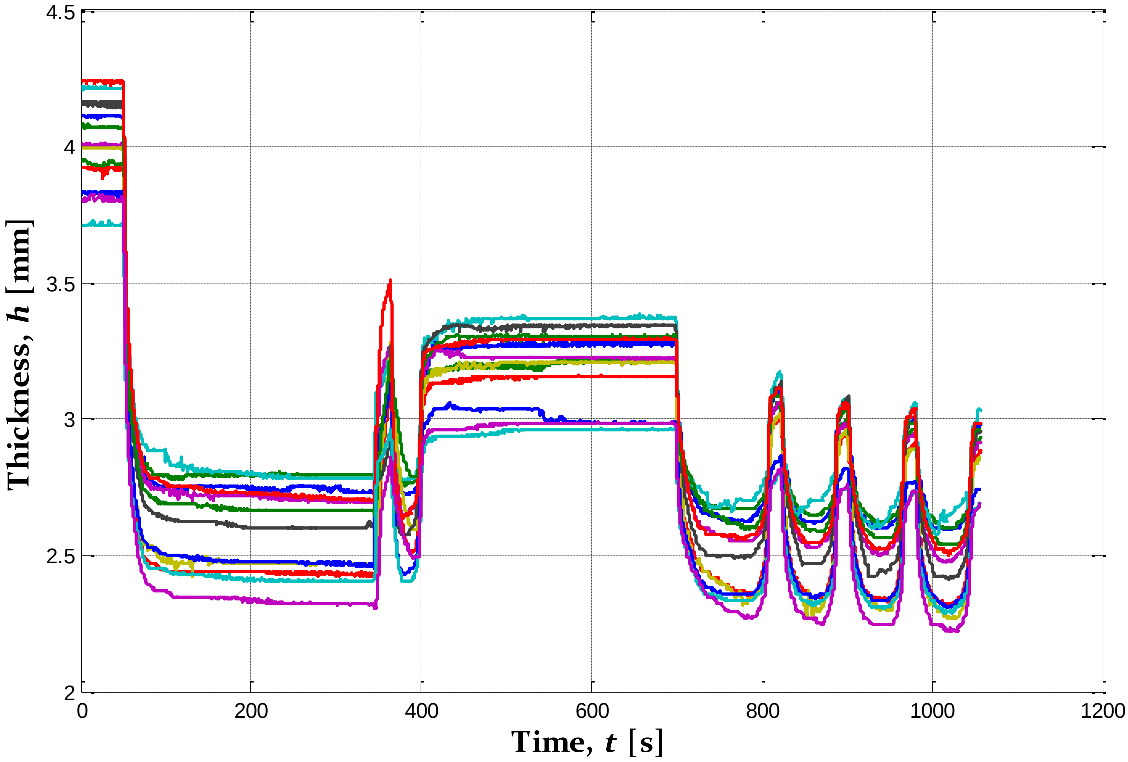

Figure B-11. Woven fabric, dP/dt = 4 kPa/s experiment thickness vs. time.

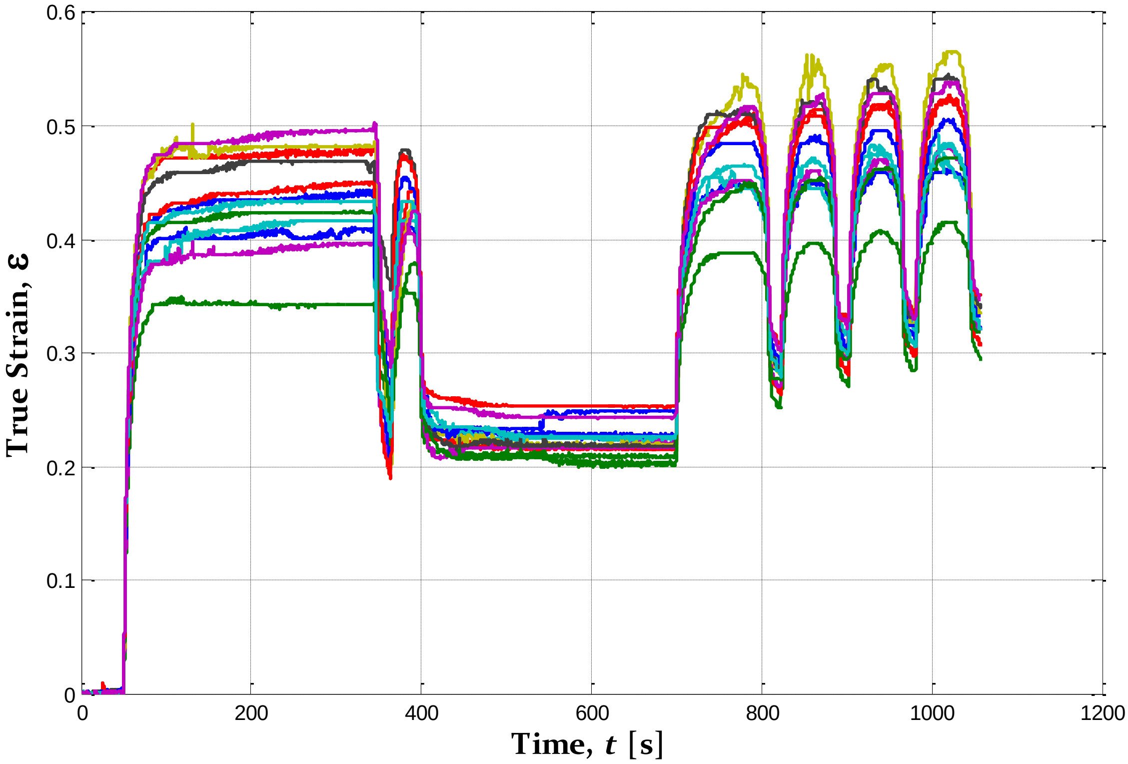

Figure B-12. Woven fabric, dP/dt = 4 kPa/s experiment true strain vs. time.

B.IV Set 5: P_{relax} = 5 kPa

i. Random

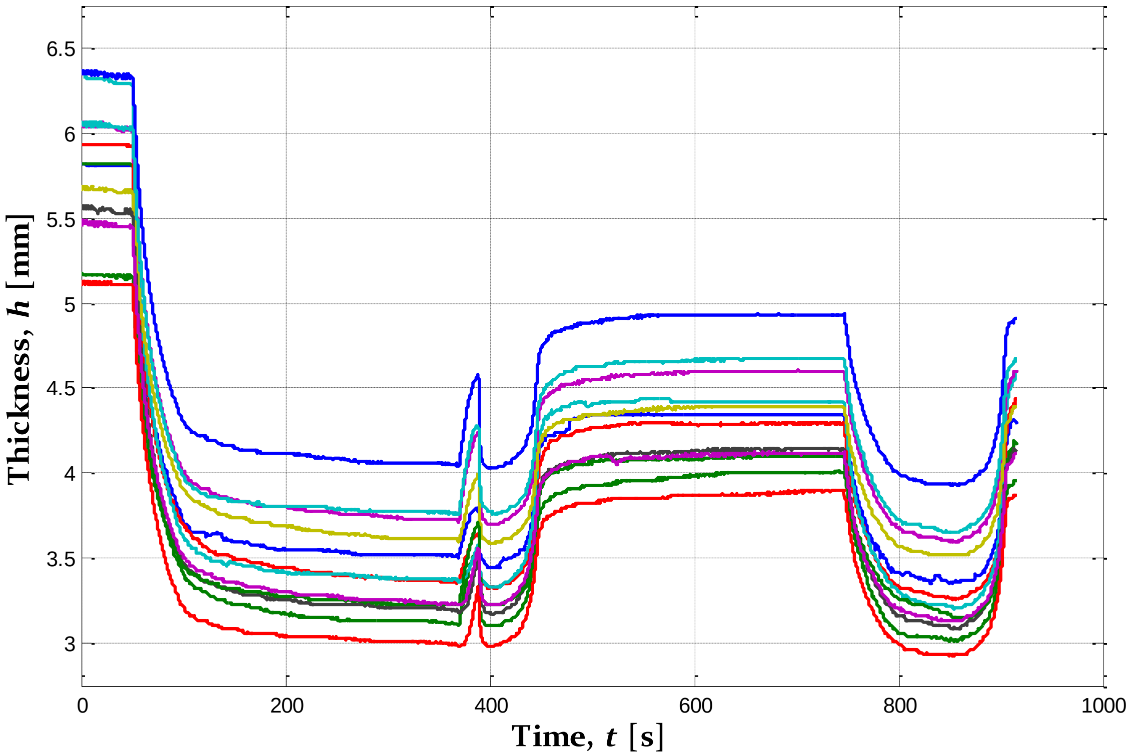

Figure B-13. Random fabric, relaxation at 5 kPa thickness vs. time.

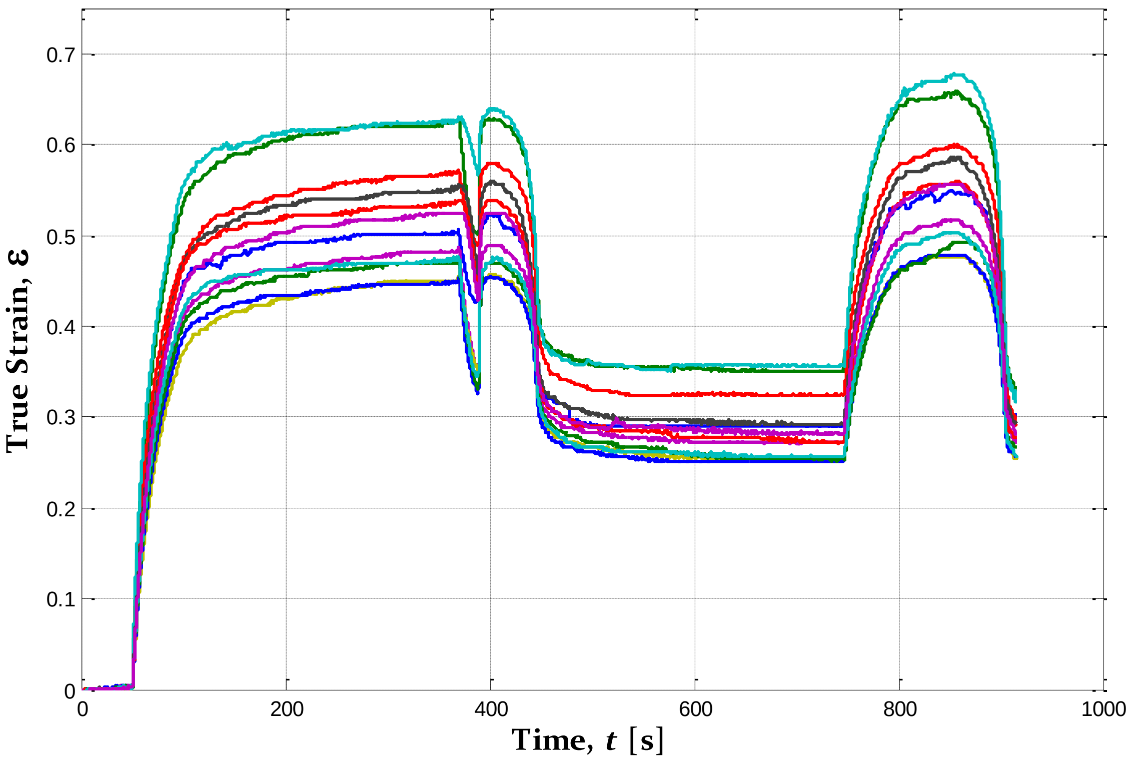

Figure B-14. Random fabric, relaxation at 5 kPa true strain vs. time.

ii. Woven

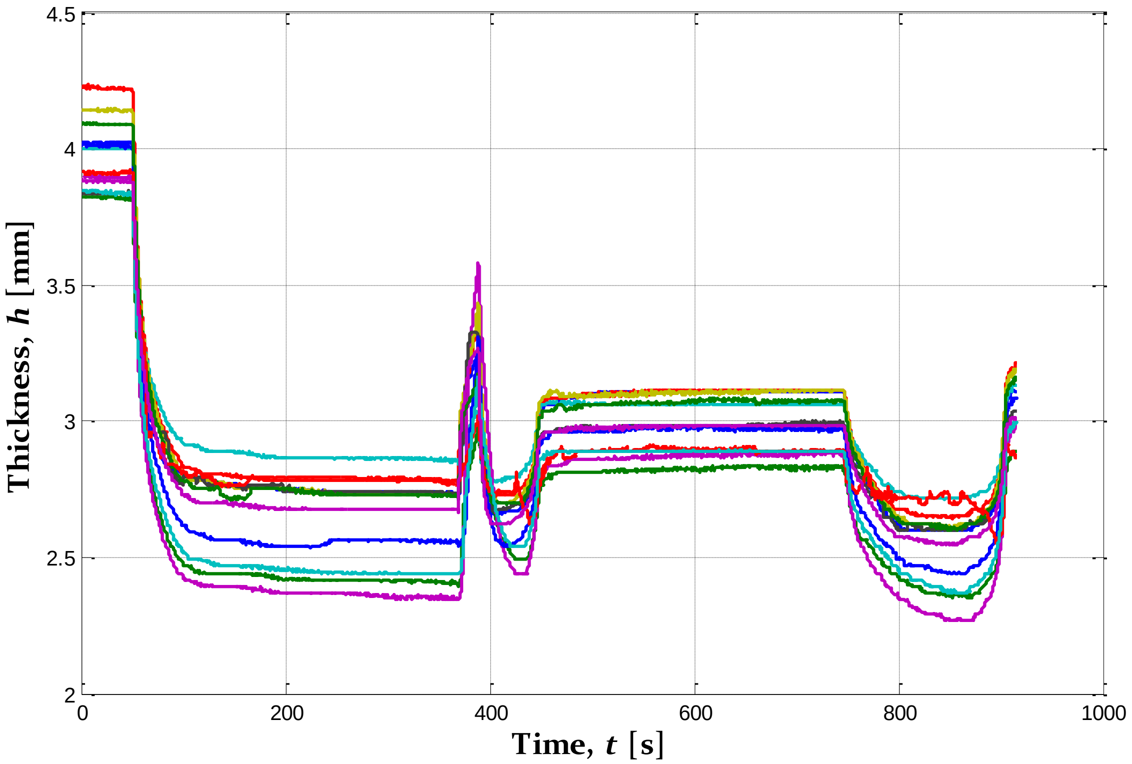

Figure B-15. Woven fabric, relaxation at 5 kPa thickness vs. time.

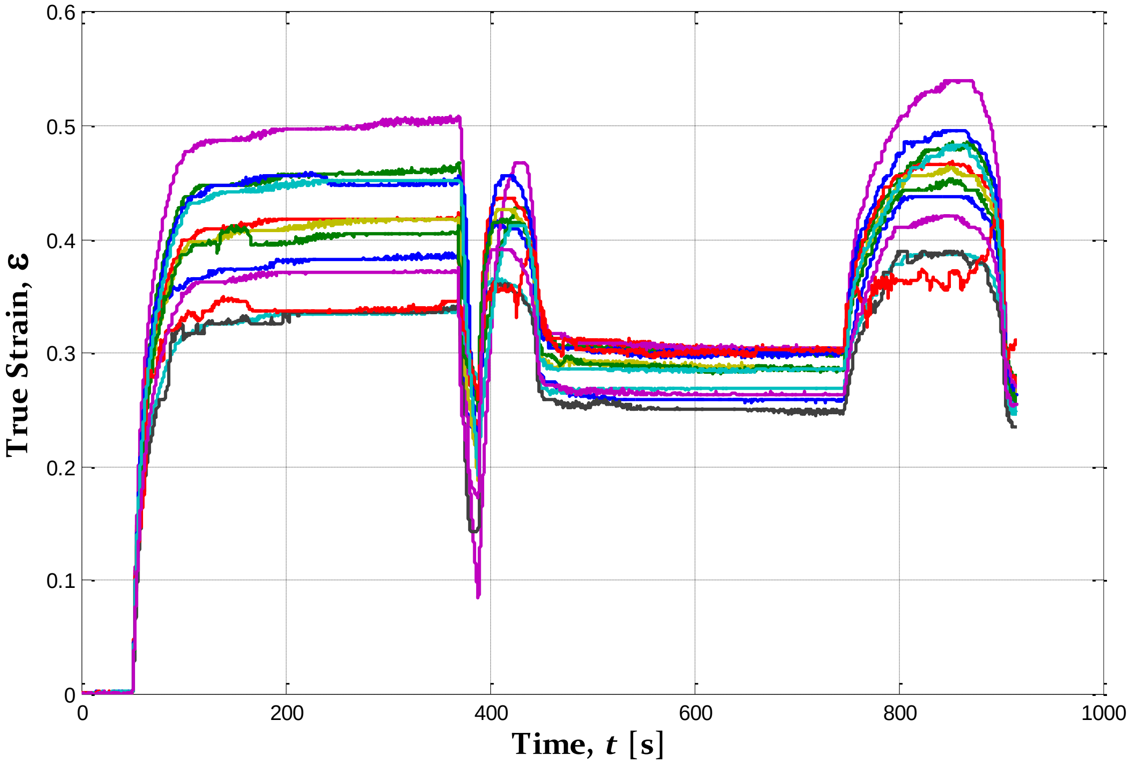

Figure B-16. Woven fabric, relaxation at 5 kPa true strain vs. time.

B.V Set 6: P_{relax} = 10 kPa

i. Random

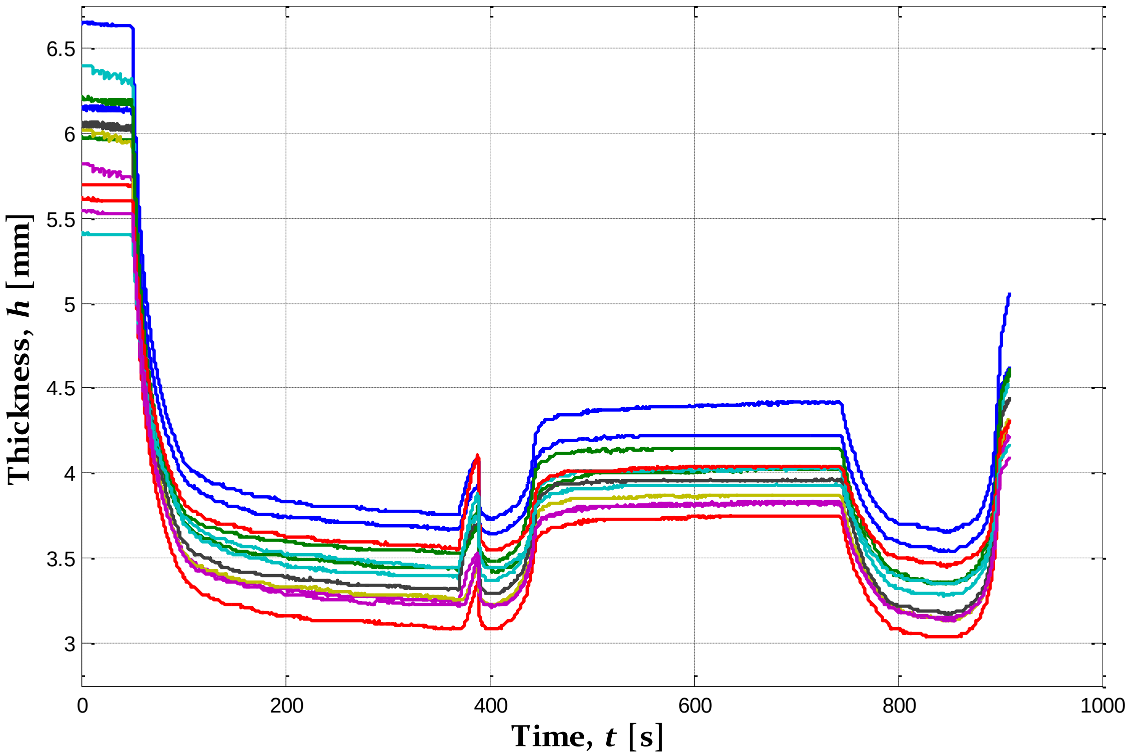

Figure B-17. Random fabric, relaxation at 10 kPa thickness vs. time.

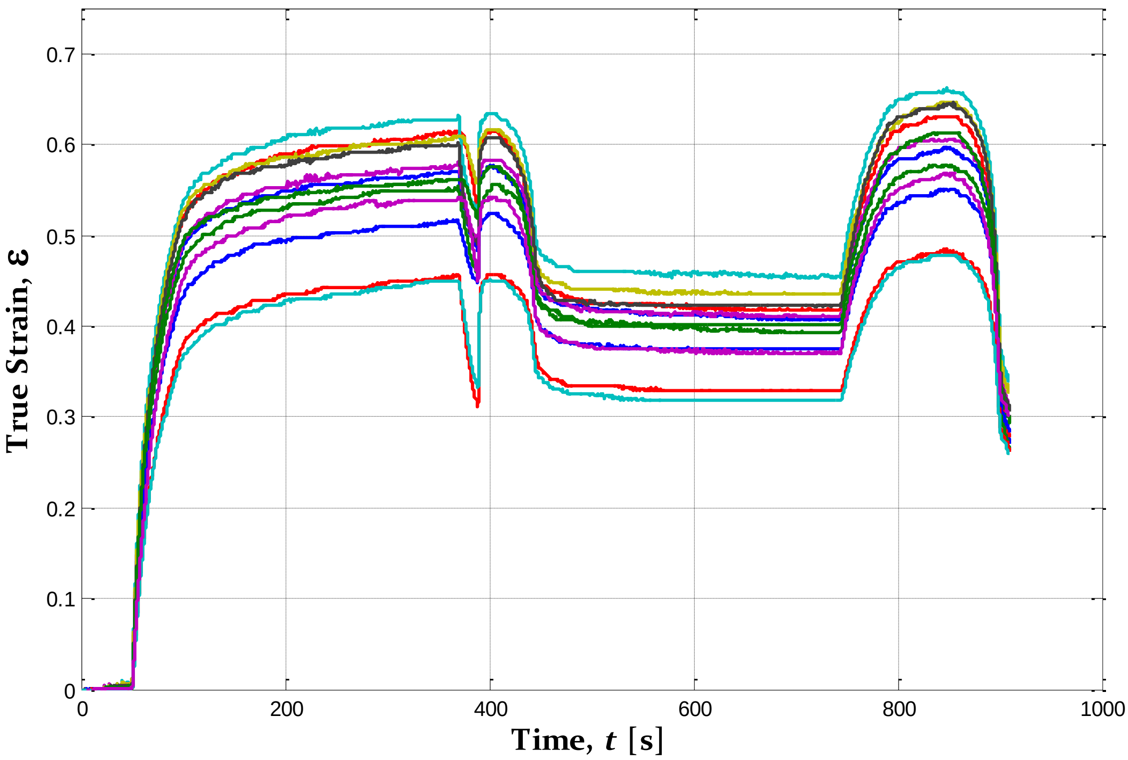

Figure B-18. Random fabric, relaxation at 10 kPa true strain vs. time.

ii. Woven

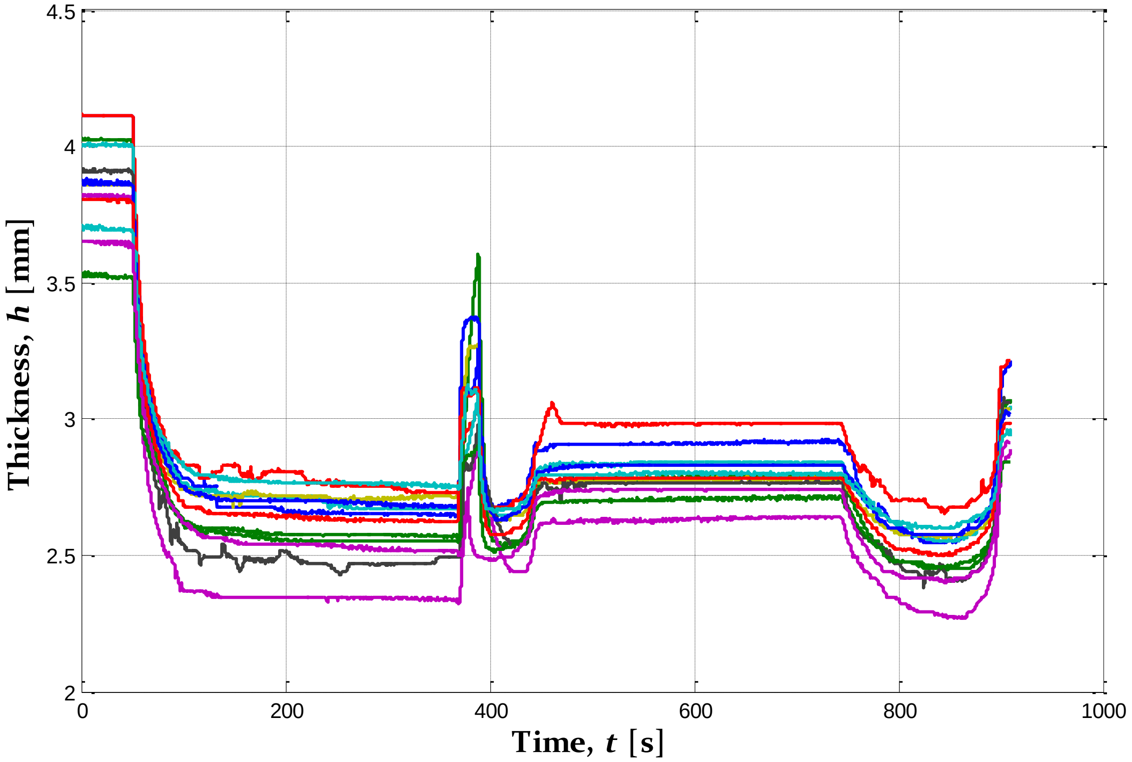

Figure B-19. Woven fabric, relaxation at 10 kPa thickness vs. time.

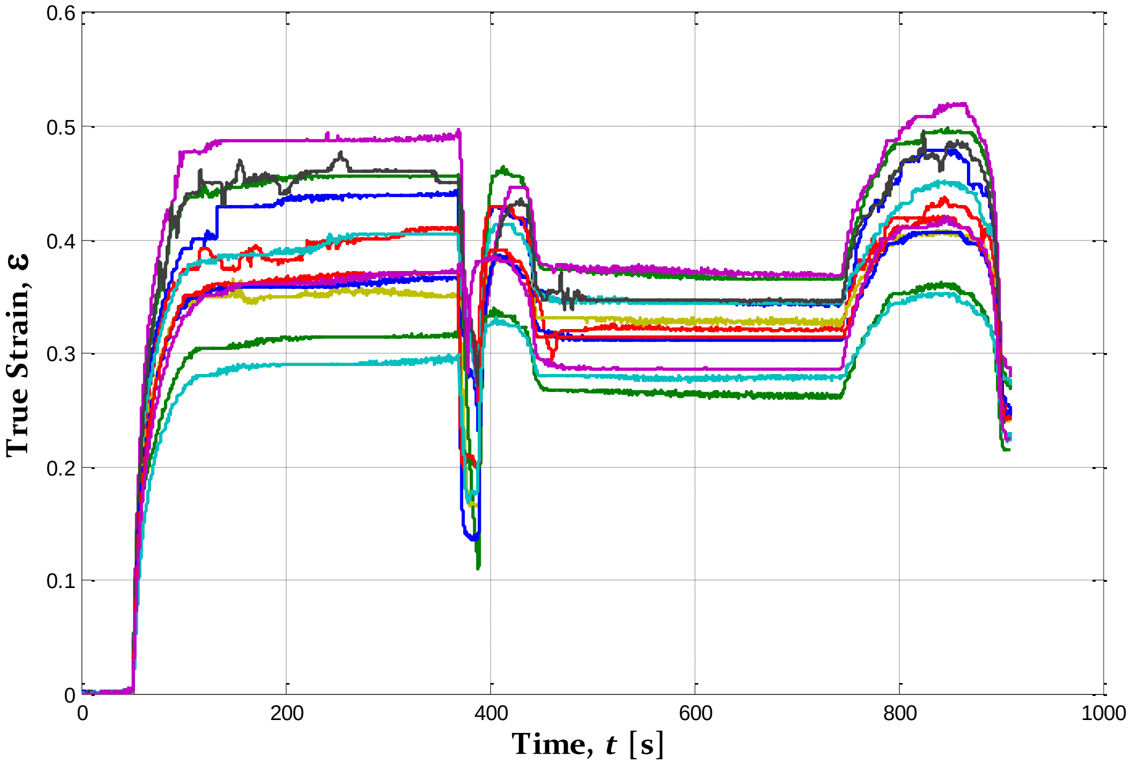

Figure B-20. Woven fabric, relaxation at 10 kPa true strain vs. time.

B.VI Set 7: P_{relax} = 40 kPa

i. Random

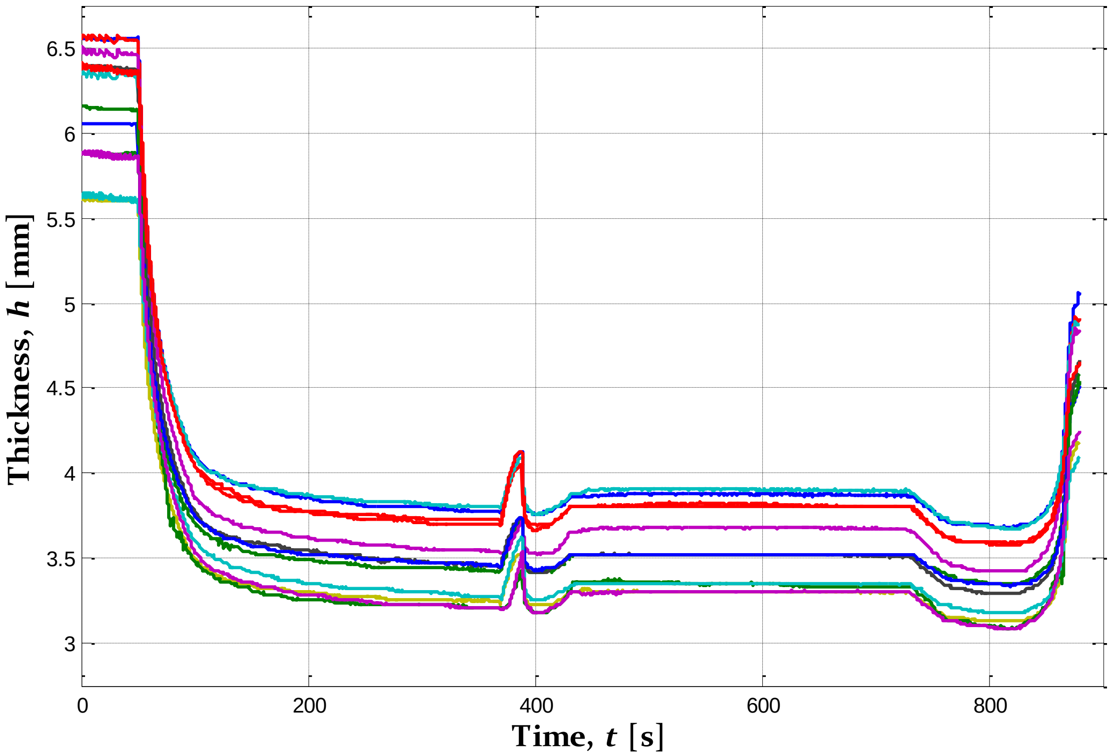

Figure B-21. Random fabric, relaxation at 40 kPa thickness vs. time.

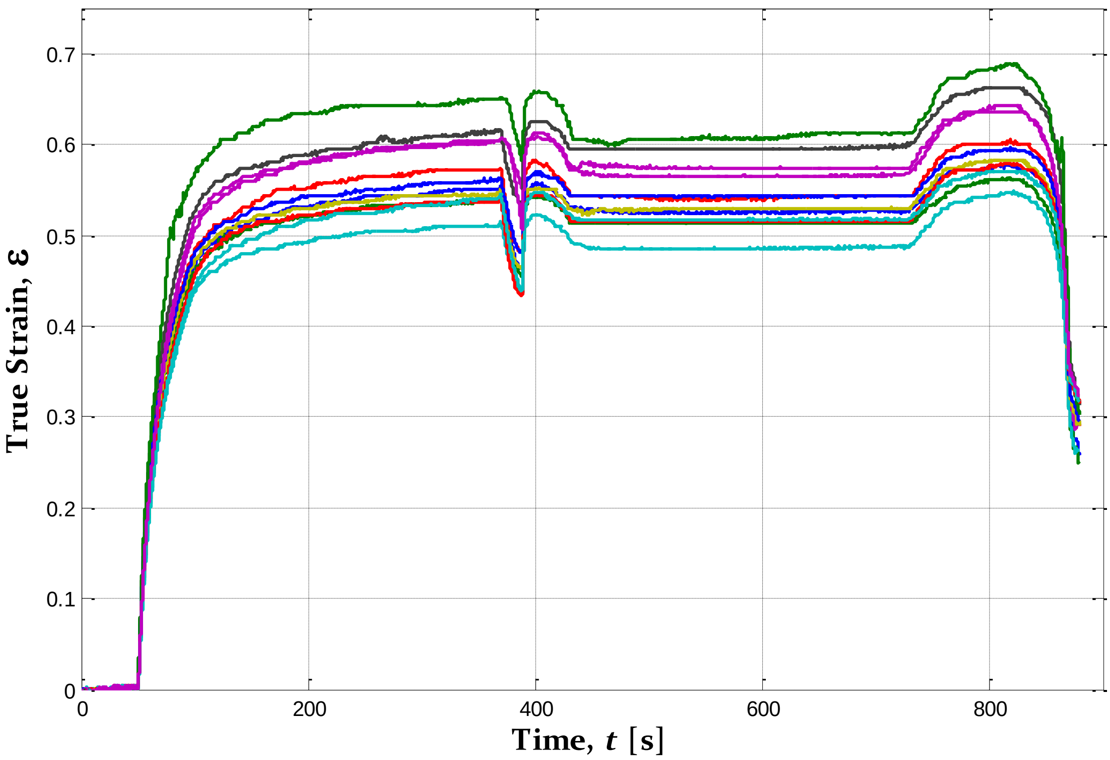

Figure B-22. Random fabric, relaxation at 40 kPa true strain vs. time.

ii. Woven

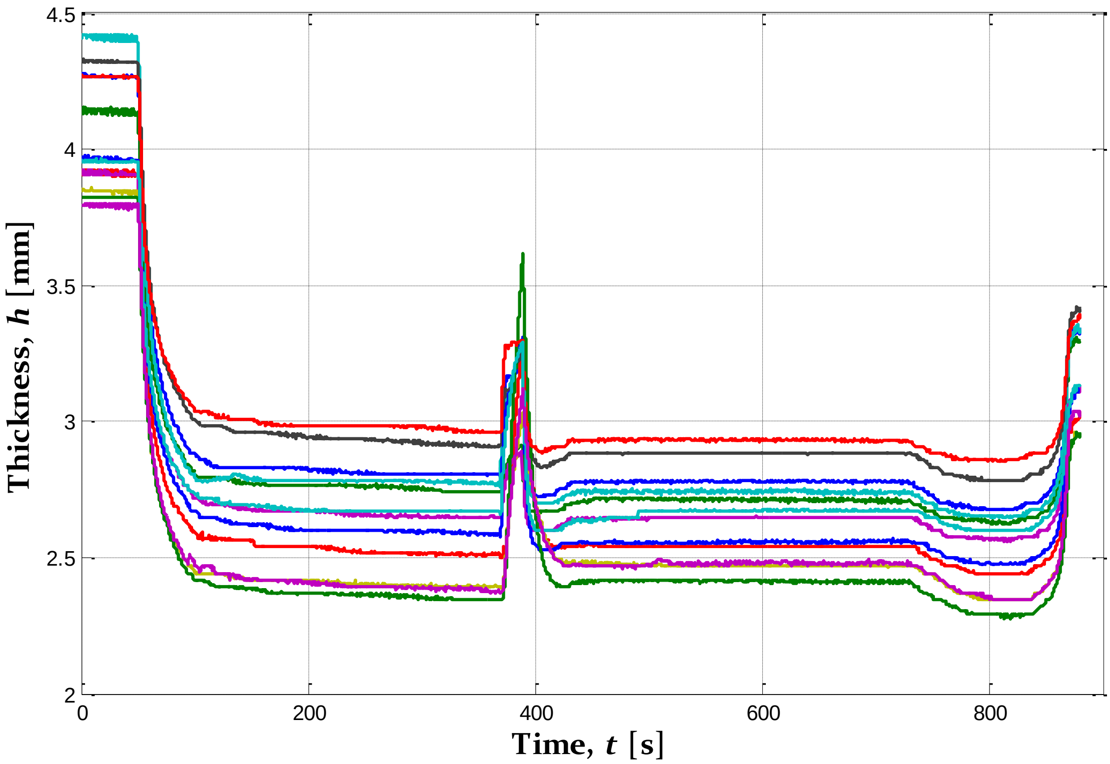

Figure B-23. Woven fabric, relaxation at 40 kPa thickness vs. time.

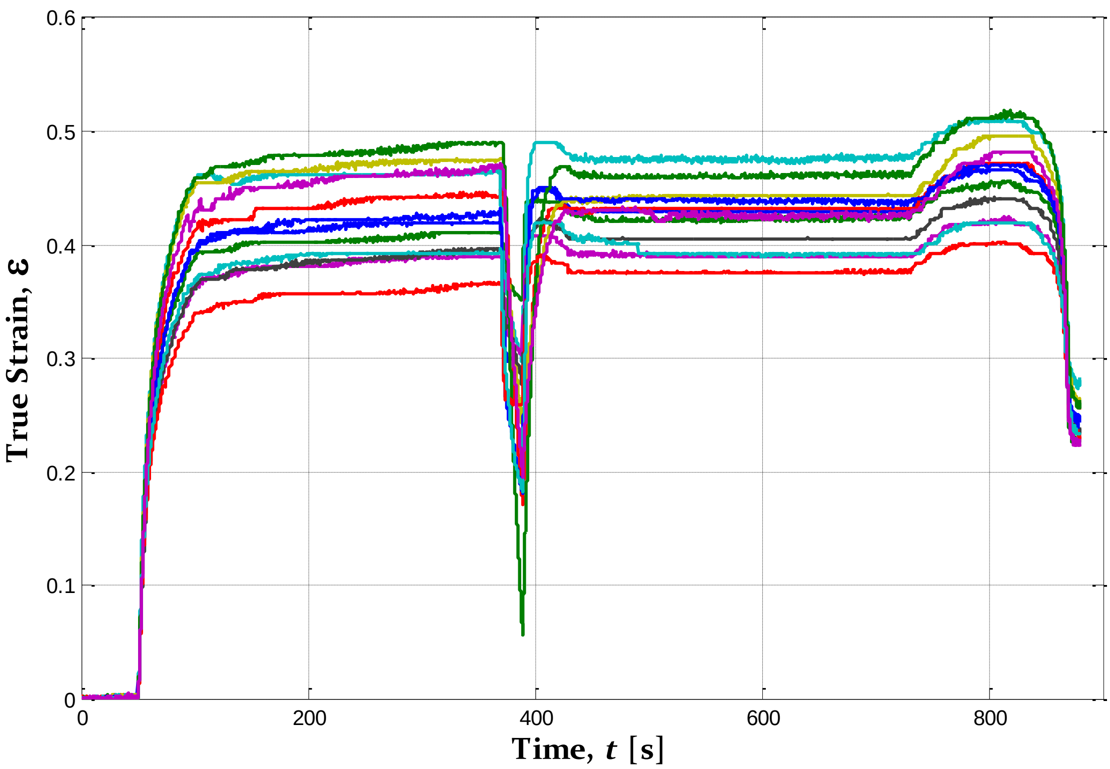

Figure B-24. Woven fabric, relaxation at 40 kPa true strain vs. time.

B.VII Set 8: $dP/dt \sim 25$ kPa/s

i. Random

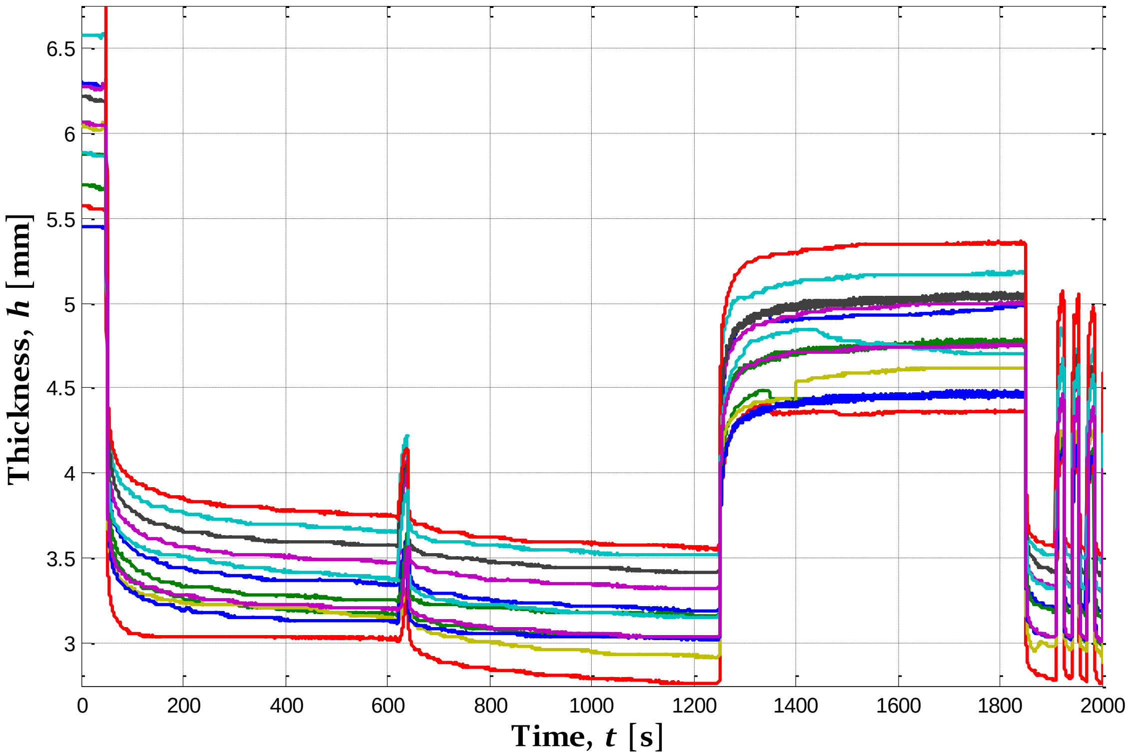

Figure B-25. Random fabric, step input thickness vs. time.

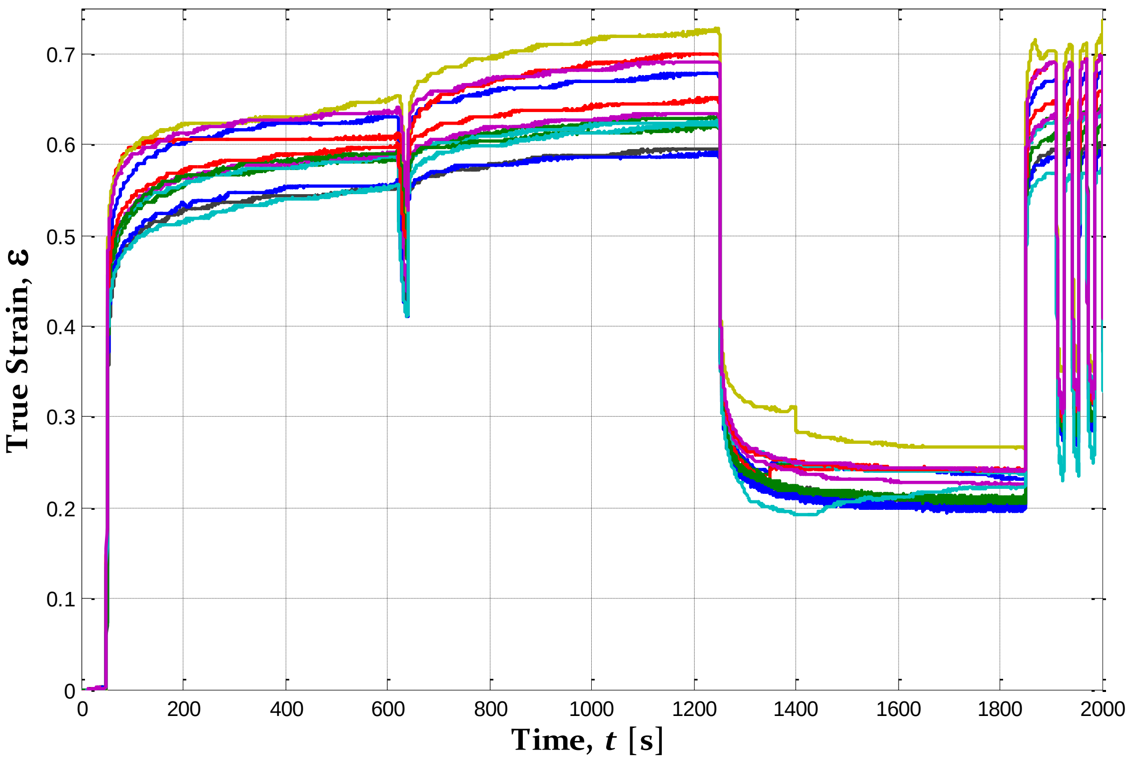

Figure B-26. Random fabric, step input true strain vs. time.

ii. Woven

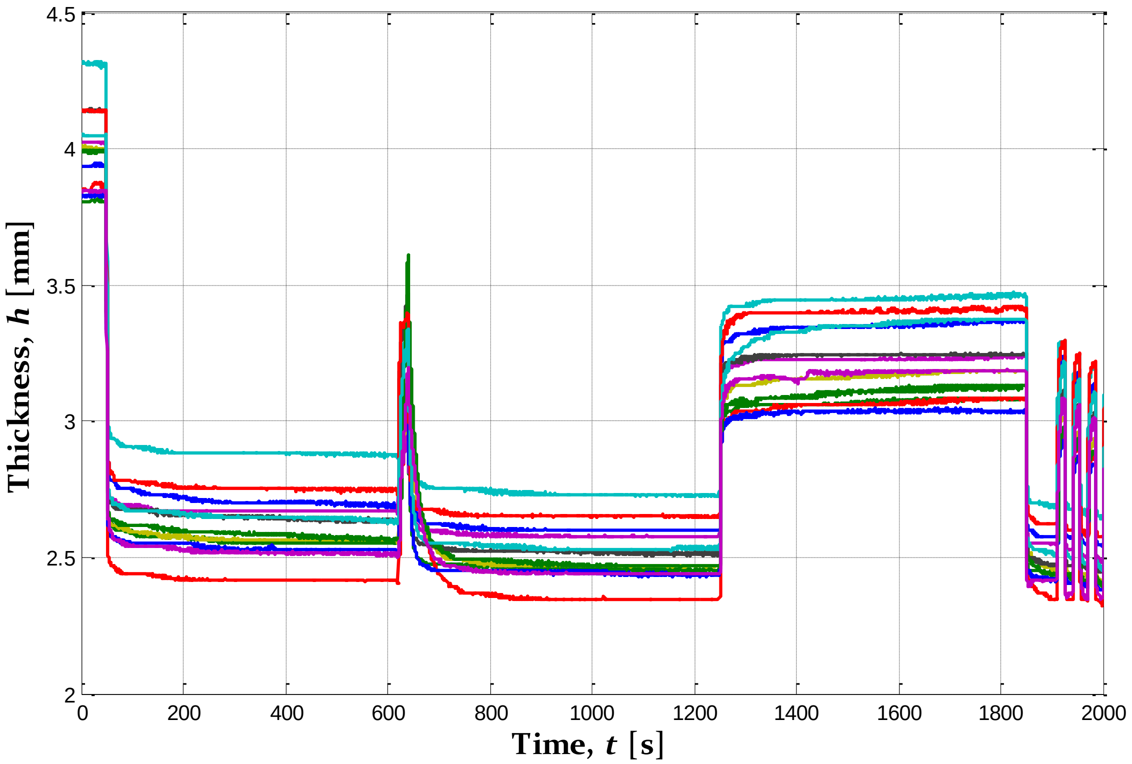

Figure B-27. Woven fabric, step input thickness vs. time.

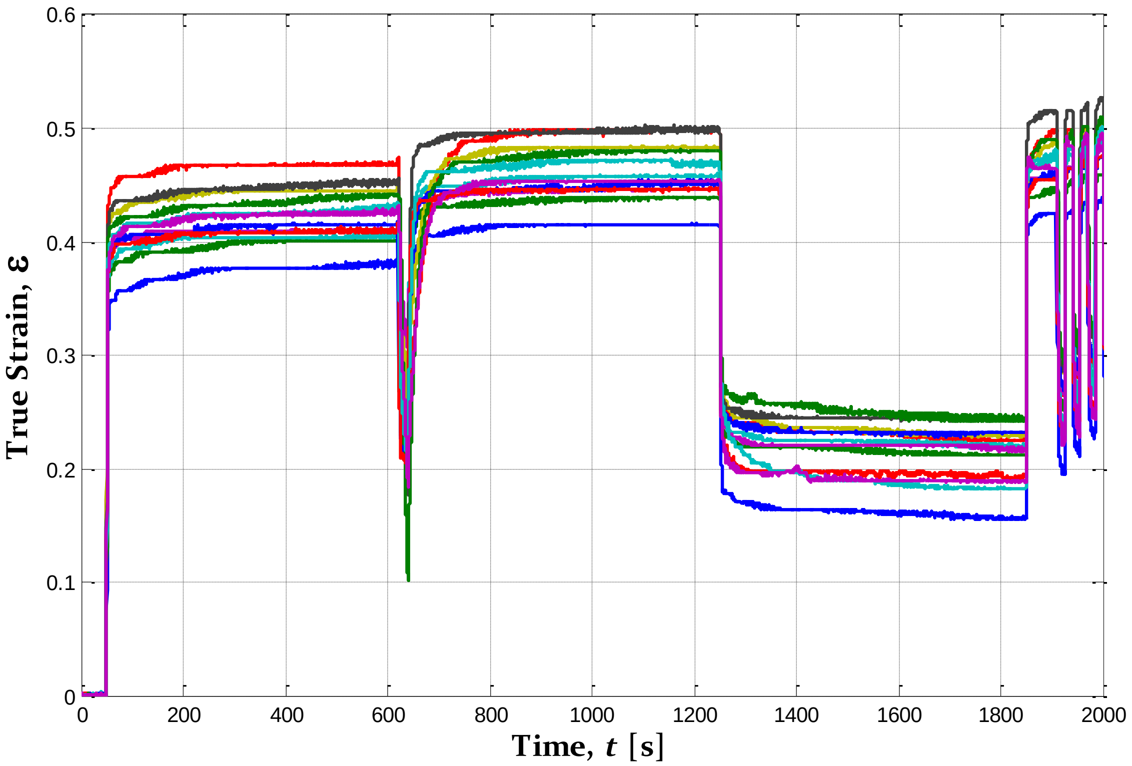

Figure B-28. Woven fabric, step input true strain vs. time.

B.VIII All sets show with error bars for random fabric

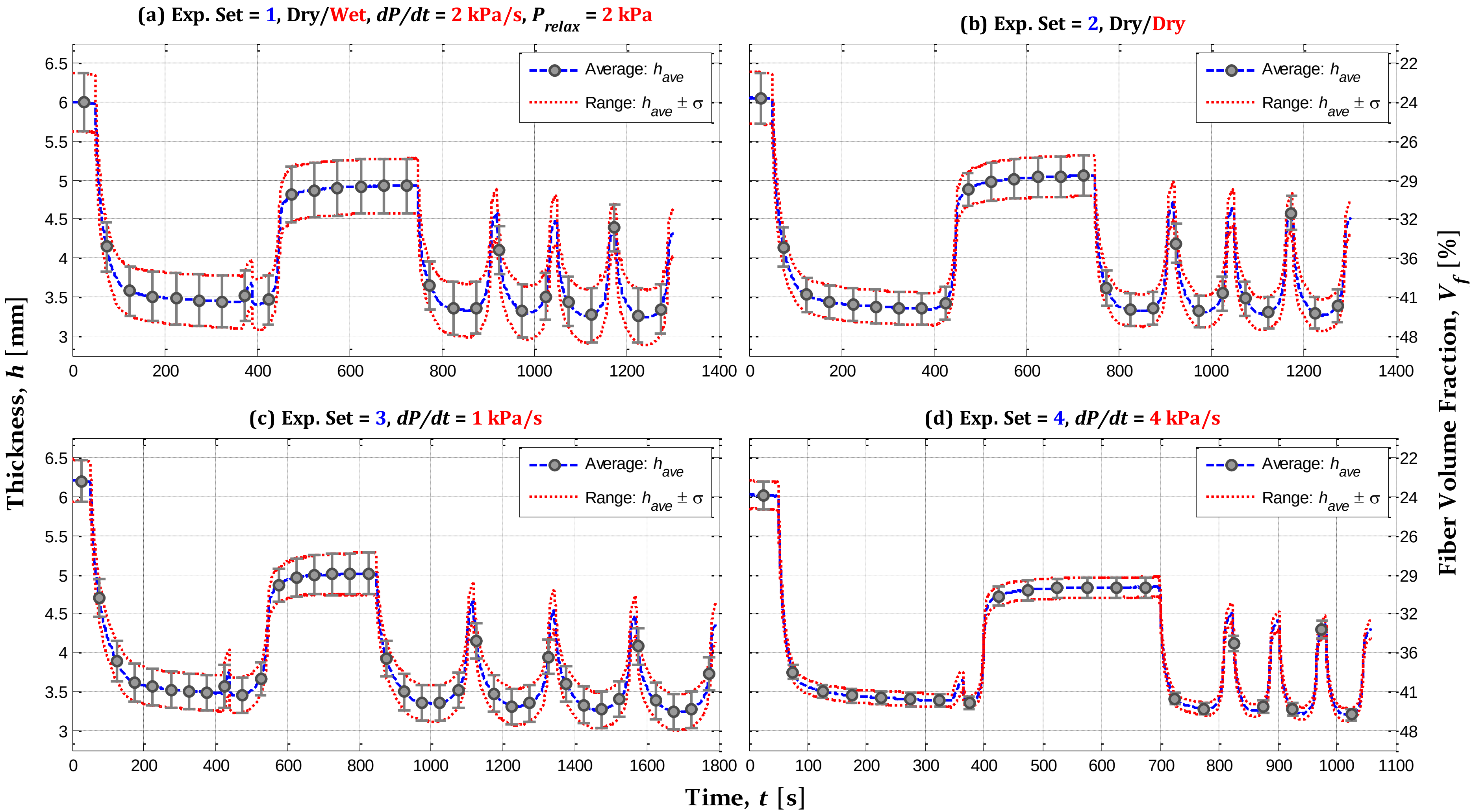

Figure B-29. Thickness vs. time for Experiment Sets 1-4 for Random fabric. In each set, 12 specimens were characterized separately.

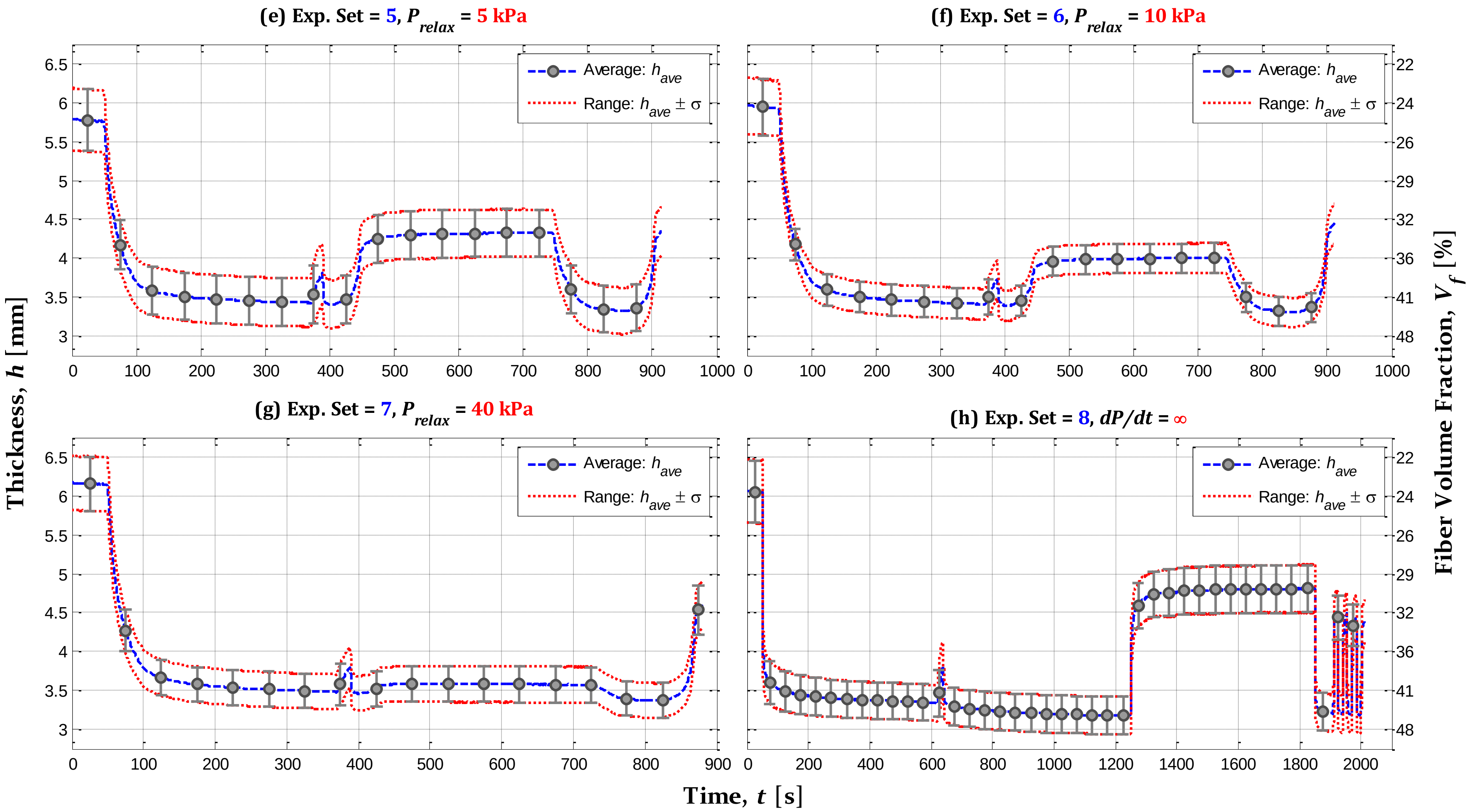

Figure B-30. Thickness vs. time for Experiment Sets 5-8 for Random fabric. In each set, 12 specimens were characterized separately.

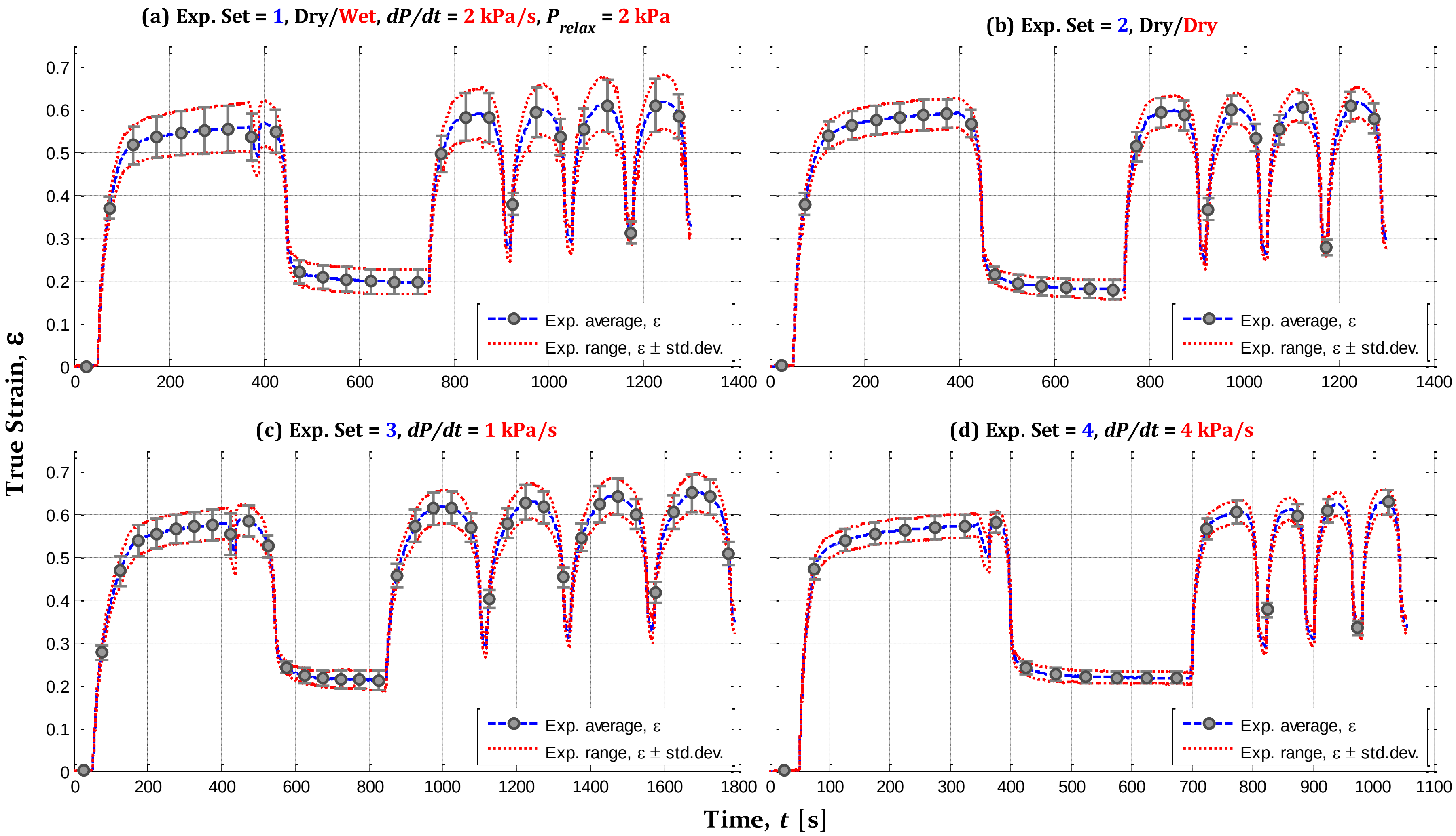

Figure B-31. True strain vs. time for Experiment Sets 1-4 for Random fabric. In each set, 12 specimens were characterized separately.

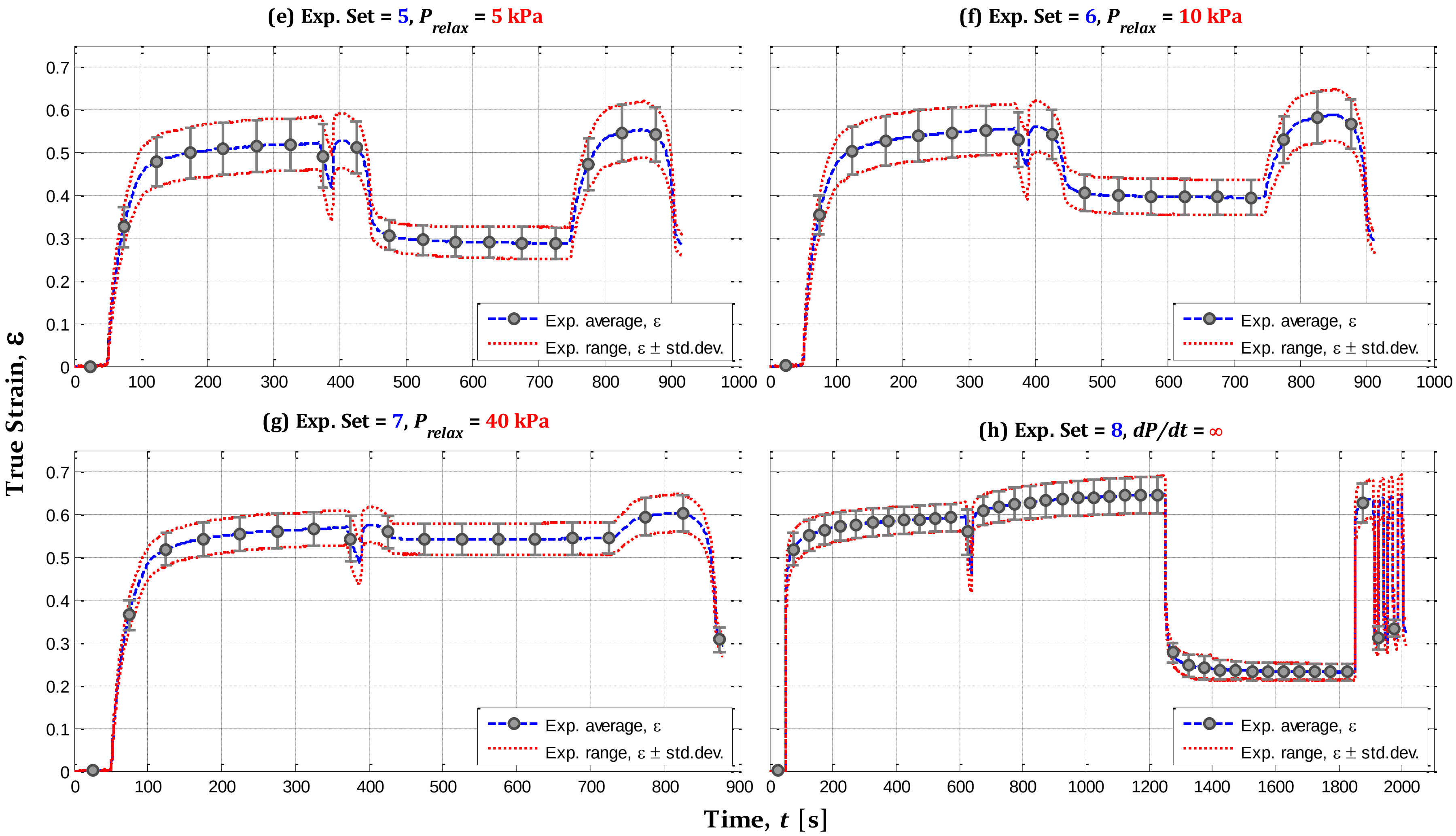

Figure B-32. True strain vs. time for Experiment Sets 5-8 for Random fabric. In each set, 12 specimens were characterized separately.

B.IX All sets show with error bars for woven fabric

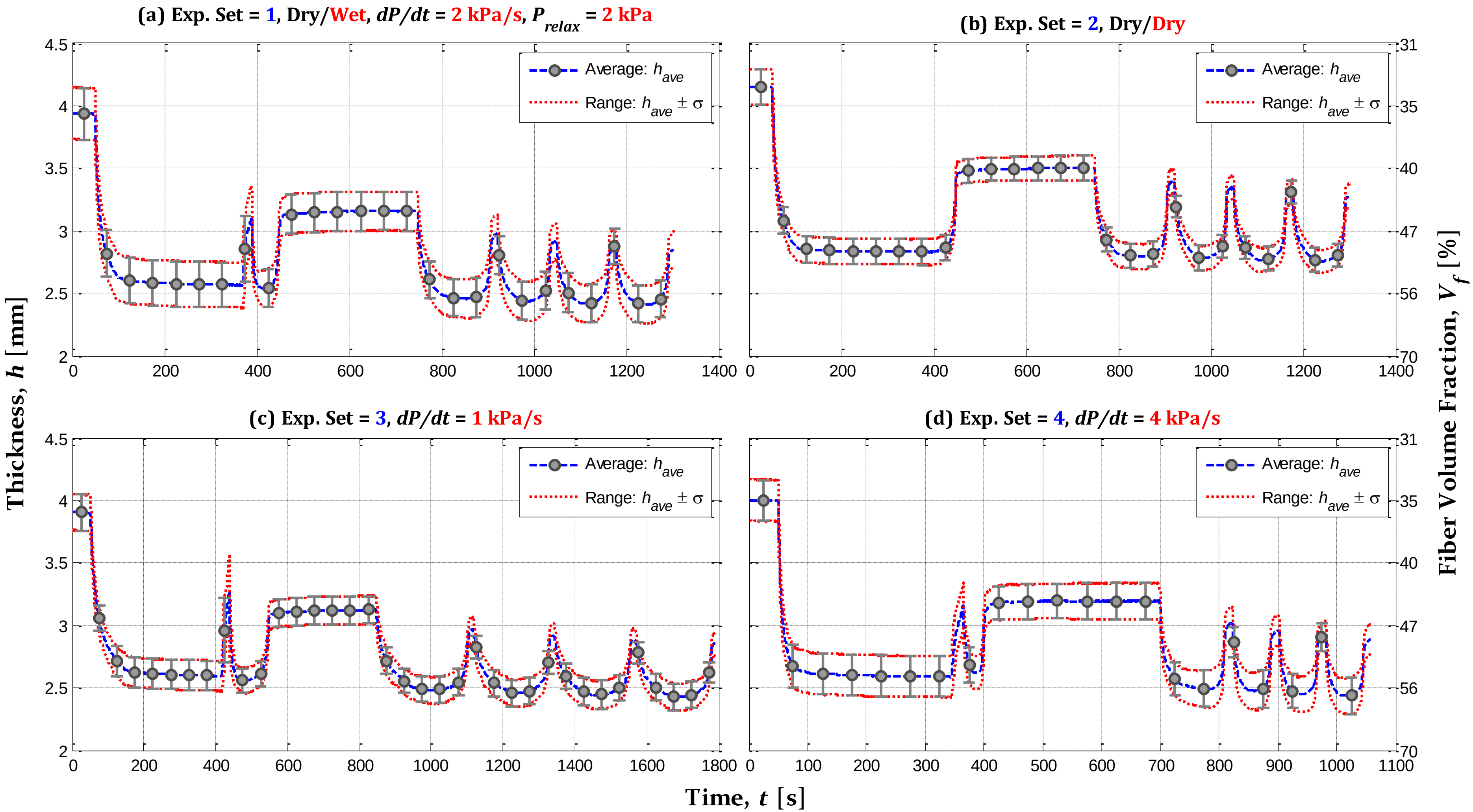

Figure B-33. Thickness vs. time for Experiment Sets 1-4 for Woven fabric. In each set, 12 specimens were characterized separately.

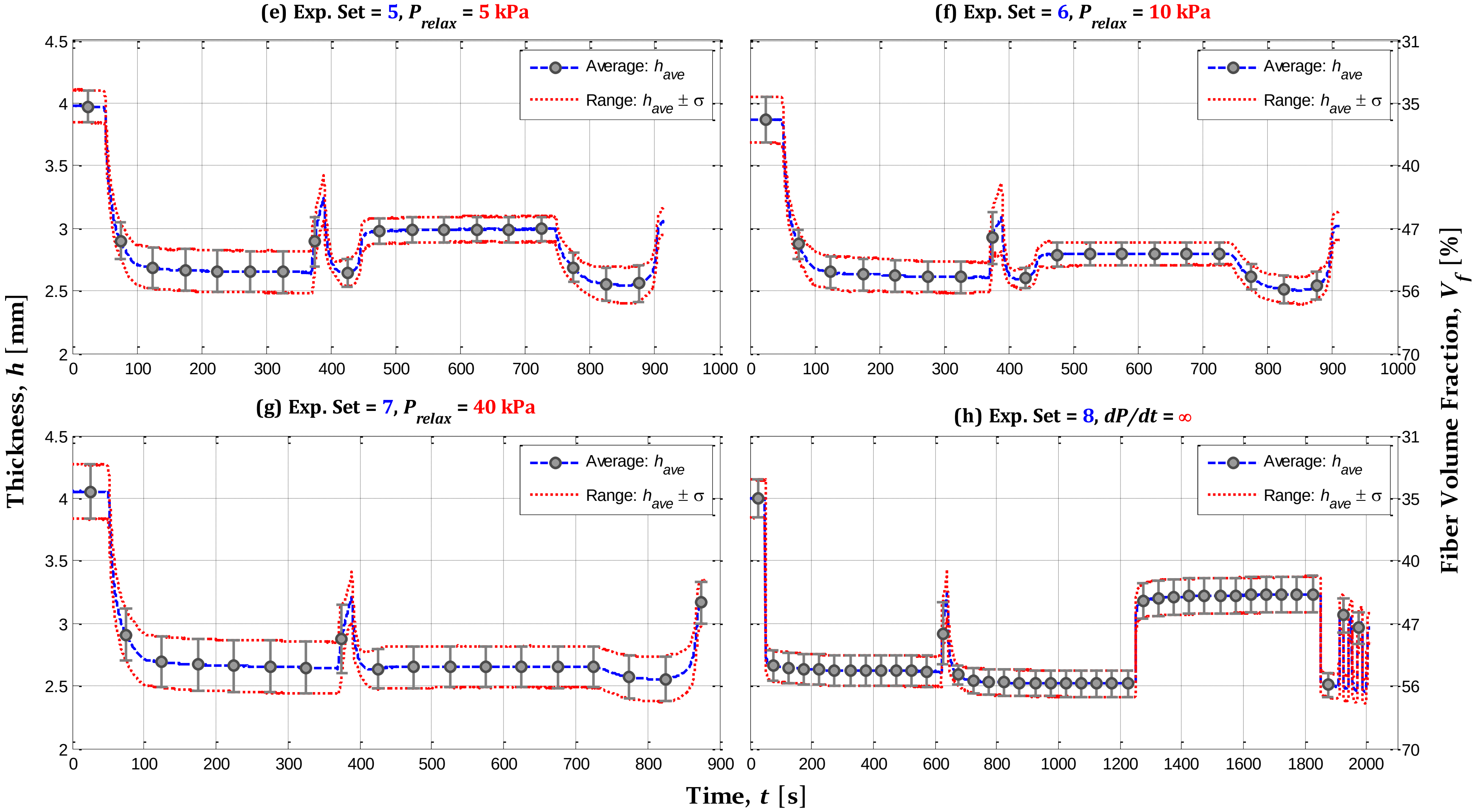

Figure B-34. Thickness vs. time for Experiment Sets 5-8 for Woven fabric. In each set, 12 specimens were characterized separately.

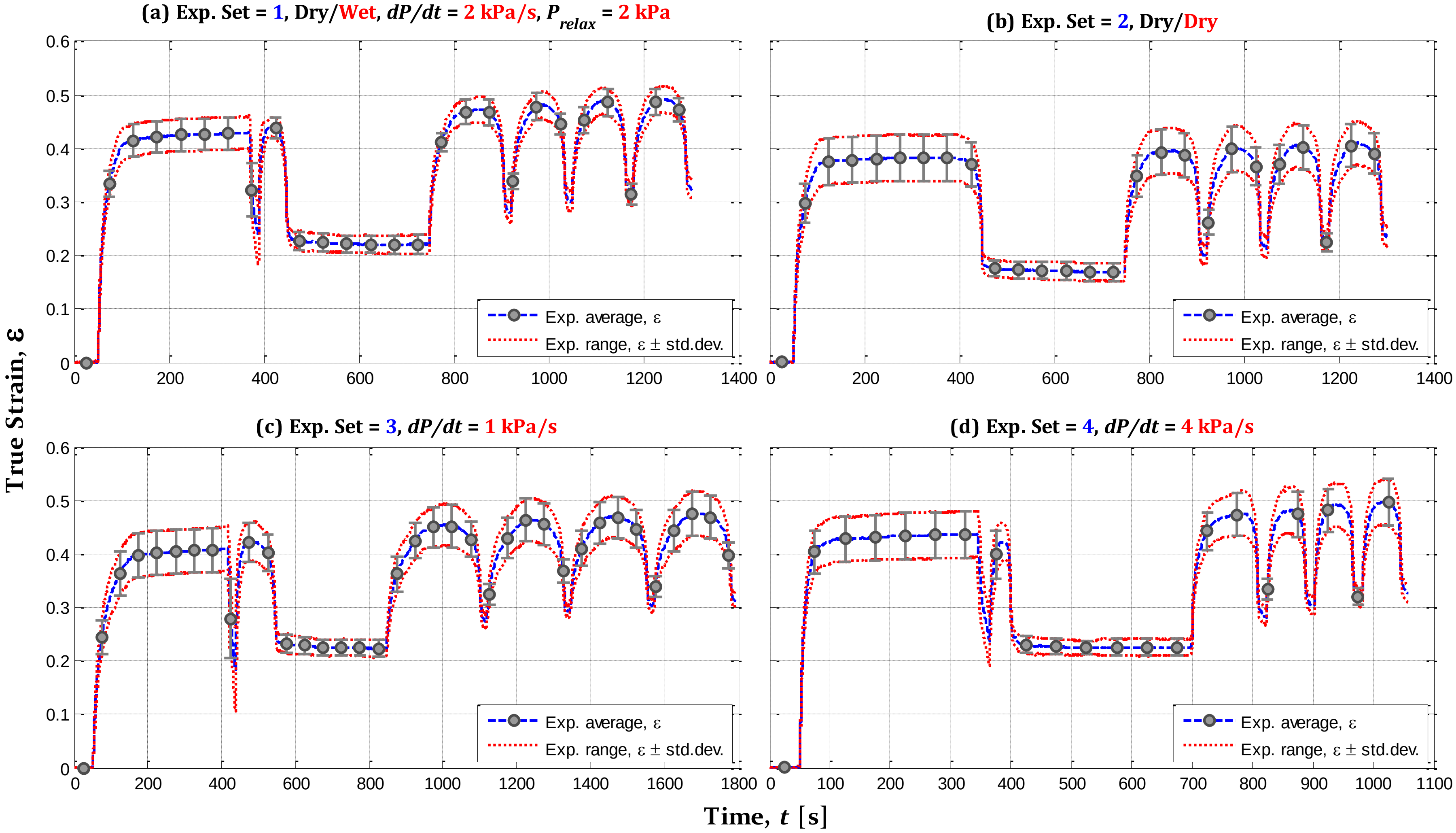

Figure B-35. True strain vs. time for Experiment Sets 1-4 for Woven fabric. In each set, 12 specimens were characterized separately.

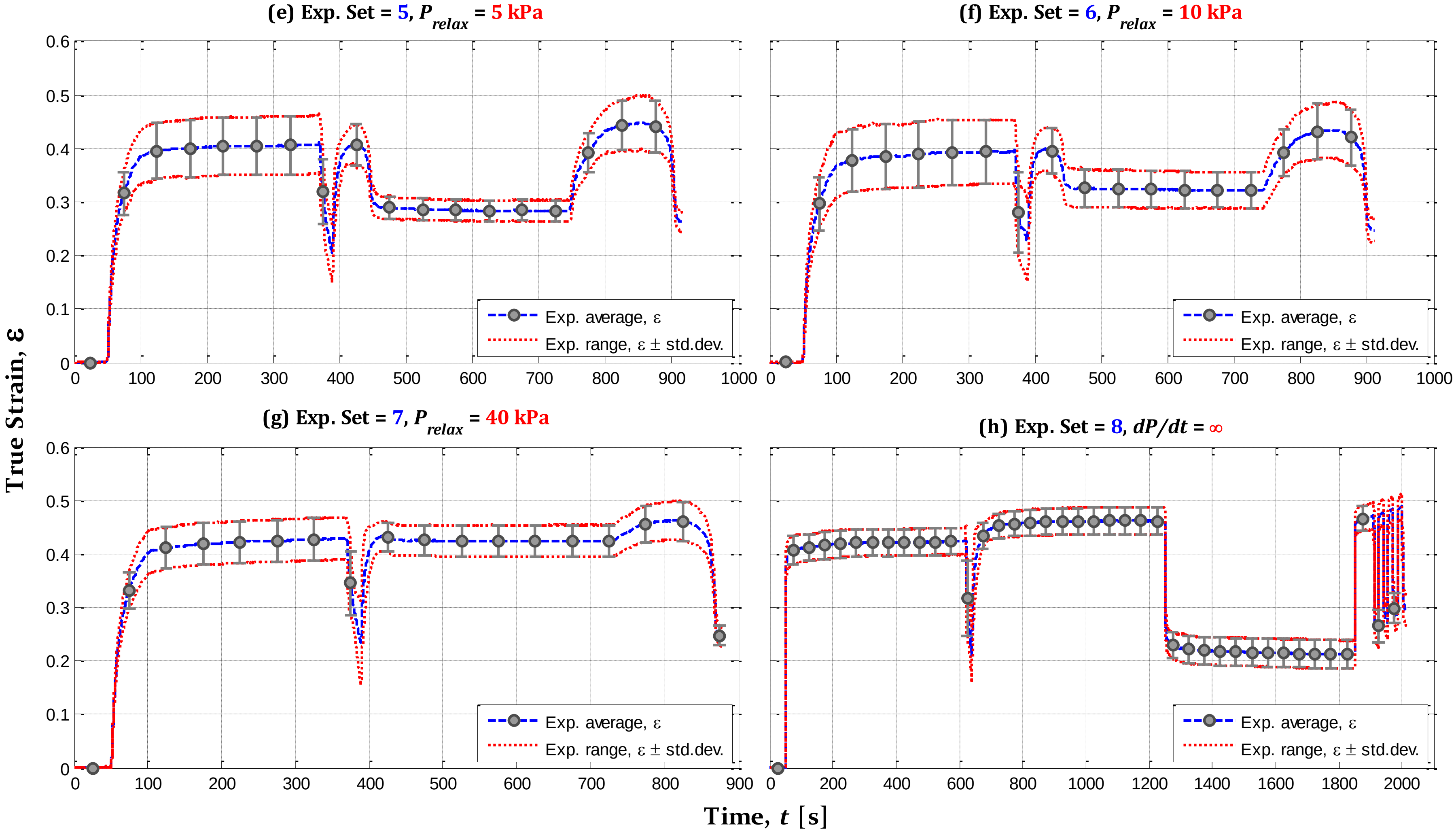

Figure B-36. True strain vs. time for Experiment Sets 5-8 for Woven fabric. In each set, 12 specimens were characterized separately.

B.X Fabric specimen variations

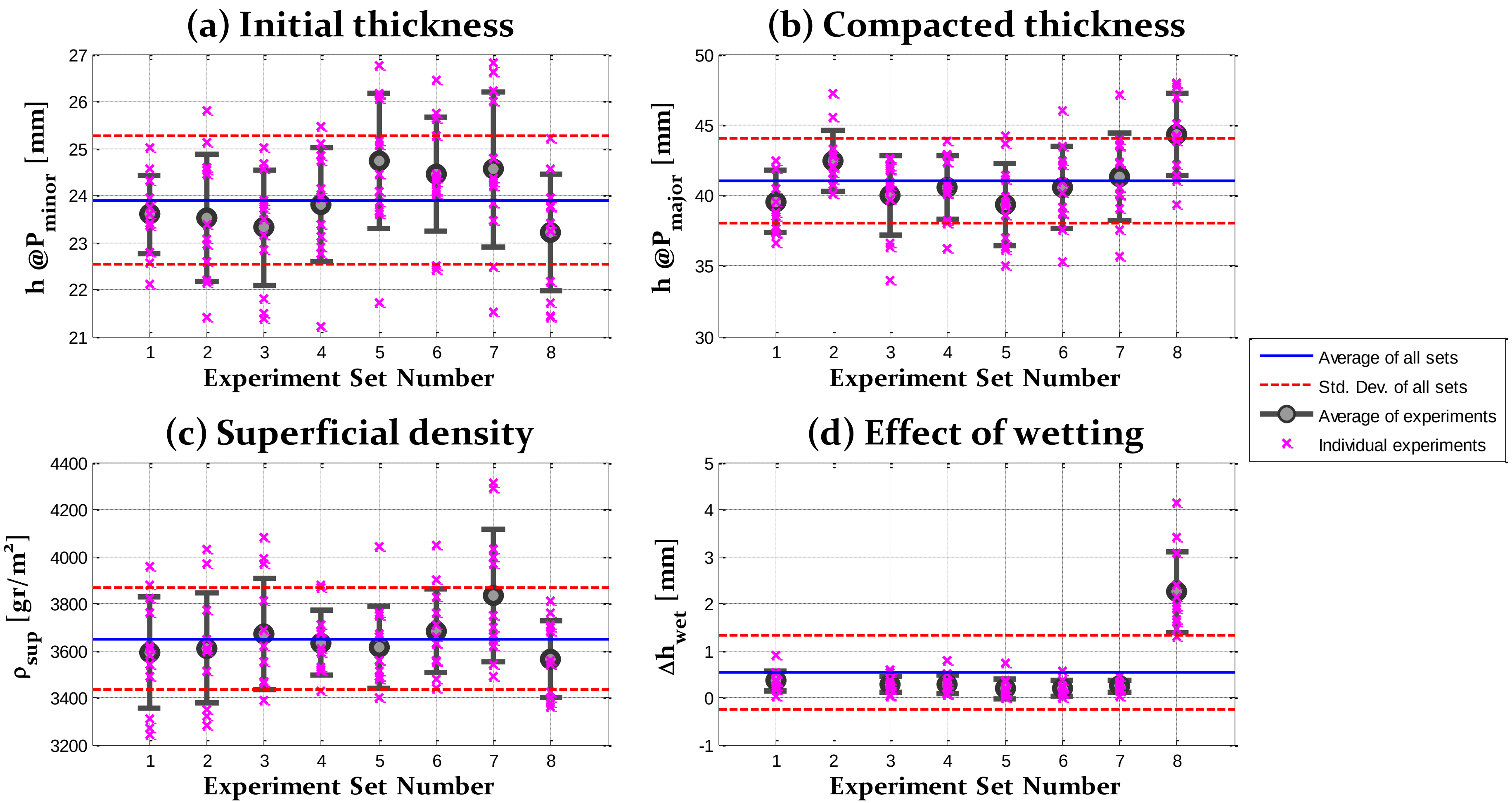

Figure B-37. Variation in fabric parameters within experiments for Random fabric.

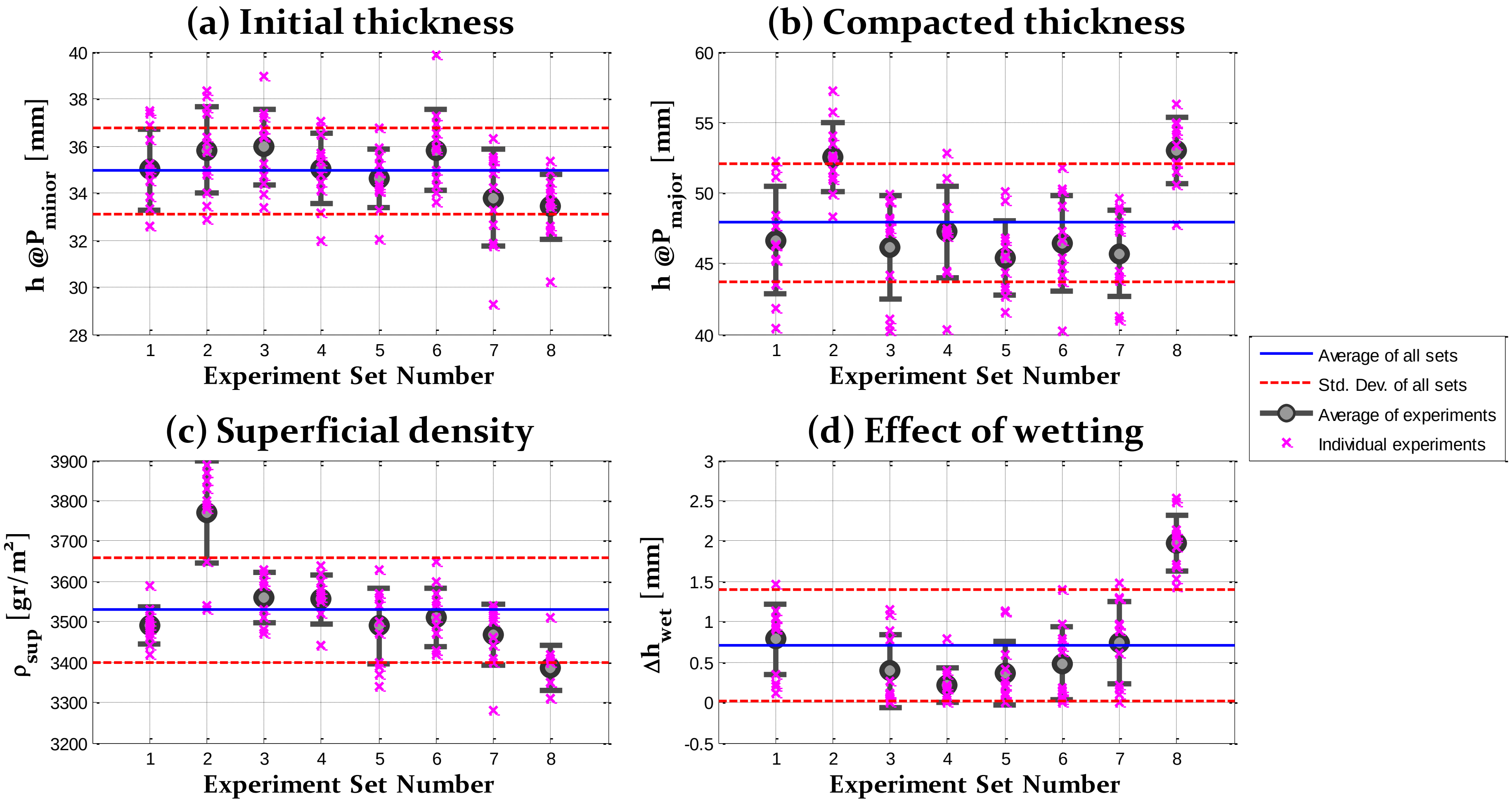

Figure B-38. Variation in fabric parameters within experiments for Woven fabric.

B.XI Change in thickness during main stages

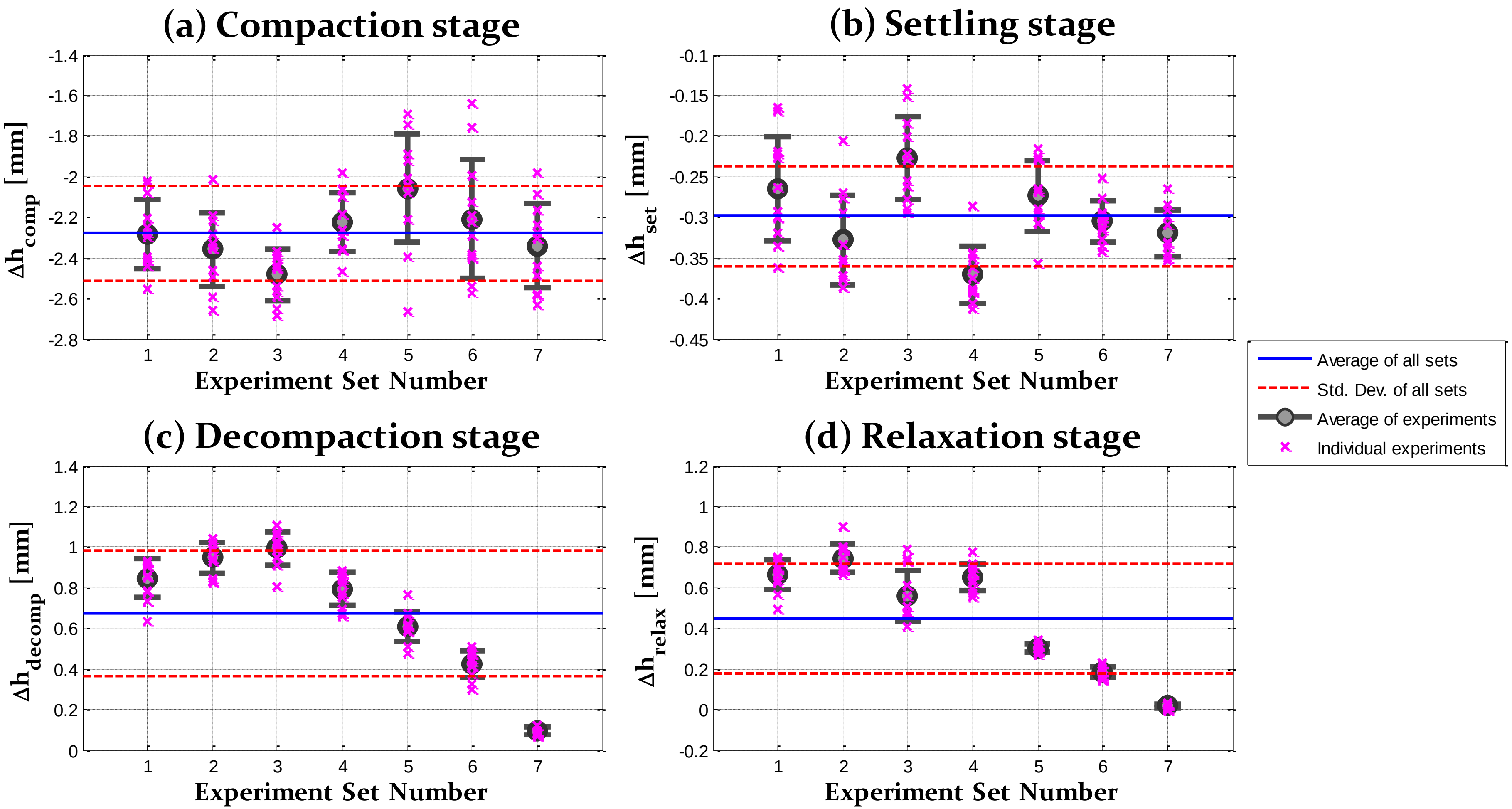

Figure B-39. Change in thickness during main stages for Random fabric excluding Experiment Set 8 (step input).

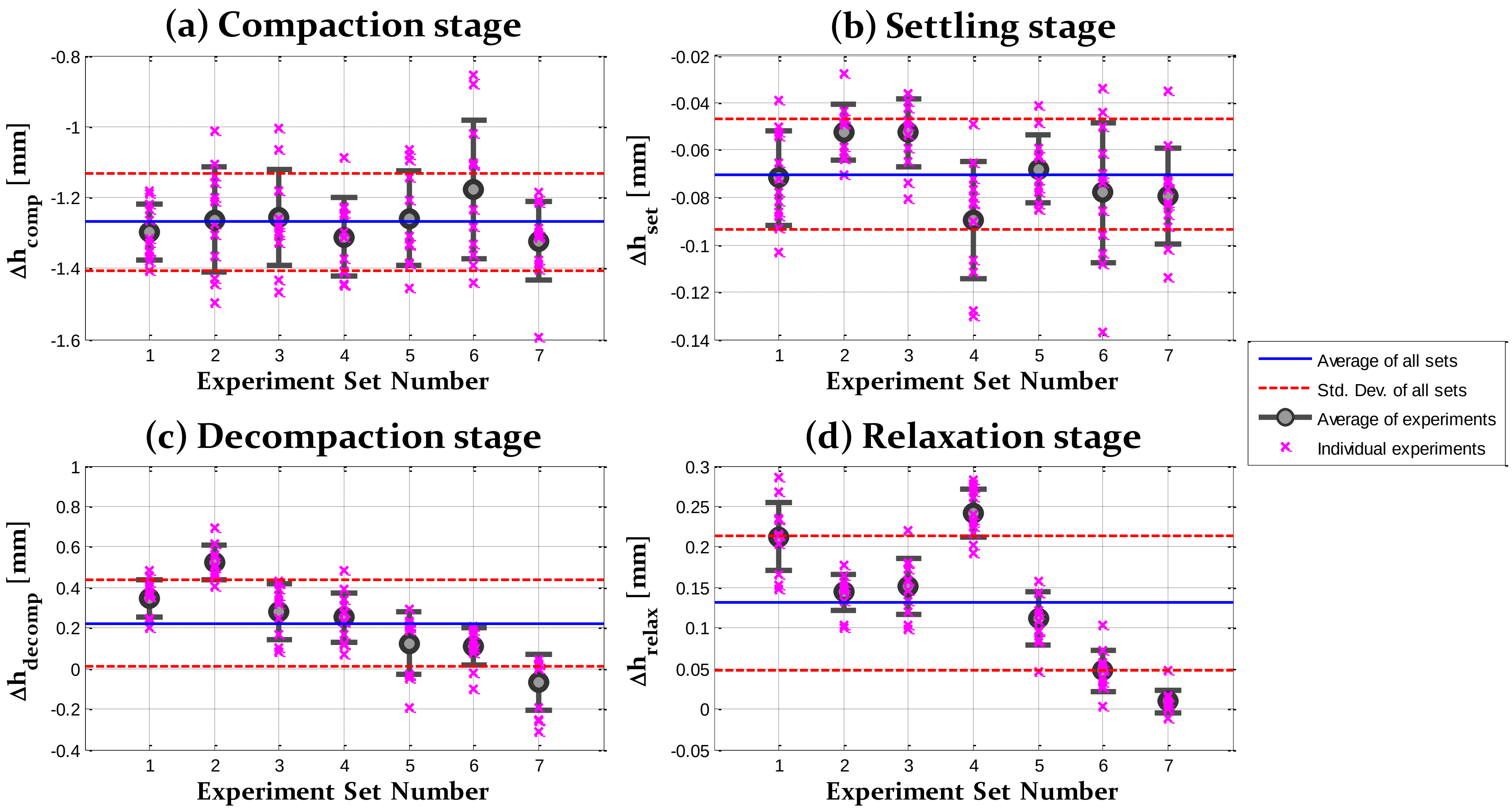

Figure B-40. Change in thickness during main stages for Woven fabric excluding Experiment Set 8 (step input).

i. Random

Exp. Set	ρ_{sup} [gr/m²]				h_{minor} [kPa] @ 2 kPa				h_{major} [kPa] @ 80 kPa			
	min	avr	max	Std. dev	min	avr	max	Std. dev	min	avr	max	Std. dev
1	2830	3390	3840	314	7.47	8.34	9.88	0.75	2.10	2.50	2.96	0.23
2	3030	3450	4210	372	7.36	9.64	12.0	1.48	2.39	2.80	3.33	0.32
3	2780	3460	4040	439	6.88	8.30	9.51	0.85	2.14	2.89	3.57	0.44
4	2720	3530	4330	460	7.16	8.40	9.30	0.69	2.25	2.90	3.50	0.40
5	2920	3530	4190	385	6.43	7.74	9.51	0.85	2.42	2.89	3.42	0.33
6	2710	3360	4070	347	7.04	8.39	10.0	0.78	2.15	2.64	3.37	0.36
7	2730	3360	4050	455	7.27	8.63	10.1	0.80	1.92	2.69	3.71	0.58
Overall	**2710**	**3440**	**4330**	**391**	**6.43**	**8.49**	**12.0**	**1.04**	**1.92**	**2.76**	**3.71**	**0.41**

ii. Woven

Exp. Set	ρ_{sup} [gr/m²]				h_{minor} [kPa] @ 2 kPa				h_{major} [kPa] @ 80 kPa			
	min	avr	max	Std. dev	min	avr	max	Std. dev	min	avr	max	Std. dev

1	3450	3650	3860	120	4.23	5.18	6.37	0.67	2.23	2.45	2.73	0.16
2	3380	3580	3760	107	4.35	4.84	5.45	0.32	4.19	4.63	5.18	0.28
3	3320	3450	3590	96	4.40	4.60	4.83	0.13	2.13	2.28	2.52	0.12
4	3160	3460	3670	139	4.54	4.73	4.97	0.16	2.23	2.35	2.47	0.10
5	3410	3560	3710	95	4.29	4.72	5.28	0.25	3.85	4.26	4.70	0.24
6	3310	3560	3740	134	4.37	4.78	5.18	0.25	2.29	2.47	2.65	0.11
7	3150	3420	3580	115	4.47	4.61	4.75	0.10	2.04	2.23	2.42	0.13
Overall	**3160**	**3460**	**3670**	**139**	**4.54**	**4.73**	**4.97**	**0.16**	**2.23**	**2.35**	**2.47**	**0.10**

Appendix C *Analytical solution for linear models*

$$\varepsilon(\sigma(t)) = L^{-1}\{L\{\sigma(t)\}\mathrm{E}(\mathrm{s})\}$$

Sample input (First 5 stages of the base experiment):

Maxwell model

$$\mathrm{E}(s) = \frac{1}{E} + \frac{1}{cs}$$

Kelvin-Voigt model

$$\mathrm{E}(s) = \frac{1}{E + cs}$$

Zener model

$$\mathrm{E}(s) = E_0 + \frac{1}{E_1} + \frac{1}{c_1 s}$$

Generalized Maxwell model

$$\mathrm{E}(s) = E_0 + \frac{E_1 c_1 s}{E_1 + c_1 s} + \frac{E_2 c_2 s}{E_2 + c_2 s} + \cdots + \frac{E_n c_n s}{E_n + c_n s}$$

Burger's model

$$\mathrm{E}(s) = \frac{1}{E_1} + \frac{1}{c_1 s} + \frac{1}{E_2 + c_2 s}$$

Appendix D *Curve fitting results*

D.I Tabulated results

i. Maxwell Model

	Set	E [kPa]	m	c [kPa.s]	R^2
Random fabric	1	1.190e3	2.95	2.225e5	0.870
	2	1.091e3	3.02	2.064e5	0.860
	3	1.138e3	3.01	2.377e5	0.821
	4	1.002e3	2.71	1.832e5	0.873
	5	1.951e3	3.36	2.901e5	0.893
	6	1.629e3	3.47	2.629e5	0.901
	7	1.581e3	3.66	3.275e5	0.899
	All	*6.832e2*	*2.38*	*2.293e5*	*0.874*

	Set	E [kPa]	m	c [kPa.s]	R^2
Woven fabric	1	2.867e3	3.02	2.392e5	0.721
	2	3.070e3	2.87	2.841e5	0.737
	3	6.124e3	3.44	2.698e5	0.574
	4	1.499e3	2.47	2.219e5	0.711
	5	2.744e3	3.17	3.711e5	0.790
	6	2.800e3	3.10	3.821e5	0.819
	7	2.643e3	3.53	6.817e5	0.803
	All	*8.083e2*	*1.92*	*2.627e5*	*0.736*

ii. Kelvin-Voigt Model

	Set	E [kPa]	m	c [kPa.s]	R^2
Random fabric	1	4.001e3	7.44	6.354e2	0.902
	2	2.505e3	7.26	6.244e2	0.917
	3	2.360e3	6.65	1.036e3	0.893
	4	4.324e3	9.41	5.385e2	0.904
	5	4.439e3	6.38	1.334e3	0.954
	6	4.786e3	8.44	1.214e3	0.947
	7	8.575e2	15.81	1.235e3	0.928
	All	*3.449e3*	*7.36*	*8.481e2*	*0.921*

	Set	E [kPa]	m	c [kPa.s]	R^2
Woven fabric	1	2.189e4	20.26	4.844e2	0.888
	2	9.346e4	23.00	4.639e2	0.928
	3	4.646e4	20.87	9.537e2	0.883
	4	2.136e2	28.75	3.313e2	0.872
	5	1.835e5	12.66	5.314e2	0.950
	6	2.624e5	17.38	6.325e2	0.951
	7	2.664e4	19.65	4.994e2	0.951
	All	*7.803e4*	*18.90*	*5.085e2*	*0.917*

iii. Zener Model

	Set	E_0 [kPa]	m_0	E_1 [kPa]	m_1	c_1 [kPa.s]	R^2
Random fabric	1	1.208e3	4.54	3.327e4	3.90	2.203e3	0.900
	2	8.014e2	4.25	4.342e4	4.33	2.654e3	0.913
	3	9.448e2	4.39	3.324e4	3.88	3.002e3	0.886
	4	1.160e3	4.78	1.712e4	3.65	2.004e3	0.912
	5	2.099e3	5.03	4.650e2	1.71	6.796e3	0.969
	6	1.108e3	4.62	1.856e2	1.28	1.014e4	0.969
	7	2.929e3	9.64	5.445e2	2.04	1.079e4	0.961
	All	*1.195e3*	*4.66*	*2.720e4*	*3.88*	*3.158e3*	*0.930*

	Set	E_0 [kPa]	m_0	E_1 [kPa]	m_1	c_1 [kPa.s]	R^2
Woven fabric	1	2.186e4	7.61	7.086e3	3.61	3.918e3	0.833
	2	1.950e4	6.26	3.655e4	3.56	2.210e3	0.942
	3	1.248e5	13.8	1.234e3	2.73	3.124e4	0.874
	4	1.294e4	5.89	3.524e4	4.09	2.975e3	0.811
	5	3.587e4	7.80	6.731e3	3.17	3.317e3	0.953
	6	6.899e4	10.0	7.012e2	2.17	6.404e4	0.965
	7	4.336e4	9.71	2.235e2	1.49	6.912e3	0.954
	All	*1.855e4*	*6.64*	*2.519e5*	*3.87*	*3.270e3*	*0.904*

iv. Generalized Maxwell Model n=2

	Set	E_0 [kPa]	m_0	E_1 [kPa]	m_1	c_1 [kPa.s]	E_2 [kPa]	m_2	c_2 [kPa.s]	R^2
Random fabric	1	1.588e3	5.57	1.667e3	3.91	3.214e4	5.777e2	1.60	5.681e2	0.947
	2	1.058e3	5.55	1.812e3	4.05	3.866e4	5.773e2	1.58	4.648e2	0.968
	3	1.193e3	5.50	1.682e3	3.91	3.655e4	6.254e2	1.53	6.753e2	0.943
	4	1.446e3	5.62	1.813e3	4.02	2.316e4	5.138e2	1.61	6.365e2	0.950
	5	1.882e3	5.21	7.281e2	2.88	3.538e4	1.418e3	2.03	1.379e3	0.982
	6	2.849e3	7.29	1.467e3	3.63	2.407e4	5.050e1	0.68	1.665e3	0.974
	7	2.048e3	11.1	1.112e3	3.20	3.630e4	1.240e2	1.13	7.286e2	0.972
	All	*1.505e3*	*5.73*	*1.733e3*	*3.78*	*3.561e4*	*5.308e2*	*1.54*	*5.283e2*	*0.962*

	Set	E_0 [kPa]	m_0	E_1 [kPa]	m_1	c_1 [kPa.s]	E_2 [kPa]	m_2	c_2 [kPa.s]	R^2
Woven fabric	1	6.443e4	13.7	4.524e4	5.39	8.989e3	3.119e2	1.24	2.776e2	0.905
	2	3.013e4	7.11	5.990e2	2.40	3.578e4	4.324e2	1.81	6.590e2	0.962
	3	5.487e4	9.38	1.475e3	2.93	2.449e4	4.838e2	1.19	3.644e2	0.885
	4	2.980e4	7.73	3.862e4	5.78	3.629e4	5.310e2	1.57	5.285e2	0.935
	5	1.332e5	12.1	8.890e3	4.66	1.511e4	1.110e2	1.05	1.043e3	0.967
	6	1.327e5	17.5	2.399e3	3.53	5.436e4	3.093e1	0.57	2.567e3	0.960
	7	4.981e4	11.2	2.031e3	3.72	4.361e4	6.670e2	1.78	9.153e2	0.966
	All	*2.963e4*	*7.73*	*3.767e4*	*5.78*	*3.561e4*	*5.309e2*	*1.57*	*5.286e2*	*0.940*

v. Generalized Maxwell Model n=3

	Set	E_0 [kPa]	m_0	E_1 [kPa]	m_1	c_1 [kPa.s]	E_2 [kPa]	m_2	c_2 [kPa.s]	E_3 [kPa]	m_3	c_3 [kPa.s]	R^2
Random fabric	1	1.531e3	5.46	1.843e3	4.01	3.022e4	4.894e2	1.58	4.935e2	1.287e4	3.66	9.710e1	0.946
	2	1.054e3	5.49	1.745e3	4.04	3.662e4	4.103e2	1.51	3.942e2	2.098e4	3.64	1.074e2	0.967
	3	1.175e3	5.50	1.638e3	3.88	3.867e4	5.050e2	1.54	5.737e2	1.450e4	3.55	9.923e1	0.944
	4	1.592e3	5.82	3.000e3	4.46	1.959e4	1.743e2	1.20	5.011e2	1.786e4	3.94	1.011e2	0.949
	5	2.376e3	5.51	1.008e3	3.13	2.299e4	5.999e2	1.57	1.299e3	1.142e3	3.28	8.083e1	0.982
	6	2.484e3	6.94	6.574e2	2.79	2.747e4	3.002e1	0.62	1.432e3	1.730e4	3.62	1.403e2	0.977
	7	9.626e2	14.1	9.681e2	3.08	3.461e4	1.016e2	1.36	8.984e2	1.599e4	0.61	1.194e2	0.964
	All	*1.446e3*	*5.62*	*1.492e3*	*3.71*	*3.516e4*	*3.248e2*	*1.49*	*6.209e2*	*1.952e4*	*3.30*	*9.515e1*	*0.961*

	Set	E_0 [kPa]	m_0	E_1 [kPa]	m_1	c_1 [kPa.s]	E_2 [kPa]	m_2	c_2 [kPa.s]	E_3 [kPa]	m_3	c_3 [kPa.s]	R^2
Woven fabric	1	3.597e4	9.23	4.087e2	3.20	3.029e3	3.817e2	1.50	5019e2	1.119e4	4.89	6.431e3	0.898
	2	7.673e4	8.59	2.349e2	2.76	3.448e3	3.768e1	0.60	4334e2	3.743e4	5.34	8.921e3	0.958
	3	6.880e4	9.97	1.521e2	3.18	2.107e3	2.169e2	0.52	2299e2	2.412e3	3.26	1.881e4	0.870
	4	2.338e4	6.52	4.123e3	5.36	2.459e3	3.889e2	1.89	2785e2	1.753e4	4.37	4.514e3	0.818
	5	1.003e5	10.7	7.815e1	1.30	9.011e2	3.384e1	0.82	6711e2	3.888e3	4.17	9.424e3	0.966
	6	8.740e4	9.47	1.040e2	2.05	3.344e2	1.291e3	0.48	1694e2	1.312e4	3.90	4.998e3	0.968
	7	5.746e4	11.3	6.716e3	4.48	2.680e3	2.131e1	0.42	3513e2	2.138e4	5.44	5.486e3	0.976
	All	*2.384e4*	*6.49*	*4.099e3*	*5.34*	*2.467e3*	*3.897e2*	*1.89*	*2800e2*	*1.743e4*	*4.23*	*4.504e3*	*0.922*

vi. Burgers Model

	Set	E_1 [kPa]	m_1	c_1 [kPa.s]	E_2 [kPa]	m_2	c_2 [kPa.s]	R^2
Random fabric	1	2.638e4	1.87	3.537e5	7.250e3	5.18	3.847e2	0.970
	2	2.833e4	2.28	2.981e5	6.319e3	4.79	3.961e2	0.939
	3	2.501e4	1.94	4.022e5	5.105e3	4.99	7.109e2	0.950
	4	2.825e4	1.80	2.825e5	8.345e3	5.47	3.188e2	0.970
	5	4.107e4	1.57	4.082e5	4.561e3	4.54	5.263e2	0.977
	6	3.562e4	1.30	3.760e5	6.305e3	5.65	6.634e2	0.970
	7	3.309e4	0.82	4.309e5	5.871e3	6.34	6.649e2	0.956
	All	*2.740e4*	*1.74*	*3.614e5*	*6.624e3*	*5.30*	*4.771e2*	*0.962*

	Set	E_1 [kPa]	m_1	c_1 [kPa.s]	E_2 [kPa]	m_2	c_2 [kPa.s]	R^2
Woven fabric	1	9.574e3	0.95	4.269e5	3.672e4	6.37	3.424e2	0.957
	2	6.957e3	0.55	5.396e5	1.818e4	5.09	3.378e2	0.939
	3	2.316e3	0.51	4.350e5	2.201e4	5.31	5.760e2	0.871
	4	6.730e3	0.53	5.311e5	1.689e4	5.88	3.046e2	0.919
	5	2.702e3	0.35	9.917e5	6.836e4	7.73	4.157e2	0.964
	6	6.027e2	0.26	5.800e5	3.741e4	6.03	2.714e2	0.970
	7	1.631e3	0.37	7.389e5	2.279e4	6.20	2.424e2	0.974
	All	*6.687e3*	*0.53*	*5.267e5*	*1.746e4*	*5.48*	*3.271e2*	*0.942*

D.II Graphical Results

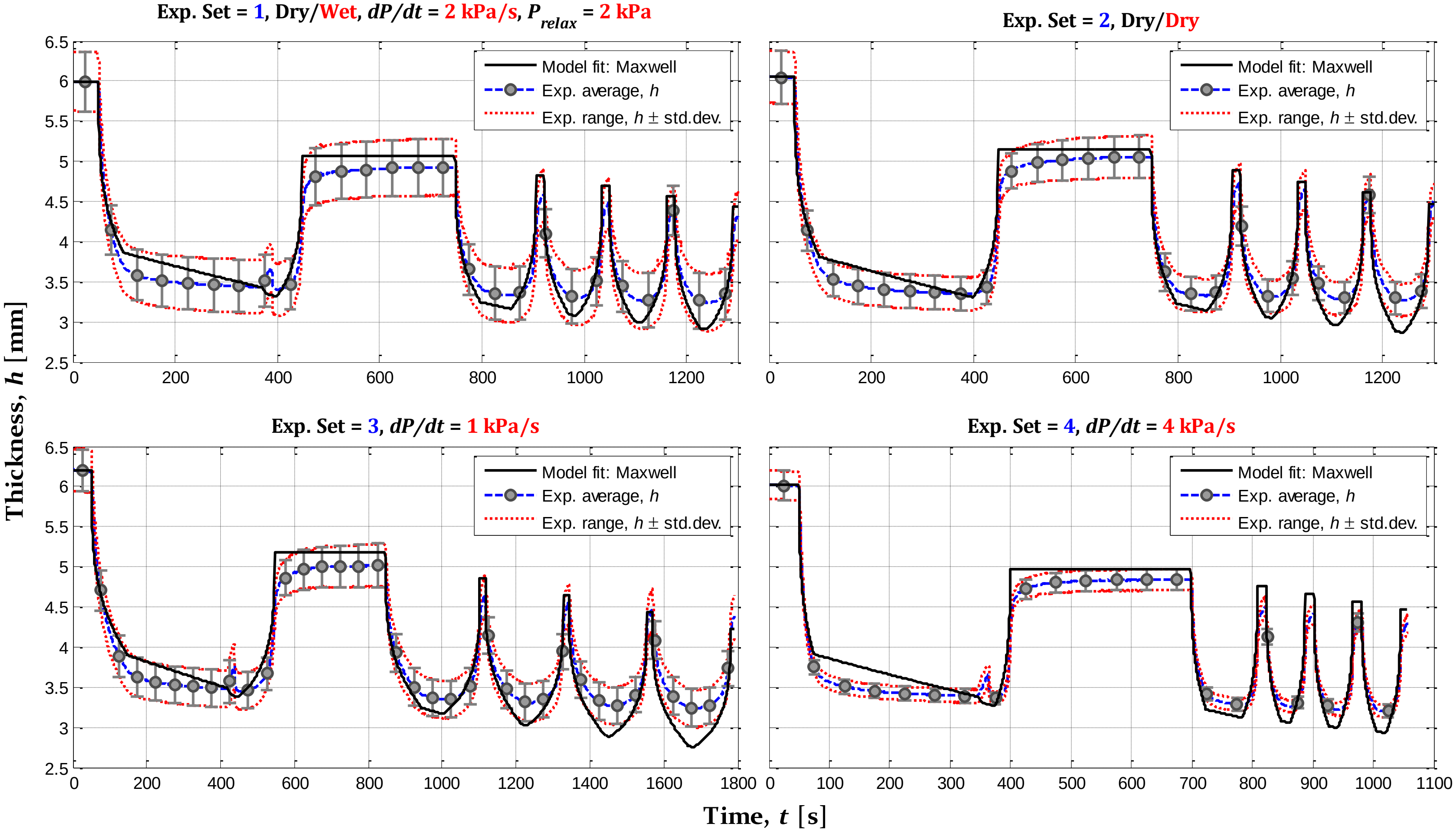

Figure D-1. Thickness graph for Random fabric using *Maxwell model* fitted to each experiment set separately using separate parameter sets.

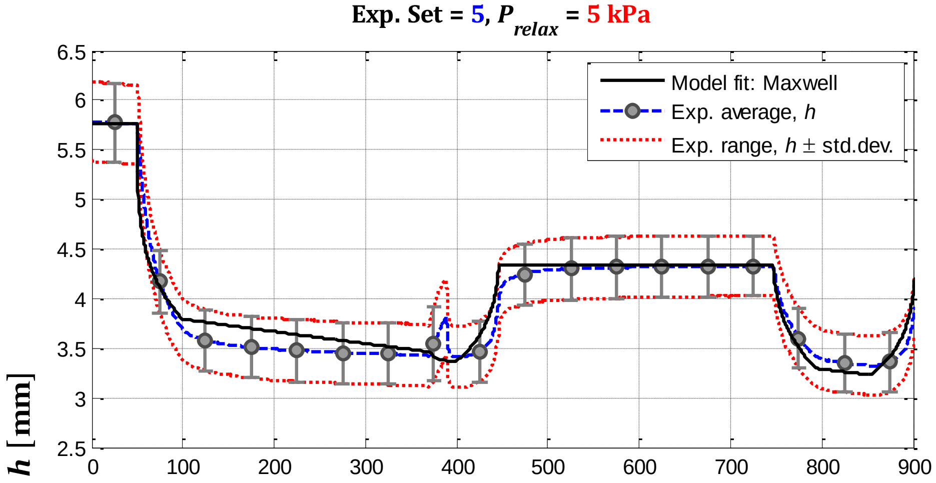

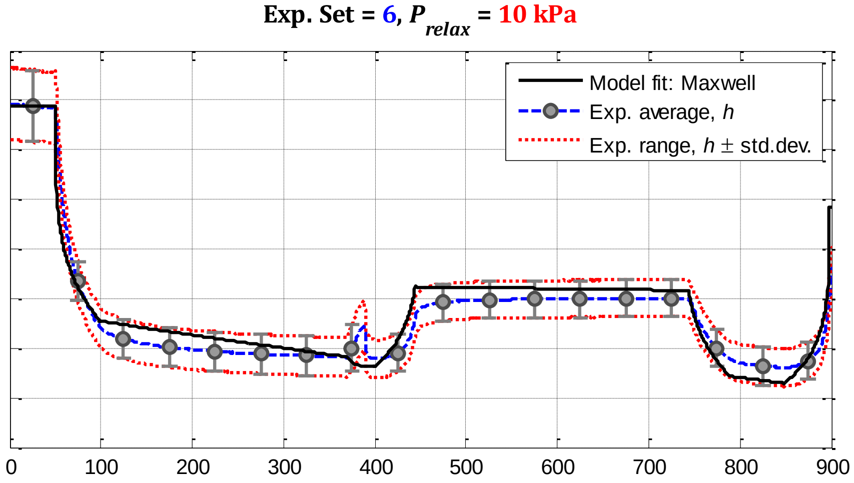

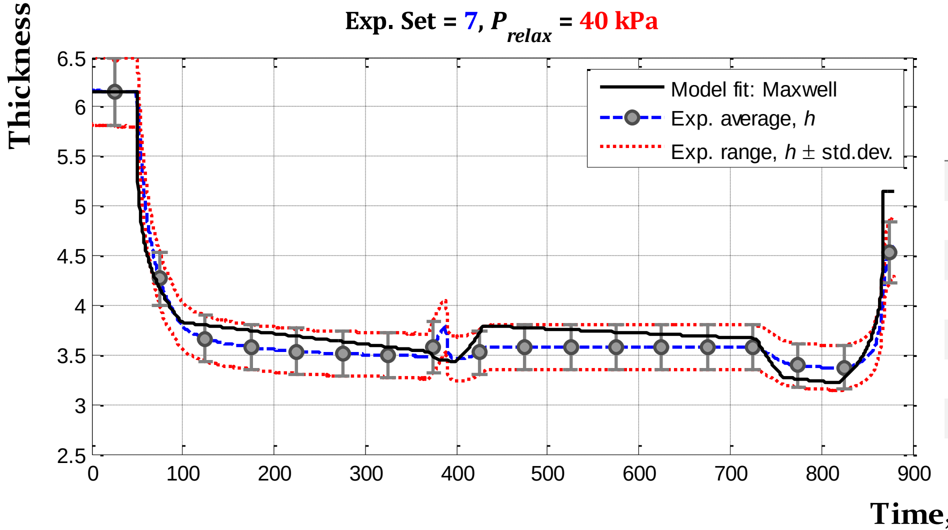

Set	*E* [kPa]	*m*	*c* [kPa.s]	R^2
1	1.190e3	2.95	2.225e5	0.870
2	1.091e3	3.02	2.064e5	0.860
3	1.138e3	3.01	2.377e5	0.821
4	1.002e3	2.71	1.832e5	0.873
5	1.951e3	3.36	2.901e5	0.893
6	1.629e3	3.47	2.629e5	0.901
7	1.581e3	3.66	3.275e5	0.899

Figure D-2. (cont.) Thickness graph for Random fabric using *Maxwell model* fitted to each experiment set separately using separate parameter sets.

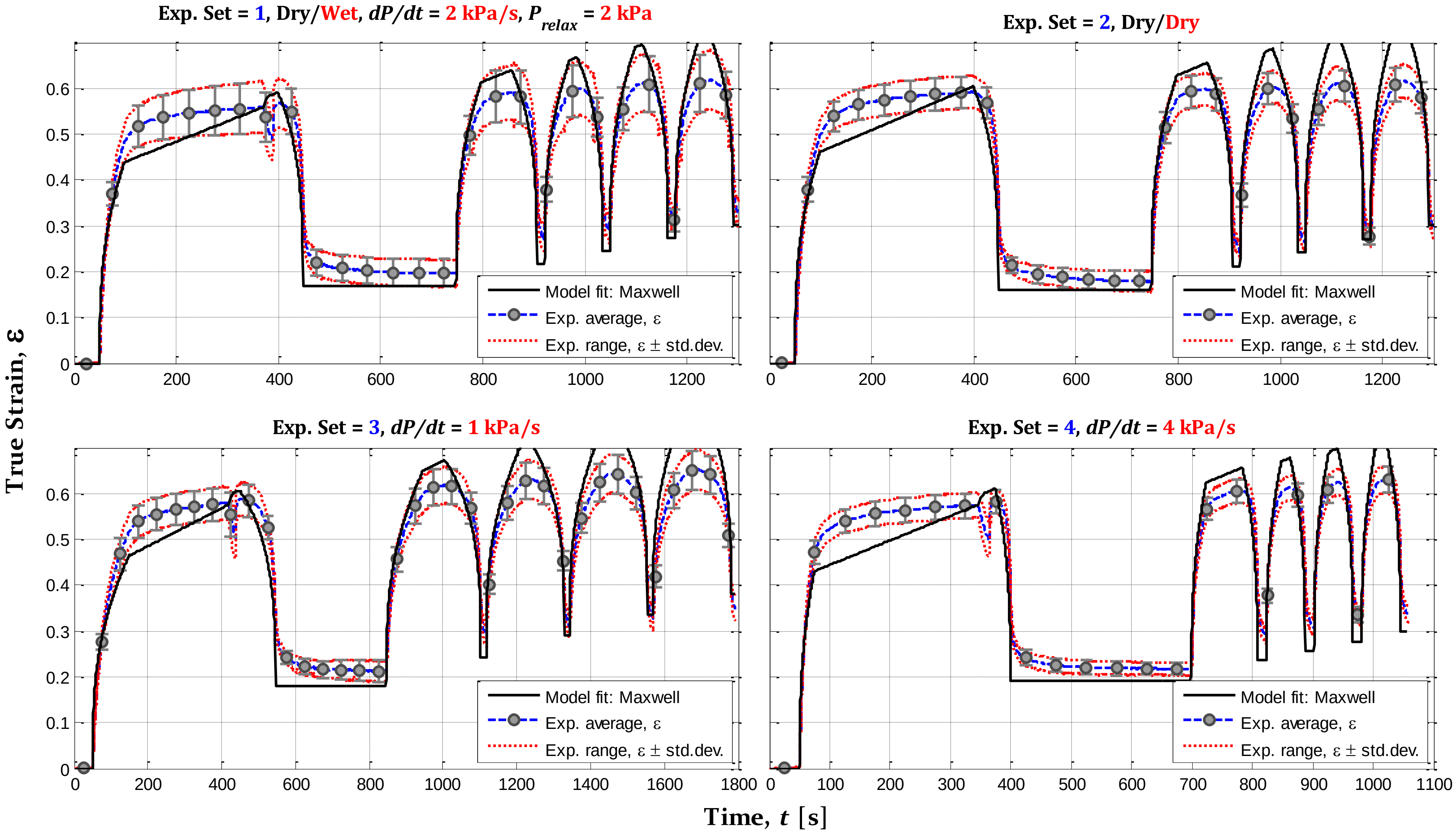

Figure D-3. Strain graph for Random fabric using *Maxwell model* fitted to each experiment set separately using separate parameter sets.

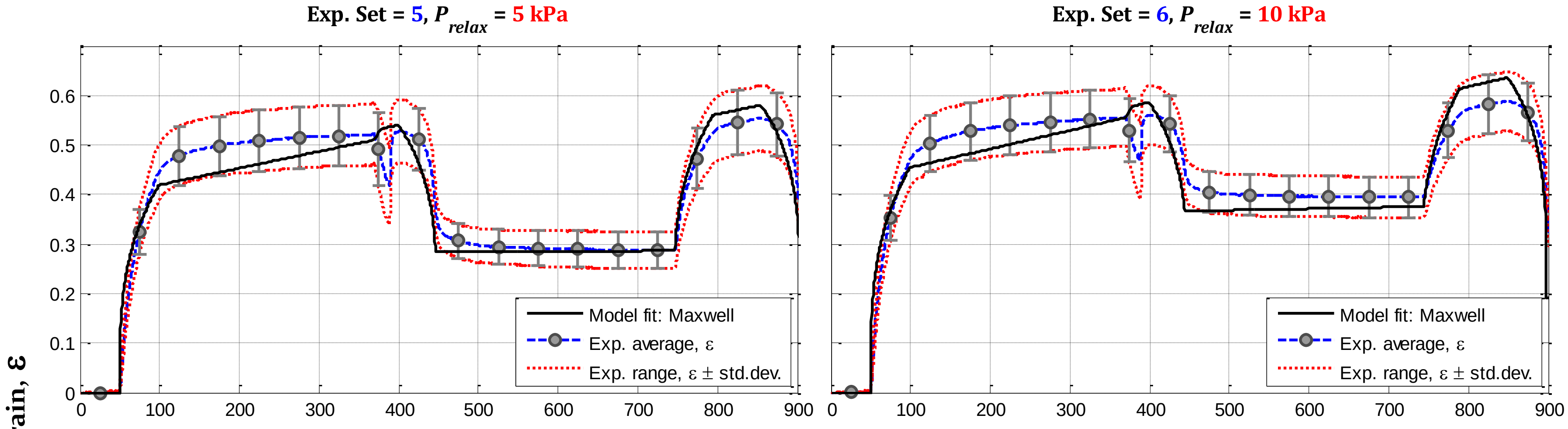

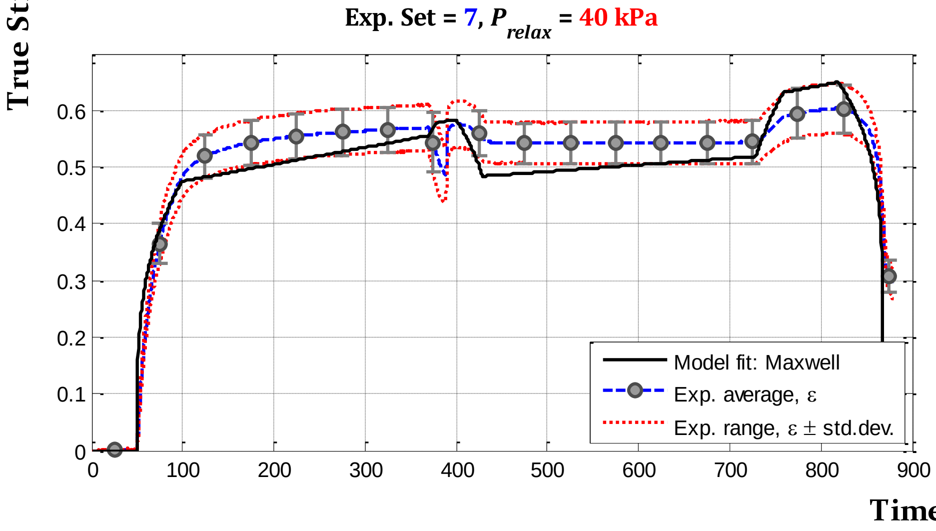

Set	*E* [kPa]	*m*	*c* [kPa.s]	R^2
1	1.190e3	2.95	2.225e5	0.870
2	1.091e3	3.02	2.064e5	0.860
3	1.138e3	3.01	2.377e5	0.821
4	1.002e3	2.71	1.832e5	0.873
5	1.951e3	3.36	2.901e5	0.893
6	1.629e3	3.47	2.629e5	0.901
7	1.581e3	3.66	3.275e5	0.899

Figure D-4. (cont.) Strain graph for Random fabric using *Maxwell model* fitted to each experiment set separately using separate parameter sets.

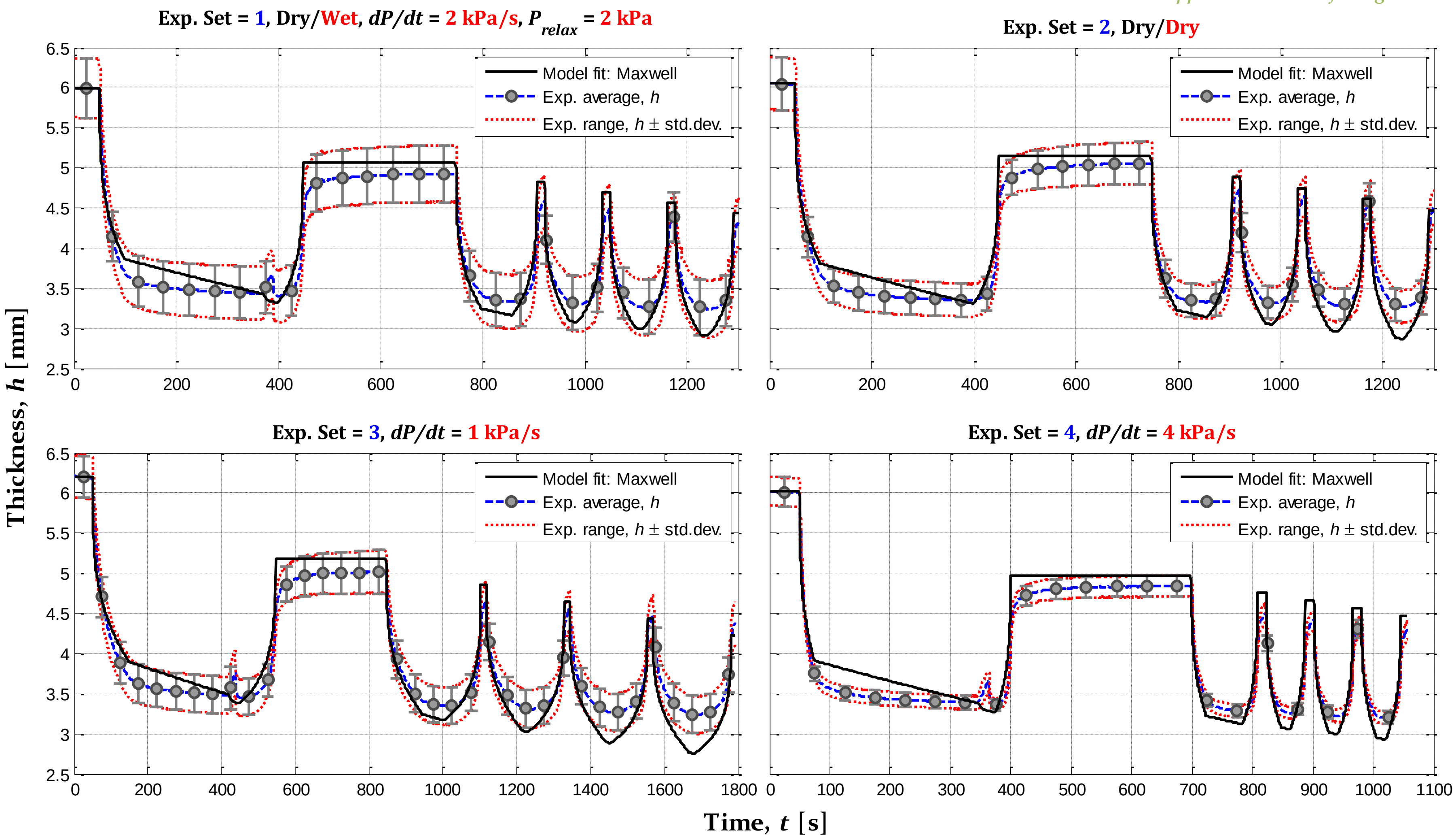

Figure D-5. Thickness graph for Random fabric using *Maxwell model* fitted to all experiment sets using a single parameter set.

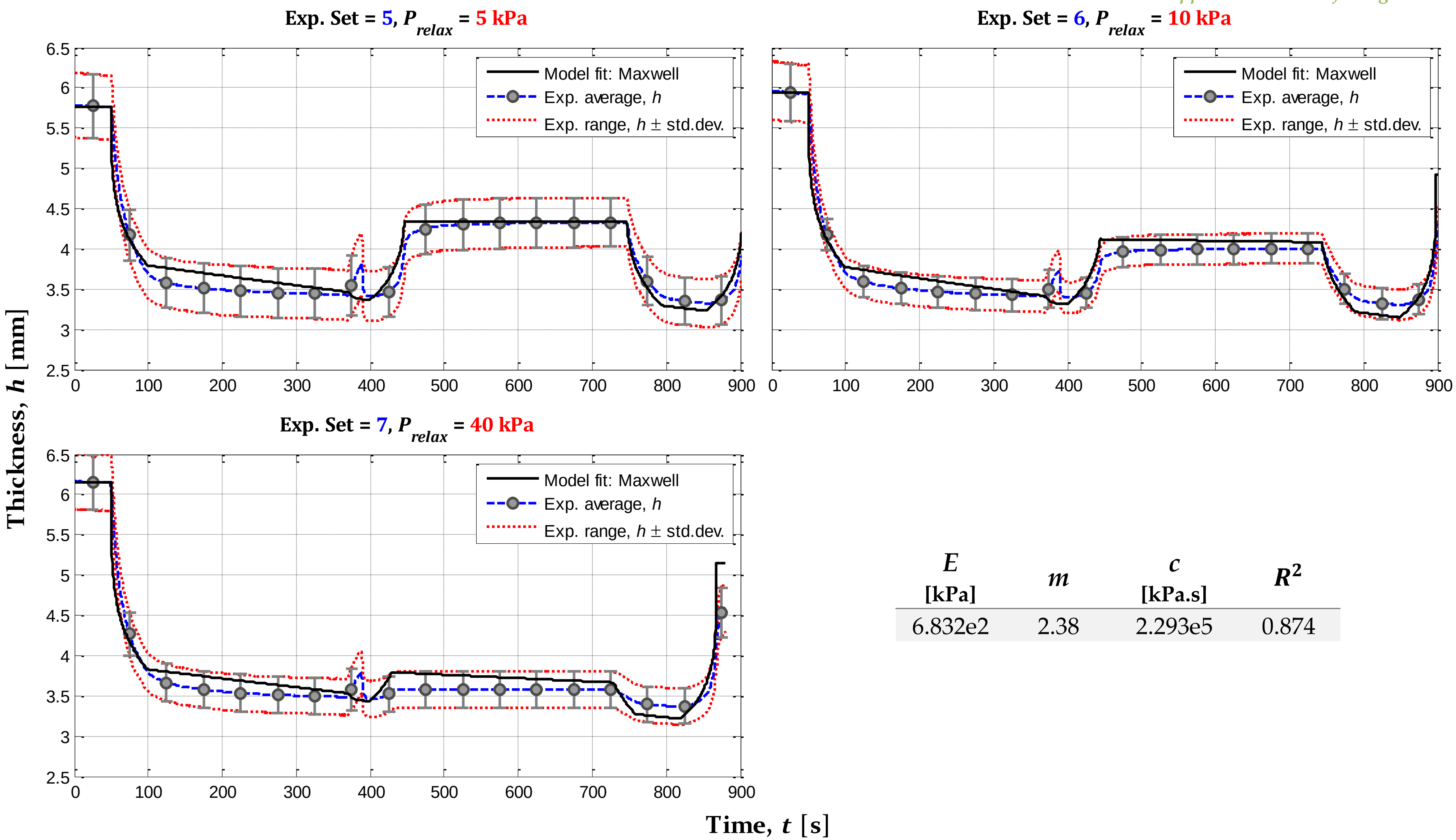

E [kPa]	m	c [kPa.s]	R^2
6.832e2	2.38	2.293e5	0.874

Figure D-6. (cont.) Thickness graph for Random fabric using *Maxwell model* fitted to all experiment sets using a single parameter set.

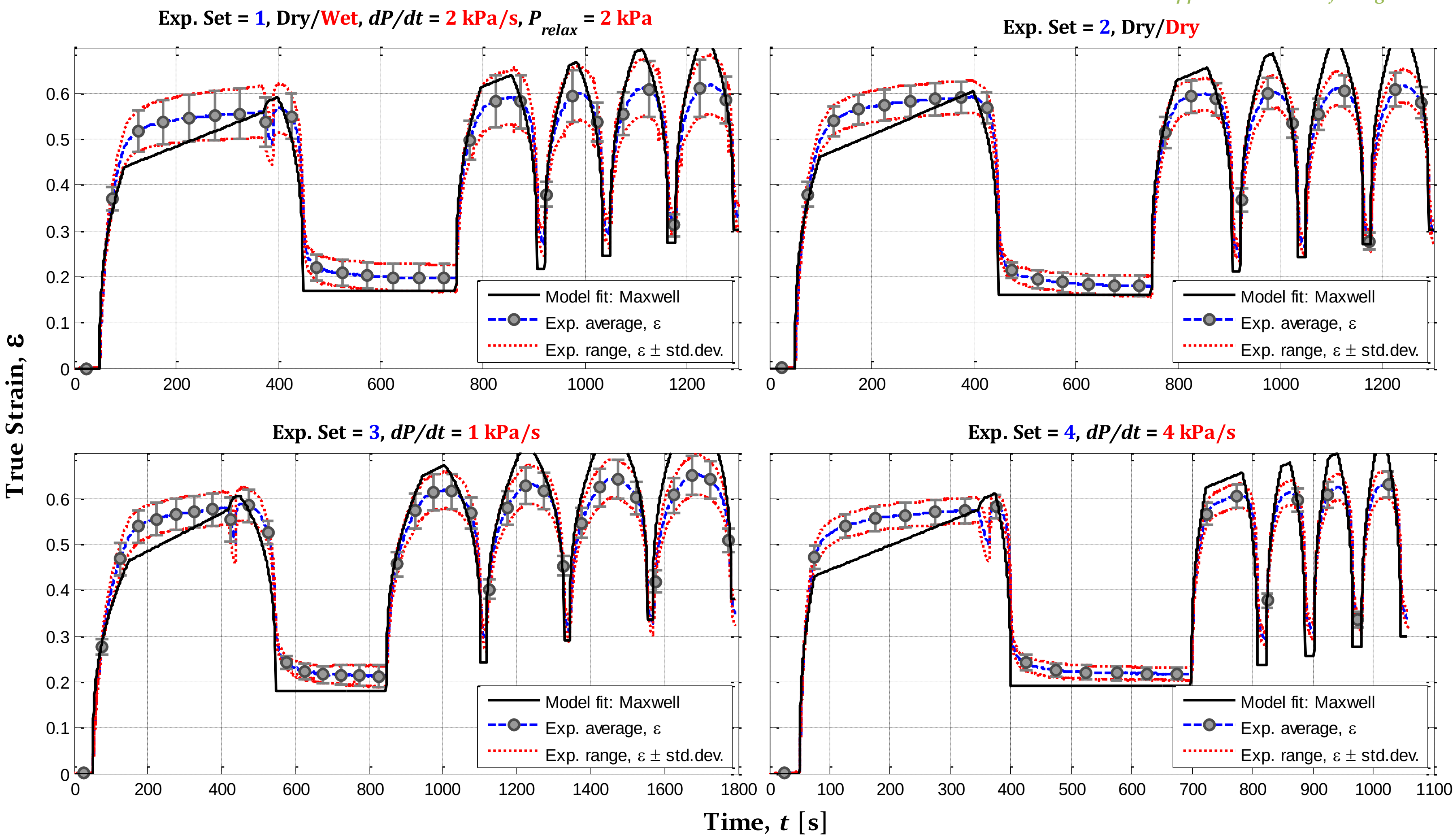

Figure D-7. Strain graph for Random fabric using *Maxwell model* fitted to all experiment sets using a single parameter set.

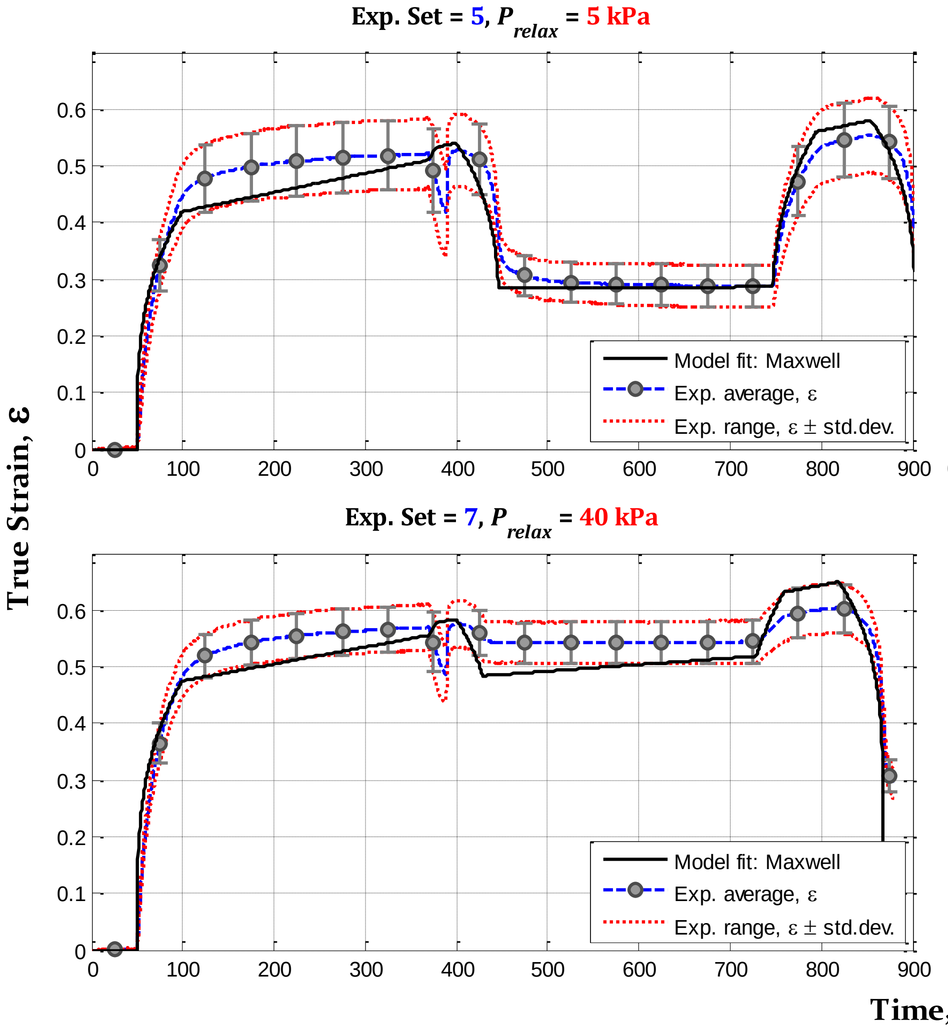

E [kPa]	m	c [kPa.s]	R^2
6.832e2	2.38	2.293e5	0.874

Figure D-8. (cont.) Strain graph for Random fabric using *Maxwell model* fitted to all experiment sets using a single parameter set.

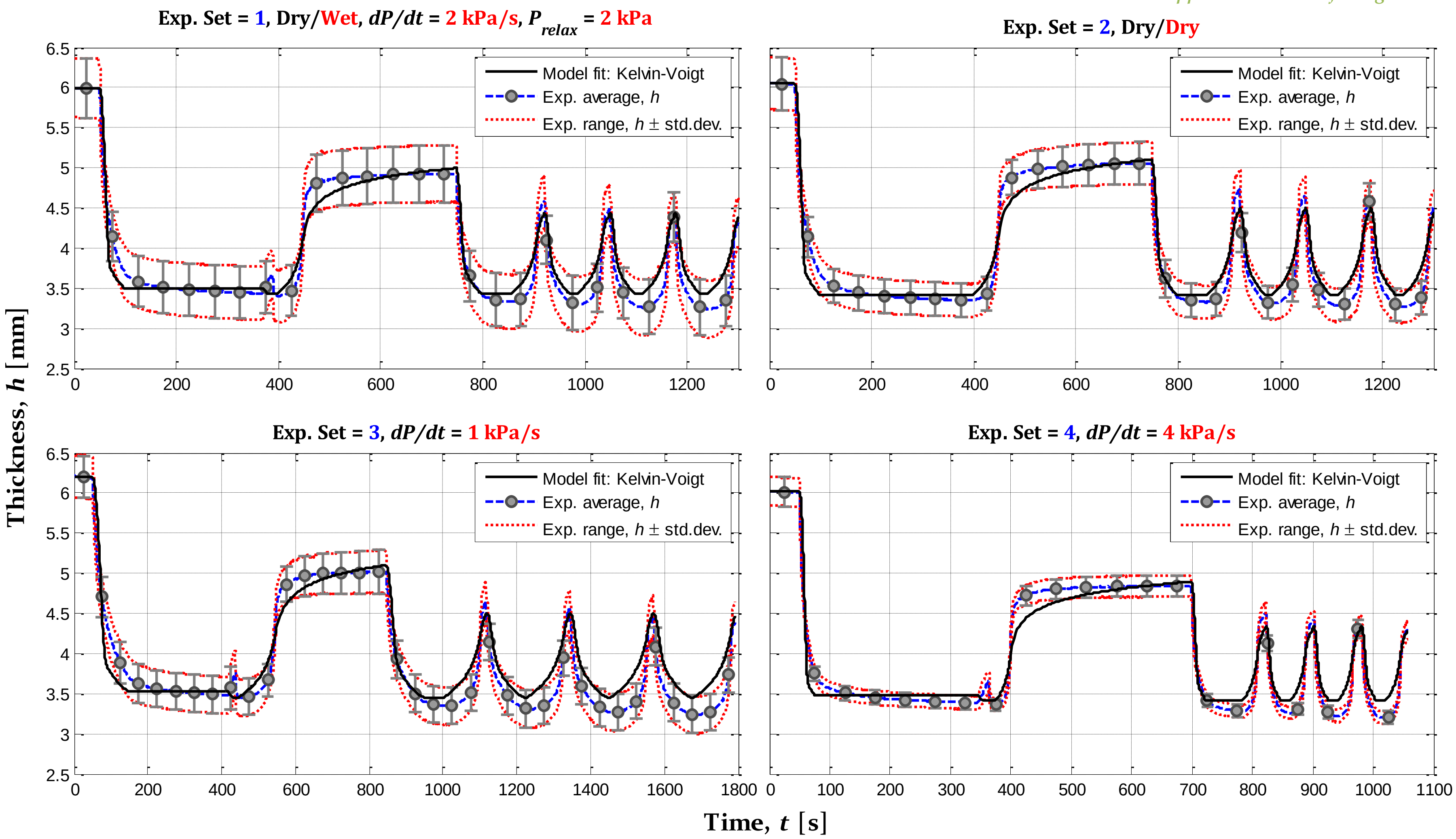

Figure D-9. Thickness graph for Random fabric using *Kelvin-Voigt model* fitted to each experiment set separately using separate parameter sets.

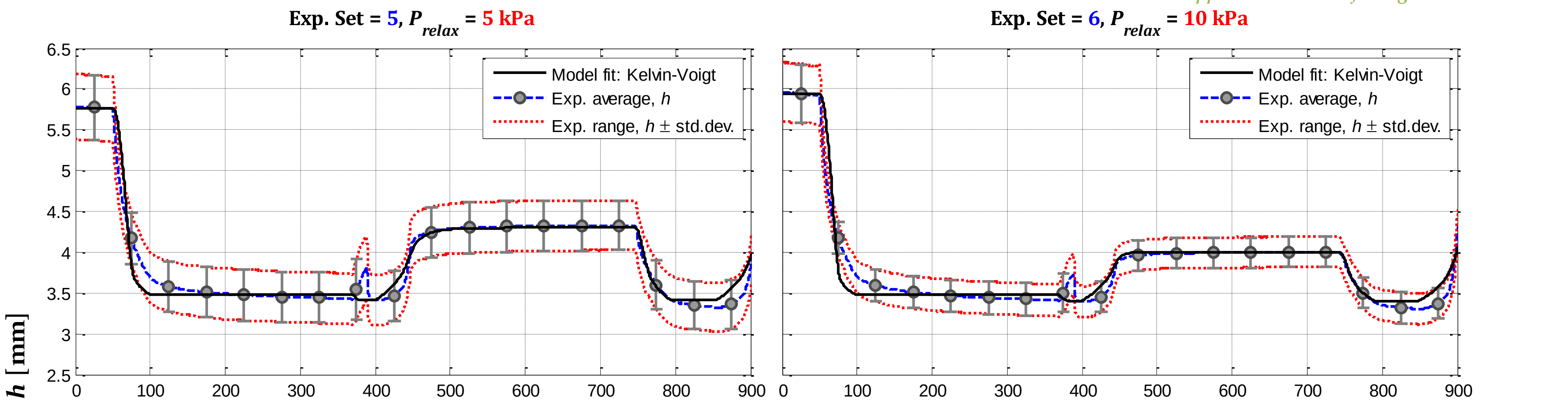

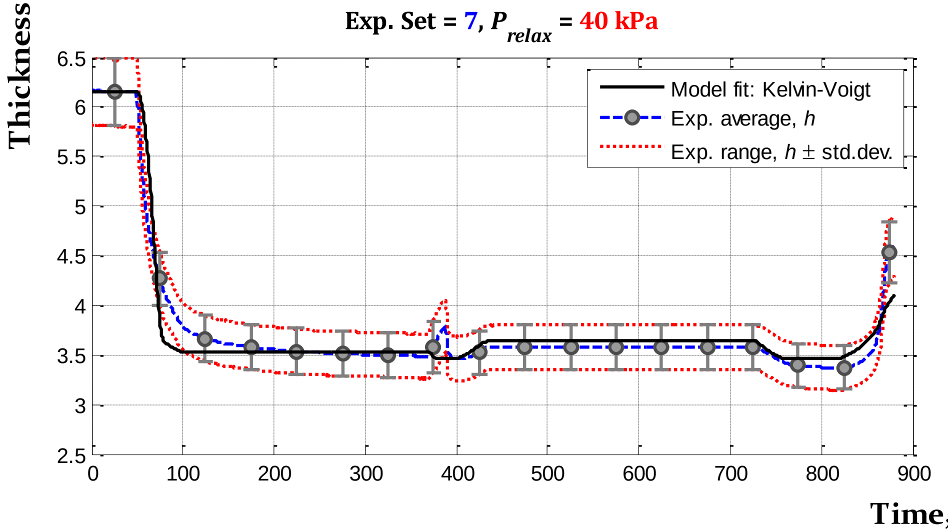

Set	*E* [kPa]	*m*	*c* [kPa.s]	R^2
1	4.001e3	7.44	6.354e2	0.902
2	2.505e3	7.26	6.244e2	0.917
3	2.360e3	6.65	1.036e3	0.893
4	4.324e3	9.41	5.385e2	0.904
5	4.439e3	6.38	1.334e3	0.954
6	4.786e3	8.44	1.214e3	0.947
7	8.575e2	15.81	1.235e3	0.928

Figure D-10. (cont.) Thickness graph for Random fabric using *Kelvin-Voigt model* fitted to each experiment set separately using separate parameter sets.

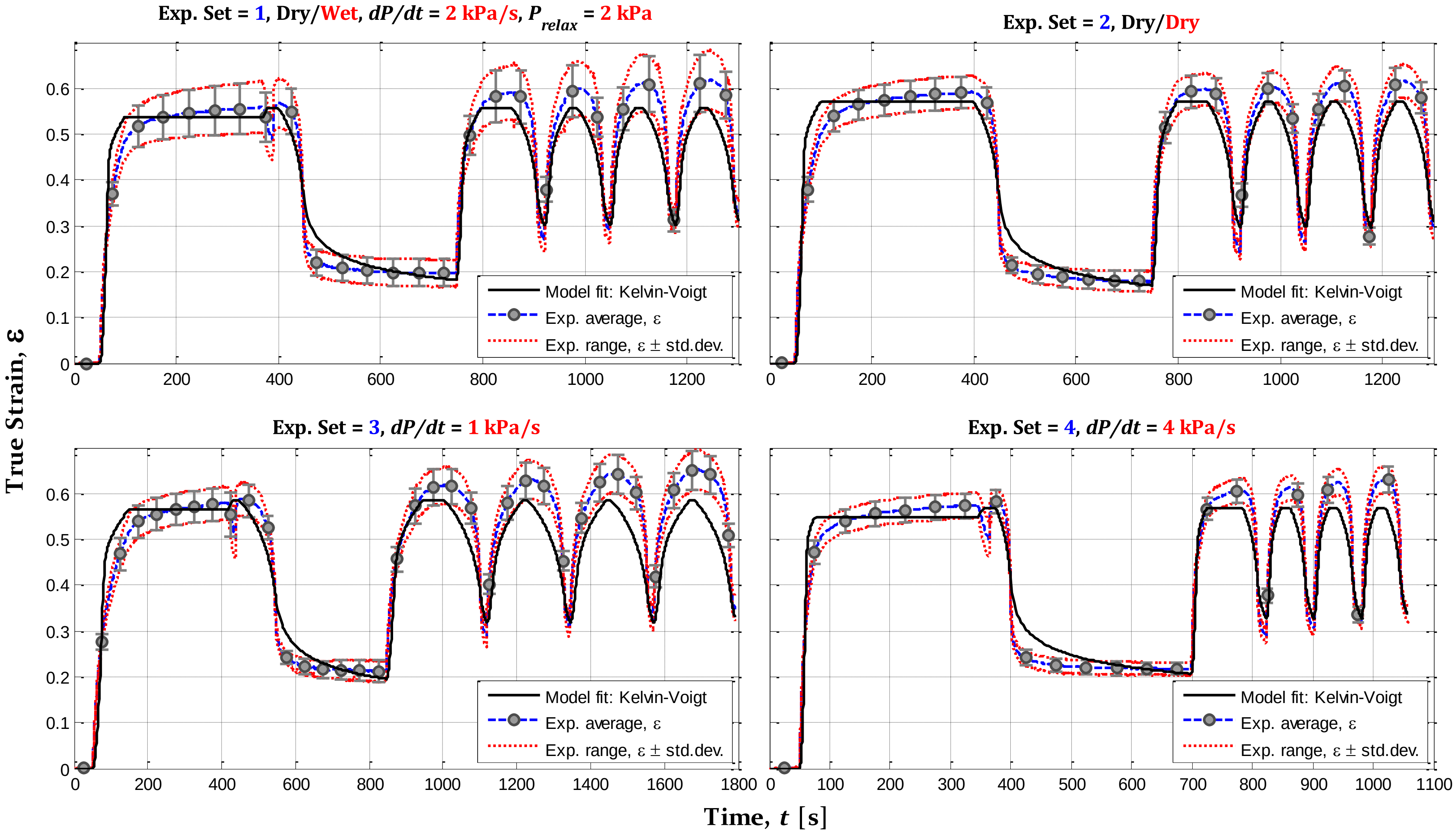

Figure D-11. Strain graph for Random fabric using *Kelvin-Voigt model* fitted to each experiment set separately using separate parameter sets.

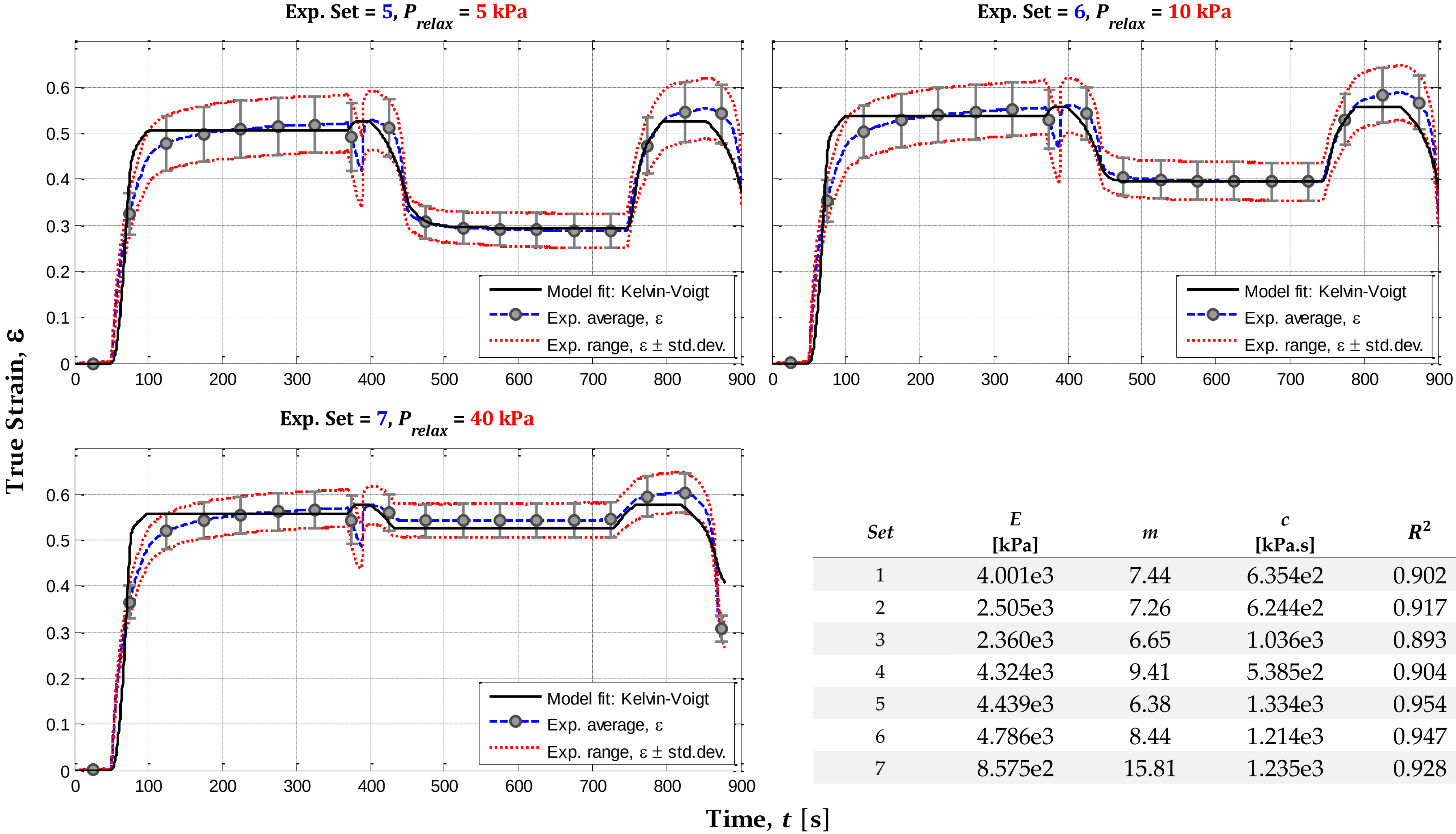

Set	*E* [kPa]	*m*	*c* [kPa.s]	R^2
1	4.001e3	7.44	6.354e2	0.902
2	2.505e3	7.26	6.244e2	0.917
3	2.360e3	6.65	1.036e3	0.893
4	4.324e3	9.41	5.385e2	0.904
5	4.439e3	6.38	1.334e3	0.954
6	4.786e3	8.44	1.214e3	0.947
7	8.575e2	15.81	1.235e3	0.928

Figure D-12. (cont.) Strain graph for Random fabric using *Kelvin-Voigt model* fitted to each experiment set separately using separate parameter sets.

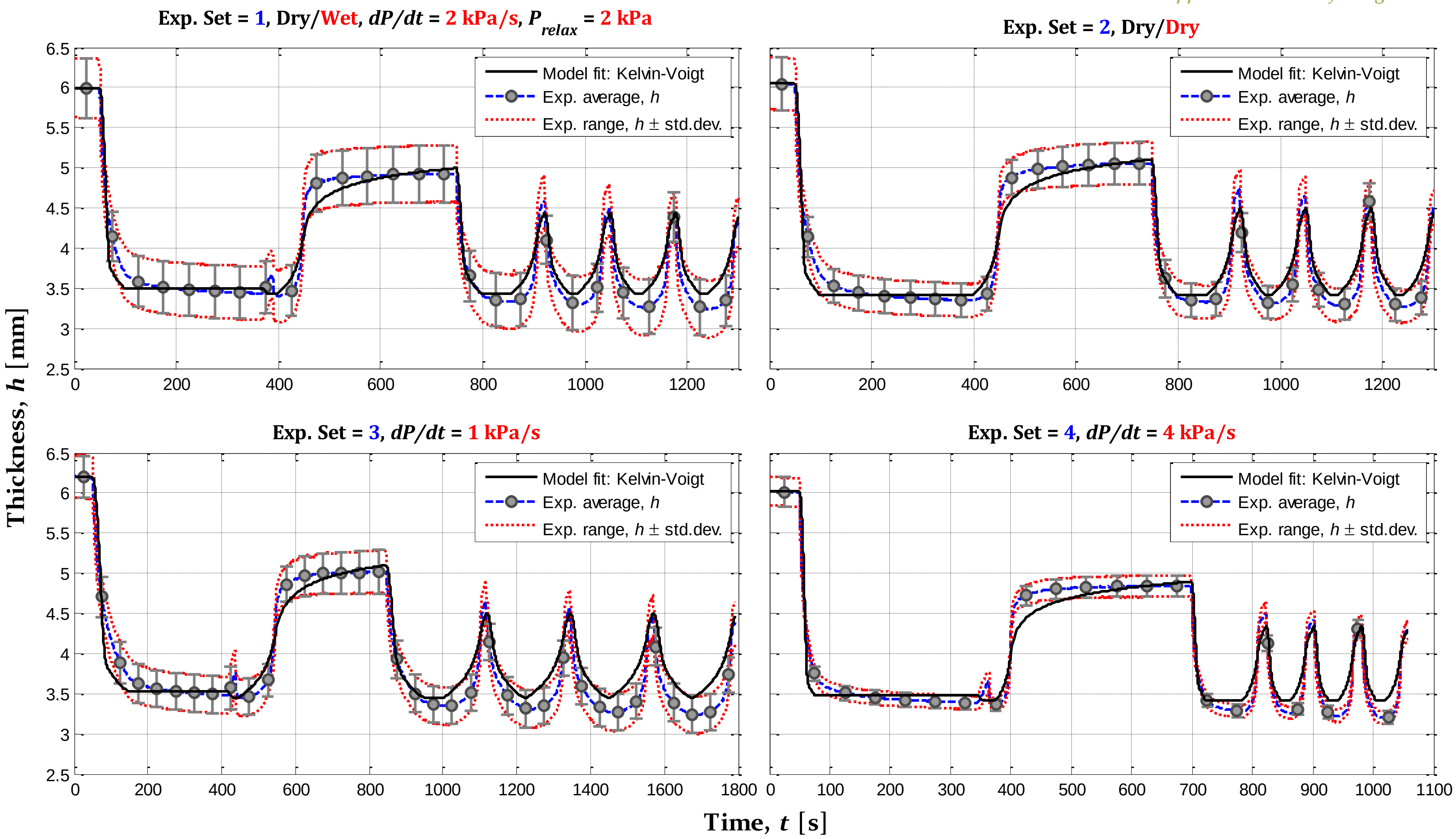

Figure D-13. Thickness graph for Random fabric using *Kelvin-Voigt model* fitted to all experiment sets using a single parameter set.

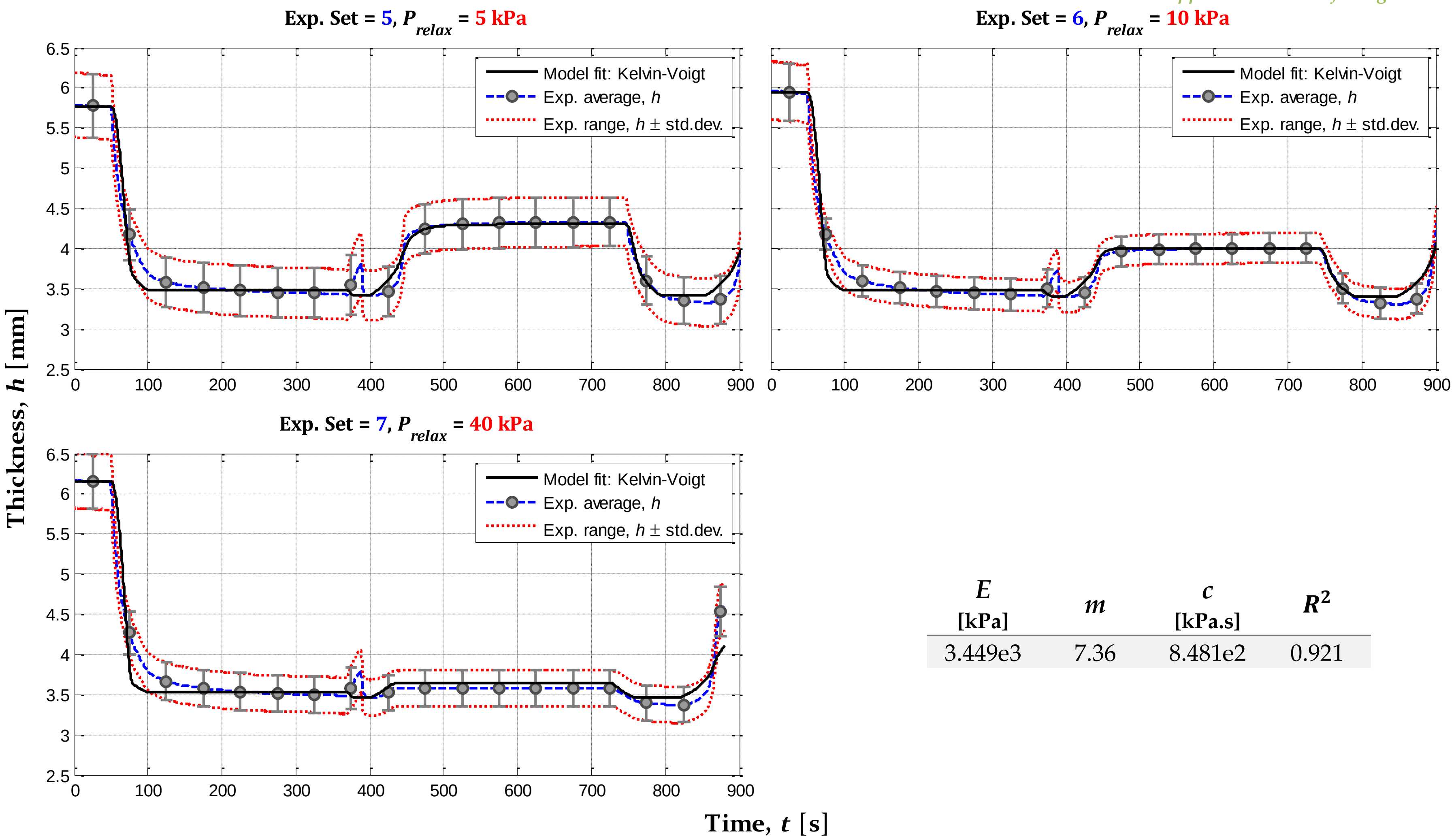

E [kPa]	m	c [kPa.s]	R^2
3.449e3	7.36	8.481e2	0.921

Figure D-14. (cont.) Thickness graph for Random fabric using *Kelvin-Voigt model* fitted to all experiment sets using a single parameter set.

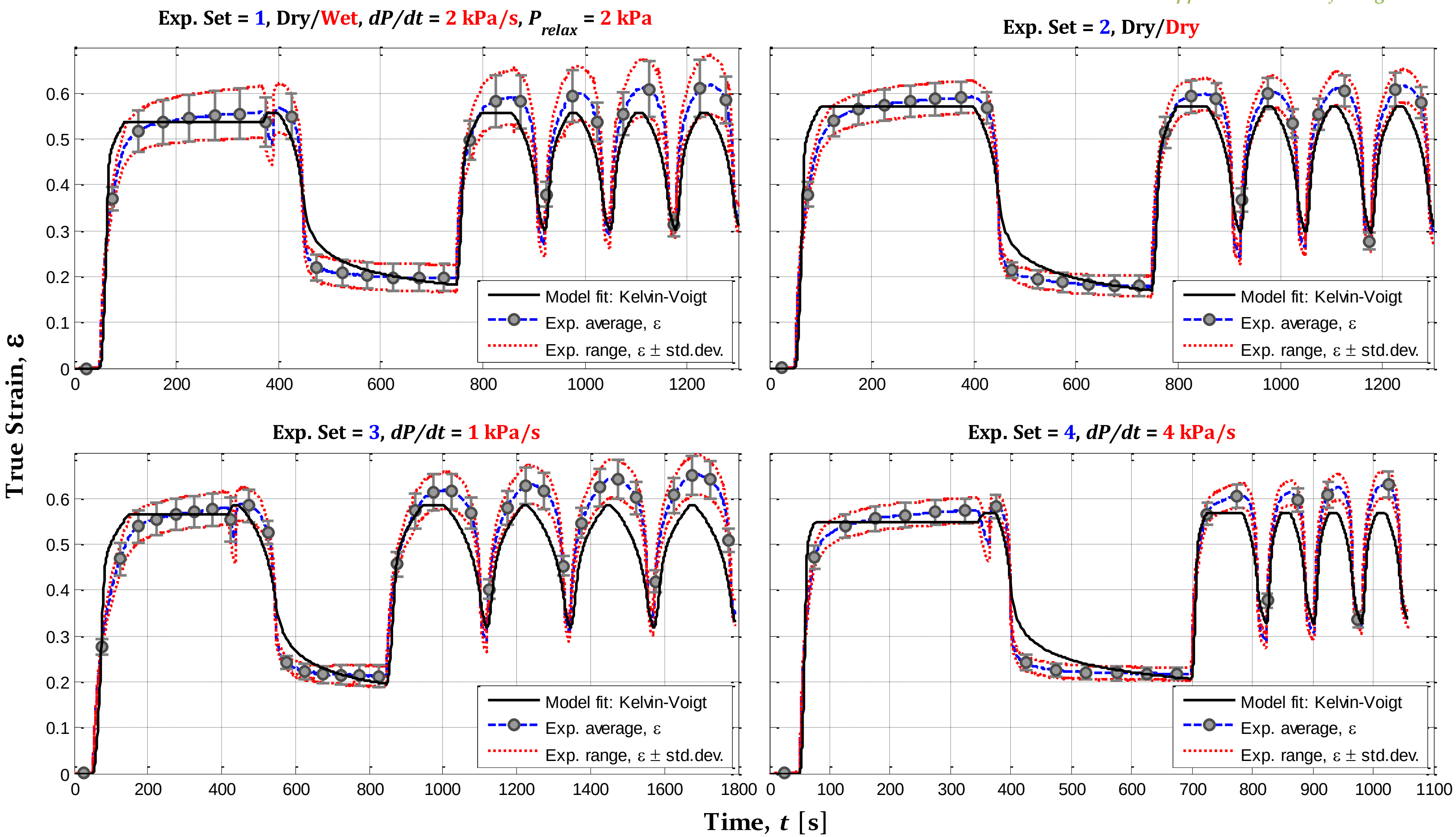

Figure D-15. Strain graph for Random fabric using *Kelvin-Voigt model* fitted to all experiment sets using a single parameter set.

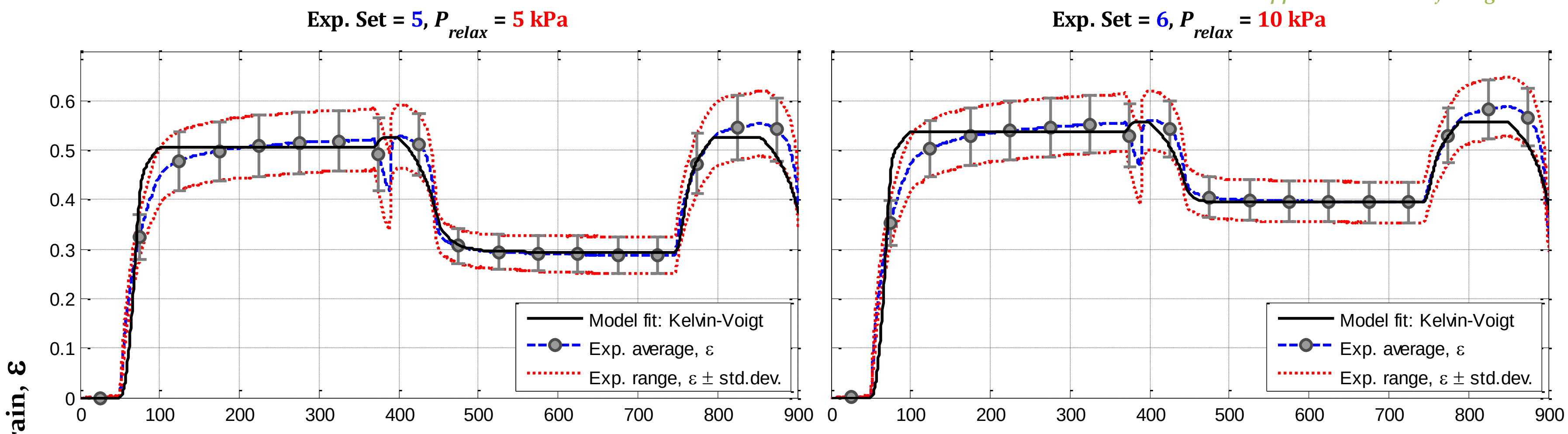

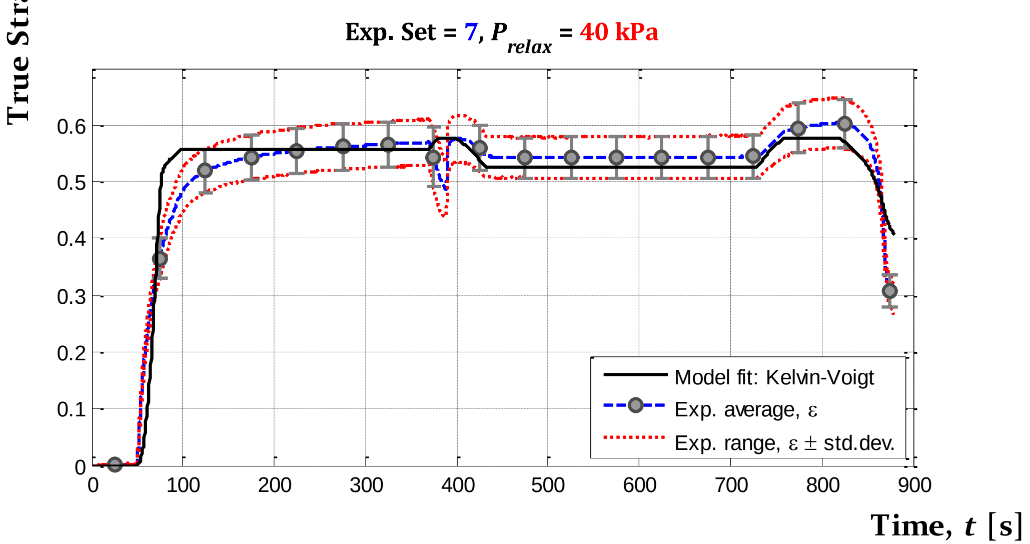

E [kPa]	m	c [kPa.s]	R^2
3.449e3	7.36	8.481e2	0.921

Figure D-16. (cont.) Strain graph for Random fabric using *Kelvin-Voigt model* fitted to all experiment sets using a single parameter set.

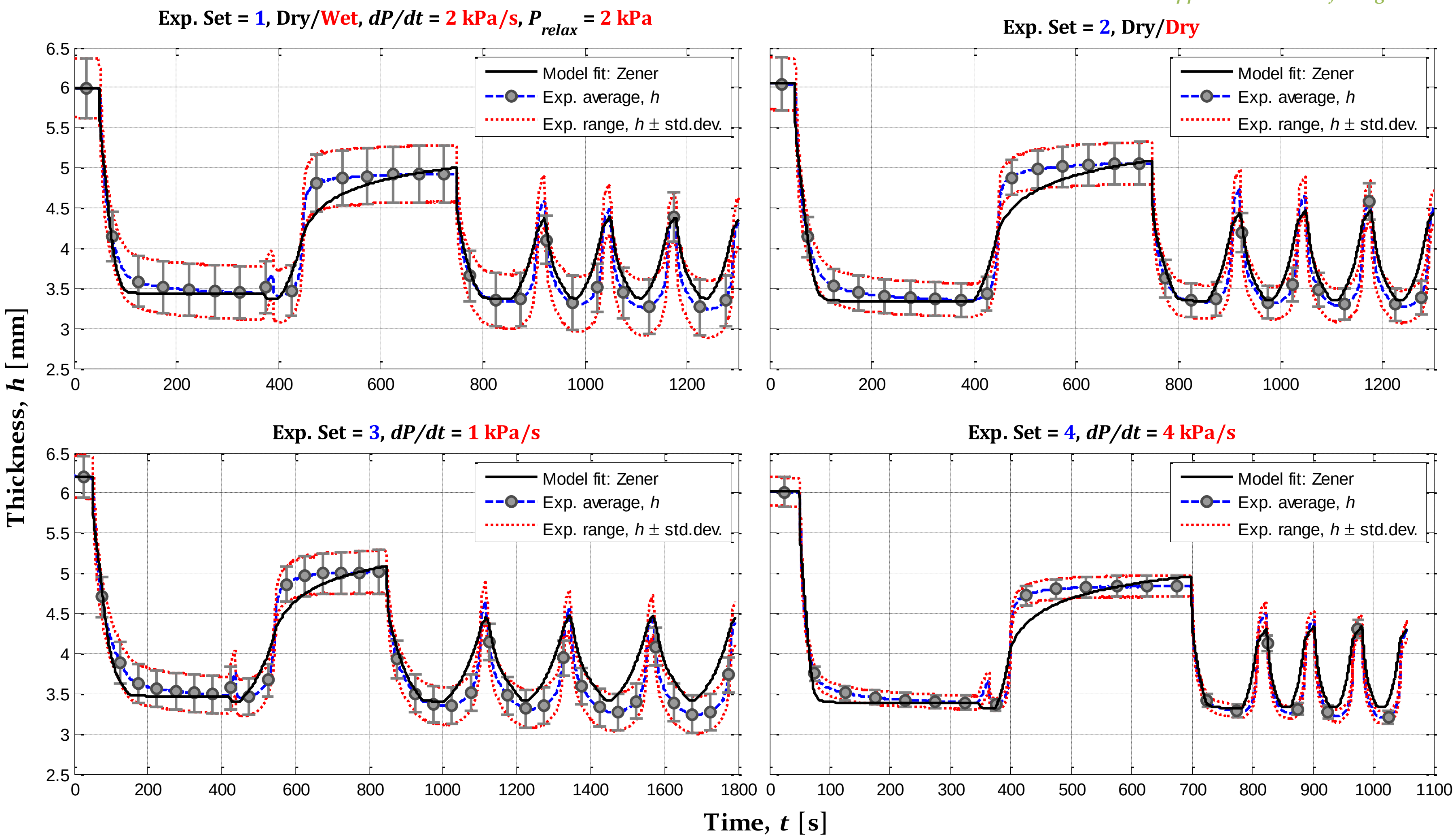

Figure D-17. Thickness graph for Random fabric using *Zener model* fitted to each experiment set separately using separate parameter sets.

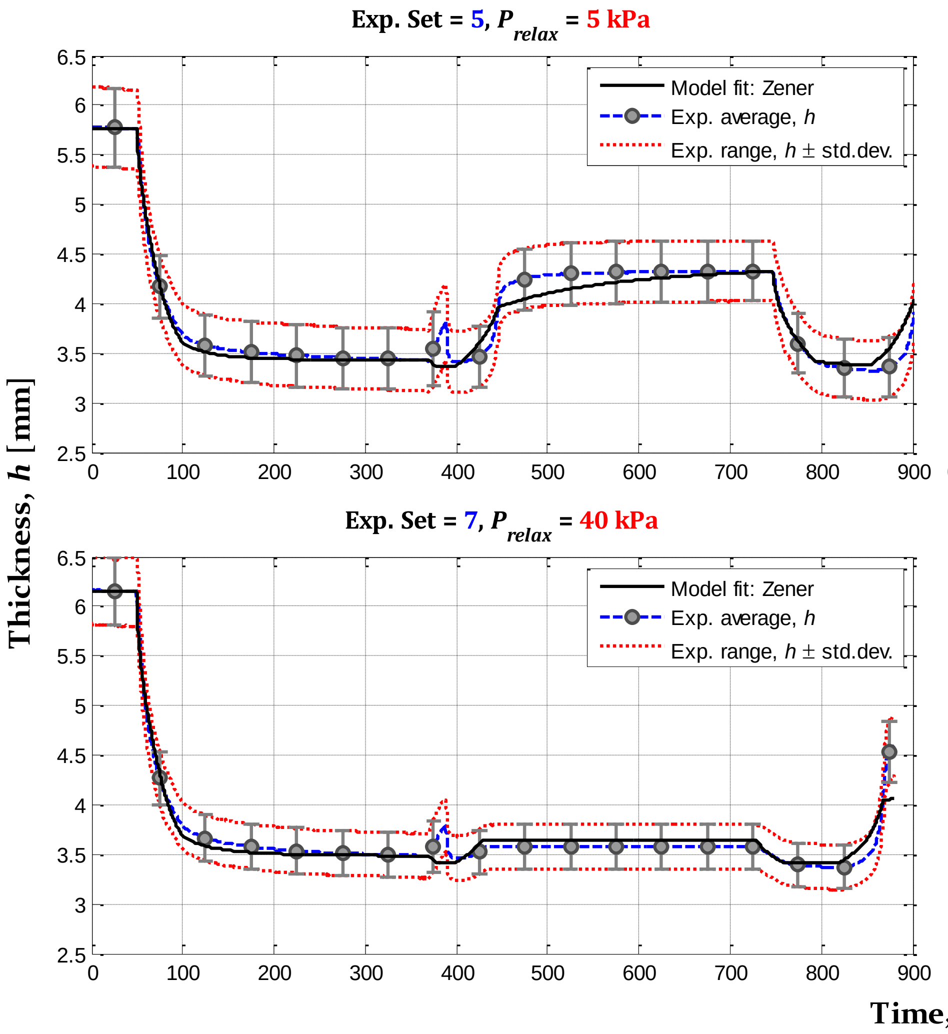

Set	*E₀* [kPa]	*m₀*	*E₁* [kPa]	*m₁*	*c₁* [kPa.s]	R^2
1	1.208e3	4.54	3.327e4	3.90	2.203e3	0.900
2	8.014e2	4.25	4.342e4	4.33	2.654e3	0.913
3	9.448e2	4.39	3.324e4	3.88	3.002e3	0.886
4	1.160e3	4.78	1.712e4	3.65	2.004e3	0.912
5	2.099e3	5.03	4.650e2	1.71	6.796e3	0.969
6	1.108e3	4.62	1.856e2	1.28	1.014e4	0.969
7	2.929e3	9.64	5.445e2	2.04	1.079e4	0.961

Figure D-18. (cont.) Thickness graph for Random fabric using *Zener model* fitted to each experiment set separately using separate parameter sets.

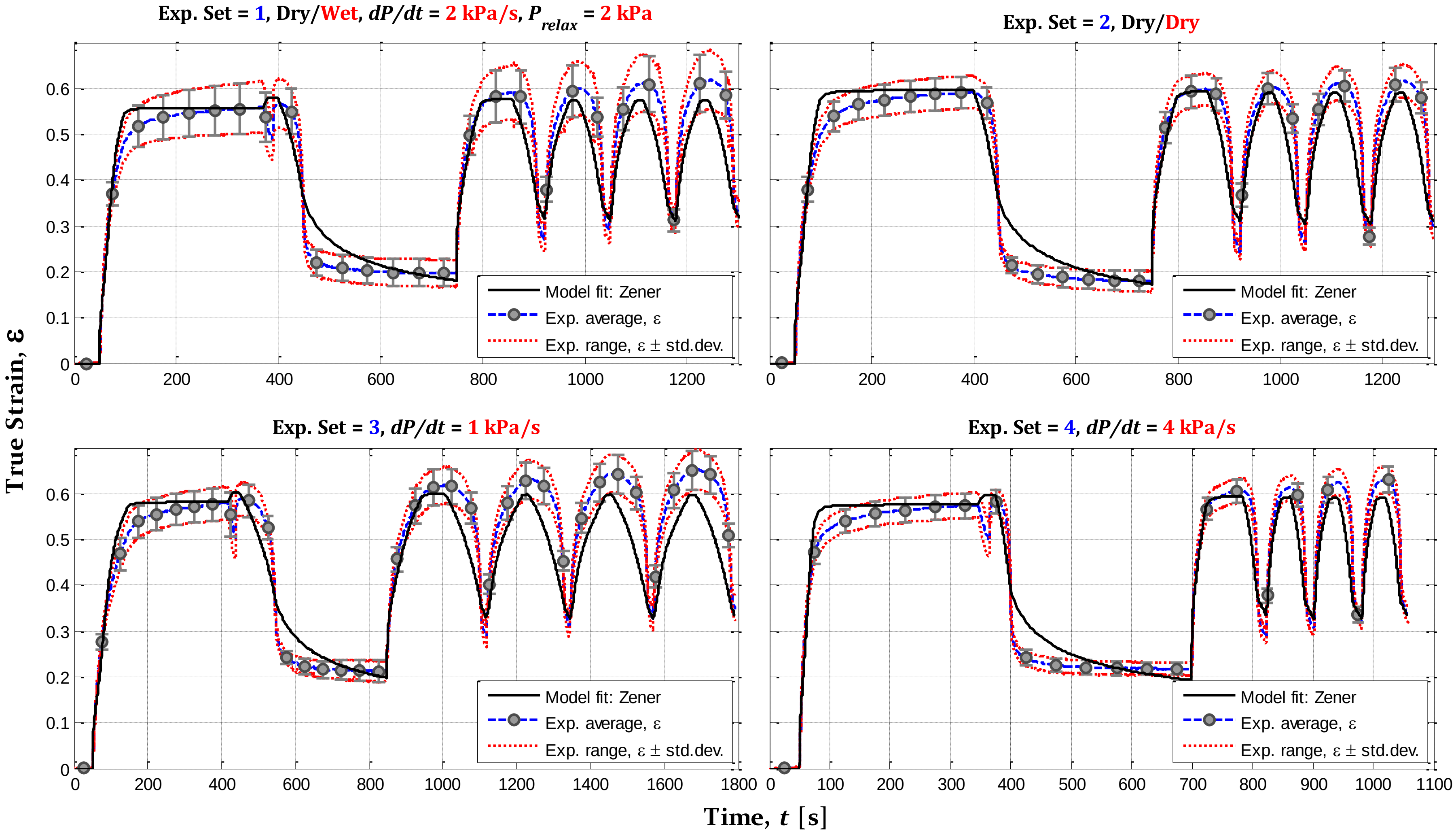

Figure D-19. Strain graph for Random fabric using *Zener model* fitted to each experiment set separately using separate parameter sets.

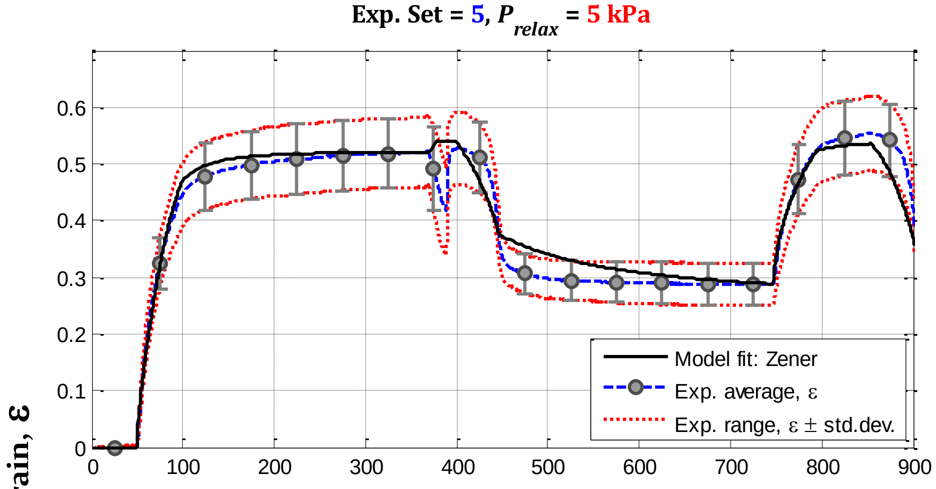

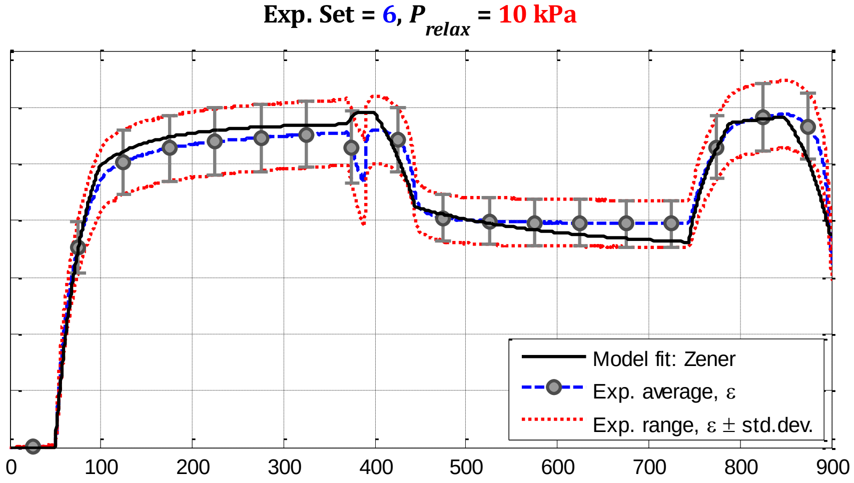

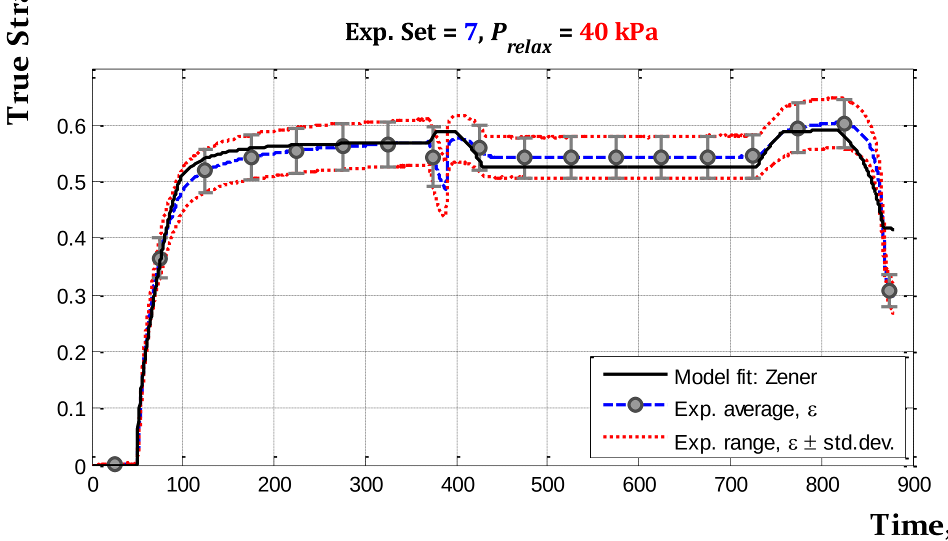

Set	E_0 [kPa]	m_0	E_1 [kPa]	m_1	c_1 [kPa.s]	R^2
1	1208.64	4.54	33279.51	3.90	2203.03	1.208e3
2	801.47	4.25	43427.70	4.33	2654.10	8.014e2
3	944.87	4.39	33249.98	3.88	3002.12	9.448e2
4	1160.42	4.78	17121.78	3.65	2004.26	1.160e3
5	2099.40	5.03	465.03	1.71	6796.42	2.099e3
6	1108.75	4.62	185.61	1.28	10142.34	1.108e3
7	2929.42	9.64	544.57	2.04	10793.49	2.929e3

Figure D-20. (cont.) Strain graph for Random fabric using *Zener model* fitted to each experiment set separately using separate parameter sets.

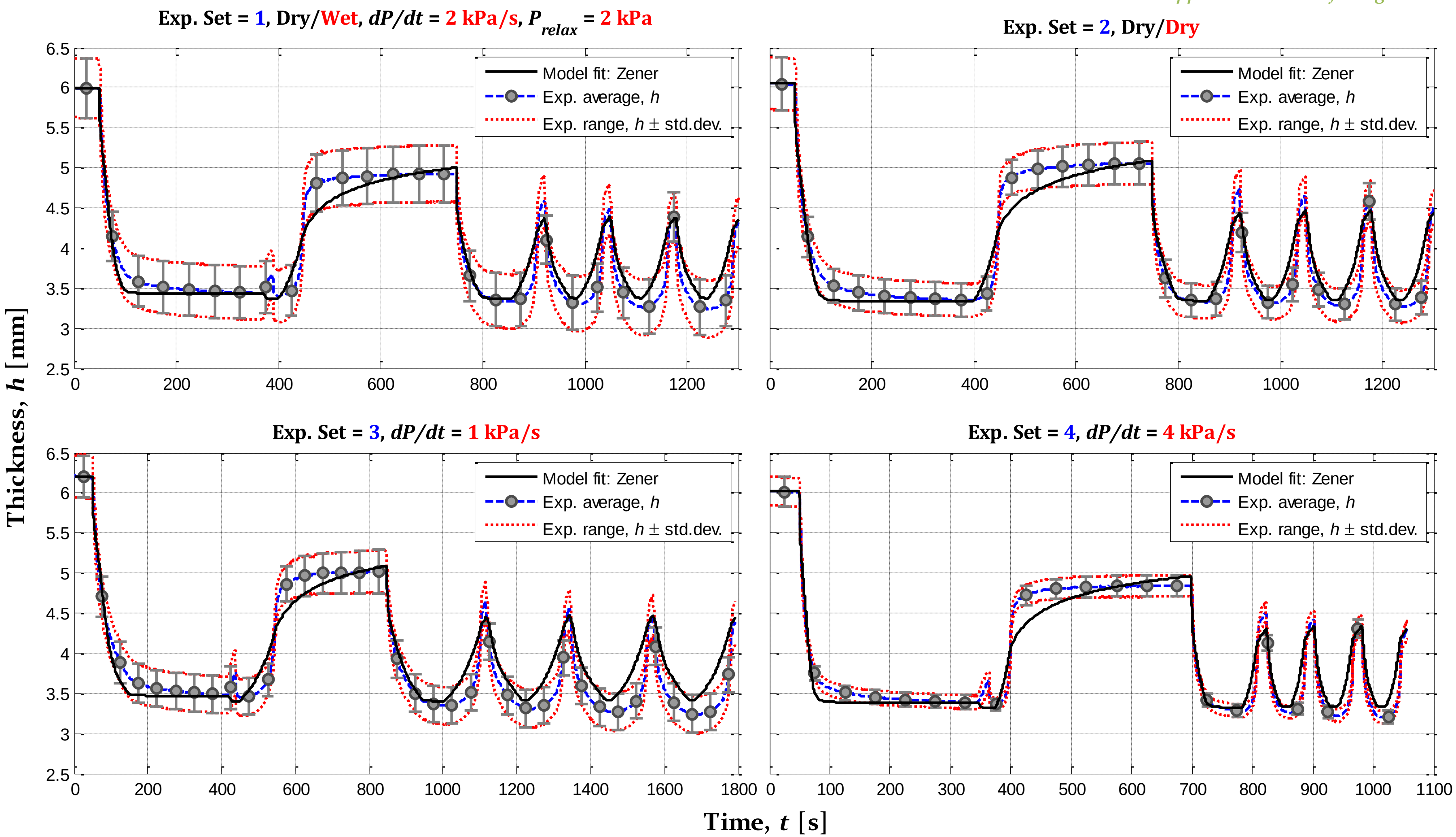

Figure D-21. Thickness graph for Random fabric using *Zener model* fitted to all experiment sets using a single parameter set.

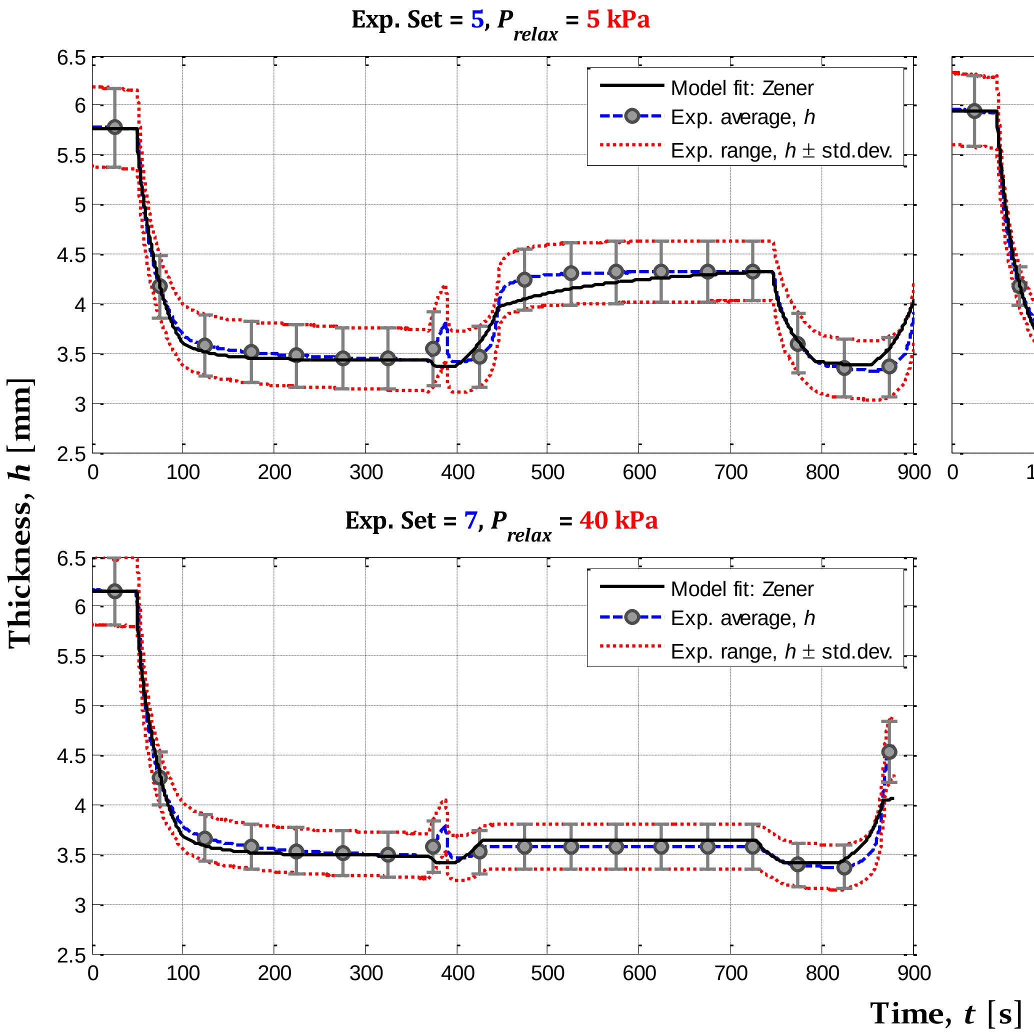

E_0 [kPa]	m_0	E_1 [kPa]	m_1	c_1 [kPa.s]	R^2
1.195e3	4.66	2.720e4	3.88	3.158e3	0.930

Figure D-22. (cont.) Thickness graph for Random fabric using *Zener model* fitted to all experiment sets using a single parameter set.

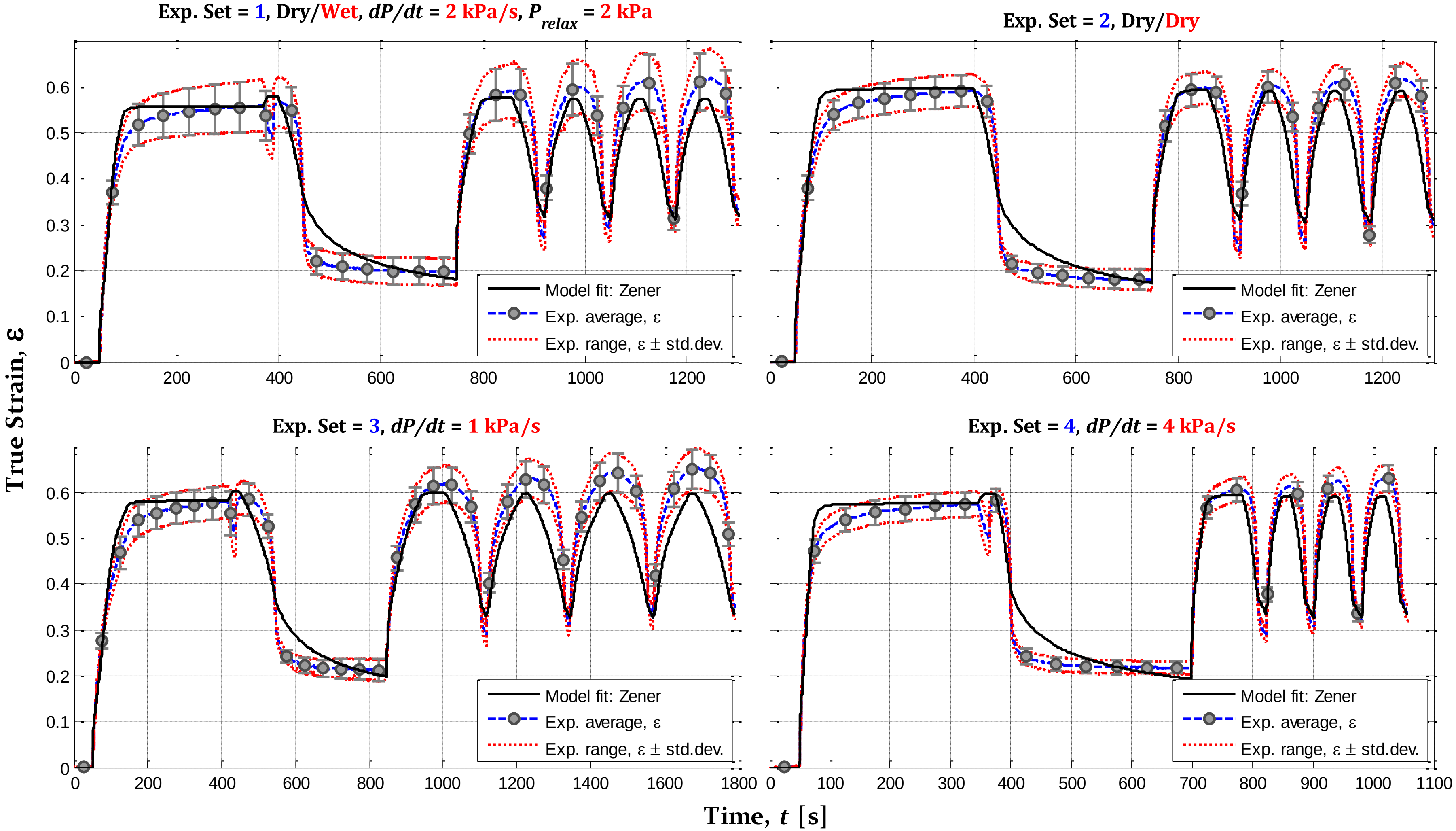

Figure D-23. Strain graph for Random fabric using *Zener model* fitted to all experiment sets using a single parameter set.

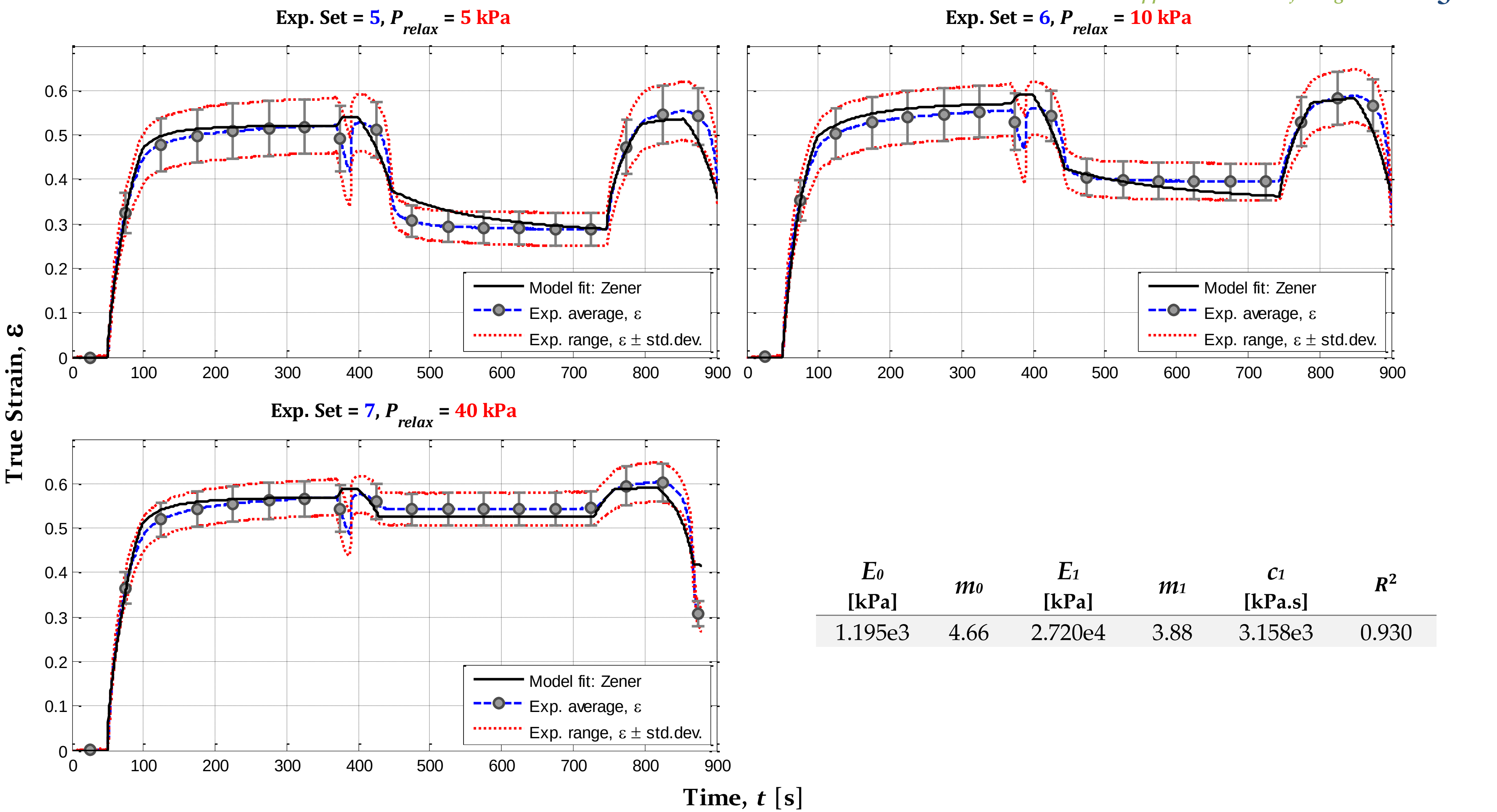

E_0 [kPa]	m_0	E_1 [kPa]	m_1	c_1 [kPa.s]	R^2
1.195e3	4.66	2.720e4	3.88	3.158e3	0.930

Figure D-24. (cont.) Strain graph for Random fabric using *Zener model* fitted to all experiment sets using a single parameter set.

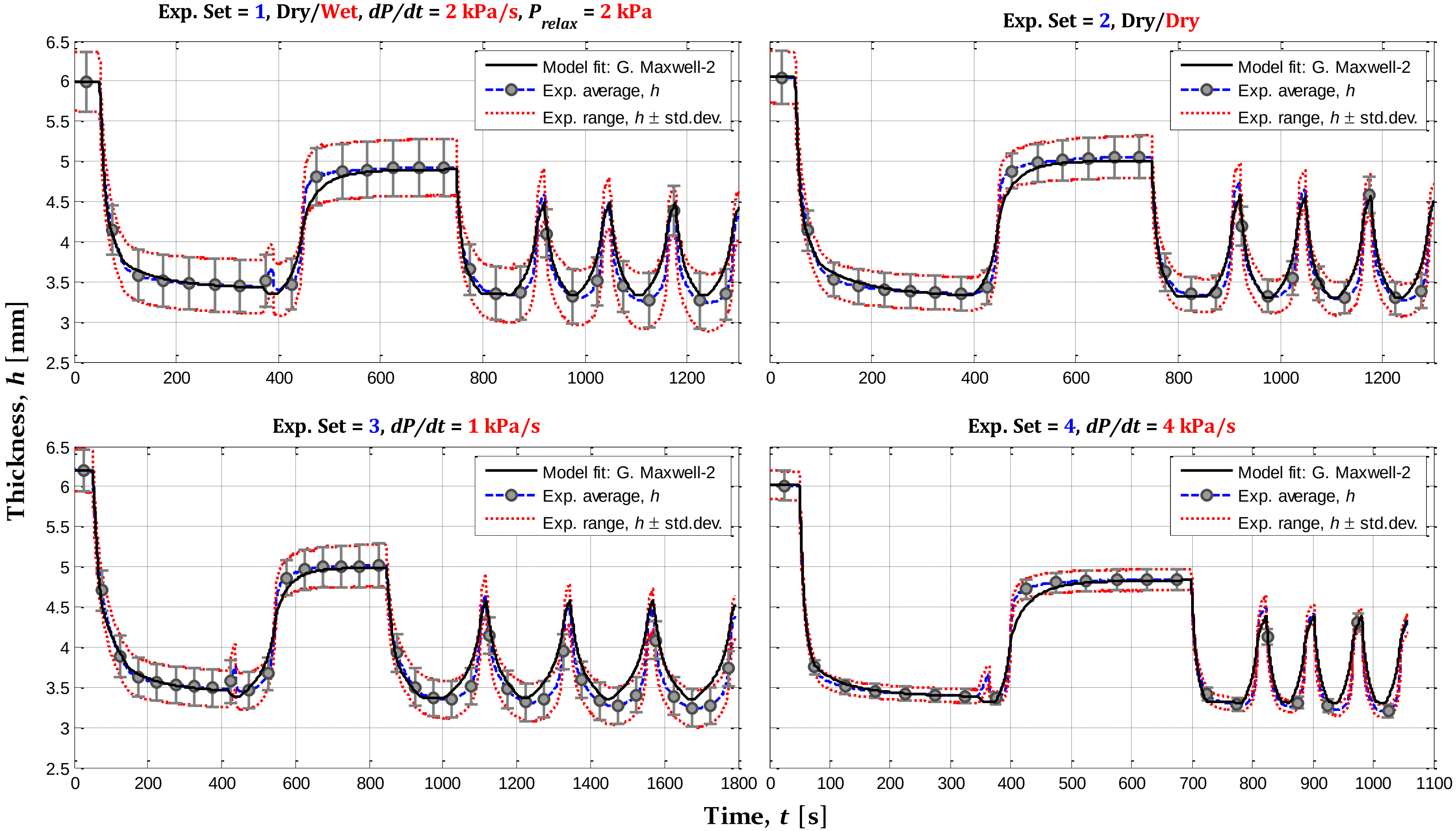

Figure D-25. Thickness graph for Random fabric using *G. Maxwell model, n=2* fitted to each experiment set separately using separate parameter sets.

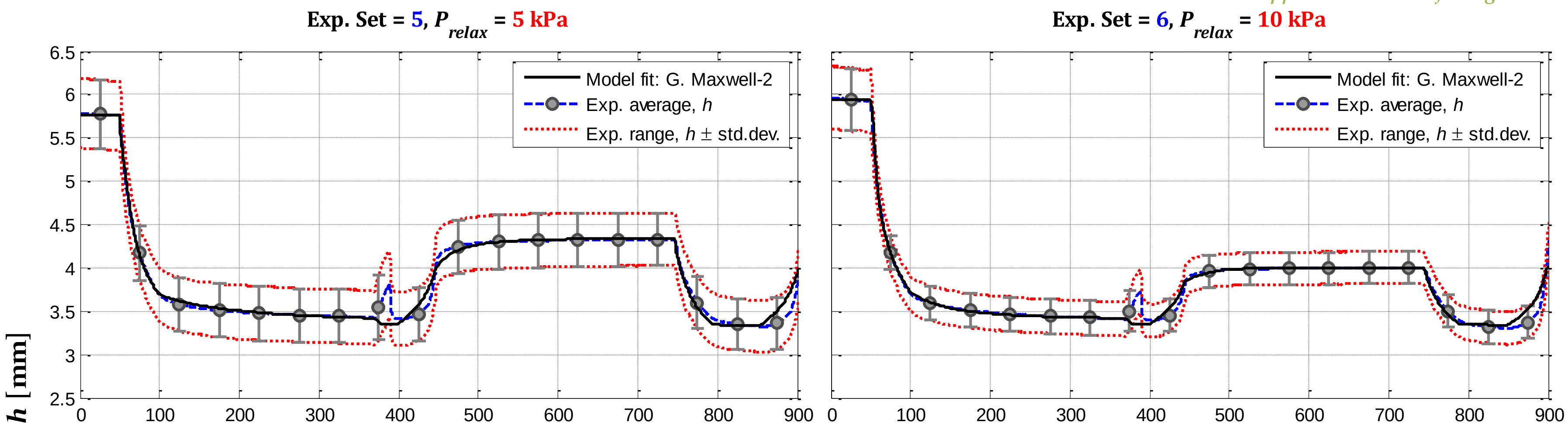

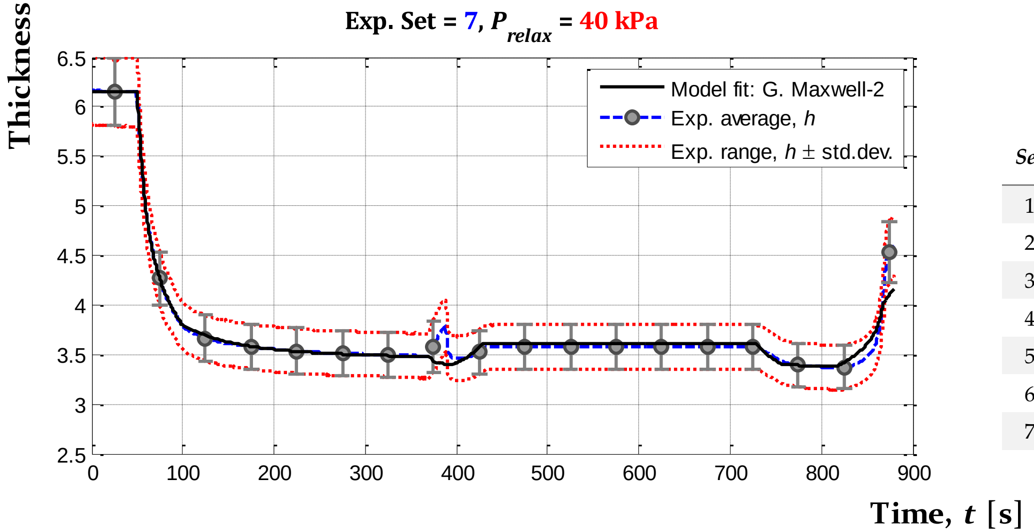

Set	E_0 [kPa]	m_0	E_1 [kPa]	m_1	c_1 [kPa.s]	E_2 [kPa]	m_2	c_2 [kPa.s]	R^2
1	1.588e3	5.57	1.667e3	3.91	3.214e4	5.777e2	1.60	5.681e2	0.947
2	1.058e3	5.55	1.812e3	4.05	3.866e4	5.773e2	1.58	4.648e2	0.968
3	1.193e3	5.50	1.682e3	3.91	3.655e4	6.254e2	1.53	6.753e2	0.943
4	1.446e3	5.62	1.813e3	4.02	2.316e4	5.138e2	1.61	6.365e2	0.950
5	1.882e3	5.21	7.281e2	2.88	3.538e4	1.418e3	2.03	1.379e3	0.982
6	2.849e3	7.29	1.467e3	3.63	2.407e4	5.050e1	0.68	1.665e3	0.974
7	2.048e3	11.1	1.112e3	3.20	3.630e4	1.240e2	1.13	7.286e2	0.972

Figure D-26. (cont.) Thickness graph for Random fabric using *G. Maxwell model, n=2* fitted to each experiment set separately using separate parameter sets.

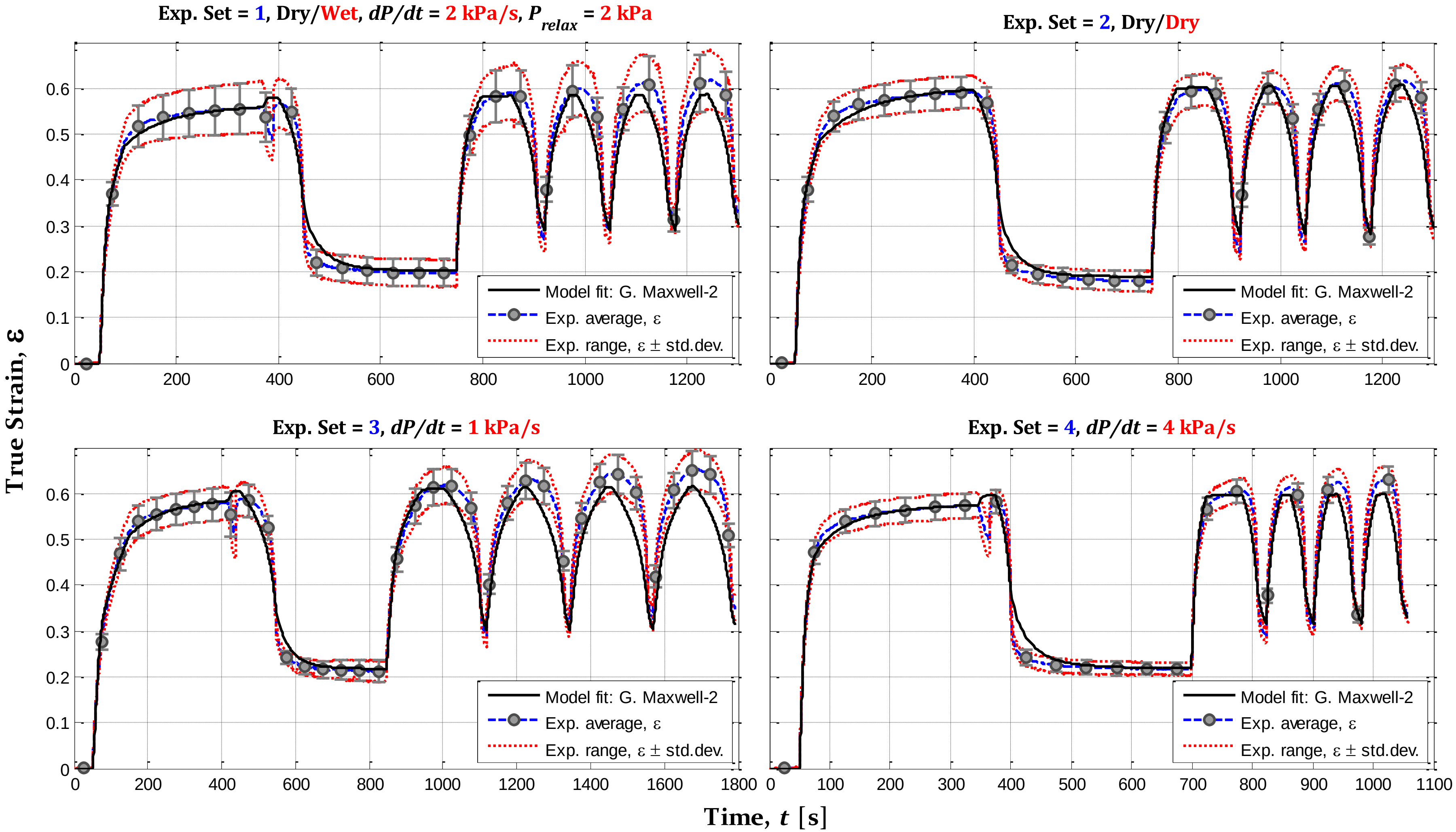

Figure D-27. Strain graph for Random fabric using *G. Maxwell model, n=2* fitted to each experiment set separately using separate parameter sets.

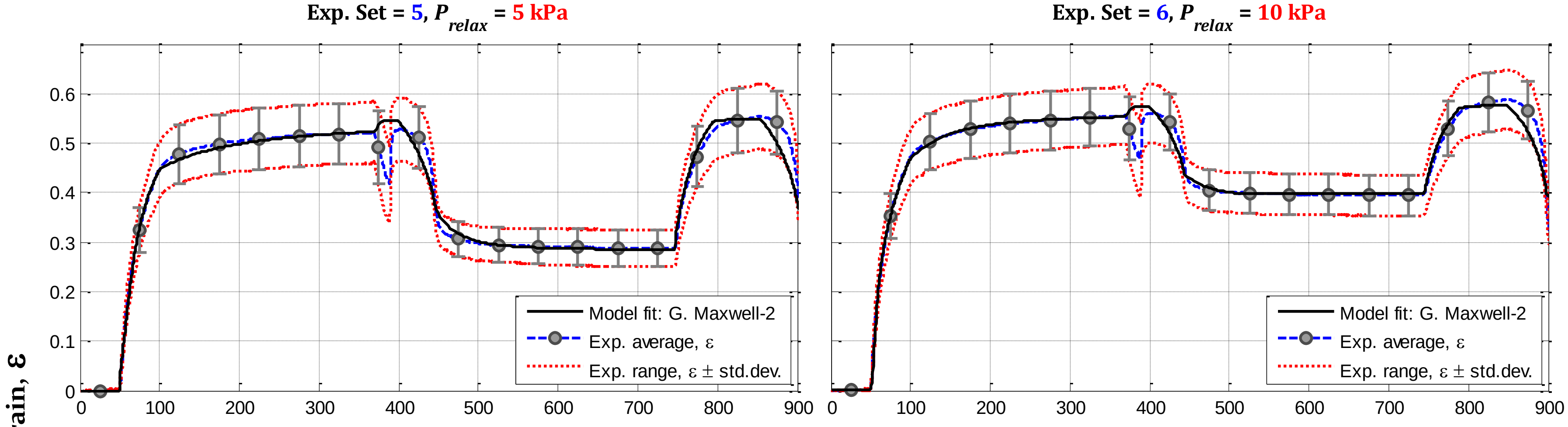

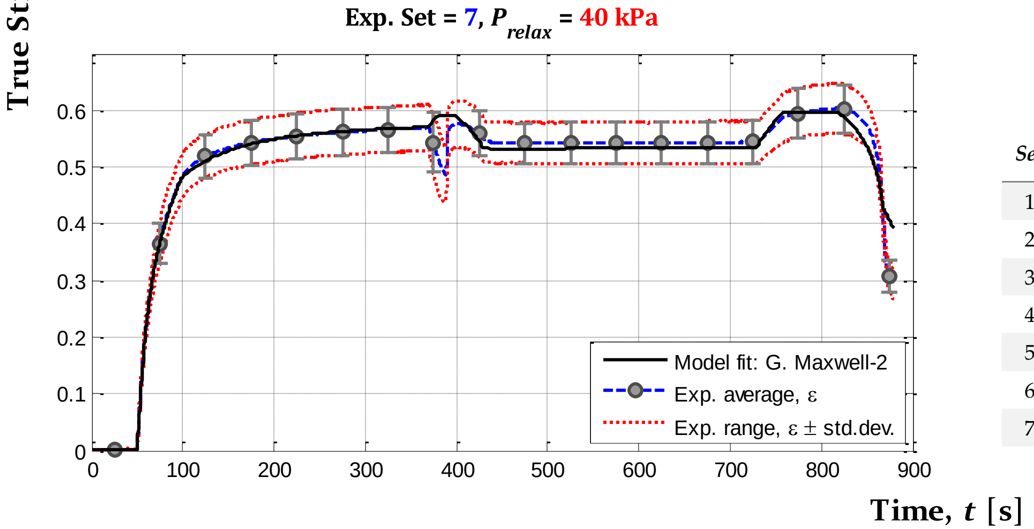

Set	E_0 [kPa]	m_0	E_1 [kPa]	m_1	c_1 [kPa.s]	E_2 [kPa]	m_2	c_2 [kPa.s]	R^2
1	1.588e3	5.57	1.667e3	3.91	3.214e4	5.777e2	1.60	5.681e2	0.947
2	1.058e3	5.55	1.812e3	4.05	3.866e4	5.773e2	1.58	4.648e2	0.968
3	1.193e3	5.50	1.682e3	3.91	3.655e4	6.254e2	1.53	6.753e2	0.943
4	1.446e3	5.62	1.813e3	4.02	2.316e4	5.138e2	1.61	6.365e2	0.950
5	1.882e3	5.21	7.281e2	2.88	3.538e4	1.418e3	2.03	1.379e3	0.982
6	2.849e3	7.29	1.467e3	3.63	2.407e4	5.050e1	0.68	1.665e3	0.974
7	2.048e3	11.1	1.112e3	3.20	3.630e4	1.240e2	1.13	7.286e2	0.972

Figure D-28. (cont.) Strain graph for Random fabric using *G. Maxwell model, n=2* fitted to each experiment set separately using separate parameter sets.

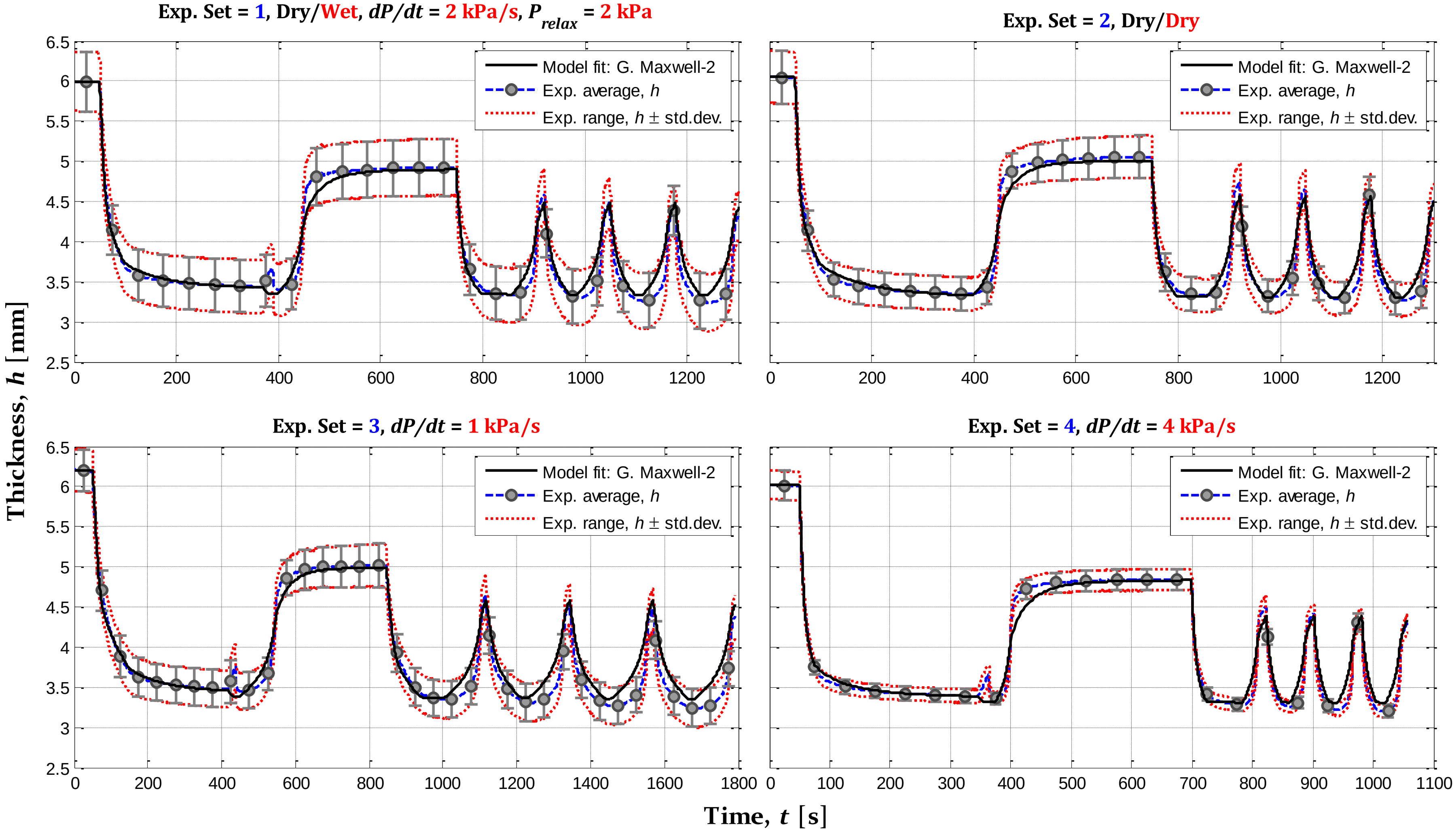

Figure D-29. Thickness graph for Random fabric using *G. Maxwell model, n=2* fitted to all experiment sets using a single parameter set.

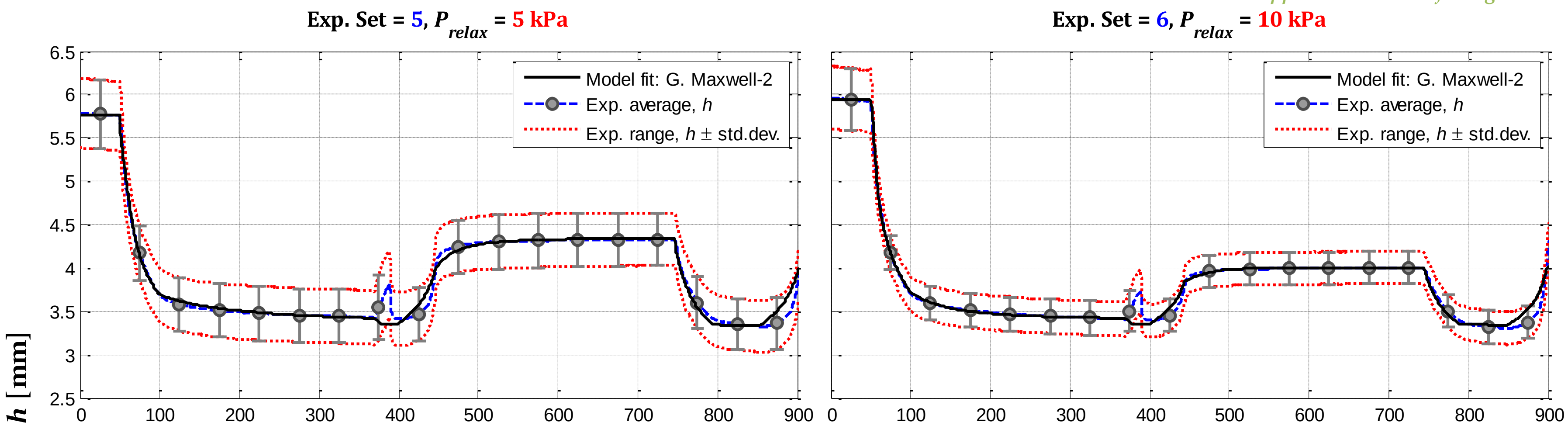

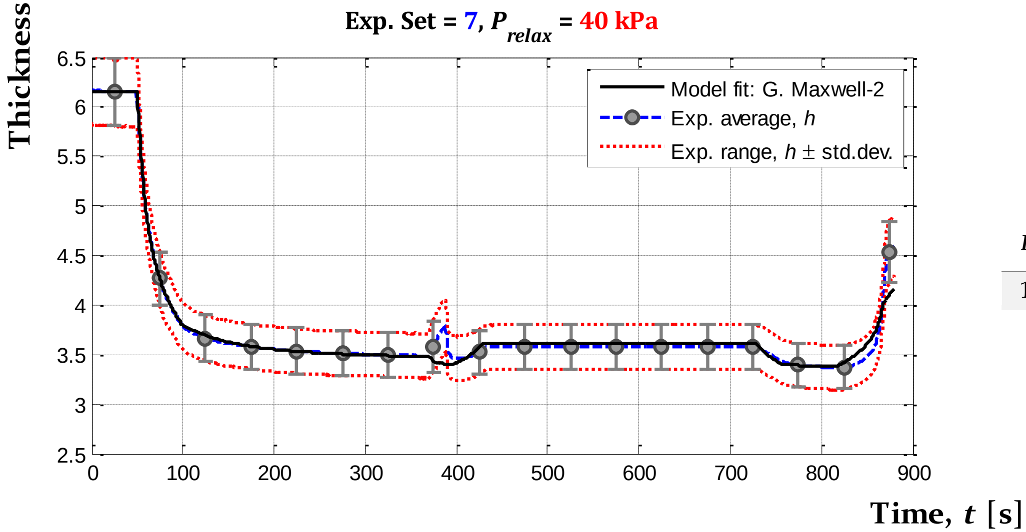

E_0 [kPa]	m_0	E_1 [kPa]	m_1	c_1 [kPa.s]	E_2 [kPa]	m_2	c_2 [kPa.s]	R^2
1.505e3	5.73	1.733e3	3.78	3.561e4	5.308e2	1.54	5.283e2	0.962

Figure D-30. (cont.) Thickness graph for Random fabric using *G. Maxwell model, n=2* fitted to all experiment sets using a single parameter set.

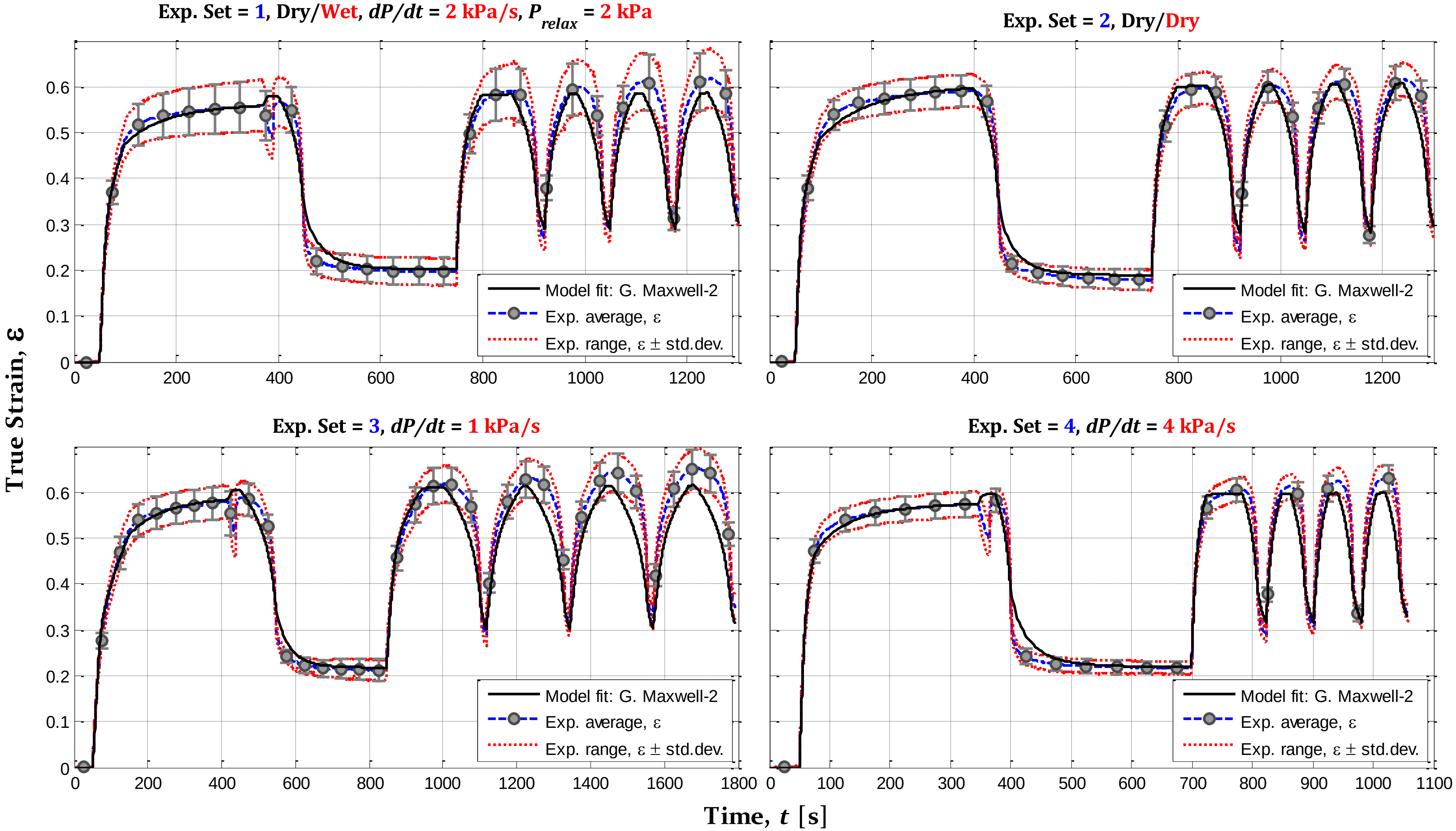

Figure D-31. Strain graph for Random fabric using *G. Maxwell model, n=2* fitted to all experiment sets using a single parameter set.

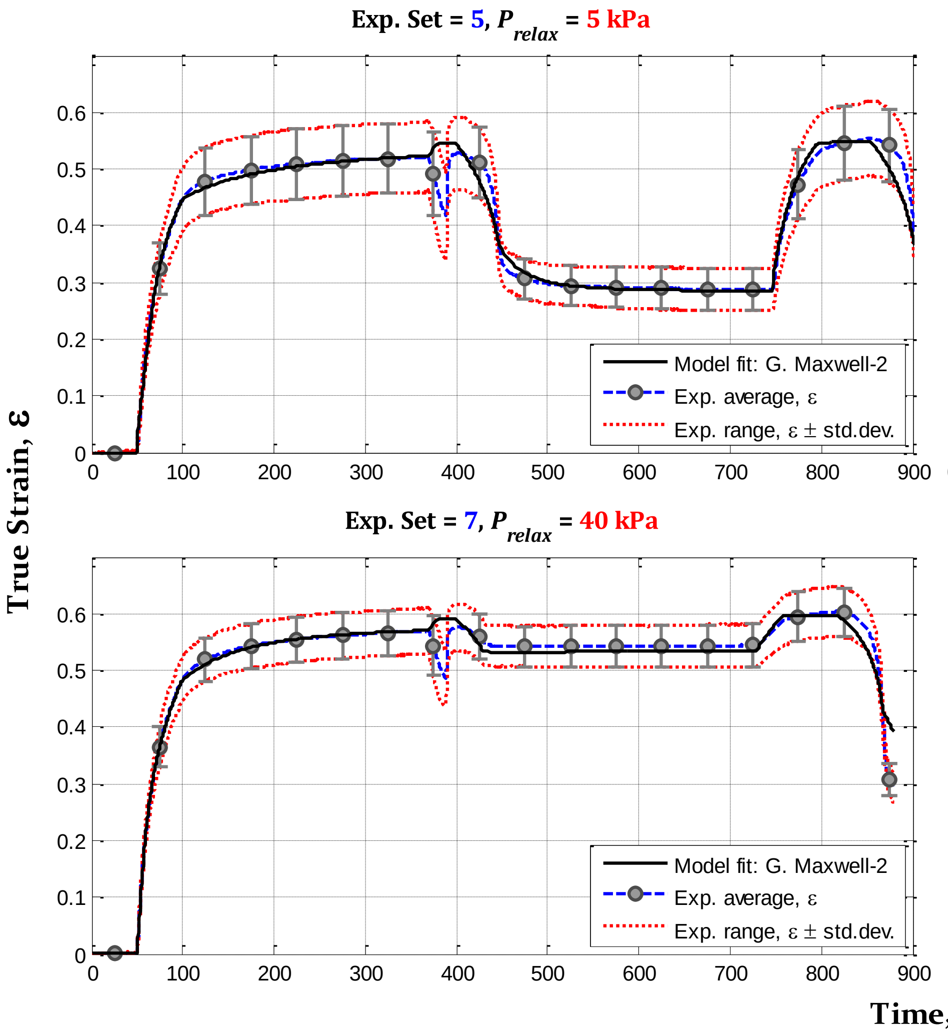

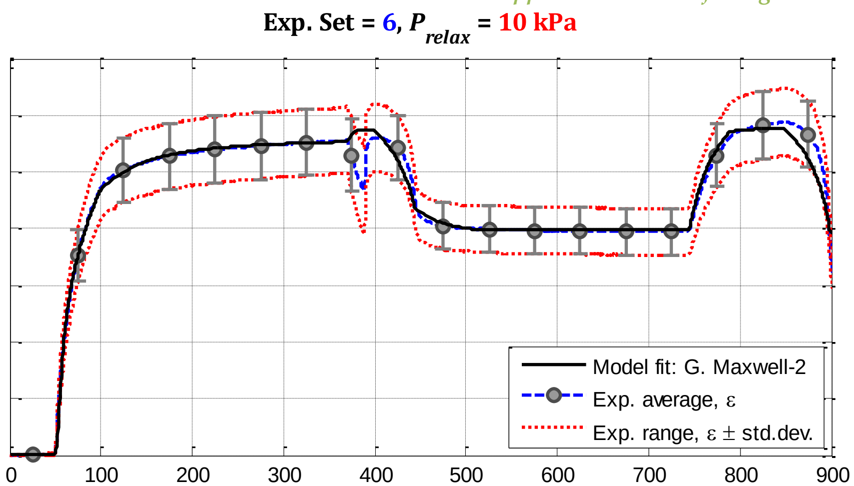

E_0 [kPa]	m_0	E_1 [kPa]	m_1	c_1 [kPa.s]	E_2 [kPa]	m_2	c_2 [kPa.s]	R^2
1.505e3	5.73	1.733e3	3.78	3.561e4	5.308e2	1.54	5.283e2	0.962

Figure D-32. (cont.) Strain graph for Random fabric using *G. Maxwell model, n=2* fitted to all experiment sets using a single parameter set.

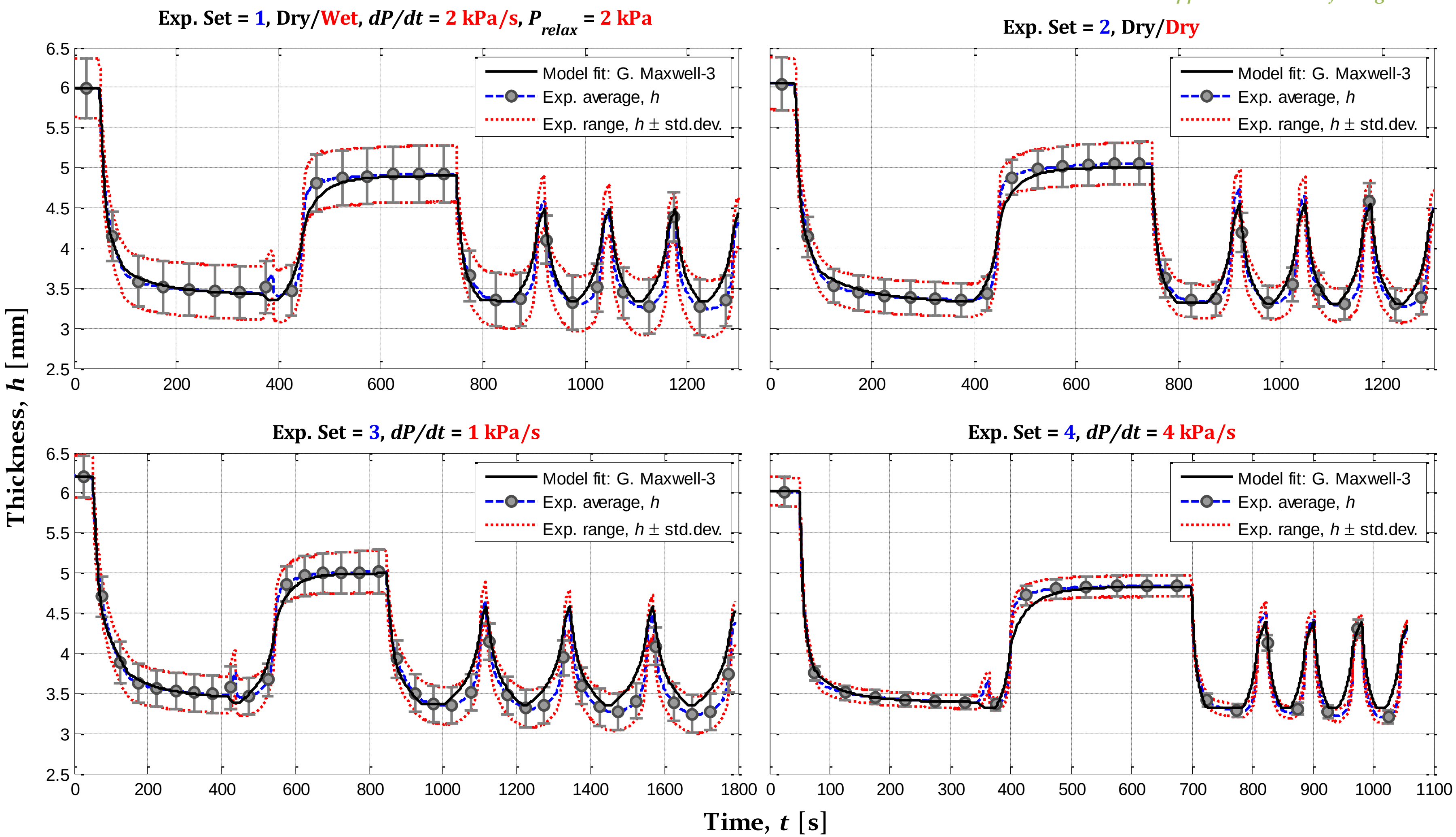

Figure D-33. Thickness graph for Random fabric using *G. Maxwell model, n=3* fitted to each experiment set separately using separate parameter sets.

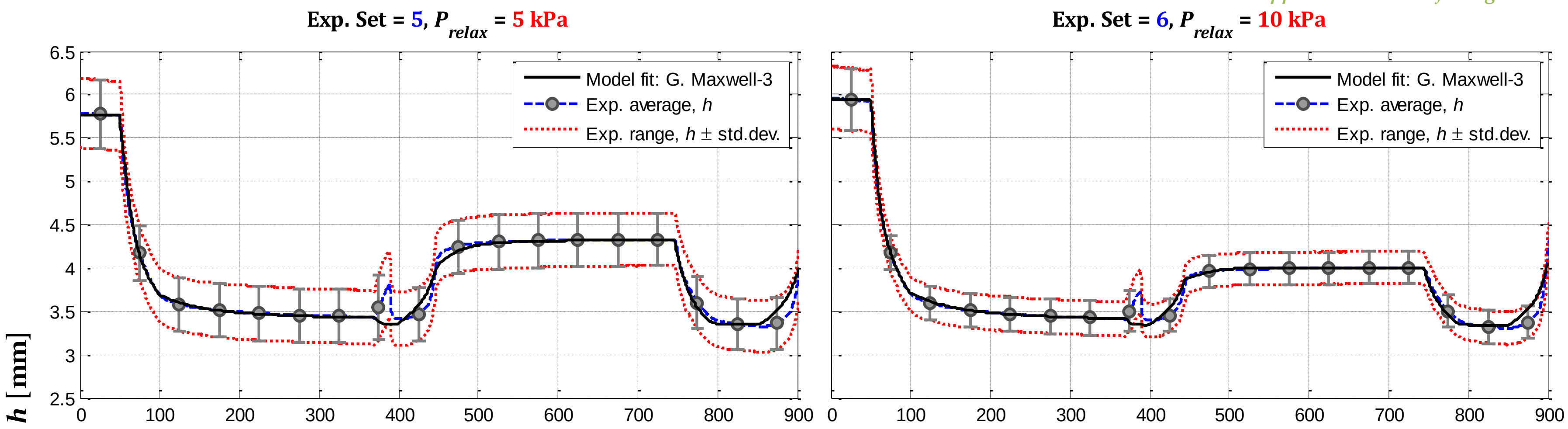

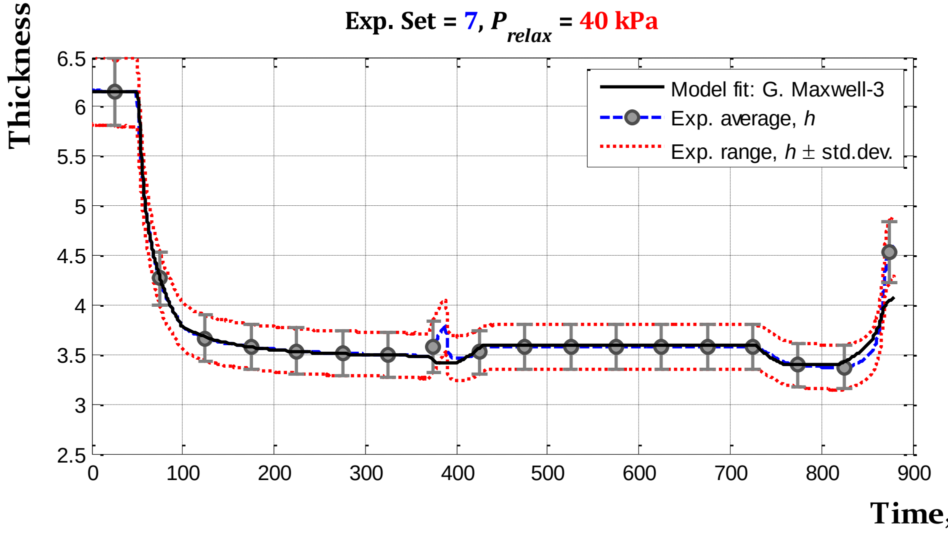

Set	E_0 [kPa]	m_0	E_1 [kPa]	m_1	c_1 [kPa.s]	E_2 [kPa]	m_2	c_2 [kPa.s]	E_3 [kPa]	m_3	c_3 [kPa.s]	R^2
1	1.531e3	5.46	1.843e3	4.01	3.022e4	4.894e2	1.58	4.935e2	1.287e4	3.66	9.710e1	0.946
2	1.054e3	5.49	1.745e3	4.04	3.662e4	4.103e2	1.51	3.942e2	2.098e4	3.64	1.074e2	0.967
3	1.175e3	5.50	1.638e3	3.88	3.867e4	5.050e2	1.54	5.737e2	1.450e4	3.55	9.923e1	0.944
4	1.592e3	5.82	3.000e3	4.46	1.959e4	1.743e2	1.20	5.011e2	1.786e4	3.94	1.011e2	0.949
5	2.376e3	5.51	1.008e3	3.13	2.299e4	5.999e2	1.57	1.299e3	1.142e3	3.28	8.083e1	0.982
6	2.484e3	6.94	6.574e2	2.79	2.747e4	3.002e1	0.62	1.432e3	1.730e4	3.62	1.403e2	0.977
7	9.626e2	14.1	9.681e2	3.08	3.461e4	1.016e2	1.36	8.984e2	1.599e4	0.61	1.194e2	0.964

Figure D-34. (cont.) Thickness graph for Random fabric using *G. Maxwell model, n=3* fitted to each experiment set separately using separate parameter sets.

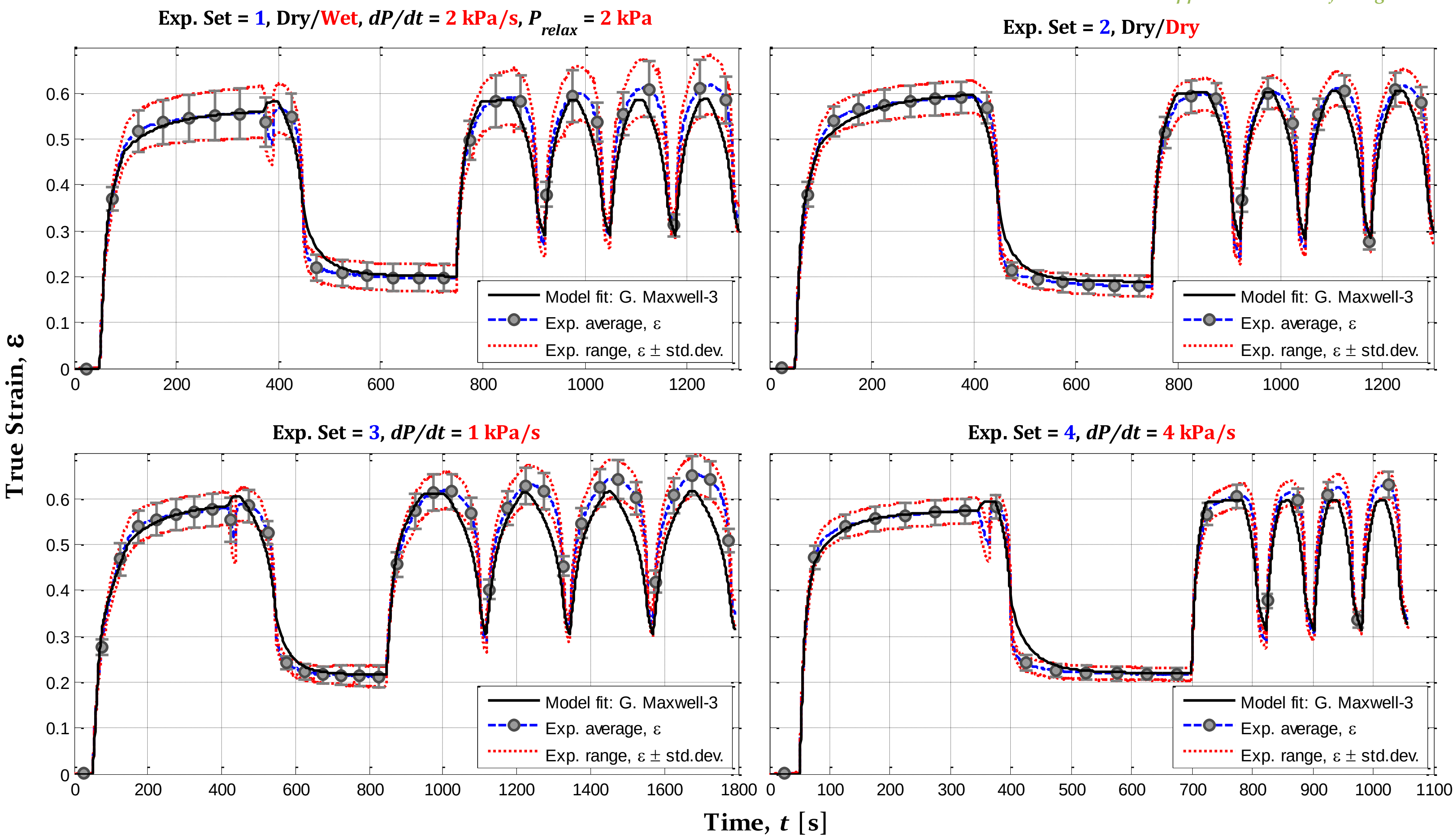

Figure D-35. Strain graph for Random fabric using *G. Maxwell model, n=3* fitted to each experiment set separately using separate parameter sets.

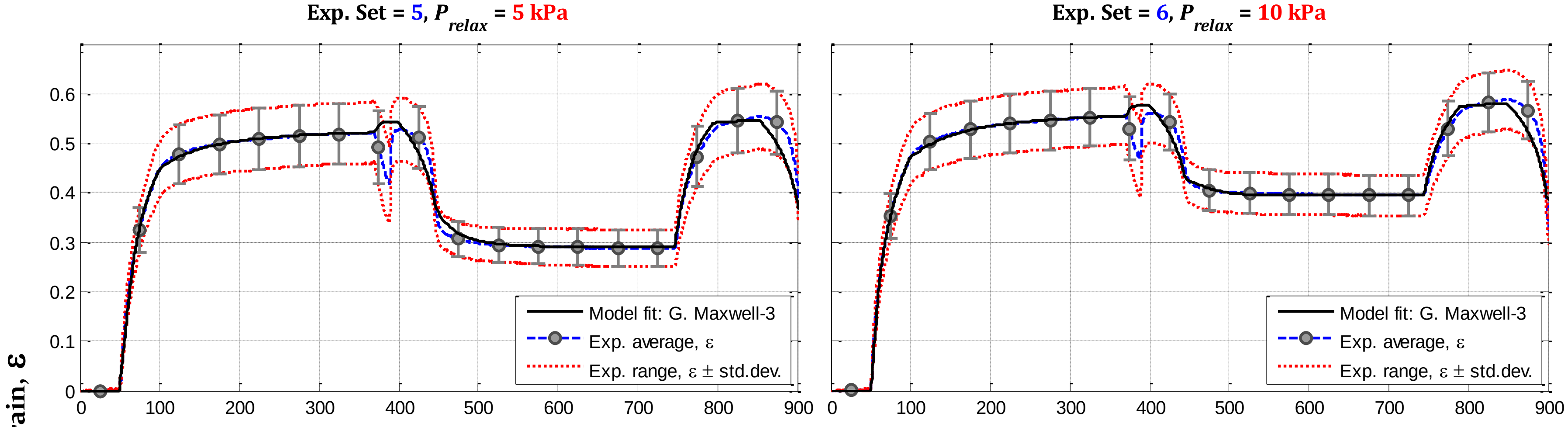

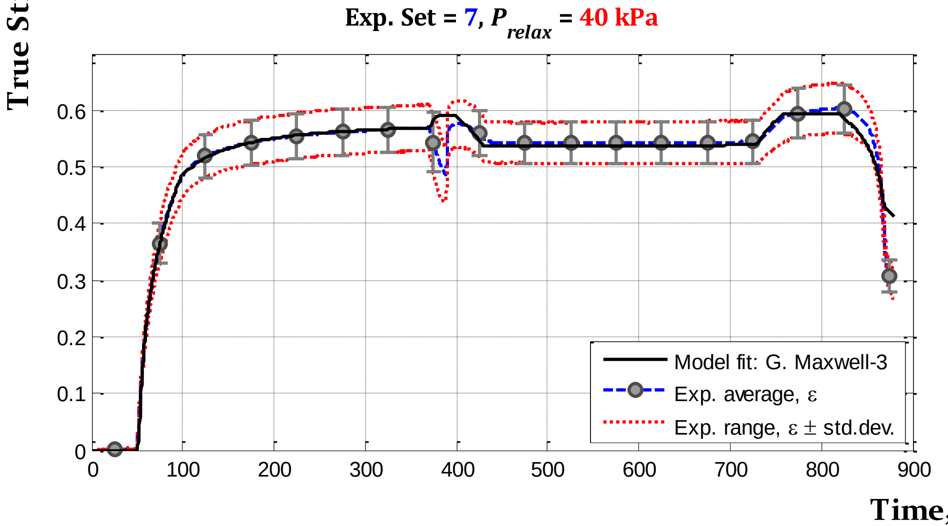

Set	E_0 [kPa]	m_0	E_1 [kPa]	m_1	c_1 [kPa.s]	E_2 [kPa]	m_2	c_2 [kPa.s]	E_3 [kPa]	m_3	c_3 [kPa.s]	R^2
1	1.531e3	5.46	1.843e3	4.01	3.022e4	4.894e2	1.58	4.935e2	1.287e4	3.66	9.710e1	0.946
2	1.054e3	5.49	1.745e3	4.04	3.662e4	4.103e2	1.51	3.942e2	2.098e4	3.64	1.074e2	0.967
3	1.175e3	5.50	1.638e3	3.88	3.867e4	5.050e2	1.54	5.737e2	1.450e4	3.55	9.923e1	0.944
4	1.592e3	5.82	3.000e3	4.46	1.959e4	1.743e2	1.20	5.011e2	1.786e4	3.94	1.011e2	0.949
5	2.376e3	5.51	1.008e3	3.13	2.299e4	5.999e2	1.57	1.299e3	1.142e3	3.28	8.083e1	0.982
6	2.484e3	6.94	6.574e2	2.79	2.747e4	3.002e1	0.62	1.432e3	1.730e4	3.62	1.403e2	0.977
7	9.626e2	14.1	9.681e2	3.08	3.461e4	1.016e2	1.36	8.984e2	1.599e4	0.61	1.194e2	0.964

Figure D-36. (cont.) Strain graph for Random fabric using *G. Maxwell model, n=3* fitted to each experiment set separately using separate parameter sets.

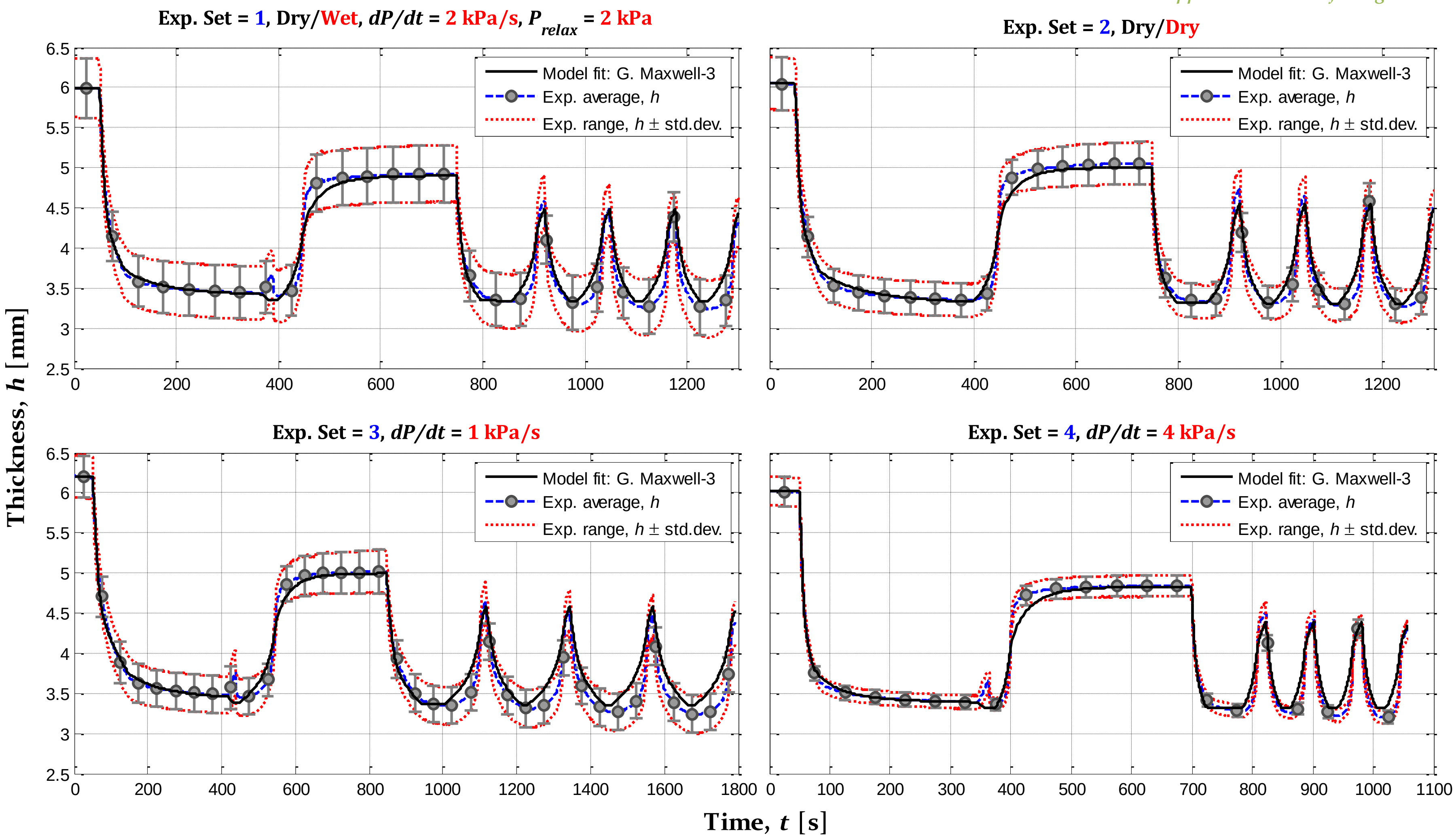

Figure D-37. Thickness graph for Random fabric using *G. Maxwell model, n=3* fitted to all experiment sets using a single parameter set.

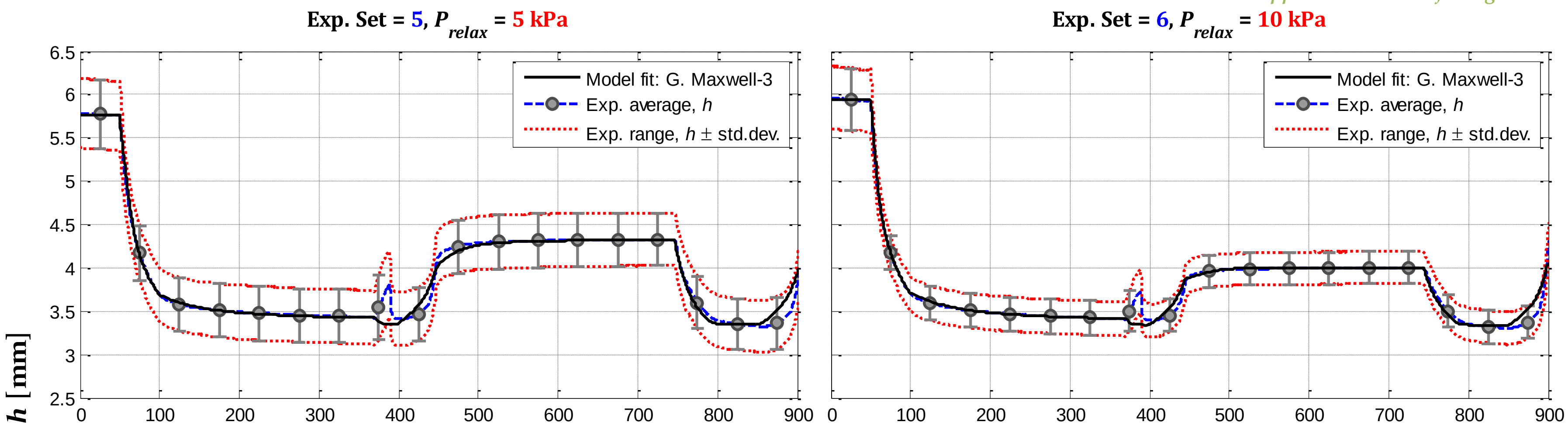

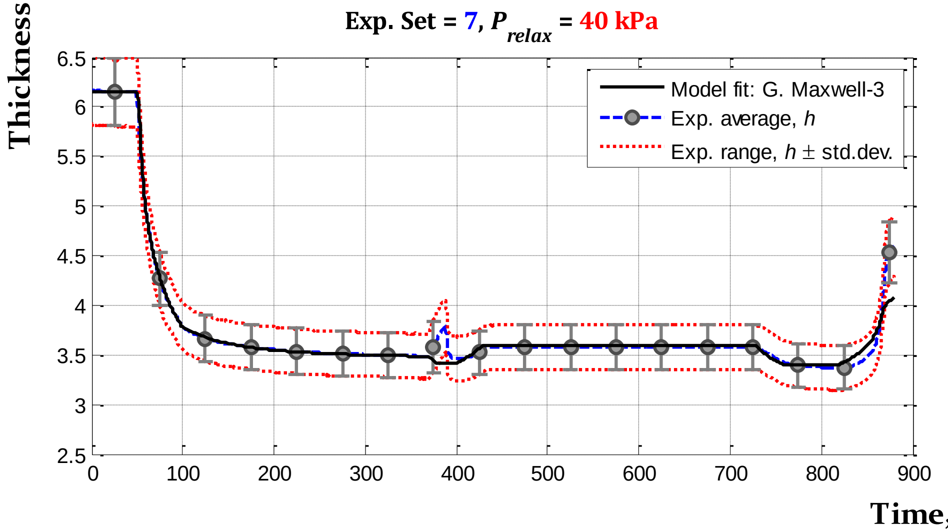

E_0 [kPa]	m_0	E_1 [kPa]	m_1	c_1 [kPa.s]	E_2 [kPa]	m_2	c_2 [kPa.s]	E_3 [kPa]	m_3	c_3 [kPa.s]	R^2
1.446e3	5.62	1.492e3	3.71	3.516e4	3.248e2	1.49	6.209e2	1.952e4	3.30	9.515e1	0.961

Figure D-38. (cont.) Thickness graph for Random fabric using *G. Maxwell model, n=3* fitted to all experiment sets using a single parameter set.

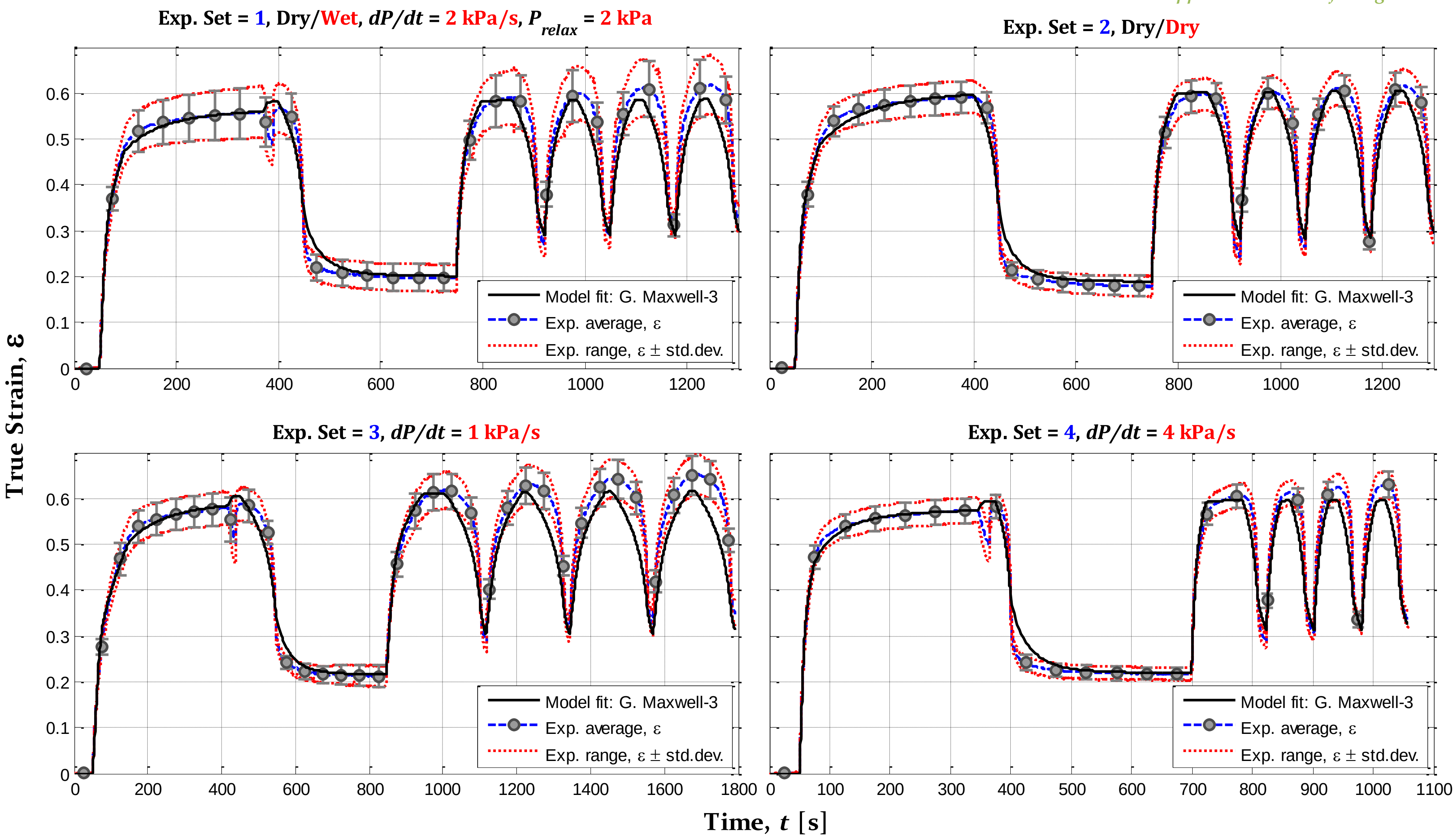

Figure D-39. Strain graph for Random fabric using *G. Maxwell model, n=3* fitted to all experiment sets using a single parameter set.

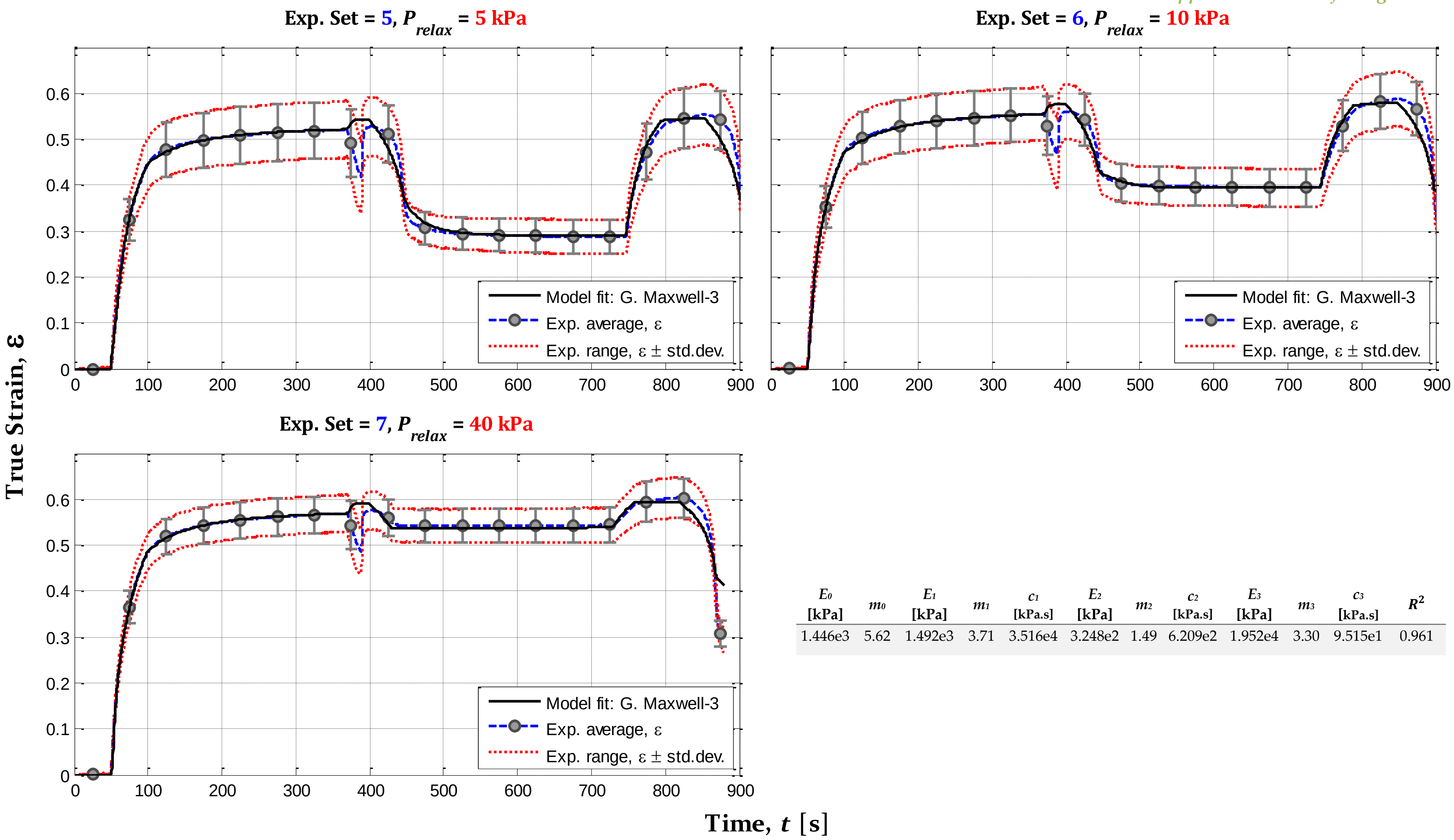

E_0 [kPa]	m_0	E_1 [kPa]	m_1	c_1 [kPa.s]	E_2 [kPa]	m_2	c_2 [kPa.s]	E_3 [kPa]	m_3	c_3 [kPa.s]	R^2
1.446e3	5.62	1.492e3	3.71	3.516e4	3.248e2	1.49	6.209e2	1.952e4	3.30	9.515e1	0.961

Figure D-40. (cont.) Strain graph for Random fabric using *G. Maxwell model, n=3* fitted to all experiment sets using a single parameter set.

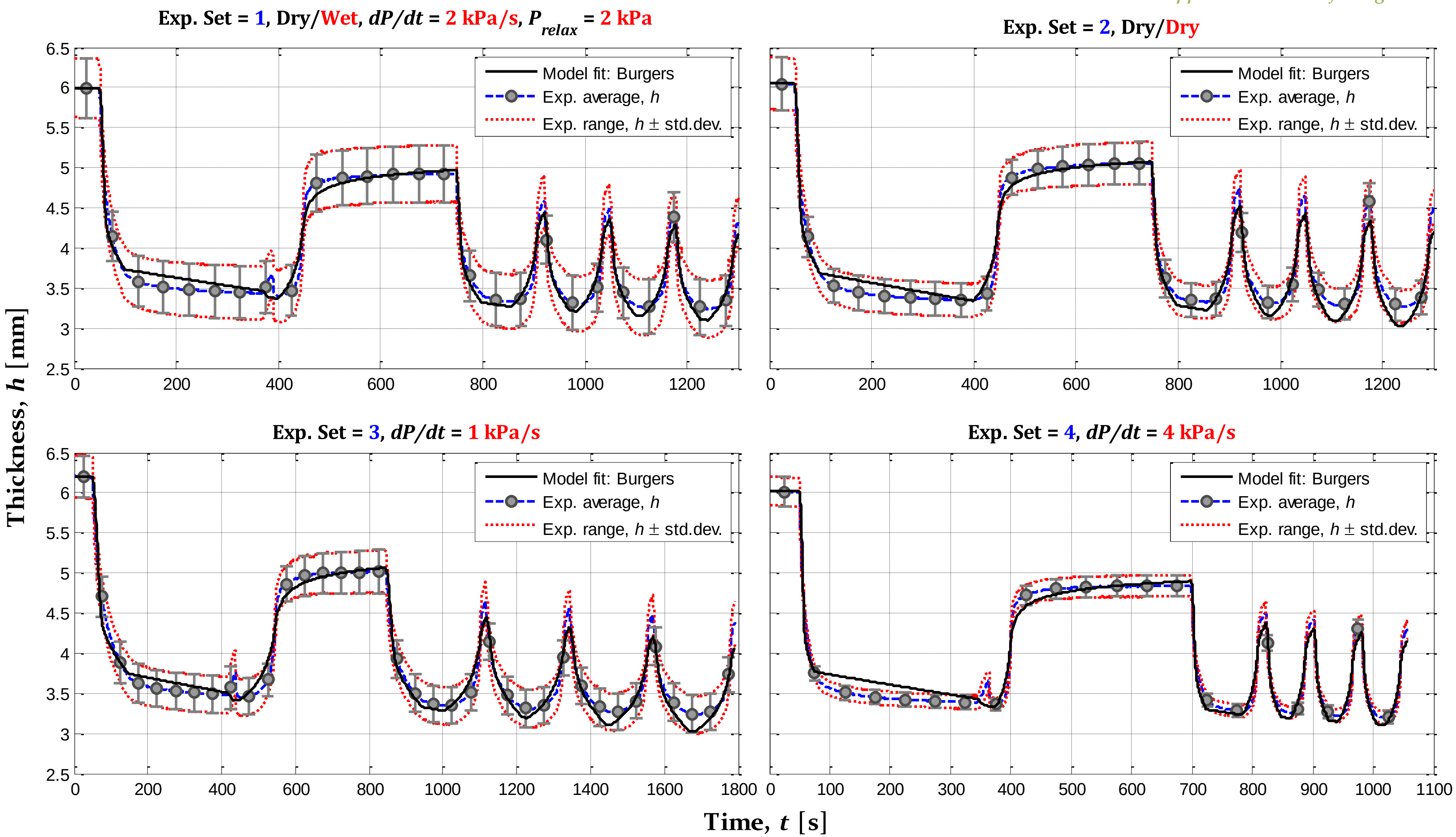

Figure D-41. Thickness graph for Random fabric using *Burgers model* fitted to each experiment set separately using separate parameter sets.

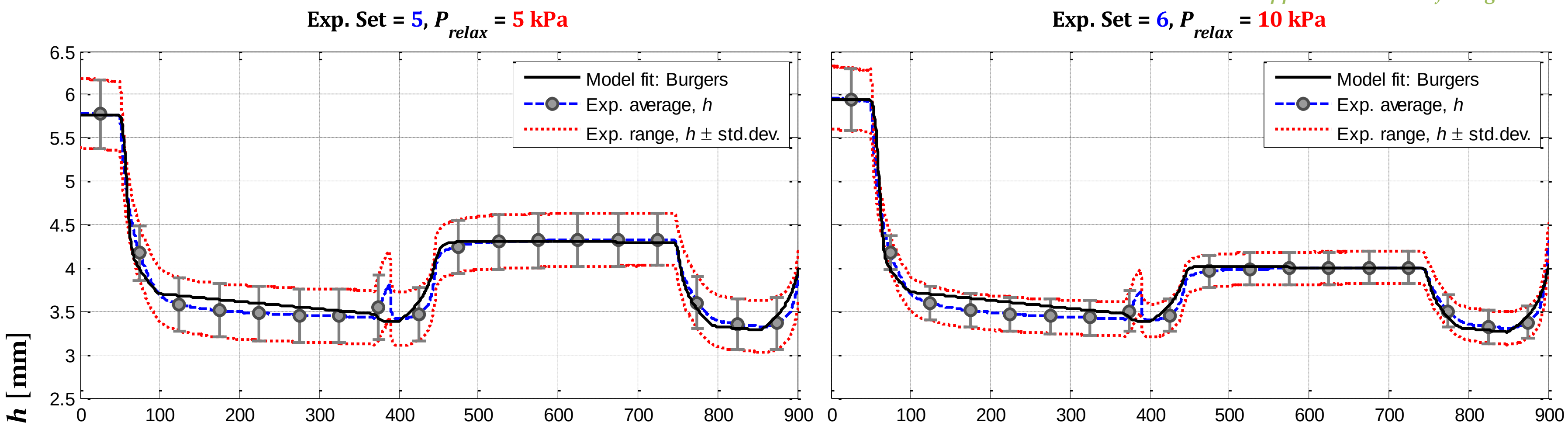

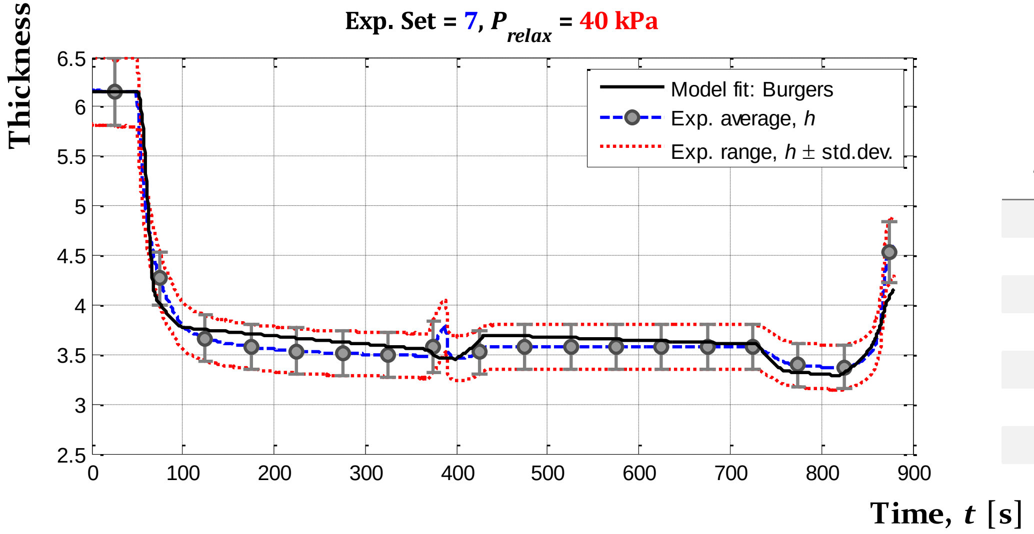

Set	E_1 [kPa]	m_1	c_1 [kPa.s]	E_2 [kPa]	m_2	c_2 [kPa.s]	R^2
1	2.638e4	1.87	3.537e5	7.250e3	5.18	3.847e2	0.970
2	2.833e4	2.28	2.981e5	6.319e3	4.79	3.961e2	0.939
3	2.501e4	1.94	4.022e5	5.105e3	4.99	7.109e2	0.950
4	2.825e4	1.80	2.825e5	8.345e3	5.47	3.188e2	0.970
5	4.107e4	1.57	4.082e5	4.561e3	4.54	5.263e2	0.977
6	3.562e4	1.30	3.760e5	6.305e3	5.65	6.634e2	0.970
7	3.309e4	0.82	4.309e5	5.871e3	6.34	6.649e2	0.956

Figure D-42. (cont.) Thickness graph for Random fabric using *Burgers model* fitted to each experiment set separately using separate parameter sets.

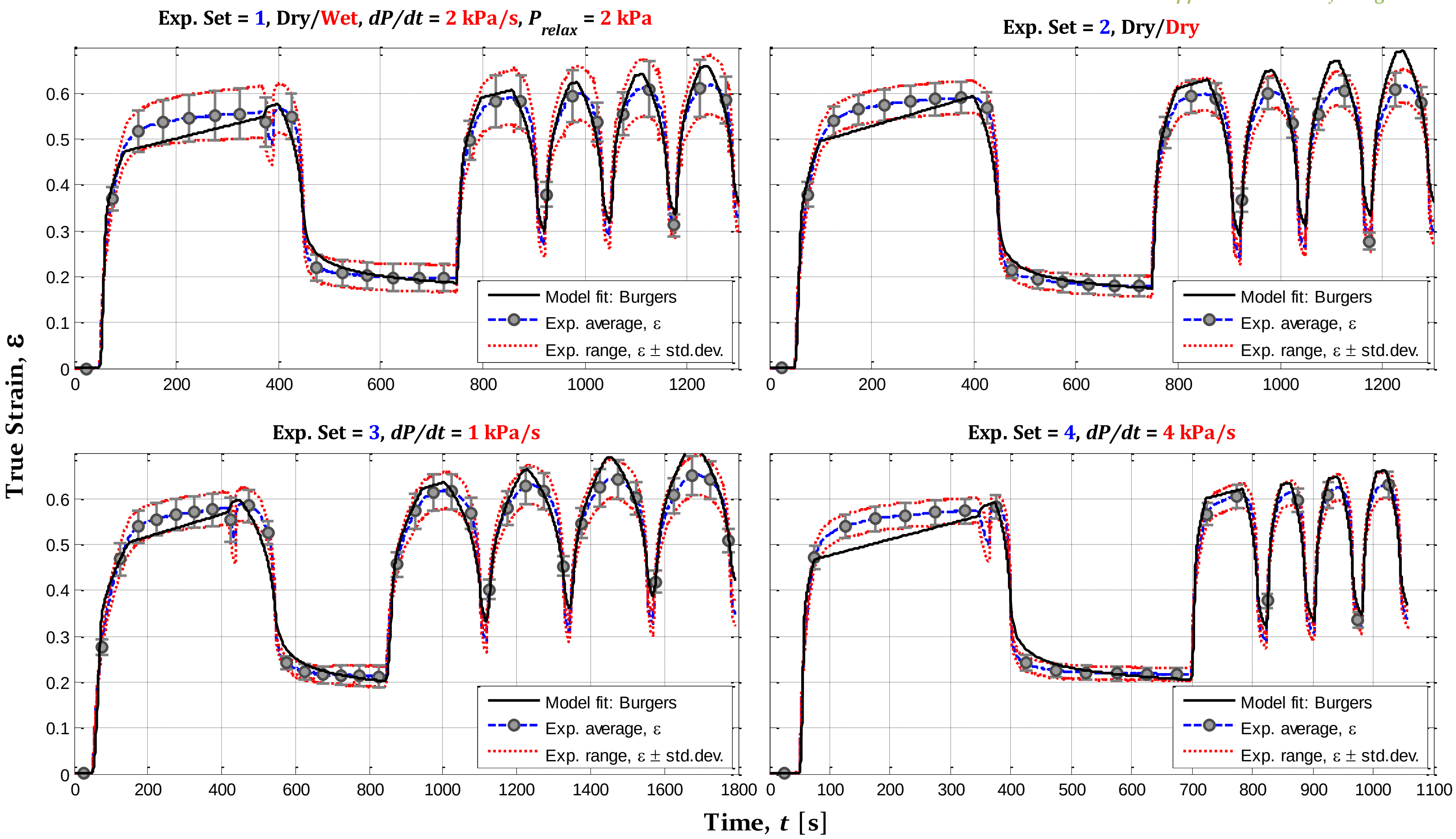

Figure D-43. Strain graph for Random fabric using *Burgers model* fitted to each experiment set separately using separate parameter sets.

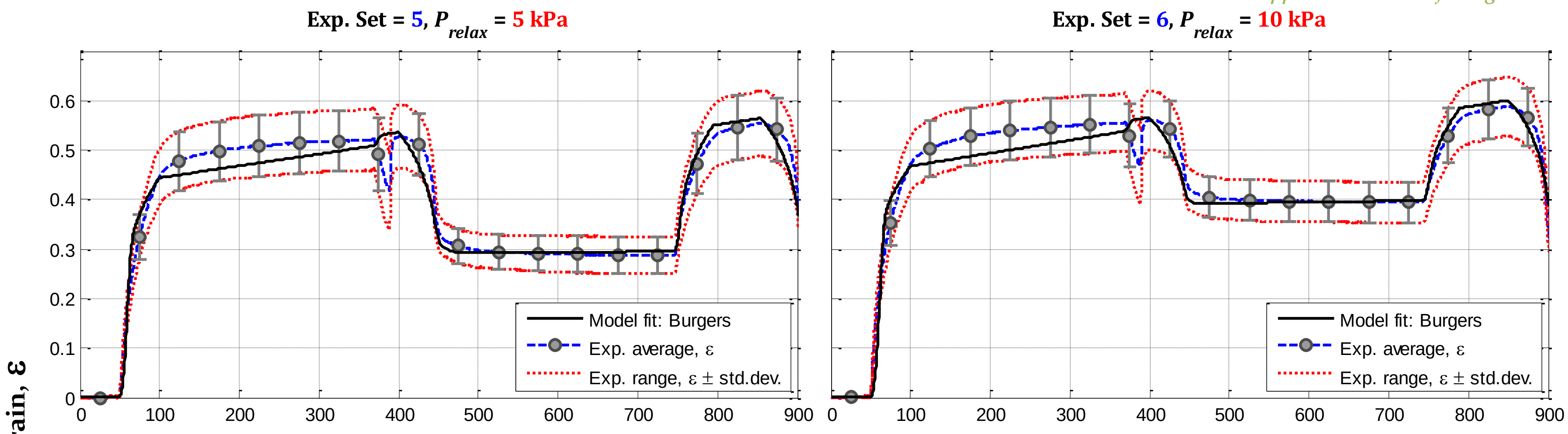

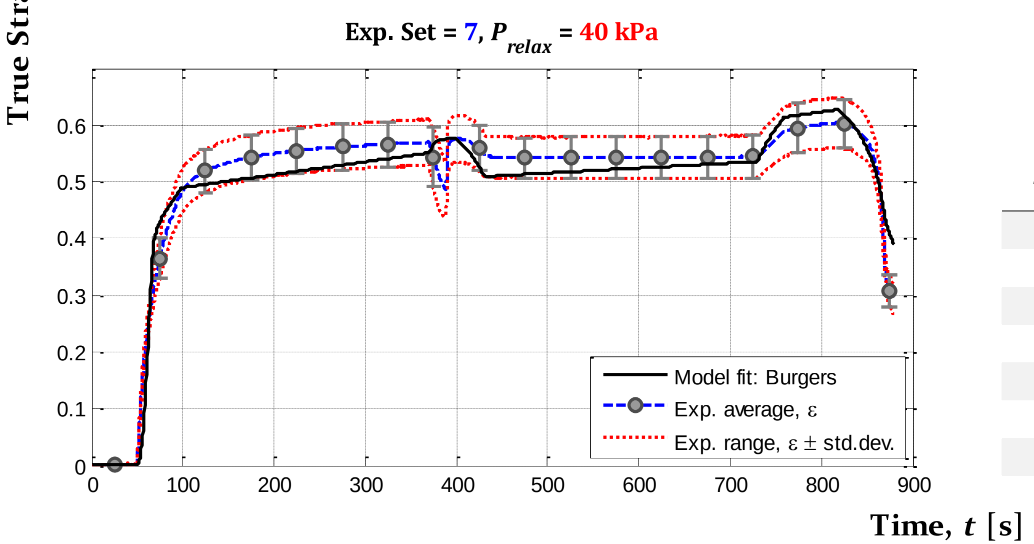

Set	E_1 [kPa]	m_1	c_1 [kPa.s]	E_2 [kPa]	m_2	c_2 [kPa.s]	R^2
1	2.638e4	1.87	3.537e5	7.250e3	5.18	3.847e2	0.970
2	2.833e4	2.28	2.981e5	6.319e3	4.79	3.961e2	0.939
3	2.501e4	1.94	4.022e5	5.105e3	4.99	7.109e2	0.950
4	2.825e4	1.80	2.825e5	8.345e3	5.47	3.188e2	0.970
5	4.107e4	1.57	4.082e5	4.561e3	4.54	5.263e2	0.977
6	3.562e4	1.30	3.760e5	6.305e3	5.65	6.634e2	0.970
7	3.309e4	0.82	4.309e5	5.871e3	6.34	6.649e2	0.956

Figure D-44. (cont.) Thickness graph for Random fabric using *Burgers model* fitted to each experiment set separately using separate parameter sets.

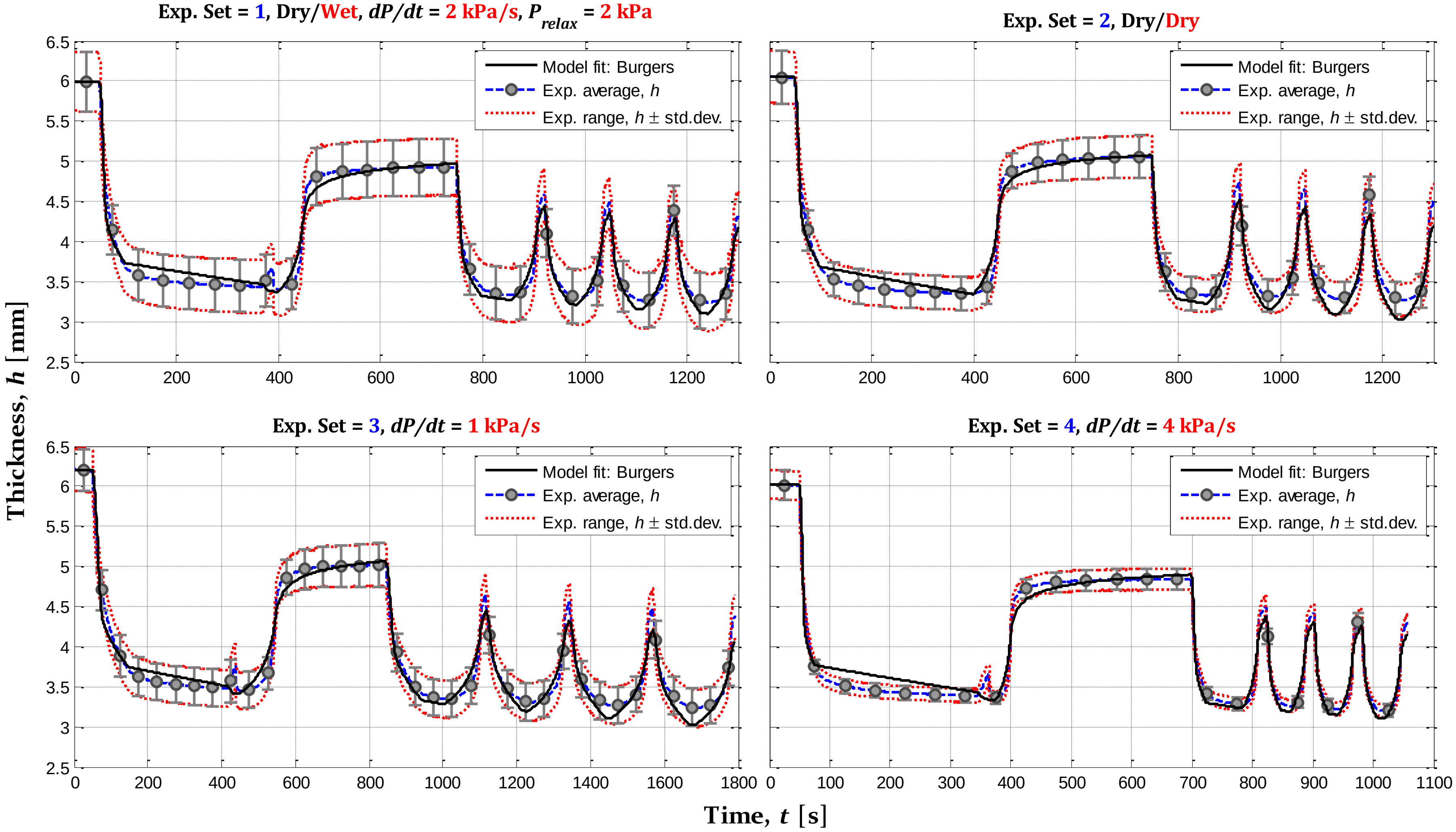

Figure D-45. Thickness graph for Random fabric using *Burgers model* fitted to all experiment sets using a single parameter set.

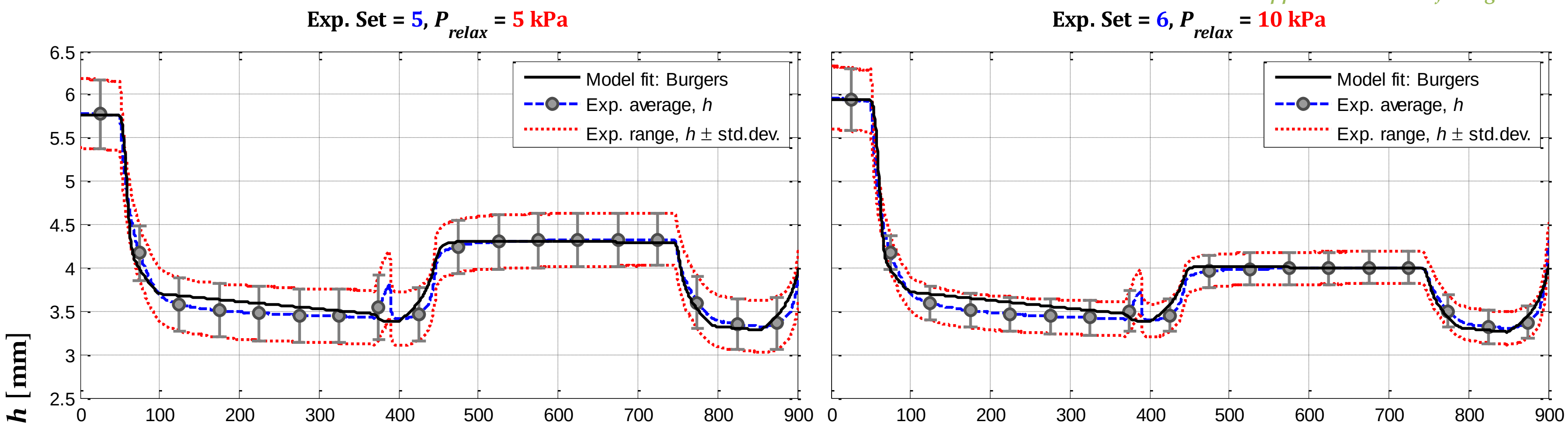

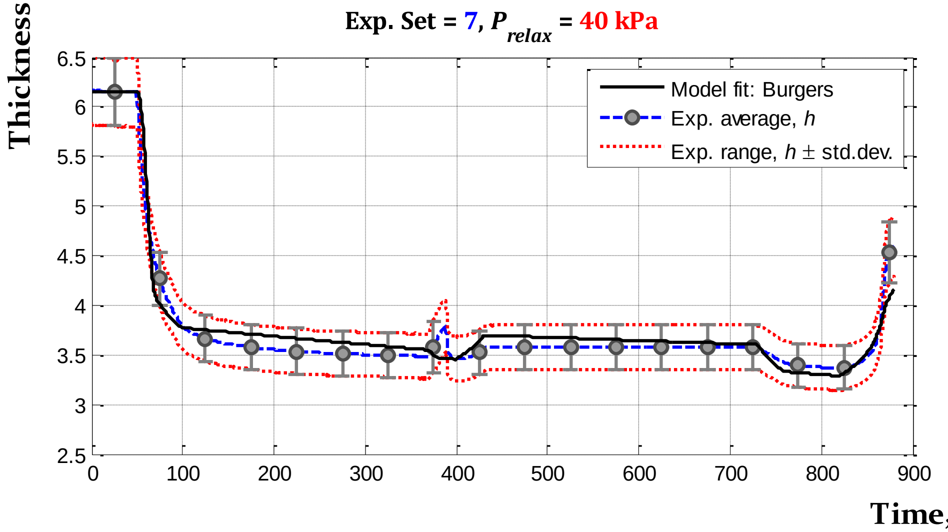

E_1 [kPa]	m_1	c_1 [kPa.s]	E_2 [kPa]	m_2	c_2 [kPa.s]	R^2
2.740e4	1.74	3.614e5	6.624e3	5.30	4.771e2	0.962

Figure D-46. (cont.) Thickness graph for Random fabric using *Burgers model* fitted to all experiment sets using a single parameter set.

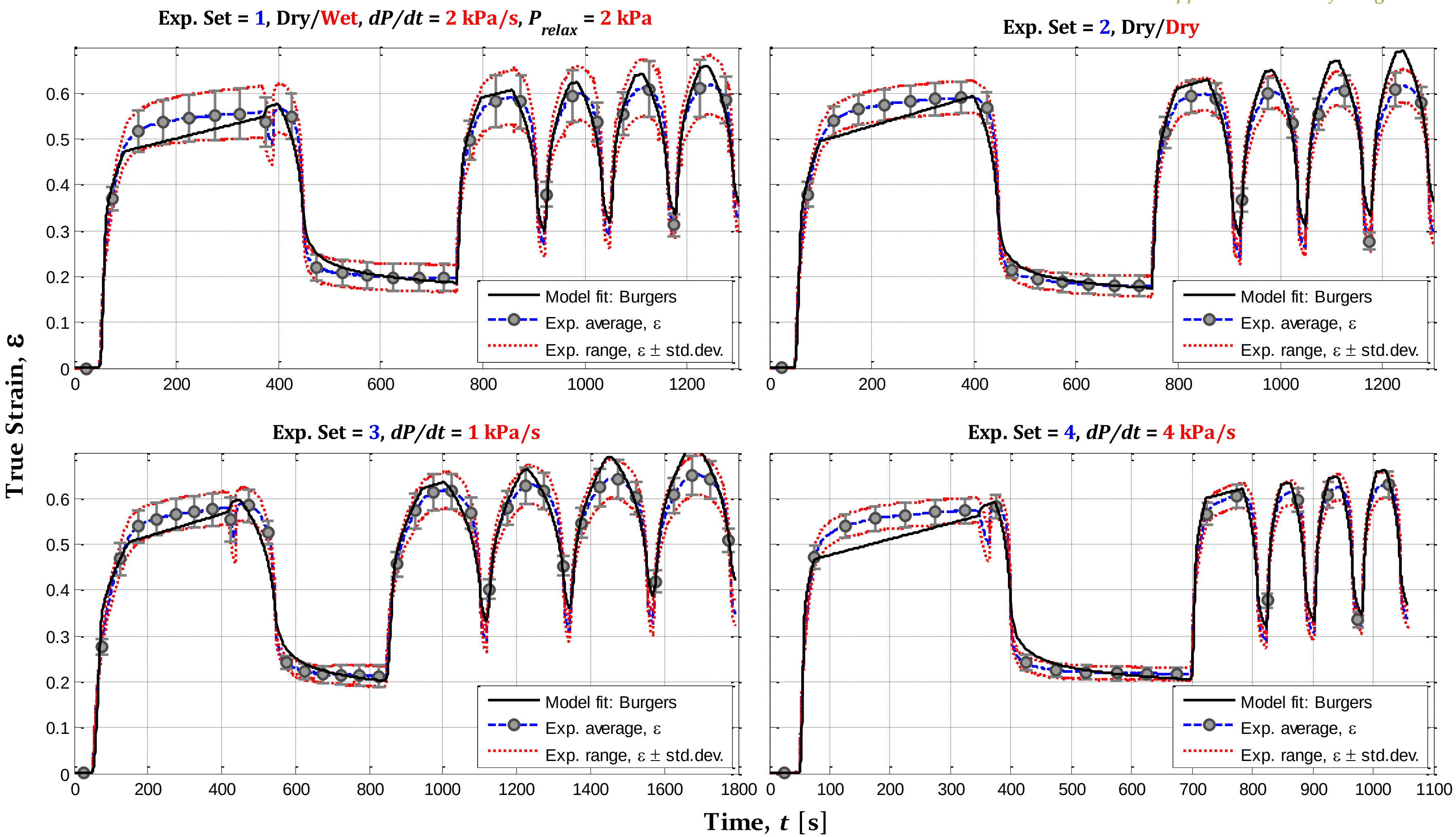

Figure D-47. Strain graph for Random fabric using *Burgers model* fitted to all experiment sets using a single parameter set.

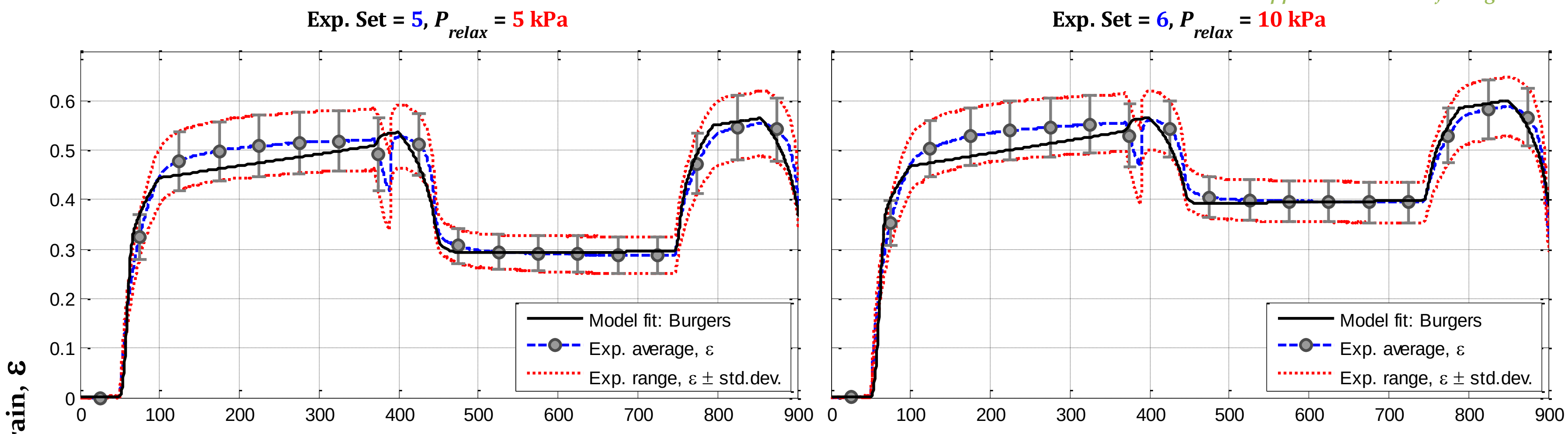

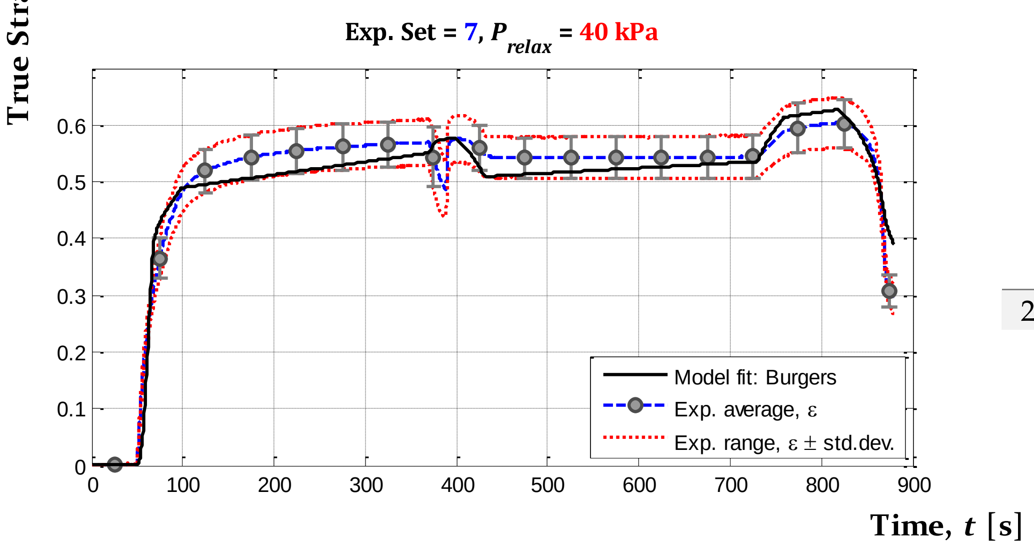

E_1 [kPa]	m_1	c_1 [kPa.s]	E_2 [kPa]	m_2	c_2 [kPa.s]	R^2
2.740e4	1.74	3.614e5	6.624e3	5.30	4.771e2	0.962

Figure D-48. (cont.) Strain graph for Random fabric using *Burgers model* fitted to all experiment sets using a single parameter set.

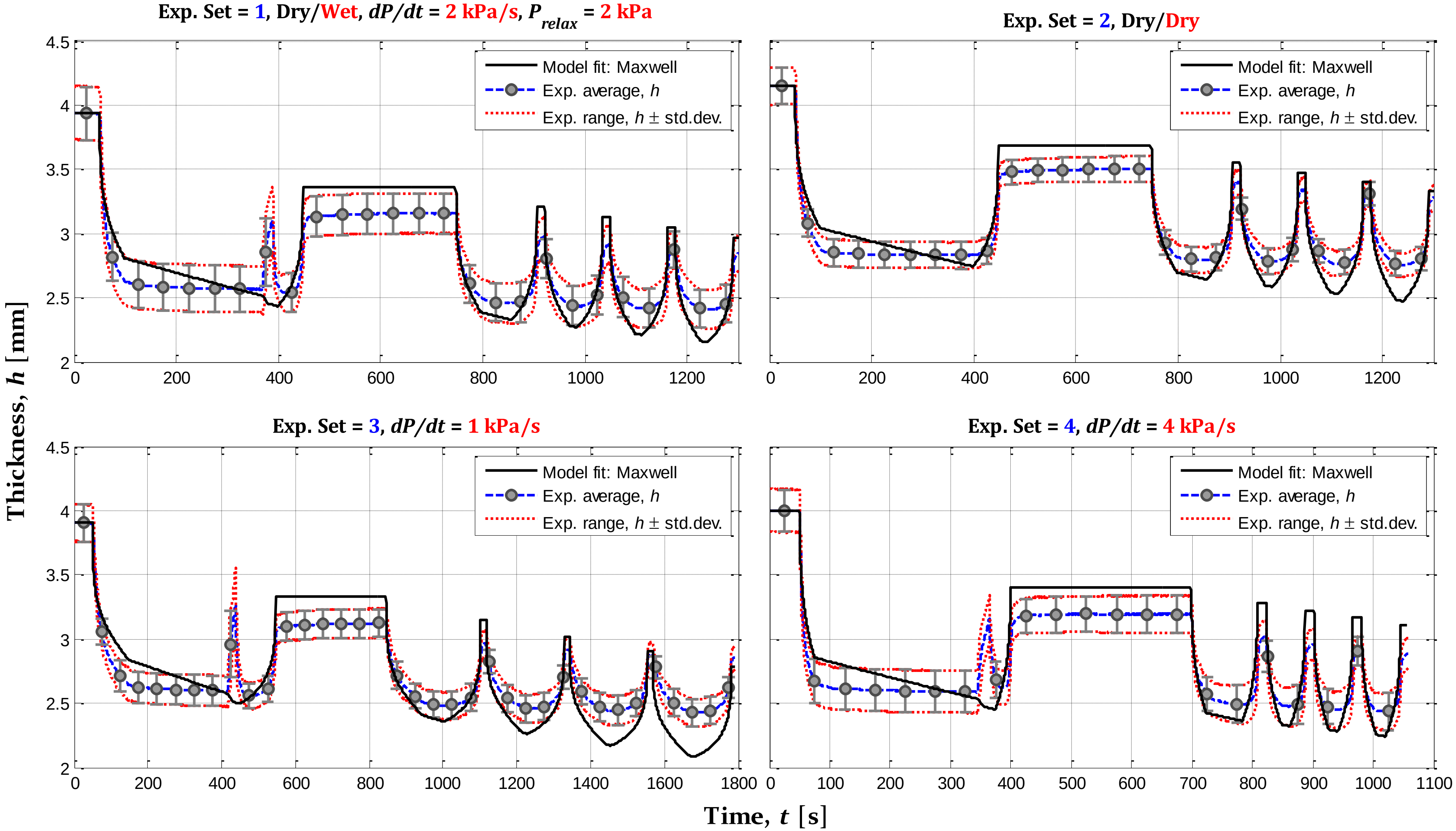

Figure D-49. Thickness graph for Woven fabric using *Maxwell model* fitted to each experiment set separately using separate parameter sets.

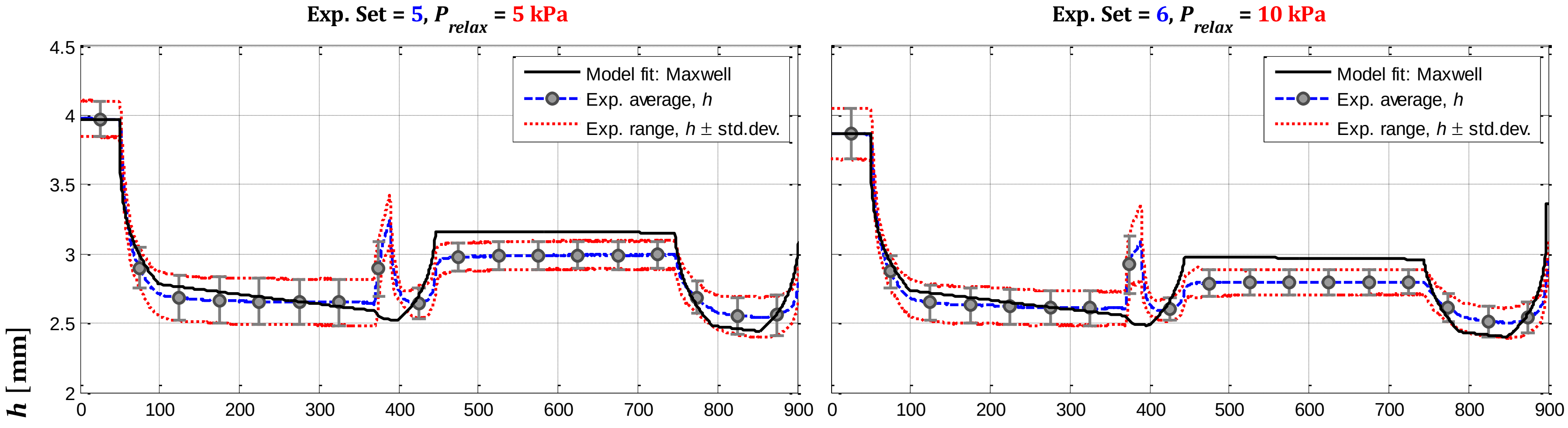

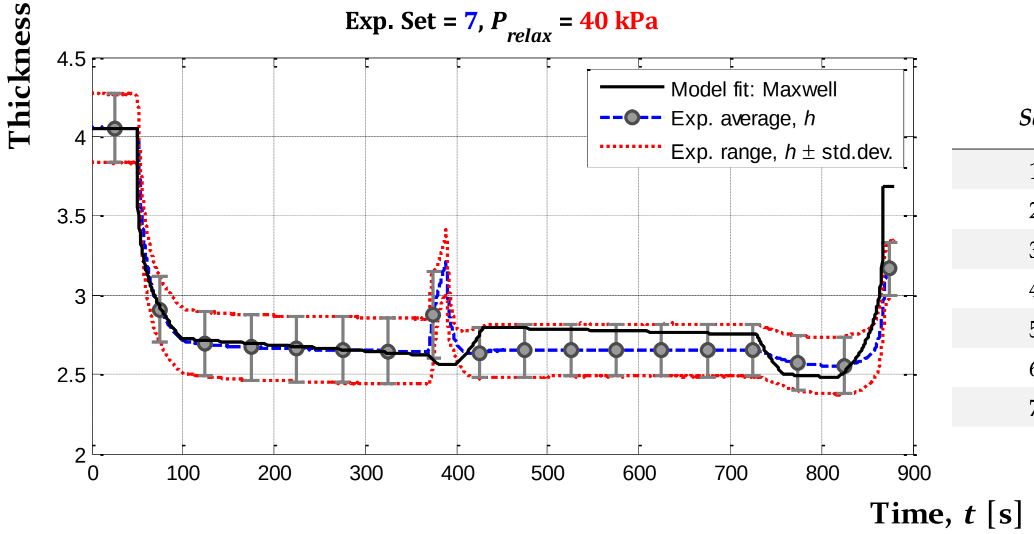

Set	*E* [kPa]	*m*	*c* [kPa.s]	R^2
1	2866.85	3.02	239162.63	0.721
2	3069.84	2.87	284060.23	0.737
3	6123.80	3.44	269744.47	0.574
4	1498.59	2.47	221829.09	0.711
5	2744.31	3.17	371089.32	0.790
6	2800.03	3.10	382065.13	0.819
7	2643.42	3.53	681664.32	0.803

Figure D-50. (cont.) Thickness graph for Woven fabric using *Maxwell model* fitted to each experiment set separately using separate parameter sets.

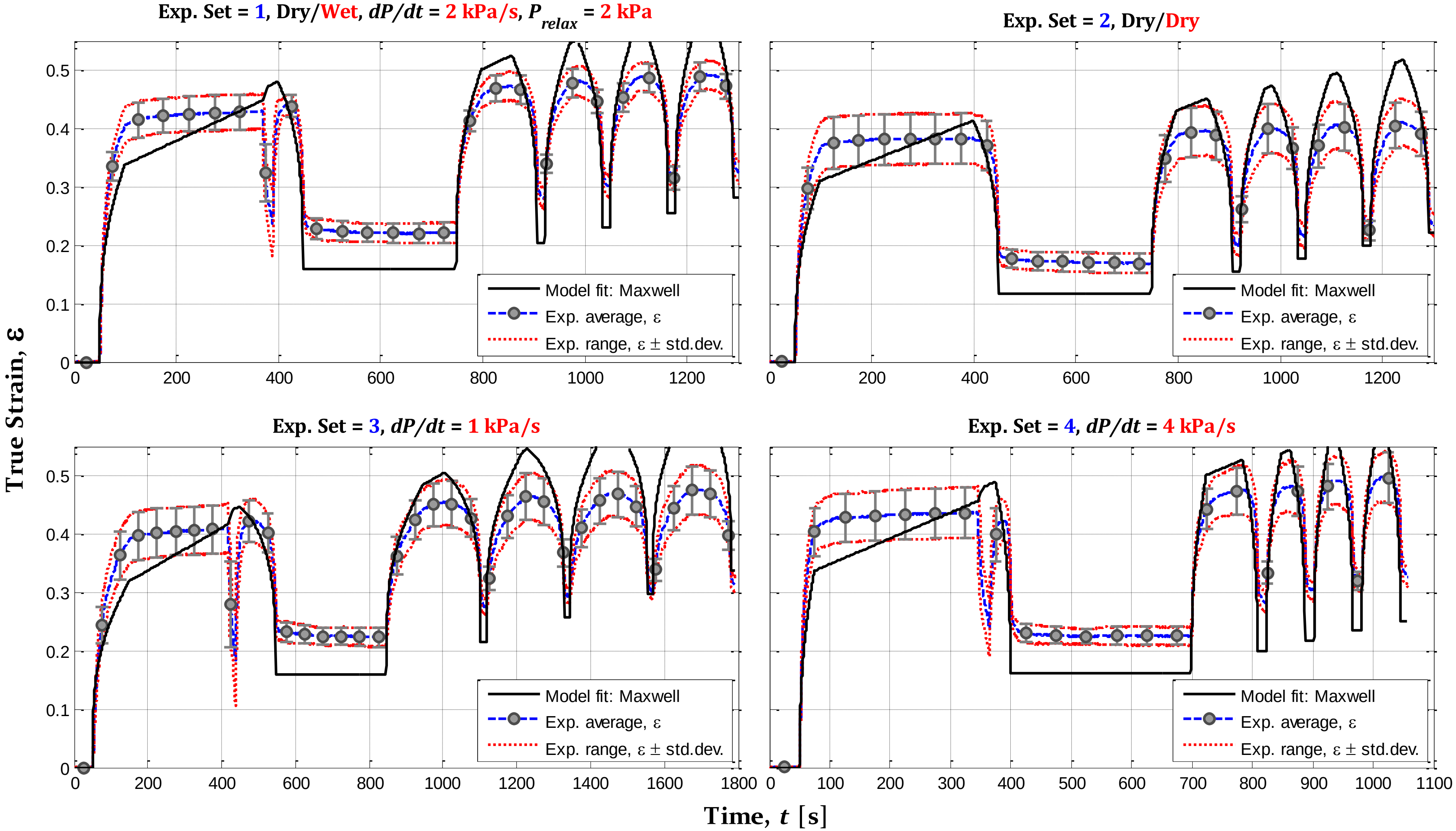

Figure D-51. Strain graph for Woven fabric using *Maxwell model* fitted to each experiment set separately using separate parameter sets.

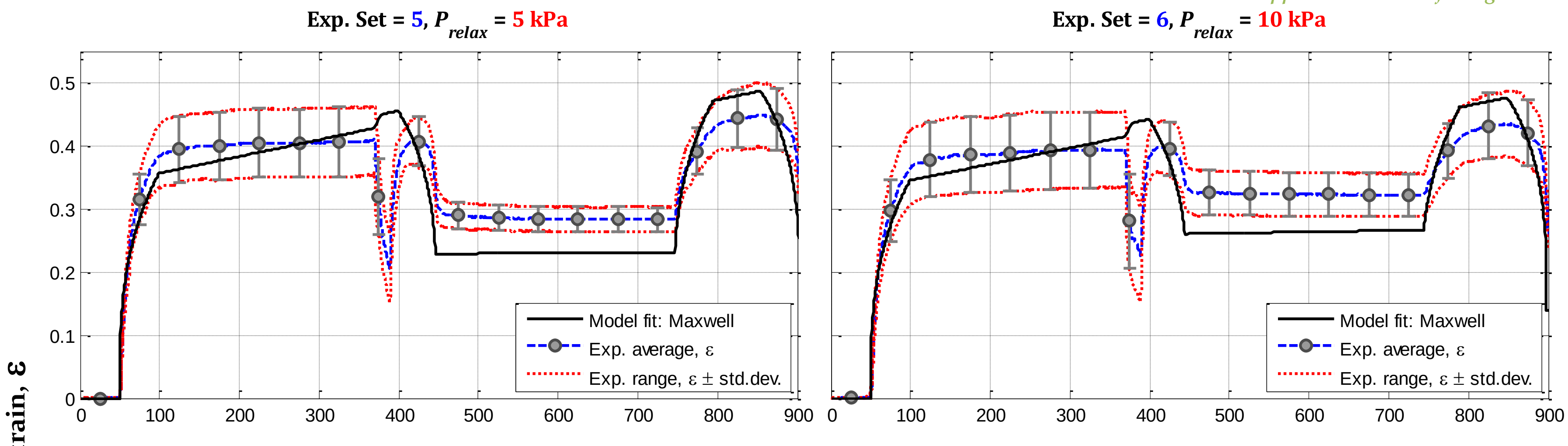

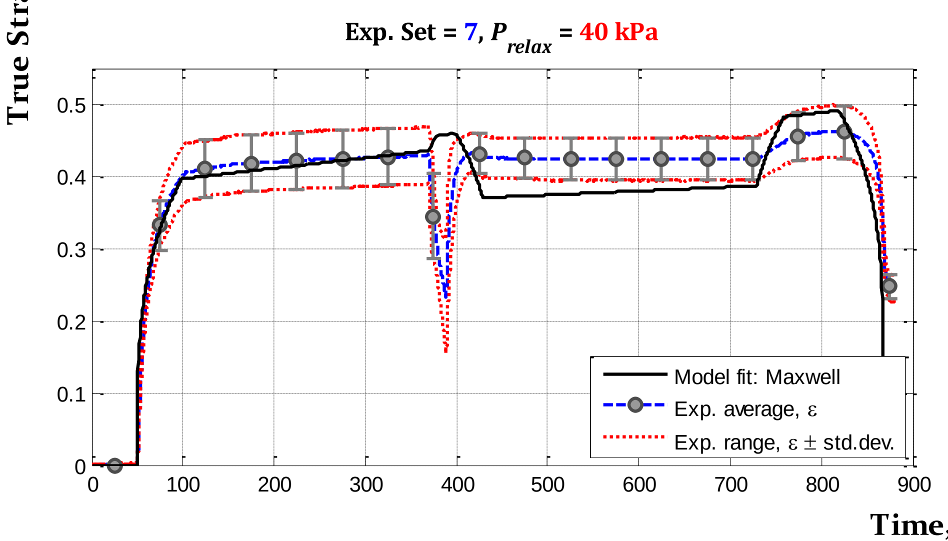

Set	*E* [kPa]	*m*	*c* [kPa.s]	R^2
1	2866.85	3.02	239162.63	0.721
2	3069.84	2.87	284060.23	0.737
3	6123.80	3.44	269744.47	0.574
4	1498.59	2.47	221829.09	0.711
5	2744.31	3.17	371089.32	0.790
6	2800.03	3.10	382065.13	0.819
7	2643.42	3.53	681664.32	0.803

Figure D-52. (cont.) Strain graph for Woven fabric using *Maxwell model* fitted to each experiment set separately using separate parameter sets.

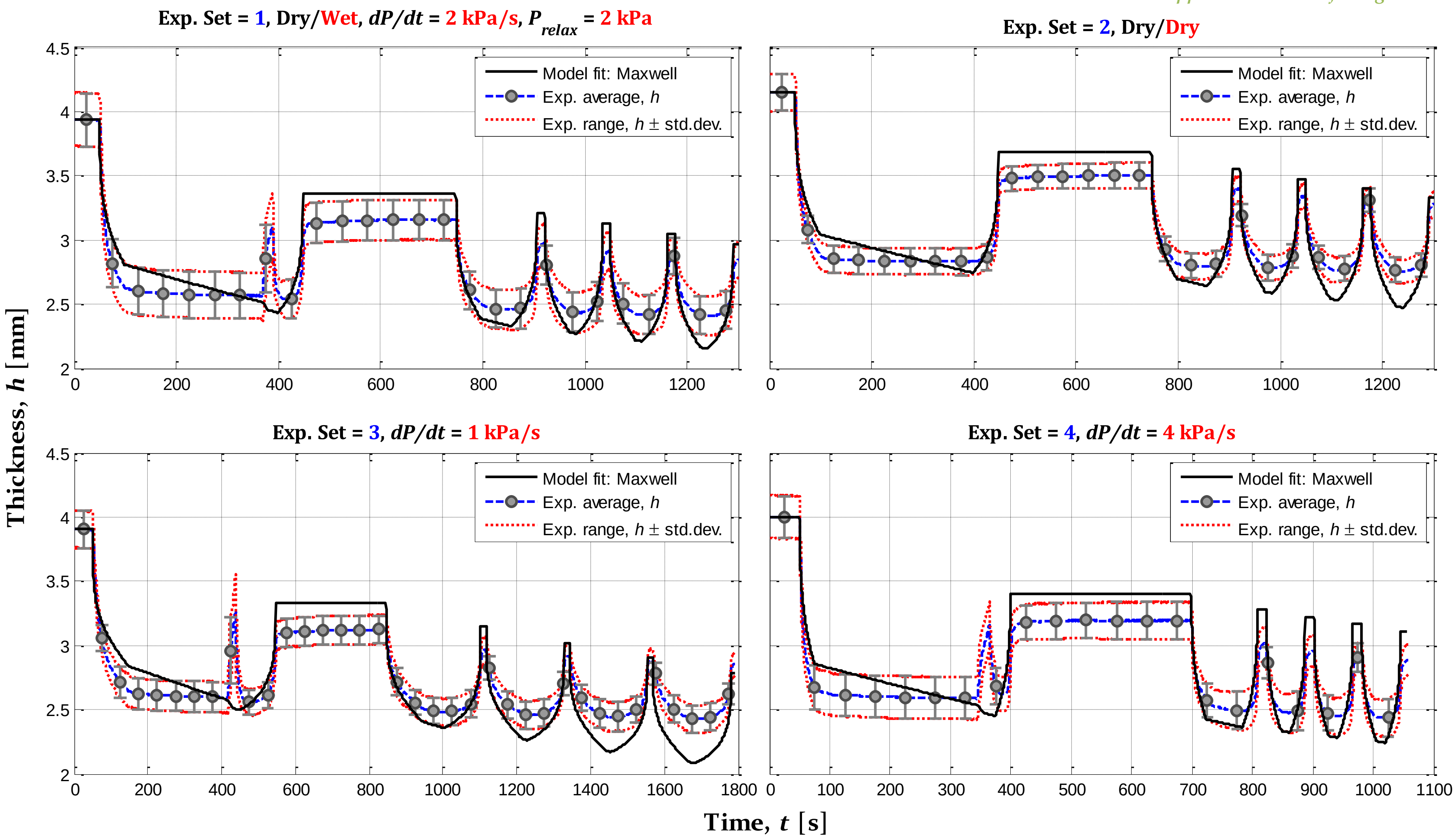

Figure D-53. Thickness graph for Woven fabric using *Maxwell model* fitted to all experiment sets using a single parameter set.

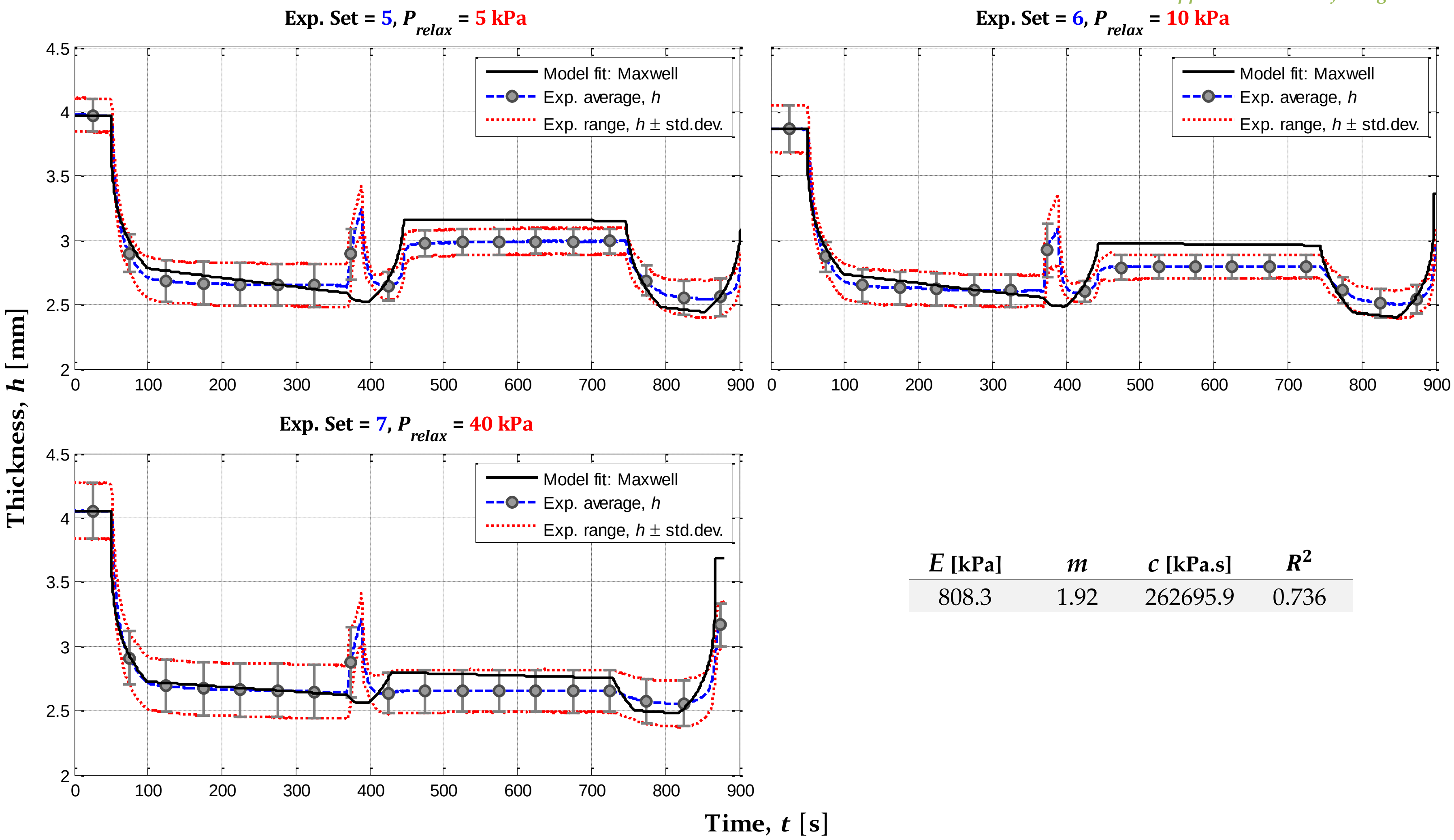

E [kPa]	m	c [kPa.s]	R^2
808.3	1.92	262695.9	0.736

Figure D-54. (cont.) Thickness graph for Woven fabric using *Maxwell model* fitted to all experiment sets using a single parameter set.

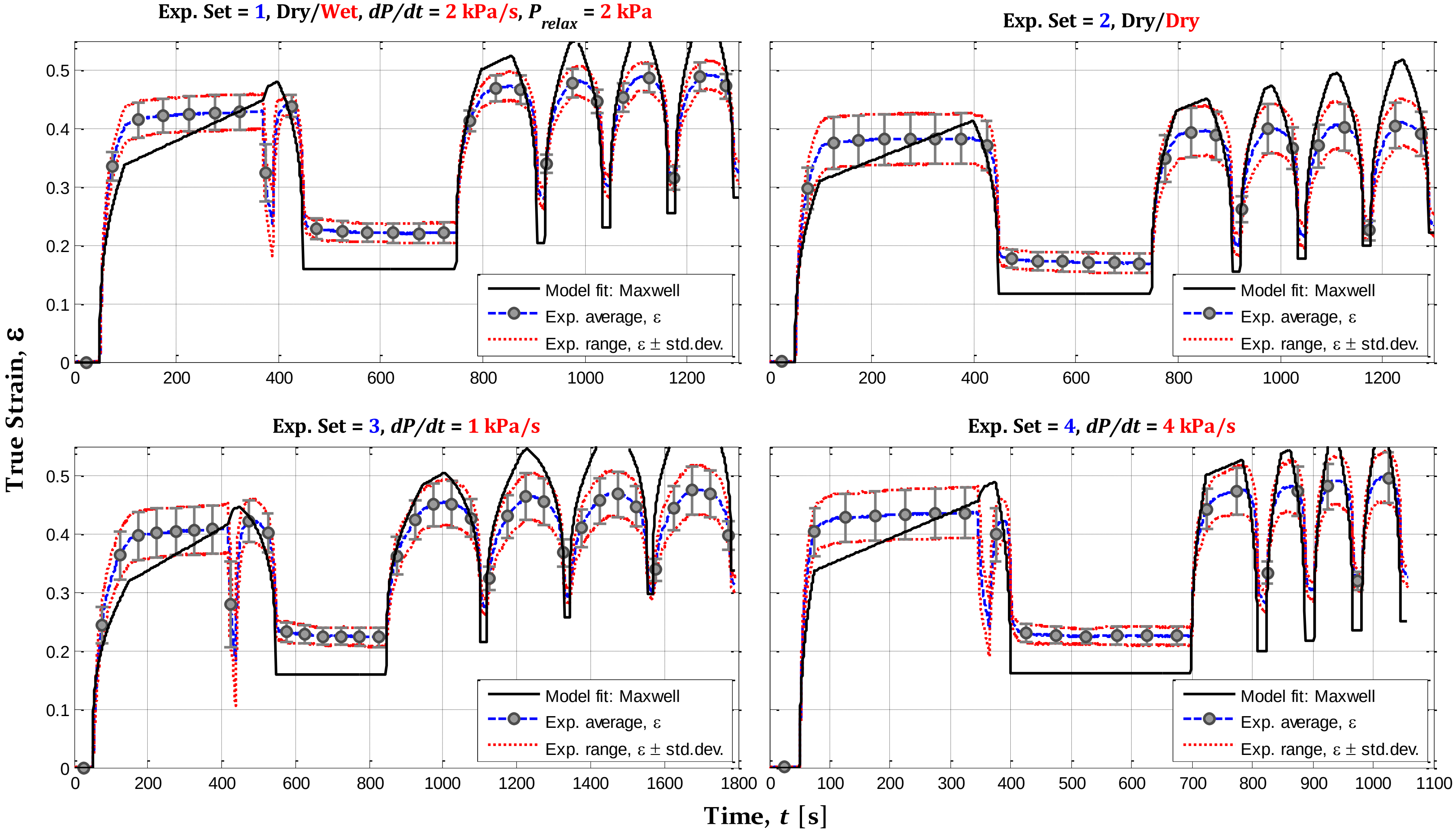

Figure D-55. Strain graph for Woven fabric using *Maxwell model* fitted to all experiment sets using a single parameter set.

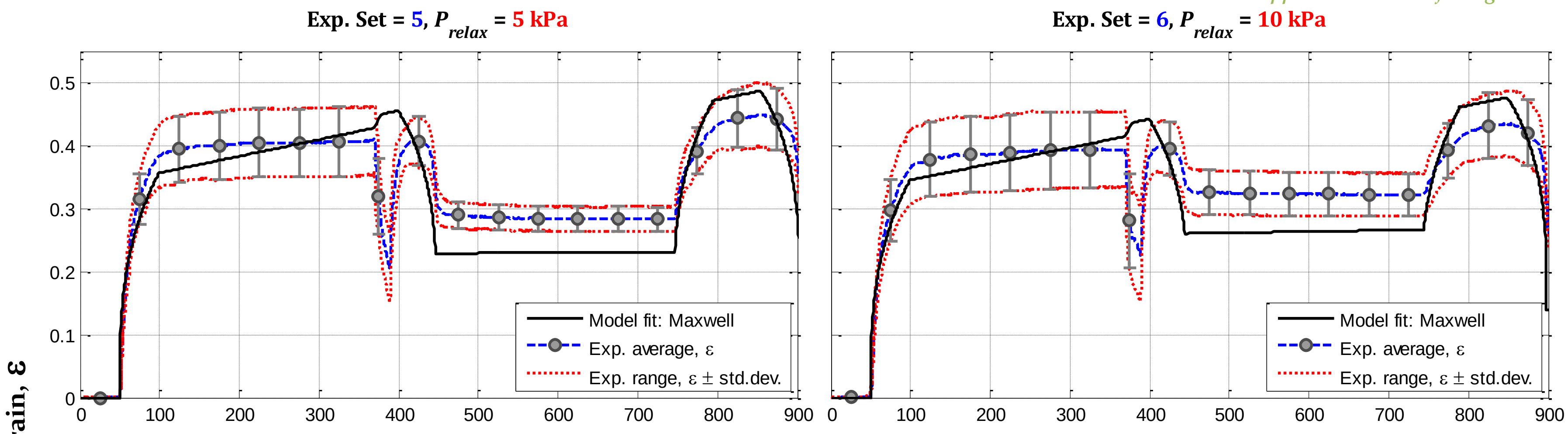

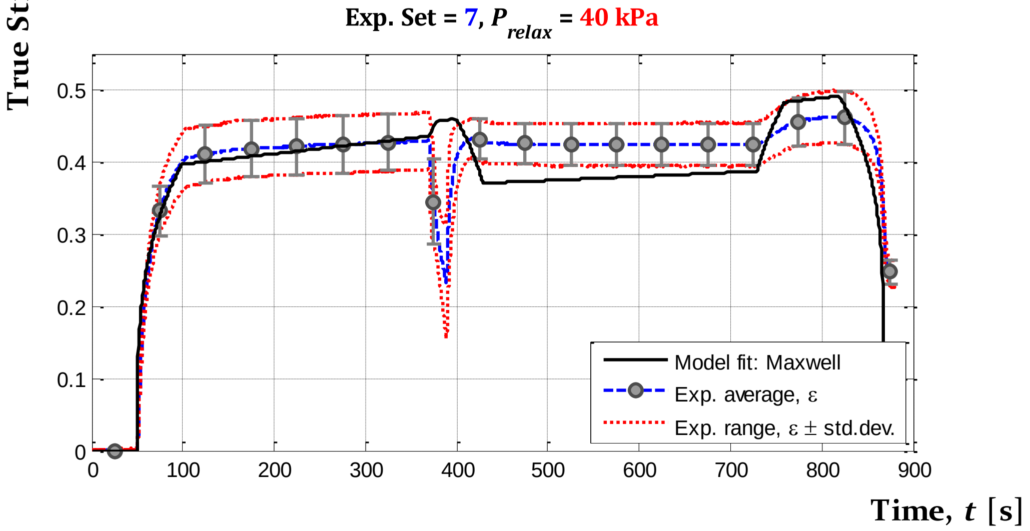

E [kPa]	m	c [kPa.s]	R^2
808.3	1.92	262695.9	0.736

Figure D-56. (cont.) Strain graph for Woven fabric using *Maxwell model* fitted to all experiment sets using a single parameter set.

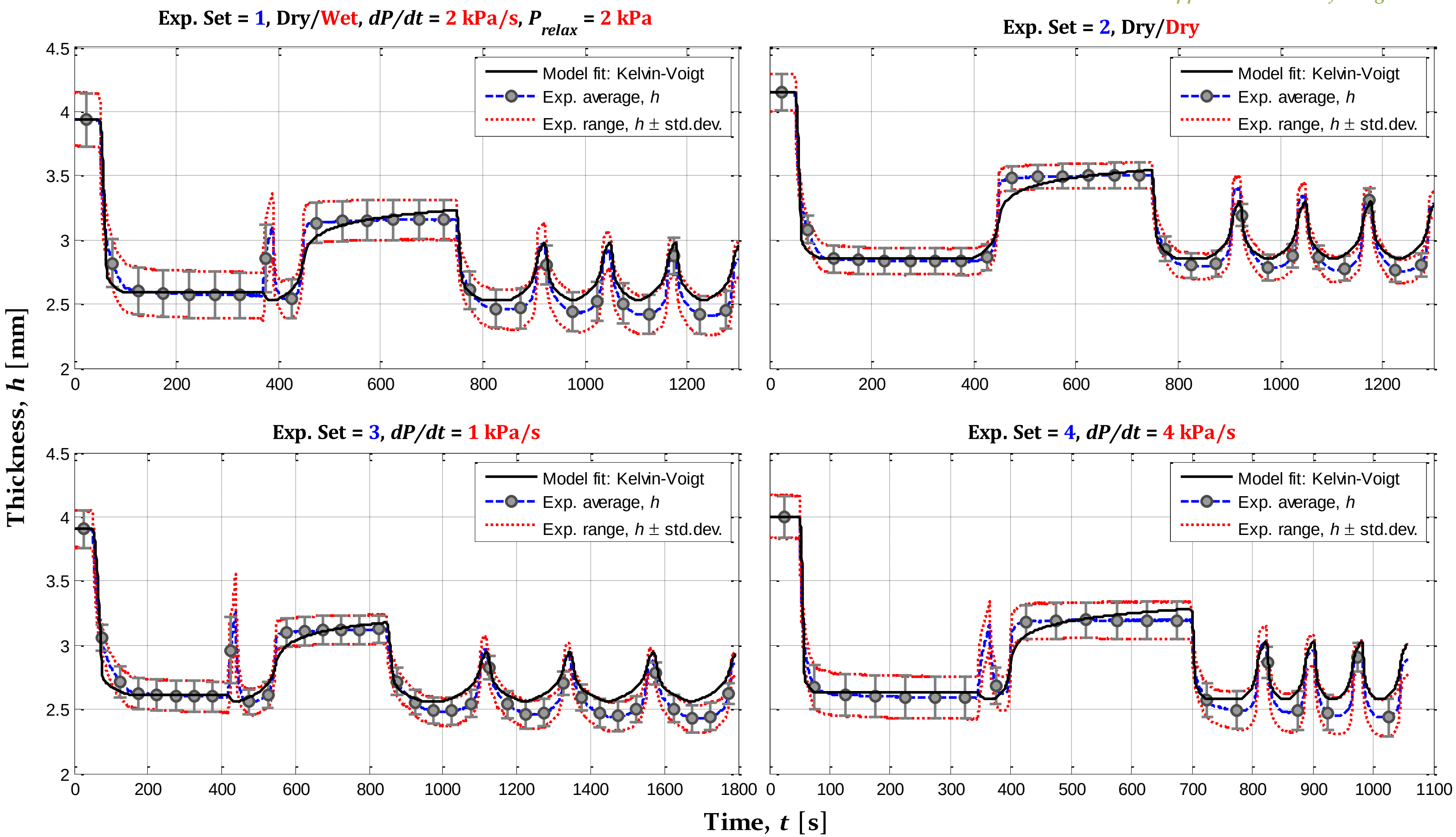

Figure D-57. Thickness graph for Woven fabric using *Kelvin-Voigt model* fitted to each experiment set separately using separate parameter sets.

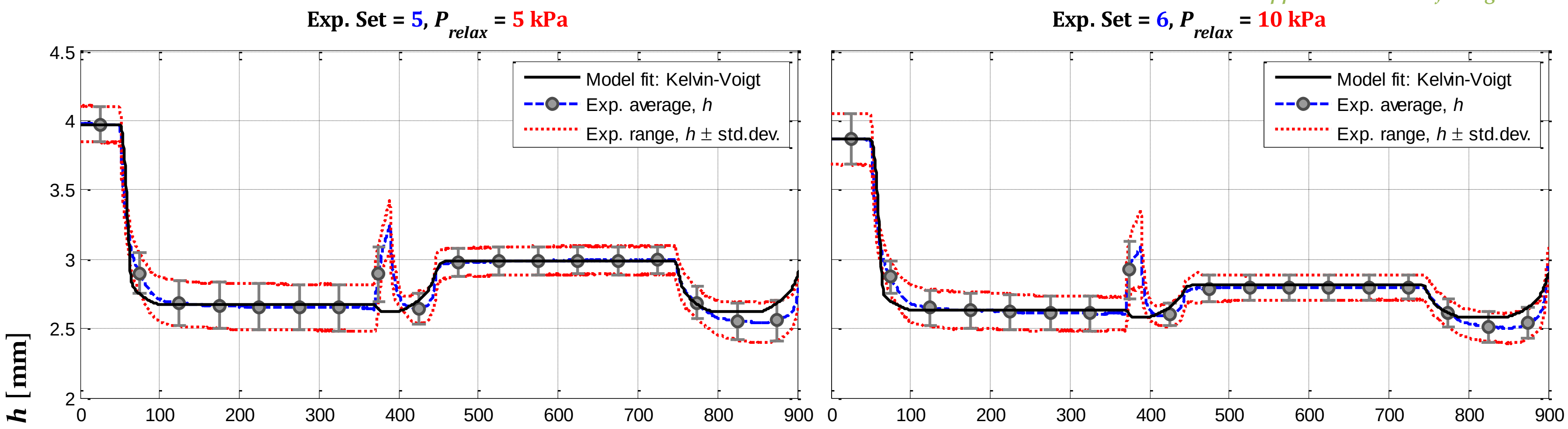

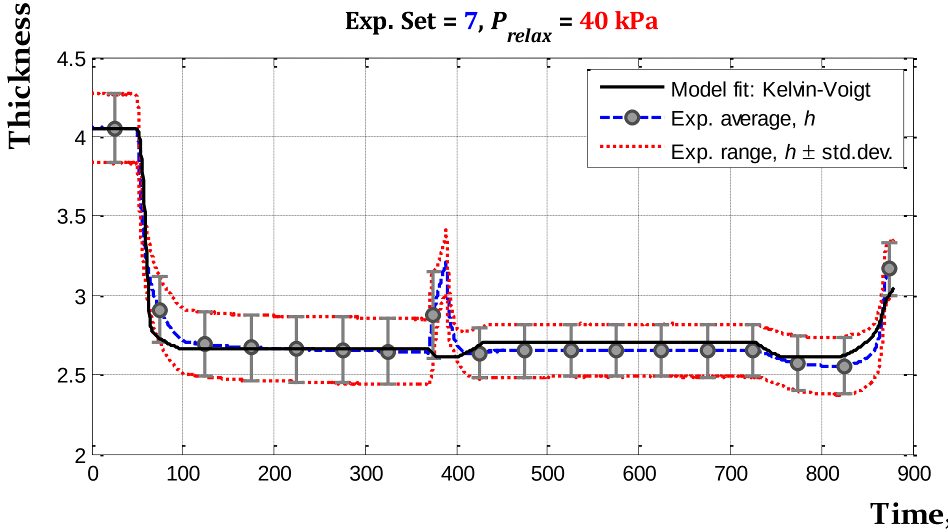

Set	*E* [kPa]	*m*	*c* [kPa.s]	R^2
1	21891.37	20.26	484.41	0.888
2	93467.47	23.00	463.90	0.928
3	46460.89	20.87	953.75	0.883
4	213.56	28.75	331.39	0.872
5	183523.52	12.66	531.43	0.950
6	262496.47	17.38	632.58	0.951
7	26640.39	19.65	499.47	0.951

Figure D-58. (cont.) Thickness graph for Woven fabric using *Kelvin-Voigt model* fitted to each experiment set separately using separate parameter sets.

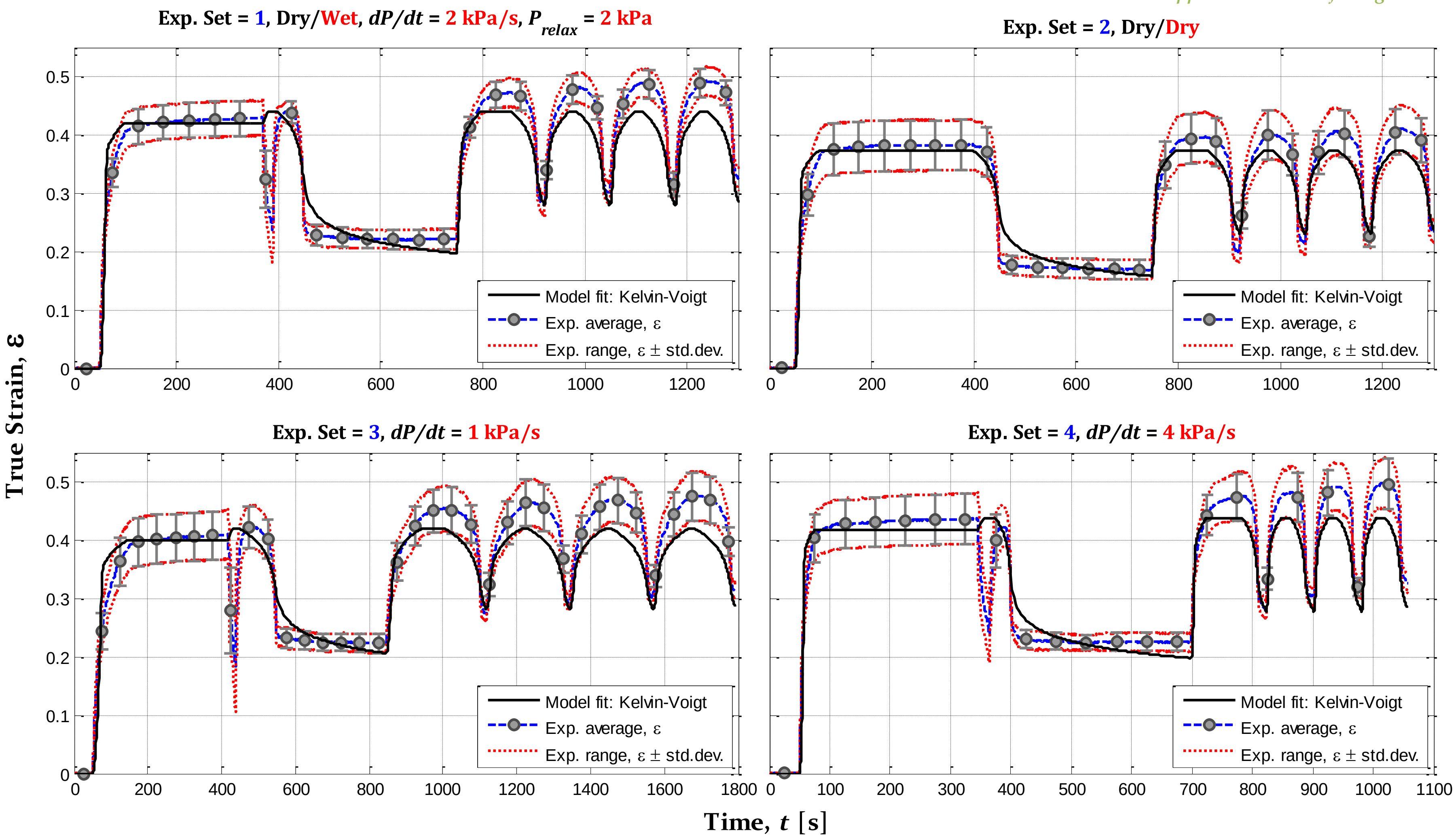

Figure D-59. Strain graph for Woven fabric using *Kelvin-Voigt model* fitted to each experiment set separately using separate parameter sets.

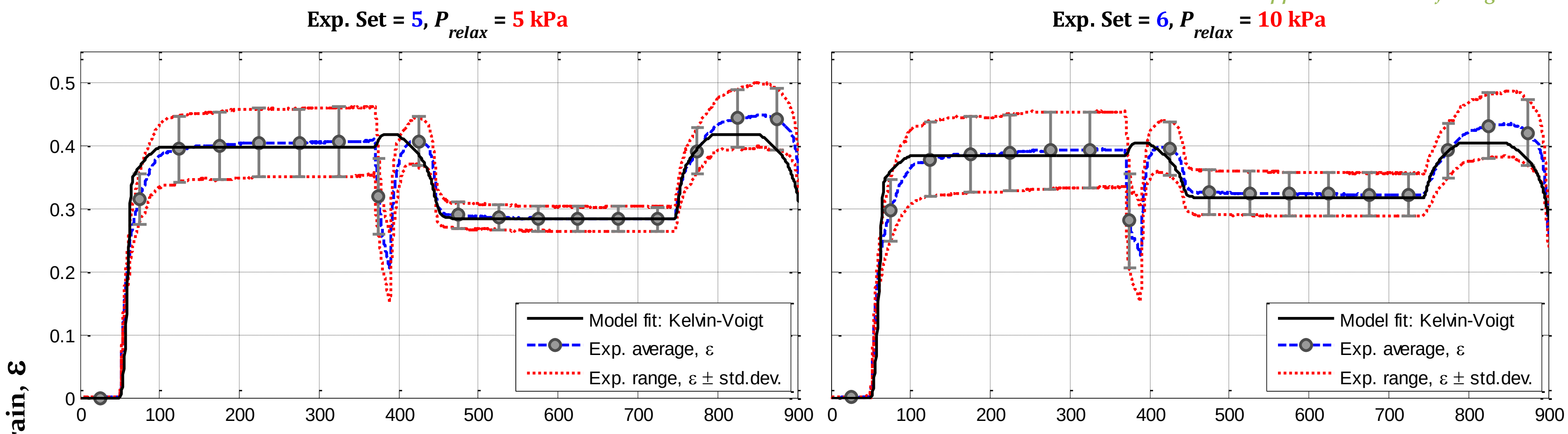

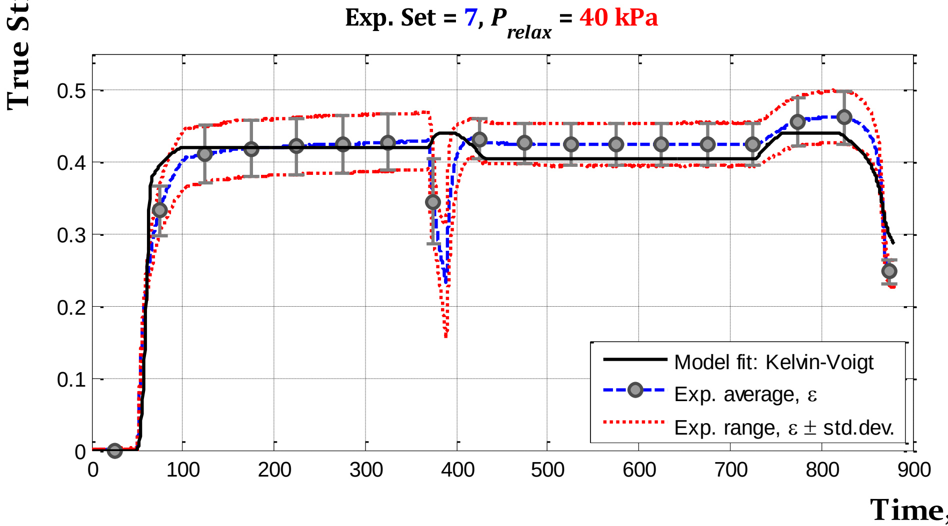

Set	*E* [kPa]	*m*	*c* [kPa.s]	R^2
1	21891.37	20.26	484.41	0.888
2	93467.47	23.00	463.90	0.928
3	46460.89	20.87	953.75	0.883
4	213.56	28.75	331.39	0.872
5	183523.52	12.66	531.43	0.950
6	262496.47	17.38	632.58	0.951
7	26640.39	19.65	499.47	0.951

Figure D-60. (cont.) Strain graph for Woven fabric using *Kelvin-Voigt model* fitted to each experiment set separately using separate parameter sets.

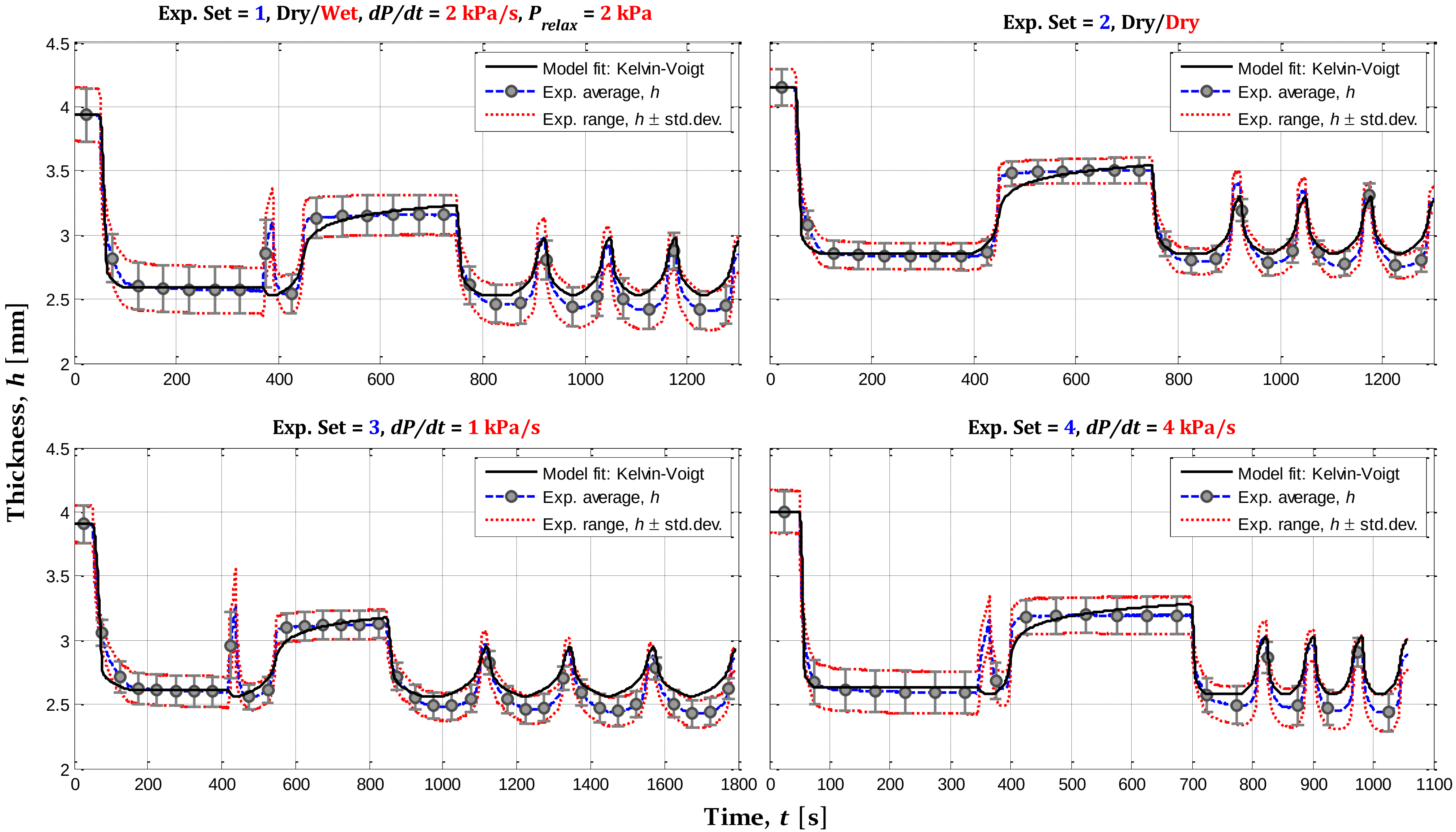

Figure D-61. Thickness graph for Woven fabric using *Kelvin-Voigt model* fitted to all experiment sets using a single parameter set.

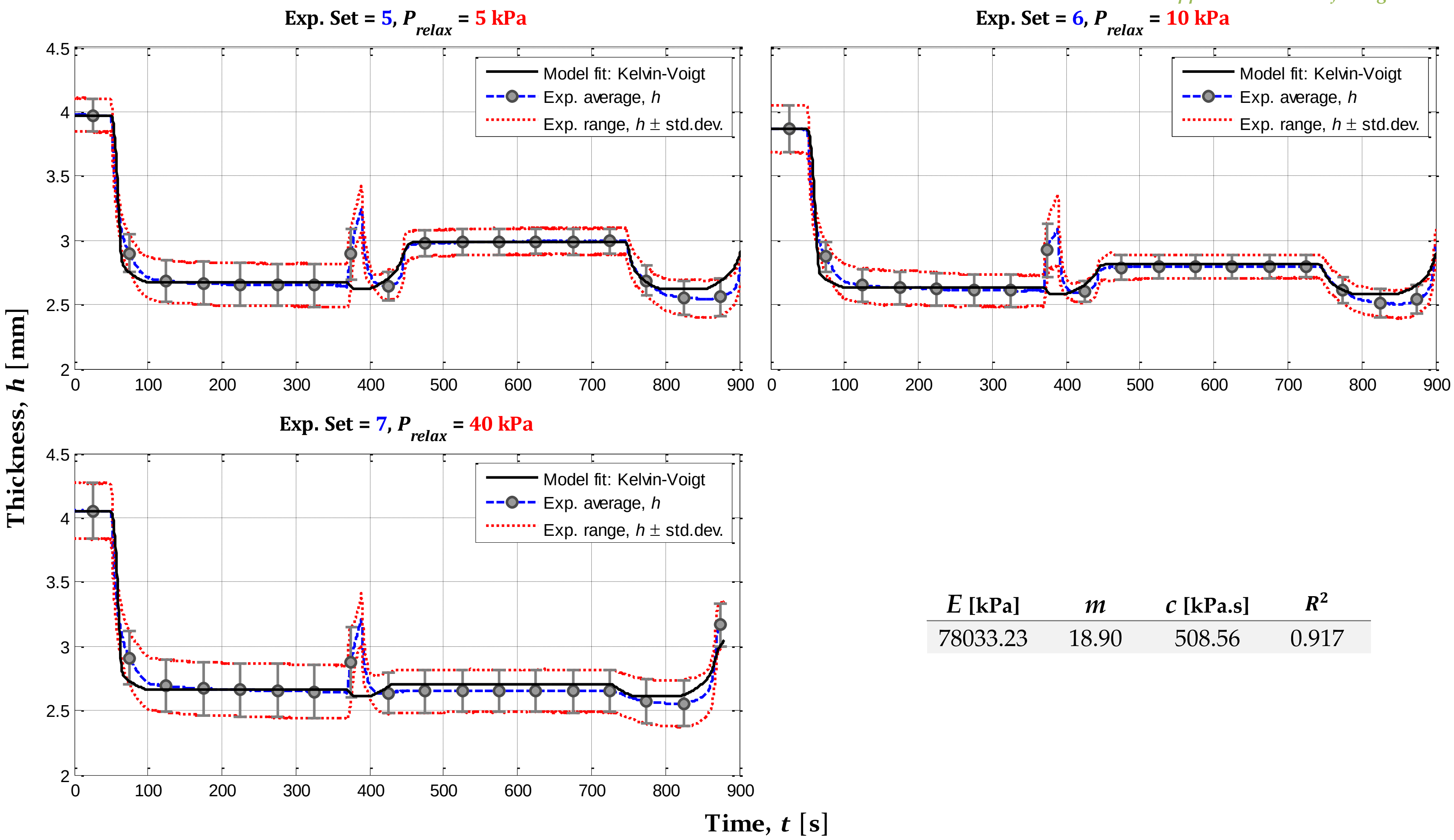

E [kPa]	m	c [kPa.s]	R^2
78033.23	18.90	508.56	0.917

Figure D-62. (cont.) Thickness graph for Woven fabric using *Kelvin-Voigt model* fitted to all experiment sets using a single parameter set.

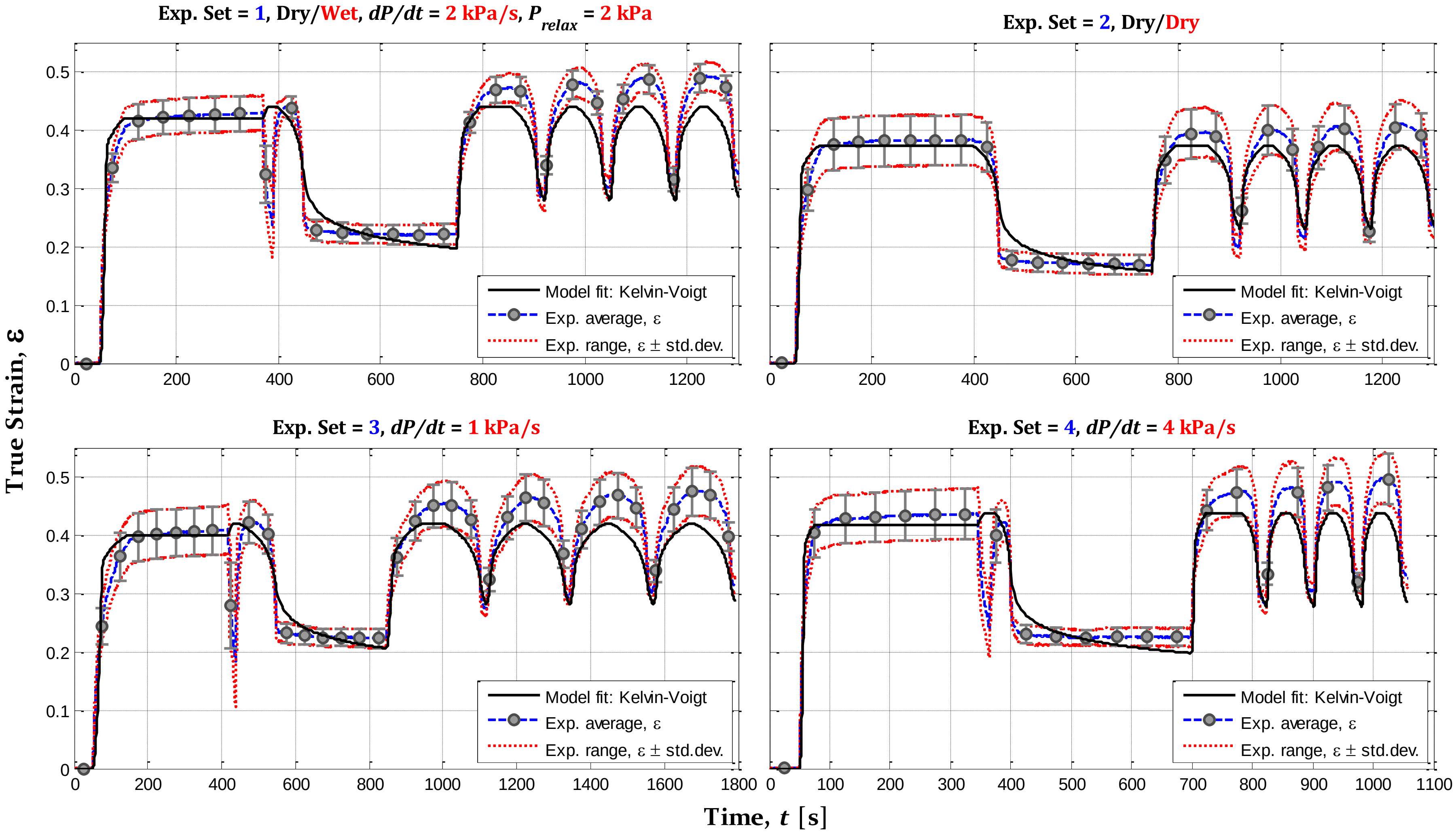

Figure D-63. Strain graph for Woven fabric using *Kelvin-Voigt model* fitted to all experiment sets using a single parameter set.

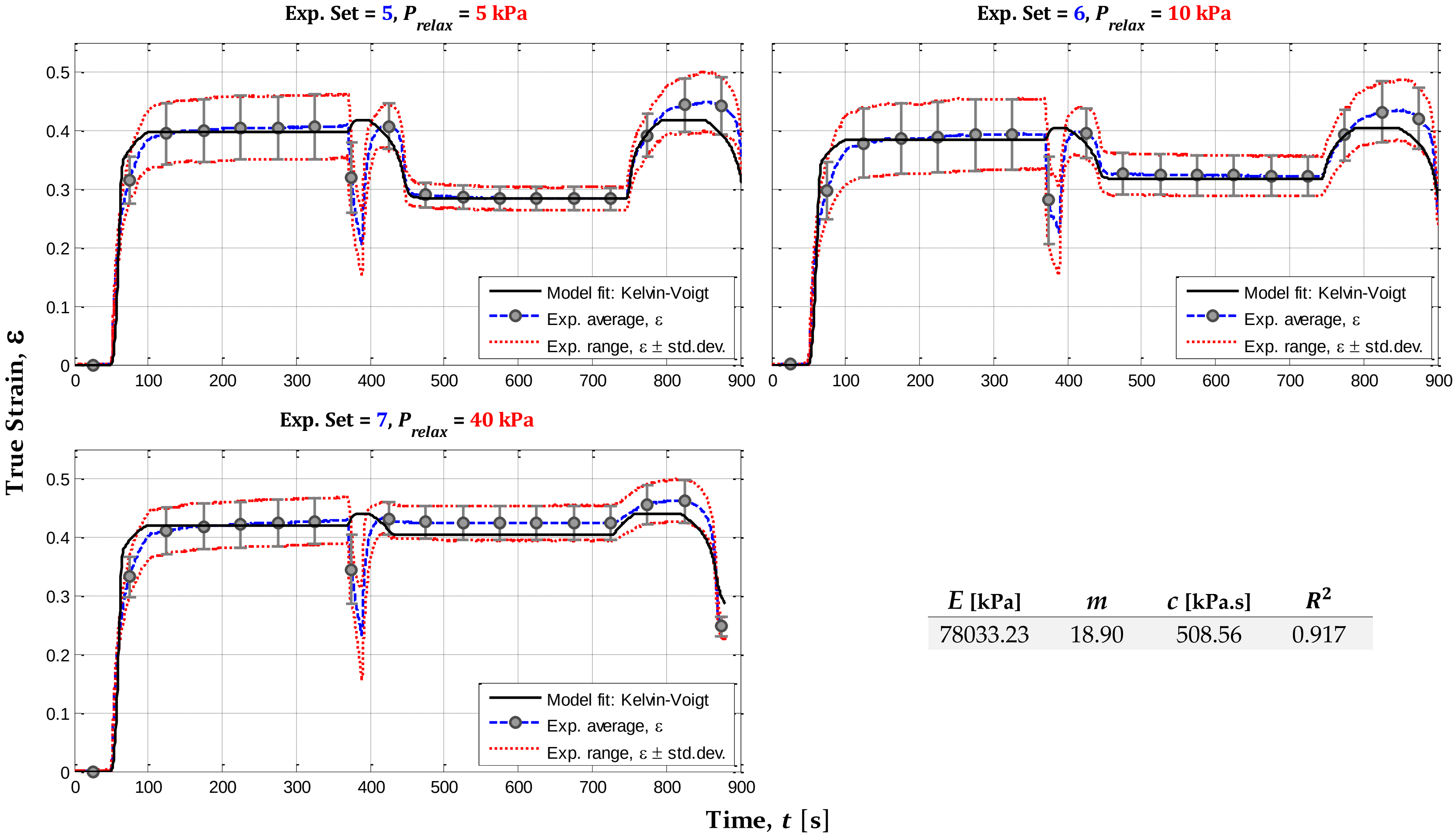

E [kPa]	m	c [kPa.s]	R^2
78033.23	18.90	508.56	0.917

Figure D-64. (cont.) Strain graph for Woven fabric using *Kelvin-Voigt model* fitted to all experiment sets using a single parameter set.

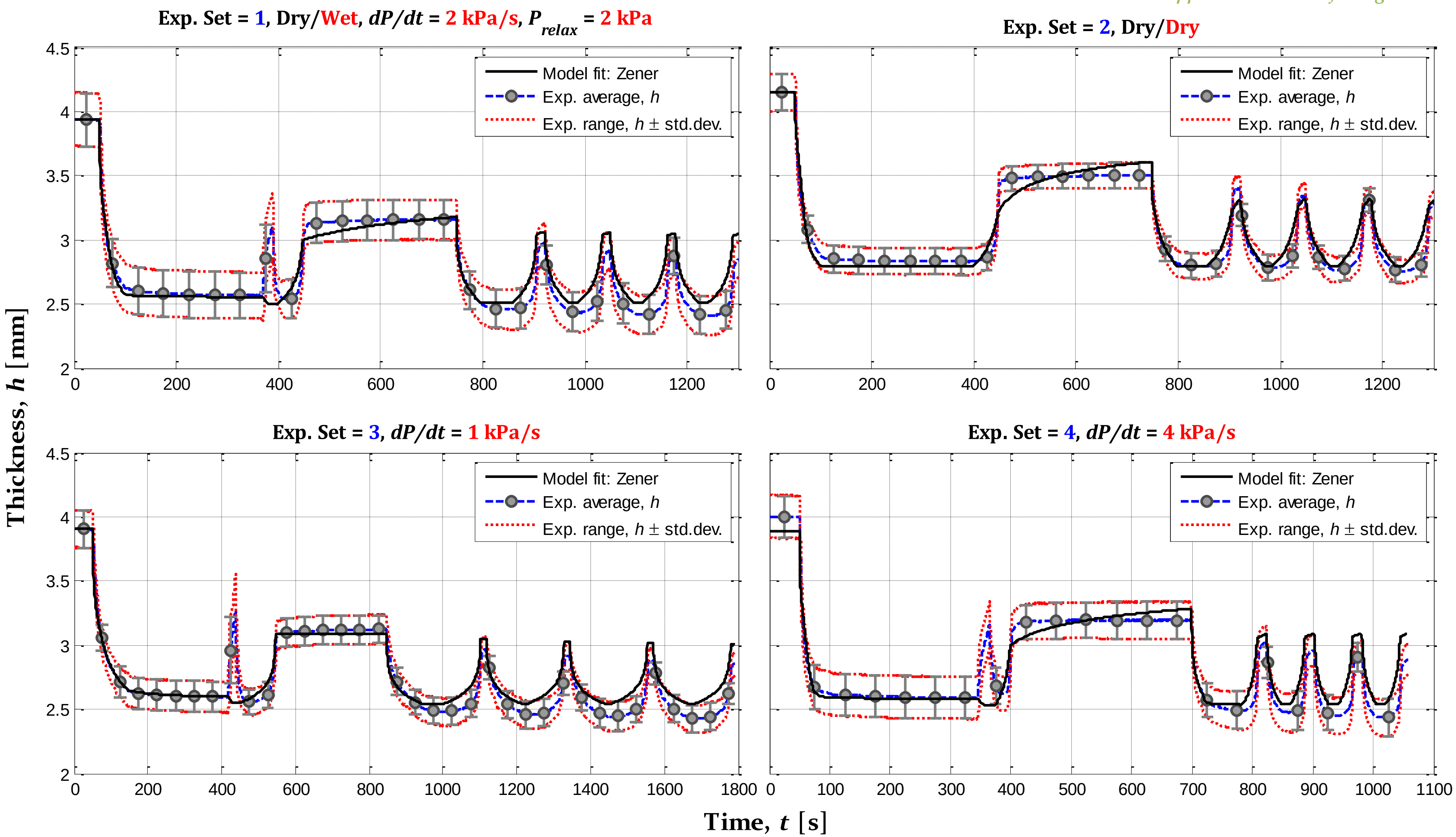

Figure D-65. Thickness graph for Woven fabric using *Zener model* fitted to each experiment set separately using separate parameter sets.

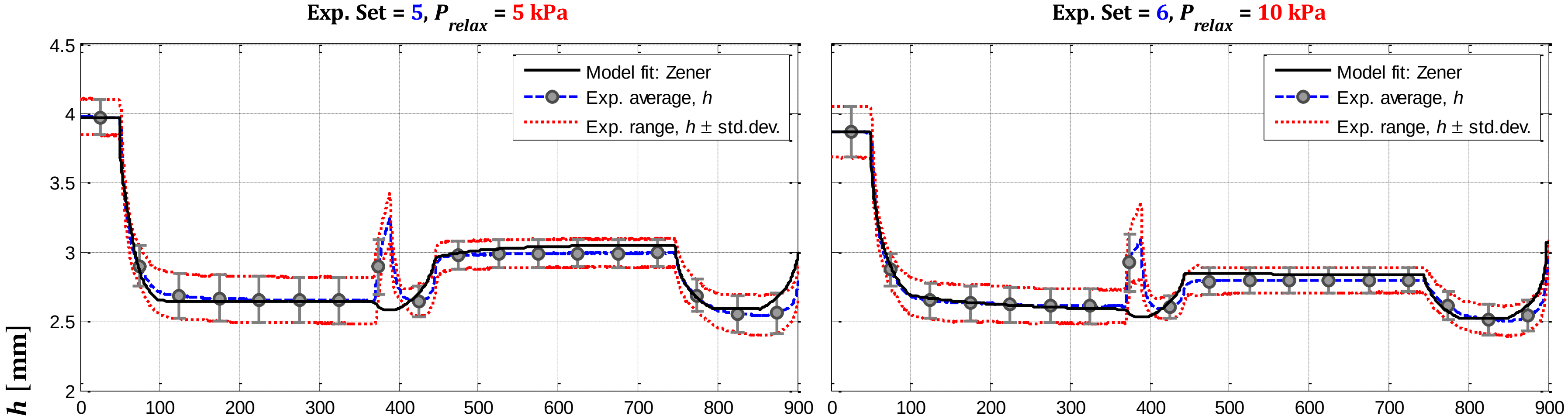

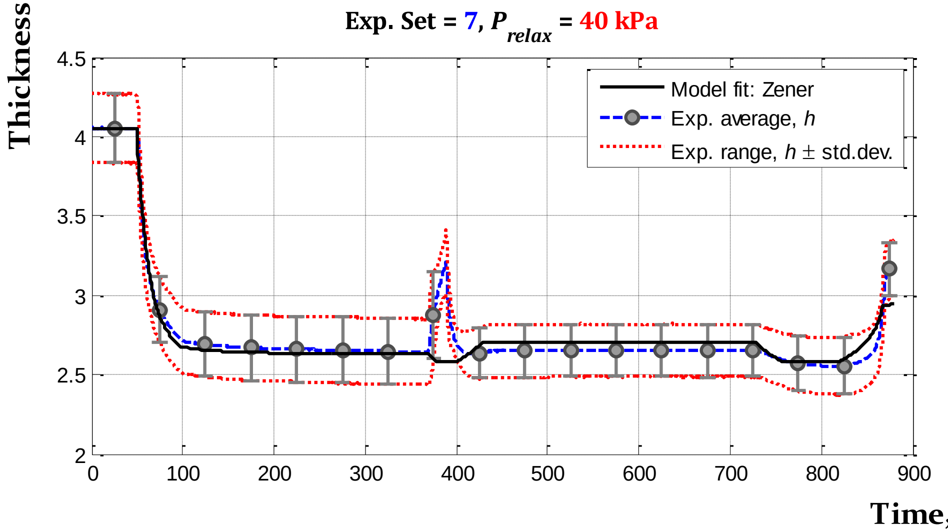

Set	E_0 [kPa]	m_0	E_1 [kPa]	m_1	c_1 [kPa.s]	R^2
1	21864.93	7.61	7086.78	3.61	3918.33	0.833
2	19503.20	6.26	36558.13	3.56	2210.28	0.942
3	124850.47	13.8	1234.45	2.73	31242.55	0.874
4	12941.47	5.89	35249.41	4.09	2975.34	0.811
5	35870.10	7.80	6731.13	3.17	3317.07	0.953
6	68991.86	10.04	701.26	2.17	64048.28	0.965
7	43365.25	9.71	223.54	1.49	6912.29	0.954

Figure D-66. (cont.) Thickness graph for Woven fabric using *Zener model* fitted to each experiment set separately using separate parameter sets.

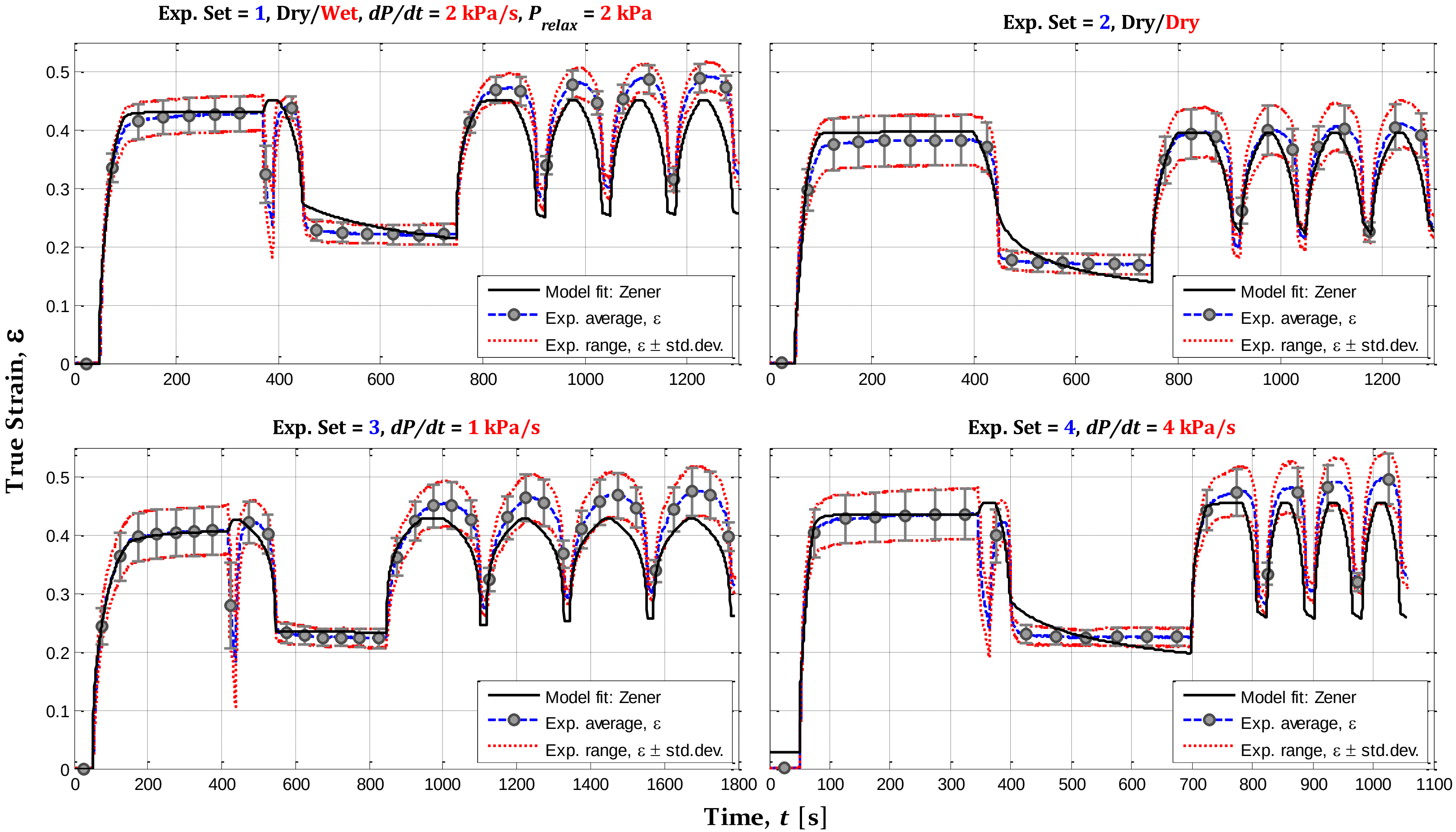

Figure D-67. Strain graph for Woven fabric using *Zener model* fitted to each experiment set separately using separate parameter sets.

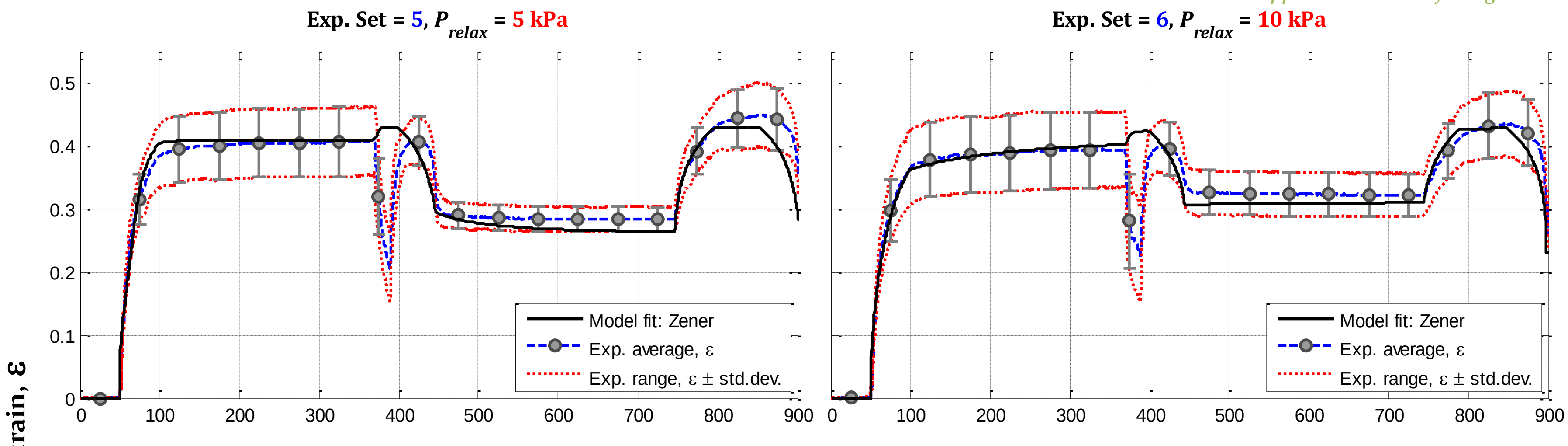

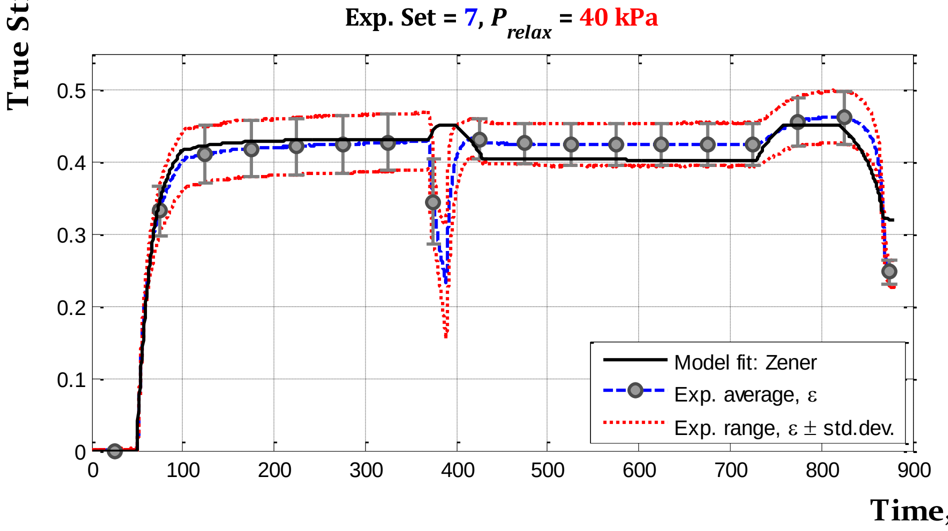

Set	E_0 [kPa]	m_0	E_1 [kPa]	m_1	c_1 [kPa.s]	R^2
1	21864.93	7.61	7086.78	3.61	3918.33	0.833
2	19503.20	6.26	36558.13	3.56	2210.28	0.942
3	124850.47	13.8	1234.45	2.73	31242.55	0.874
4	12941.47	5.89	35249.41	4.09	2975.34	0.811
5	35870.10	7.80	6731.13	3.17	3317.07	0.953
6	68991.86	10.04	701.26	2.17	64048.28	0.965
7	43365.25	9.71	223.54	1.49	6912.29	0.954

Figure D-68. (cont.) Strain graph for Woven fabric using *Zener model* fitted to each experiment set separately using separate parameter sets.

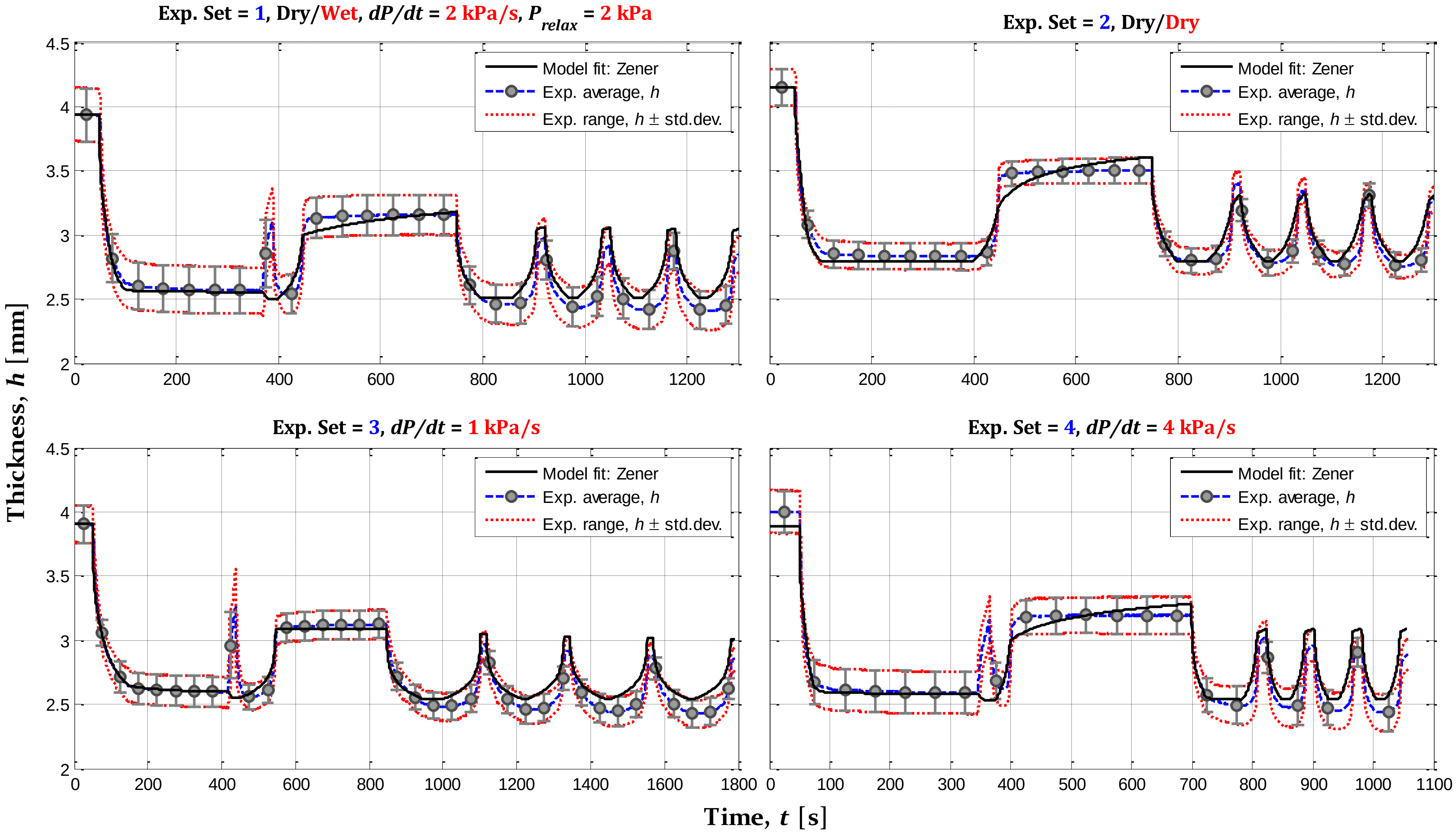

Figure D-69. Thickness graph for Woven fabric using *Zener model* fitted to all experiment sets using a single parameter set.

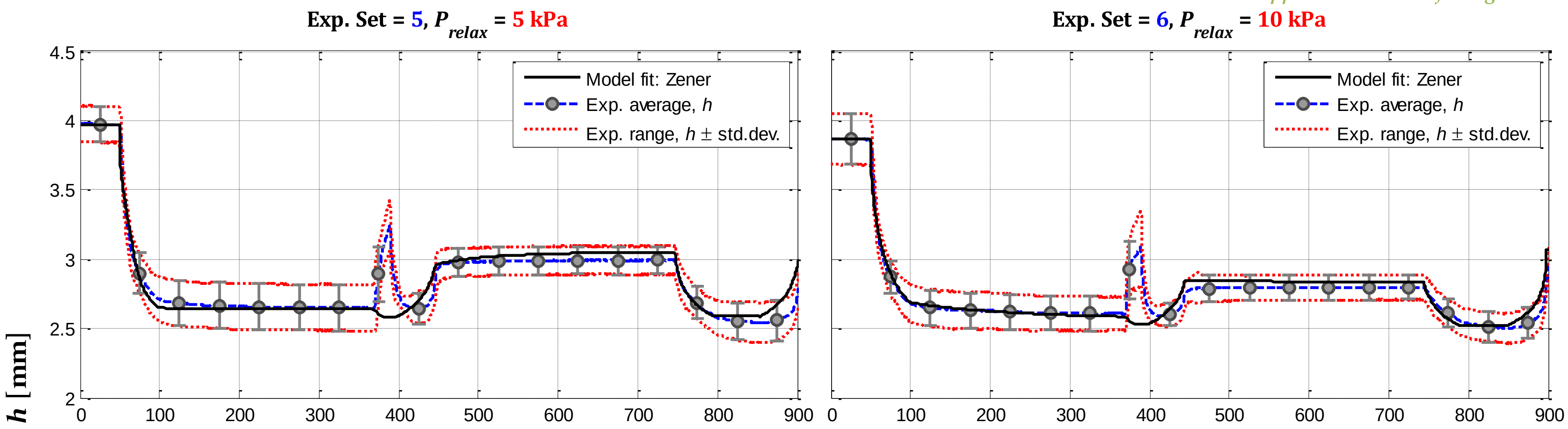

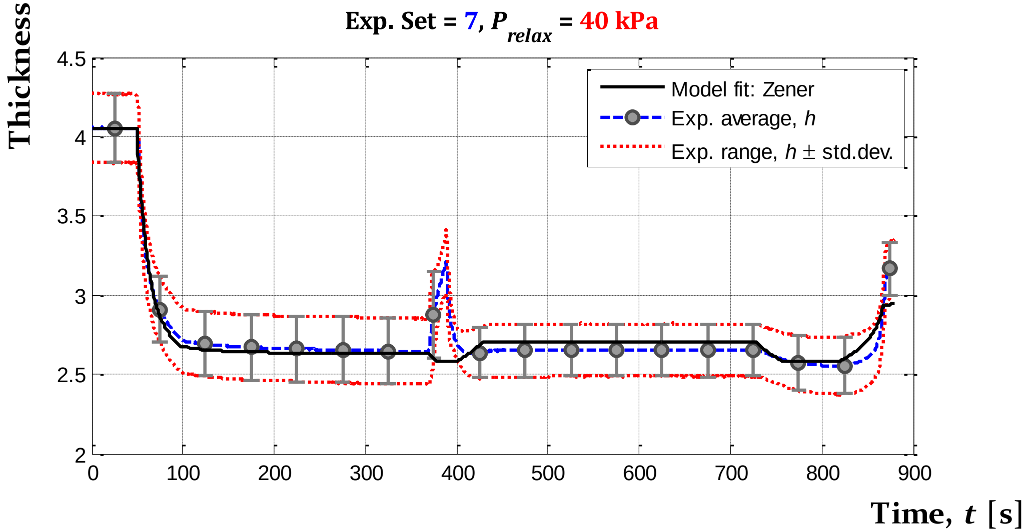

E_0 [kPa]	m_0	E_1 [kPa]	m_1	c_1 [kPa.s]	R^2
18557.40	6.64	25192.02	3.87	3270.73	0.904

Figure D-70. (cont.) Thickness graph for Woven fabric using *Zener model* fitted to all experiment sets using a single parameter set.

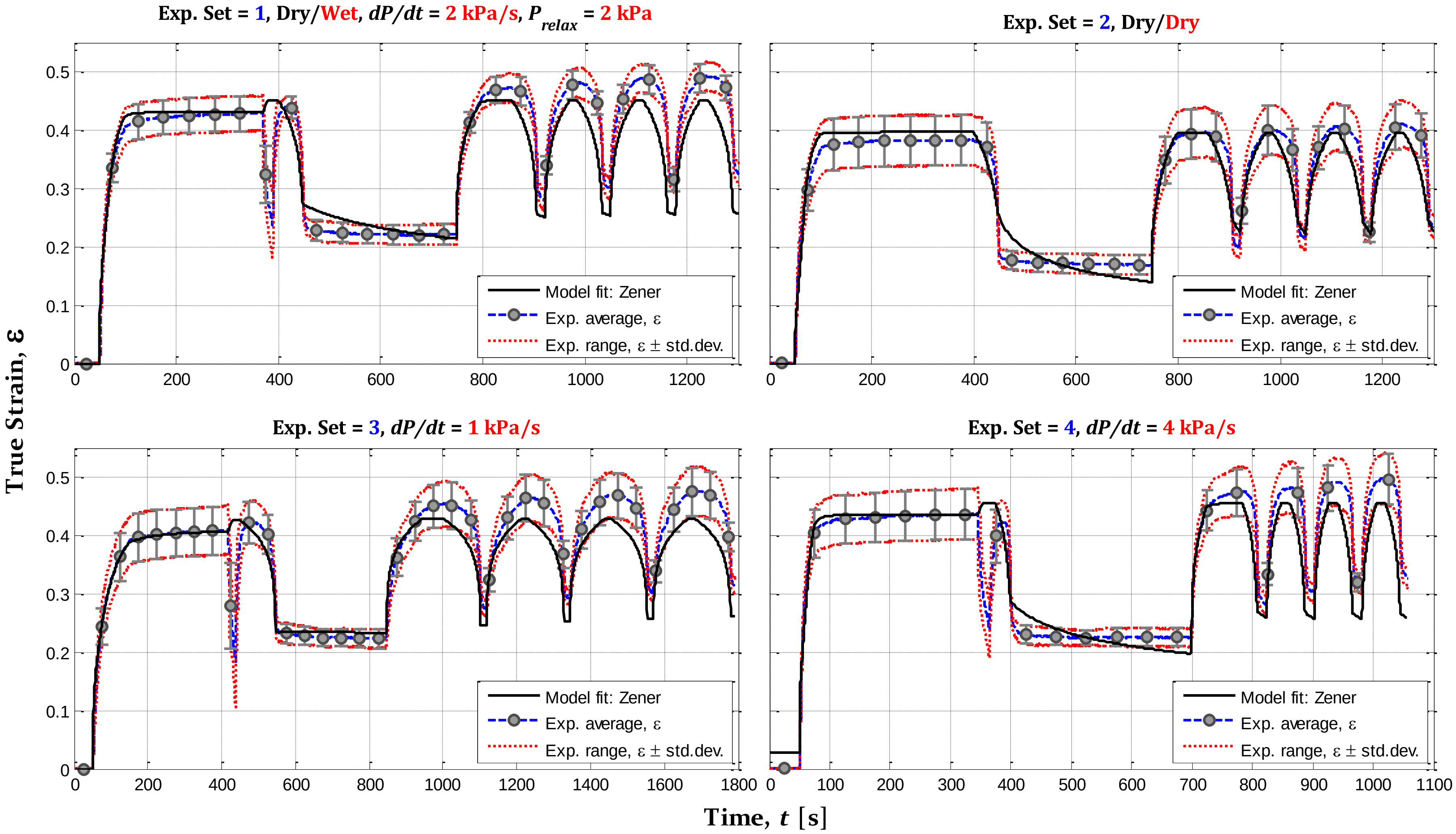

Figure D-71. Strain graph for Woven fabric using *Zener model* fitted to all experiment sets using a single parameter set.

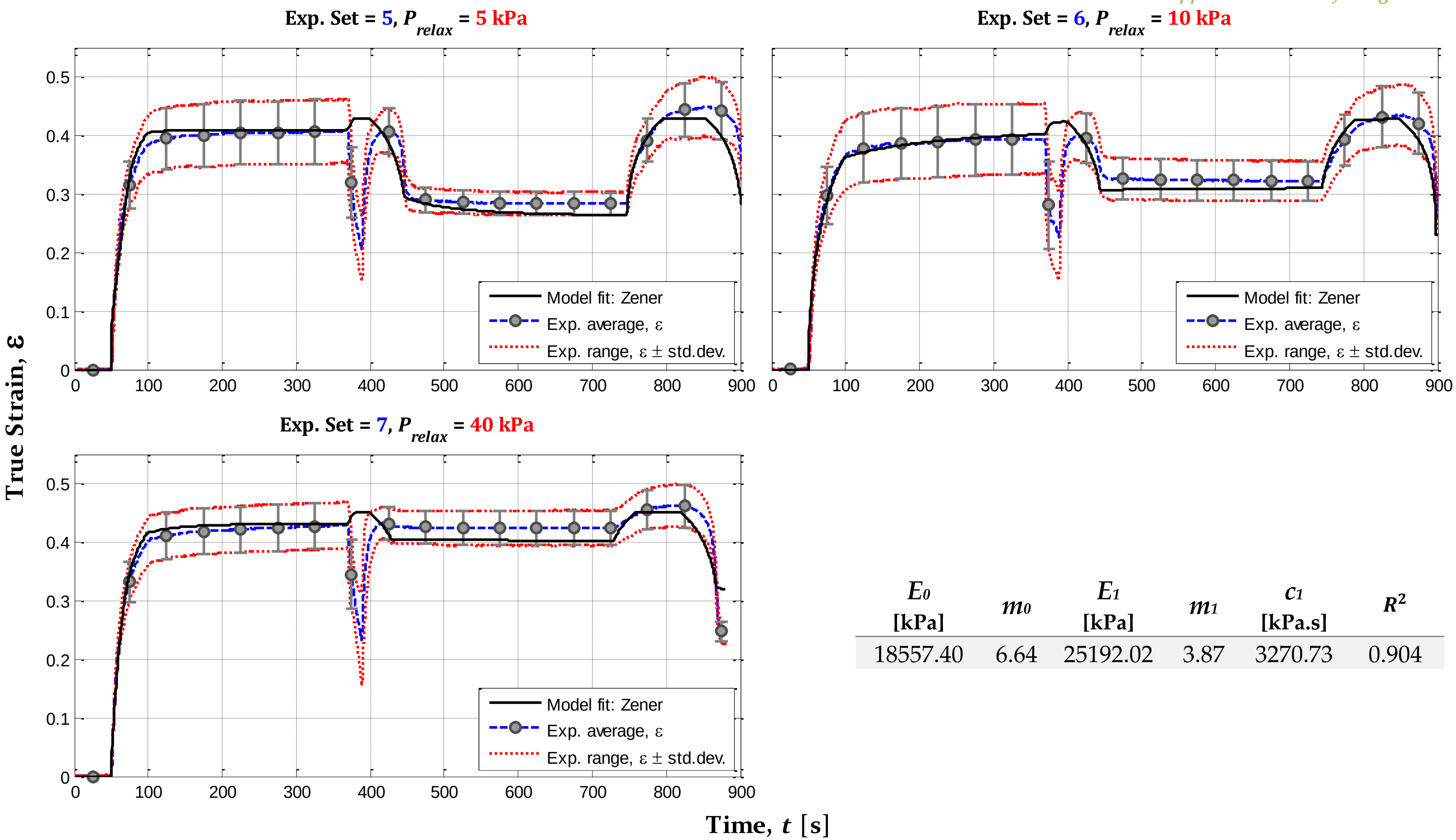

E_0 [kPa]	m_0	E_1 [kPa]	m_1	c_1 [kPa.s]	R^2
18557.40	6.64	25192.02	3.87	3270.73	0.904

Figure D-72. (cont.) Strain graph for Woven fabric using *Zener model* fitted to all experiment sets using a single parameter set.

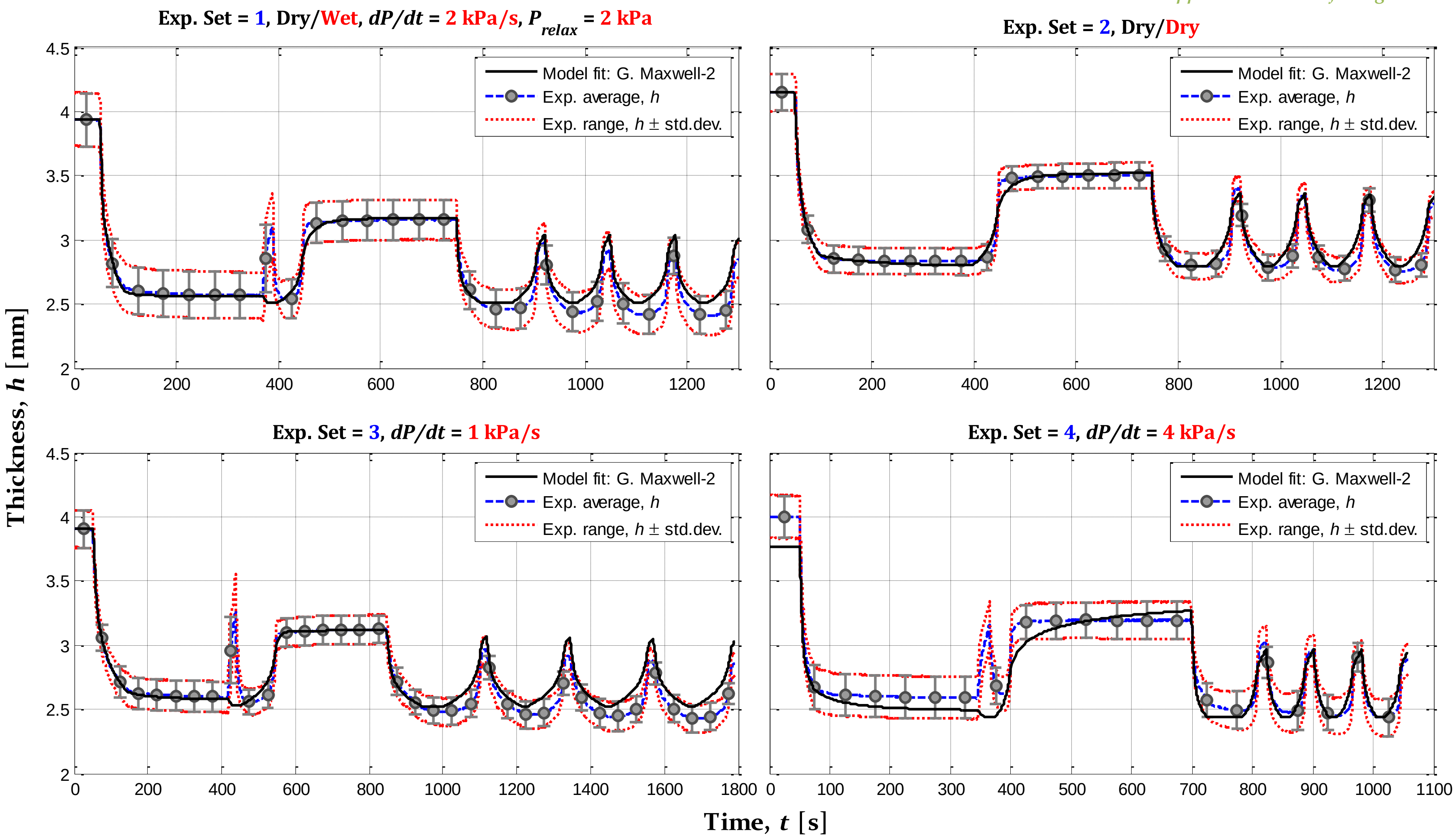

Figure D-73. Thickness graph for Woven fabric using G. Maxwell model, n=2 fitted to each experiment set separately using separate parameter sets.

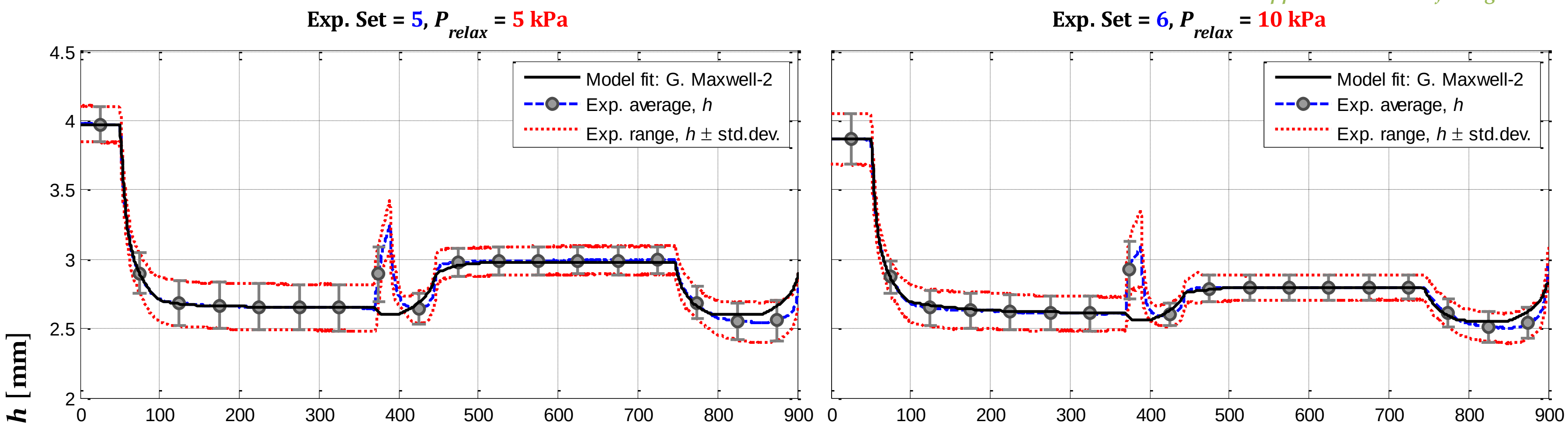

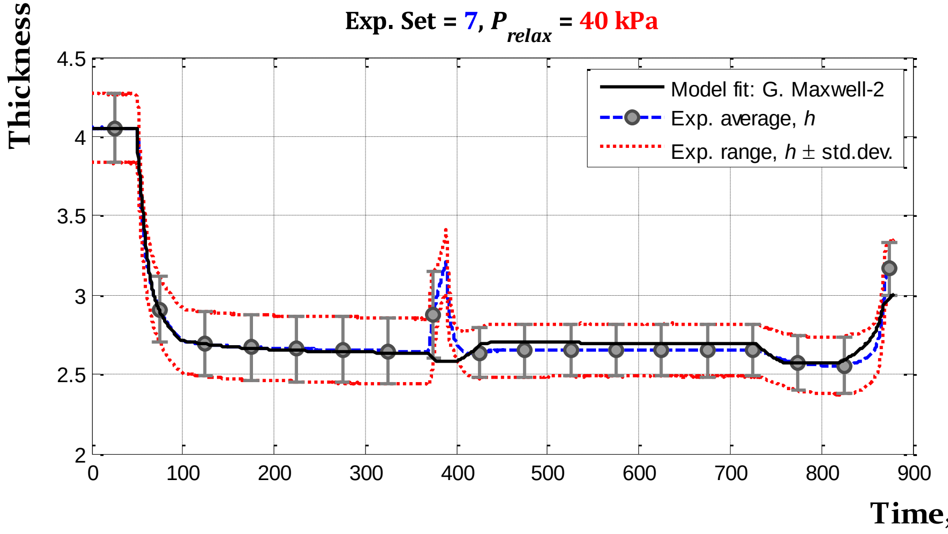

Set	E_0 [kPa]	m_0	E_1 [kPa]	m_1	c_1 [kPa.s]	E_2 [kPa]	m_2	c_2 [kPa.s]	R^2
1	64430.39	13.78	45248.11	5.39	8989.46	311.95	1.24	277.63	0.905
2	30136.94	7.11	599.63	2.40	35783.96	432.41	1.81	659.03	0.962
3	54875.39	9.38	1475.57	2.93	24494.64	483.83	1.19	364.41	0.885
4	29801.24	7.73	38624.26	5.78	36292.99	531.05	1.57	528.59	0.935
5	133246.14	12.14	8890.30	4.66	15114.35	111.07	1.05	1043.35	0.967
6	132788.98	17.56	2399.39	3.53	54360.97	30.93	0.57	2567.79	0.960
7	49818.35	11.28	2031.77	3.72	43617.20	667.00	1.78	915.39	0.966

Figure D-74. (cont.) Thickness graph for Woven fabric using *G. Maxwell model, n=2* fitted to each experiment set separately using separate parameter sets.

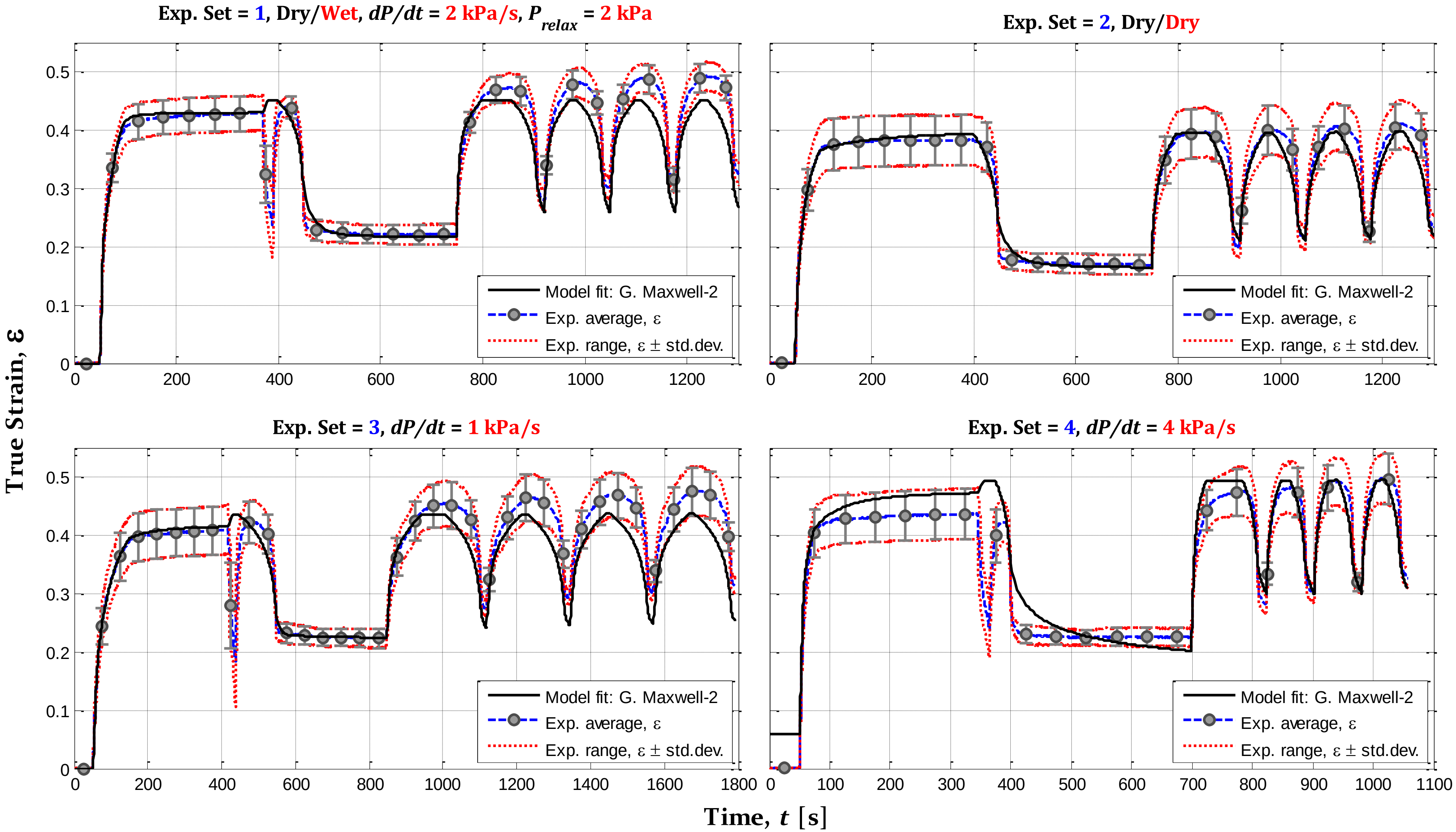

Figure D-75. Strain graph for Woven fabric using *G. Maxwell model, n=2* fitted to each experiment set separately using separate parameter sets.

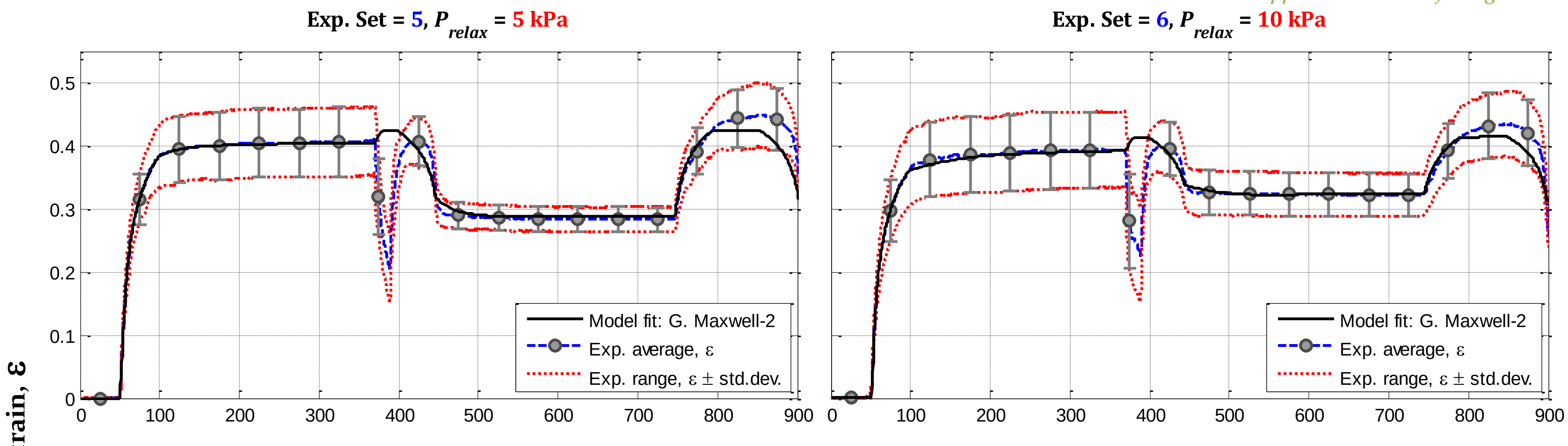

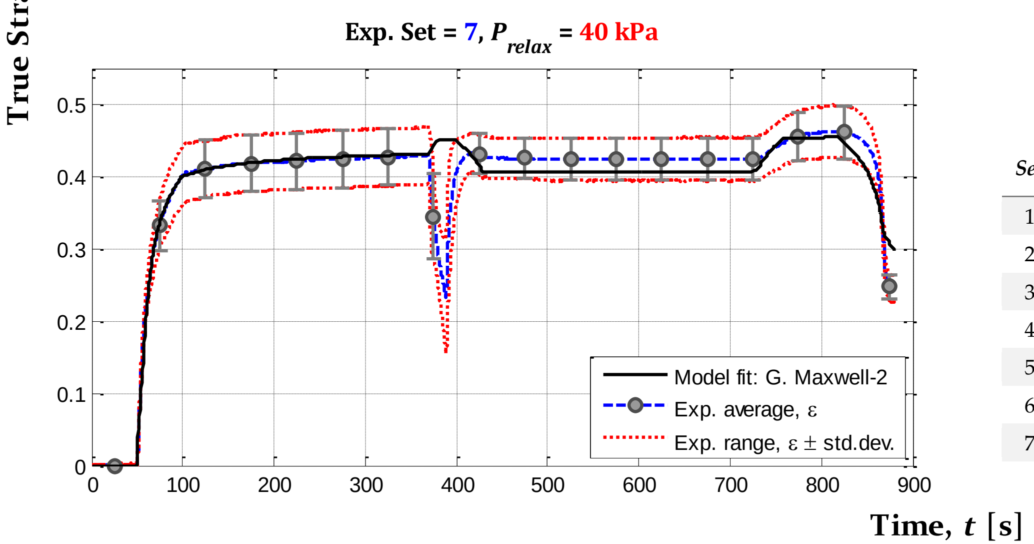

Set	E_0 [kPa]	m_0	E_1 [kPa]	m_1	c_1 [kPa.s]	E_2 [kPa]	m_2	c_2 [kPa.s]	R^2
1	64430.39	13.78	45248.11	5.39	8989.46	311.95	1.24	277.63	0.905
2	30136.94	7.11	599.63	2.40	35783.96	432.41	1.81	659.03	0.962
3	54875.39	9.38	1475.57	2.93	24494.64	483.83	1.19	364.41	0.885
4	29801.24	7.73	38624.26	5.78	36292.99	531.05	1.57	528.59	0.935
5	133246.14	12.14	8890.30	4.66	15114.35	111.07	1.05	1043.35	0.967
6	132788.98	17.56	2399.39	3.53	54360.97	30.93	0.57	2567.79	0.960
7	49818.35	11.28	2031.77	3.72	43617.20	667.00	1.78	915.39	0.966

Figure D-76. (cont.) Strain graph for Woven fabric using *G. Maxwell model, n=2* fitted to each experiment set separately using separate parameter sets.

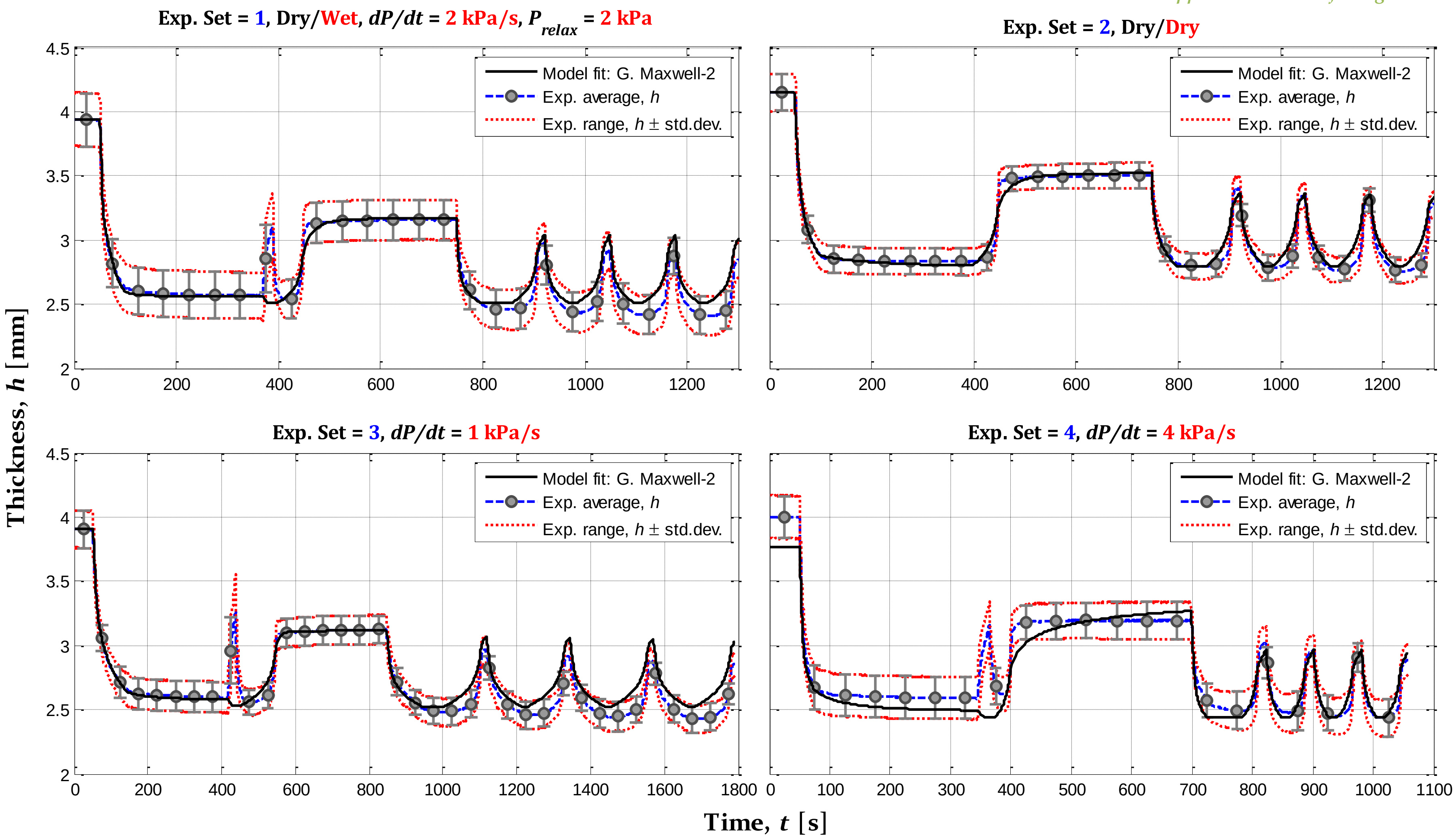

Figure D-77. Thickness graph for Woven fabric using G. Maxwell model, n=2 fitted to all experiment sets using a single parameter set.

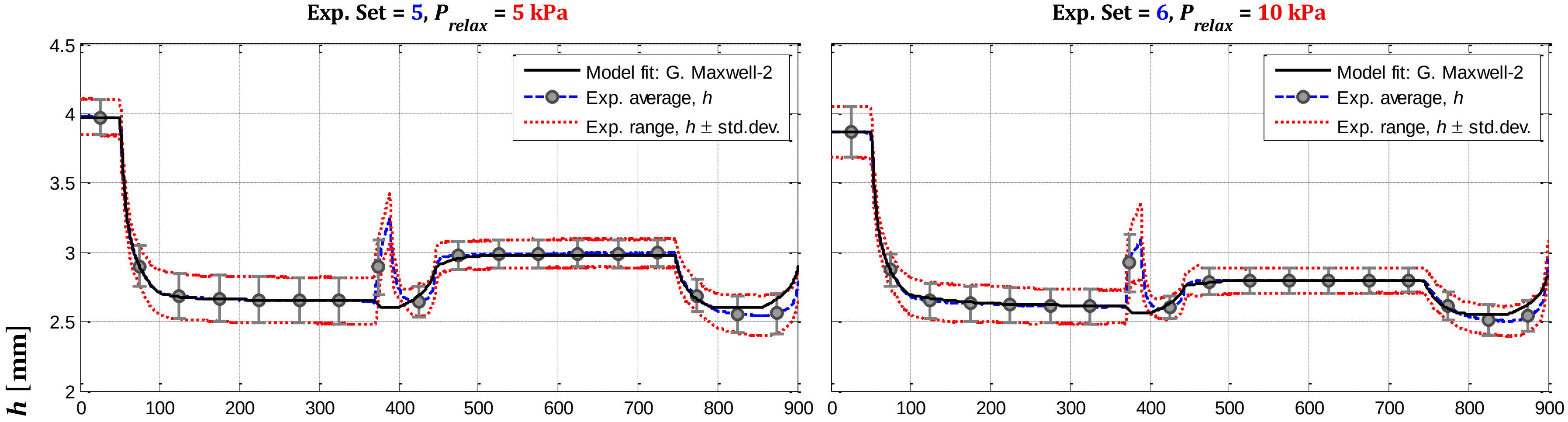

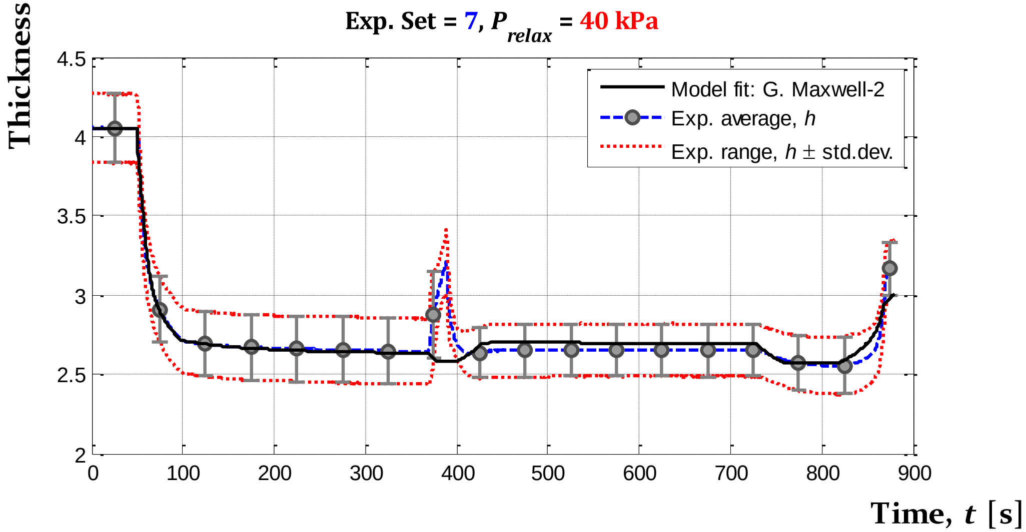

E_0 [kPa]	m_0	E_1 [kPa]	m_1	c_1 [kPa.s]	E_2 [kPa]	m_2	c_2 [kPa.s]	R^2
29632.48	7.73	37673.18	5.78	35616.33	530.92	1.57	528.68	0.940

Figure D-78. (cont.) Thickness graph for Woven fabric using *G. Maxwell model, n=2* fitted to all experiment sets using a single parameter set.

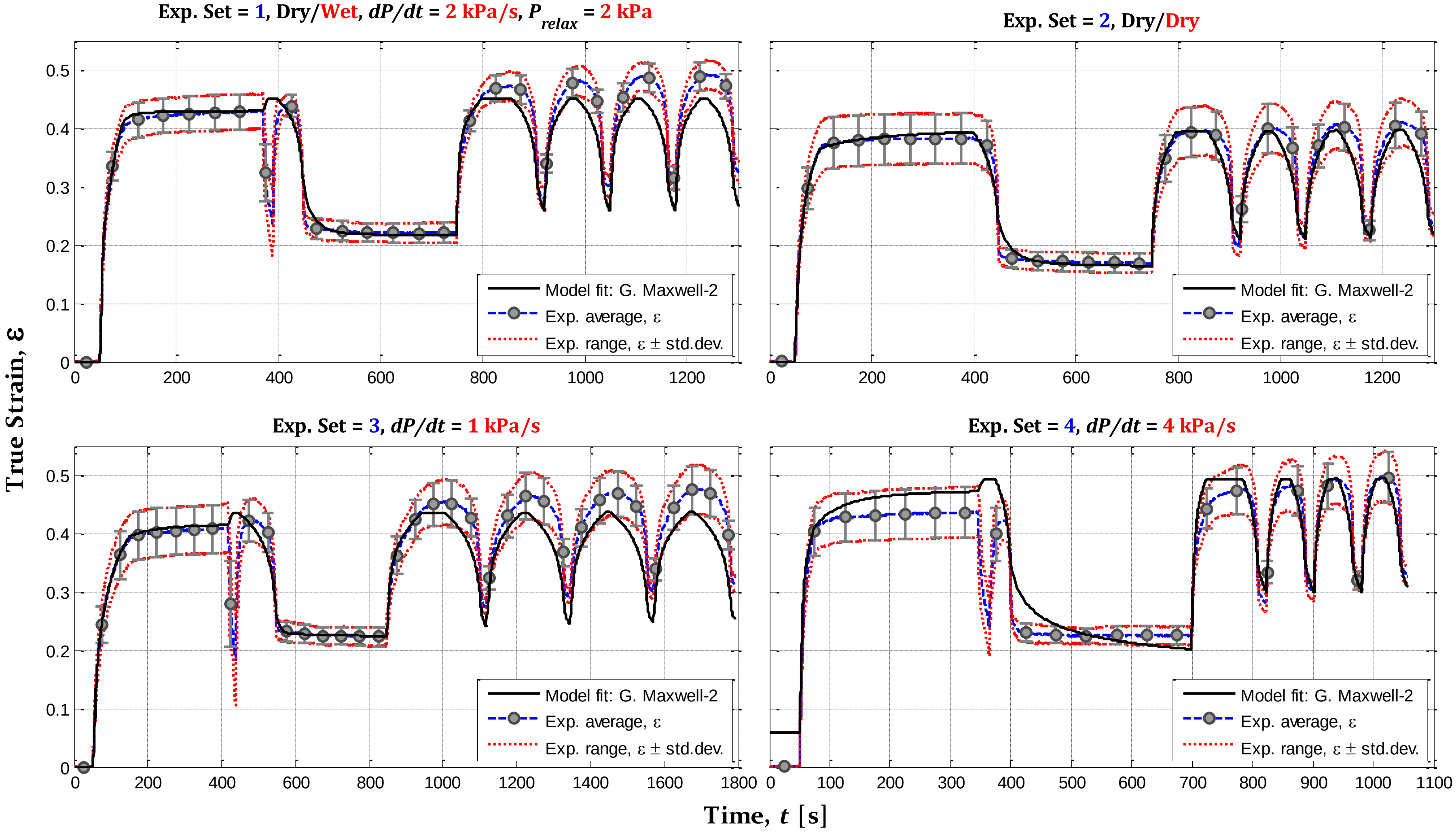

Figure D-79. Strain graph for Woven fabric using *G. Maxwell model, n=2* fitted to all experiment sets using a single parameter set.

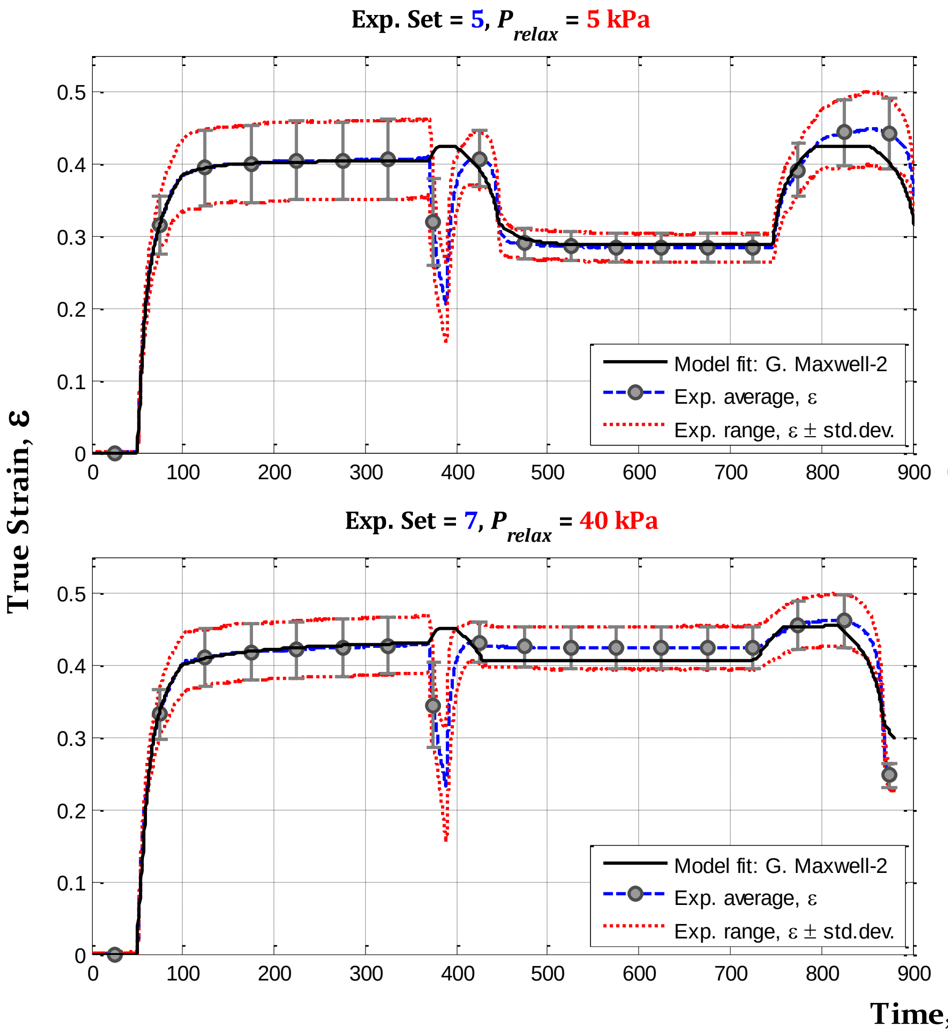

E_0 [kPa]	m_0	E_1 [kPa]	m_1	c_1 [kPa.s]	E_2 [kPa]	m_2	c_2 [kPa.s]	R^2
29632.48	7.73	37673.18	5.78	35616.33	530.92	1.57	528.68	0.940

Figure D-80. (cont.) Strain graph for Woven fabric using *G. Maxwell model, n=2* fitted to all experiment sets using a single parameter set.

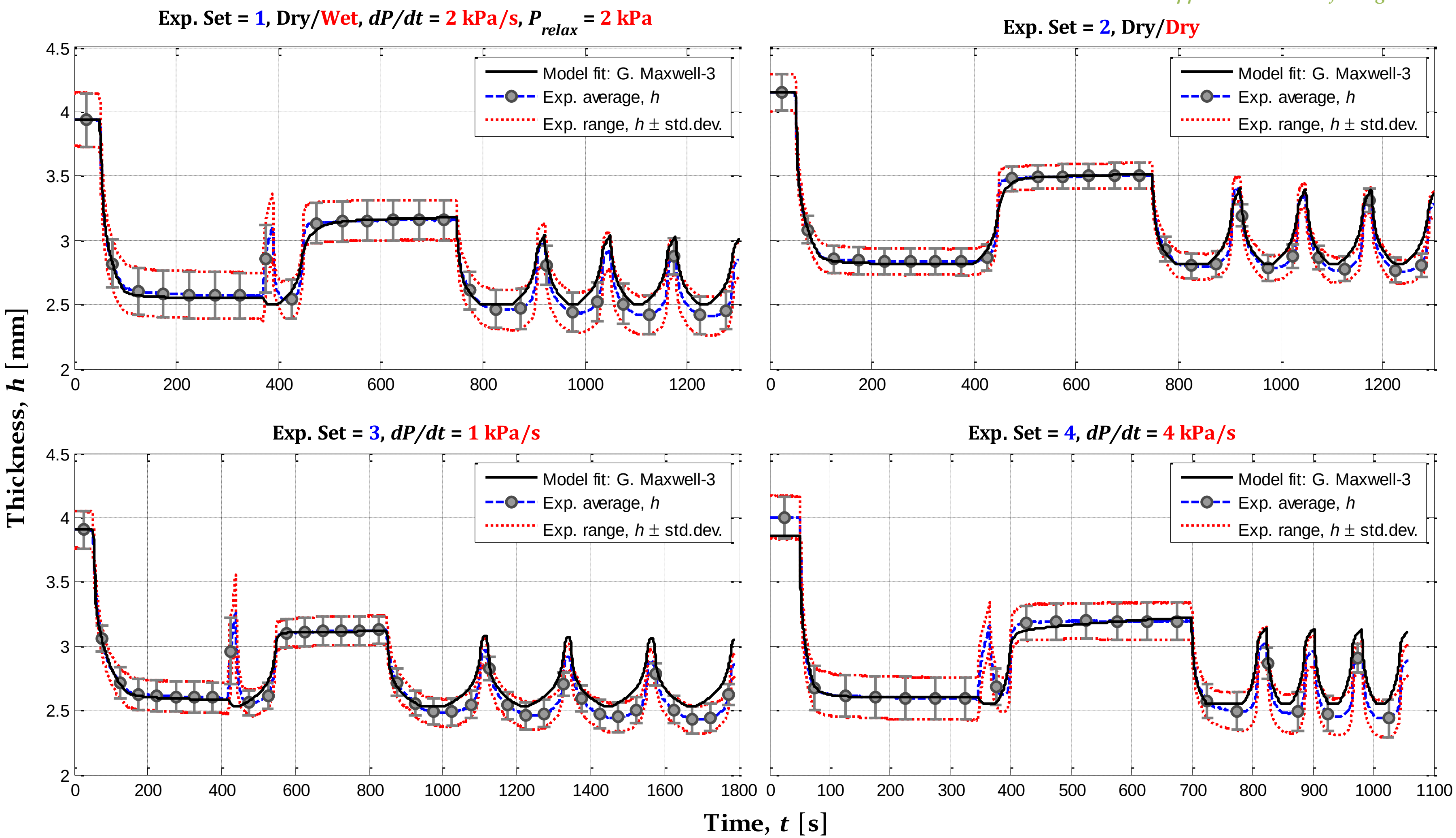

Figure D-81. Thickness graph for Woven fabric using G. Maxwell model, n=3 fitted to each experiment set separately using separate parameter sets.

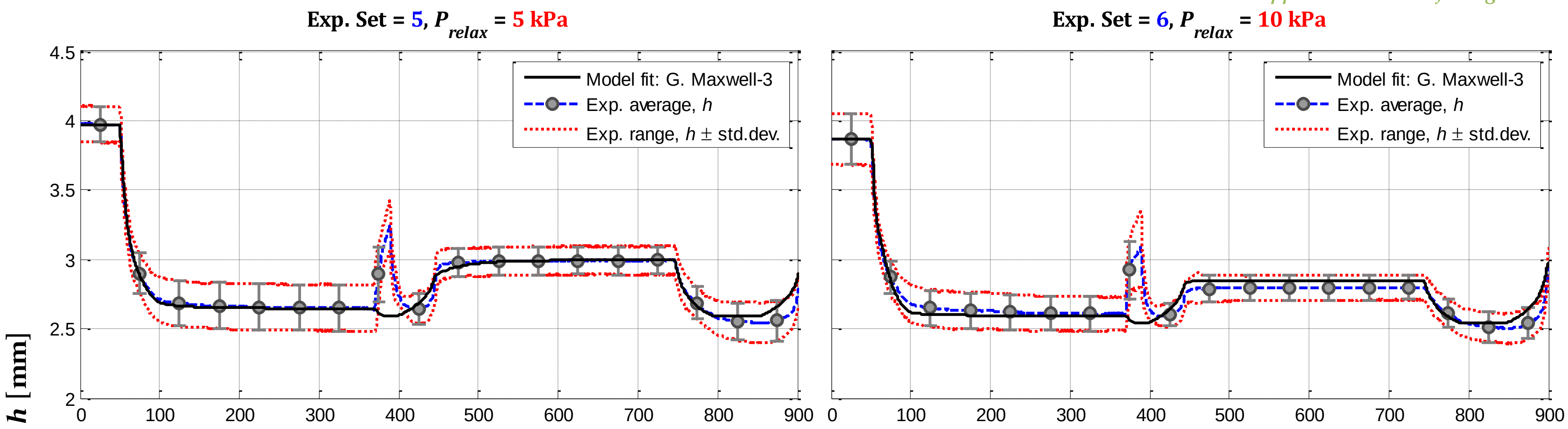

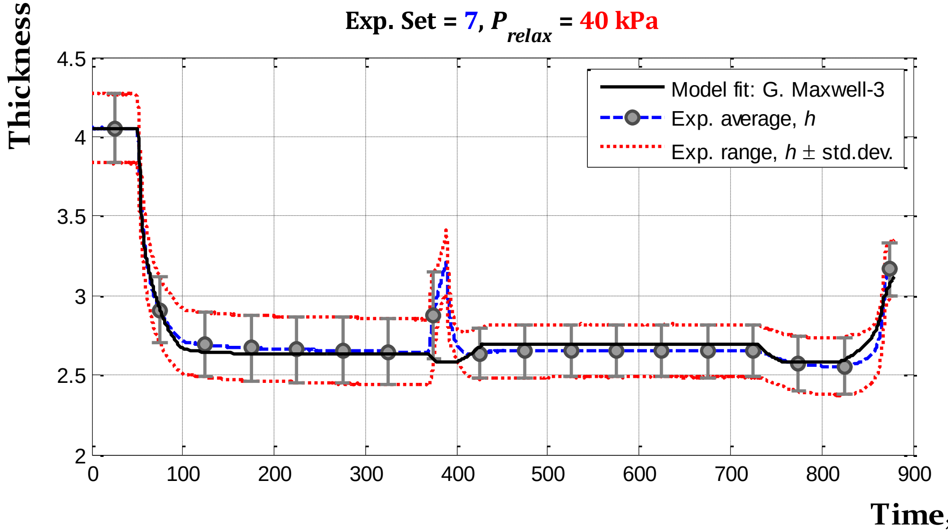

Set	E_0 [kPa]	m_0	E_1 [kPa]	m_1	c_1 [kPa.s]	E_2 [kPa]	m_2	c_2 [kPa.s]	E_3 [kPa]	m_3	c_3 [kPa.s]	R^2
1	35973.74	9.23	408.77	3.20	3029.97	381.70	1.50	501.98	11192.43	4.89	6431.45	0.898
2	76732.22	8.59	234.91	2.76	3448.77	37.68	0.60	433.42	37438.00	5.34	8921.22	0.958
3	68807.83	9.97	152.10	3.18	2107.25	216.92	0.52	229.98	2412.77	3.26	18813.58	0.870
4	23388.22	6.52	4123.18	5.36	2459.83	388.90	1.89	278.50	17534.91	4.37	4514.47	0.818
5	100320.6 3	10.79	78.15	1.30	901.16	33.84	0.82	671.10	3888.81	4.17	9424.17	0.966
6	87406.75	9.47	104.02	2.05	334.45	1291.57	0.48	169.44	13120.04	3.90	4998.61	0.968
7	57463.53	11.34	6716.45	4.48	2680.51	21.31	0.42	351.36	21386.24	5.44	5486.12	0.976

Figure D-82. (cont.) Thickness graph for Woven fabric using *G. Maxwell model, n=3* fitted to each experiment set separately using separate parameter sets.

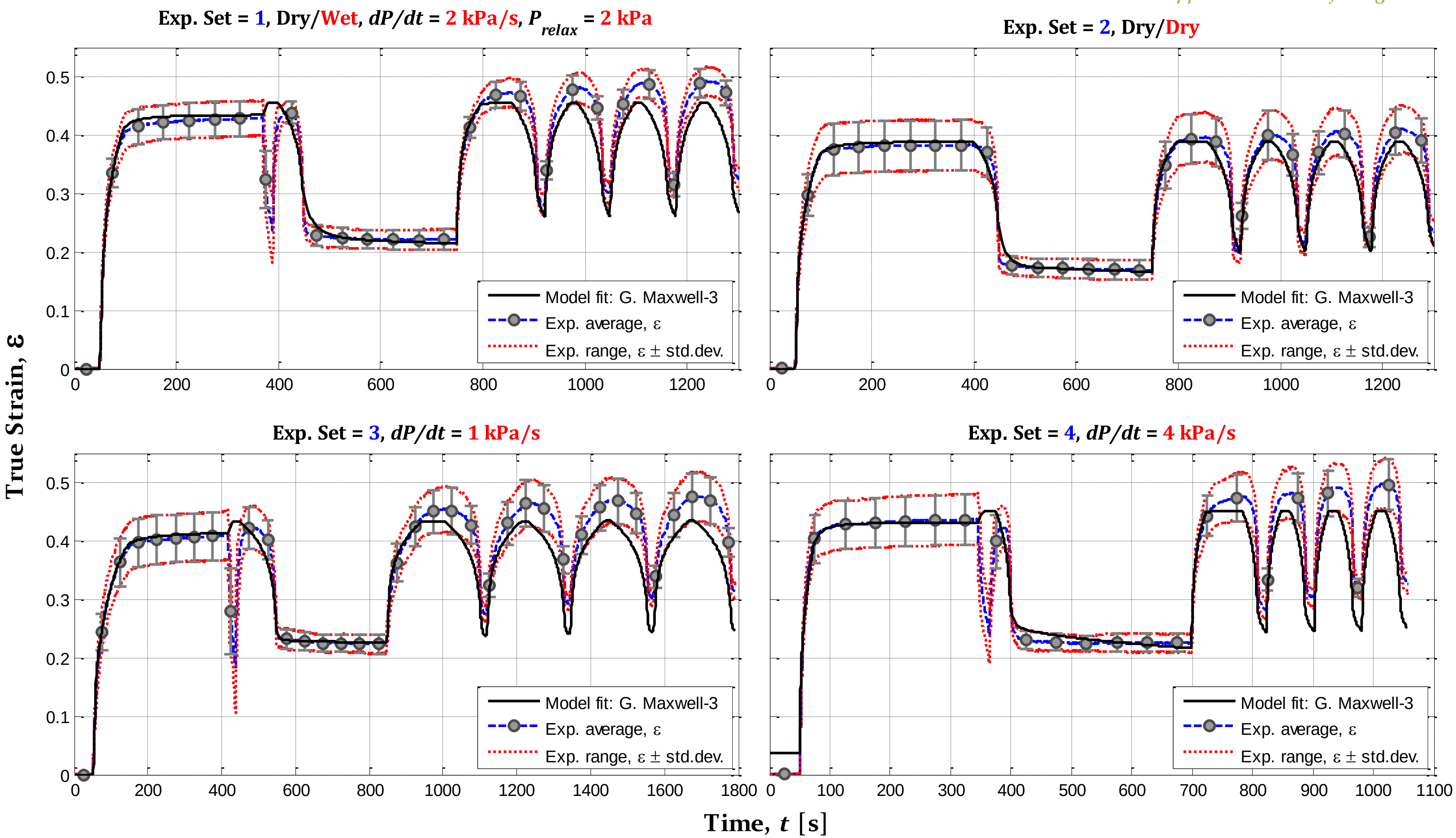

Figure D-83. Strain graph for Woven fabric using *G. Maxwell model, n=3* fitted to each experiment set separately using separate parameter sets.

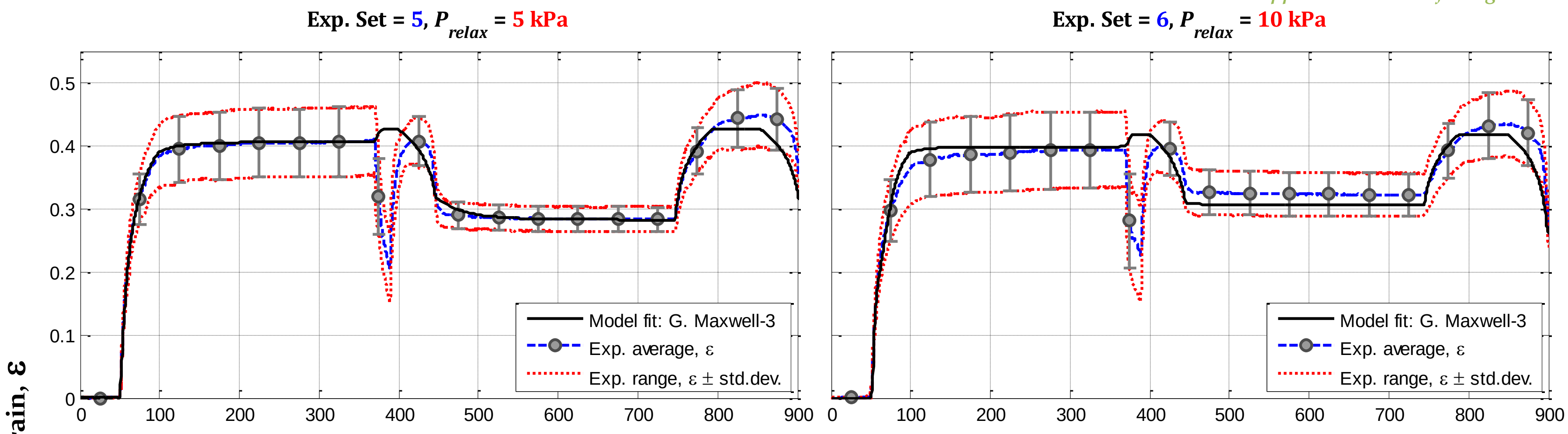

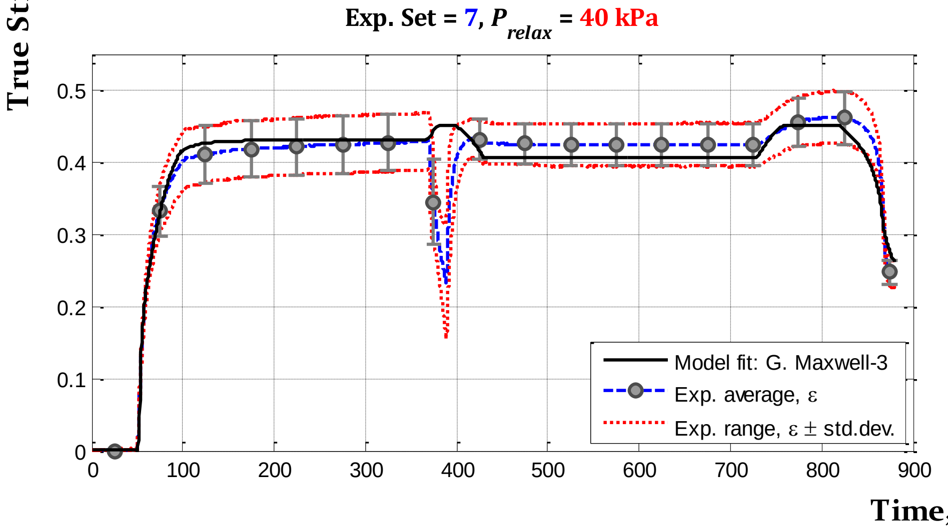

Set	E_0 [kPa]	m_0	E_1 [kPa]	m_1	c_1 [kPa.s]	E_2 [kPa]	m_2	c_2 [kPa.s]	E_3 [kPa]	m_3	c_3 [kPa.s]	R^2
1	35973.74	9.23	408.77	3.20	3029.97	381.70	1.50	501.98	11192.43	4.89	6431.45	0.898
2	76732.22	8.59	234.91	2.76	3448.77	37.68	0.60	433.42	37438.00	5.34	8921.22	0.958
3	68807.83	9.97	152.10	3.18	2107.25	216.92	0.52	229.98	2412.77	3.26	18813.58	0.870
4	23388.22	6.52	4123.18	5.36	2459.83	388.90	1.89	278.50	17534.91	4.37	4514.47	0.818
5	100320.63	10.79	78.15	1.30	901.16	33.84	0.82	671.10	3888.81	4.17	9424.17	0.966
6	87406.75	9.47	104.02	2.05	334.45	1291.57	0.48	169.44	13120.04	3.90	4998.61	0.968
7	57463.53	11.34	6716.45	4.48	2680.51	21.31	0.42	351.36	21386.24	5.44	5486.12	0.976

Figure D-84. (cont.) Strain graph for Woven fabric using *G. Maxwell model, n=3* fitted to each experiment set separately using separate parameter sets.

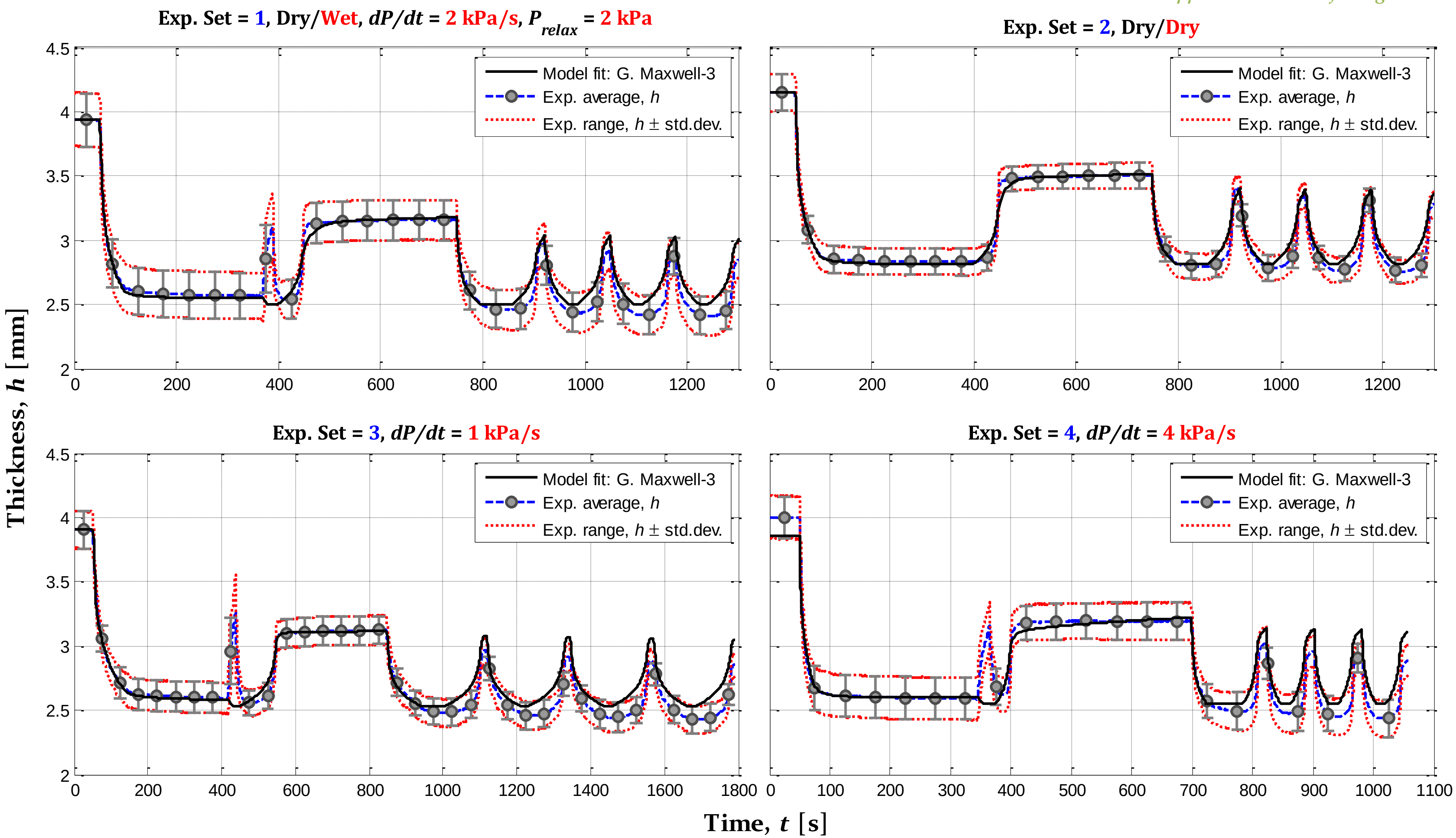

Figure D-85. Thickness graph for Woven fabric using G. Maxwell model, n=3 fitted to all experiment sets using a single parameter set.

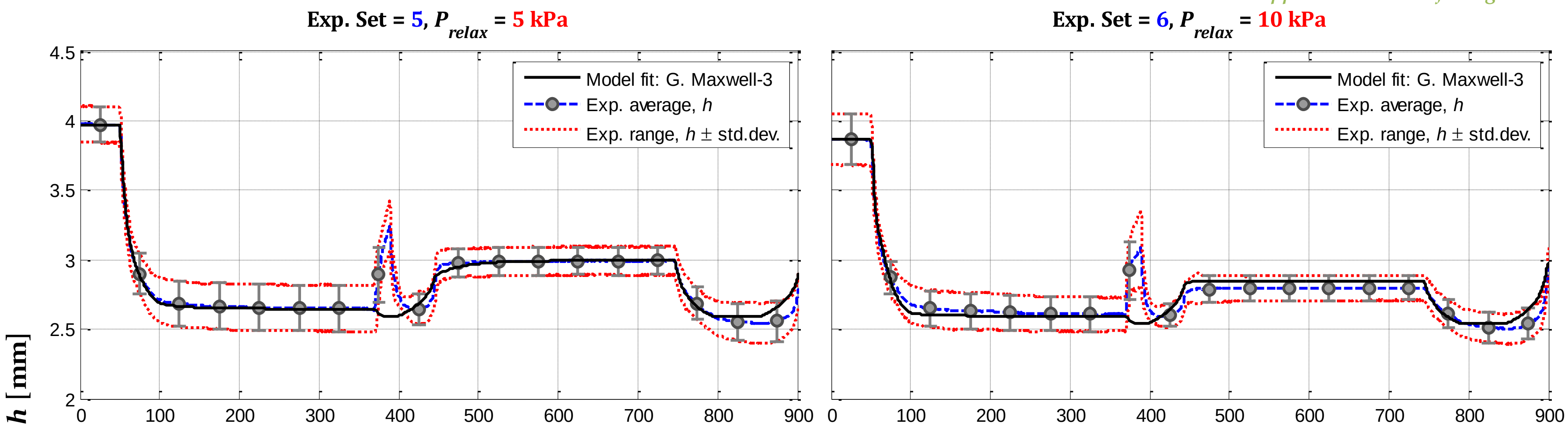

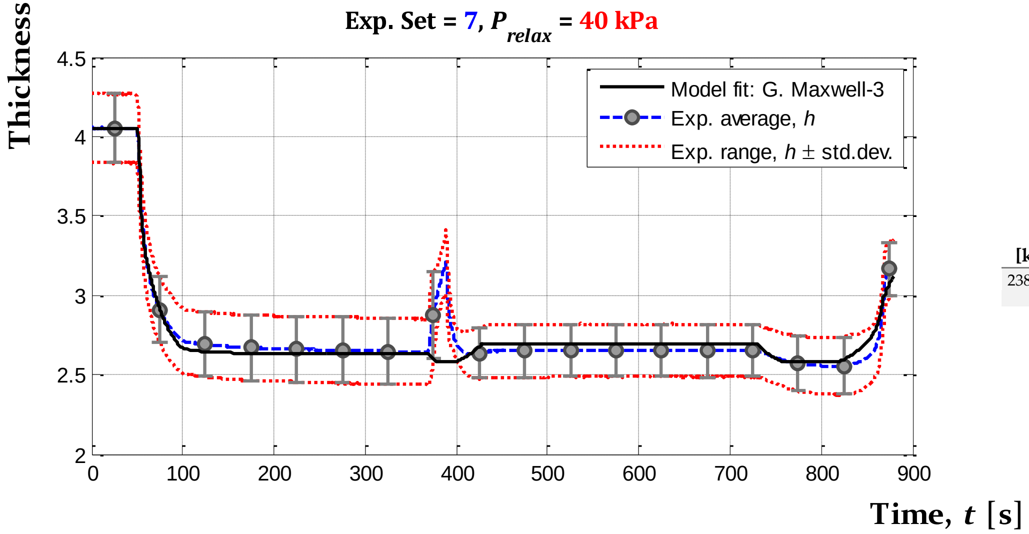

E_0 [kPa]	m_0	E_1 [kPa]	m_1	c_1 [kPa.s]	E_2 [kPa]	m_2	c_2 [kPa.s]	E_3 [kPa]	m_3	c_3 [kPa.s]	R^2
23844.50	6.49	4099.72	5.34	2467.15	389.71	1.89	280.07	17435.14	4.23	4504.44	0.922

Figure D-86. (cont.) Thickness graph for Woven fabric using *G. Maxwell model, n=3* fitted to all experiment sets using a single parameter set.

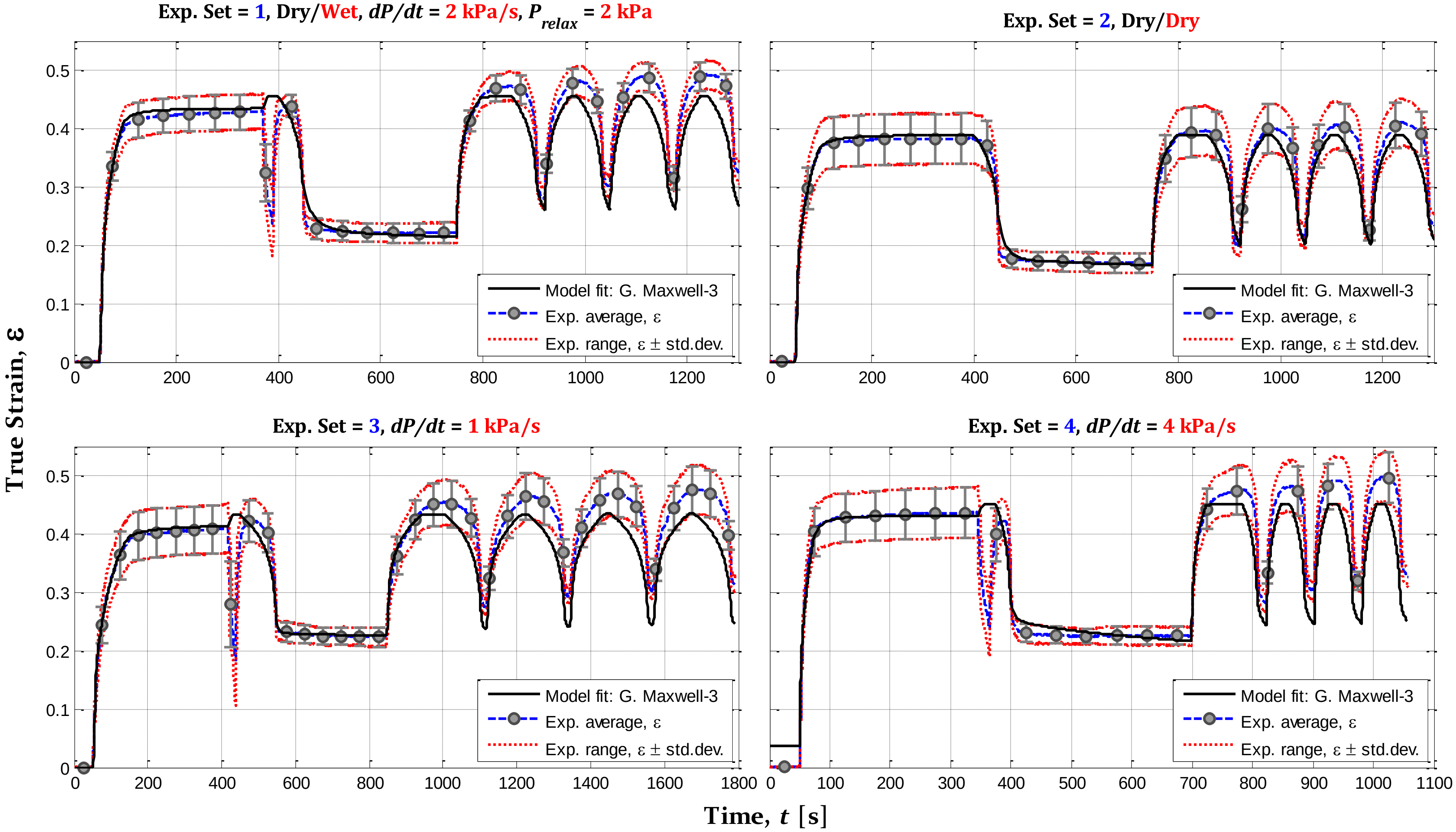

Figure D-87. Strain graph for Woven fabric using *G. Maxwell model, n=3* fitted to all experiment sets using a single parameter set.

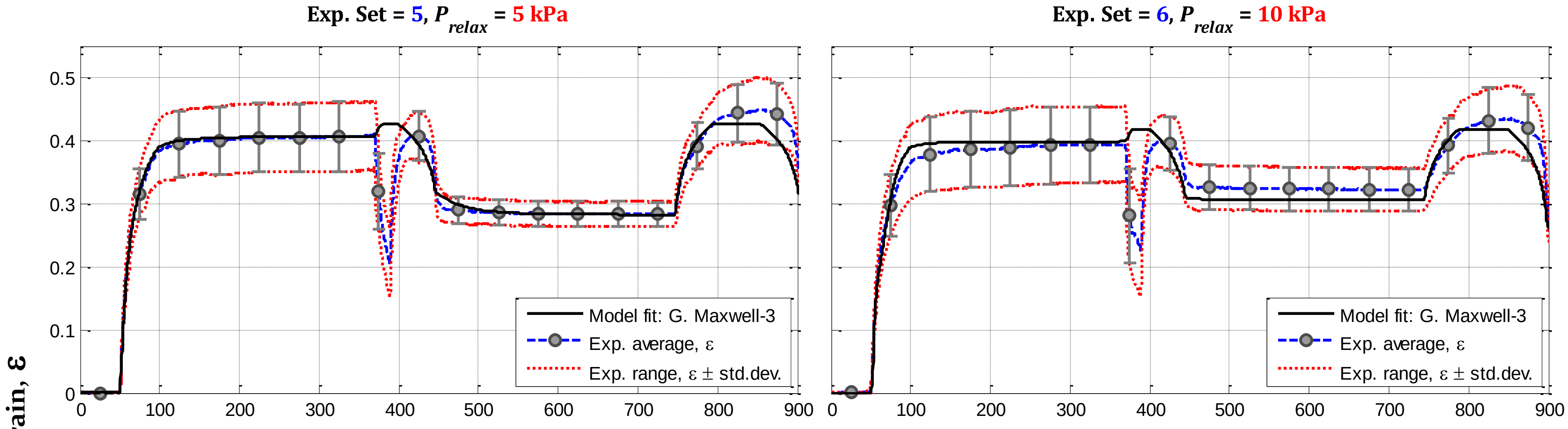

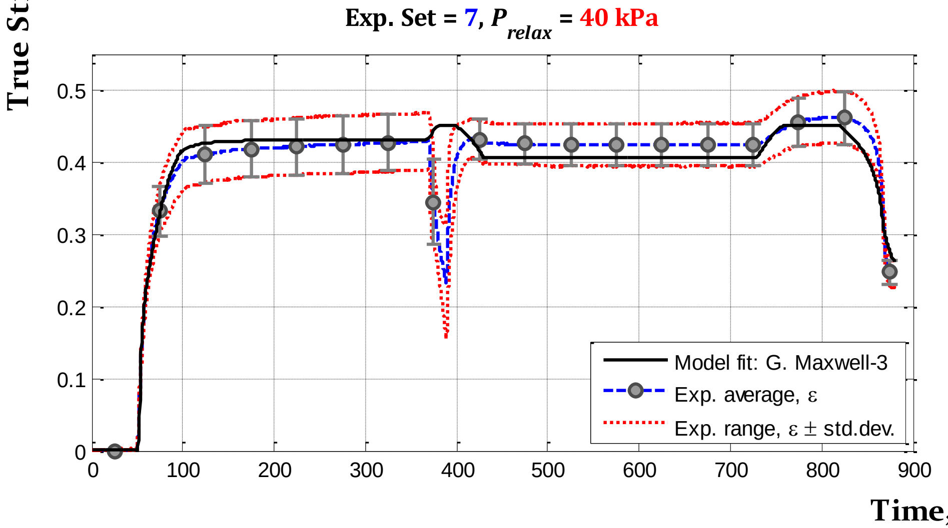

E_0 [kPa]	m_0	E_1 [kPa]	m_1	c_1 [kPa.s]	E_2 [kPa]	m_2	c_2 [kPa.s]	E_3 [kPa]	m_3	c_3 [kPa.s]	R^2
23844.50	6.49	4099.72	5.34	2467.15	389.71	1.89	280.07	17435.14	4.23	4504.44	0.922

Figure D-88. (cont.) Strain graph for Woven fabric using *G. Maxwell model, n=3* fitted to all experiment sets using a single parameter set.

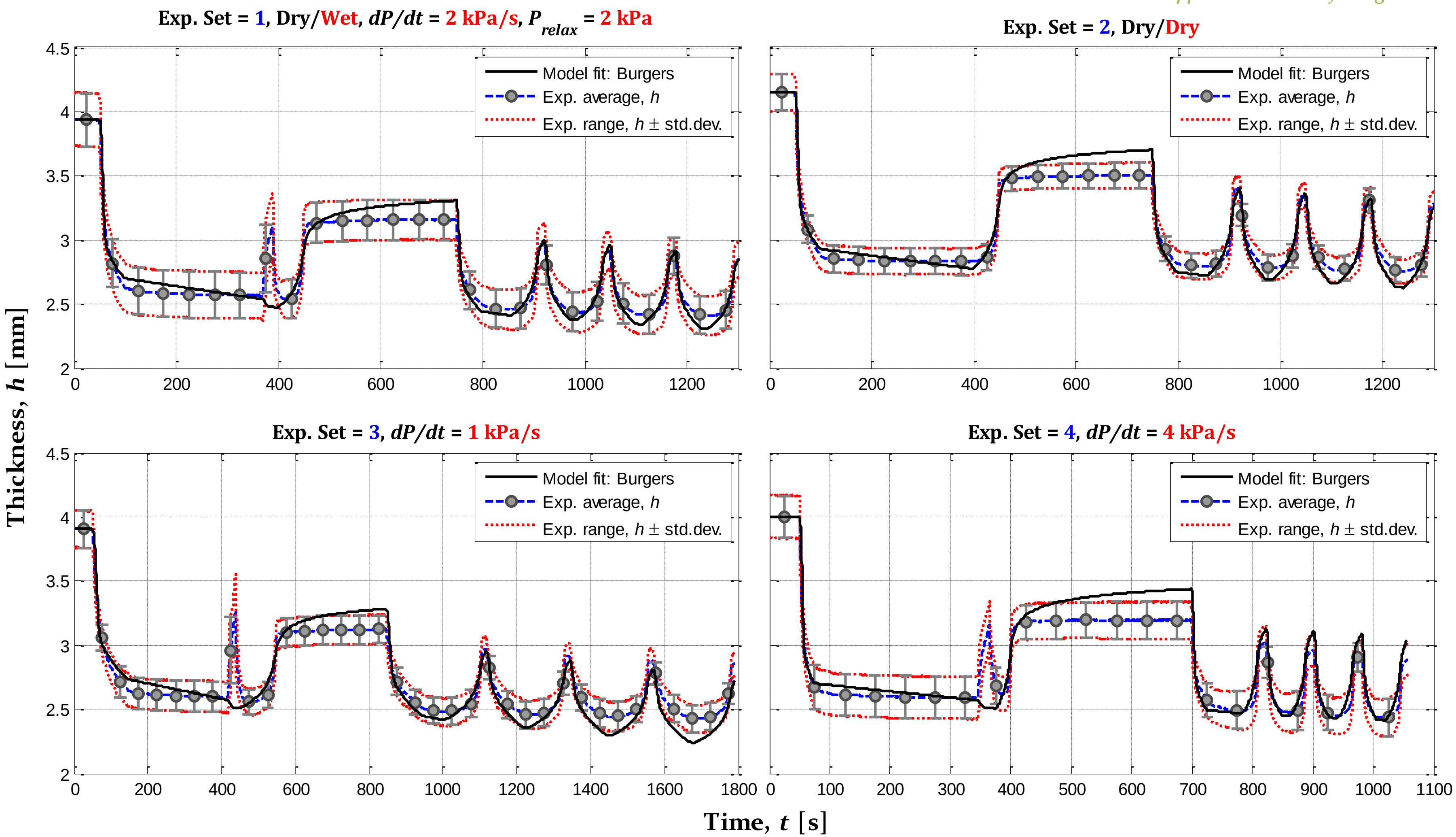

Figure D-89. Thickness graph for Woven fabric using *Burgers model* fitted to each experiment set separately using separate parameter sets.

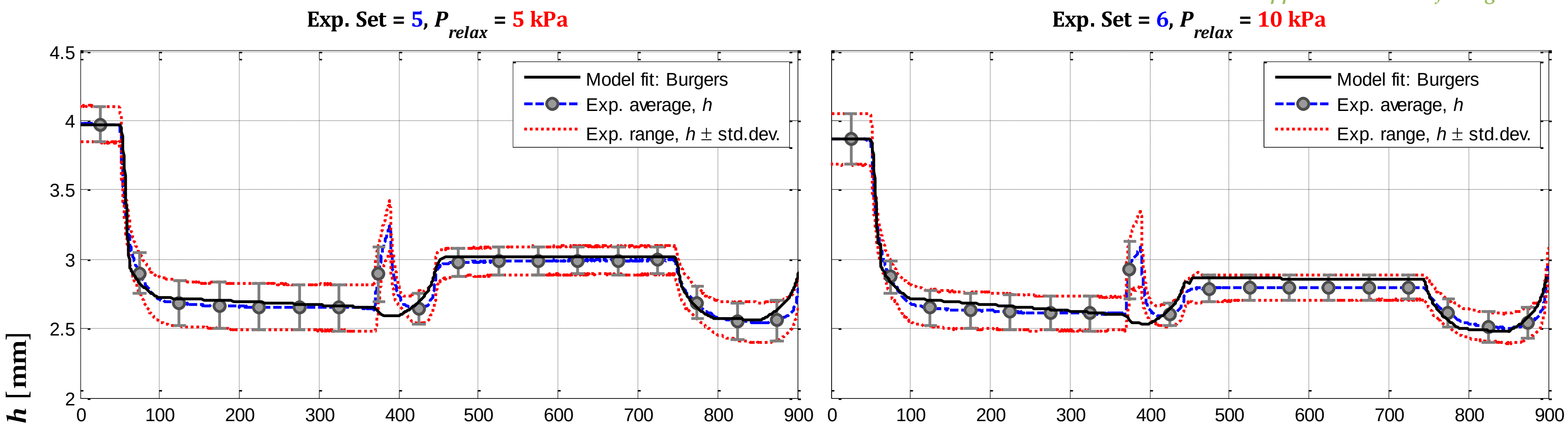

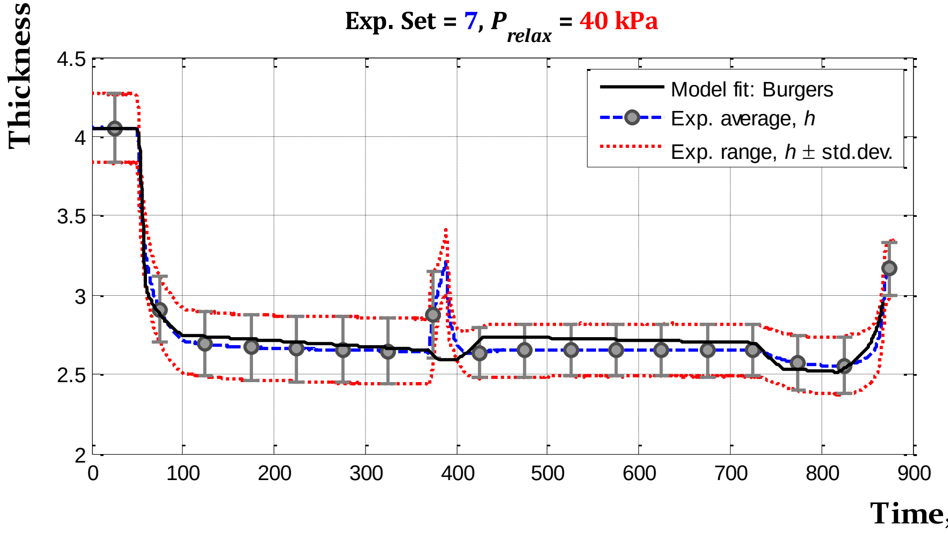

Set	E_1 [kPa]	m_1	c_1 [kPa.s]	E_2 [kPa]	m_2	c_2 [kPa.s]	R^2
1	9574.32	0.95	426976.60	36724.54	6.37	342.40	0.957
2	6957.58	0.55	539688.35	18187.19	5.09	337.82	0.939
3	2316.71	0.51	435051.78	22011.61	5.31	576.05	0.871
4	6730.59	0.53	531170.75	16897.46	5.88	304.64	0.919
5	2702.20	0.35	991732.37	68362.87	7.73	415.76	0.964
6	602.76	0.26	580002.11	37412.88	6.03	271.46	0.970
7	1631.22	0.37	738976.60	22791.27	6.20	242.44	0.974

Figure D-90. (cont.) Thickness graph for Woven fabric using *Burgers model* fitted to each experiment set separately using separate parameter sets.

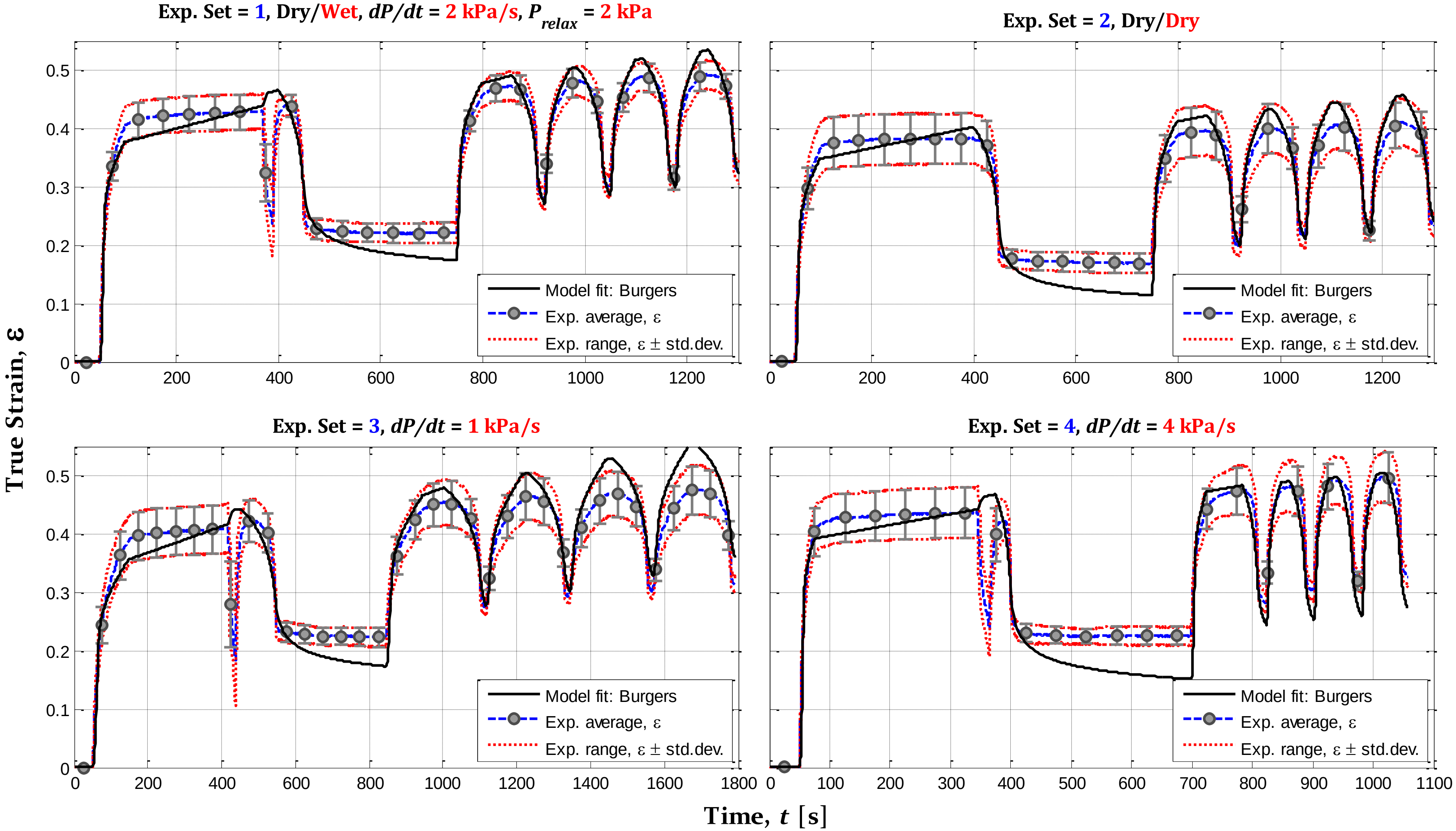

Figure D-91. Strain graph for Woven fabric using *Burgers model* fitted to each experiment set separately using separate parameter sets.

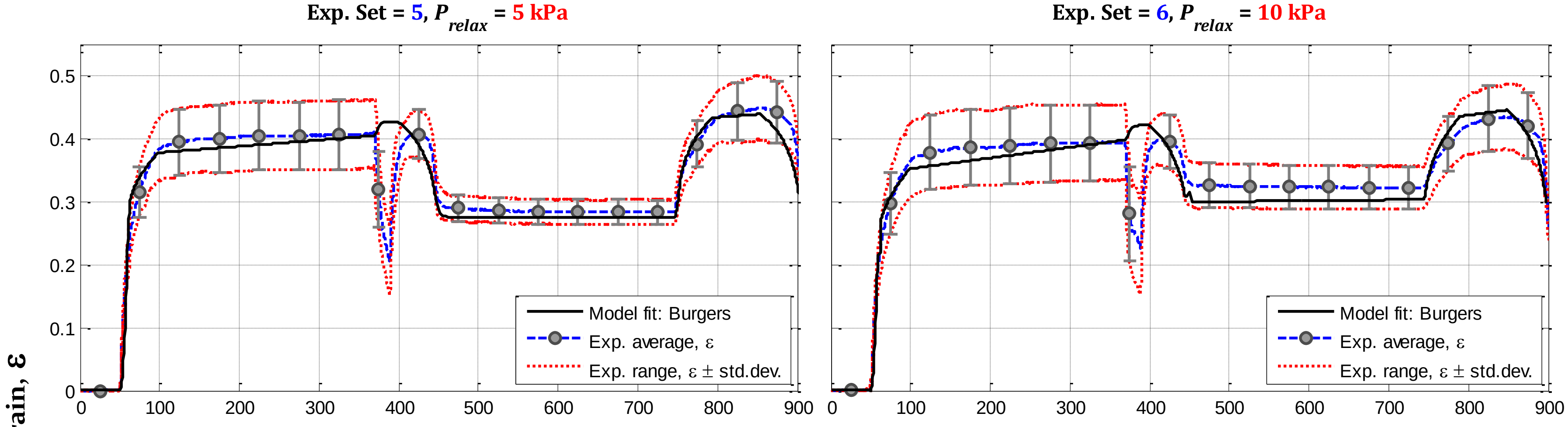

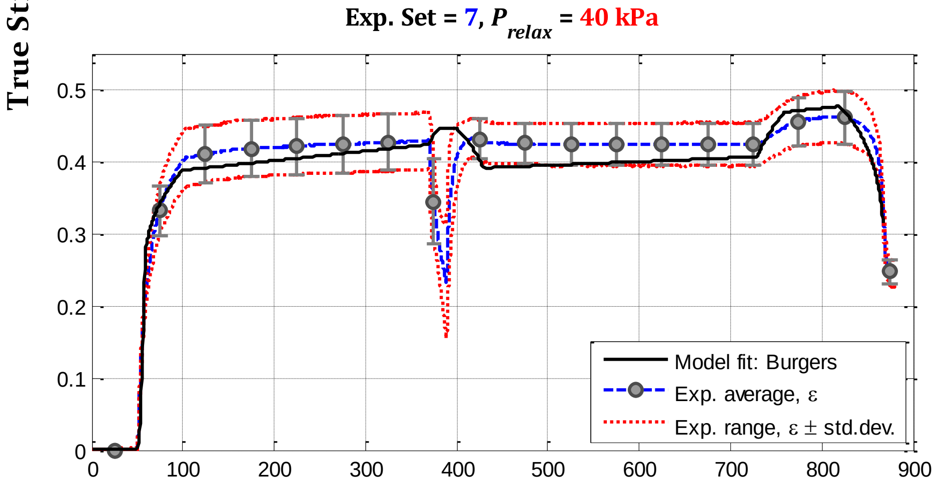

Set	E_1 [kPa]	m_1	c_1 [kPa.s]	E_2 [kPa]	m_2	c_2 [kPa.s]	R^2
1	9574.32	0.95	426976.60	36724.54	6.37	342.40	0.957
2	6957.58	0.55	539688.35	18187.19	5.09	337.82	0.939
3	2316.71	0.51	435051.78	22011.61	5.31	576.05	0.871
4	6730.59	0.53	531170.75	16897.46	5.88	304.64	0.919
5	2702.20	0.35	991732.37	68362.87	7.73	415.76	0.964
6	602.76	0.26	580002.11	37412.88	6.03	271.46	0.970
7	1631.22	0.37	738976.60	22791.27	6.20	242.44	0.974

Figure D-92. (cont.) Thickness graph for Woven fabric using *Burgers model* fitted to each experiment set separately using separate parameter sets.

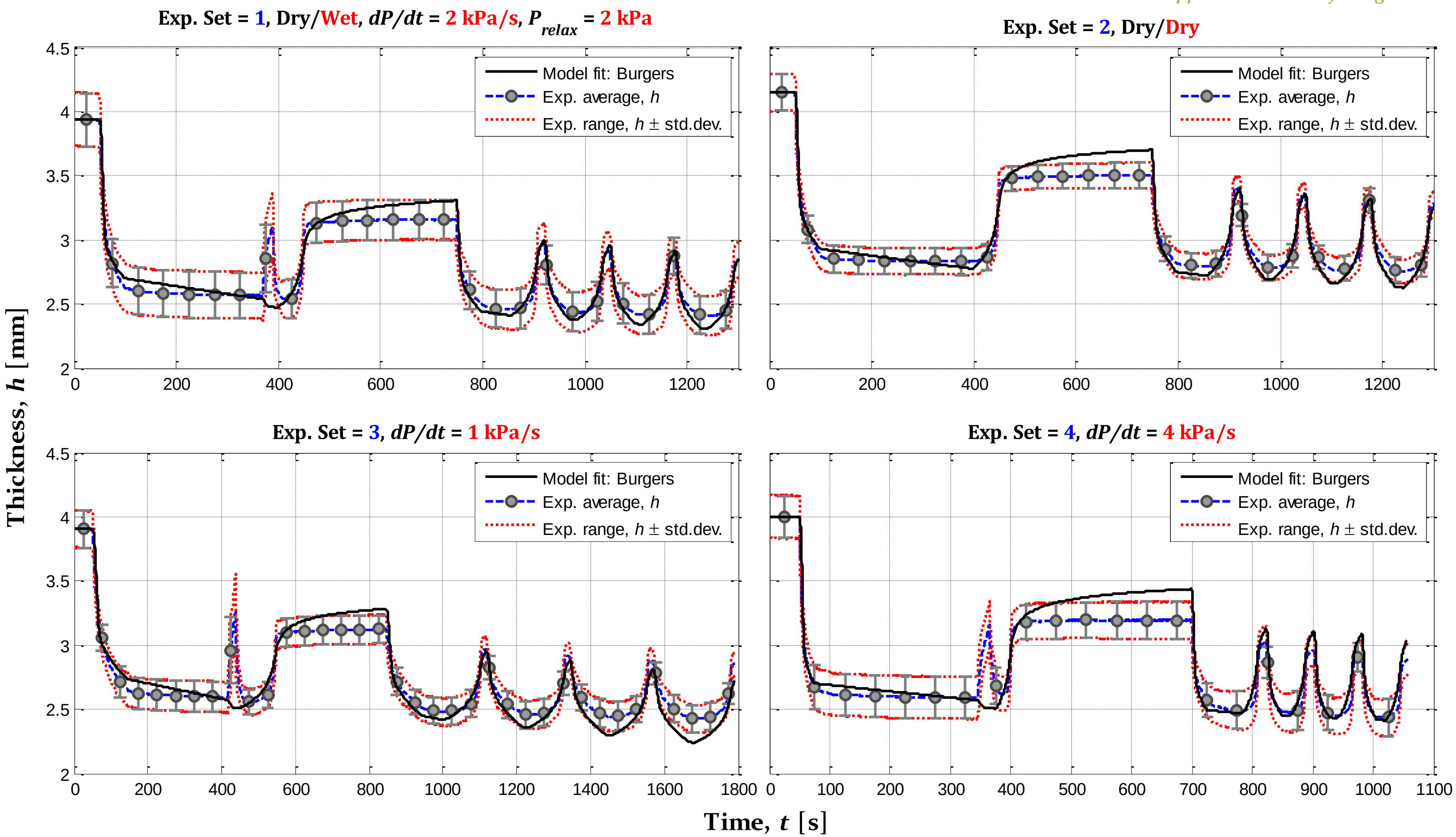

Figure D-93. Thickness graph for Woven fabric using *Burgers model* fitted to all experiment sets using a single parameter set.

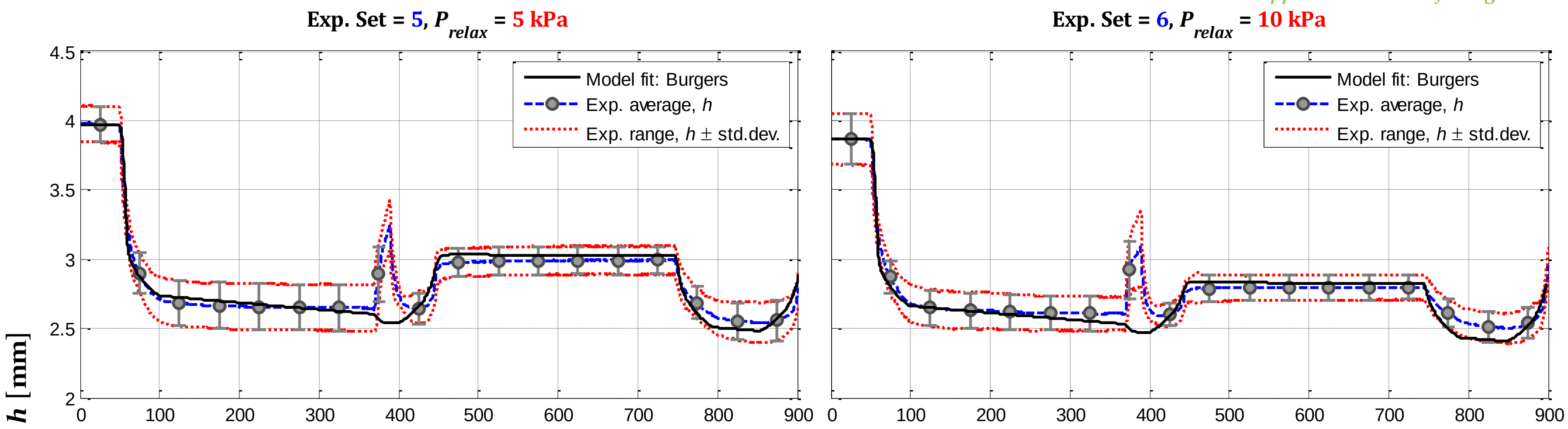

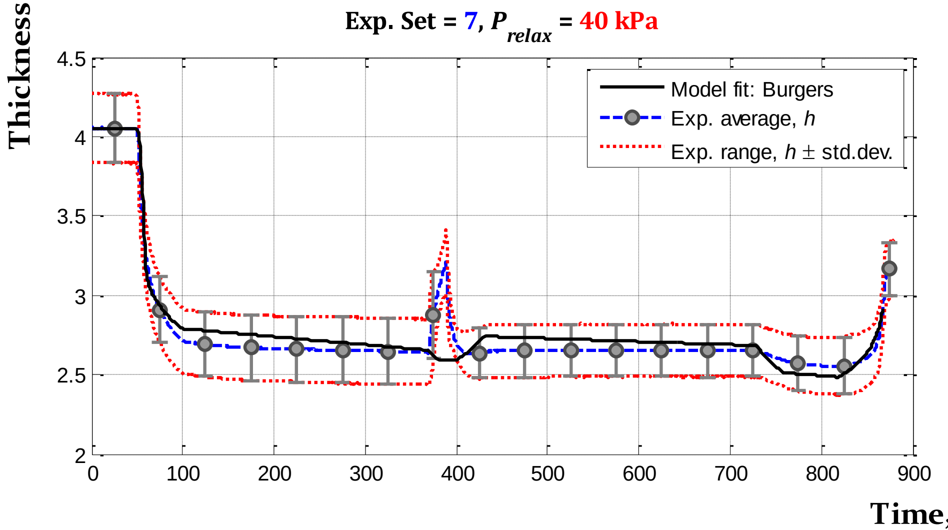

E_1 [kPa]	m_1	c_1 [kPa.s]	E_2 [kPa]	m_2	c_2 [kPa.s]	R^2
6687.68	0.53	526710.07	17468.58	5.48	327.16	0.942

Figure D-94. (cont.) Thickness graph for Woven fabric using *Burgers model* fitted to all experiment sets using a single parameter set.

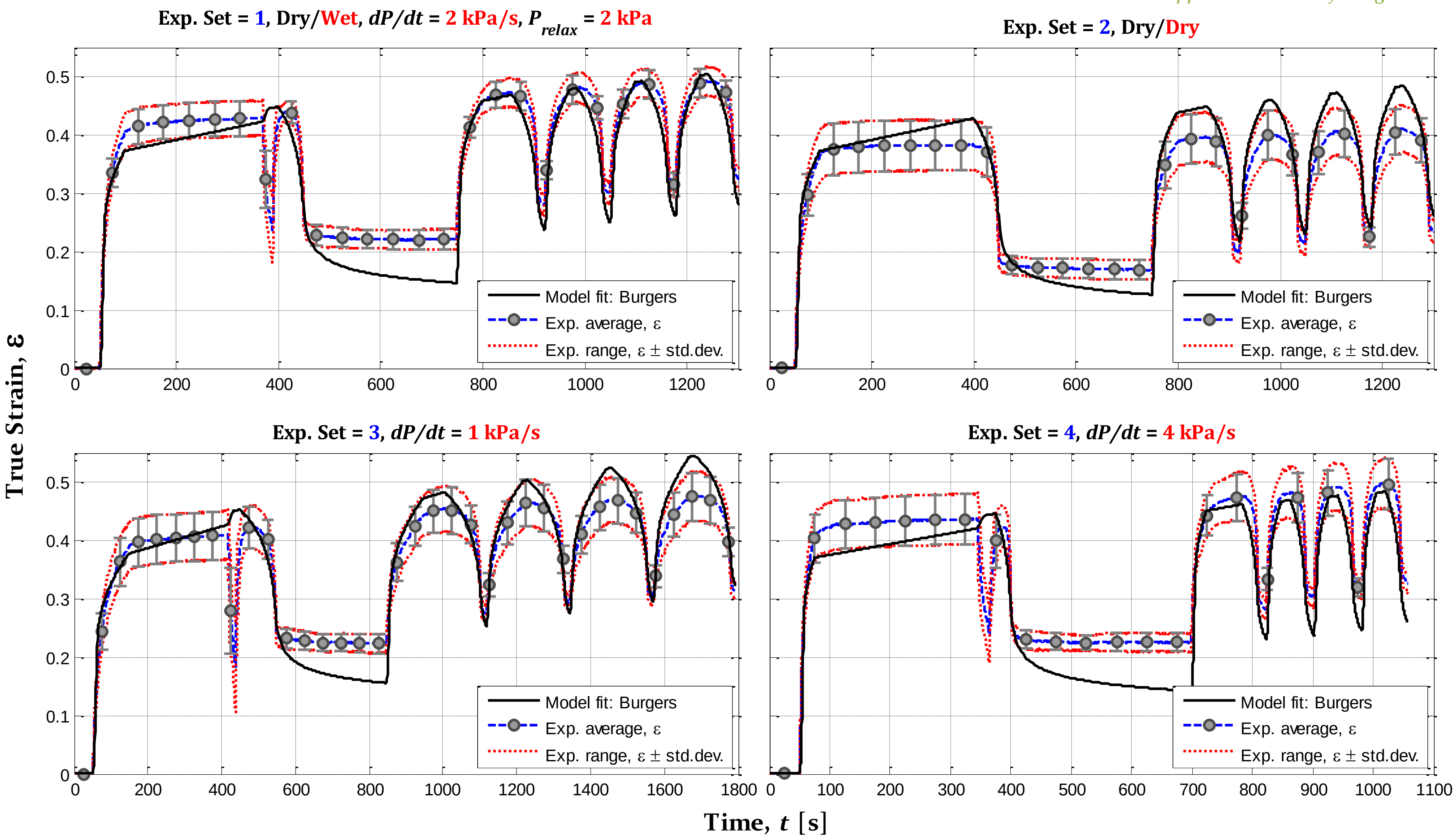

Figure D-95. Strain graph for Woven fabric using *Burgers model* fitted to all experiment sets using a single parameter set.

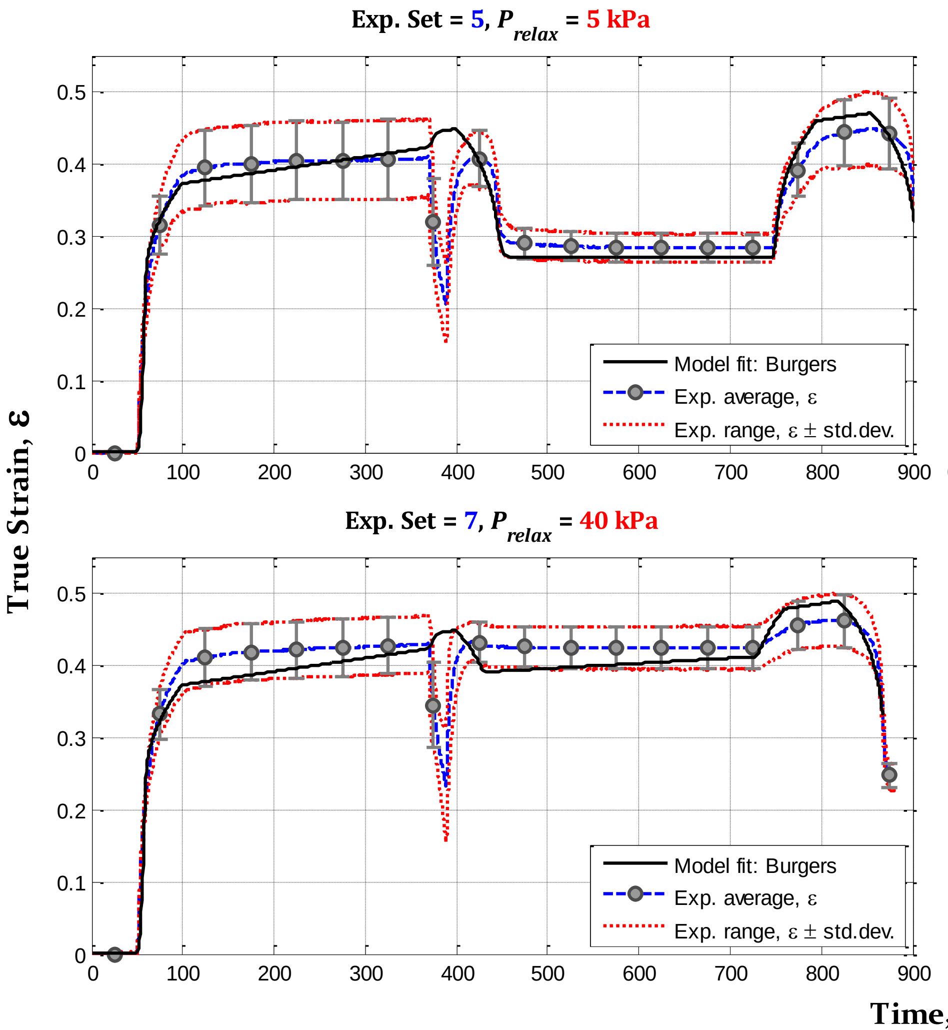

E_1 [kPa]	m_1	c_1 [kPa.s]	E_2 [kPa]	m_2	c_2 [kPa.s]	R^2
6687.68	0.53	526710.07	17468.58	5.48	327.16	0.942

Figure D-96. (cont.) Strain graph for Woven fabric using *Burgers model* fitted to all experiment sets using a single parameter set.

Appendix E *Elastic model*

E.I Tabulated results

	Set	E [kPa]	m	R^2
Random fabric	1	9.885e2	3.80	0.079
	2	8.011e2	3.82	0.087
	3	8.330e2	3.82	0.066
	4	8.719e2	3.69	-0.021
	5	2.874e3	4.84	0.580
	6	2.915e3	5.39	0.573
	7	8.045e2	3.77	0.610
	All	*1.198e3*	*4.18*	*0.282*

	Set	E [kPa]	m	R^2
Woven fabric	1	6.907e3	5.02	-0.530
	2	7.864e3	4.61	-0.154
	3	9.595e3	5.13	-0.534
	4	6.061e3	4.83	-0.597
	5	7.467e4	7.17	0.492
	6	9.920e4	7.26	0.524
	7	5.205e3	4.74	0.615
	All	*1.455e4*	*5.61*	*-0.026*

E.II Graphical Results

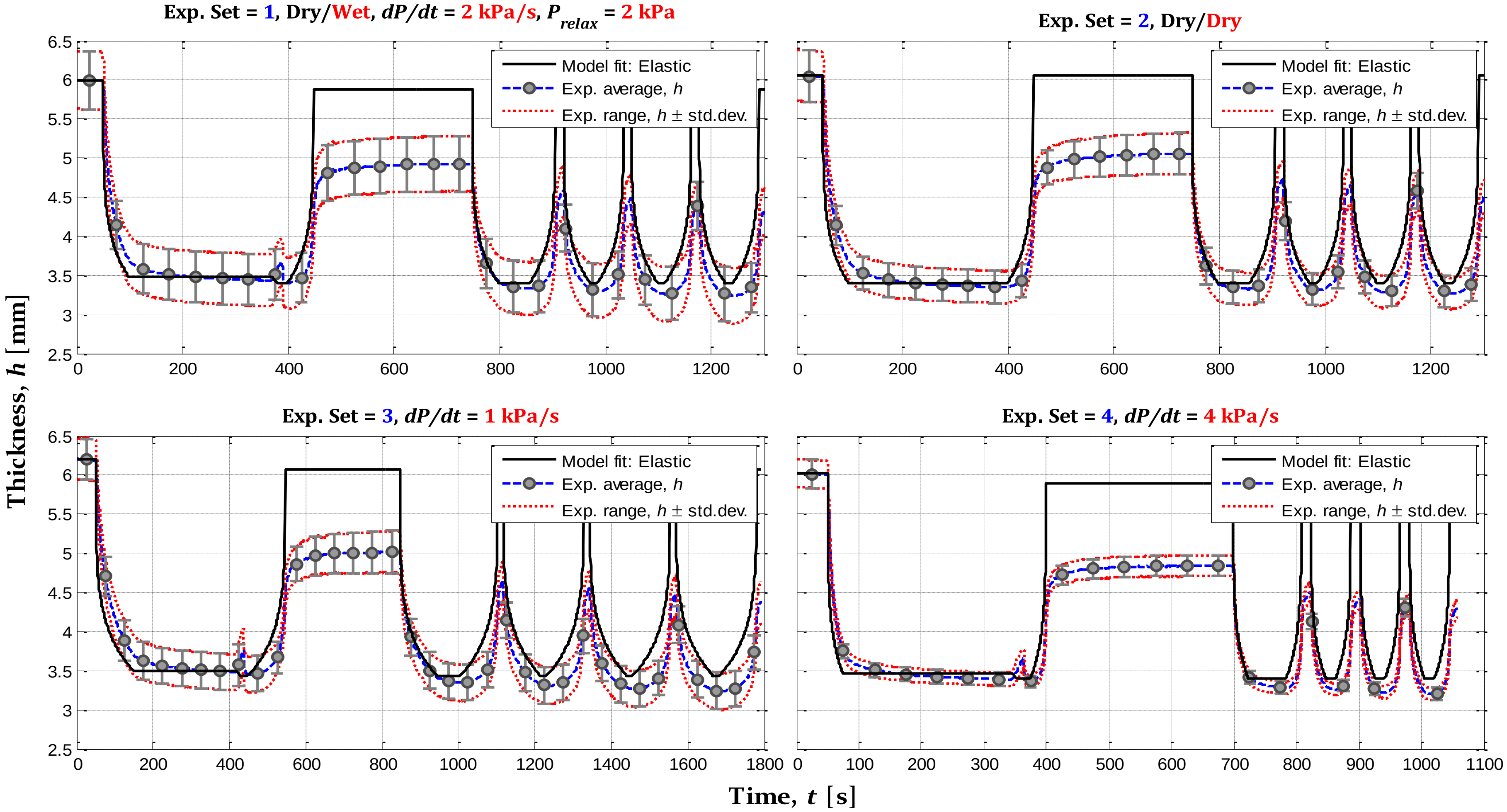

Figure E-1. Thickness graph for Random fabric using *elastic model* fitted to each experiment set separately using separate parameter sets.

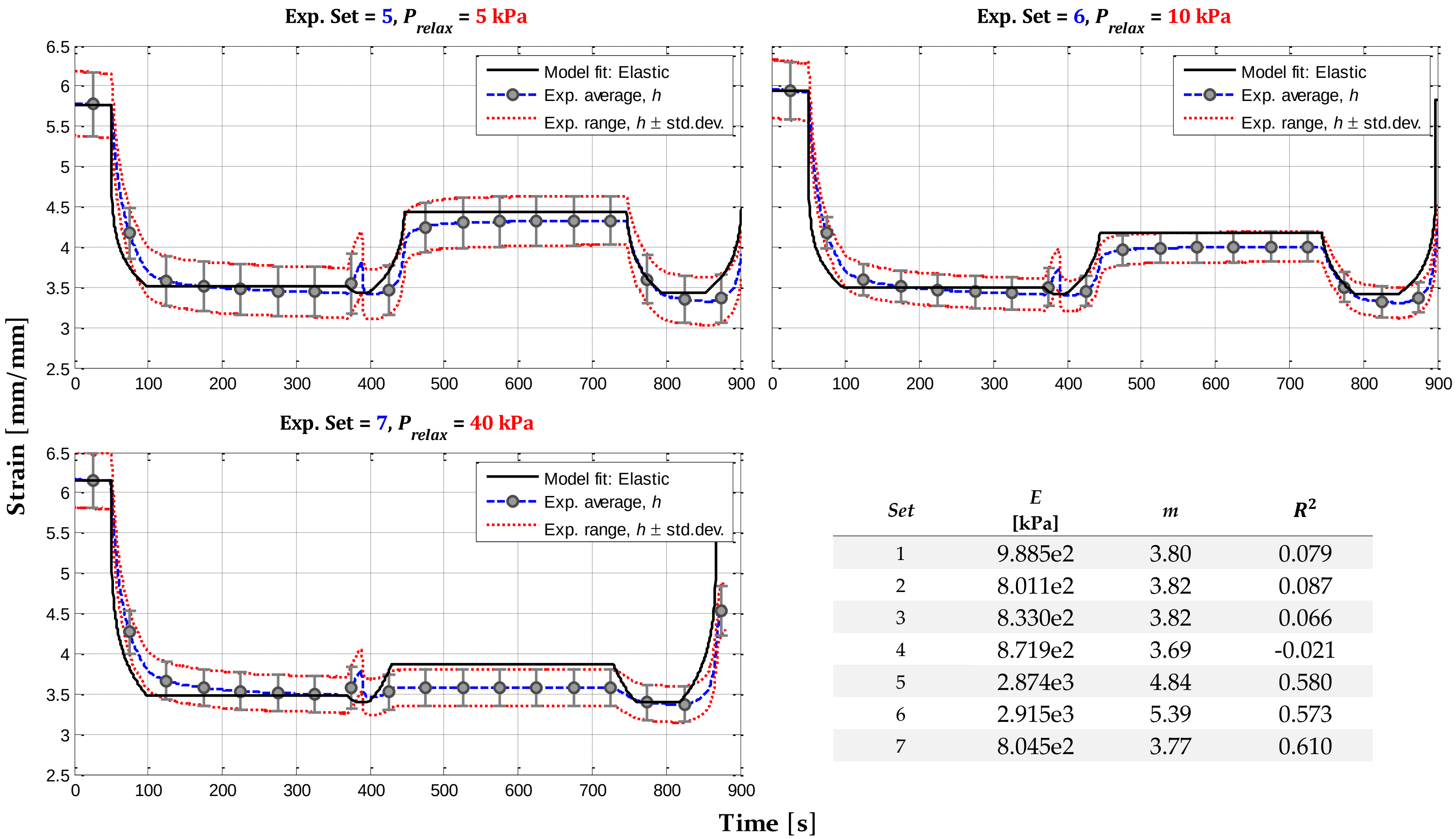

Set	*E* [kPa]	*m*	R^2
1	9.885e2	3.80	0.079
2	8.011e2	3.82	0.087
3	8.330e2	3.82	0.066
4	8.719e2	3.69	-0.021
5	2.874e3	4.84	0.580
6	2.915e3	5.39	0.573
7	8.045e2	3.77	0.610

Figure E-2. (cont.) Thickness graph for Random fabric using *elastic model* fitted to each experiment set separately using separate parameter sets.

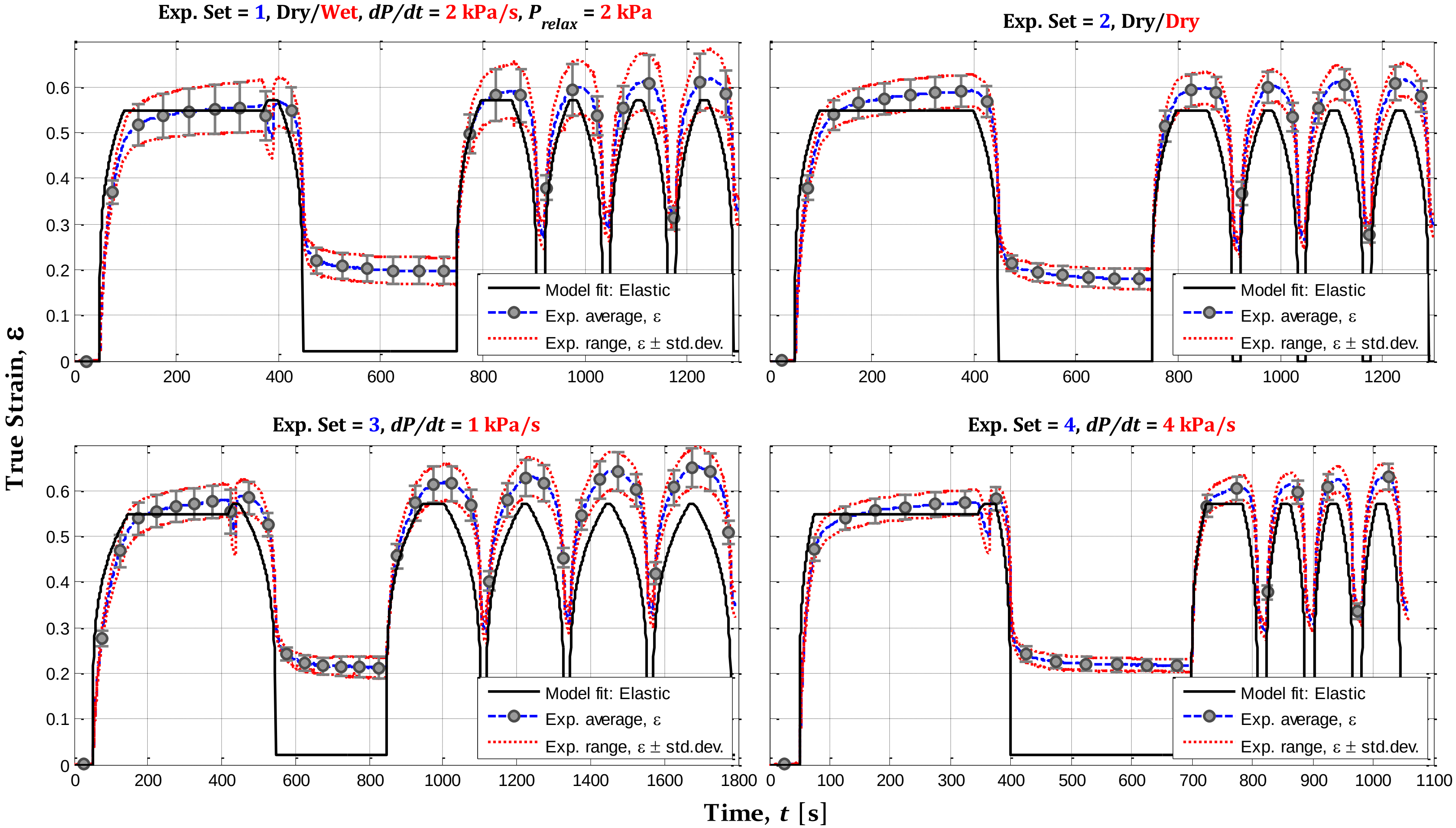

Figure E-3. Thickness graph for Random fabric using *elastic model* fitted to all experiment sets using a single parameter set.

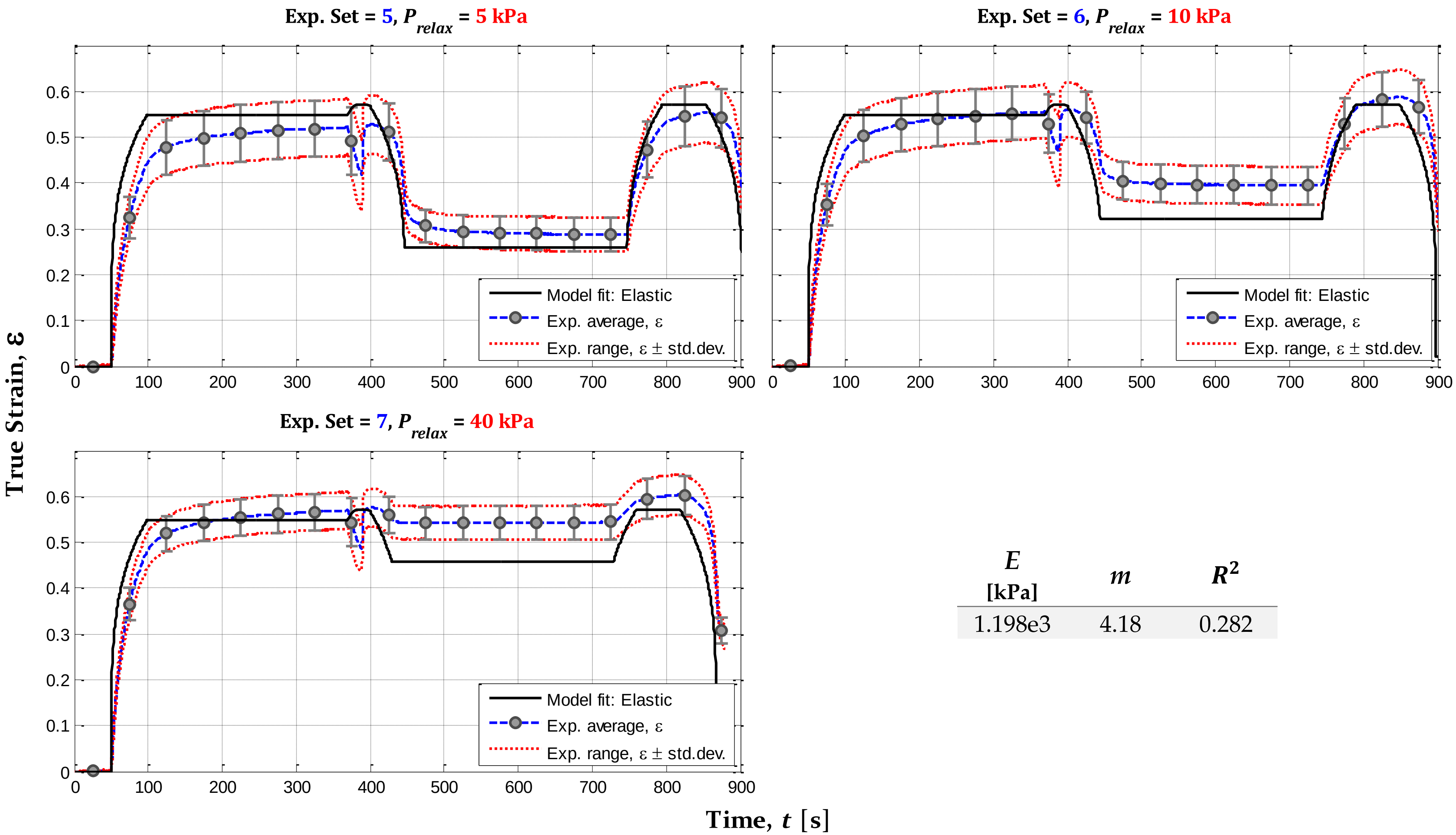

E [kPa]	m	R^2
1.198e3	4.18	0.282

Figure E-4. (cont.) Thickness graph for Random fabric using *elastic model* fitted to all experiment sets using a single parameter set.

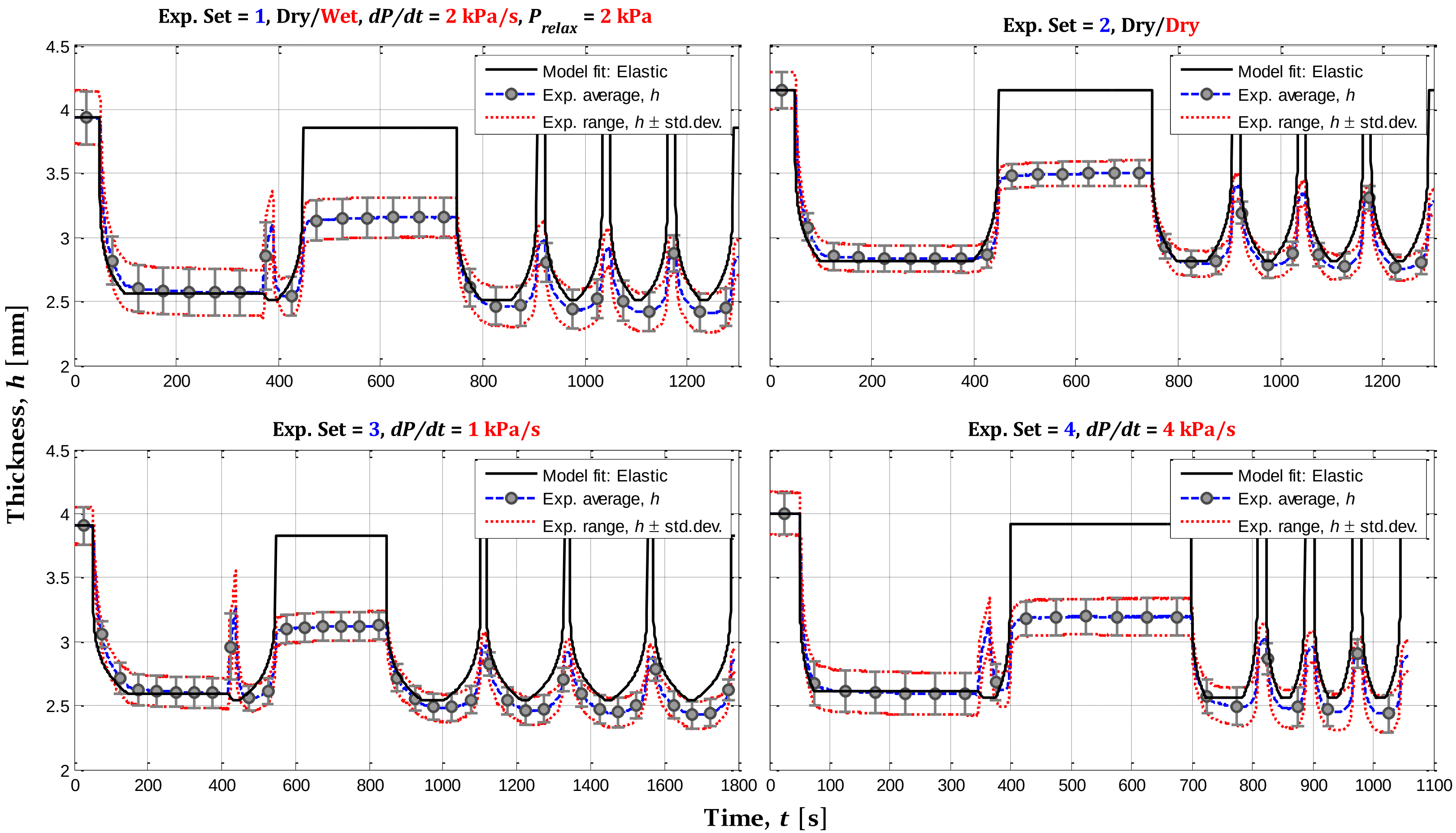

Figure E-5. Thickness graph for Woven fabric using *elastic model* fitted to each experiment set separately using separate parameter sets.

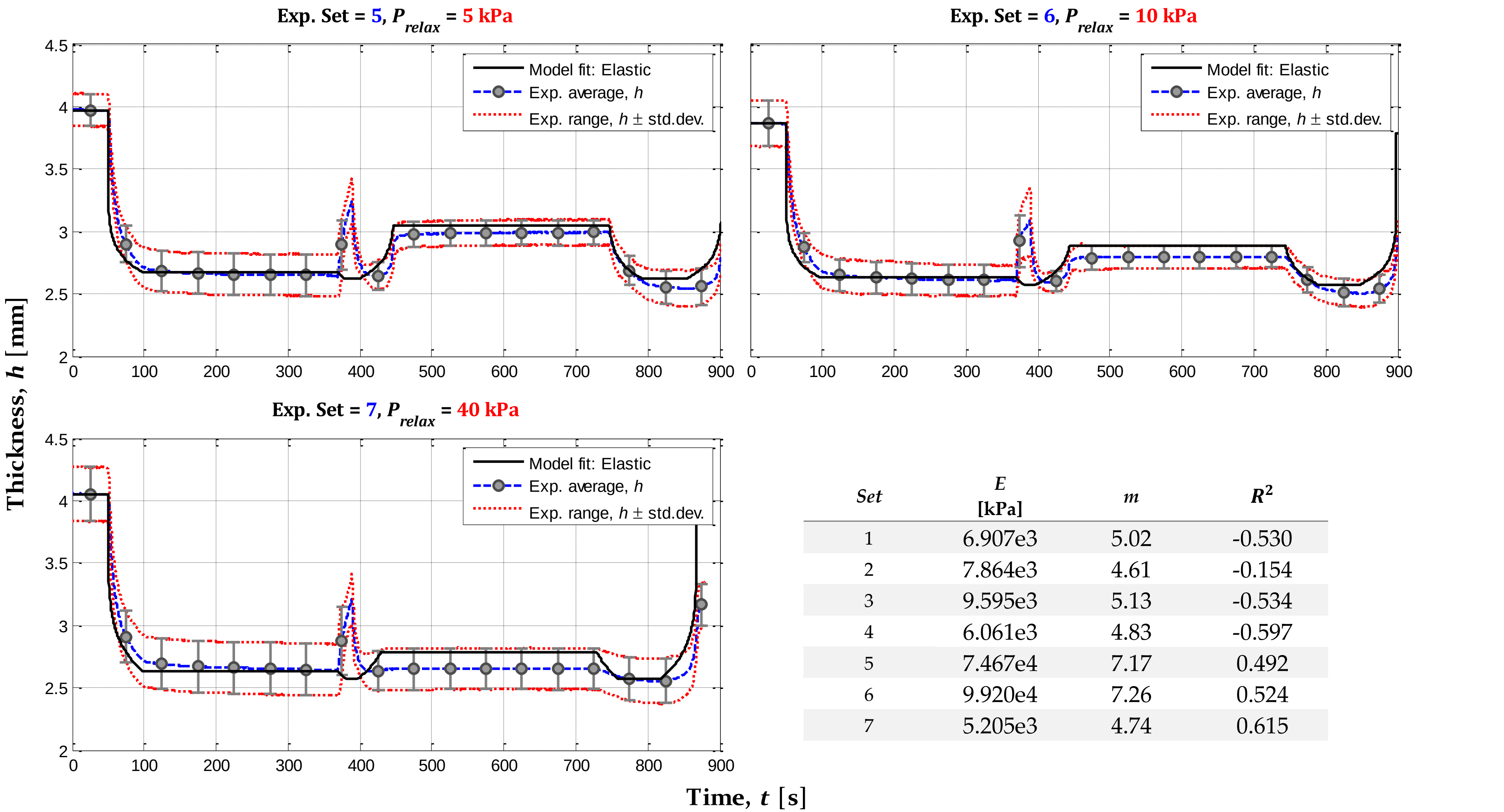

Set	*E* [kPa]	*m*	R^2
1	6.907e3	5.02	-0.530
2	7.864e3	4.61	-0.154
3	9.595e3	5.13	-0.534
4	6.061e3	4.83	-0.597
5	7.467e4	7.17	0.492
6	9.920e4	7.26	0.524
7	5.205e3	4.74	0.615

Figure E-6. (cont.) Thickness graph for Woven fabric using *elastic model* fitted to each experiment set separately using separate parameter sets.

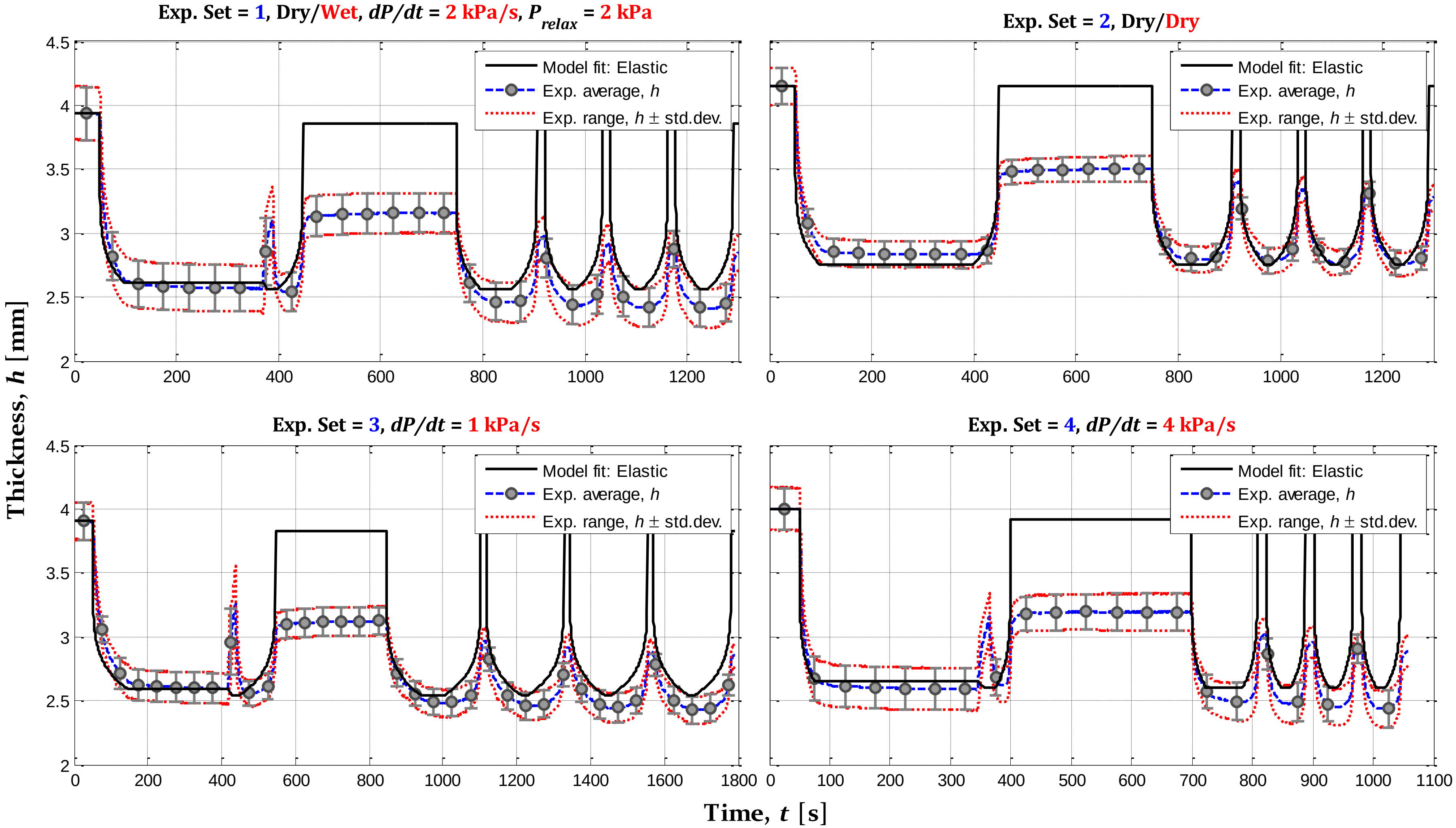

Figure E-7. Thickness graph for Woven fabric using *elastic model* fitted to all experiment sets using a single parameter set.

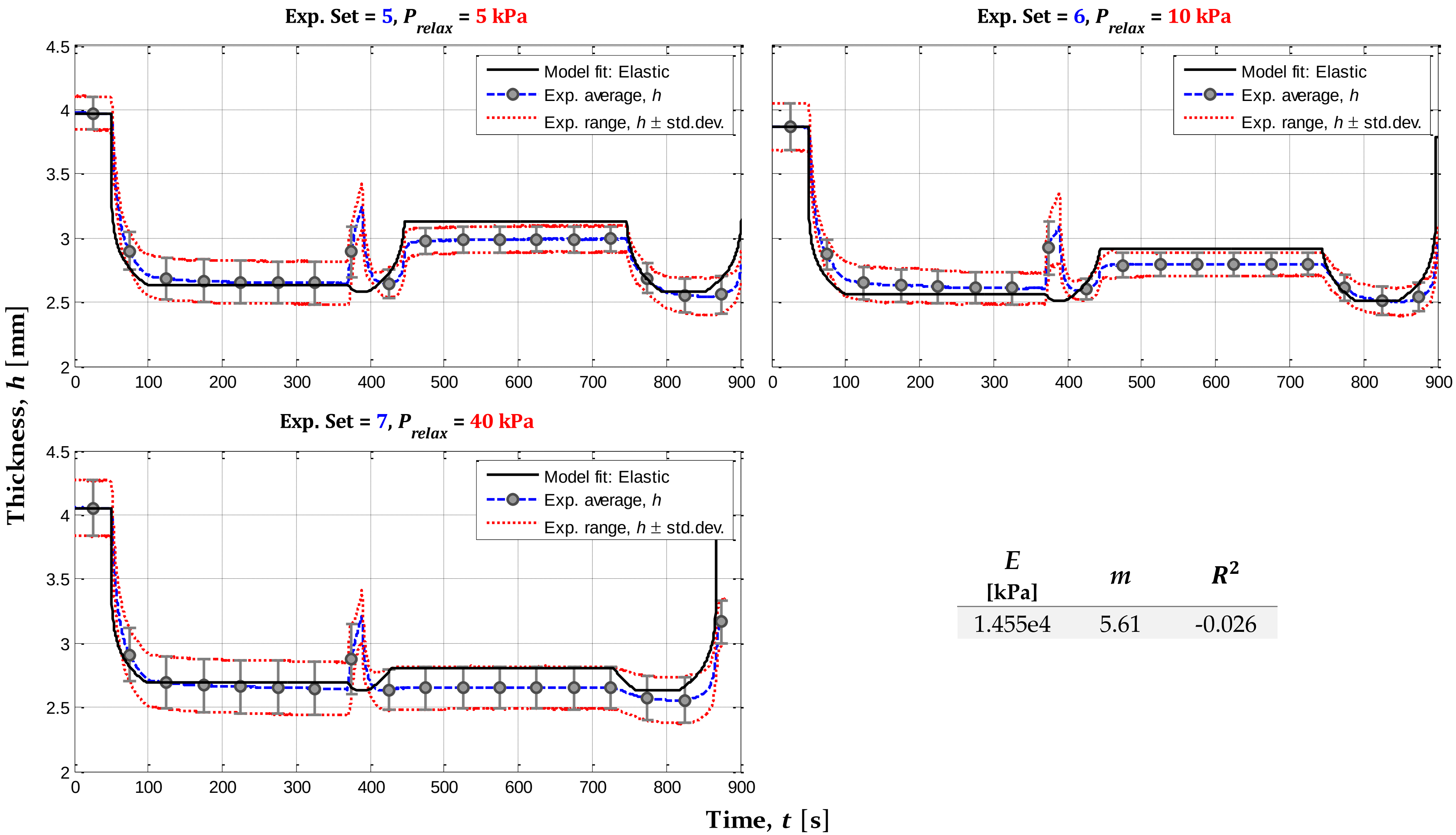

E [kPa]	m	R^2
1.455e4	5.61	-0.026

Figure E-8. (cont.) Thickness graph for Woven fabric using *elastic model* fitted to all experiment sets using a single parameter set.